

1127-21

JOURNAL OF 1-16 COLLOID SCIENCE

Editor-in-Chief

VICTOR K. LA MER, Columbia University, New York

Advisory Board

C. O. BECKMANN
KATHARINE B. BLODGETT
K. F. BONHOEFFER
M. L. CORRIN
P. J. W. DEBYE
JOHN T. EDSALL
I. FANKUCHEN
JOHN D. FERRY
A. R. GORDON
WILFRIED HELLER
ERIC HUTCHINSON
JOHN G. KIRKWOOD
E. C. LINGAFELTER
L. G. LONGSWORTH
J. W. MCBAIN

J. TH. G. OVERBEEK
R. RUYSSSEN
E. K. RIDEAL
WILLIAM SEIFRIZ
LEO SHEDLOVSKY
THEODORE SHEDLOVSKY
ROBERT SIMHA
JACINTO STEINHARDT
THE SVEDBERG
HUGH S. TAYLOR
ARNE TISELIUS
ROBERT D. VOLD
BERNARD VONNEGUT
RALPH W. G. WYCKOFF
BRUNO H. ZIMM

VOLUME 7

1952

ACADEMIC PRESS INC., PUBLISHERS
NEW YORK, N. Y.

Copyright, 1952, by Academic Press Inc.
Made in United States of America

DIELECTRIC CHARACTERISTICS OF PIGMENT DISPERSIONS

Andries Voet and Louis R. Suriani

Research Department, J. M. Huber Corporation, Borger, Texas

Received October 12, 1951

I. INTRODUCTION

The dielectric characteristics of nonaqueous dispersions of materials of high dielectric constants dispersed in media of low dielectric constants have been previously reported (1). Data were obtained for dispersions in a quiescent state as well as when subjected to shear. This method yielded general conclusions about the shape, orientation, and agglomeration of the particles in the dispersion and gave a more complete account of the process of formation and destruction of particle structures in concentrated dispersions than was hitherto possible by means of rheological methods.

The materials previously investigated were metallic pigments and carbon black. Furthermore, titanium dioxide and similar materials of a high dielectric constant were studied. Dispersions were prepared in mineral or vegetable oils.

The present investigation is an extension of previous work to dispersions of colored pigments, many of which have a dielectric constant of the same order of magnitude as the dispersion medium. A series of organic and inorganic colored pigments were dispersed in three vehicles, namely a medium-bodied linseed oil, a heavy mineral oil, and a limed rosin-mineral oil varnish. The dielectric constants were determined at rest as well as when subjected to shear, in dispersions of different concentrations.

II. THEORETICAL PART

The dielectric constant ϵ of a dispersion of spherical particles of a dielectric constant ϵ_p , dispersed in a volume fraction v in a medium of a dielectric constant ϵ_M , has been derived theoretically by Bruggeman (2). More recently, a somewhat refined calculation has been introduced by Boettcher (3). From extensive investigations by Van Vessel (4), it appears that both equations, which do not differ greatly, are in satisfactory agreement with experiments on powdered ionic crystals, provided certain precautions, to be discussed later, are taken.

The equation derived by Boettcher is as follows:

$$\frac{\epsilon - \epsilon_M}{3\epsilon} = v \frac{\epsilon_p - \epsilon_M}{\epsilon_p + 2\epsilon} \quad [1]$$

This equation may be written in the following form:

$$\frac{\epsilon_M}{\epsilon} = 1 - 3v \frac{\epsilon_p - \epsilon_M}{\epsilon_p + 2\epsilon}, \quad [2]$$

$$\epsilon = \epsilon_M \frac{1}{1 - 3v \frac{\epsilon_p - \epsilon_M}{\epsilon_p + 2\epsilon}}. \quad [3]$$

For a small value of v , the following approximation holds:

$$\epsilon = \epsilon_M \left(1 + 3v \frac{\epsilon_p - \epsilon_M}{\epsilon_p + 2\epsilon} \right). \quad [4]$$

For $\epsilon_p/\epsilon_M \gg 1$

$$\epsilon = \epsilon_M(1 + 3v). \quad [5]$$

This equation is valid for particles with a high dielectric constant dispersed in a vehicle with a low dielectric constant. The identical equation may be derived from Bruggeman's equation by applying the same limiting conditions.

For $\epsilon_p/\epsilon_M = 1$, we find:

$$\epsilon = \epsilon_M. \quad [6]$$

For $\epsilon_p/\epsilon_M \simeq /$, and v is small, we may replace ϵ in the right hand side of Eq. [4] with ϵ_M , resulting in the following approximation:

$$\epsilon = \epsilon_M \left(1 + 3v \frac{\epsilon_p - \epsilon_M}{\epsilon_p + 2\epsilon_M} \right) \quad [7]$$

or,

$$\epsilon = \epsilon_M(1 + kv), \quad [7a]$$

whereby

$$k = 3 \frac{\epsilon_p - \epsilon_M}{\epsilon_p + 2\epsilon_M}. \quad [7b]$$

For nonspherical particles the problem becomes rather complex. Calculations by Polder and Van Santen (5) have shown that the dielectric constant of a dispersion of nonspherical particles is only slightly affected by the particle shape when particle and medium have dielectric constants of the same order of magnitude. Large deviations from Boettcher's equation due to the nonspherical shape of the particles, however, are to be expected when the particles have a considerably higher dielectric constant than the medium.

It was shown experimentally that for dispersions of particles with a large dielectric constant the following relationship generally holds for concentrations up to about 10% by volume (1):

$$\epsilon = \epsilon_M(1 + 3fv), \quad [8]$$

where f is a form factor. For spherical particles, $f = 1$; while for non-spherical particles, $f > 1$.

If particle agglomeration occurs, the shape of the complex formed differs from the shape of the original particles. The change in shape due to agglomeration leads to a change in dielectric constant. The following relationship appears to be valid (1):

$$\epsilon = \epsilon_M(1 + 3a_v f v), \quad [9]$$

whereby a_v is the agglomeration factor corresponding to each concentration v . A method for determining a_v is by measuring dielectric constants first in a quiescent liquid, allowing agglomeration to take place. The measurements are then repeated in liquids subjected to shear, which destroys the agglomeration mechanically, reducing the agglomeration factor to unity.

In addition, orientation of nonspherical particles in the direction of the electric field appeared to lead to an increased dielectric constant, while a decrease in dielectric constant was observed for orientation of nonspherical particles perpendicular to the electric field. These observations are in complete accord with the theory of Bruggeman. This was recently confirmed by orientation of ferromagnetic particles in a magnetic field (6).

While the dielectric characteristics yield valuable information about the inner structure of a dispersion of particles of a dielectric constant high compared to the dielectric constant of the medium, the following investigation has been carried out with the object of studying the inner structure of dispersions of particles in media of dielectric constants of a comparable magnitude.

III. EXPERIMENTAL PART

A. Materials

The following commercial pigments were dispersed in three vehicles: Monastral Blue, Milori Blue, Barium Lithol Resinated, Barium Lithol Unresinated, Chrome Yellow, and Benzidine Yellow.

The vehicles used were a mineral oil, a heat-bodied linseed oil, and a limed rosin-mineral oil varnish. While dispersions were also made in a solution of a maleic-modified rosin in diethylene glycol, the conductivity and the loss angle of the latter dispersions were so high as to make the dielectric data completely meaningless, since extrapolation to infinite wavelength could not be attempted.

The pigments were first mixed in the vehicles in the highest concentration used. The mixtures were passed repeatedly over a three-roller mill until additional passes did not reduce the residue retained on a No. 325 screen. In all cases the percentage of residue retained was less than 0.001%.

All other concentrations were made by reducing the highest concentration with the calculated amount of vehicle, followed by extensive mixing by means of an electric stirrer. All dispersions were aged at least 48 hr. before any measurements were taken.

B. Apparatus and Method

The capacitance bridge used to measure the capacitance of the solutions was substantially the same as that previously described. As a cell, however, the cup and bob assembly of a high-shear variable-speed precision rotational viscometer was used, basically as described by Buchdahl *et al.* (7), but redesigned to have the bob and cup of the cell electrically insulated from each other. The accuracy of the instrument was materially improved by mounting the bob unit, by means of brass sleeves, on the cup-retaining cylinder. In addition, a closed unit is formed, eliminating solvent evaporation. The same cell was also used for conductivity measurements.

The instruments allowed capacitance measurements with an accuracy of $\pm 0.5\%$. Varying rates of shear could be obtained up to 660 sec.^{-1} , for materials of a viscosity up to 1000 poises, with an over-all accuracy of $\pm 0.5\%$ in shearing stresses.

The temperature was kept constant at 30.0°C. during the experiment by means of an electrically controlled thermostat.

Capacitance measurements were initially made at different frequencies. It appeared, however, that at 5000 cycles the maximum values of the dielectric constants were obtained, outside of the dielectric dispersion range. Conductivity measurements showed that the systems investigated have a low conductivity, of the order of $10^{-12} \text{ ohm}^{-1} \text{ cm.}^{-1}$. The conductivity is little affected by the application of shearing stresses.

While the cell of the rotational viscometer is suitable to show differences in dielectric constants between sheared and quiescent dispersions, it appears that absolute values of the dielectric constants are not entirely reliable, in view of the large correction for "lead capacity," caused by the unavoidable presence of the rotating mechanism. In several instances absolute values of the dielectric constants of quiescent dispersions were corrected by checking the data by means of a conventional three-electrode cell.

In order to apply any of the theoretical equations, it is necessary to know the dielectric constant of the pigments used, the value of which is not indicated in the literature. It was therefore decided to measure the dielectric constants directly in air. The pigment powders were densely packed, until a density of at least 50% of the actual density was reached.

Following the work of Van Vessem (4), a large cell was constructed, of an inner diameter of 8.8 cm. and an outer diameter of 10.2 cm. with a

height of 10 cm. This was done to eliminate the so called "grain" effect. For a proper calculation of the dielectric constant from Boettcher's equation it is necessary that the pigment particles in the packed powder be very small compared to the cell dimensions. Actually the rotating cell, of an inner diameter of 1.10 cm. and a clearance of 0.05 cm., does not fulfill these requirements. The use of the large cell is therefore advantageous for air-packed powders containing comparatively large particle clusters.

The pigments dispersed in the vehicles with the aid of a three-roller mill all have very fine particles, usually less than $1\ \mu$ in diameter. For these dispersions the rotating cell is satisfactory. Moreover, the three-electrode cell, with dimensions considerably larger than the rotating cell, was used to check the data obtained.

The calculations of the dielectric constants of the pigments in air must be carried out with the aid of one of the equations previously discussed. Although Polder and Van Santen (5) state that Boettcher's equation is a satisfactory approximation for powders of nonspherical particles of a small dielectric constant suspended in air, we have also used the so-called immersion method for measuring the dielectric constants of powders of a low dielectric constant.

The immersion method is based on Eq. [6], which indicates that the dielectric constant of a dispersion is independent of the concentration of the dispersed phase provided the dielectric constants of both phases are equal. One condition must be satisfied, however, that the conductivities of both phases do not differ markedly, since in that case complications arise due to electric charges set up at the phase boundaries.

The pigments investigated were dispersed in various mixtures of vehicles until a combination was found, generally by interpolation of the data, in which the dielectric constant of the dispersion was equal to the dielectric constant of the medium at every concentration. In that case the dielectric constant of the pigment is also equal to the dielectric constant of the vehicle.

This method yields more accurate results than the previously mentioned method, in view of the nonspherical character of the pigment particles. It was found that the conductivity of most of the densely packed pigments was relatively low, of the order of 10^{-11} – 10^{-12} ohm $^{-1}$ cm. $^{-1}$, while a small dielectric loss angle was found. The vehicles used were castor oil, linseed oil, and a mineral oil, and their mixtures. It was not possible to use liquids with a higher dielectric constant, which eliminated a check on the dielectric constants of Milori Blue and Chrome Yellow. The highest value obtained for a vehicle was that of castor oil, 4.20, in view of the fact that all of the other liquids tried did not fulfill the requirements, such as satisfactory dispersing characteristics for the pigments, absence of chem-

ical reactivity, very low conductivity, and a small dielectric loss angle. The only satisfactory vehicles were those indicated previously.

The dielectric data for pigments obtained by means of the immersion method are thus the more reliable.

C. Data

1. *Dielectric Constants of Pigments.* The following Table I indicates the values for the dielectric constants of pigments as found with both methods.

TABLE I
Dielectric Constant

Pigment	Air-packed powders	Immersed powders
Benzidine Yellow	2.93	3.55
Barium Lithol Resinated	4.71	4.40
Barium Lithol Unresinated	4.05	4.01
Milori Blue	18.3	—
Monastral Blue	4.85	—
Chrome Yellow	—	—

The values obtained for air-packed powders have been calculated from Boettcher's equation, while the immersion method does not require any special calculation.

The conductivity of the Chrome Yellow powder was too high to yield significant data. Its dielectric behavior appears to be comparable to materials with a high dielectric constant.

From the data it appears that the Boettcher equation applied to air-packed powders yields data in reasonable accord with the immersion method only for Barium Lithol Unresinated. There is a marked deviation for Barium Lithol Resinated and a large discrepancy for Benzidine Yellow. This indicates that the Boettcher equation, derived for spherical particles, is not always satisfactory for the nonspherical pigment particles, even for those with a low dielectric constant. The values for Monastral Blue and Milori Blue, obtained by means of the Boettcher equation from data of packed powders, are therefore not very reliable.

D. Dielectric Constants of Dispersions

For each vehicle-pigment combination the relationship between the dielectric constant and the concentration by volume of the pigment has been determined for both quiescent and sheared dispersions. The rate of shear applied was in every case high enough to yield the lowest obtainable value of the dielectric constant. This means that upon further increase of the shearing stress no additional change in the dielectric constant was observed. The shearing stress rate necessary to reach the minimum dielectric constant was less than 100 sec.⁻¹ in each case.

Figure 1 indicates the rest values of the dielectric constants for pigments dispersed in linseed oil. Figure 2 indicates the corresponding shear values. It must be remarked that there is also a very small difference in rest and shear values of the dielectric constant of the pure vehicle.

It may be observed that the relationships uncovered are linear over the lower range of concentrations, indicating the validity of Eq. [7].

It may also be seen that the slopes of the lines differ for dispersions at rest and subjected to shear in the range of linear relationship, indicating

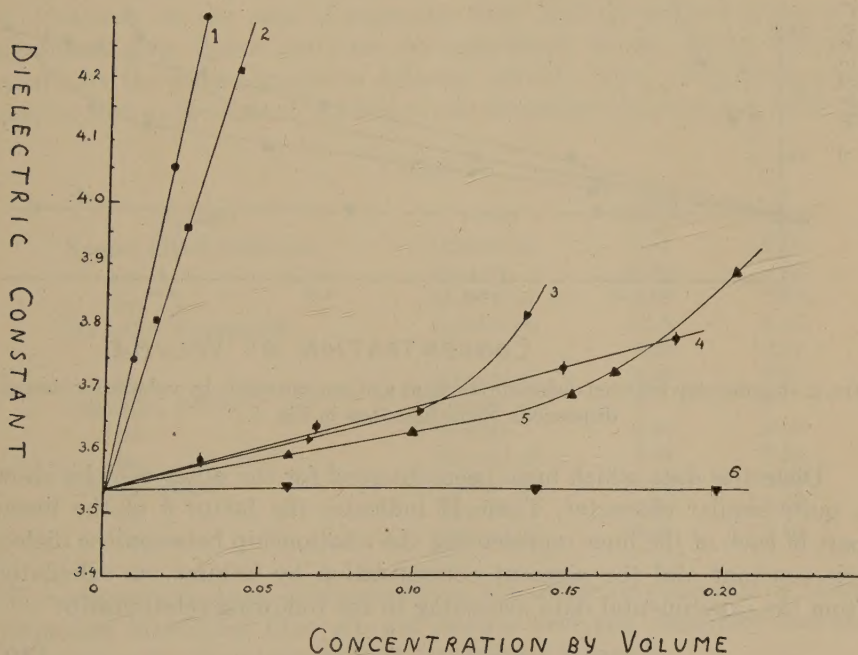


FIG. 1. Relationship between dielectric constant and concentration by volume for quiescent dispersions. ● 1, Milori Blue; □ 2, Chrome Yellow; ► 3, Monastral Blue; ◆ 4, Barium Lithol Unresinated; ▲ 5, Barium Lithol Resinated; and ▽ 6, Benzidine Yellow.

an orientation of nonspherical particles due to the applied stresses. In general, linearity persists over a rather wide range of concentrations. In the sheared dispersions this linearity appears to be valid up to a somewhat higher concentration than in the quiescent dispersions, indicating the existence of particle agglomeration in the quiescent dispersions at higher concentrations (1).

It must be remarked, however, that the effects are much smaller in these dispersions than in those with particles of a high dielectric constant. For Chrome Yellow, Eq. [5] appears to be approximately valid.

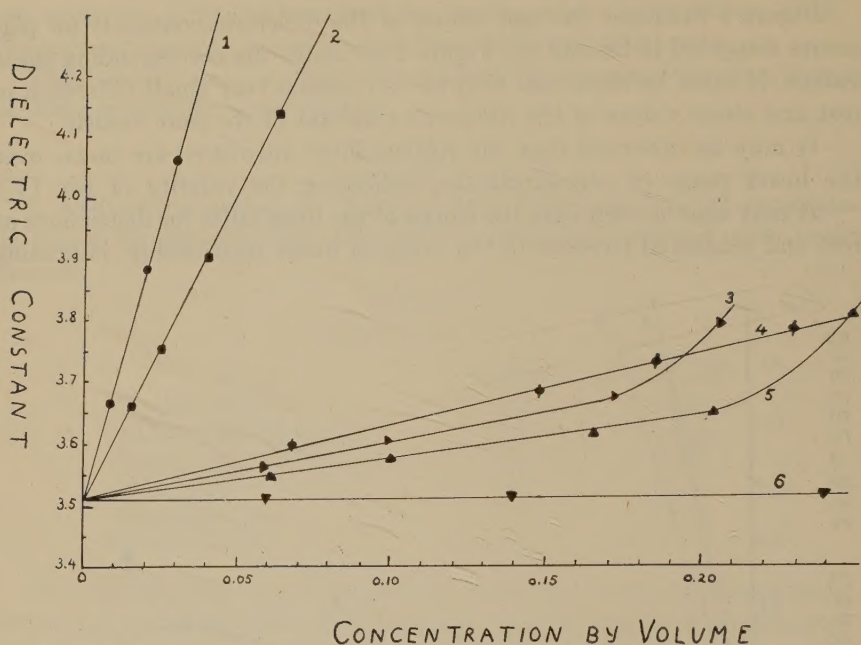


FIG. 2. Relationship between dielectric constant and concentration by volume for sheared dispersions. Same legend as in Fig. 1.

Dielectric data which have been obtained for the other vehicles show a quite similar character. Table II indicates the factor k of the linear part of each of the lines representing the relationship between the dielectric constant and the pigment concentration by volume, as calculated from the experimental data according to the following relationship:

$$\epsilon = \epsilon_M(1 + kv). \quad [10]$$

The theoretical Eq. [7], derived as an approximation of the Boettcher Eq. [1] appears to be of the same general form as the experimental Eq. [10]. We may thus compare the values of k found experimentally with those calculated from Eq. (7a).

TABLE II

Vehicle	Condition	Milori Blue	Chrome Yellow	Ba Lithol Resinated	Monastral Blue	Benzidine Yellow	Ba Lithol Unresinated
Linseed oil	Rest	7.16	4.84	0.28	0.37	0	0.38
Linseed oil	Shear	5.29	2.90	0.19	0.29	0	0.33
Varnish	Rest	8.48	4.92	0.64	0.89	0.61	0.73
Varnish	Shear	5.56	3.09	0.55	0.82	0.55	0.59
Mineral oil	Rest	3.24	4.54	0.59	0.42	0.33	0.85
Mineral oil	Shear	2.26	3.10	0.50	0.40	0.29	0.71

The following Table III indicates the comparison between calculated and observed values, in the absence of agglomeration, for sheared dispersions, the latter obtained from Table II in which the corresponding values for quiescent dispersions are also given. The values of the dielectric constants were obtained with the immersion method.

These data indicate that the agreement between calculated and observed values is not very good. On the other hand, however, the calculated values are not greatly out of line and the deviations result, most likely, from the nonspherical character of the particles.

Contrary to the case of pigments with high dielectric constants, a significant form factor could not be established, in view of the different results for the same pigment in different vehicles. Again, this discrepancy may be due to the lack of validity of the Boettcher equation as a result of

TABLE III

Pigment	Vehicle	k calculated	k observed
Barium Lithol Resinated	Linseed oil	0.17	0.19
Do.	Varnish	0.58	0.55
Do.	Mineral oil	0.66	0.50
Ba Lithol Unresinated	Linseed oil	0.15	0.33
Do.	Varnish	0.48	0.59
Do.	Mineral oil	0.58	0.71
Benzidine Yellow	Linseed oil	0	0
Do.	Varnish	0.34	0.55
Do.	Mineral oil	0.42	0.29
Chrome Yellow	Linseed oil	3.00	2.90
Do.	Varnish	3.00	3.09
Do.	Mineral oil	3.00	3.10

the nonspherical shape of the particles. The dielectric constants of Milori Blue and Monastral Blue are not known with any reliability and the calculations for these pigments have not been included.

SUMMARY

Dielectric constants have been determined for various colored pigments dispersed in different vehicles.

The theoretically predicted linearity between dielectric constant and concentration by volume has been observed for the lower concentration range. The agreement between calculated and observed values of the slopes is only fair, most likely because of the nonspherical character of the particles, which cause the fundamental Boettcher relationship to have a limited applicability only.

While the dielectric characteristics of dispersions of pigments of a high dielectric constant dispersed in vehicles of a low dielectric constant allow important conclusions about the internal structure of the dispersions, such

appears not to be the case with the present data for dispersions of pigments in vehicles of dielectric constants of the same order of magnitude. This is due to the smallness of the effect and the lack of a precise theory.

REFERENCES

1. VOET, A., *J. Phys. & Colloid Chem.* **51**, 1037 (1947).
2. BRUGGEMAN, D. A. G., *Ann. Physik* (5) **24**, 636 (1935).
3. BOETTCHER, C. J. F., *Rec. trav. chim.* **64**, 47 (1945).
4. VAN VESSEM, J. C., Thesis, Utrecht, Netherlands, 1947.
5. POLDER, D., AND VAN SANTEN, J. H., *Physica* **12**, 257 (1946).
6. VOET, A., AND SURIANI, R., *J. Colloid Sci.* **6**, 155 (1951).
7. BUCHDAHL, R., *et al.*, *Rev. Sci. Instruments* **18**, 168 (1947).

SOLUBILITY OF POLYMETHYL METHACRYLATE AND POLYVINYL ACETATE ¹

Hubert Daoust² and Marcel Rinfret

Institut de Chimie, Université de Montréal, Montreal, Canada

Received August 2, 1951

INTRODUCTION

The purpose of this work was to find a number of good solvents for polymethyl methacrylate and polyvinyl acetate. Moreover, we have tried to find possible correlations among intrinsic viscosity, cohesive energy density, dipole moment, and dilution ratio. A further requirement was that the chosen solvents should have values of refractive index below, near, and above those of the polymers because of their intended use in light-scattering studies.

Solubility of High Polymers

The study of the solubility of high polymers may be compared, with some restrictions, to that of low-molecular-weight molecules. For low-molecular-weight substances, we know from the mass of available data, that (a) a similar chemical structure of solute and solvent favors solubility, (b) similar polarities and similar cohesive energy densities (CED's) favor solubility, (c) the higher the melting point of the solute, the lower will be its solubility in a liquid solvent, (d) solubility decreases as the temperature of the solvent is lowered, and (e) solubility also decreases as the molecular weight of the solute increases.

The work of van Laar, Hildebrand, and Scatchard (8) on solubility yields useful information on the solvent power of a liquid solvent for a given solute by comparing their CED's. Gee (5) has extended this concept to nonpolar, noncrystalline polymers. According to him, the CED of a polymer is equal to the midpoint of CED's of solvents in which the polymer is soluble. In the case of a polar polymer, the polarity will give better information on the choice of solvents. If a polymer has polar groups in its chain, the polarities of which are similar to that of the solvent, solution will be facilitated. Hydrogen bonding is particularly

¹ The authors are pleased to acknowledge the financial assistance of the Associate Committee on Synthetic Rubber Research of the National Research Council of Canada.

² This paper is taken in part from a thesis submitted by Hubert Daoust for the M. Sc. degree in Chemistry, Université de Montréal, April, 1951.

important in the case of polar polymers; thus, the solubility of polymethyl methacrylate in chloroform may be explained by hydrogen bonding (13). Polarity is not sufficient to produce solubility; it is necessary, according to Spurlin (14), that the polymer and the solvent be different in their "basic" or "acidic" character, i.e., that one be an electron "acceptor" and the other an electron "donor."

The solvent power of a liquid solvent for a given polymer can be estimated by the viscosity behavior of the dilute solution. We know, from the Huggins-Kraemer viscosity relationship, that

$$\frac{\eta_{sp}}{c} = [\eta] + ac,$$

where η_{sp} = specific viscosity, c = concentration (g./100 ml.), $[\eta]$ = intrinsic viscosity, and a = slope of the viscosity curve; this term depends on the interaction between solute molecules.

For sufficiently dilute solutions, it has been found that $a = k'[\eta]^2$, where k' is a constant for a polymer in a given solvent; the value of k' for a linear polymer in a good solvent is usually between 0.3 and 0.4 (4). In a poor solvent, k' has a higher value. Intrinsic viscosity depends on the nature of the solvent and the solute. According to generally accepted theory (1,2), a long hydrocarbon chain takes a random coiled form intermediate between the spherical and linear forms. In a good solvent, the flexible molecule is extended and the intrinsic viscosity is high; the molecule is tightly coiled or compact in a poor solvent and the intrinsic viscosity is low.

There is another simple method for estimating solvent power: the dilution-ratio method. A determination is made of the amount of some nonsolvent that must be added to cause initial turbidity. Presumably, the solvent to which the largest amount of nonsolvent is added before precipitation occurs is the best. However, this method is not as precise as the viscosity method, because on addition of diluent the solvent power may pass through a maximum before decreasing.

Refractive Index Increments of Dilute Polymer Solutions

The refractive index of a polymer solution will increase if the refractive index of the polymer is higher than that of the solvent and vice versa. The ratio $\Delta n/c$ may be regarded as a constant for a polymer in solution in a given solvent for sufficiently high molecular weights and sufficiently low concentrations. When white light is used, the value of Δn corresponds very closely to that which would be obtained by using sodium D light (for white light, average $\lambda = 5600$ Å.; and for sodium D light, $\lambda = 5893$ Å.) (16).

EXPERIMENTAL

An unfractionated sample of polyvinyl acetate (from Bakelite Corp.) of average molecular weight 170,000 and an unfractionated sample of polymethyl methacrylate (from Eimer and Amend) of average molecular weight 250,000 were used. The following solvents: toluene, benzene, chlorobenzene, bromobenzene, ethylene chloride, trichloroethylene, and chloroform bought as reagent chemicals were distilled through a high-efficiency column (12). The other solvents, *s*-tetrachloroethane, *p*-dioxane, 1,1,2-trichloroethane, acetophenone, *o*-dichlorobenzene, cyclohexanone, 1,2,4-trichlorobenzene, methanol, and *n*-heptane were used after a simple distillation.

A new type of Ubbelohde suspended-level viscometer modified by Henderson and Legge (7) was used for the viscosity determinations. This type of viscometer has dimensions such that one can neglect the kinetic energy corrections and has a large reservoir of 100 ml. capacity in which one can make the dilutions without the necessity of rinsing and drying it at each dilution. Moreover, with that type of viscometer, flow time is independent of the volume of liquid introduced into it (15). For each viscosity determination, the viscometer was rinsed out three times with pure solvent and then clamped into a thermostat the temperature of which was maintained at $25.00 \pm 0.01^\circ\text{C}$. At least 5 ml. of pure solvent was introduced into the viscometer, and after 10 min. the flow time was determined. The flow-time determination was repeated three times until it checked within 0.1 sec. Then, the pure solvent was removed, the viscometer was dried, and exactly 6 ml. of an approximately 0.7% filtered solution of polymer was introduced into the viscometer. The flow time of the solution was determined with the same precautions as for pure solvent. Successive amounts of 2 ml. (0.525%), 4 ml. (0.35%), and 12 ml. (0.175%) of pure solvent were introduced in the viscometer and the flow time for each dilution was determined. After each addition of solvent, the solution was made homogeneous by blowing dried air gently through it. The solution was drawn out and the viscometer rinsed thrice with pure solvent after each completed experiment.

The method employed to determine the refractive index increments is given by Weissberger (16) and the apparatus used (a Rayleigh interferential refractometer) is described by G. Goyer (9). It is a high-precision apparatus. The initial concentration of the solutions used for these determinations was also 0.7% and the temperature range was between 22 and 25°C .

For the dilution-ratio method, exactly 0.5% solutions were prepared. Ten ml. of each solution was successively introduced in a round-bottomed 50-ml. flask, and the nonsolvent was added drop by drop from a burette with constant stirring until incipient turbidity. Before the use of a

nonsolvent, one has to check its miscibility with all the investigated solvents in all proportions and at both cold and room temperatures.

N.B. Concentration of solutions used for viscosity and $\Delta n/c$ determinations were checked by evaporation after each experiment.

RESULTS

Tables I and II show the intrinsic viscosities and k' values of the two polymers in 16 solvents, along with the dipole moment and the square root of the cohesive energy density of each solvent; this last value is

TABLE I
Solubility Data for Polymethyl Methacrylate

Solvent	δ_0^a	μ^a	[η]	k'	Volume	
					<i>n</i> -Heptane ml.	Methanol ml.
<i>s</i> -Tetrachloroethane	9.7	1.95	1.33	0.32	11.9	36.2
Chloroform	9.3	1.10	1.27	0.32	17.5	33.8
<i>p</i> -Dioxane ^b	10	0.4	1.05	0.29	5.9	23.1
1,1,2-Trichloroethane	9.6	1.55	1.02	0.34	10.8	31.1
Benzene ^b	9.15	0	1.02	0.29	4.4	21.2
Ethylene chloride	9.8	1.75	0.97	0.40	9.2	28.2
Acetophenone	10.2	2.97	0.89	0.30	7.0	27.2
<i>o</i> -Dichlorobenzene	10	2.25	0.88	0.41	7.2	21.0
Bromobenzene	9.9	1.51	0.88	0.32	6.2	20.9
Chlorobenzene	9.5	1.55	0.81	0.37	5.9	24.4
Trichloroethylene	9.3	0.94	0.76	0.39	5.7	22.2
Cyclohexanone ^b	9.9	2.8	0.70	0.52	5.8	25.0
Toluene	8.9	0.52	0.69	0.34	2.3	19.9
1,2,4-Trichlorobenzene	10.1	1.25	<i>I</i>	—	—	—
Methanol	14.6	1.64	<i>I</i>	—	—	—
<i>n</i> -Heptane	7.45	0	<i>I</i>	—	—	—

^a Dipole moment in Debye units. These values are taken from SIDGWICK, N. V., HAMPSON, G. G., AND MARSDEN, R. J. B., *A Table of Dipole Moments*. Gurney and Jackson, London, 1934.

^b Intrinsic viscosities and k' values for *p*-dioxane, benzene, and cyclohexanone have been calculated from the results given by Alfrey, Goldberg, and Price (2).

^c Delta values are taken from Hildebrand and Scott (8) for most of the solvents, and are calculated with the aid of Hildebrand's rule (8) for the rest.

expressed as δ_0 (solubility parameter). In the same tables are listed the results from the dilution-ratio method. Figures 1 and 2 show the specific viscosity curves of polymethyl methacrylate and polyvinyl acetate in six solvents to illustrate the degree of precision obtained.

Values of refractive index increments of the two polymers in a few solvents are listed for white light in Table III, along with the refractive index of the pure solvents for the sodium D line. Figure 3 shows the $\Delta n/c \times 10^3$ variation for the two polymers in pure solvents for white light.

TABLE II
Solubility Data for Polyvinyl Acetate

Solvent	δ_0^a	μ^a	$[\eta]$	k'	Volume of <i>n</i> -heptane ml.
Chloroform	9.3	1.10	1.14	0.37	17.9
<i>s</i> -Tetrachloroethane	9.7	1.95	1.06	0.35	11.9
1,1,2-Trichloroethane	9.6	1.55	1.06	0.34	9.4
Ethylene chloride	9.8	1.75	0.99	0.35	9.3
Trichloroethylene	9.3	0.94	0.85	0.37	6.5
Acetophenone	10.2	2.97	0.80	0.40	7.0
<i>p</i> -Dioxane	10	0.4	0.78	0.35	6.1
Cyclohexanone	9.9	2.8	0.76	0.19	6.2
Chlorobenzene	9.5	1.55	0.74	0.37	5.4
Benzene	9.15	0	0.70	0.36	3.7
<i>o</i> -Dichlorobenzene	10	2.25	0.65	0.54	5.8
Bromobenzene	9.9	1.51	0.59	0.45	5.3
1,2,4-Trichlorobenzene	10.1	1.25	0.58	0.62	4.0
Toluene	8.9	0.52	0.56	0.07	2.7
Methanol	14.6	1.64	0.45	0.40	—
<i>n</i> -Heptane	7.45	0	<i>I</i>	—	—

^a Dipole moment in Debye units. These values are taken from SIDGWICK, N. V., HAMPSON, G. G., AND MARSDEN, R. J. B., A Table of Dipole Moments. Gurney and Jackson, London, 1934.

^c Delta values are taken from Hildebrand and Scott (8) for most of the solvents, and are calculated with the aid of Hildebrand's rule (8) for the rest.

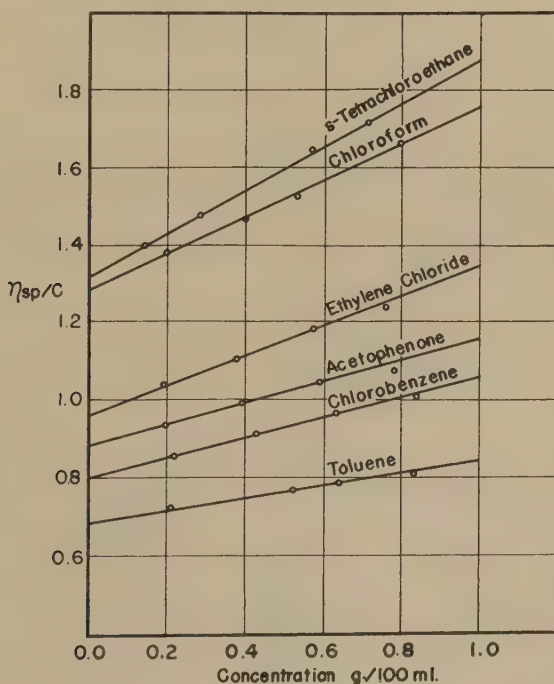


FIG. 1. Viscosity of polymethyl methacrylate in pure solvents.

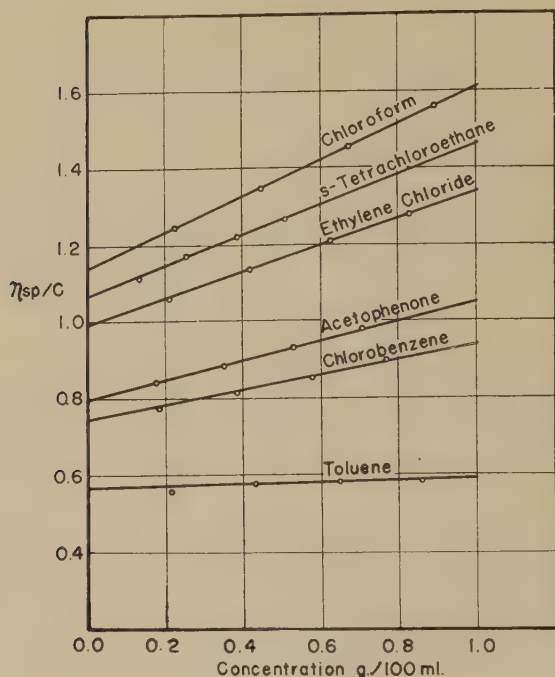


FIG. 2. Viscosity of polyvinyl acetate in pure solvents.

DISCUSSION

Flory-Huggins' statistical thermodynamic theory (8) predicts the approximate range of the solubility parameters δ_0 of good solvents for a homogeneous high-molecular-weight polymer. Such a polymer is expected to be completely miscible in solvents which satisfy the condition, for the solubility parameter of the polymer δ_p :

$$(\delta_p - 1.1) < \delta_0 < (\delta_p + 1.1).$$

If we take the higher limit of δ_0 as 10.2 (see Tables I and II) we find

TABLE III

$(\Delta n/c) \times 10^3$ Values for White Light

Solvent	n_D^t	Polymethyl methacrylate $(\Delta n/c) \times 10^3$	Polyvinyl acetate $(\Delta n/c) \times 10^3$
<i>p</i> -Dioxane	1.4221 ²⁰	52.07	32.45
Chloroform	1.4427 ²⁵	49.43	
1,1,2-Trichloroethane	1.4719 ²⁰	24.45	
Toluene	1.49385 ²⁵		-19.76
Benzene	1.49807 ²⁵		-25.68
Chlorobenzene	1.52215 ²⁵	-10.56	-39.70
Bromobenzene	1.5576 ²⁵	-36.26	

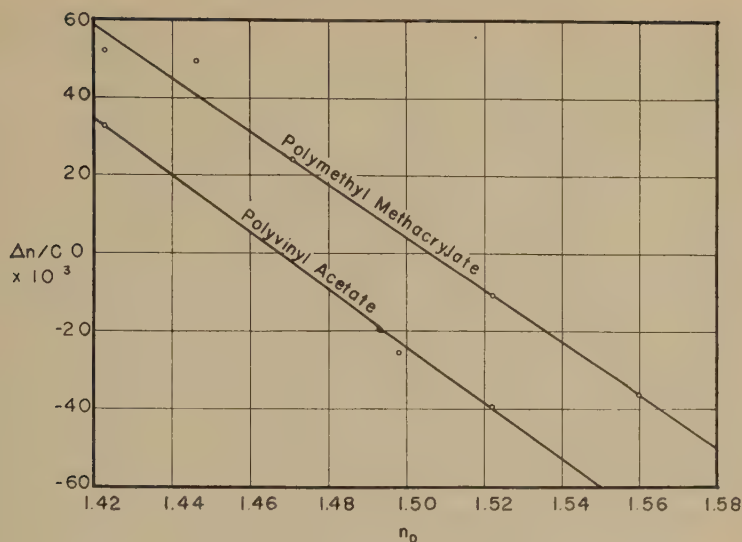


FIG. 3. Variation of $\frac{\Delta n}{C} \times 10^3$ for white light with the refractive index of the pure solvents for the sodium D line.

δ_p to be 9.1 which gives about 83 for the cohesive energy density of both polymers. Meares (11) also found 83 for the CED of polyvinyl acetate.

The CED concept may give a good explanation for the solvent power of nonpolar or slightly polar and neutral solvents (no "acidic" or "basic" character) as in the case of benzene, *p*-dioxane, and toluene. The solubility parameter of *n*-heptane is out of the predicted limits of δ_o -values, and the solubility tests show that it is a nonsolvent for the two polymers.

However, agreement of CED is not sufficient to explain the classification of the solvent with respect to those two polymers; Spurlin's point of view, based on the theory of Lewis, gives a better explanation than the CED concept for the solvent power of polar solvents. Polymethyl methacrylate and polyvinyl acetate have carbonyl groups which show a "basic" character and therefore can donate to an electron-acceptor solvent. If a solvent shows an "acidic" character or can accept from an electron donor, there is a solvation phenomenon and the solubility increases. The solvation may explain the great solubility of the two polymers in the halogenated aliphatic compounds, because the negative charge is carried by the halogens and the positive charge is carried by the hydrogen atoms which show the "acidic" character. Such is the case with chloroform, *s*-tetrachloroethane, 1,1,2-trichloroethane, ethylene chloride, and trichloroethylene, which are among the best solvents for the two polymers. Acetophenone and the halogenated aromatics show "basic" character because the positive charge is carried by the benzene ring and there is no acid hydrogen.

The cohesive energy density of methanol is so far from that of polymethyl methacrylate and polyvinyl acetate that it would not be expected to dissolve those two polymers. But methanol dissolves polyvinyl acetate and is a nonsolvent for polymethyl methacrylate. This fact may be explained by the polarity of methanol and the difference between the flexibility of the polymeric chains. Thus, the dipole moment per monomer unit is 2.3×10^{-18} e.s.u. for polyvinyl acetate (9) and around 1.4×10^{-18} e.s.u. for polymethyl methacrylate (10); the dipole moment of the free monomer molecule is approximately 1.8×10^{-18} e.s.u. for both polymers. The difference between the dipole moment of the monomer unit and the free monomer molecule depends on the free rotation of the polar group. For polyvinyl acetate, the high value of the dipole moment is due to the carbonyl group being attached to the polymeric chain by a flexible oxygen hinge. The orientation of the dipole is consequently much less dependent on the convolutions of the chain than if the dipole were attached directly to a chain carbon atom. For polymethyl methacrylate, the highly polar carbonyl group is attached to a chain carbon, and the weaker methoxy group is relatively free from the steric hindrance imposed by the chain configuration. Apparently, the methyl group on the same carbon which carries the polar group stiffens the chain so that free rotation is very much reduced (10).

The dilution-ratio method is not satisfactory for finding the best solvents in the case of polymethyl methacrylate. But in the case of a flexible polymer like polyvinyl acetate, this method seems to be very useful for a rapid investigation of solubility, since it classifies the solvents in the same order as the intrinsic viscosity (Table II).

Tables I and II show that most of the k' values are between 0.3 and 0.4 for the best solvents; but, there are some irregularities with cyclohexanone and toluene for polyvinyl acetate because the k' values decrease instead of increasing. Among the investigated liquids, none is a really poor solvent; toluene which is one of the poorest solvents used for the two polymers, gives an intrinsic viscosity which is about one half of that given by the best solvent in both cases; whereas the solvents chosen by Alfrey, Goldberg, and Price (2), in their study of dilute-solution viscosity of polymethyl methacrylate, give an intrinsic viscosity value for the best one about four times that of the poorest one, and their k' values are between 0.29 and 1.38.

Figure 3 shows that the refractive index for the sodium D line is about 1.505 for polymethyl methacrylate and 1.47 for polyvinyl acetate.

SUMMARY

Intrinsic viscosities and k' values have been determined for polymethyl methacrylate and polyvinyl acetate. The cohesive energy density is 83

for both polymers. The best solvents for these two polymers are those that show an "acidic" character. The dilution-ratio method may serve for a rapid investigation of the solubility of polyvinyl acetate. The refractive index (for the sodium D line) is approximately 1.505 for polymethyl methacrylate and 1.47 for polyvinyl acetate.

REFERENCES

1. ALFREY, T., JR., BARTOVICS, A., AND MARK, H., *J. Am. Chem. Soc.* **64**, 1557 (1942).
2. ALFREY, T., JR., GOLDBERG, A. I., AND PRICE, J. A., *J. Colloid Sci.* **5**, 251 (1950).
3. ALFREY, T., JR., *J. Colloid Sci.* **2**, 99 (1947).
4. BAWN, C. E. H., *The Chemistry of High Polymers*. Butterworths, London, 1948.
5. GEE, G., *Trans. Faraday Soc.* **40**, 463 (1944).
6. GOYER, G., M.Sc. Thesis. University of Montreal, 1948.
7. HENDERSON, D. A., AND LEGGE, N. R., Report to the Research Projects Subcommittee on Synthetic Rubber. Polymer Corp. Ltd., Sarnia, Ont., April 17, 1950.
8. HILDEBRAND, J. H., AND SCOTT, R. L., *Solubility of Nonelectrolytes*. Reinhold, New York, 1950.
9. MEAD, D. J., AND FUOSS, R. M., *J. Am. Chem. Soc.* **63**, 2839 (1941).
10. MEAD, D. J., AND FUOSS, R. M., *J. Am. Chem. Soc.* **64**, 2389 (1942).
11. MEARES, P., *Trans. Faraday Soc.* **47**, 703 (1951).
12. RINFRET, M., *Ann. Acfas* **15**, 62 (1949).
13. SCHMIDT, A. X., AND MARLIES, C. A., *Principles of High Polymer Theory and Practice*. McGraw-Hill, New York, 1948.
14. SPURLIN, H. M., *J. Polymer Sci.* **3**, 714 (1948).
15. UBBELOHDE, L., *Ind. Eng. Chem.* **9**, 85 (1937).
16. WEISSBERGER, A., *Physical Methods of Organic Chemistry*. Interscience, New York, 1949.

STUDY OF THE EXTINCTION COEFFICIENTS OF GELS DURING MUTUAL GELATION

Mata Prasad and V. Swaminathan

Chemical Laboratories, Institute of Science, Bombay, India

Received August 6, 1951

ABSTRACT

Extinction coefficients during the mutual gelation of sols of negatively charged nickel hydroxide and positively charged stannic hydroxide have been measured. The results indicate a close similarity between this type of gelation with that obtained by (a) the addition of electrolytes to sols or (b) metathetical reaction.

INTRODUCTION

The study of the optical properties of colloidal systems has a decided advantage over other methods inasmuch as the systems can be investigated without disturbing the internal equilibrium. Therefore extinction coefficients of different gel-forming mixtures of sols of stannic and nickel hydroxides were determined with a view to obtaining some information about the different stages involved in mutual gelation.

EXPERIMENTAL

The extinction coefficients were measured by means of Nutting's photometer used in conjunction with the Hilger wavelength spectrometer in the same manner as described by Prasad and co-workers (4). The gel-forming mixtures were prepared by mixing 5.0 ml. of stannic hydroxide sol with different volumes of dialyzed or undialyzed nickel hydroxide sol, and the total volume in each case was made up to 10 ml. by the addition of distilled water. The gel-forming mixtures were transferred to the optical cell which was thoroughly cleaned and dried beforehand. The stop watch was started simultaneously with the mixing of the sols. The readings were taken on the logarithmic scale at intervals of 1 min. by equalizing the intensity of light of the two beams in the green region of the spectrum ($\lambda = 5430$ A.). The effects of (a) time, (b) volume of the sol, and (c) dialysis of the nickel hydroxide sol on the extinction coefficients were determined systematically.

The sols of stannic and nickel hydroxides used were the same as described in the previous investigation.

The results obtained are given in Tables I, II, and III in which t denotes the time of setting.

TABLE I

Extinction Coefficients

Time min.	Ml. of nickel hydroxide, undialyzed			
	0.7	0.8	0.9	1.0
2	0.0111	0.0444	0.0444	—
3	0.0677	0.0677	0.0667	0.0222
4	0.0889	0.0677	0.0778	0.0778
5	0.1000	0.0677	0.0778	0.1000
6	0.1000	0.0677	0.0778	0.1111
				0.1333
7	0.1000	0.0677	0.0778	0.1333
8	0.1000	0.0677	0.0778	0.1333
<i>t</i> (min.)	60	30	13	7

TABLE II

Extinction Coefficients

Time min.	Ml. of nickel hydroxide sol dialyzed for 1 day			
	1.1	1.2	1.3	1.4
2	—	0.0222	0.0333	0.0889
3	0.0333	0.0444	0.1110	0.1333
4	0.0389	0.1110	0.1333	0.1444
5	0.0444	0.1270	0.1444	0.1444
6	0.0444	0.1333	0.1556	0.1444
<i>t</i> (min.)	22	13	8	6

TABLE III

Extinction Coefficients

Time min.	Ml. of nickel hydroxide sol dialyzed for 2 days			
	2.0	2.1	2.2	2.3
1	0.0110	0.0221	0.0221	0.1110
2	0.0220	0.0333	0.0445	0.1332
3	0.0330	0.0446	0.0667	0.1444
4	0.0442	0.0611	0.1110	0.1500
5	0.0667	0.0722	0.1332	0.1556
6	0.1000	0.0880	0.1332	0.1556
7	0.1000	0.0880	0.1332	0.1556
<i>t</i> (min.)	12	10	7	6

DISCUSSION OF RESULTS

It will be seen that the extinction coefficients of the several gel-forming mixtures increase with time, in most cases slowly in the beginning of gel-formation and rapidly later on, and finally reach a constant value. However, in some cases the increase is quite rapid from the very early stages. The curves obtained by plotting the values of the extinction coefficients against time are continuous, smooth, and S-shaped. In some cases the final value of the extinction coefficient is reached rather too suddenly and hence the curve bends sharply at this stage. This point has been carefully examined by repeating the experiments several times and also by determining the extinction coefficients long after the gel had set. In all such

cases the final values were found to be the same as the constant values given in the tables. The observed increase in the values of the extinction coefficient during the setting of the gels shows that the intensity of light scattered by the system increases during the setting process. This conclusion has been qualitatively verified by the direct measurement of the intensity of light scattered by a gel-forming system undergoing gelation. Hence it is concluded that when the transparent sol of positively charged stannic hydroxide is admixed with the negatively charged sol of nickel hydroxide, the entities, consisting mainly of the disperse phases in the two sols, formed on account of the neutralization of the electric charges on the particles either by the mutual adsorption of the oppositely charged micelles or by the interaction of the stabilizing electrolytes present in the two sols or by both, continuously agglomerate together. These aggregates become simultaneously highly hydrated, and the hydrated micelles combine to form the ultimate gel particles which enclose the rest of the dispersion medium and cause the setting of the gel. Thus it appears that the mechanism of the formation of gels by mutual gelation is similar to that observed in the formation of gels by (a) the addition of electrolytes to sols or (b) metathetical reaction, or (c) the cooling of the solution of an organic or inorgano-organic substance in a suitable solvent.

The extinction coefficients of the various gel-forming mixtures were measured from the time of mixing the constituents of the gel-forming mixture until they had set to a gel. The extinction coefficient-time curves therefore represent graphically the changes which take place in the gel-forming system during the process of setting. The continuous nature of these curves indicates that the various processes, namely, (a) the coagulation of the colloidal particles of the two sols, (b) the increase in the size of the coagulated particles, (c) the increase in their hydration, and (d) the formation of the ultimate structure of the gel, involved in gel-formation, take place continuously, and perhaps to a certain extent simultaneously. These observations are in agreement with those made by Prasad and co-workers (4).

It will be seen that the extinction coefficients of the different gel-forming mixtures attain a constant value long before the gels set. This observation is similar to that made by Prasad and Guruswamy (5) in the case of thorium molybdate gels, but is contrary to those of Prasad and co-workers and Gaokar who found that the values of the extinction coefficient or the opacity of the gel-forming mixture of silicic acid (4) and zirconium borate and molybdate (2) gels become constant only at the time of setting of the gels determined either by Fleming's or Hurd and Letteron's method.

The aforesaid observations bring out that when the two sols are mixed, the potential of the particles is first reduced to a minimum value

and hence the rate of coagulation is slow and the values of the extinction coefficients are small in the earlier stages of gelation. Subsequently the particles begin to agglomerate and hence the changes in the values of the extinction coefficients are large, and attain a constant value when the maximum coalescence of particles has taken place. Since the gel is not set at the stage when the coagulation is complete, that is, when the values of the extinction coefficients become constant, it appears that the hydration of the particles of the coagulum and the linking up of the hydrated particles which are the essential factors for the formation of gels do not take place sufficiently rapidly, and that in these two processes no change in the extinction coefficient takes place since there is no difference in the refractive indices of the water attached to the micelles and the "free" water.

It will be generally observed that the addition of increasing amounts of the nickel hydroxide sol to a fixed volume of the stannic hydroxide sol increases the rate of change of the extinction coefficient. This conclusion is not strictly true as some irregularities are observed in the case of undialyzed sols and those dialyzed for 2 days. Similarly, the final values of the extinction coefficients of all the set gels obtained by the addition of increasing amounts of nickel hydroxide sol do not follow a regular order in the above named cases; they first decrease and then increase. It may be that these peculiarities are caused by the several or the combined action of the four factors mentioned in the earlier paper, which bring about mutual gelation.

Prakash (3) has pointed out that large changes in the transparency of gels take place on using progressively more dialyzed sols. Hence gels were prepared by mixing the same volume of the undialyzed and dialyzed sol of nickel hydroxide with a fixed volume of stannic hydroxide sol. These mixtures set after a long time, approximately 24 hrs., and hence it was not possible to study the changes in the extinction coefficients of these mixtures with time. However, extinction coefficients of the set gels were measured, and it was found that their values in all cases were nearly the same. The visual observations of these gels also indicated no change in transparency or opacity.

It has been established that the process of gelation is to a certain extent analogous to that of coagulation (7,1). Hence the applicability of Smoluchowski's theory (7) of kinetics of coagulation to the gels formed by mutual gelation was examined. The theory requires that the coagulation curves obtained by the addition of different concentrations of the coagulant must be similar in shape and affinity to each other. If, therefore, a particular value of the extinction coefficient is shown by various mixtures at time t_1, t_2, t_3 , etc., then according to the theory

$$t_1:t_2:t_3:\dots = T_1:T_2:T_3:\dots$$

where T_1 , T_2 , T_3 , etc., are constants. The ratio of T_1 , T_2 , T_3 must therefore be a fixed ratio, independent of the absolute values of the extinction coefficients. Values were therefore chosen from the curves in which the extinction coefficients have been plotted against time and the corresponding ratios were calculated. It has been found that the relation is obeyed approximately only in the case of gels obtained by using the stannic hydroxide and nickel hydroxide sols dialyzed for 1 day.

REFERENCES

1. DE JONG, B., *Z. physik. Chem.* **130**, 208 (1927).
2. GAOKAR, private communication.
3. PRAKASH, S., *J. Phys. Chem.* **36**, 2483 (1932).
4. PRASAD, M., *et al.*, *J. Phys. Chem.* **36**, 1324 (1932).
5. PRASAD, M., AND GURUSWAMY, S., *Proc. Indian Acad. Sci.* **19**, 47 (1944).
6. PRASAD, M., AND MODAK, K. V., *Proc. Indian Acad. Sci.* **15**, 445 (1942).
7. SMOLUCHOWSKI, M. V., *v.*, *Physik. Z.* **17**, 557 (1916); *Z. physik. Chem.* **92**, 129 (1917).

STUDIES IN MUTUAL GELATION

Mata Prasad and V. Swaminathan

Chemical Laboratories, Institute of Science, Bombay, India

Received August 6, 1951

ABSTRACT

Mutual gelation of negatively charged nickel hydroxide sol with positively charged sols of copper hydroxide, stannic hydroxide, and ferric phosphate has been thoroughly studied. Increase of temperature decreases the time of setting by enhancing the agglomeration of the particles. It is concluded that the process of mutual gelation is not controlled merely by the neutralization of opposite electrical charges; but other factors also play an important role. Further, it is found that the coagulation of the sol of the gel-forming substance consequent on the neutralization, should take place under suitable environment in order to ensure gel formation.

INTRODUCTION

It is known that a certain amount of an electrolyte has to be added to a sol before any turbidity due to coagulation becomes visible. Similarly, mutual coagulation takes place only when two sols containing oppositely charged particles are mixed in certain proportions (1,2,23,33). Weiser and Chapman (35) have called the limits of these proportions the zone of flocculation, the width of which depends mainly upon the charges of the particles in the two sols and their hydration; it is a minimum when the charges are a maximum. If these limits are exceeded either partial or no coagulation takes place (5).

Mutual coagulation is therefore analogous to the coagulation of sols by electrolytes. The work of Joshi and co-workers (19) on viscosity measurements during the coagulation of sols by electrolytes and mutual coagulation of sols has established this analogy. Hence, mutual coagulation has been considered to be predominantly due to the neutralization of the charges carried by the particles in the two sols (3,36). However, other factors, such as (a) the mutual adsorption of colloidal particles, (b) the interaction between stabilizing ions, and (c) the presence of the excess of free electrolytes in the sols, have been found to play an equally important part in some cases (10,15,16,20,34,35).

When electrolytes are added to some sols, gels instead of precipitates are obtained (24,30,31). It is, therefore, obvious that gels should be formed when oppositely charged sols are mixed in certain definite proportions. Hauser and Hirshon (12) have shown from the viscosity-time curves

obtained during the gelation of (a) hydrogen bentonite sol and ferric chloride and (b) ferric hydroxide-hydrogen bentonite sols that the two processes of the gel formation are similar, though not identical. Hauser and Reed (14) have reported that thixotropic gels are obtained by mixing dialyzed iron or aluminum oxide sols (+ve) with the sol of hydrogen bentonite (-ve). They have also found that the addition of increasing amounts of ferric hydroxide sol lowers the thixotropic setting time and an increase in temperature increases it. However, it is not clear whether the gels obtained by them are of the same type as obtained by Prasad and co-workers (27), that is, are transparent or translucent and are so stiff that they will not flow out of the container when it is inverted. Prasad and Mehta (29) and Prasad and Chhaya (26) have recently prepared several gels, probably for the first time, by mixing together suitable volumes of oppositely charged sols, dialyzed or undialyzed. They have determined the volume limits of a sol, dialyzed to different extents, which would give transparent or translucent gels with a fixed volume of the oppositely charged sol. They have also measured the time of setting (t) of these gels at a constant temperature and have found that the experimental results are reproduced by the equation $t = Ra^{-m}$, where R and m are constants. Prasad and Chhaya (26b) have also measured the time of setting at several temperatures and have found that for the same gel-forming system the plots of $\log t$ against $\frac{1}{T_{(\text{Abs.})}}$ are parallel straight lines.

The values of Q , the heat of activation, have been calculated according to Arrhenius' equation and found to be nearly constant for the same system. They have thus established the similarity between the mechanism of the formation of gels by mixing oppositely charged sols, called by them "mutual gelation," and those prepared either by the addition of electrolytes to sols or by metathetical reactions.

It is obvious that few observations have been made and little systematic work has been done on the formation of gels by mixing two oppositely charged sols. The authors have prepared some new gels by the method of mutual gelation and have determined their time of setting which has been pointed out by Prasad (25) to be the characteristic property of gels and have also systematically studied the process of mutual gelation by following the effects of (a) charge on the colloidal particles, (b) temperature, and (c) extent of dialysis of the sols on gelation.

EXPERIMENTAL AND OBSERVATIONS

1. Preparation of Sols

(a) Nickel hydroxide sol was prepared by the method of Prasad and Mehta (29). The sol was dialyzed for 1, 2, and 3 days, and the undialyzed and the dialyzed samples of sols were stored in Jena glass bottles, labeled

A , A_1 , A_2 , and A_3 , respectively. One liter of the sol was found to contain nickel hydroxide corresponding to 3.4 g. nickel (estimated by dimethylglyoxime method). The colloid content of the four samples was found to be practically constant.

(b) Copper hydroxide sol was prepared by Mittra's method (21). The sol was dialyzed for a long time and was found to contain 4.458 g. of copper oxide/l. It was labeled as B .

(c) Ferric phosphate sol was prepared by the method of Prakash and Dhar (24). The sol was found to be slightly opaque, and contained ferric phosphate corresponding to 2.38 g. ferric oxide/l. It was labeled as C .

(d) Stannic hydroxide sol was prepared by the method of Dhar and Vardhanam (7). The sol was purified by dialysis and the dialyzed sample was found to contain 14.0 g. stannic oxide/l. It was labeled as D .

2. Measurement of Cataphoretic Speed

The cataphoretic speeds of the sols were measured by Mukherjee's apparatus enclosed in an electrically controlled thermostat maintained at $30 \pm 0.5^\circ\text{C}$. The upper liquid was a dilute solution of HCl (Merck's extra pure) whose conductivity was nearly the same as that of the sol and whose density was slightly lower than that of the sol. The sol was colored by neutral red; 0.01 ml. of 1% solution of the dye was added to 40 ml. of the sol. A current from a constant voltage source of 100 v. was passed through the sol for 15 min. and then for the same time in the reverse direction; the movement of the boundary was noted in each case. The difference between the two readings was never more than 3-4%. The mean of the two readings was used for the calculation of the cataphoretic speed (v) in cm./sec./v. from the relation,

$$v = \frac{V}{d} \times \frac{m}{t}$$

in which d = distance between the side tubes in cm.,

V = potential applied at the boundary of the sol or between the two side tubes, in volts,

m = displacement of the boundary in cm., and

t = time in seconds for which the potential V was applied.

The values of V and d were determined from separate experiments and were found to be 6.06 v. and 4.2 cm., respectively.

3. Behavior of Gels Obtained by Mutual Gelation

The gels obtained by mixing copper and nickel hydroxide sols were bluish in color and underwent syneresis to a considerable extent. They were translucent or transparent according as the undialyzed or dialyzed sol of nickel hydroxide was used; further, their transparency increased on

using the nickel hydroxide sol dialyzed for longer intervals. The gels obtained by mixing sols of (a) nickel hydroxide and ferric phosphate and (b) nickel and stannic hydroxides were milky and colored grass-green. These gels also were synergetic and translucent or transparent depending upon the extent of dialysis of the nickel hydroxide sol.

4. *Measurement of the Time of Setting*

Miss Nathan's modification (22) of Hurd and Letteron's method was used for the measurement of the time of setting.

(a) *Effect of the Volume of the Gelating Sols on the Time of Setting.* To determine this effect several test tubes were filled with 5.0 ml. of one sol. In another set of test tubes, known volumes (measured by a micropipet reading up to 0.01 ml.) of the oppositely charged sols were taken and were made up to 5.0 ml. by the addition of distilled water. The test tubes were well corked and were placed in an air thermostat kept at a constant temperature for half an hour. The contents of the two test tubes were then thoroughly mixed and the mixture was poured into a small weighing bottle. The glass rod was kept in position in the gel-forming mixture by means of a support and the stop watch was started simultaneously to note the time of setting. When the glass rod could remain in its position without the aid of the mechanical support, the time indicated on the stop watch was taken as the time of setting. To increase the accuracy of the measurement, several readings were taken, each time disturbing the gel-forming mixture as few times as possible. The minimum time observed was taken as the time of setting of the gel.

(b) *Effect of Temperature on the Time of Setting.* The time of setting (t) of a gel depends upon the temperature ($T_{(Abs.)}$) at which it is measured (9,17,28). Szegvari and Shaleck (32), Hauser and Reed (13), and Broughton and Squires (4) could satisfactorily express their results by the empirical expression $\log t = AT + B$, where A and B are constants; while Hurd and Letteron (18) and Prasad and co-workers (27) have found that the time of setting (t) obeys the Arrhenius equation and have calculated the heats of activation for the gels studied by them (18, 27). The time of setting of the gels prepared by mutual gelation was therefore measured at different temperatures and attempts were made to examine the applicability of the two relations.

(c) *Effect of the Dialysis of a Sol on the Time of Setting.* Purity of a sol plays a very important part in the formation of gels and in determining their time of setting. Dube (8) has found that the rate of formation of ferric arsenate and phosphate gels with respect to the concentration of KCl increases as the sols are more and more dialyzed. Gaokar (11) has found that increasing concentrations of electrolytes are required to cause the setting of increasingly dialyzed sols of zirconium borate and zirconium

molybdate in the same time; that is, the time of setting is considerably decreased toward the same concentration of electrolytes on increasing the extent of the dialysis of the sols. Therefore, wherever possible, the influence of dialysis on the time of setting of the gels studied in this investigation was also systematically examined.

RESULTS

The results for the cataphoretic velocities are given in Table I and those obtained for the time of setting at various temperatures, using the

TABLE I
Cataphoretic Speeds of Sols

Label	Sol	m	$v \times 10^4$
A	Nickel hydroxide sol undialyzed	0.385	6.17
A ₁	Do. 1 day dialyzed	0.510	8.18
A ₂	Do. 2 days dialyzed	0.630	10.10
A ₃	Do., 3 days dialyzed	0.225	3.61
B	Copper hydroxide	0.785	12.59
C	Ferric phosphate	0.250	4.01
D	Stannic hydroxide	0.510	8.18

TABLE II

Time of Setting of (B) Copper Hydroxide Sol (+ve), and (A, A₁, A₂) Nickel Hydroxide Sol (-ve)

A = 5.0 ml.				A ₁ = 5.0 ml.				A ₂ = 5.0 ml.			
B	t ₂₅	t ₄₀	t ₄₅	B	t ₂₅	t ₄₀	t ₄₅	B	t ₂₅	t ₄₀	t ₄₅
ml.				ml.				ml.			
3.1	17' 0"	16' 11"	15' 14"	2.5	18' 20"	17' 45"	16' 0"	2.0	19' 0"	17' 52"	16' 30"
3.2	10' 18"	10' 5"	9' 52"	2.6	10' 21"	10' 0"	8' 46"	2.1	10' 47"	10' 28"	9' 32"
3.3	4' 54"	4' 30"	4' 18"	2.7	5' 50"	5' 15"	5' 0"	*2.2	*4' 30"	*3' 45"	*3' 15"
3.4	*2' 23" ^a	*1' 15"	*1' 2"	2.8	*1' 8"	*1' 1"	*0' 52"	*2.3	*1' 55"	*1' 36"	*1' 15"
3.5	*0' 42"	*0' 33"	*0' 29"	2.9	*0' 39"	*0' 31"	*0' 25"	2.4	*0' 53"	*0' 45"	*0' 35"
3.6	*0' 30"	*0' 15"	*0' 12"	3.0	*0' 14"	*0' 11"	*0' 9"	2.5	*0' 26"	*0' 18"	*0' 15"

^a For values marked with an asterisk, see text. All times shown are *minutes* (') and *seconds* (").

TABLE III

Time of Setting of (C) Ferric Phosphate Sol (+ve), and (A, A₁, A₂) Nickel Hydroxide Sol (-ve)

A = 5.0 ml.				A ₁ = 5.0 ml.				A ₂ = 5.0 ml.			
C	t ₂₅	t ₃₀	t ₄₀	C	t ₂₅	t ₃₅	t ₄₅	C	t ₂₅	t ₃₅	t ₄₅
ml.				ml.				ml.			
3.5	0' 38"	4' 30"	2 hrs.	3.5	1' 10"	1' 30"	5' 0"	4.0	2' 45"	2' 52"	3' 1"
3.6	0' 27"	2' 6"	45' 0"	3.6	*0' 50"	*1' 5"	*3' 0"	4.1	2' 20"	2' 30"	2' 40"
3.7	0' 20"	1' 6"	16' 0"	3.7	*0' 37"	*0' 46"	*1' 50"	4.2	1' 55"	2' 3"	2' 20"
3.8	0' 15"	0' 40"	6' 0"	3.8	*0' 28"	*0' 35"	*1' 5"	4.3	1' 32"	1' 42"	2' 7"
3.9	*0' 10" ^a	*0' 20"	*2' 20" ^a	3.9	*0' 21"	*0' 24"	*0' 30"	4.4	*1' 12"	*1' 22"	*2' 4"
4.0	*0' 6"	*0' 15"	*1' 13"	4.0	*0' 15"	*0' 17"	*0' 20"	4.5	*0' 52"	*1' 6"	*2' 2"

^a For values marked with an asterisk, see text. All times shown are *minutes* (') and *seconds* (").

TABLE IV

Time of Setting of (D) Stannic Hydroxide Sol (+ve), and (A, A₁, A₂) Nickel Hydroxide Sol (-ve)

D = 5.0 ml.				D = 5.0 ml.				D = 5.0 ml.			
A	t ₃₀	t ₃₅	t ₄₀	A ₁	t ₃₀	t ₃₅	t ₄₀	A ₂	t ₃₀	t ₃₅	t ₄₀
ml.				ml.				ml.			
1.0	5' 40''	4' 40''	2' 40''	1.4	5' 15''	3' 30''	2' 30''	2.0	11' 20''	8' 15''	5' 30''
1.1	2' 40''	1' 50''	1' 10''	1.5	3' 0''	1' 40''	1' 32''	2.1	*9' 15''	*6' 15''	*4' 7''
1.2	1' 5''	0' 45''	0' 34''	1.6	2' 0''	1' 11''	0' 58''	2.2	*7' 30''	*5' 2''	*3' 13''
1.3	*0' 46'' ^a	*0' 23''	0' 13''	1.7	*1' 20''	*0' 46''	0' 35''	2.3	*6' 2''	*3' 55''	*3' 35''
1.4	*0' 33''	*0' 16''	0' 9''	1.8	*0' 54''	*0' 30''	*0' 21''	2.4	*4' 35''	*3' 5''	*2' 7''
1.5	*0' 25''	*0' 11''	0' 5''	1.9	*0' 39''	*0' 21''	*0' 15''	2.5	*3' 40''	*2' 30''	*1' 51''

^a For values marked with an asterisk, see text. All times shown are *minutes* (') and *seconds* (").

undialyzed and the dialyzed sols of nickel hydroxide are given in Tables II to IV in which *t* denotes the time of setting of the gel at the temperature in degrees centigrade indicated by the suffix.

On adding different volumes of the copper hydroxide and ferric phosphate sols to the nickel hydroxide sol dialyzed for 3 days gelation either did not take place or was delayed too long. In a few cases mutual coagulation actually took place. On adding different volumes of the nickel hydroxide sol dialyzed for 3 days to 5.0 ml. of the stannic hydroxide sol either homogeneous mixtures were obtained which did not set to a gel even after a long time or mutual coagulation of the sols took place.

DISCUSSION OF RESULTS

1. Cataphoretic Velocities

Table I shows that the cataphoretic speed, that is, the density of charge on the colloidal particles of the nickel hydroxide sol increases, reaches a maximum, and then decreases as the sol is progressively dialyzed. These results are similar to those obtained by Desai and co-workers (5) and can be explained on their hypothesis according to which the oppositely charged ions are removed at first and the similarly charged ions are removed subsequently during dialysis.

The cataphoretic speed of the copper hydroxide sol is much higher than those of the other sols. It was found that (a) even on prolonged dialysis the stabilizing ions could not be completely removed from the copper hydroxide sol, and (b) the viscosity of the sol was not different from that of water. The latter observation shows that it behaves like a typical lyophobic sol, probably due to the high adsorbability of the stabilizing ions. These observations also bring out that the high charge on the colloidal particles is responsible for low hydration and low viscosity of the sol (6).

2. Time of Setting

(a) *Effect of Volumes of Sols on the Time of Setting.* It will be seen from the results given in Tables II to IV that the time of setting of gels obtained by the mutual gelation of sols of (a) nickel and copper hydroxides (b) nickel hydroxide and ferric phosphate, and (c) nickel and stannic hydroxides, decreases at first rapidly and then slowly as increasing amounts of oppositely charged sols are added to a fixed volume of either nickel hydroxide or stannic hydroxide sols. The curves obtained by plotting the time of setting against the volumes of oppositely charged sols are steep in the earlier stages and later gradually tend to run parallel to the volume axis.

Prasad and Hattiangdi (27) have shown that their results on the time of setting (t) of silicic acid gels can be expressed by the relation $(t - \alpha c^m)(t - \beta c^n) = 0$, where c represents the concentrations of ammonium acetate solutions added to the same solution of sodium silicate and α , β , m , and n are constants. Paine (22a) observed a similar relation for the coagulation of certain sols of inorganic substances. Later, Prakash and co-worker (24) found that the relation $t = R a^{-m}$ holds good in the case of several inorganic gels formed by the addition of electrolytes to sols. This relation also holds good in the case of gels formed by the mutual gelation of sols [cf. Prasad and Mehta (29)].

It has been found that the relation $t = R a^{-m}$ is also followed in the case of the several gels obtained in this investigation. The plots for $\log t$ against $\log a$ (a being the volume of the oppositely charged sol) lie on a pair of intersecting straight lines. The values of t were calculated from the values of m_1 and $\log R_1$ and m_2 and $\log R_2$ (the latter being marked with an asterisk in the tables) for corresponding values of a and were found to be in good agreement with the observed ones in most cases. The observation that pairs of straight lines are obtained indicates that the mechanism of the formation of the gels obtained by using varying volumes of oppositely charged sols is not quite the same.

(b) *Effect of Temperature on the Time of Setting.* It will be observed from Tables II and IV that the time of setting of the gels obtained by the mutual gelation of (a) nickel hydroxide ($-ve$) and copper hydroxide ($+ve$) sols and (b) stannic hydroxide ($+ve$) and nickel hydroxide ($-ve$) sols decreases as the gel-forming solutions are allowed to set at higher temperatures. However, Table III shows that the time of setting of the gels obtained by mixing sols of nickel hydroxide ($-ve$) and ferric phosphate ($+ve$) increases with an increase in the temperature of setting.

The change in temperature, in general, causes a variation in (a) the solubility of the disperse phase, (b) the degree of hydrolysis of the gel-forming substance, (c) the hydration of the particles of the disperse phase, and (d) the rate of coagulation of the colloidal system. The setting time

is a complicated function of all these factors. With the exception of those gel-forming substances which undergo marked hydrolysis with rise in temperature the rate of coagulation in gel-forming systems is markedly increased on raising the temperature. With rapid decrease in charge on coagulation, the viscosity and the hydration of the particles also increase rapidly and hence a gel sets in a comparatively shorter time at higher temperatures. Since the agglomeration tendency of the particles is favored at higher temperatures, the gels obtained at higher temperatures are more opalescent. The sols which undergo hydrolysis at higher temperatures become stable toward coagulation and, as such, the gel takes more time to set. In accordance with these arguments the decrease in the time of setting of the gels of (a) nickel hydroxide-copper hydroxide and (b) stannic hydroxide-nickel hydroxide is due to an increase in the agglomeration tendency of the colloidal particles at higher temperatures; the increase in the time of setting of the gels of nickel hydroxide-ferric phosphate is probably due to the hydrolysis of ferric phosphate at higher temperatures. Further, in cases of gels obtained by mutual gelation the time of setting would depend upon the hydration developed by different phases.

The application of Arrhenius' equation to the gel-forming systems studied in this investigation was examined by plotting the values of $\log t$ against $1/T_{(\text{Abs.})}$ for each gel-forming mixture. It was found that all the plotted points for gel-forming mixtures containing the same volume of one sol and different volumes of the other do not lie on straight lines in some cases and sets of parallel straight lines in others. Hence, it was not possible to calculate the values of Q , the heat of activation, involved in the formation of these gels.

3. Mechanism of Mutual Gelation

Several factors involved in the process of mutual gelation are mentioned on p. 25. Hence, in the following an attempt has been made to examine the mechanism of mutual gelation in the light of these factors.

(a) *Interaction Between Stabilizing Ions.* It will be seen from the discussion on the increase in the density of charge on nickel hydroxide sol on dialysis that comparatively fewer hydroxyl ions are removed during the first 2 days than the oppositely charged ions. Hence one can assume that the concentration of OH^- ions either remains practically constant or decreases to a small extent during the dialysis of the nickel hydroxide sol. Now if the removal of the stabilizing ions of the oppositely charged sols due to their interaction is mainly responsible for the instability of sols on mixing, then the volume of the positively charged sol required to bring about the gelation with a fixed volume of the negatively charged nickel hydroxide sol undergoing dialysis should either remain unaltered or decrease with an increase in the extent of dialysis. To see how far this

assumption is correct, the volumes of the oppositely charged sols of copper hydroxide, ferric phosphate, and stannic hydroxide required to bring about the formation of gels with nickel hydroxide sol, undialyzed and dialyzed to different extents, in 2 min. have been computed from the data given in Tables II to IV and are given in Table V.

It will be seen from Table V that the quantities of the copper hydroxide sol required to bring about the gelation with the same amount of nickel hydroxide sol in 2 min. at all the temperatures studied decrease as the latter is dialyzed more and more. This indicates that the concentration of OH^- ions in nickel hydroxide sol particles decreases on dialysis. This effect is confirmed from the observation that the amounts of nickel

TABLE V

(a) *Nickel Hydroxide (A) and Copper Hydroxide (B) Gels*

Temp. °C.	Ml. of B for 5 ml. of A dialyzed for		
	0 day	1 day	2 days
35	3.44	2.79	2.29
40	3.35	2.77	2.26
45	3.34	2.76	2.23

(b) *Nickel Hydroxide (A) and Ferric Phosphate (C) Gels*

Temp. °C.	Ml. of C for 5 ml. of A dialyzed for		
	0 day	1 day	2 days
25	3.31	3.39	4.18
35	3.61	3.45	4.22
45	3.92	3.68	4.60

(c) *Nickel Hydroxide (A) and Stannic Hydroxide (D) Gels*

Temp. °C.	For 5 ml. of D, ml. of A dialyzed for		
	0 day	1 day	2 days
30	1.14	1.60	2.70
35	1.08	1.47	2.56
40	1.05	1.45	2.45

hydroxide sol required to bring about the formation of gels with 5.0 ml. of stannic hydroxide sol in 2 min. increase as the nickel hydroxide sol is dialyzed further. The results for the nickel hydroxide-ferric phosphate gels show that the volume of the ferric phosphate sol required to bring about the gelation with 5 ml. of the nickel hydroxide sol in 2 min. first decreases and then increases as more and more dialyzed nickel hydroxide sol is used. The first decrease is in conformity with the principle laid down above, but the subsequent increase would seem to be anomalous unless it is assumed that the product of the interaction taking place between the ions stabilizing the nickel hydroxide and the ferric phosphate sols increases the stability of the nickel hydroxide sol dialyzed for 2 days, or that the anomaly is due to some other factors.

(b) *Effect of Free Electrolytes in the Sols.* The effect of the presence of free electrolytes in the sols as a factor affecting the process of mutual gelation could not be very considerable since this complication was greatly reduced by dialyzing the sols to a fair extent. However, the difference in the behavior of (a) nickel hydroxide-copper hydroxide and nickel hydroxide-stannic hydroxide gel-forming systems and (b) nickel hydroxide-ferric phosphate gel-forming systems may indicate that the free electrolytes play some, though a small, role in mutual gelation.

(c) *Mutual Adsorption of Colloidal Particles.* The effect of this factor would be to cause the neutralization of the charges on the colloidal particles of the oppositely charged sols. The greater the force of attraction between them, the greater would be the possibility of mutual agglomeration. Hence if fixed volumes of (a) the positively charged sols and (b) the negatively charged sol of nickel hydroxide dialyzed to different extents are taken, the time of setting of gels should decrease continuously. The data of Table VI show that this is not true in all cases.

TABLE VI

Days of dialysis of nickel hydroxide sol	0	1	2
Time of setting for			
(a) 5 ml. of nickel hydroxide and 2.5 ml. of copper hydroxide sols at 35°	>>20 min.	18 min. 20 sec.	0 min. 26 sec.
(b) 5 ml. of nickel hydroxide and 3.5 ml. of ferric phosphate sols at 25°	0 min. 38 sec.	1 min. 10 sec.	>>3 min.
(c) 5 ml. of stannic hydroxide and 1.50 ml. of nickel hydroxide sols at 30°	0 min. 25 sec.	3 min.	>>12 min.

(d) *Electrical Neutralization of Charge.* This would depend upon the adsorbability of the oppositely charged ions of the electrolytes by the particles of each sol in the mixture, as well as on the adsorption of the oppositely charged particles of one sol by those of the other. Assuming that the number of particles per milliliter of nickel hydroxide sol remains unaltered on dialysis, it is clear that if the neutralization of the charges carried by the oppositely charged sols is the main factor which brings about the gelation, then the volume of the nickel hydroxide sol required to cause the gelation with a given volume of the positively charged sol should continuously decrease or the volume of the positively charged sol required to cause the gelation with a given volume of the nickel hydroxide sol should continuously increase, according as the nickel hydroxide sol, undialyzed or dialyzed for 1 and 2 days, is used. It will be seen from Table V that the hypothesis of neutralization of charge seems to fit in only in the case of nickel hydroxide-ferric phosphate system, because as

the nickel hydroxide sol of greater cataphoretic velocity is employed, larger quantities of the ferric phosphate sol are required to bring about the gelation in the same time. Hence it appears that the neutralization of opposite electric charges is not necessarily a dominant factor in the process of mutual gelation although it cannot be denied that this factor is not without its effect in all cases.

It will be seen from the above discussion that the process of gel formation by mixing oppositely charged sols is not controlled solely by the neutralization of opposite electric charges, but other factors mentioned above also play an important part. Possibly the process of chemical interaction between stabilizing ions supplements the neutralization of the electrical charges of the oppositely charged particles. It has been noted that no gel is obtained on mixing the nickel hydroxide sol dialyzed for more than 2 days with stannic hydroxide, ferric phosphate, or copper hydroxide sols. Instead, the system tends to coagulate. The only obvious reason for this is that the stabilizing ions and free electrolytes have been largely removed from the nickel hydroxide sol during the long period of dialysis. These observations thus bring out that mere coagulation of the sol of the gel-forming system does not determine the formation of gels; it is necessary that the coagulation of the sol of the gel-forming substance should take place under certain environments which, though not absolutely determinate, should prevail in these systems.

REFERENCES

1. BECHHOLD, H., *Z. physik. Chem.* **48**, 385 (1904).
2. BILLITZER, J., *Z. physik. Chem.* **51**, 148 (1905).
3. BILTZ, W., *Ber.* **38**, 148 (1905).
4. BROUGHTON, G., AND SQUIRES, L., *J. Phys. Chem.* **40**, 1041 (1936).
5. DESAI, B. N., *et al.*, *J. Univ. Bombay* **6**, 50 (1937); *ibid.* **8**, 134 (1939); *ibid.* **9**, 69 (1940); *J. Indian Chem. Soc.* **16**, 645 (1939).
6. DHAR, N. R., *et al.*, *J. Phys. Chem.* **26**, 701 (1922); *ibid.* **28**, 313 (1924); *ibid.* **31**, 649 (1927).
7. DHAR, N. R., AND VARDHANAM, C. I., *J. Indian Chem. Soc.* **20**, 159 (1943).
8. DUBE, H. L., *Proc. Indian Acad. Sci.* **11**, 331 (1940).
9. FLEMMING, W., *Z. physik. Chem.* **41**, 427 (1902).
10. FREUNDLICH, H., AND NATHANSOHN, A., *Kolloid-Z.* **28**, 258 (1920); *ibid.* **29**, 16 (1921).
11. GAO KAR, H. D., M.Sc. Thesis, Univ. Bombay, 1945.
12. HAUSER, E. A., AND HIRSHON, S., *J. Phys. Chem.* **43**, 1015 (1939).
13. HAUSER, E. A., AND REED, C. E., *J. Phys. Chem.* **41**, 911 (1937).
14. HAUSER, E. A., AND REED, C. E., *J. Phys. Chem.* **41**, 929 (1937).
15. HAZEL, F., AND MCQUEEN, D. M., *J. Phys. Chem.* **37**, 571 (1933).
16. HAZEL, F., *J. Phys. Chem.* **42**, 409 (1938).
17. HOLMES, H. N., *J. Phys. Chem.* **22**, 516 (1918).
18. HURD, C. B., AND LETTERON, H. A., *J. Phys. Chem.* **36**, 604 (1932).
19. JOSHI, S. S., *et al.*, *J. Indian Chem. Soc.* **10**, 329 (1933); *ibid.* **10**, 599 (1933); *ibid.* **11**, 133 (1934); *ibid.* **11**, 555 (1934).
20. LOTTERMOSER, A., *Kolloid-Z.* **6**, 78 (1910).

21. MITTRA, R. N., *J. Indian Chem. Soc.* **16**, 175 (1939).
22. NATHAN, A., *J. Indian Chem. Soc.* **20**, 159 (1943).
- 22a. PAINE, H. H., *Kolloidchem. Beihefte* **4**, 24 (1912); *Proc. Cambridge Phil. Soc.* **16**, 430 (1912).
23. PICTON, H., AND LINDER, S. E., *J. Chem. Soc.* **71**, 568 (1897).
24. PRAKASH, S., AND DHAR, N. R., *J. Indian Chem. Soc.* **6**, 391 (1929).
25. PRASAD, M., Presidential Address., *Proc. Indian Sci. Cong.*, Part II, 1941.
26. PRASAD, M., AND CHHAYA, B. N., *Proc. Indian Acad. Sci.* **32**, 74 (1950).
27. PRASAD, M., *et al.*, *J. Indian Chem. Soc.* **6**, 653 (1929); *J. Univ. Bombay* **7**, 132 (1938).
28. PRASAD, M., *et al.*, *Proc. Indian Acad. Sci.* **3**, 107 (1936); *J. Indian Chem. Soc.* **16**, 117 (1939).
29. PRASAD, M., AND MEHTA, S. D., *Current Sci. (India)* **12**, 19 (1943); *J. Indian Chem. Soc.* **20**, 166 (1943).
30. PRASAD, M., AND MEHTA, S. D., *Proc. Natl. Acad. Sci. U. S.* **13**, 78 (1943).
31. PRASAD, M., AND MODAK, K. V., *Proc. Indian Acad. Sci.* **12**, 235 (1940).
32. SHALECK, E., AND SZEGVARI, A., *Kolloid-Z.* **32**, 318 (1923); *ibid.* **33**, 326 (1924).
33. TEAGUE, O., AND BUXTON, H. H., *Z. physik. Chem.* **60**, 489 (1907).
34. THOMAS, A. W., AND JOHNSON, L., *J. Am. Chem. Soc.* **45**, 2532 (1923).
35. WEISER, H. B., AND CHAPMAN, T. S., *J. Phys. Chem.* **35**, 543 (1931); *ibid.* **36**, 713 (1932).
36. WINTGEN, R., AND LÖWENTHAL, H., *Z. physik. Chem.* **109**, 39 (1924).

THE ELECTROCHEMISTRY OF PERMSELECTIVE PROTAMINE COLLODION MEMBRANES. III. THE ELECTRICAL RESISTANCE OF SEVERAL TYPES OF PERMSELECTIVE PROTAMINE COLLODION MEMBRANES IN SOLUTIONS OF VARIOUS ELECTROLYTES¹

Karl Sollner² and Harry P. Gregor³

Department of Physiology, University of Minnesota, Minneapolis, Minnesota; and the Laboratory of Physical Biology, National Institute of Arthritis and Metabolic Diseases, National Institutes of Health, Public Health Service, Federal Security Agency, Bethesda, Maryland

Received September 24, 1951

The rates of establishment of final, stable concentration potentials across several types of permselective protamine collodion membranes and the final, stable concentration potentials themselves were dealt with in two preceding papers (1,2). This communication presents a similar, general survey on the electrical resistance of the same types of permselective protamine collodion membranes in various electrolytes at different concentrations. In content and presentation it is strictly analogous to the preceding paper on the conductance of the permselective collodion membranes; many details described there are omitted here (3).

A. THE TIME REQUIRED FOR THE ESTABLISHMENT OF THE FINAL, STABLE ELECTRICAL RESISTANCE OF PERMSELECTIVE PROTAMINE COLLODION MEMBRANES

I

The membranes used were prepared according to the previously described method (4). Highly porous three-layer collodion membranes are cast on the outside of rotating tubes and immersed for at least 24 hr. in buffered protamine sulfate solutions.⁴ These membranes are dried in

¹ Based on a portion of a thesis submitted by Harry P. Gregor to the Graduate School of the University of Minnesota, 1945, in partial fulfillment of the requirements for the Ph.D. degree.

² Present address: Laboratory of Physical Biology, National Institute of Arthritis and Metabolic Diseases, National Institutes of Health, Bethesda 14, Maryland.

³ Present address: Polytechnic Institute of Brooklyn, Brooklyn, New York.

⁴ The authors wish to express their thanks to Eli Lilly and Company for kindly furnishing the protamine sulfate used in the present work.

air of controlled humidity and in most instances dried a second time after removal from the glass tubes on which they were cast (4). Their designation follows the previously established usage; a membrane, e.g., designated as Hum 58—Shr 58 is one which was dried at 58% relative humidity on its casting tube and without this support (i.e., "shrunk") at the same relative humidity.

The rates of establishment of final, stable resistances across membranes can be studied in principle under two different conditions (1,3,5). A membrane having its fixed, cationic groups compensated for electrically with critical ions of one type is brought in contact with a solution having some other critical ion (anion), or a membrane is immersed in a solution which has the same species of anions as are carried as counter ions by the fixed, cationic wall groups.

It is very difficult, if not impossible, to bring protamine collodion membranes into a well-defined basic state (with the fixed, cationic wall groups compensated for electrically by hydroxyl ions), which would correspond to the previously used (1,3) standard acidic state. Treatment of the protamine membranes with hydroxide solutions, followed by exhaustive washing, is not desirable because of decomposition effects. Leaching with water to displace by hydrolysis the last species of anions with which the dissociable wall groups were saturated would be expected to be a slow and inefficient process because of the fairly strong base strength of the protamine and the concomitant low degree of hydrolysis of its salts. In either case significant quantities of bicarbonate ions are liable to be picked up by the membrane from the distilled water or the air, unless extreme precautions are taken. Water-washed protamine membranes can thus be expected to hold as the counter ions of their fixed wall groups variable ratios of hydroxyl and bicarbonate ions. In addition, nitrite and nitrate ions may also be present, originating from the unavoidable, though very slow, hydrolysis of the cellulose nitrate (which is likely to be accelerated in the presence of the basic protamine).

For the present purpose it seemed fully satisfactory to carry out the rate studies on protamine membranes in the state which results from prolonged washing with distilled water, since it was shown in the preceding paper on permselective collodion membranes that presaturation of the dissociable wall groups of the membrane with the critical species of ions under consideration is not an important factor in determining the rates at which final, stable membrane resistances are established.

The experimental technique was exactly as described in the preceding communication (3). All data on the time effect reported for one type of membrane were obtained with a single membrane specimen, which before use had been aged by at least 3 days' immersion in 0.1 *N* potassium chloride solution.

TABLE I

The Time Required for the Establishment of the Final, Stable Electrical Resistance of Various Permselective Protamine Collodion Membranes in Solutions of Different Electrolytes at Several Concentration Levels
($t = 25.0 \pm 0.1^\circ\text{C.}$)

Membrane	Hum 20—Shr 20			Hum 58—Shr 58			Hum 58		
Conc. of solution, equiv./l.	0.001	0.01	0.1	0.001	0.01	0.1	0.001	0.01	0.1
KCl									
	$\Omega/100 \text{ cm.}^2$								
Time min.									
5	58.6	26.6	10.4	24.7	6.9	1.3	13.2	2.8	0.5
15	58.5	25.0	8.0	23.4	5.4	1.2	11.4	2.4	0.4
30	55.8	23.4	6.9	23.9	4.9	1.0	11.5	2.2	0.4
60	53.6	21.1	6.1	22.7	4.2	0.9	10.3	2.0	0.4
120	53.0	18.7	4.8	20.2	3.5	0.7	9.0	1.9	0.5
180	54.0	18.9	4.6	19.3	3.1	0.6	9.1	2.0	0.4
240	53.8	19.3	4.5	19.6	3.0	0.7	9.0	2.0	0.4
300	54.5	19.0	4.5	19.2	3.2	0.6	8.5	2.0	0.4
360	53.6	18.8	4.5	19.2	3.2	0.6	9.0	1.9	0.4
KIO ₃									
	$\Omega/100 \text{ cm.}^2$								
5	159.0	138.5	42.8	60.2	16.7	8.3	27.5	10.5	3.4
15	155.3	130.5	38.3	57.5	16.1	7.0	23.7	9.1	2.8
30	134.8	91.3	34.9	57.0	15.0	6.2	21.8	7.7	2.4
60	125.1	81.4	32.3	52.6	12.6	5.1	19.9	5.9	2.0
120	123.7	78.0	29.9	45.0	12.2	4.8	17.7	5.4	1.6
180	118.3	75.2	28.9	40.1	11.5	4.3	17.0	5.0	1.5
240	114.8	71.1	28.0	39.8	11.0	4.3	15.0	4.6	1.5
300	107.2	70.2	27.5	40.2	11.2	4.2	14.6	4.8	1.5
360	102.5	70.0	27.3	39.1	11.1	4.3	14.4	4.7	1.5
420	102.3	70.0	27.3	39.5	11.1	4.3	15.0	4.7	1.5
1200	101.7	—	—	39.7	—	—	13.9	—	—
MgCl ₂									
	$\Omega/100 \text{ cm.}^2$								
5	79.9	28.4	26.7	38.6	15.3	2.4	16.7	6.4	0.8
15	79.1	26.8	23.3	36.7	13.0	2.2	16.6	5.9	0.7
30	76.1	25.5	19.4	36.9	11.7	2.0	17.1	5.0	0.7
60	75.2	24.7	17.6	36.9	9.3	1.7	16.3	3.7	0.5
120	74.8	24.1	16.7	36.3	8.1	1.5	15.6	3.3	0.5
180	—	23.4	15.0	—	8.2	1.4	—	3.1	0.5
240	75.8	23.1	14.9	36.5	7.7	1.4	16.4	3.2	0.5
300	74.9	23.3	15.0	36.6	7.9	1.4	16.1	3.0	0.5
360	75.4	23.3	14.6	36.9	7.9	1.4	15.8	3.1	0.5

Table I summarizes the resistances as a function of time for three types of permselective protamine membranes with three concentrations of potassium chloride, potassium iodate, and magnesium chloride. The experimental data are expressed in ohms/100 cm². Resistances of 10 ohms and greater are accurate within ± 3 to $\pm 5\%$; values below 10 Ω have a probable error of $\pm 0.5 \Omega$.

II

The periods of time in which the final, stable electrical resistances are established vary from about 15 min. to many hours. There is some indication that equilibration is reached somewhat faster with membranes of relatively high porosity. Differences between the two electrolytes with the same critical ion, potassium chloride and magnesium chloride, are small; a large noncritical ion does not seem to retard the establishment of the equilibrium to a significant extent. With a large critical ion, the iodate ion, equilibration is considerably slower, this difference between small and large critical ions being much more pronounced than with the collodion membranes (3). The concentration of the solution in contact with the membrane seems to be of little significance. The differences found between different electrolytes with the same membrane are of about the same magnitude as in the case of the establishment of final, stable concentration potentials. The differences between the various membranes with the same electrolyte are less pronounced than in the latter case.

It will be noted that stable resistances are obtained more slowly with the protamine collodion membranes than with the collodion membranes (3). This is paralleled by the differences in the rates at which final, stable potentials are established in the two cases (1,5). The cause of this difference cannot be attributed to any specific known factor, such as differences in the absolute magnitude of the resistance of the two types of membranes. One might be inclined to correlate it with the presumably higher ion-exchange capacity of the protamine membranes.

A comparison of the periods of time necessary to establish the final equilibrium resistance of the membranes with those previously reported for the establishment of stable, well-defined concentration potentials across the same types of membranes in the same electrolytes (1), shows as good an agreement as can be expected in view of the limited accuracy of the time-resistance data. This is in contrast to the results obtained with the permselective collodion membranes with which the establishment of the stable resistances requires longer periods than those necessary for reaching final, stable concentration potentials. A satisfactory explanation for this difference in the behavior of the collodion and protamine collodion membranes is lacking.

With regard to the question of the rates of establishment of equilibrium resistances in the case of protamine membranes which previously have

undergone ion exchange with the critical species of ions under consideration, the same conclusions can be drawn from Table I as were drawn in the case of the collodion membranes (3). Prior saturation of the wall groups with the critical ions can be expected to be of no practical significance.

B. THE EQUILIBRIUM RESISTANCE OF PERMSELECTIVE PROTAMINE COLLODION MEMBRANES IN SOLUTIONS OF VARIOUS ELECTROLYTES

I

Hardly any data on the resistance of electropositive membranes of highest ionic selectivity and low resistance can be found in the literature, except those by Gregor and Sollner (4,6,7).

The equilibrium resistances per unit area (cm^2), $^*\rho$, of three types of permselective protamine collodion membranes in solutions of six electrolytes are given in Table II. The experiments on one type of membrane were performed with a single membrane specimen in order to ensure a strict comparability of the data. The accuracy of the data of Table II can be estimated to be about $\pm 3\%$ with membranes of a unit area resistance of $1000\ \Omega$ and higher; values below $1000\ \Omega$ have a probable error of not more than $\pm 30\ \Omega$.

Column 1 of Table II names the electrolytes with which the membranes are equilibrated; col. 2 gives the concentration of the various solutions; col. 3 the specific resistances, ρ_s , of the latter; col. 4 gives the specific resistance of the solutions, ρ_s , divided by the transference number of its anion, t_- , i.e., the reciprocal of that part of the specific conductivity of the solution which is due to the anion; cols. 5, 6, and 7 present the unit area resistance, $^*\rho$, in ohms/ cm^2 of membrane, the ratios of each two adjacent figures pertaining to different concentrations of the same electrolyte being added in parentheses. Column 8 gives one example of the ratios of the unit area resistances of two different membranes equilibrated with solutions of the same electrolytes at the same concentrations.

II

Table II, even if limited in scope, shows the range of resistances that can be expected with permselective protamine collodion membranes prepared strictly according to the previously described methods (4).

As with the permselective collodion membranes, there was a time interval of about 8 months between the preparation of the membranes used for the equilibrium resistance measurements of Table II and of those used in the rate studies of Table I. The resistances at equilibrium conditions given in Table II for various electrolytes deviate considerably in several instances from the corresponding values of Table I. These differences indicate the variations which exist between membranes prepared

TABLE II

The Unit Area Resistances, $\ast\rho$, of Various Permselective Protamine Collodion Membranes in Equilibrium with Solutions of Several Electrolytes

($t = 25.0 \pm 0.1^\circ\text{C}.$)

1	2	3	4	5	6	7	8
Solution				Unit area resistance			Hum 20— Shr 20 $\ast\rho_{\text{ex}}$
Electro- lyte, x	Concen- tration, c	Specific resistance, ρ_s	$\frac{\rho_s}{t}$	Hum 20—Shr 20 $\ast\rho_{\text{ex}}$	Hum 58— Shr 58 $\ast\rho_{\text{ex}}$	Hum 58 $\ast\rho_{\text{ex}}$	Hum 58 $\ast\rho_{\text{ex}}$
	<i>equiv./l.</i>			$\Omega/\text{cm.}^2$ <i>ratio</i>	$\Omega/\text{cm.}^2$ <i>ratio</i>	$\Omega/\text{cm.}^2$ <i>ratio</i>	
KCl	0.001	6780	13300	7830	2010	1240	6.3
	0.01	693	1360	3930 (2.0)	400 (5.0)	200 (6.2)	20
	0.1	78	153	1180 (3.3)	120 (3.3)	30 (6.7)	39
LiCl	0.001	8760	13130	9080	3120	2450	3.7
	0.01	935	1395	4980 (1.8)	750 (4.2)	390 (6.3)	13
	0.1	105	154	1660 (3.0)	160 (4.7)	60 (6.5)	28
MgCl ₂	0.001	7870	12900	35400	4260	2170	16
	0.01	862	1403	8330 (4.3)	830 (5.1)	370 (5.9)	23
	0.1	99	152	2110 (4.0)	150 (5.5)	60 (6.2)	35
KF	0.001	7840	19100	13700	2410	1760	7.8
	0.01	811	1930	6740 (2.0)	500 (4.8)	310 (5.7)	22
	0.1	91	212	2250 (3.0)	160 (3.1)	50 (6.2)	45
KAc	0.001	8750	24350	22300	3010	2070	11
	0.01	925	2640	11000 (2.0)	1310 (2.3)	730 (2.8)	15
	0.1	104	307	6320 (1.7)	560 (2.3)	290 (2.5)	22
K ₂ SO ₄	0.001	6820	13170	45700	6540	2380	19
	0.01	746	1446	39500 (1.16)	2830 (2.3)	550 (4.3)	72
	0.1	91	178	36400 (1.09)	1560 (1.8)	120 (4.6)	303

under the same nominal conditions but at different times and from different batches of collodion and protamine. Membranes which are prepared simultaneously from the same preparations show a much better agreement in their resistances.

The data of Table II will now be considered from the same angles, according to the various variables, as were the analogous data in the preceding paper.

The comparison of the resistances of the *different* types of membranes equilibrated with solutions of the *same* electrolytes at the *same* concentration shows that with all the 18 solutions used (6 electrolytes at 3

concentrations) the resistance of the different membranes—in agreement with prior observations (4)—decreases in the sequence: Hum 20—Shr 20, Hum 58—Shr 58, Hum 58. The relative differences between the resistances of the various membranes are the greater, the higher the concentration of the solutions, as is evident from the representative ratio figures of col. 8.

The comparison of the resistance of the *same membranes* equilibrated with solutions of *different concentrations* of the *same electrolytes* shows that $\ast\rho$ is the greater the more dilute the solution. The variation in $\ast\rho$ with varying concentrations of the solutions is not nearly as great as the variation in the specific resistance of the latter, ρ_s , as can be seen from a comparison of col. 3 of Table II with the $\ast\rho$ values of cols. 5 to 7 or with the corresponding ratio figures in parentheses. Since the conductance of the membranes is due largely to the critical ions, the comparison of $\ast\rho$ with the corresponding values of ρ_s/t_- of col. 4 might be more pertinent (3).

The comparison of the resistance of the *same membranes* in equilibrium with solutions of the *same concentration* (normality) of *different electrolytes* shows the following:

With the three chlorides, $\ast\rho$ increases in the sequence potassium chloride, lithium chloride, magnesium chloride. In other words, the larger the noncritical ion (and the higher its valence) the higher the resistance. This result is analogous to that found with the denser collodion membranes (3).

With potassium fluoride and potassium acetate, $\ast\rho$ is with all membranes and at all concentrations higher than with potassium chloride. The ratios $\ast\rho_{KF}/\ast\rho_{KCl}$ and $\ast\rho_{KA}/\ast\rho_{KCl}$ are, however, in several instances significantly smaller than would be expected on the basis of the specific resistance, ρ_s , of the corresponding solutions (col. 3), or the values ρ_s/t_- of column 4. The cause of this is probably to be found in the anomalies of the chemistry of the fluorides and the hydrolysis of potassium acetate. Hydrolysis also may be responsible for the unexpectedly high resistances of all membranes in the 0.1 N potassium acetate solutions.

With potassium sulfate the membranes show a resistance considerably greater than that observed with univalent anions, the relative difference being greater with the denser membranes.

The comparison of the *concentration functions of the resistance of the same membranes equilibrated with solutions of different electrolytes* is based on the three vertical rows of figures given in parentheses in cols. 5 to 7 of Table II, which present the ratios of the $\ast\rho$ values for the same membranes at different concentrations of the same electrolytes. These figures show with all three membranes a fair degree of uniformity of the concentration function with all electrolytes having a univalent critical ion. With

potassium sulfate there is much less change in $\kappa\rho$ with a change in the concentration of the outside solution than in the former cases, particularly with the densest membrane. These observations are strictly analogous to the corresponding ones made with the collodion membranes.

The quantitative comparison of the *concentration function of the resistance of different membranes equilibrated with solutions of the same electrolytes* is based on a comparison of the ratios of the unit area resistances of the same membranes at different concentrations of the same electrolytes. An inspection of the (horizontal rows of) ratio figures in parentheses shows that the relative changes in membrane resistance with changes in the concentration of the solutions are the smaller the denser the membranes. Of particular interest is the membrane Hum 20—Shr 20 in the potassium sulfate solutions: in this instance the resistance of the membrane changes by only about 25% with a hundred fold change in concentration of the adjacent solution. As before, these results are strictly analogous to the corresponding observations on permselective collodion membranes.

This discussion of the resistance data of Table II may be concluded appropriately with a *comparison of the regularities found here for the protamine collodion membranes and those reported in the preceding paper for the permselective collodion membranes* (3). Such a comparison shows that the dependence of the membrane resistance upon the various variables—porosity of the membranes, size and valence of the ions of the electrolyte, and the electrolyte concentration—closely follows the same pattern with the two types of membranes without any significant discrepancy. This parallelism of the data strongly suggests that the physical mechanisms involved are essentially identical with the two types of membranes. This makes it possible to discuss jointly the equilibrium resistances of the two types of membranes from a more general, theoretical point of view.

III

The discussion of the experimental data on the resistance of permselective collodion and protamine collodion membranes will be confined to the correlation of these data with certain conclusions from the basic concepts of the fixed charge theory. No attempt will be made to expand the formal treatment of the theory, given by Teorell (8) and by Meyer and Sievers (9), to the problem of the resistance of membranes of ideal ionic selectivity. It might be added that a formal treatment of membrane resistance in general, strictly from the point of view of the Teorell, Meyer-Sievers formulation of the fixed charge theory was recently announced by Schmid in a preliminary paper (10). It seems doubtful whether any such straightforward extension of the theory could be applicable to mem-

branes of ideal ionic selectivity. Moreover, the available experimental data are inadequate for a crucial test of any such extension of the theory. We, therefore, prefer to postpone a mathematical development of the theory until more adequate experimental data will be available.

In a discussion of the factors which determine the resistance of membranes equilibrated with electrolyte solutions it will frequently be more convenient to refer to membrane conductance than to membrane resistance, the former being the reciprocal of the latter; the term more appropriate in any particular connection will be used.

According to the fixed charge theory the transport of electricity across a membrane is due to the movement of the counter ions of the fixed, charged wall groups, and to the "nonexchange electrolyte," both anions and cations, which enters the membrane to a varying degree, dependent on the concentration of the adjacent solution. The concentration of this "nonexchange electrolyte" in the pores of the membrane may be assumed to be governed by a distribution function which is closely analogous to a Donnan distribution, and actually has been introduced as such in the fixed charge theory (8,9), where the fixed dissociable wall groups act as the nondiffusible species of ions. In the case of real heteroporous membranes, in addition to electric blocking of pores steric hindrance must be considered. Here certain pores or parts of pores of a membrane which are accessible to ions below a certain size are inaccessible to larger ions. "Critical" ions as well as "noncritical" ions may thus be excluded from certain pathways or parts of pathways across the membrane which are accessible to smaller ions. If the critical ions are too large to enter certain pores, they cannot act there as counter ions of the fixed wall groups, and the ion of water, H_3O^+ or OH^- , as the case may be, must be assumed to occupy these positions (11). Nonexchange electrolyte can enter only those pores or parts of pores which permit the entry of both anions and cations—electroneutrality must be maintained.

The ions of each movable ionic species within a (hypothetical) homogeneous pore contribute toward the over-all conductance of the membrane according to their number, their mobility, and the "degree of dissociation" of the surface compounds which they form with the fixed, charged wall groups.

With pores of uneven diameter the conductance at each cross-sectional plane along the axis of the pore is determined by the number of movable critical and noncritical ions times their respective ionic conductances,⁵ the total resistance of the pore being the sum of the resistances of the

⁵ To which extent the movement of the counter ions of fixed wall groups which are far apart from each other may be helped by the presence of nonexchange electrolyte is at present a matter of speculation; the nonexchange electrolyte may help considerably to bridge the gap between the movable counter ions which oscillate around their fixed wall groups (12,13).

sequence of volume elements of different properties.⁶ The resistance of membranes with inhomogenous pores is consequently a complicated function of the structure of the membrane, the concentration of the solution with which the membrane is equilibrated, and of the properties of the critical as well as noncritical ions of the electrolyte under consideration.

The situation prevailing in an inhomogenous pore can be visualized with the aid of the highly schematic Fig. 1, which represents the simple case of absence of steric hindrance.

The cross-hatched parts in Fig. 1 indicate the solid wall material of the membrane. The fixed charged groups on the pore walls are represented by flat protuberances; the charge of these fixed anionic groups in the dissociated state is indicated by a minus sign; the thin-line half-circles around the wall groups indicate the spheres of effective electrostatic repulsion between these groups and univalent anions in solution. The variously inscribed solid circles represent the hydrated size of the respective ions in solution. The thin-line circles around the anions indicate the spheres of effective electrostatic repulsion between these ions and the fixed wall groups or other ions of the same sign in solution. The dotted-line circles around the cations represent the spheres of repulsion between the cations. The spheres of repulsion of the various univalent ions are assumed to be of the same magnitude. An ion in solution cannot approach another ion or a fixed, charged wall group of the same sign more closely than the distance defined by the sum of the radii of their two spheres of repulsion. Ions of one sign of charge can approach ions of the opposite sign including fixed, charged wall groups up to the point of contact (indicated in the figure by the contact of solid lines), since spheres of electrostatic repulsion are not operative between charged units of the opposite sign. Likewise, ions may approach to the point of bodily contact the charge-free parts of a pore wall. With the symbols defined, Fig. 1 is virtually self-explanatory.

In spite of its obvious shortcomings, this simple and undoubtedly incomplete picture of the physical basis of membrane conductance leads to some clear-cut conclusions concerning certain idealized, limiting cases.

For example, with electrolytes with which steric hindrance does not come into play with a given membrane, all the potentially dissociable wall groups of the latter, as stated before, are compensated for electrically by the critical species of ions in the system. The theory further predicts that with solutions below a certain concentration virtually no nonexchange electrolyte enters the pores. In this latter instance, the conductance of the membrane would be due entirely to the counter ions of the fixed

⁶ This situation is basically different from that prevailing in the case of the concentration potential, where the narrowest part of the pore which carries a charged wall group is of paramount importance (14).

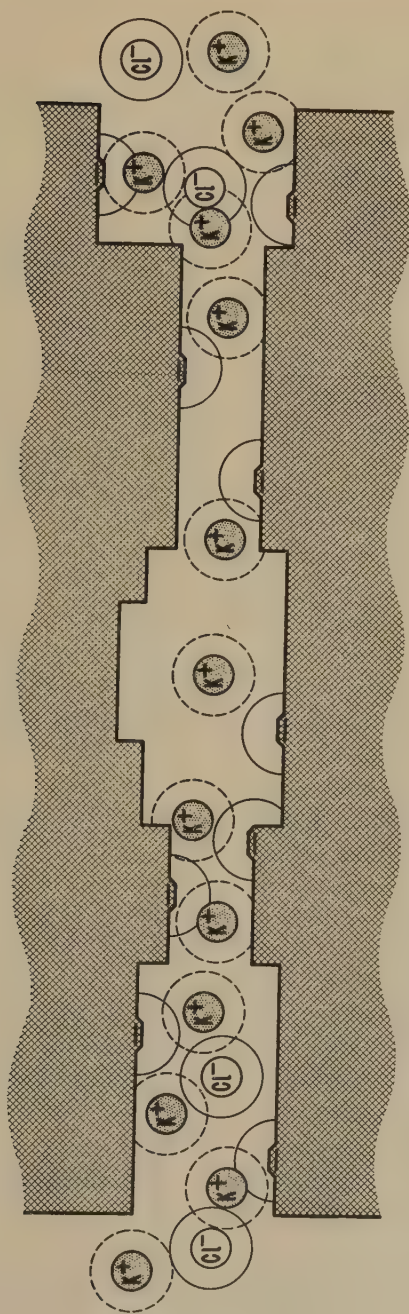


FIG. 1. The distribution of ions in an inhomogeneous pore of an electronegative membrane according to the fixed charge theory.

wall groups, and thus independent of the concentration (below the limiting concentration) of the outside solution.⁷

If the noncritical species of ions in solution is excluded from the pore system of the membrane, the membrane conductance in the presence of a given critical ion can be expected to be independent of the nature of the noncritical ion of the electrolyte in the solution.

With regard to the ratios of the magnitude of the membrane conductances in the presence of different critical ions, none of which must suffer any steric hindrance, the theory leads to this prediction: Under conditions where the conductance of the counter ions (surface conductance) is the total conductance of the membranes, its magnitude should be proportional to the equivalent ionic conductivity (in free solution) of the counter ions, provided that the degrees of dissociation of the compounds formed by the wall groups and the various counter ions are virtually the same.

In this connection it is interesting to note that Heymann and O'Donnell have measured the resistances of cation exchangers, the fixed dissociable groups of which were compensated for by various cations (15). For this purpose compressed plugs of granular ion exchangers were equilibrated with various electrolyte solutions, the excess of the latter and the nonexchange electrolyte within the individual granules being removed by prolonged washing with large quantities of distilled water. Under these conditions the conductance of the ion exchangers divided by the mobility of the various ions was virtually constant in the case of the Li^+ , Na^+ , K^+ , and NH_4^+ ions. In the case of the hydrogen ion the ratio was significantly less. With heavy-metal and polyvalent ions complicated relationships were found which Heymann and O'Donnell rightly attribute primarily to the varying degrees of dissociation.

Another limiting case occurs (in the absence of steric hindrance) with electrolyte concentrations which are sufficiently high to swamp any specific membrane effect. Here the contribution of the counter ions toward the total membrane conductance is negligible, the conductance being due essentially to the nonexchange electrolyte. In this case the membrane conductance in solutions of different concentrations of the same electrolyte or of different electrolytes should be proportional to the specific conductance of these solutions. This situation arises readily with membranes of high porosity even at moderate electrolyte concentrations.

The comparison of these general deductions from the fixed charge theory and of the data in the Tables II of this and the preceding paper

⁷ In the language of surface chemistry, the "surface conductance" of the pore walls is, under these conditions, the total conductance of the membrane. The higher the charge density on the pore walls of the membrane and the lower its porosity (within certain limits), the higher will be the limiting concentration of the outside solution below which virtually the entire conductance of a membrane is surface conductance.

(3) shows in several instances a noticeable approach of the experimentally studied situations toward the simple limiting conditions which could be treated theoretically. Some such cases have been indicated previously in the special discussion parts which follow the two tables; some additional examples can be found by a careful examination of the data.

The trend of the experimental data clearly indicates that the investigated concentration range is too narrow to encompass those very low and very high concentrations, within which the limiting situations arise in full clarity. In any further resistance studies it will, therefore, be necessary to extend the range of investigated concentrations considerably, particularly in the direction of lower concentrations. A greater variety of electrolytes should be studied; of particular interest would be the numerous univalent inorganic anions, of about equal size but greatly different adsorbabilities (7,16). Likewise, the study of membrane resistance in the simultaneous presence of two species of critical ions (in various concentration ratios) can be expected to shed much light on the intricacies of the electrical and geometrical structure of the membranes. Quantitative determinations should be made in all instances, both of the quantities of critical *and* of noncritical ions which under the various conditions are contained in the membrane (17). In these investigations the newer types of strong acid, negative membranes will be particularly interesting and useful (3,18,19), as well as the corresponding strong base, positive membranes which undoubtedly will become available in the near future.⁸ Their

⁸ The future improvement of the permselective positive membranes will follow similar lines as those indicated previously for the negative membranes (3).

The mechanical strength of the permselective protamine collodion membranes (which are not weakened by an oxidation process) is fully satisfactory and does not require any improvement, at least for laboratory purposes. The main shortcoming of the currently available permselective protamine membranes is their unavoidable, inherent leak of (univalent) noncritical ions, though this deficiency is not quite as large as was previously assumed on the basis of data on concentration potentials in potassium chloride chains which were not corrected for the asymmetry of the liquid junction potentials (3). (The data previously given for 2:1 and 10:1 concentration ratio chains are too low by 0.3 and 1.1 mv., respectively.) Some improvement of the ionic selectivity of the protamine membranes may conceivably be obtained by the use of more highly purified preparations of protamine, or by decarboxylation of the latter; more promising seems to be the chemical blocking, by esterification, of the free carboxyl groups of the protamine molecules.

An increase in the basicity of the fixed wall groups in the positive membranes over that of the amino groups of the protamine would be highly desirable, though it is not as necessary as the corresponding improvement of the negative membranes. The incorporation of tertiary amines or, much better, of quaternary ammonium bases in the pore walls of the membranes should lead to a satisfactory solution of this problem. In this connection a paper by Albrink and Fuoss should be mentioned (20). With the art of preparing true anion exchangers (not acid adsorbers) making rapid progress in recent years, it soon should be not too difficult to find some anion-exchange material which

high unit area exchange capacity (charge density), by virtually absolute exclusion of the noncritical ions even at high concentrations, can be expected to simplify many experimental problems and the theoretical evaluations of experimental data.

In all such further resistance studies it will be advisable to improve the conductance cells, as suggested previously (21), or, for precise measurements, to use flat, not test tube-shaped membranes (17). More important, it should be carefully determined whether or not the resistance of the various types of membranes as determined by the Kohlrausch alternating current method is in all instances identical with their direct-current resistance, the number and accuracy of direct tests in this direction being at present inadequate (17,22).⁹

Even a cursory reflection on the foregoing general statements leads to the conclusion that at least certain aspects of the physical chemistry of membranes tend to merge with the physical chemistry of ion exchangers; the work of Heymann and O'Donnell is a good example in this respect (15). Any progress in this latter, rapidly expanding and deepening field is bound to promote an understanding of the behavior and actions of membranes in electrolytic systems. Ion exchangers of known structure, charge density, acid or base strength, etc., might easily yield certain results which are not readily obtainable with membranes.

This promotion of understanding in one field by the progress in the other, however, can be expected to be by no means a one-sided process. The systematic introduction of the study of concentration potentials, conductance (and conductivity), and, last but not least, of the bi-ionic potential (16) into the investigation of ion exchangers is bound to clarify greatly the latter field.

SUMMARY

1. The periods of time required in which final, stable electrical resistances are established with three electrolytes—potassium chloride, potassium iodate, and magnesium chloride—across three types of permselective protamine collodion membranes vary from about 15 min. to many hours,

could be used for the preparation of strong base type permselective collodion base membranes which would be the electropositive analog of the recently described strong acid type permselective collodion base membranes (18,19).

⁹ In the measurement of the resistance of permselective collodion and protamine collodion membranes with the conventional Kohlrausch method (1000 cycles/sec.) sharp minima are obtained in the majority of instances without the use of any capacitors in the circuit, in infrequent instances by the use of small capacitances ($\ll 0.1 \mu\text{f}/100 \text{ cm.}^2$). With the newer type of ion exchanger-collodion base membranes, considerable capacitances are required in order to obtain sharp minima (19). Here the identity of 1000 cycles a. c. "resistance" and d. c. resistance seems to be questionable. It, therefore, will be advisable to have recourse to the more elaborate methods of impedance measurements as used by Cole (23), Goldman (24), Albrink and Fuoss (20), and Teorell (25).

being somewhat longer, for unknown causes, than in the case of the analogous permselective collodion membranes. The influence of the ionic properties of the electrolytes with which the membranes are equilibrated on the rates of equilibration closely resembles that observed with the permselective oxidized collodion membranes.

2. The final, stable resistances of three types of permselective protamine collodion membranes equilibrated with solutions of six electrolytes at six concentrations were measured and tabulated. The data are evaluated as to the differences of the various types of membranes, the influence of the concentration on membrane resistance, the influence of the nature of the electrolyte, and various concentration functions. The regularities found are strictly analogous with those observed with permselective oxidized collodion membranes.

3. The experimental data on equilibrium resistance of permselective collodion and protamine collodion membranes given in this and in the preceding paper are discussed jointly from the point of view of the basic concept of the fixed charge theory of electrochemical membrane behavior. Various complications which arise with real membranes which are heteroporous and have inhomogenous pores are sketched. Certain cases of membrane behavior under limiting conditions as to concentration of the adjacent solutions, the nature of the critical ions, etc., are discussed and compared to the experimental results.

4. The direction of further fruitful investigations on membrane resistance is pointed out and the increasing number of points of close contact and even of overlapping between the physical chemistry of membranes and studies on ion exchangers is indicated.

REFERENCES

1. SOLLNER, K., AND GREGOR, H. P., *J. Phys. & Colloid Chem.* **54**, 325 (1950).
2. SOLLNER, K., AND GREGOR, H. P., *J. Phys. & Colloid Chem.* **54**, 330 (1950).
3. SOLLNER, K., AND GREGOR, H. P., *J. Colloid Sci.* **6**, 557 (1951).
4. GREGOR, H. P., AND SOLLNER, K., *J. Phys. Chem.* **50**, 88 (1946).
5. SOLLNER, K., AND GREGOR, H. P., *J. Phys. Chem.* **50**, 470 (1946).
6. GREGOR, H. P., Ph.D. Thesis, University of Minnesota, 1945.
7. SOLLNER, K., *J. Electrochem. Soc.* **97**, 139C (1950).
8. TEORELL, T., *Proc. Soc. Exptl. Biol. Med.* **33**, 282 (1935); *Proc. Natl. Acad. Sci. U. S.* **21**, 152 (1935).
9. MEYER, K. H., AND SIEVERS, J.-F., *Helv. Chim. Acta* **19**, 649 (1936); MEYER, K. H., *Trans. Faraday Soc.* **33**, 1073 (1937).
10. SCHMID, G., *Z. Elektrochem.* **54**, 424 (1950).
11. BETHE, A., AND TOROPOFF, TH., *Z. physik. Chem.* **88**, 686, (1914); **89**, 597 (1915).
12. JENNY, H., *J. Phys. Chem.* **40**, 501 (1936); JENNY, H., AND OVERSTREET, R., *J. Phys. Chem.* **43**, 1185 (1939).
13. GREGOR, H. P., GUTOFF, F., AND BREGMAN, J. I., *J. Colloid Sci.* **6**, 245 (1951).
14. SOLLNER, K., *J. Phys. Chem.* **49**, 265 (1945).
15. HEYMANN, E., AND O'DONNELL, I. J., *J. Colloid Sci.* **4**, 405 (1949).

16. SOLLNER, K., *J. Phys. & Colloid Chem.* **53**, 1211, 1226 (1949).
17. GREEN, A. A., WEECH, A. A., AND MICHAELIS, L., *J. Gen. Physiol.* **12**, 473 (1929).
18. SOLLNER, K., AND NEIHOF, R., *Arch. Biochem. Biophys.* **33**, 166 (1951).
19. NEIHOF, R., in preparation.
20. ALBRINK, W. S., AND FUOSS, R. M., *J. Gen. Physiol.* **32**, 453 (1949).
21. GREGOR, H. P., AND SOLLNER, K., *J. Phys. Chem.* **50**, 53 (1946).
22. CARR, C. W., AND SOLLNER, K., *J. Gen. Physiol.* **28**, 119 (1944).
23. COLE, K. S., *J. Gen. Physiol.* **15**, 641 (1932); COLE AND COWORKERS, *J. Gen. Physiol.* **18**, 877 (1935); **19**, 609, 625 (1936); **21**, 189 (1937); **21**, 583, 591, 757 (1938); **22**, 37 (1938); **22**, 649 (1939); **24**, 551 (1941); **25**, 765 (1942); and other papers.
24. GOLDMAN, D. E., *J. Gen. Physiol.* **27**, 37 (1943).
25. TEORELL, T., *Acta Physiol. Scand.* **10**, 243 (1945); **12**, 235 (1946).

STUDIES ON POLYELECTROLYTES. I. SODIUM CARBOXYMETHYLCELLULOSE

Sadhan Basu* and Pares Ch. Das Gupta

Indian Association for the Cultivation of Science, Calcutta, India

Received July 18, 1951

ABSTRACT

Various physicochemical properties of sodium carboxymethylcellulose solutions, namely, viscosity, pH-effect, salt-effect, and conductivity have been measured. The peculiar characteristics of these solutions compared to those of neutral polymers on the one hand and strong electrolyte on the other have been attributed to the polyelectrolytic nature of sodium carboxymethylcellulose. A critical discussion has shown that only by the folding chain theory could all the experimental results be satisfactorily explained.

INTRODUCTION

Of all the water-soluble cellulose ethers, the sodium salt of carboxymethylcellulose has come to occupy a unique position in industry as a challenging substitute for natural gums. The diverse uses to which this single substance can be put have been summarized by Caldwell and Watters (1); these cover almost the whole field from detergents to medicine via the paper, ceramic, and textile industries. As with all other commercially important high-molecular-weight substances, practice has far surpassed theory in this case. The only recorded data on the physicochemical properties of the sodium carboxymethylcellulose solution are those of Brown and Haughton (2). These data are very meager and the explanation advanced to account for certain characteristic features of the solution requires reconsideration in view of the recent theoretical development of the physical chemistry of polyelectrolytes (3, 4). Further, the physicochemical study of the sodium carboxymethylcellulose solution is of great importance since it is structurally similar to polyuronic acid, of which numerous derivatives are widely distributed in nature and play important roles as protective fluids due to some peculiar characteristics of their solutions.

THEORETICAL

By the term polyelectrolyte is meant a high-molecular-weight substance that is simultaneously also an electrolyte containing a number of ionizable groups distributed along the polymer chain. The carboxymethyl-

* Present address: Department of Chemistry, Indiana University, Bloomington, Indiana.

cellulose is a compound of cellulose in which some of the cellulose —OH groups have been converted into a structure of the type $\text{—O—CH}_2\cdot\text{COOH}$. In addition, the high molecular weight of the cellulose chain makes carboxymethylcellulose a polyelectrolyte according to Fuoss's definition (4). There is a fundamental difference between simple electrolytes and polyelectrolytes. In a simple electrolyte the positive and negative ions are capable of independent motion; in solution, therefore, there is on an average an equal number of positive and negative charges per unit volume. In a polyelectrolyte on the other hand, a number of similar charges are bound to the same chain and the maximum possible separation among them is obtained only when the chain is fully extended. In solution, therefore, some of the similar charges exist in clusters with intervening solvent molecules containing only oppositely charged particles.

The geometrical configuration of such a compound is also quite different from that of a neutral polymer. In a neutral polymer, the chain is coiled up in solution, the extent of coiling being determined by the kinetic energy and internal Brownian movement. The coiling will not vary appreciably with concentration, at least not in very dilute solution in a good solvent. In the case of a polyelectrolyte, however, at infinite dilution all the ionizable groups will be dissociated and the polymer chain will be left fully charged. The repulsion between similarly charged centers on the chain will cause it to assume a fully stretched configuration accompanied by maximum possible charge separation. As the concentration is increased some of the oppositely charged ions will be drawn back on the polymer chain owing to high charge density on the polymer, thereby neutralizing some of the charges on the chain, which will then assume a less extended configuration owing to diminution in the intramolecular coulombic repulsion. Thus, as the concentration is progressively increased, the coiling of the chain becomes increasingly predominant, till at last the limit is reached when all the groups are undissociated and the coiling is maximum.

This change in polymer coil will be accompanied by a change in the hydrodynamic volume units and consequently will be reflected in those properties of solution where movements of the polymer unit are an important factor, e.g., viscosity, conductivity, etc.

With these introductory observations we pass on to the considerations of various physicochemical characteristics of a sodium carboxymethylcellulose solution and see how far they can be explained by the foregoing assumptions. It may be added in this connection that it has been amply demonstrated that cellulose derivatives, gums, alginates, and pectinates dissolve molecularly in solution, the colloidal aspects of such solutions in dilute regions being due to colloidal dimensions of the molecules themselves (5).

EXPERIMENTAL

Material

The sodium carboxymethylcellulose used was a commercial sample of medium viscosity (about 60 c.p. in 1% solution; M.W. 40,000 to 60,000), purified by solution, filtration, and reprecipitation. The sample had a substitution of about 0.38, determined by potentiometric titration of free acid with alkali in water, checked against the ash value of the sodium salt. The samples must be perfectly free from electrolytes and great precautions must be taken to avoid any contamination with electrolytes during the course of work, since the properties of sodium carboxymethylcellulose (hereafter called SCMC) are profoundly modified in the presence of electrolytes.

In preparing the solution, SCMC was shaken with water, allowed to stand at room temperature for about 48 hours and then filtered through hardened filter paper. Heating of the solution above 60°C. was scrupulously avoided.

Measurement of Viscosity

The viscosity measurements were taken in an Ostwald viscometer having a flow time of 76 sec. with water, at a temperature of 35°C. ± 0.01 .

Measurement of Conductance

Conductance was measured on a direct reading bridge of philosophic type with a magic eye outfit for determining the balance point. The applied cell voltage was about 2.0 and the measurements were taken at a frequency of 1000 c.p.s. The conductivity cell was a Kohlrausch type of parallel plate fixed electrode cell, having a cell constant of 0.7247 checked against 0.01 *N* KCl solution.

RESULTS

The viscometric measurements of the solutions of SCMC at different concentrations in water dioxane mixtures were made at 35°C. and the calculated values of reduced viscosity ($\eta_{sp/c}$, where $\eta_{sp} = \eta/\eta_0 - 1$, η and η_0 being the viscosities of solution and solvent, respectively) are summarized in Table I and the corresponding curves are given in Fig. 1.

The values given in Table I show that there is an enormous depression of reduced viscosity of SCMC solution as the percentage of dioxane is increased in the solution. The three solvents used had dielectric constants of 78, 62.8, and 52.7, respectively. The curves in Fig. 1 show that $\eta_{sp/c}$ rises sharply in dilute region, sharpness decreasing with increasing dioxane content of the solution.

Viscosity of a solution was measured at constant concentration of SCMC with increasing and diminishing pH. The SCMC (0.04%) solution

TABLE I
Viscosities of SCMC Solutions

In water ($\epsilon = 78$)		In 1:4 dioxane:water mixture ($\epsilon = 62.8$)		In 1:2 dioxane:water mixture ($\epsilon = 52.7$)	
Conc. %	η_{sp}/c	Conc. %	η_{sp}/c	Conc. %	η_{sp}/c
0.070	63.50	0.0530	20.28	0.0430	16.46
0.053	63.11	0.0215	21.62	0.0215	19.62
0.040	68.00	0.0081	29.00	0.0108	23.53
0.023	76.63	0.0035	37.71	0.0054	27.90
0.013	93.18	—	—	—	—

has a pH of 6.8 in water. In one experiment the pH was increased by gradual addition of sodium hydroxide, and subsequently diminished step by step by acid in one case and dialysis in other, to pH 6.8. In another experiment the pH of the original solution was diminished below 6.8 by hydrochloric acid and again increased step by step to pH 6.8 by sodium hydroxide, viscosity being determined at each step. The results are summarized in Table II and the corresponding graphs are given in Fig. 2.

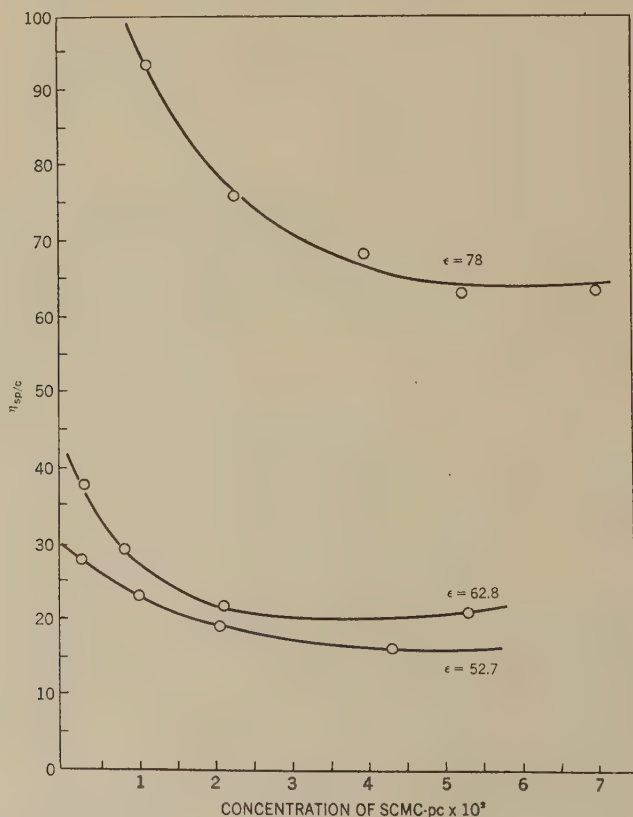


FIG. 1

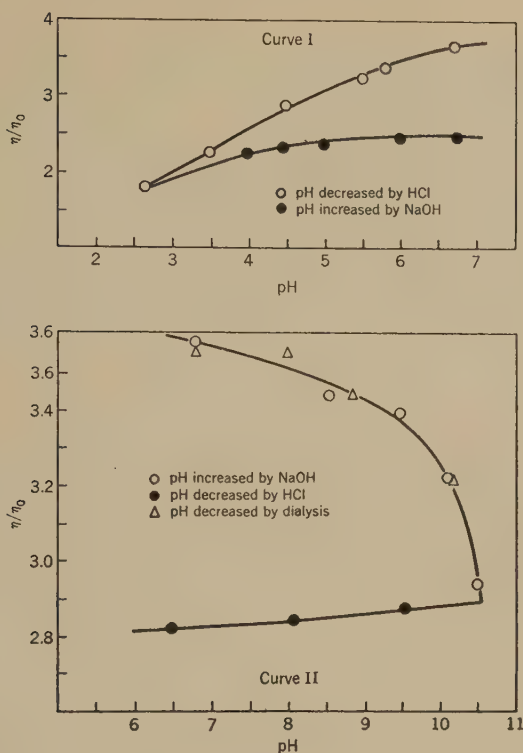


FIG. 2

TABLE II

pH-Viscosity Measurements of SCMC Solution (pH 6.8)

In alkaline region	pH increasing by NaOH		pH diminishing by HCl		pH diminishing by dialysis	
	pH	η/η_0	pH	η/η_0	pH	η/η_0
	6.80	3.58	9.60	2.87	10.10	3.21
	8.80	3.44	8.10	2.84	8.88	3.44
	9.50	3.39	6.80	2.82	8.00	3.55
	10.10	3.22			6.80	3.55
	10.54	2.93				
In acid region	pH diminishing by HCl		pH increasing by NaOH			
	pH	η/η_0	pH	η/η_0		
	6.80	3.67	4.0	2.25		
	5.80	3.35	4.4	2.30		
	5.50	3.28	5.1	2.39		
	4.52	2.90	6.1	2.43		
	3.52	2.29	6.7	2.45		
	2.68	1.82				

While reducing the pH by dialysis (using membrane quality Cellophane) a fall in the concentration of the solution was expected due to osmosis. In order to correct for this effect, concentration was determined at each stage while working with dialyzed samples. It has been found, however, that there was no change in the concentration even after 6 hours dialysis, which was the time required to bring back the pH from

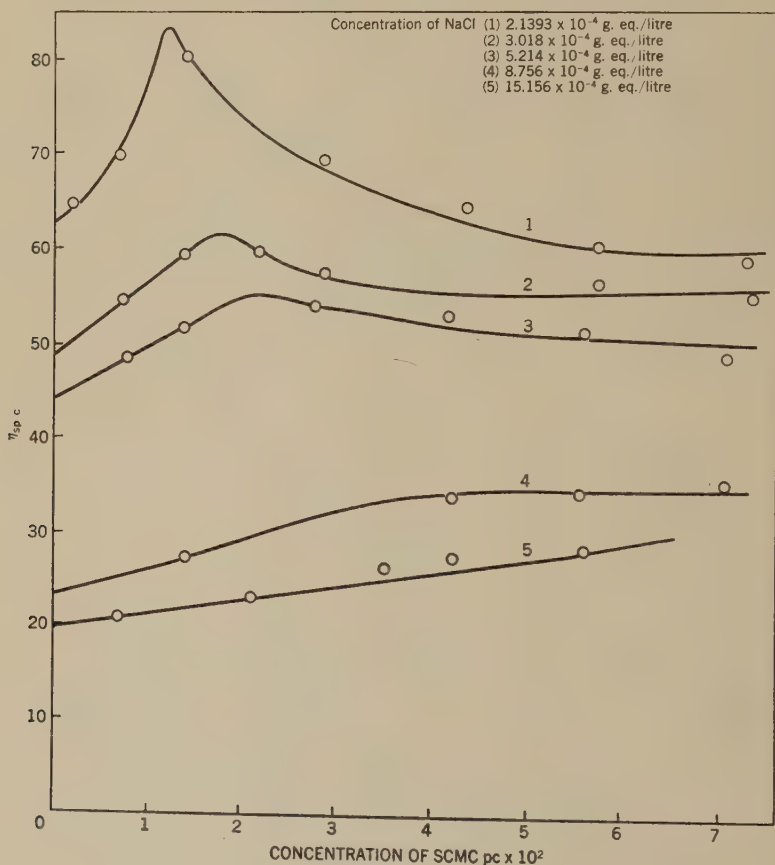


FIG. 3

10.5 to 6.8. This may be expected since firstly the compound was a high molecular one and secondly the solution was very dilute and had a vanishingly small osmotic pressure.

The measurements of reduced viscosity of solutions at different concentrations of SCMC were done at constant sodium chloride concentration, the results of which are given in Table III for five different sodium chloride concentrations and the corresponding graphs are given in Fig. 3.

TABLE III

Viscosity of SMC Solution in Presence of Sodium Chloride

Conc. of SMC %	Conc. of NaCl in g. equivalent per liter $\times 10^4$	η_{sp}/c	Remarks
0.0882	2.1393	55.64	
0.0735		58.42	
0.0588		60.87	
0.0441		64.55	Maximum at
0.0294		69.40	2.2341×10^{-4} g.
0.0147		80.66	equivalent SMC
0.0072		70.26	per liter
0.0022		65.57	
0.0882	3.018	53.31	
0.0735		54.94	
0.0588		56.40	
0.0441		58.34	Maximum at
0.0294		57.27	3.562×10^{-4} g.
0.0221		59.84	equivalent SMC
0.0142		59.48	per liter
0.0074		54.83	
0.0994	5.214	45.33	
0.0852		47.62	
0.0710		48.89	
0.0568		51.24	Maximum at
0.0497		53.94	4.418×10^{-4} g.
0.0426		53.02	equivalent SMC
0.0284		54.24	per liter
0.0142		51.71	
0.0071		48.76	
0.0852	8.756	35.53	
0.0710		35.01	
0.0568		34.58	
0.0426		33.79	
0.0142		27.77	
0.0753	15.156	30.51	
0.0568		28.64	
0.0426		27.10	
0.0355		26.32	
0.0213		22.91	
0.0071		20.39	

It becomes evident from Table III that the viscosity of SMC solution is decreased by added NaCl and that the decrease increases with increasing concentration of NaCl. The curves at three NaCl concentrations, namely, 2.139×10^{-4} , 3.018×10^{-4} , and 5.214×10^{-4} g. equivalent

TABLE IV
Viscosity of SCMC in Presence of Neutral Salts

Conc. of SCMC %	Conc. of added salt g. equivalent per liter $\times 10^4$	η_{sp}/c	Remarks
0.074	3.223 (Na_2SO_4)	24.28	
0.049		26.89	Maximum at 4.831×10^{-4} g. equiv. of SCMC per liter
0.033		28.48	
0.022		29.50	
0.015		27.80	
0.010		25.60	
	23.861 (Na_2SO_4)		
0.099		16.46	
0.066		15.90	
0.044		16.36	
0.029		16.04	
0.019		14.87	
	4.156 (KCl)		
0.0990		33.13	
0.0880		34.37	
0.0770		34.84	
0.0660		36.90	Maximum at 3.632×10^{-4} g. equiv. of SCMC per liter
0.0550		36.63	
0.0440		39.90	
0.0330		42.21	
0.0220		45.13	
0.0110		44.64	
0.0050		40.90	
	18.642 (KCl)		
0.0768		28.36	
0.0640		28.21	
0.0517		26.87	
0.0256		26.22	
0.0128		24.27	
	1.736 (MgCl_2)		
0.1003		33.89	
0.0668		31.96	
0.0445		32.58	Maximum at 4.21×10^{-4} g. equiv. of SCMC per liter
0.0296		39.42	
0.0197		44.21	
0.0131		32.58	
0.0087		22.98	
	13.03 (MgCl_2)		
0.1003		12.73	
0.0668		10.77	
0.0445		9.43	
0.0296		8.44	

ent per liter, respectively, show well-defined maxima at a concentration of SCMC where the equivalent concentration of Na from SCMC becomes nearly equal to that from NaCl, as shown in Table III. At higher NaCl concentration the $\eta_{sp}/c - c$ curves become similar to that for neutral polymer. Similar measurements were taken with three other electrolytes, namely, Na_2SO_4 , KCl, and MgCl_2 , the data for which are given in Table IV and the curves in Fig. 4. The curves show that in these cases also maximum appears at low cation concentrations and at higher electrolyte concentration the $\eta_{sp}/c - c$ curves become linear having a positive slope with concentration axis.

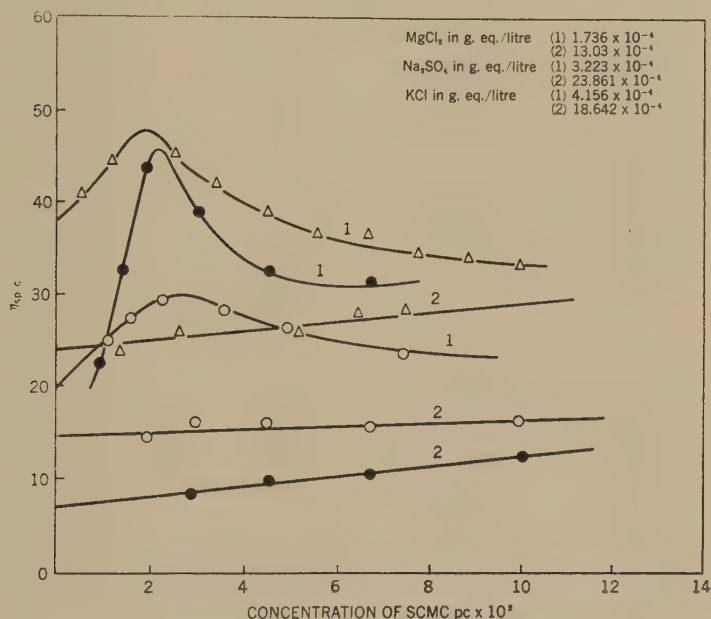


FIG. 4

The results of conductivity measurements of the solution of SCMC in water and water-dioxane mixtures are summarized in Table V and the corresponding $\Lambda - \sqrt{c}$ curves are given in Fig. 5.

The $\Lambda - \sqrt{c}$ curves given in Fig. 5 show that they are not linear with a downward slope, as is the case with strong electrolytes, nor do they tend to approach a limiting value at extremely low dilution as is the case with colloidal electrolytes. If $\log \Lambda$ is plotted against $\log c$, linear curves, as is the case with pyridonium polyelectrolyte, are not obtained with SCMC solution. Fuoss (3) has shown that when the percentage of vinyl pyridine was low in the co-polymer of pyridine and styrene, the polyelectrolytes

obtained from such compounds by treating them with methyl bromide also failed to give a linear $\log \Lambda - \log c$ plot in a solution of nitromethane-dioxane mixture. In our case the failure to give a linear plot may also be due to rarity of ionizable groups on the polymer chain.

TABLE V
Conductivity of SCMC Solution

Conc. in g. equivalent per liter	\sqrt{c}	Specific con- ductivity $\times 10^4$	Λ
In water ($\epsilon = 78$)			
0.00551	0.0742	10.21	185.2
0.00371	0.0609	7.246	195.3
0.00247	0.0497	4.529	183.3
0.00164	0.0405	3.294	200.8
0.00109	0.0330	2.337	214.4
0.00073	0.0270	1.811	247.8
0.00048	0.0221	1.393	286.7
0.00032	0.0180	1.115	344.2
0.00021	0.0146	0.9410	439.7
0.00014	0.0118	0.8052	571.1
In 1:4 dioxane:water ($\epsilon = 62.8$)			
0.00444	0.0663	5.575	125.5
0.00356	0.0597	4.831	135.7
0.00214	0.0463	3.45	160.9
0.00128	0.0358	2.337	182.6
0.00075	0.0274	1.726	224.8
0.00045	0.0212	1.421	315.7
In 1:2 dioxane:water ($\epsilon = 52.7$)			
0.00247	0.0497	3.37	136.5
0.00164	0.0405	2.337	142.5
0.00109	0.0330	1.705	156.4
0.00073	0.0270	1.317	180.5
0.00048	0.0219	1.098	228.8
In 1:1 dioxane:water ($\epsilon = 40.1$)			
0.00278	0.0527	2.499	89.89
0.00185	0.0430	1.916	103.0
0.00123	0.0351	1.407	114.4
0.00083	0.0288	1.051	126.6
0.00055	0.0235	0.7964	144.7
0.00036	0.0189	0.6412	178.1

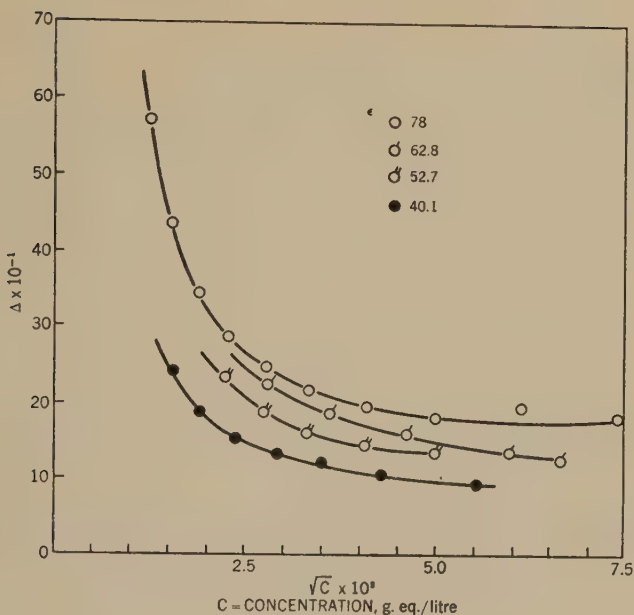


FIG. 5.

DISCUSSION

Viscosity and Concentration

The most interesting property which distinguishes a polyelectrolyte from other neutral polymers is the way in which the reduced viscosity (η_{sp}/c) is dependent on concentration. For a neutral polymer, the curve $\eta_{sp}/c - c$ is linear in the dilute region, having a positive slope with the c -axis, while for the polyelectrolyte $\eta_{sp}/c - c$ rises rapidly with diminishing concentration. Exactly similar behavior is noticeable with $\eta_{sp}/c - c$ curves of SCMC solutions (Fig. 1), which may be explained according to Fuoss's concept as due to increased intramolecular coulombic repulsion with increased electrolytic dissociation of the SCMC. This type of behavior has also been observed with polyvinyl pyridonium methyl bromide by Fuoss (3, 4), for sodium pectinates by Pals and Herman (6), for pneumococcus polysaccharide by Heidelberger and Kendall (7), for sodium polyacrylate by Staudinger (8) and for hyaluronic acid by Balazs and Laurent (9).

Further, according to Fuoss (3), the rise in the $\eta_{sp}/c - c$ curve at lower dilution will be proportional to the dielectric constant of the medium, since coulombic interaction will be strongly dependent on the dielectric constant and consequently the extent of coiling of the polymer chains will also vary with the dielectric constant of the medium. The $\eta_{sp}/c - c$ curves for SCMC solution containing different amounts of dioxane and with dielectric constants of 78, 62.8, and 52.7, respectively, are given in

Fig. 1, which shows that the rapid rise in $\eta_{sp}/c - c$ curve diminishes appreciably with diminishing dielectric constant.

The viscosity concentration relation $\eta_{sp}/\sqrt{c} = A + B\sqrt{c}$ that has been deduced for simple electrolytes (10) holds in this case with fairly long range of approximation only. Fuoss (4) has proposed an empirical equation for the reduced viscosity (η_{sp}/c) - concentration relation which has been found to hold good for all the polyelectrolytes studied by him, and which takes into account both molecular-weight effect and coulombic-interaction effect on the viscosity of polyelectrolyte solutions. The equation may be written as

$$\eta_{sp}/c = \frac{A}{1 + Bc^{\frac{1}{3}}} + D,$$

where A depends on the molecular weight and B on the dielectric constant of the medium. The significance of the term D is not very clear, although it is known that its value is also dependent on the dielectric constant and equals η_{sp}/c when c becomes ∞ . The values of B/A and D as calculated by Fuoss's method (3) from various η_{sp}/c and c (see Table I) values in water and water-dioxane mixtures are given in Table VI.

TABLE VI

Solvents		B/A	D
Water	78.0	0.12	30
Water-dioxane 4:1	62.8	0.46	8
Water-dioxane 2:1	52.7	0.64	10

One peculiarity noted in this case was that the value of D did not vary in a regular way with the dielectric constant. It is, however, evident that B/A increases with a decrease in dielectric constant, as has also been observed with pyridonium compounds by Fuoss. Since the molecular weight of SCMC does not change in different solvents the increase in the value of B/A may be attributed to the increase in the value of B , i.e., the increase in coulombic interaction effect.

Viscosity and pH

A very characteristic property of SCMC solution is the dependence of viscosity on pH. The viscosity-pH curve given in Fig. 2 (curve 2) shows that with increasing pH the viscosity falls, slowly at first then rapidly as the pH goes above 9.5. Brown and Houghton (2) have explained this observation on the assumption that the alkali added to raise the pH of the solution goes to form a salt with cellulosic-OH groups. They suggested that if the pH could be diminished again by adding successive quantities of HCl, the curve could be retraced. In performing the operation we noticed that the viscosity remained constant instead of rising (Fig. 2, curve

2), actually showing a slight fall with diminishing pH. When, however, the pH diminution was achieved by dialyzing out the alkali added, the curve was nicely retraced. Further, when increasing amounts of NaCl were added to a solution of SCMC, keeping the concentration of SCMC constant, the viscosity showed a fall with increasing Na-ion concentration. This shows that it is the Na-ion and not alkali or pH that was responsible for the fall in viscosity. In fact, this type of behavior is expected of SCMC if it be a polyelectrolyte. The addition of Na-ion to the solution of SCMC forces some of the dissociated Na-ion of SCMC to be drawn back to the polymer chain, causing the chain to assume a less extended configuration owing to the reduction in the net negative charge on the chain, hence the fall in viscosity. In diminishing the pH by neutralizing the alkali with HCl no change in Na-ion concentration occurs, consequently, no change in polymer coil takes place. When the pH fall takes place due to dialysis there is a reduction in Na-ion concentration in solution, hence increase in viscosity owing to the better dissociation of SCMC molecule with the consequent uncoiling of the polymer chain. The sharp fall in viscosity takes place at the pH where the Na-ion concentration has increased sufficiently to cause almost all the SCMC molecules to become more or less undissociated and thus to assume a coiled up configuration. The pH at which this fall takes place varies slightly with concentration of SCMC in solution; for a 0.04% solution it is at 9.4 while for 0.5% solution it is at 10.5, as is to be expected if our explanation is correct. Brown and Houghton (2) also obtained the sharp fall in viscosity at about 11.5 pH with 1% solution of medium viscosity SCMC.

When HCl is added to a solution of SCMC (6.8 pH) to diminish the pH, the viscosity curve also shows a similar fall (Fig. 2, curve 1). It has been observed that with dilute solution of SCMC (about 0.04% solution) the pH could be reduced to as low a value as 2.5 without causing any separation of the free acid. When the pH was again increased by neutralizing the acid with NaOH the viscosity actually increased although the original curve was not retraced. In this region, where the solution contains free acid, CMC, the fall in viscosity is due to decreased dissociation of the free acid in presence of added H-ion. When NaOH is added, Na-ion is neutralized, but the increase in Na-ion does not exert any marked influence on the dissociation of free acid, hence the viscosity rises. When, however, the alkali concentration becomes sufficient to convert at least some of the CMC molecules into its sodium salt, the effect of NaCl on the solution viscosity again becomes operative and consequently the viscosity fails to regain its original value. In the case of concentrated solutions of SCMC (0.5%), the pH-viscosity curves also showed similar characteristics, i.e., at about 10.5 pH there was a sharp fall in viscosity, which remained constant on reversing the pH with acid. When the pH fall was

achieved by dialysis, the viscosity increased with diminishing pH, but the original curve with increasing pH was not exactly retraced owing to dilution of the solution by osmosis.

Viscosity and Added Electrolyte

The addition of simple electrolytes has been found to have a marked effect on the reduced viscosity of polyelectrolytes as observed by Fuoss (3, 4) and Pals and Hermann (6). In the present investigation the viscosity of SCMC solution in the presence of different amounts of NaCl was measured and the $\eta_{sp/c} - c$ curves are given in Fig. 3. It may be noted that with only 2.139×10^{-4} g. equivalents of NaCl per liter the sharp rise in $\eta_{sp/c} - c$ curve vanishes, the curve showing a well-defined maximum which appears when the stoichiometric concentration of Na-ion from the polymer is nearly equal to that from the added NaCl (Table III). With increasing concentration of NaCl the maximum shifts towards higher concentration of SCMC until at last it vanishes completely and the curves resemble those of a neutral polymer. If the intercept on the $\eta_{sp/c}$ -axis be interpreted as the measure of the volume of the polymer in solution, we see that the added electrolyte compresses the hydrodynamic volume enormously since the intrinsic viscosity diminishes considerably in the presence of the electrolyte. Fuoss (3) has attributed this to mass action effect, increase in free cation concentration enhancing the association of the Na-ion to the polymer chain, thereby reducing the intramolecular coulomb repulsion with consequent coiling up of the molecules. Confining our attention to the top curve in Fig. 3, we observe that at the maximum point in the curve, the concentration of Na-ion from SCMC is approximately equal to that from the added NaCl. Below this concentration of SCMC the added Na-ion is in excess of that from SCMC, hence almost all the SCMC molecules remain undissociated and the $\eta_{sp/c} - c$ curve resembles a neutral polymer curve, i.e., a $\eta_{sp/c} - c$ curve with a positive slope with the c -axis. Above this concentration of SCMC the added Na-ion concentration is less than that from the SCMC, hence some of the SCMC molecules can dissociate and the curve resembles the reduced viscosity ($\eta_{sp/c}$) concentration curves for polyelectrolytes, i.e., a curve sloping downward and concave to the c -axis. As the concentration is increased the maximum shifts (other curves in Fig. 3) to higher concentration of SCMC (so as to furnish an equivalent amount of Na-ion to that from NaCl) until at last the concentration of the added ion becomes so high as to keep almost all the SCMC molecules undissociated over the concentration range studied. Similar effects are noticeable with other neutral electrolytes, e.g., Na_2SO_4 , KCl, MgCl_2 , the maximum occurring near about the equivalent concentration with KCl, but at a value higher than one-third and much less than one-half the equivalent concentration with MgCl_2 .

These observations show that the salt effect cannot be attributed simply to mass action phenomena. The ionic strength of the added electrolyte is most probably responsible in some way for this effect. The ionic strength of the MgCl_2 solution is three times the KCl solution of the same equivalent concentration, consequently the maximum with MgCl_2 occurs at a concentration of about one-third the value for KCl, i.e., at an equal ionic strength. Furthermore, the ionic strength effect alone cannot account for all the facts, as is shown by the behavior of Na_2SO_4 solution where the maximum appears at a concentration much higher than the concentration of equal ionic strength, yet at the same time at a much lower concentration than the equivalent one (Table IV). This shows that the mass-action effect has some sway over one phenomenon at least. Nothing, however, can be said with certainty for the agreement in all cases is very approximate and a quantitative formulation is not yet forthcoming.

Conductance

A polyelectrolyte obviously presents an entirely different charge distribution in solution from that of a simple electrolyte like NaCl. In very dilute NaCl solution a microscopic volume element will always contain, on an average, an equal number of positive and negative ions, whereas in the case of sodium carboxymethylcellulose, a polyelectrolyte, a similar test volume will contain only cations, and when encountered with a chain, will contain only anions with a high negative charge density. The conductance characteristics of such solution will therefore exhibit some special features not shared by simple electrolytes.

Above about 4.8×10^{-4} g. equivalent of SCMC per liter equivalent conductance remains nearly constant, changing but slowly with increasing concentration; as concentration decreases into a very dilute range, the equivalent conductance begins to increase at a very rapid rate. At moderate concentration, the relative ionic concentration is fairly well buffered, that is, as more polyelectrolyte is added the degree of association remains practically constant. The polymer chain represents a region of high charge density and consequently the oppositely charged sodium ions are attracted, some of which are actually paired off with COO-groups while others form a space charge of screened sodium ion atmosphere around the polymer chain. These clusters form the mobile kinetic units, the net charge on them being the difference between the number of COO-groups on the chain and the paired Na-ions. At moderate concentrations a Na-ion can escape from the field of one polymer ion and be captured in time by another chain; so a polymer chain contains a steady number of Na-ions on the average. In dilute solution, however, once a sodium ion escapes from the polymer chain, the chance of its coming back to a polymer chain diminishes as the concentration is reduced. Consequently, the net charge

on the polymer chain will increase with diminishing concentrations and as a result the equivalent conductance increases as we pass on to more dilute solutions.

If this contention for the conductance behavior of SCMC be justified, then the measurement of conductance of mixtures of polyelectrolyte and simple electrolyte will show that the sum of the conductances of the components is greater than the conductance of a mixture, since in presence of added electrolyte some of the SCMC will be undissociated. This has been confirmed nicely for a mixture of SCMC and NaCl as given in Table VII.

It may be mentioned that when two simple electrolytes are mixed the specific conductivity of the mixture will be less (or sometimes greater) than the sum of the specific conductivities of the individual electrolytes owing to mutual interaction of the ion atmospheres, but the difference will be

TABLE VII
Conductivity of SCMC Solution in NaCl Solution
Specific conductivity of NaCl = $1.317 \times 10^{-4}(\rho)$

Concentration of SCMC (%)	Sp. conductance of SCMC soln. $\times 10^4 (\rho_1)$	Sp. conductance of SCMC in NaCl soln. $\times 10^4$ (observed)	Sum of the sp. conductances of SCMC and NaCl soln. $\times 10^4 (\rho + \rho_1)$	Lowering of sp. conductance (%)
0.270	9.29	10.04	10.607	5.0
0.135	4.529	5.575	5.846	4.6
0.068	2.337	3.370	3.654	7.7
0.034	1.260	2.337	2.577	9.4
0.017	0.6528	1.811	1.97	8.1
0.008	0.3534	1.542	1.67	7.8

very small. This is well illustrated by the results of A. E. Stearn (11), where in the equimolecular mixture of sodium and potassium halides (chlorides, bromides, and iodides) in the concentration range of 0.1 to 0.5 (*N*) the percentage lowering of specific conductivity (calculated from the results of A. E. Stearn, 11) ranges from -0.05 to 0.467. In solutions as dilute as those used by us the difference between the two values will be vanishingly small. In our case, however, even in dilute solution, the difference between the two values ranges from 5 to 9%, progressively increasing with dilution over the range of concentration of SCMC studied. This justifies, at least qualitatively, our assumption of the diminution of the dissociation of SCMC in the presence of NaCl.

It has been found by McBain and Searles (12) for a number of colloidal electrolytes that disperse to subultimate units in aqueous solution, that the conductivity of a colloidal electrolyte and a simple electrolyte is more than additive in the dilute region. Hartley (13) suggested an ex-

planation for this on the basis of counter ions associated with colloidal particles forming separate locally-neutralized systems. In the present case, however, the observation is exactly the reverse, i.e., the conductivities are less than additive. The explanation suggested appears to be most logical and in conformity with fundamental theory of dissociation of electrolytes and their mutual interaction.

Concluding Remarks

There are three possible ways of explaining the peculiar viscous behavior of a colloidal system. For example, it may be ascribed to the presence of either electrical charges (better known as Smoluchowski's electroviscous effect (14), associated poly-ions (better known as Staudinger's swarm effect), or flexible chain molecules (better known as Fuoss' folding-chain effect). Markovitz and Kimball (15) have recently shown that all the peculiarities in the viscous behavior of sodium polyacrylate solution can only be explained by the folding-chain theory. In fact, it was suggested long ago by Mark and Meyer (16) and reiterated recently by the same authors (17) and by Goldacre and Lorch (18) that most probably the change in shape and size of the dissolved molecules plays a prominent role in the determination of viscosity of colloidal solutions that disperse to ultimate units in solution. On this assumption, they explained the increasing viscosity of protein solutions on either side of isoelectric pH.

Recently Hartly (5) also stressed the importance of change in size and shape of colloidal particles, which are molecularly dispersed in solution, in determining the various physicochemical behavior of their solutions, particularly viscosity. However, he also stressed the importance of the electroviscous effect, which is generally superimposed on the folding-unfolding effect in dilute regions, admitting at the same time that the second effect becomes the dominating factor in the case of extremely long chain molecules. In addition Hartly (5) emphasized the importance of viscometric investigations on solutions of long-chain compounds of known structure in order to elucidate various peculiarities of colloidal solutions, particularly molecular colloids. Of late it has been shown by Herman and Overbeek (19) and by Arnold and Overbeek (20) that the contribution of Smoluchowski's (14) electroviscous effect in determining the viscosity characteristic of polyelectrolytes is appreciable only to a very low degree of ionization (less than 0.2). The reason for this effect is threefold: (1) a rigid spherical structure was assumed in Smoluchowski's deduction, (2) Debye and Bueche (21) have shown that in such deductions both the electrical charge and the potential on the particle should be low, and (3) the thickness of the ion atmosphere around each charged spot should be greater than or equal to the distance between the charge centers. None of

these conditions is obeyed by the polyelectrolyte solution over an appreciable range of concentration.

In the case of dilute solutions of sodium carboxymethylcellulose, although the rapid rise in reduced viscosity (η_{sp}/c) with diminishing concentration can also be explained by the electrical theory and the swarm theory, the effect of neutral electrolytes on the shape of η_{sp}/c vs. c curve, particularly the hump, cannot be explained by these theories. These facts can be explained more or less completely only by the folding chain theory, as has already been done. It is true that the theoretical calculation of viscosity increase with extent of stretching obtainable from Debye's equation (21) for viscosity of chain molecules does not agree well with experimental results (15). This however, does not invalidate the folding-chain hypothesis, since at present there is no way to determine the extent of coiling or uncoiling with a fair degree of accuracy by any experimental means.

ACKNOWLEDGMENT

Thanks are due to Prof. Santi R. Palit, Indian Association for the Cultivation of Science, Calcutta-32, for his keen interest and constant encouragement during the course of this investigation.

REFERENCES

1. CALDWELL, W. A., AND WATTERS, A. J., *Research* **1**, 251 (1947-48).
2. BROWN, C. J., AND HOUGHTON, A. A., *J. Soc. Chem. Ind.* **99**, 254 (1941).
3. FUOSS, R. M., AND CATHERS, G. I., *J. Polymer Sci.* **4**, 97, 121 (1949).
4. FUOSS, R. M., AND STRAUSS, U. P., *J. Polymer Sci.* **3**, 246, 602 (1948).
5. HARTLEY, G. S., *Quart. Rev. Chem. Soc.* **2**, 152 (1948).
6. PALS, D. T. F., AND HERMAN, J. J., *J. Polymer Sci.* **3**, 897 (1948).
7. HEIDELBERGER, M., AND KENDALL, F. E., *J. Biol. Chem.* **95**, 127 (1932).
8. STAUDINGER, H., *Die hochmolekularen organischen Verbindungen*, Part II D, Springer, Berlin, 1932.
9. BALAZS, E. A., AND LAURENT, T. C., *J. Polymer Sci.* **6**, 665 (1951).
10. FALKENHAGEN, H., AND VERNON, E. L., *Physik. Z.* **33**, 140 (1932).
11. STEARN, A. E., *J. Am. Chem. Soc.* **44**, 670 (1922).
12. MCBAIN, J. W., AND SEARLES, J., *J. Phys. Chem.* **40**, 493 (1936).
13. HARTLEY, G. S., *Trans. Faraday Soc.* **39**, 247 (1943).
14. SMOLUCHOWSKI, M., *Kolloid Z.* **18**, 190 (1916).
15. MARKOVITZ, H., AND KIMBALL, G. E., *J. Colloid Sci.* **5**, 136 (1950).
16. MARK, H., AND MEYER, K. H., *Der Aufbau der hochpolymeren organischen Naturstoffe*, p. 232. Leipzig, 1930.
17. MEYER, K. H., AND MARK, H., *Nature* **167**, 736 (1951).
18. GOLDACRE, R. J., AND LORCH, I. J., *Nature* **166**, 497 (1950).
19. HERMAN, J. J., AND OVERBEEK, J. T. G., *Rec. trav. chim.* **67**, 761 (1948).
20. ARNOLD, R., AND OVERBEEK, J. T. G., *Rec. trav. chim.* **69**, 192 (1950).
21. DEBYE, P., AND BUECHE, A. M., *J. Chem. Phys.* **16**, 573 (1948).

THE MEASUREMENT OF LIGHTSCATTERING INTENSITIES ACCORDING TO BRICE ¹

W. F. H. M. Mommaerts ²

*Department of Biochemistry, Duke University School of Medicine,
Durham, North Carolina*

Received November 19, 1951

INTRODUCTION

Interest in the study of the lightscattering characteristics of colloidal systems has emphasized the need for a convenient method for measuring the intensity of scattered light on an absolute scale. A photometer for that purpose has been designed by Brice *et al.* (1, 7), who have carefully evaluated all aspects of the method in order to obviate recourse to standardization with reference fluids. However, in view of the limited experience available, and the criticism brought forward against parts of Brice's procedure (5), it was thought useful to apply some experimental tests to this system of measurement. This was done by measuring the light scattered by solutions of various concentrations of colloidal silica, "Ludox" ³ in the Brice instrument, as well as the transmittance of these solutions in a spectrophotometer. After application of appropriate corrections, the turbidity values obtained with the two methods were compared. It was only intended to use the colloid as a convenient medium for performing this comparison; no studies of a more fundamental nature were envisaged. During the progress of this work, similar measurements were reported by Doty and Steiner (4), who obtained the same final result in studies with systems requiring larger corrections than needed in the present work, and restricted to lower turbidity values.

DEFINITIONS

The turbidity of a system is defined as the conservative absorption coefficient in the expression $I = I_0 e^{x\tau}$. In light scattering measurements one obtains primarily a value for Rayleigh's ratio, e.g., at an angle of 90° with the primary beam:

$$R_{90} = \frac{i_{90} r^2}{I_0}, \quad [1]$$

¹ This investigation was supported by Research Grant No. H-221 from the National Heart Institute of the National Institutes of Health, U. S. Public Health Service.

² This work was done during the tenure of an Established Investigatorship of the American Heart Association.

³ Dr. J. T. Edsall directed the writer's attention to this substance.

where i_{90} is the intensity of light measured in the direction 90° at a distance r from the scattering element, and I_0 is the irradiance of the incident light. From Rayleigh's ratio, the turbidity is then obtained as follows:

$$\tau = \frac{16\pi}{3} R_{90}. \quad [2]$$

This relation, however, is only valid when the scattered light is completely polarized, and when its radial distribution is symmetrical with respect to the 90° direction. Doty and Edsall (3) have stressed that these conditions are usually not fulfilled, for which reason they recommend employment of Rayleigh's ratio for the expression of experimental results.

As an alternative system, it is proposed to use the "apparent turbidity," defined by the expression:

$$\tau' \equiv \frac{16\pi}{3} R_{90} \quad [3]$$

from which the true turbidity can be obtained by application of the correction factors (Doty and Steiner, 4) for depolarization and dissymmetry:

$$\tau = f_p \cdot f_z \cdot \tau'. \quad [4]$$

It is believed that the use of τ' rather than R_{90} is advantageous since it is related to the true turbidity by correction factors which usually do not differ greatly from unity and which are employed in a manner analogous to the use of activity coefficients.

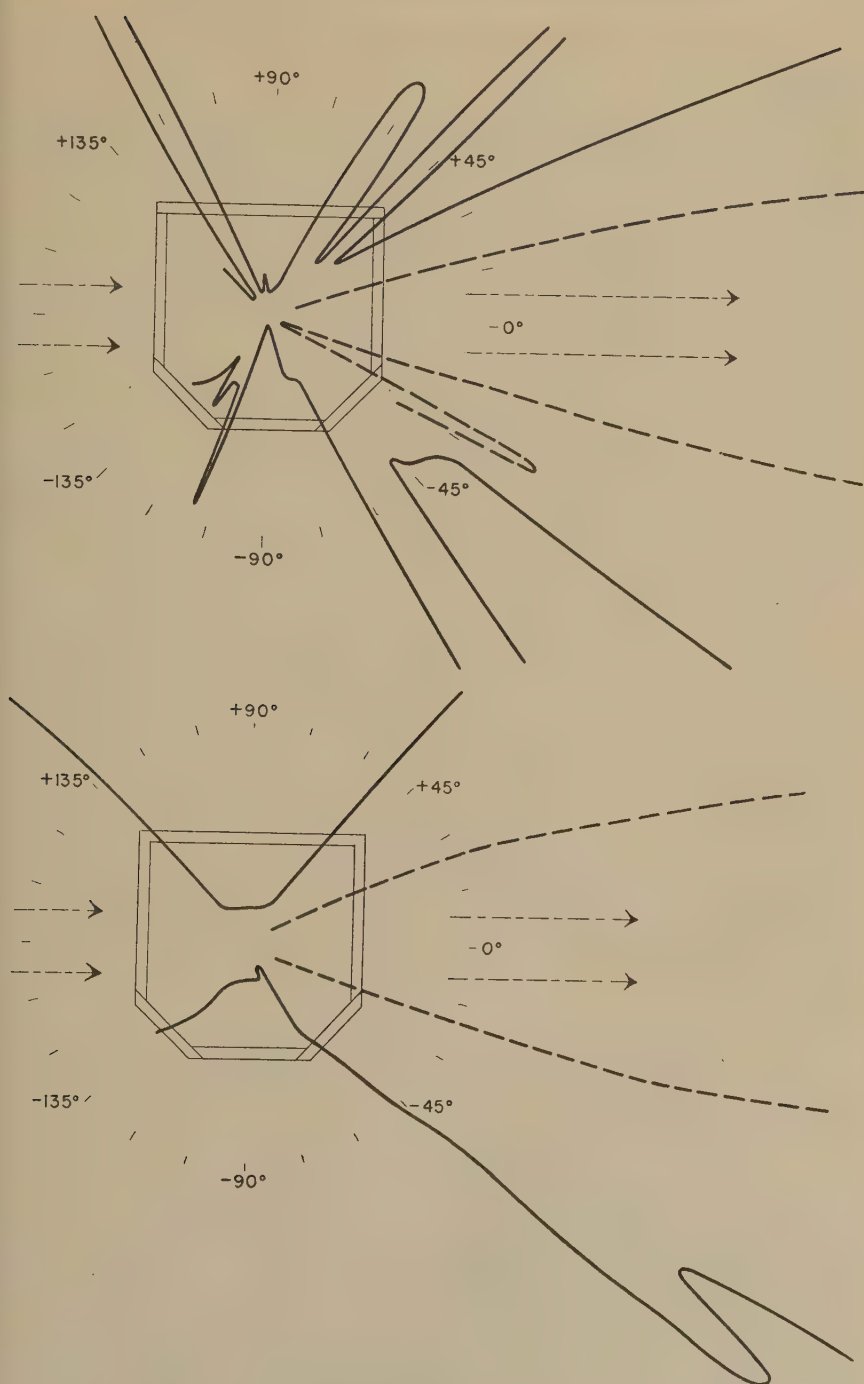
EXPERIMENTAL

Measurement of Lightscattering Intensities

The experiments were performed with the Brice instrument,⁴ slightly modified by the introduction of a 1×10 mm. vertical slit immediately in front of the envelope of the AH-3 mercury arc.

The detector, a 1P21 photomultiplier cell, differs in sensitivity with respect to horizontally and vertically polarized light. While this effect is far less than in case of simple photocells (e.g., Hughes and DuBridge, 6), it still amounts to about 3% in the apparatus used in this study. Conventionally, this difference is eliminated by an opal glass depolarizer in front of the photocell, which reduces the impinging intensity ten- to twentyfold. Since there is no selective sensitivity with respect to left-versus righthand circularly-polarized light, a quarterwave plate has been employed in the diagonal position in front of the detector. This completely abolishes the differential sensitivity for the green light of the mercury arc, for which the retardation amounts to exactly one-quarter wave. In

⁴ Constructed by Phoenix Precision Instrument Co., Philadelphia.



FIGS. 1 and 2. Light intensities (in polar coordinates) under various angles around the semi-octagonal scattering cuvet (Empty, Fig. 1; water-filled, Fig. 2). The dashed curve is drawn on a scale 100-fold reduced in comparison to the scale of the drawn curve.

the blue region, a difference of about 0.3% remains, which can usually be neglected.

The use of square and semi-octagonal cells instead of the elaborate cells with Wood's horns (2) gives rise to the question whether the measurements are affected by spurious radiation originating by reflection at the surfaces. A number of measurements have been undertaken to study the angular pattern of light intensities around the semi-octagonal cuvet.

As shown in Fig. 1, the radiation distribution for the empty vessel is extremely complex, and bears little recognizable relationship to the geometrical shape of the cell. (The effect of the blackened junctions between the fused windows, however, can be distinguished.) For the cell filled with solvent (Fig. 2), the pattern is simpler. Close to the 90° direction, the angular intensity function is quite regular, and corresponds approximately to the theoretical $(1 + \cos^2 \theta)$ relation. In the 135° and particularly the 45° directions, however, the intensity varies more sharply with the angle. This may, in part, be ascribed to residual dust in the solutions, yet it is also obvious that the accurate alignment of the container is critical in dissymmetry measurements at low levels of turbidities.

Of greater practical importance is the comparison of measurements on binary systems with those on the solvent. The latter measurement assumes the significance of a correction to be applied to the results obtained with solutions, evaluating not only the contribution which the solvent makes toward the total turbidity, but also the effect of the spurious light. These corrections were found to be negligible at turbidity levels above 10^{-2} but become increasingly important at lower turbidities.

It has furthermore been tested whether the same solution, if measured in differently shaped vessels, gives the same values. Such comparisons were made at various turbidity levels, using the 4-cm. semioctagonal, and 2- and 3-cm. square cells. No systematic variations were encountered, e.g. in the following series of comparisons between two sizes of square cells:

MEASURED TURBIDITY							
2-cm. cell	0.128	0.0501	0.0270	0.0145	0.00616	0.00346	0.00144
3-cm. cell	0.130	0.0500	0.0268	0.0141	0.00606	0.00346	0.00141

Transmittance Measurements

These determinations were performed at various wavelengths in the Beckman Quartz Spectrophotometer, in cells 100-mm. long. The beam was limited before and after passage through the solution by centrally placed round diaphragms 5 mm. in diameter. This dimension was arbitrarily chosen. It was maintained after Doty and Steiner (4) found that below a 4 mm. diameter the turbidity measured in systems with pronounced forward scattering was independent of the opening of the beam,

and that an error of 2% was introduced by complete omission of the diaphragms.

Turbidity values for the wavelengths of the mercury arc were then found by interpolation.

RESULTS

The Ludox preparation was obtained in the form of a 30% aqueous solution⁵; since it was only intended to obtain systems of varying turbid-

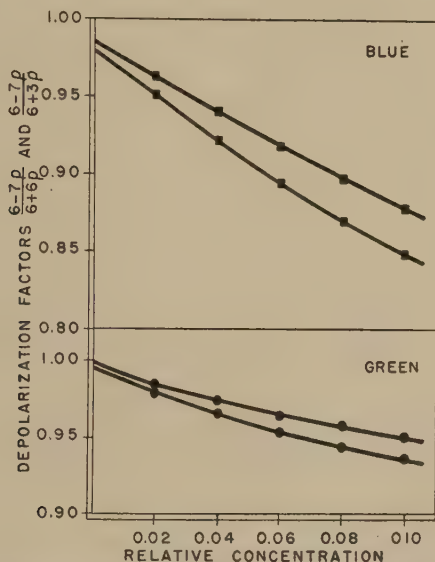


FIG. 3. Depolarization values of "Ludox" solutions at various concentrations, for blue and green light. Depolarization factors $(6 - 7\rho)/(6 + 6\rho)$ (lower curve of each graph) and $(6 - 7\rho)/(6 + 3\rho)$ (upper curve).

ity values, the concentrations will be expressed on a relative scale, the stock solution being unity.

Measurements of the dissymmetry gave an average value of $Z = 1.02$, without a clear concentration dependency, within the limits of error. This yields a dissymmetry correction factor f_z of 1.01 to 1.02.

The depolarization values are considerable, and show a strong dependence on the concentration. Depolarizations of both unpolarized and vertically polarized incident light were measured, and the latter were entered into the term $[\rho] = 2\rho_v(1 - \rho_v)$, following Zimm *et al.* (8). The depolarization factors according to Cabannes and Debye $(6 - 7\rho)/(6 + 6\rho)$ and

⁵ Kindly made available by Dr. H. H. Snyder of E. I. DuPont de Nemours and Co., Inc.

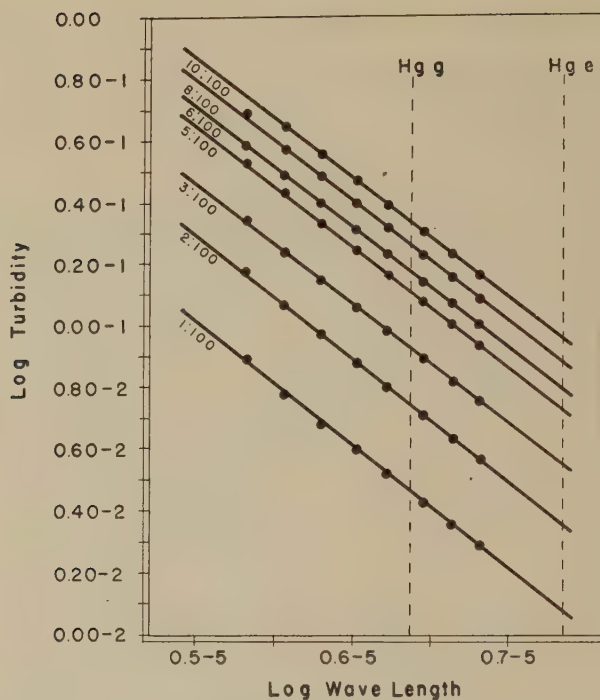


FIG. 4. Turbidity (determined from transmittance measurements) as a function of wavelength for "Ludox" solutions of various relative concentrations.

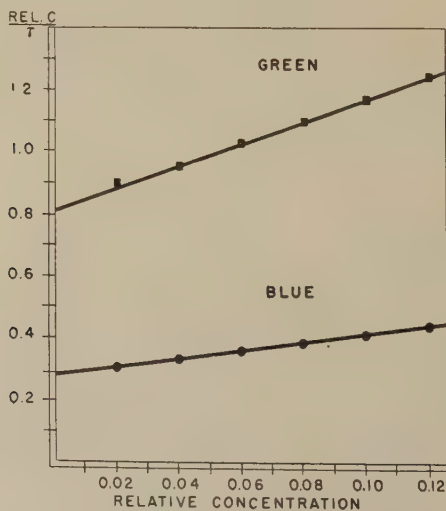


FIG. 5. Reciprocal turbidity plot for "Ludox" solutions of various concentrations.

$(6 - 7\rho)/(6 + 3\rho)$, respectively, were calculated both for ρ_u and $[\rho]$. The values plotted in Fig. 3 were obtained for $[\rho]$; for ρ_u , the values are a few per cent higher.

Values for τ' were computed from the scattering measurement according to Brice, and were converted into τ according to equation [4].

Typical results of transmittance measurements are given in Fig. 4. It is seen that the turbidity is proportional to λ^b , the values of b scattering between 3.95 and 4.02, with an average of about 3.98, so that $\beta = 4 - b$ is of the order of 0.02. It was not found possible to determine β with good accuracy, but the order of magnitude indicated is compatible with the

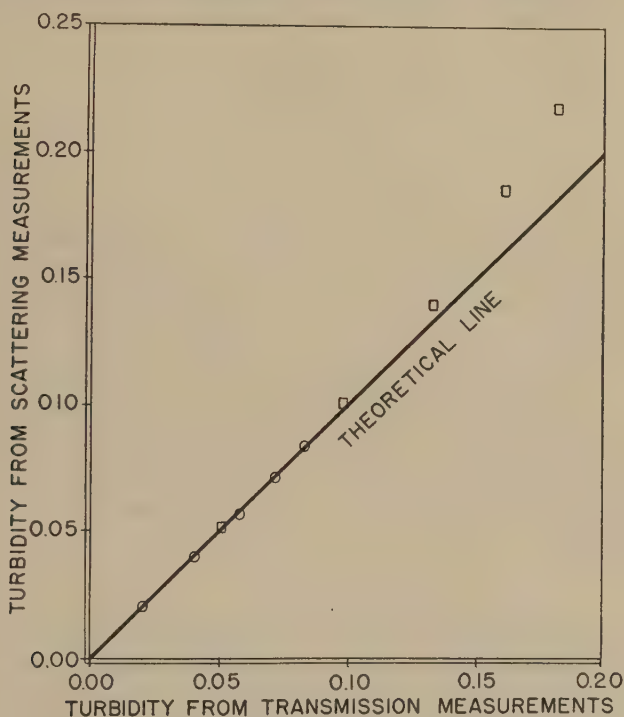


FIG. 6. Comparison of turbidity values obtained by transmission and scattering measurements.

measured scattering dissymmetry, according to the tabulations given by Doty and Steiner (4).

As shown in Fig. 5 by the plot of $(\text{rel. conc.})/\tau$ versus the concentration, the system follows the traditional type of concentration dependency, with a positive value for the osmotic factor.

For final comparison of the results obtained, the turbidities measured by transmittance and those derived from scattering measurements, each

subjected to the proper corrections, are plotted against each other in Fig. 6. The depolarization corrections used are those obtained upon extrapolation toward zero concentration. The effect of these corrections is very small, and the dissymmetry corrections are entirely negligible. It is seen that up to about $\tau = 0.1$ a very close correspondence is obtained. In more turbid systems, the scattering measurements give increasingly higher values, due to the effect of secondary scattering and other circumstances. If the depolarization corrections are based upon the actual values at the relevant concentrations, the correspondence between the two sets of measurements at higher turbidities becomes better. This is probably due to the large depolarization of the repeatedly diffused light; this type of depolarization correction, therefore, partly corrects for the secondary scattering, but has no rigorous meaning.

DISCUSSION

As the previous presentation shows, it is possible to obtain identical values of the turbidity of a system, whether derived from transmittance or from scattering measurements, if the latter are evaluated according to Brice *et al.* Similar results have recently been obtained by Doty and Steiner for a few solutions of linear polymers at lower turbidities. In their case, the dissymmetry corrections were considerable, the depolarization factors small. In the present example, the effect of depolarization was likewise small, that of dissymmetry negligible. The present experimental tests, therefore, prove the applicability of Brice's system for performing absolute lightscattering measurements, without uncertainty due to significant corrections.

SUMMARY

A number of technical details of the measurement of lightscattering intensities is discussed. The use of a quarter wave plate instead of an opal glass depolarizer in photoelectric measurements is proposed.

A study is made of some lightscattering characteristics of the colloidal silica, "Ludox." This system is shown to have negligible scattering dissymmetry and low depolarization (as far as not caused by secondary scattering).

Turbidity values have been determined by scattering measurements according to Brice *et al.*, and by transmittance measurements. The values obtained by these two measurements are in agreement. The validity of the Brice system of scattering measurements has hereby been confirmed.⁶

⁶ The author is indebted to Dr. B. A. Brice for his careful revision of the manuscript of this paper.

REFERENCES

1. BRICE, B. A., HALWER, M., AND SPEISER, R., *J. Optical Soc. Am.* **40**, 268 (1950).
2. CABANNES, J., *La diffusion moléculaire de la lumière*. Presses Universitaires, Paris, 1929.
3. DOTY, P., AND EDSALL, J. T., *Advances in Protein Chem.* **6**, 37 (1951).
4. DOTY, P., AND STEINER, R. F., *J. Chem. Phys.* **18**, 1211 (1950).
5. HERMANS, J. J., AND LEVINSON, S., *J. Optical Soc. Am.* **41**, 460 (1951).
6. HUGHES, A. L., AND DUBRIDGE, L. A., *Photoelectric Phenomena*. McGraw-Hill, New York, 1932.
7. SPEISER, R., AND BRICE, B. A., *J. Optical Soc. Am.* **36**, 364a (1946).
8. ZIMM, B., STEIN, R. S., AND DOTY, P., *Polymer Bull.* **1**, 90 (1945).

ADSORPTION OF VAPORS BY SILICA GELS OF DIFFERENT STRUCTURES

F. E. Bartell and John E. Bower

Department of Chemistry, University of Michigan, Ann Arbor, Michigan

Received November 19, 1951

INTRODUCTION

The use of the Gibbs adsorption equation for the evaluation of free surface energy changes that occur during adsorption of vapors had until recently been applied rigorously only to nonporous solids. This method has now been extended (1, 2) to apply to the case of porous adsorbents and, moreover, it has been shown how it should be possible to determine the specific surface areas of porous adsorbents from free energy considerations. To test further the general validity of this method, a study has been made in the present research of porous adsorbents (silica gels) which differed from each other in pore radius, pore volume, and in surface area but which were of the same chemical character. These silica gels were used with a series of adsorbate liquids with properties which, it was believed, would cause them to give quite different interaction energies with a given adsorbent. It was found that the free surface energy changes which occurred when unit area of the clean porous solid surface was replaced by a unit area of solid-liquid or solid-saturated vapor interface were independent of the precise structure and of the apparent density of the solid.

EXPERIMENTAL

Materials

Liquids selected as adsorbates formed zero contact angles with silica, they had a fairly large range of surface tension values, were such as should give a fairly wide range of energy changes on contact with a siliceous surface, and each liquid had an appreciable vapor pressure at room temperature. These liquids were water, methyl alcohol, ethyl alcohol, *n*-propyl alcohol, benzene, hexane, and carbon tetrachloride. Each organic liquid received final purification by fractionation and by vigorous dehydration. The water was re-distilled from an alkaline permanganate solution. Each liquid was sealed under vacuum into its sample tube after having been de-aerated by a freezing process.

Three quite different silica gels were procured and are referred to as Gels No. 1, No. 2, and No. 3. Gels No. 1 and No. 3 were prepared by the hydrolysis of silicon tetrachloride. Gel No. 1 was identical with that described and employed by Bartell and Dobay (3) and gel No. 3 was identical with that employed by Bartell and Donahue (4). Gel No. 2 was a commercial product which had been prepared from sodium silicate. It was purified by refluxing with nitric acid and repeated flushing with distilled water. The specific surface area of each gel was determined by the BET nitrogen adsorption method, using 16.2 \AA^2 as the molecular area of nitrogen. At least three separate determinations were made for each gel. The pore volume of each gel was estimated from the apparent density as determined by mercury displacement. Gels No. 1, No. 2, and No. 3 were found to have BET specific surface areas (a) of 320, 355, and $455 \text{ m}^2/\text{g}.$, respectively, and pore volumes (V_p) of 1.16, 0.43, and 1.01 cc./g. , respectively.

Apparatus

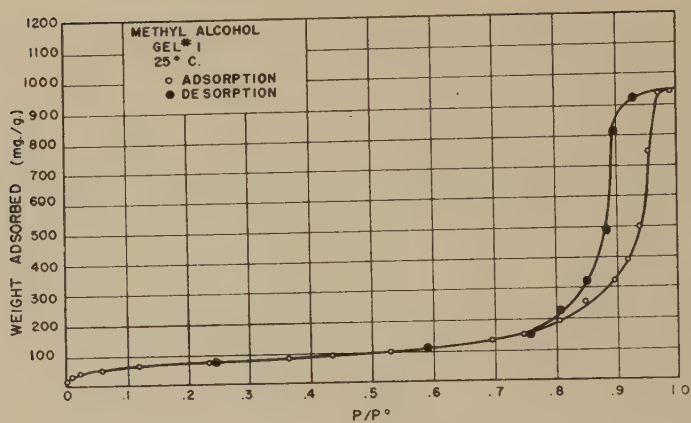
The apparatus and techniques used to determine the low-temperature nitrogen adsorption isotherm data from which the specific surface areas were calculated were the same as those described by Emmett (5) and by Bartell and Dodd (6). A nitrogen vapor pressure thermometer was used to obtain the temperature of the liquid air bath and to give directly the saturation vapor pressure of nitrogen at that temperature.

The data for the isothermals for the adsorption of the various organic liquids and of water on the silica gels were obtained gravimetrically by means of McBain-Bakr quartz spiral balances (7). The gravimetric apparatus and specialized techniques were very similar to those described by Bartell and Dobay (3).

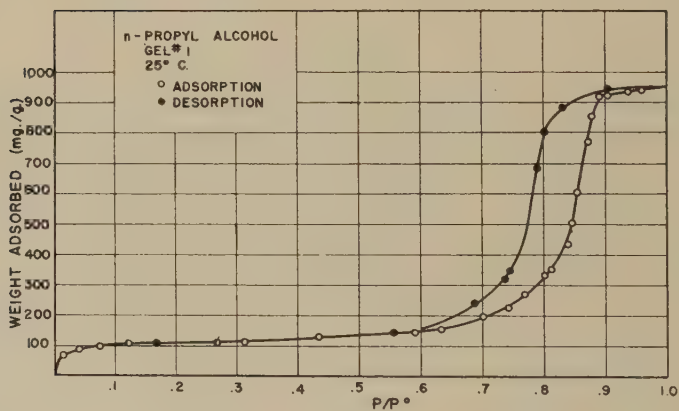
The vapor pressure was controlled by precise control of the temperature of the liquid adsorbate sample. Multiple adsorbent tubes made possible the simultaneous determination either of isotherms of a given liquid on different samples of the same gel or of isotherms of a given liquid on different gels.

The adsorption data obtained for each of the three gels are presented graphically in Figs. 1 and 2.

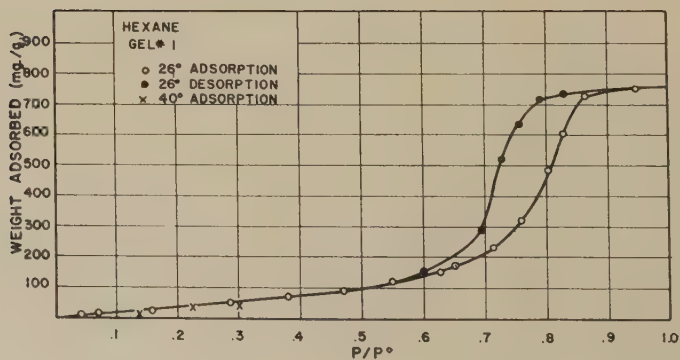
In all cases the weights adsorbed per gram of gel (x/m) are numerical averages of at least two independent determinations. The accuracy of the data in the high pressure range depends primarily upon the temperature control of the liquid adsorbate, i.e., any inaccuracy will be principally in the abscissa (p/p^0). In the low pressure range any inaccuracy will be principally in the ordinate (x/m).



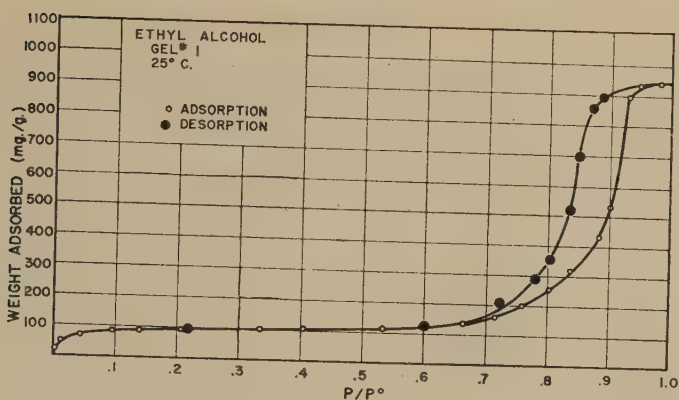
A



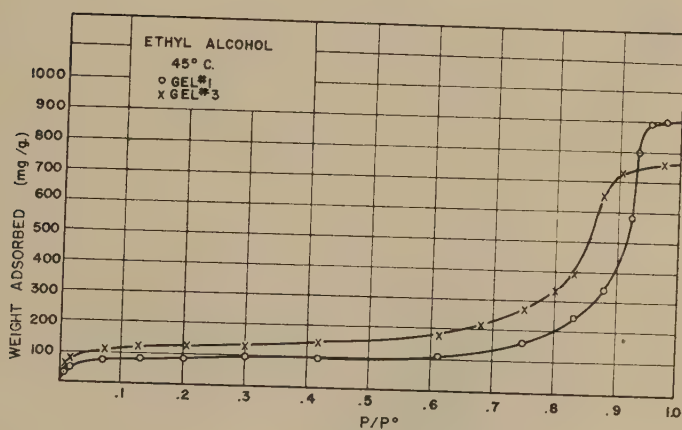
B



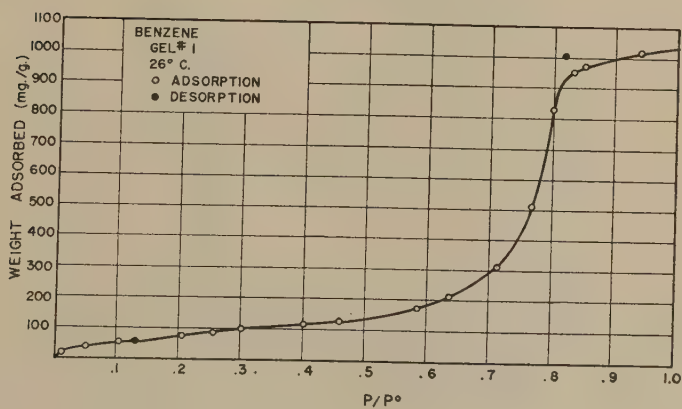
C



D



E

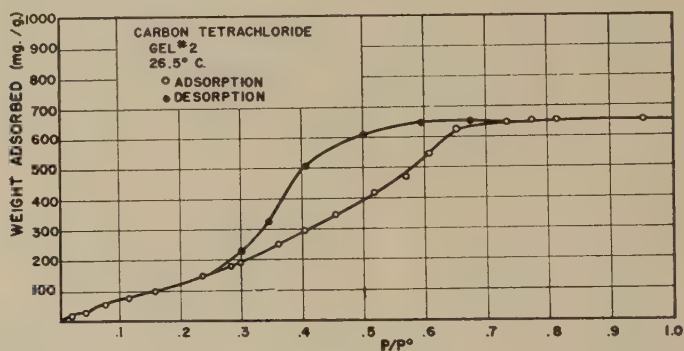


F

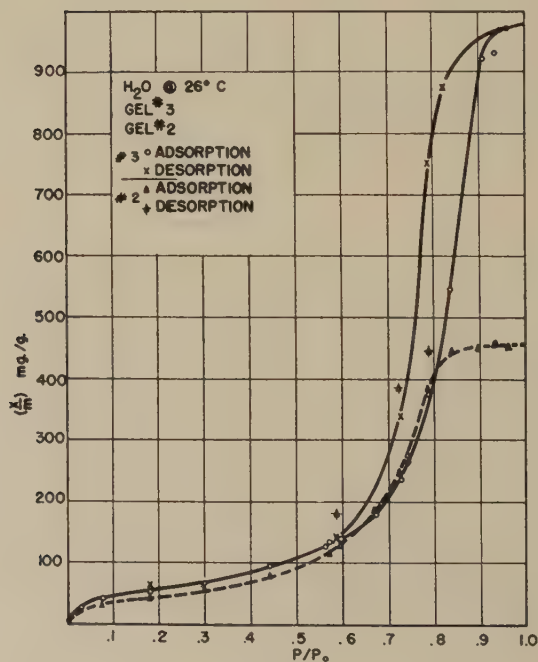
FIG. 1. Adsorption isotherms. Different organic liquids on silica gel.

Theoretical

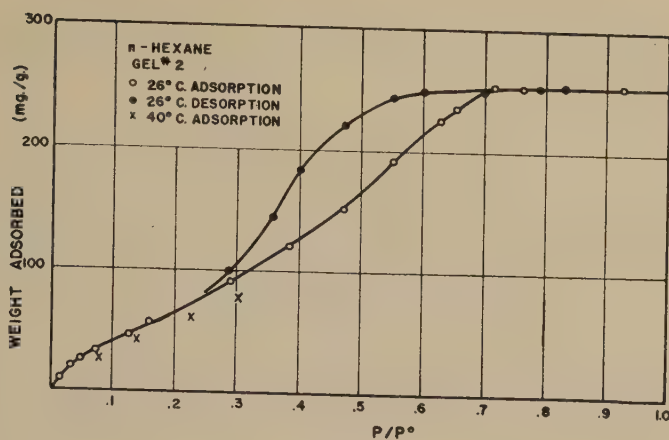
The use of the Gibbs adsorption equation as an indirect method of determining free surface energy changes occurring during adsorption was first proposed by Bangham and Razouk (8, 9, 10). Details of the procedure and formulations usually employed may be found in the papers of Boyd and Livingston (11) and of Harkins and Jura (12).



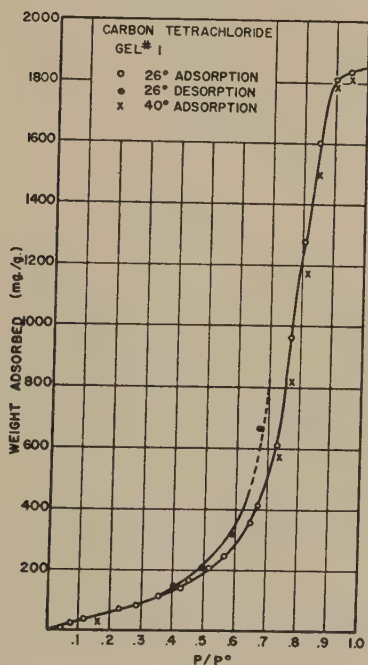
A



B



C



D

FIG. 2. Adsorption isotherms. Different liquids on silica gel.

Recently Dobay, Fu, and Bartell (1) and Fu and Bartell (2) have shown that for adsorption by porous adsorbents the methods and formulations of the theory must be modified somewhat. The lowering of the free surface energy ϕ at $P/P^0 = 1$ was demonstrated to be equal to the adhesion tension (A) of the liquid adsorbate against the solid (defined by

the equation $(\gamma_{S_0} - \gamma_{SL})$.^{*} By employing the Gibbs equation the following formulation was developed:

$$\phi_S = A = (\gamma_{S_0} - \gamma_{SL}) = \frac{RT}{Ma} \int_{P/P_0=0}^{P/P_0=1} \frac{x}{m} d \ln P/P_0. \quad [1]$$

With the use of equation [1] the work of spreading, W_S , (or the "initial spreading coefficient," $\gamma_{S_0} - \gamma_{SL} - \gamma_{LV^0}$) and the work of adhesion W_a (or $\gamma_{S_0} + \gamma_{LV^0} - \gamma_{SL}$) can be evaluated for liquids which form no angle of contact. The total free surface energy lowering which occurs when the adsorption by a porous solid is carried to saturation pressure is visualized as being composed of two terms: first, that representing the replacement of the clean solid surface by a solid-liquid and a liquid-vapor interface, and second, that representing the destruction of the liquid-vapor interface due to further "adsorption" and filling of the capillaries with liquid. The calculations are simplified by employment of a *hypothetical* process whose end states are identical with those of the actual process (1). The total free energy lowering at saturation may then be written as:

$$\phi_S = \frac{RT}{Ma} \int_{P/P_0=0}^{P/P_0=(P/P_0)_b} \frac{x}{m} d \ln P/P_0 + \frac{RT}{Ma} \int_{P/P_0=(P/P_0)_b}^{P/P_0=1} \frac{x}{m} d \ln P/P_0, \quad [2]$$

where $(P/P_0)_b$ represents that reduced pressure (less than $P/P_0 = 1$) at which a liquid film has been formed. The first term in equation (2) is interpreted to represent the energy change $(\gamma_{S_0} - \gamma_{SL} - \gamma_{LV^0})$ which is equal to $(\gamma_{S_0} - \gamma_{SV^0})$ if $\theta = 0^\circ$.[†] The second term represents the destruction of unit area of liquid surface and should therefore be equal to γ_{LV^0} . A graph of ϕ vs. P/P_0 reveals the composite nature of the total free energy changes, ϕ_S , and permits the individual quantities $\phi = (\gamma_{S_0} - \gamma_{SV^0})$, $\phi_S = (\gamma_{S_0} - \gamma_{SL})$ and γ_{LV^0} to be evaluated. That is:

$$\phi_S - \phi_b = \gamma_{LV^0}. \quad [3]$$

It was found (2) that a plot of $\log \phi$ vs. $\log P/P_0$ permitted the intersection point to be more accurately determined.

^{*} The following symbols are employed: γ = any surface tension, interfacial tension, or free surface energy. Subscripts S_0 , SL , SV^0 represent solid-vacuum, solid-liquid, and solid-saturated vapor interfaces, respectively. Adhesion tension (A) is defined as $(\gamma_{S_0} - \gamma_{SL})$. Spreading coefficient is defined as $(\gamma_{S_0} - \gamma_{SL} - \gamma_{LV^0})$. ϕ = lowering of free surface energy per cm^2 of solid. ϕ_S represents the lowering of free surface energy per cm^2 at $(P/P_0)_b$. x/m = weight of vapor adsorbed per gram of gel. M = molecular weight of adsorbate. a = specific surface area.

[†] Also according to Young's equation $(\gamma_{SV^0} - \gamma_{SL}) = \gamma_{LV^0} \cos \theta$.

If the surface area is unknown and is to be determined then equation [2] may be written

$$\phi_S = \frac{RT}{M} \int_{P/P_0=0}^{P/P_0=(P/P_0)_b} \frac{x}{m} d \ln P/P_0 + \frac{RT}{M} \int_{P/P_0=(P/P_0)_b}^{P/P_0=1} \frac{x}{m} d \ln P/P_0 \quad [4]$$

$$a\phi_S = a\phi_b + a\gamma_{LV}^0$$

$$\frac{a\phi_S - a\phi_b}{\gamma_{LV}^0} = a. \quad [5]$$

That the energy change (ϕ_b) corresponding to $(\gamma_{S_0} - \gamma_{SV}^0)$ should occur at some pressure less than the saturation pressure (P^0) during adsorption by a porous solid is to be expected since in small capillaries liquid and vapor are at equilibrium at pressures much lower than the saturation pressure of bulk liquid at that temperature (Kelvin equation).

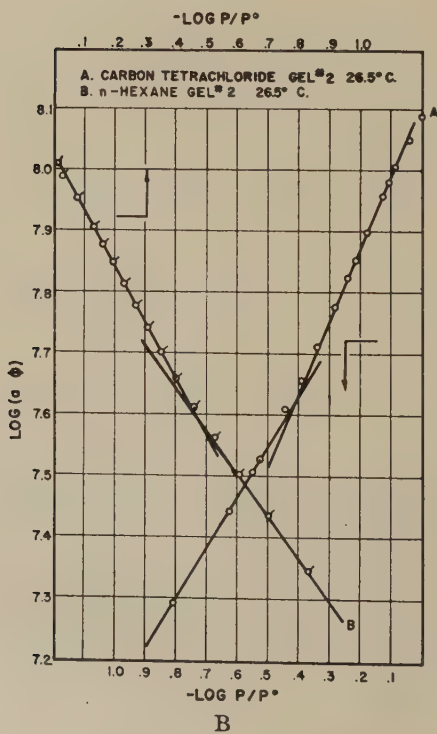
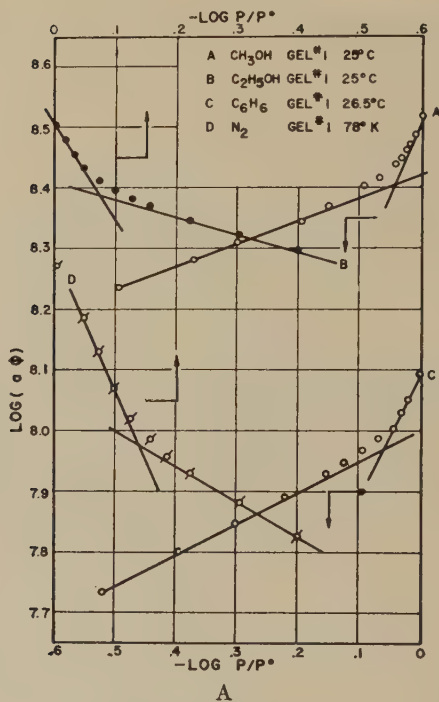
Free Surface Energy Changes

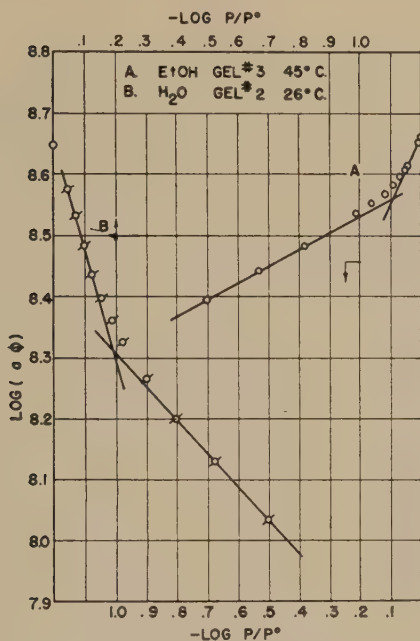
The Adhesion Tension, Spreading Coefficient and Work of Adhesion

Employing the equations discussed above the quantity $a\phi$ was determined by graphical integration. Graphs of $\log a\phi$ versus $\log P/P^0$ are shown in Fig. 3. The plots seem to indicate quite clearly that two disparate phenomena occur consecutively. The value of $a\phi$ at the intersection point corresponds to the energy change $a(\gamma_{S_0} - \gamma_{SL} - \gamma_{LV}^0)$, which is equivalent to $a(\gamma_{S_0} - \gamma_{SV}^0)$ if there is no angle of contact. The intersection point represents that reduced pressure at which a film of sufficient thickness has formed in the "average" capillary so that capillary condensation can begin.

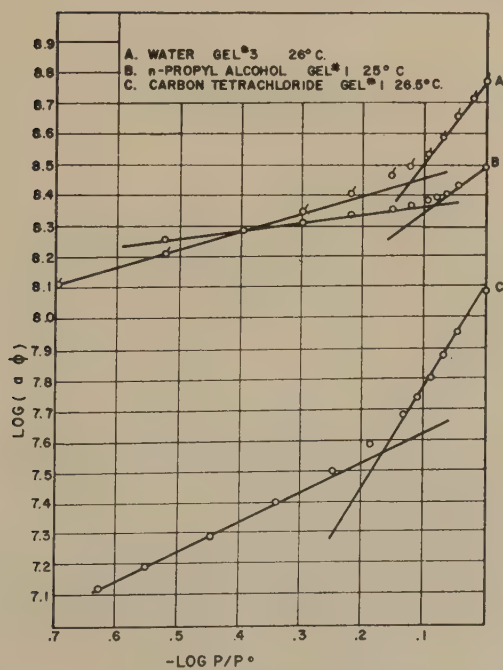
The value of $(a\phi)$ at $P/P^0 = 1$ represents $a(\gamma_{S_0} - \gamma_{SL})$ or aA . Dividing this value by the previously determined BET specific surface area gave the value of the adhesion tension, and by subtracting γ_{LV}^0 , the initial spreading coefficient recorded in columns 4 and 5 of Table I. In column 6 are recorded the values for the work of adhesion $(\gamma_{S_0} - \gamma_{SL} + \gamma_{LV}^0) = A + \gamma_{LV}^0$.

Although gels No. 1, No. 2 and No. 3 differed in method of preparation, in pore radii, and in pore volume, and although the isothermals were strikingly different in shape, the values of the adhesion tensions and of the spreading coefficients calculated for the same adsorbate on the different gels were in fairly good agreement. It may be concluded, therefore, that the siliceous surfaces must be quite similar in nature, differing only in specific surface area. The relative order of the energy changes meas-





C



D

FIG. 3. Free surface energy changes as related to relative pressures. $\text{Log}(a\phi)$ vs. $\text{Log } P/P^\circ$.

TABLE I
Free Surface Energy Changes

Adsorbent	Adsorbate	Temperature °C.	Adhesion tension $\frac{A}{\gamma SL}$ ergs/cm. ²	Initial spreading coefficient ($Wa = Wc$) ^c ($\gamma_{SL} - \gamma_{SV}$) ^a ergs/cm. ²	Work of adhesion W_a ($A + \gamma_{LV}$) ⁰ ergs/cm. ²
Gel No. 1	CH ₃ OH	25	102.7	79.7	124.9
	C ₂ H ₅ OH	25	99.9	76.9	122.2
	C ₂ H ₅ OH	45	97.5	76.7	117.3
	<i>n</i> -C ₃ H ₇ OH	25	97.1	73.3	120.5
	C ₆ H ₆	26.5	58.6	29.7	86.9
	C ₆ H ₆	40	54.9	26.9	81.2
	CCl ₄	26.5	38.4	11.5	64.5
	CCl ₄	40	37.7	11.8	62.1
	<i>n</i> -C ₆ H ₁₄	26.5	31.0	11.7	48.8
	N ₂	-195	(39) ^a	(29) ^a	(47.8)
Gel No. 3	C ₂ H ₅ OH	45	101.1	80.0	121.7
	H ₂ O	26	(129) ^b	(61.4) ^b	(200.8)
Gel No. 2	CCl ₄	26.5	35.0	11.9	61.1
	<i>n</i> -C ₆ H ₁₄	26.5	28.8	11.7	46.6
	H ₂ O	26	(125) ^b	(57.8) ^b	196.8

^a Insufficient data in very low pressure region for accurate results.

^b Zero point in doubt, i.e., the isotherm is not reversible in the low pressure region.

^c $W_c = 2\gamma_{LV}$ ⁰ the work of cohesion, and $Wa - Wc = W_s$, which is work of spreading.

ured was the same as that which had previously been found for siliceous material by entirely different methods (13-19).

Surface Area

The specific surface areas of each of the three gels were determined by application of equation [5]. The values so determined for each gel are listed in Table II. The area values calculated using surface tension values of liquids which varied from 8.8 dynes/cm. to 72 dynes/cm. show sufficiently good agreement to attest to the soundness of the method. Calculations of surface area by this method employing adsorption data available in the literature gave equally good results (20).

It may be noted that this method of area evaluation is analogous in theory to the "absolute" method of Harkins (21) for the determination of the surface area of powders.

In the "absolute" method the heat evolved (H) on destroying an adsorbed liquid film which covers the solid is measured calorimetrically. The total enthalpy change is then divided by the surface enthalpy of the liquid per square centimeter (h), where $h = \gamma - T \frac{d\gamma}{dT}$. The area of the liquid film destroyed (equal approximately to the area of the solid) is thus of

tained since $H = ah$. In the Fu and Bartell method, the total free surface energy lowering during destruction of such a liquid film is calculated through the use of Gibbs equation and division of this value by the free surface energy per square centimeter of the liquid (numerically equal to the surface tension) gives the area of the surface destroyed. Thus, Harkins employed total energy considerations and Fu and Bartell free energy considerations.

The values of the specific areas determined by the latter method are seen to be in reasonable agreement with those determined by the BET

TABLE II
*Specific Surface Area of Silica Gels No. 1, No. 2, and No. 3
by the Method of Fu and Bartell*

Adsorbate	Temperature °C.	Surface area (m. ² /g.)	
GEL No. 1			
CH ₃ OH	25	338	a = BET nitrogen (320 m. ² /g.)
C ₂ H ₅ OH	25	327	
<i>n</i> -C ₃ H ₇ OH	25	326	
C ₂ H ₅ OH	25	317	
C ₆ H ₆	26.5	329	
<i>n</i> -C ₈ H ₁₄	26.5	334	
CCl ₄	26.5	327	
N ₂	-195	342	
GEL No. 2			
<i>n</i> -C ₆ H ₁₄	26.5	342	a = BET nitrogen (355 m. ² /g.)
CCl ₄	26.5	316	
H ₂ O	26	329	
GEL No. 3			
C ₂ H ₅ OH	45	477	a = BET nitrogen (455 m. ² /g.)
H ₂ O	26	433	

method. Good agreement was also obtained between these values and the area obtained by dividing twice the liquid volume "adsorbed" at saturation by the dry radius of the capillary pores, i.e., $a = 2V_s/\text{radius}$. (This dry radius was determined by adding the calculated multilayer thickness at the inception of capillary condensation to the radius calculated by the Kelvin equation using the P/P^0 value of the steepest point of the desorption curve.) For example, the "average" Kelvin radius for gel No. 1 was found to be 60.5Å. and the multilayer thickness at the inception of capillary condensation in the average pore was calculated to be 9.8Å. whence

the dry radius was 70.3A. Since the average liquid volume at saturation was 1.17 cc./g., the area so calculated for gel No. 1 was 333 m.²/g.

SUMMARY

1. Isothermals were obtained at 25°C. for the adsorption of the vapors of methyl alcohol, ethyl alcohol, *n*-propyl alcohol, benzene, carbon tetrachloride, hexane, and water by silica gels of different apparent densities. For certain of these systems additional isotherms at 40 or 45°C. were obtained.

2. The specific surface area of each gel was determined by three independent methods as follows: (a) by application of the BET equation to the low temperature nitrogen adsorption isotherms, (b) by the method based upon the assumption of the existence of uniform circular capillaries (i.e., $a = \frac{2V_s}{\text{radius}}$), and (c) by treatment of the gravimetric data according to the free surface energy method of Fu and Bartell.

3. For each system the values of the adhesion tension, work of adhesion, and initial spreading coefficient were calculated from the adsorption data by means of the Gibbs equation which interrelates surface area, surface tension, surface excess and chemical potential.

4. It was found that the free surface energy changes which occurred when unit areas of the different porous solids were replaced by unit areas of given solid-liquid or solid-saturated vapor interfaces were independent of the apparent densities of the adsorbent, i.e., the adhesion tension values calculated for a given liquid against a series of silica gels which differed in average pore radius, pore volume, and specific surface area were practically the same.

5. Inasmuch as six different organic liquids, possessing widely different surface tensions as well as widely different interaction energies against silica gave for a given gel similar values for surface area, which values were in good agreement with values obtained with other accepted methods, it appears justifiable to conclude that the free surface energy method of Fu and Bartell is generally applicable.

REFERENCES

1. DOBAY, D., FU, Y., AND BARTELL, F. E., *J. Am. Chem. Soc.* **73**, 308 (1951).
2. FU, Y., AND BARTELL, F. E., *J. Phys. & Colloid Chem.* **55**, 662 (1951).
3. BARTELL, F. E., AND DOBAY, D., *J. Am. Chem. Soc.* **72**, 4388 (1950).
4. BARTELL, F. E., AND DONAHUE, D. J., *J. Phys. Chem.* (in press).
5. EMMETT, P. H., *Advances in Colloid Sci.* **1**, 1-36 (1942).
6. BARTELL, F. E., AND DODD, C., *J. Phys. & Colloid Chem.* **54**, 114 (1950).
7. MCBAIN, J. W., AND BAKER, A. M., *J. Am. Chem. Soc.* **48**, 690 (1926).
8. BANGHAM, D. H., *Trans. Faraday Soc.* **33**, 805 (1937).
9. BANGHAM, D. H., AND RAZOUK, R. I., *Trans. Faraday Soc.* **33**, 1459 (1937).
10. BANGHAM, D. H., AND RAZOUK, R. I., *Proc. Roy. Soc. London* **A166**, 572 (1938).

11. BOYD, G. E., AND LIVINGSTON, H. K., *J. Am. Chem. Soc.* **64**, 2383 (1942).
12. JURA, G., AND HARKINS, W. D., *J. Am. Chem. Soc.* **66**, 1356 (1944).
13. BARTELL, F. E., AND MERRILL, E. J., *J. Phys. Chem.* **36**, 1178 (1932).
14. BARTELL, F. E., AND OSTERHOF, H. J., *J. Phys. Chem.* **37**, 543 (1933).
15. BARTELL, F. E., AND WHITNEY, C. E., *J. Phys. Chem.* **36**, 3115 (1932).
16. BARTELL, F. E., AND ALMY, E. G., *J. Phys. Chem.* **36**, 475 (1932).
17. BARTELL, F. E., AND FU, Y., Colloid Symposium Annual. Seventh Colloid Symposium Monograph. John Wiley, New York, 1930, p. 135.
18. PATRICK, W. A., AND GRIMM, F. E., *J. Am. Chem. Soc.* **43**, 2144 (1921).
19. BOYD, G. E., AND HARKINS, W. D., *J. Am. Chem. Soc.* **64**, 1190 (1942).
20. BOWER, J. E., Thesis, Univ. of Michigan (1951).
21. HARKINS, W. D., AND JURA, G., *J. Am. Chem. Soc.* **66**, 1362 (1944).

MORPHOLOGIC CHANGES IN GELLED SYNTHETIC LATICES ¹

Samuel H. Maron and Carl Moore

*Physical Chemistry Laboratory, Department of Chemistry and Chemical Engineering,
Case Institute of Technology, Cleveland, Ohio*

Received December 12, 1951

INTRODUCTION

In two earlier papers from this laboratory (1, 2) a method for concentrating synthetic latices by controlled gelation of latex-electrolyte mixes and their subsequent filtration was described. During the development of this process wide variations in filtration rates were observed for gelled latex samples prepared under different conditions, the rates ranging all the way from rapid filtration to complete non-filterability. Such behavior suggested the possibility that the variations noted were due to differences in the character of the particles present in the latex mixes. Preliminary microscopic observations disclosed the fact that in some mixes a characteristic oölitic or "fish-egg" structure was present, while this structure was totally absent in other mixes prepared under different conditions. Consequently the microscopic study was extended to careful visual observation of the phenomena involved in the various stages of the process and their photomicrographic recording. The results of this study are described in the present paper.

APPARATUS AND TECHNIQUE

A Bausch and Lomb standard research microscope was employed for all visual observations. For the photomicrographic phase of the study the same instrument, fitted with a Leitz Micro-Ibso attachment and a 35 mm. Leica camera, was found very suitable. The illumination was generally supplied by a Spencer standard microscope lamp equipped with a 100-watt bulb. When a more intense light source was needed, or one of lower wavelength for greater resolution, a Bausch and Lomb carbon arc microscope lamp was substituted.

The film employed was the fast emulsion Kodak Super XX, or, when a finer grain was required, Kodak Panatomic X. Fine grain developers were used throughout for developing the film.

¹ This research was sponsored by the Reconstruction Finance Corporation, Synthetic Rubber Division, as part of the Government Synthetic Rubber Program, and was first reported in December, 1945.

Since all the phenomena observed here appear below room temperature provision had to be made for keeping the latex samples cool during observation and photographing. For this purpose was constructed an aluminum cold stage through which precooled water could be circulated by means of a small centrifugal pump. The stage consisted of an aluminum block through which were drilled horizontal holes for passage of cold water, and a vertical $\frac{3}{4}$ -inch hole for light passage. Into the top of the block was milled an inch-wide slot for holding the microscope slide. By regulating the temperature of the circulating water, the cold stage could be kept at any temperature and for any length of time desired.

The photomicrographs were enlarged to final magnifications as high as 3400 diameters for study and particle size measurement. For the latter purpose a micrometer scale on a slide was photographed through the microscope and enlarged under the same conditions as photographs of the latex samples. The enlargement served then as a calibration scale for direct measurement of particle size.

The technique utilized in mounting samples for observation was the "hanging drop" method common in biological work. It consisted of using a slide having a small depression in it, over which a cover glass was fitted. A drop or smear of the sample was suspended from the cover glass into this depression, and examination of the specimen was made through the cover glass.

BEHAVIOR OF SYNTHETIC LATEX-ELECTROLYTE MIXES ON COOLING

When a synthetic rubber latex with suitably adjusted pH, soap, and electrolyte content is cooled with agitation, a viscous gel is formed at a definite temperature called the *gel point*. This temperature varies with the soap content, pH, and total solids of the adjusted latex, as well as with the type and concentration of electrolyte present. As the gel is cooled further with stirring, its viscosity continues to increase until at a characteristic temperature called the *thin point* it suddenly drops, and the mass becomes fluid. When conditions are properly adjusted, cooling of the thinned mass with agitation to 2–8°C. produces a mix with good filterability.

Microscopic examination of a latex-electrolyte mix being cooled *without agitation* has revealed that at a particular temperature Brownian motion of the visible particles ceases, and the sample gels. As a result of gelation less light is transmitted, and the latex appears to consist of a mosaic of dark particles embedded in a continuous and more transparent matrix. As the temperature is lowered this structure persists, and no further changes are observed unless the sample is allowed to remain at the lower temperature for some time. In the latter instance a small amount of serum is formed by syneresis, but the gel does not break up.

It is not possible to observe continuously the behavior on cooling of an agitated latex-electrolyte mix. Consequently samples were taken at various stages of cooling, placed on the cold stage, and these examined or photographed. Such samples, taken from latex of suitably adjusted pH, soap, and electrolyte content, showed that initially a gel structure similar to the one described above is obtained. However, as cooling progresses to several degrees below the gel point and the thinning stage is reached, the transparent matrix begins to disintegrate into irregular clumps of gel floating in a continuous liquid phase. Under the influence of agitation this structure readily changes to a mass of spheroidal particles surrounded by clear serum. These spheroids are stable, and remain as such unless the

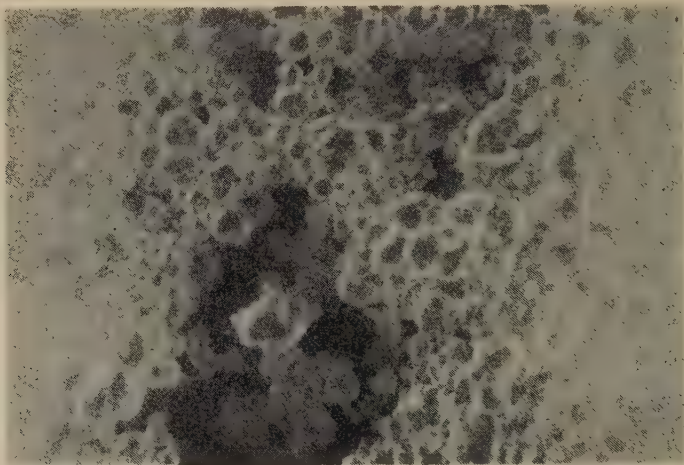
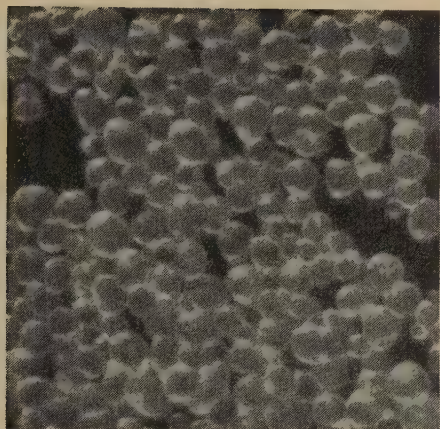


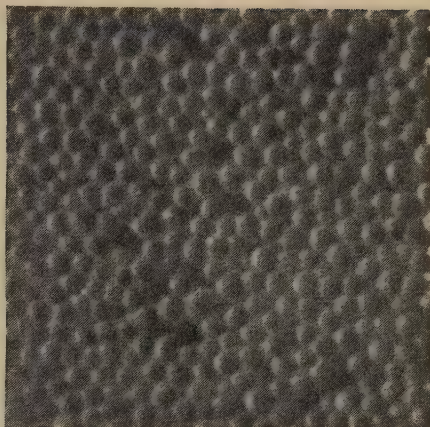
FIG. 1. Spheroidal particles forming in gelled type III GR-S latex (reflected light, $360\times$).

temperature is raised too far or it is lowered below the freezing point of the system.

A photomicrograph showing the disintegration of gel into clumps and serum and the incipient formation of spheroids is given in Fig. 1. The sample is a Type III GR-S latex containing sodium carbonate as the added electrolyte. Spheroids resulting from processing a Type II latex containing the same electrolyte and a Type III latex with sodium pyrophosphate are depicted in Fig. 2. Similar oölitic structure has been observed also in other latices containing various electrolytes and treated in the same manner, namely, GR-S 10, Buna S-3 (both German and American made), Hycar OR, and the redox formula "cold rubber" latex. In GR-S 10 and Hycar OR, however, the particles photographed were considerably smaller in size than in Types II and III latices. Other latices, such as Neoprene and vinyl chloride, were unstable to electrolyte when



Type II



Type III

FIG. 2. Oölitic particles in thinned type II and type III GR-S latex (reflected light, 330 \times).

cooled or did not yield spheroids, and hence they were not studied further.

Such spheroidal structure was found only in cooled latex-electrolyte mixes which filtered well on a cold Büchner funnel. Batches which did not filter gave instead of spheroids a gel structure such as shown in Fig. 3. Here the gel is continuous, serum is absent, and the mass exhibits no tendency to thin out on further cooling. These observations establish a direct connection between filterability and the presence of spheroidal particles. It was also noted that samples containing large spheroids

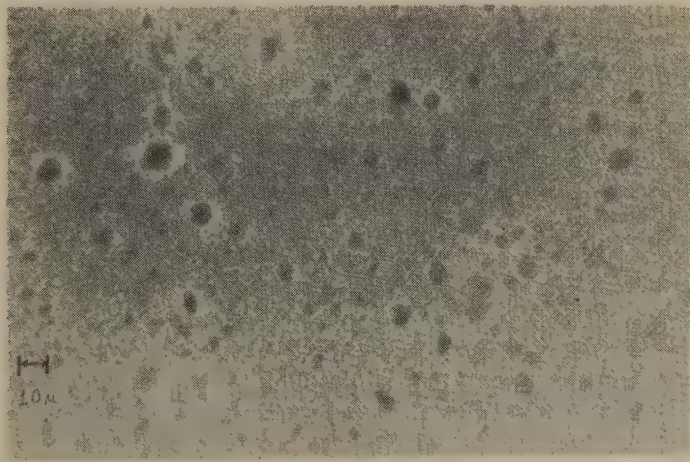


FIG. 3. Appearance of a nonfiltering type III GR-S latex mix (reflected light, 360 \times).

filtered more rapidly than those containing small ones. The slow filtration was due not only to the small size of the spheroids, but also to the fact that small spheroids tended to be matted together by smaller pieces of gel. Such matting tied up serum and interfered with the filtration.

The size of spheroids has been found to range from 1–20 μ , and to depend upon the manner of preparation, soap and electrolyte contents of the latex, and particularly the polymer content of the latex-salt mix. When the rubber content of the mix fell much below about 25%, it was virtually impossible to induce formation of the proper spheroid structure. Further, use of low rubber contents with some latices yielded concentrates of poor stability and final solids contents of only 50% or less.

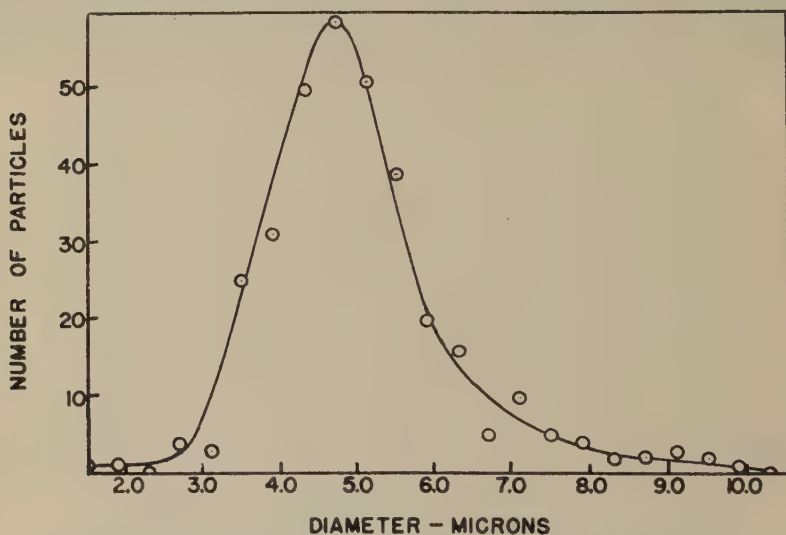


FIG. 4. Distribution of spheroid diameters in a type III GR-S latex mix.

In Fig. 4 is shown a size-distribution curve for spheroids prepared in a Type III GR-S latex containing added sodium chloride. The total number of particles measured on photomicrographs of the chilled latex was 400. The number average diameter for the sample shown in Fig. 4 is 5.2 μ . The optimum size average for most rapid filtration was found to be 10–15 μ . Larger size spheroids offer no advantage, and, in fact, slow down the filtration somewhat. An additional factor found to influence the filtration rate was uniformity of size—the more uniform the size of the particles in any given range the more rapid the filtration rate.

STABILITY AND STRUCTURE OF THE SPHEROIDS

The oölitic structure was found to persist during filtration and could be discerned in the cold gel retained on the filter paper after removal of

the serum by suction. However, upon warming either filtered or unfiltered latex mixes to room temperature, the spheroids disappeared and latex sols were again obtained. This behavior immediately rules out any possibility that the spheroids are particles of coagulated rubber. It suggests instead that they are temporary agglomerates of colloidal polymer particles existing only at the lower temperatures and in the presence of the proper electrolyte content. Microscopic observations at higher magnifications readily bear out this fact. By examining the spheroids with transmitted axial illumination it was found that the large particles are not solid but consist of still finer particles held together by a transparent phase. The photomicrograph in Fig. 5, at a magnification of 1400, illustrates this observation.

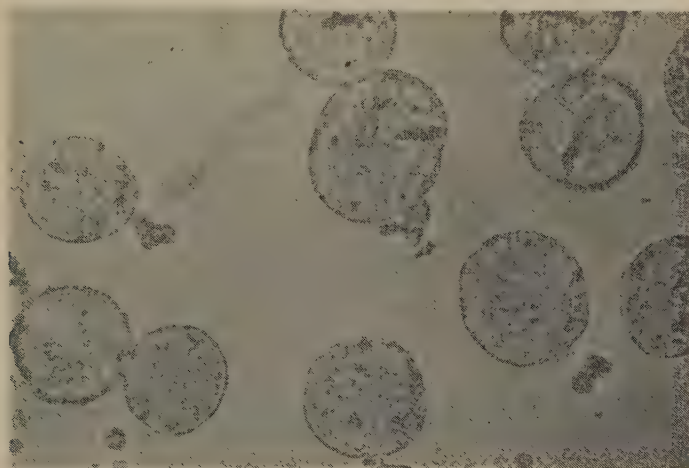


FIG. 5. Inner structure of spheroids in type III GR-S latex mix (transmitted light, 1100 \times).

Further verification of the existence of finer particles within the spheroids was obtained by adding a dye such as methylene blue to the latex prior to cooling and gelation. This dye, adsorbed on the surface of the particles within the spheroids, made them stand out more distinctly for observation.

The inner structure of spheroids makes understandable their disintegration on warming into stable latices containing particles not far different in size from those present prior to processing. Since spheroid formation results apparently from temporary agglomeration of individual latex particles into clusters on gelation and thinning, the reversal of the process on heating yields again essentially the original latex particles.

In the latices dealt with here the average particle size ranged from 700–1000 Å. However, since the particle size distribution of synthetic

lattices is quite broad, many particles are of a size several times the average and fall within the range visible in the ordinary microscope. We believe that these large particles are the ones observed within the spheroidal particles.

Attempts were made to ascertain whether the spheroids are electrically charged. No migration was observed under the microscope with applied potentials as high as 25 volts per centimeter, nor could the spheroids be electrodeposited. Hence it must be concluded that the spheroids are either uncharged, or too heavy to migrate under the experimental conditions.

BREAKDOWN OF THE SPHEROIDS

Since no agitation is required for breakdown of the spheroids on warming, it is possible to follow the disintegration under the microscope. At temperatures considerably below that for disintegration (but above freezing), the spheroids are distinct in outline when viewed with transmitted light, and only the large latex particles within the globules are visible. However, as the temperature is raised slowly the spheroids begin to cloud up, become translucent, and more particles become visible. Although no change in size is apparent, a loosening of the inner structure of the polymer particles and soap gel occurs, which allows more particles to become distinct. As the warming continues a temperature is finally reached at which the outline of the spheroids becomes indistinct and disappears. At this stage the darker particles observable within the spheres by transmitted light start to exhibit Brownian motion, slowly diffuse into the surrounding serum, and are lost on complete disintegration. Figure 6 shows a photomicrograph taken during the early stages of disintegration

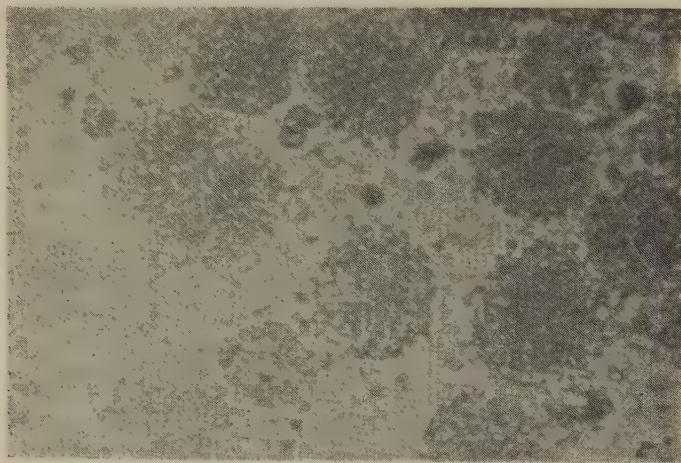


FIG. 6. Type III GR-S latex spheroids in process of disintegration on warming (transmitted light, 1090 \times).

of a field of view similar to that given in Fig. 5 and photographed under the same conditions. In this figure the disappearance of outline of the spheroids and the broadening of their field as a result of diffusion of the particles are readily evident.

Observation of spheroids during disintegration and in the presence of new surroundings has revealed other interesting facts about their behavior. If at the stage of initial breakdown shown in Fig. 6 the temperature be lowered, the fine particles which have not as yet diffused away coalesce again into a coherent and translucent mass of definite distinctness. However, the new mass formed is no longer consistently spheroidal in shape, but shows an irregularity dependent upon the stage of disintegration by diffusion of the original spheroid. On increase in temperature the new irregular-shaped particle behaves like the parent spheroid and readily disintegrates.

If the cold serum in which the spheroids float is diluted with cold, distilled water to about 70% of its original electrolyte strength, disintegration of the spheres may also be induced. This observation relates directly the stability of the structure to the electrolyte strength of the serum, as well as to the temperature. It might also be conjectured that the soap content of the serum may be critical. However, it has been shown (2) that about 90% of the soap is retained in the gel portion of filtered latex, and is presumably bound in the spheroidal globules along with an appropriate amount of water and electrolyte. Prolonged filtration with suction of a processed latex has yielded a residue which contained about 75% polymer. The remainder of the gel mass was evidently soap gel and water not removable by filtration. A fraction of the initial electrolyte also remains with the gel. Analyses indicate that the ratio of electrolyte to water in the gel phase is approximately the same as in the serum.

SUMMARY

A photomicrographic study was made of the transformations undergone by synthetic latices during concentration by a method involving electrolyte addition, gelation, cooling and subsequent filtration. This investigation has disclosed that in latex-salt mixes suitably adjusted and processed for concentration a characteristic structure is present consisting of quite uniform spheroids suspended in a medium of clear serum. This spheroidal structure has been found to be essential for filterability, the rate of filtration being the faster the larger and more uniform the spheroids.

During filtration only serum is removed, the spheroids remaining as a residue. On warming the filter residue the spheroidal particles disintegrate to give again a latex free of coagulum.

Photomicrographic study has shown that the spheroids consist of small particles of apparently polymer, embedded in a transparent matrix of presumably soap gel. When the spheroids are warmed the gel breaks down, and the particles diffuse into and are dispersed in the surrounding medium. These phenomena indicate that the spheroids are temporary low temperature agglomerates of rubber and soap which disintegrate into finer latex particles as soon as the temperature is raised above a critical point. The stability of the spheroids is dependent principally upon electrolyte content, temperature and the amount and type of emulsifier present.

The above structure has been found in processed and filterable Type II, Type III, GR-S 10, Buna S-3, Hycar OR, and "cold rubber" latex-electrolyte mixes.

REFERENCES

1. MARON, S. H., AND MOORE, C., *India Rubber World* **116**, No. 6, 789 (1947).
2. MARON, S. H., MOORE, C., KINGSTON, J. G., ULEVITCH, I. N., TRINASTIC, J. C., AND BORNEMAN, E. H., *Ind. Eng. Chem.* **41**, 156 (1949).

Book Reviews

Adhesion and Adhesives. Edited by N. A. DE BRUYNE AND R. HOUWINK. Elsevier Publishing Co., New York, Amsterdam, London, and Brussels, 1951. xv + 517 pp. Price \$10.00.

This is probably the most extensive treatment of adhesion and adhesives in any language. It contains nine chapters compiled by N. A. de Bruyne, F. Chapman, W. R. Lewis, and C. Mylonas from England, C. P. Fritzius, J. Hoekstra, R. Houwink, R. N. J. Saal, G. Salomon, W. J. K. Schönlaue, and A. J. Staverman from Holland, and E. D. Cornwell, W. M. Lee, and J. H. Wills from the United States.

A contributing cause of the impressive length of the book is that it deals also with some topics hardly connected with adhesives. Thus the first two chapters discuss intermolecular attraction. The attraction between two arrays of different molecules is often termed adhesion. This adhesion is related to the adhesion operating in glued joints about as closely as is horsepower to powers of numbers and to great powers. Nevertheless the confusion between the two adhesions persists and caused the inclusion of the first two chapters in the volume under review. The rest of the volume is a good proof for the two adhesions being entirely different, since the molecular forces described in the beginning of the book are hardly ever mentioned in the later chapters and the strength of joints is (quite correctly) correlated with stress distribution and similar causes not on a molecular scale.

Chapter 3 is a sound review of the rheology of adhesives. Chapter 4, on the stress distribution in joints, is the most valuable part of the book for a scientist. It is more than a mere review and includes also some unpublished material.

The following chapters deal with "Technological Aspects," namely, with animal glues, vegetable adhesives, synthetic resin adhesives, asphaltic bitumens, inorganic adhesives and cements, rubbery adhesives, adhesion in soldered joints, and the physical testing of adhesion and adhesives. As in many other books produced by coöperative effort, the treatment is very uneven, depending on the background of the author. Thus the section on animal glues contains scarcely any chemistry or physics (but includes uses of gelatin other than as adhesive) while the section on bitumen may be classified as a rheological paper. The section on sodium silicate discusses a host of United States patents, while 28 of the 32 references to soldered joints are from British sources, and no patent literature is considered.

As might be expected, there are overlaps between chapters written by different authors and there are also omissions, for every author believed that the subject belonged to another chapter. Thus the relation between thickness and strength of adhesive joints is treated twice (in Chapters 3 and 4). Breaking stress depends on thickness (a) because of the greater probability of flaws in bigger specimens, (b) because the conditions of setting are different in specimens of different sizes, and (c) because the stress distribution during test may depend on the dimensions of the joint. All three groups of causes usually operate in every joint. Presumably the authors of Chapters 3 and 4 agree with this view. However, the emphasis placed on one group in one chapter and on another group in the other chapter may mislead many readers into believing that the three groups are mutually exclusive and that one author contradicts the other. Omissions may be exemplified by the absence of tests on adhesion of asphalt to stone; these tests could suit-

ably be described either in the section on asphalt or together with other tests, but the reviewer could not find them anywhere.

Some of the chapters had to be translated and the translator did not always succeed with scientific terms. Thus (p. 34) velocity of shear, rate of shear, and rate of flow are said to be identical, and the inverse of viscosity is called mobility instead of fluidity.

As the above observations show, the book is not perfect. Nevertheless, the wealth of knowledge displayed in it (partly from unaccessible European publications) and the high scientific quality of some chapters are such that I shall turn to it first whenever I need information on adhesives and their action.

The printing and binding are good. There are 205 instructive figures.

J. J. BIKERMAN, Woodside, Long Island, N. Y.

The Pectic Substances. By Z. I. KERTESZ. Interscience Publishers, Inc., New York, 1951. 640 pp. Price \$13.50.

Pectins, although substances of considerable theoretical and practical interest, have not been critically or comprehensively reviewed for many years. This book will be a welcome addition to libraries of food technologists and carbohydrate chemists. It contains over two thousand references (some duplications) with critical comment and for that reason alone will serve a valuable purpose.

The style is informative with sufficient speculation by the author to stimulate the imagination. Different sides of debatable issues are discussed to enable the reader to decide whether he agrees with the author's conclusions. A more impartial treatment of some of these issues would improve the book.

Generally, this book is well-written and reflects the extensive experience of the author but the sections dealing with colloidal properties are not equal to the standards of the rest of the book. These sections are more polemical than the facts warrant. Surprisingly only about seven pages are devoted to the gel properties, one of the most important physical properties of pectin. While emphasis is placed on colloidal properties of pectin, there is little discussion of its effect on pectin extraction from plant materials. There are also occasional errors in interpretation.

The book is recommended to chemists interested in polysaccharides and pectic enzymes. The colloid chemist will find it valuable for its references and as source book for further research problems.

HARRY S. OWENS, Albany, California

Die Makromolekulare Chemie, Band VI, Staudinger Festband, März 1951. Herausgegeben von E. HUSEMANN. Verlag Karl Alber Freiburg, München, 317 pp.

This reviewer has already performed on another occasion the pleasant duty of emphasizing the general importance of this special volume of the *Makromolekulare Chemie*, which celebrates the 70th birthday of the distinguished founder of this branch of chemistry and presents a very interesting and stimulating cross-section of the present state of our knowledge in this field.

Nine of its twenty-six articles are devoted to polysaccharides with special emphasis on cellulose and its derivatives. Foremost here are problems of the morphology and crystallinity of natural and regenerated fibers and of the existence of weak bonds in the chain molecules of these substances. Nine other contributions deal with the investigation of macromolecules in the dissolved state and comprise studies of osmotic pressure, turbidity, diffusion, sedimentation and viscosity of homopolymer polymers in non-polar solvents and of polyelectrolytes and other water-soluble macromolecules in water. Five papers are concerned with the description of work on the synthesis of certain polymers on the mechanism of polymerization reactions and of the kinetics of the degradation of

proteins. Three articles are of a more general nature; they discuss the importance of macromolecules as building materials in nature and industry, the process of inorganic and organic condensation and the significance of the relaxation spectrum of highpolymers in the solid state. The volume contains a wealth of new experimental and theoretical progress and well fulfills its purpose of paying homage to one of the most distinguished and successful pioneers in the chemistry of macromolecules.

H. MARK, Brooklyn, N. Y.

Amino Acids and Proteins. Theory. Methods. Application. Compiled and edited by DAVID M. GREENBERG, Ph.D. Charles C Thomas, Springfield, Illinois, 906 pp., 99 illustrations. Price \$15.00.

Comment on this huge volume should include an indication of the audience at which it is aimed, and how useful this audience will find it. It is not easy, however, to make a just appraisal, in this respect, of this splendid expensive example of the bookmaker's art. Contrary to the jacket blurb, not all the 15 contributors are "the *foremost* authorities in the special fields covered." They are better characterized as a group of competent workers, principally located at, or originating from, the West Coast, many of them students or associates of the late C. L. A. Schmidt. Indeed, in many respects, the volume gives the impression of a latter-day version of his own compendious volume on the same subject issued some twelve years ago by the same publisher.

Individual chapters deal with Properties of Amino Acids (E. E. Howe); Methods of Determination of Amino Acids (H. S. Olcott); The Preparation of Amino Acids and Polypeptides (S. Archer); The Synthesis of Labeled Alpha Amino Acids (J. C. Reid and B. M. Tolbert); Isolation of Amino Acids (M. S. Dunn and L. B. Rockland); Classification, Purification, and Isolation of Proteins (H. L. Fevold); Determination of the Molecular Size of Proteins (H. P. Lundgren and W. H. Ward); Amphoteric Properties of Amino Acids and Proteins (D. M. Greenberg); Criteria of the Purity of a Protein (Choh Hao Li); Chemical Reactions of Proteins (H. Fraenkel-Conrat); Nutritional Applications of the Amino Acids (H. J. Almquist); Chemistry of Antibodies (D. H. Campbell and F. Lanni); Bio-chemical Applications of Proteins and Peptides (D. M. Greenberg); and the Metabolism of Amino Acids and Proteins (H. Tarver). There is an excellent general subject index, and extensive author indices at the end of each chapter. The book is unusually well provided with summary tables which provide very general coverage of the literature.

It will be noted that there are obvious and serious omissions: there is no general discussion of protein denaturation, its concomitant phenomena and their significance; little explicit treatment of protein structure beyond the polypeptide chain; nothing on bond-lengths, bond-angles; very little on light scattering; x-ray crystallography; streaming double-refraction; molecular shape; and practically no discussion of the large amount of work in recent years on the fibrous proteins. The literature coverage on recent papers is very incomplete—possibly because many of the contributions seem to have been prepared originally at least three years ago.

The treatment of the material included is in most cases exhaustive rather than critical. In a number of places quite old physicochemical material is presented and seriously discussed alongside more recent work which should have led to complete disregard of the older interpretations.

The book is unique in the amount of detail included. Much of its very substantial bulk is the direct result of page after page of detailed instructions as to how, e.g., to use particular instruments (some of them now widely familiar), or how to prepare particular proteins. In at least one place identical material is given at length in two different chapters. Since most of this material is readily available in the literature, the decision to

include it, in word-for-word detail, thus adding materially to the size and expense of the volume, must be viewed as a clue to the audience which the volume is intended to serve. Possibly this audience is a young generation of students at the threshold of graduate instruction, anxious to expedite its direct contact with the material of research without too-great coping with the labyrinth of literature research. Such an audience will undoubtedly find the volume extremely convenient, and make extended use of it. It is an unusual decision however to combine a "theoretical" text and a laboratory manual in a single cover. The absence of an acceptable laboratory manual in this all-encompassing and difficult chemical field may, however, well justify it.*

No review of this book would be complete without mention of the unusual excellence of one of the contributions. The reviewer found the clearly written, carefully organized "Chemistry of the Antibodies," by Campbell and Lanni, altogether rewarding.

JACINTO STEINHARDT, Cambridge, Mass.

Metallurgical Thermochemistry. By O. KUBASCHESKI AND E. LL. EVANS. Academic Press Inc., New York, 1951. xi + 368 pp. Price \$6.00.

It is the stated intention of the authors that this monograph should serve as an introduction to metallurgical thermochemistry and as a reference source (1) for experimental research scientists who measure fundamental data and (2) for process metallurgists seeking solutions to practical problems on the basis of available information. While it is probable that the book will serve its dual purposes, it is not certain that it will serve these purposes equally well for the two groups of readers toward whom it is aimed.

The theoretical basis of chemical thermodynamics and solution theory is the subject of the first chapter. The common thermodynamic functions are defined, and it is shown how the values of these functions may be computed from thermal measurements and equilibrium studies. An excellent contribution of this section is the statement of the most useful thermodynamic equations in such form that the experimentally measured quantities appear in just the way they are determined by usual experimental practice. This should help to minimize the chance of computational errors.

The second section is devoted to experimental techniques with somewhat greater emphasis being placed upon calorimetric methods than on the determination of electromotive force, distribution between condensed phases, and gas phase equilibria. Spectroscopic methods are excluded from the discussion. This chapter, which presupposes a considerable acquaintance with calorimetry, seems to be aimed at a higher level of prior information on the part of the reader than the preceding chapter, which assumes only a sketchy background of thermodynamics. Since the book is intended for the metallurgist, it seems far safer to assume the sketchy background in thermodynamics than any acquaintance with calorimetry. A moderate expansion of the introductory material in the second chapter should widen the circle of readers to include those who would profit most from this book.

The third chapter describes procedures for estimating thermochemical values for which measurements are not available or for checking doubtful experimental values. Such procedures should prove useful in the design of apparatus for making precise determinations or process equipment in which equilibria are to be established. The authors' claims for the empirical correlations seem to be sufficiently conservative to prevent unwarranted confidence in the results of any single "educated guess." The emphasis on the use of several independent estimates is commendable.

* The recent book of Haurowitz "Chemistry and Biology of Proteins" (Academic Press) is an excellent first approximation to the text-book presentation of the subject matter.

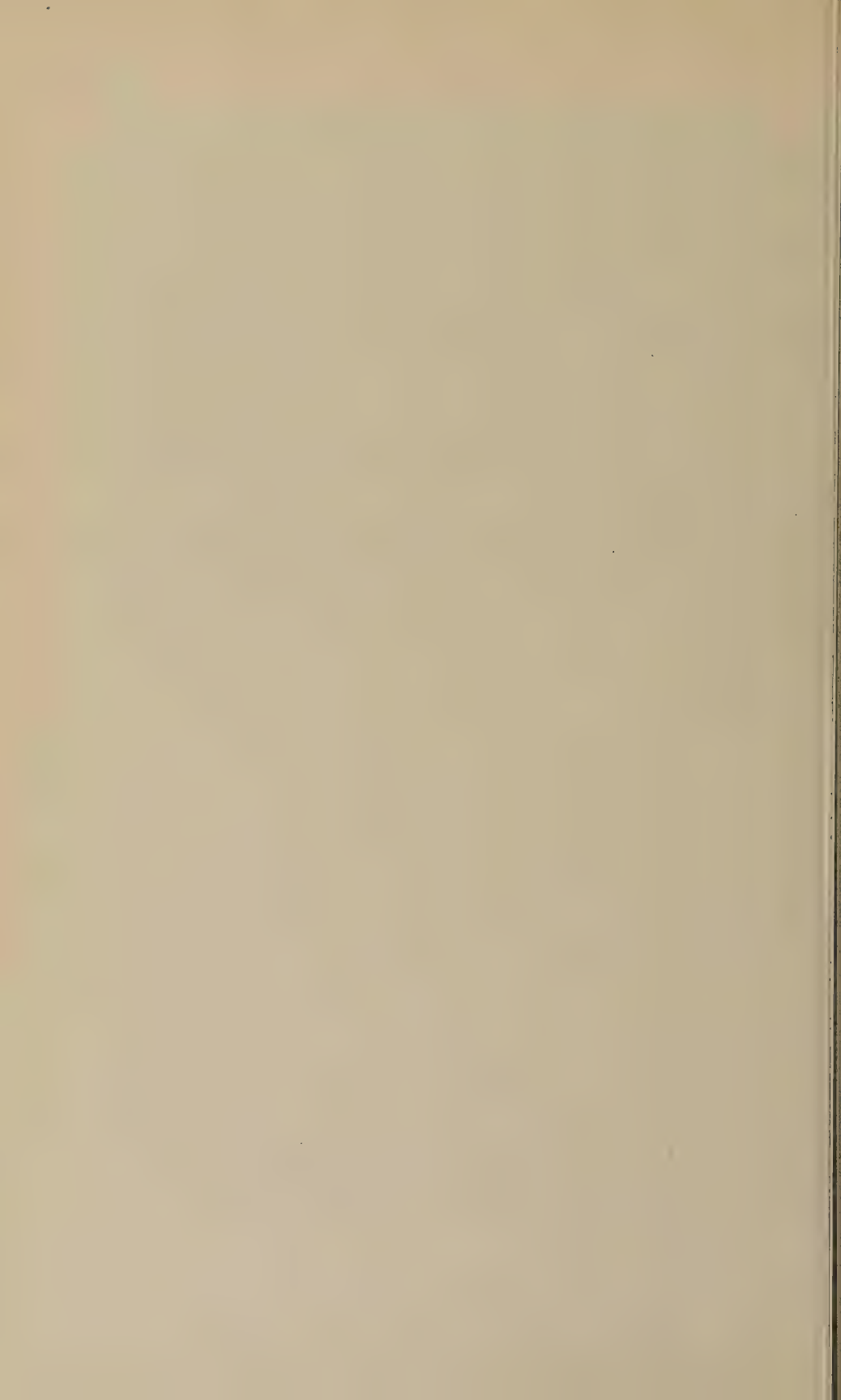
Section four contains extensive tables giving critically chosen thermodynamic (and some structural) data for many inorganic substances of interest in metallurgy. Such generous limits of error have been set that it is very unlikely that these limits will be exceeded by revision of accepted values due to future experiments.

In the final part six metallurgical problems are discussed from the thermodynamic point of view employing the tabulated data. The references are listed separately rather than as footnotes throughout the book. Name and subject indices complete the volume.

It is easier to find points about the book to commend than items to criticize. For instance, the words of caution concerning the calculation of activities from equilibrium diagrams on page 50 and the warnings about the pitfalls in the over-interpretation of slag-metal equilibria on page 52 seem very appropriate to the intent of this book and the needs of the hour. On the other hand, it seems to this reviewer that there is nothing thermochemistry needs so little as the introduction of proper adjectives such as Raoultian and Henrian to apply to activity coefficients referred to the pure component and infinitely dilute solution, respectively, as the standard state. It would seem adequate to identify the standard state once for each component in each solution. If the statement is unambiguous there will be no ambiguity in the subsequent use of the unmodified expression "activity coefficient."

For a first edition, the typographical errors noted were few and inconsequential. The diagrams, which were chosen well and used generously, contributed much to the exposition, although in one or two instances slightly larger reproduction would have improved the visibility of detail. *Metallurgical Thermochemistry* should prove a useful addition to the bookshelf of the metallurgist or inorganic chemist concerned with this intensely active field.

C. ERNEST BIRCHENALL, Pittsburgh, Pennsylvania



THE SPREADING OF LIQUIDS ON LOW-ENERGY SURFACES.

II. MODIFIED TETRAFLUOROETHYLENE POLYMERS¹

H. W. Fox and W. A. Zisman

Naval Research Laboratory, Washington, D. C.

Received June 11, 1951; revised September 28, 1951 and January 18, 1952

INTRODUCTION

The regularities found in our earlier study (1) on the spreading of a variety of liquids on smooth surfaces of polytetrafluoroethylene (TFE) led us to investigate other low energy solids. In particular, the effect of introducing either chlorine or hydrogen into tetrafluoroethylene to replace fluorine was expected to cause an increase in the work of adhesion and the spreading coefficient for every liquid. A series of interpolymers of tetrafluoroethylene and chlorotrifluoroethylene and a 50:50 interpolymer of tetrafluoroethylene and ethylene, obtained through the courtesy of the Du Pont Company, were studied. The final member of the perhalogenated series was polychlorotrifluoroethylene commercially designated as Kel-F. The wettability of these polymers by a variety of pure liquids is the subject of this paper.

In the previous study of TFE (1) it had been shown that the contact angles of the higher boiling liquids were the same in air (at 20°C.) as in air saturated with the vapor in question. A similar experiment on Kel-F and on the 50:50 copolymer of tetrafluoroethylene and ethylene (TFE-E) established that the same situation held for such liquids when placed upon these materials (the least fluorinated of the polymers). This means that for the polymers of this study, f_{SV}° , the free energy decrease on immersion of solid in saturated vapor (or what is often called the equilibrium spreading pressure, π_E) in the corrected Young-Dupré equation for the work of adhesion

$$W_A = f_{SV}^{\circ} + \gamma_{LV}^{\circ}(1 + \cos \theta_E) \quad [i]$$

can be neglected for nonspreading liquids. Thus to a good approximation, for the higher boiling liquids which do not spread on these solid surfaces, W_A is given by

$$W_A = \gamma_{LV}^{\circ}(1 + \cos \theta_E), \quad [ii]$$

¹ The opinions or assertions contained in this paper are the authors' and are not to be construed as official or reflecting the views of the Navy Department.

where γ_{LV° is the surface tension of the liquid and θ_E is the contact angle of the liquid in equilibrium with the solid and its own vapor. This equation applied for TFE to liquids as volatile as heptane, and to liquids as volatile as methylene iodide for all the surfaces of this study.

As Bangham and Razouk have pointed out (2), f_{SL} , the free energy decrease on immersion of the solid in a liquid ($f_{SL} \equiv \gamma_{S^\circ} - \gamma_{SL}$), can be expressed as

$$f_{SL} = f_{SV^\circ} + \gamma_{LV^\circ} \cos \theta_E. \quad [\text{iii}]$$

When f_{SV° is negligible, it follows that

$$f_{SL} = \gamma_{LV^\circ} \cos \theta_E. \quad [\text{iv}]$$

This expression can be applied as a useful approximation for the systems discussed here.

The initial and final spreading coefficients S_{LV°/S° and S_{LV°/SV° given by Boyd and Livingston (3) are

$$S_{LV^\circ/S^\circ} = \gamma_{S^\circ} - \gamma_{SL} - \gamma_{LV^\circ}. \quad [\text{v}]$$

$$S_{LV^\circ/SV^\circ} = \gamma_{SV^\circ} - \gamma_{SL} - \gamma_{LV^\circ}. \quad [\text{vi}]$$

Applying the modified Young equation

$$\gamma_{SV^\circ} - \gamma_{SL} = \gamma_{LV^\circ} \cos \theta_E \quad [\text{vii}]$$

to Eq. [vi], the following convenient expression results for the final spreading coefficient:

$$S_{LV^\circ/SV^\circ} = \gamma_{LV^\circ} (\cos \theta_E - 1). \quad [\text{viii}]$$

Another useful relation involving the spreading coefficients is

$$S_{LV^\circ/S^\circ} - S_{LV^\circ/SV^\circ} = \gamma_{S^\circ} - \gamma_{SV^\circ} = f_{SV^\circ}. \quad [\text{ix}]$$

Hence, when $f_{SV^\circ} = 0$, $S_{LV^\circ/SV^\circ} = S_{LV^\circ/S^\circ}$. In general

$$S_{LV^\circ/S^\circ} = W_A - W_C, \quad [\text{x}]$$

where W_C , which equals $2\gamma_{LV^\circ}$, is the work of cohesion. Since

$$W_A = \gamma_{LV^\circ} + \gamma_{S^\circ} - \gamma_{SL} = \gamma_{LV^\circ} + f_{SL}, \quad [\text{xi}]$$

by subtracting W_C it follows from [x] that

$$S_{LV^\circ/S^\circ} = f_{SL} - \gamma_{LV^\circ}. \quad [\text{xii}]$$

Where f_{SL} is constant for a group of liquids, it is seen from the form of Eq. [xii] that a plot of S_{LV°/S° vs. γ_{LV° would be a straight line with a negative 45° slope; from [xi] it is evident that a plot of W_A vs. γ_{LV° would be a straight line with a positive 45° slope. In both cases, the intercept of the 45° line with the axis of ordinates has the value of f_{SL} .

MATERIALS AND PROCEDURES

The polymers used were thin translucent sheets up to 0.050-inches thick. Cleaning the sheets in hot acid caused them to warp so that a modification of the acid-cleaning method employed on TFE was adopted. The polymer sheet was boiled in nitric-sulfuric acid (1:2) and rinsed by boiling in three successive changes of grease-free distilled water. When dry it was placed between two blocks of thick, scratch-free plate glass (previously acid-cleaned) and pressed at 150°C. and about 1000 lbs./sq. in. The pressure was maintained while the heat was shut off and the system allowed to cool to room temperature. The sheet was not removed from between the glass plates until ready to be used. This procedure produced flat, glossy, uncontaminated surfaces on which contact angles were readily measured. Furthermore, the contact angles from specimen to specimen of the same polymer showed good reproducibility. The TFE-E, which is attacked by oxidizing acids, was prepared by removing from a piece of the polymer of suitable size, a layer 1-2-mm. thick with a grease-free microtome blade. The resultant clean, flat surface was pressed against a previously acid-cleaned glass plate. The plate was heated to just above the softening point of the polymer and then cooled rapidly to room temperature while maintaining the pressure. This treatment produced flat, glossy surfaces with no visible evidences of crystallinity. Again the surfaces were kept in contact with the glass until used. TFE-E surfaces, on separation from the glass, developed a static charge which interfered with the placement of drops. This difficulty was resolved by placing the charged surfaces near an alpha-particle source for about 5 minutes.

The same liquids were used as before (1) since they conveniently cover the available range of surface tensions and boiling points and permit a direct comparison with the previous results on TFE. Every quoted value for the contact angle is the result of at least four separate measurements of the advancing angle. Great care was exercised to ensure that the surfaces were smooth so as to avoid frictional and other irreversible effects as much as possible. A primary drop was placed carefully on the surface under study and small amounts of additional liquid were added to the drop. The correct value was assumed when the contact angle did not change with successive increases in the size of the drop. In this way, the advancing contact angle was obtained with the system as close as possible to mechanical equilibrium (4). The maximum deviation from the mean for a single set of measurements was in general less than $\pm 2^\circ$ and in most cases as low as $\pm 1^\circ$. All measurements were made at 20°C. and 50% relative humidity.

Measurements were made on the series of copolymers of tetrafluoroethylene and chlorotrifluoroethylene containing by weight the following proportions of the two monomers respectively: 98-2, 90-10, 80-20, 60-40,

TABLE I
Surface Energy Relations of Some Liquids on Fluorinated Copolymers (20°C.)

Liquid	80-20 copolymer				60-40 copolymer				Kel-F				TFE-E			
	γ_{LV}^o dynes cm.	θE	$\gamma \cos \theta$ dynes cm.	$\frac{\gamma(1+\cos \theta)}{\text{ergs cm.}^2}$	$\frac{SLV^o/SP^o}{\text{ergs cm.}^2}$	θE	$\gamma \cos \theta$ dynes cm.	$\frac{\gamma(1+\cos \theta)}{\text{ergs cm.}^2}$	θE	$\gamma \cos \theta$ dynes cm.	$\frac{\gamma(1+\cos \theta)}{\text{ergs cm.}^2}$	$\frac{SLV^o/SP^o}{\text{ergs cm.}^2}$	θE	$\gamma \cos \theta$ dynes cm.	$\frac{\gamma(1+\cos \theta)}{\text{ergs cm.}^2}$	$\frac{SLV^o/SP^o}{\text{ergs cm.}^2}$
<i>n</i> -Alkanes																
Hexadecane	27.6	37	22.0	49.6	— 6.5	24	25.2	52.8	Spr	12	27.0	54.6	12	27.0	54.6	0.6
Tetradecane	26.7	35	21.9	48.6	— 4.8	23	24.6	51.3	Spr	9	26.4	53.1	9	26.4	53.1	0.3
Dodecane	25.4	35	20.8	46.2	— 4.6	19	24.0	49.4	Spr	Small angle						
Decane	23.9	27	21.3	45.2	— 2.6	5	23.8	47.7	Spr							
Nonane	22.9	26	20.6	43.5	— 2.3	Spr			Spr							
Heptane	20.3	8	20.1	40.4	— 0.2	Spr			Spr							
Hexane	18.4	Spr														
di(<i>n</i> -alkyl)Ethers																
Octyl	27.7	43	20.3	48.0	— 7.4	29	24.2	51.9	Spr	16	26.6	54.3	16	26.6	54.3	1.1
Heptyl	27.0	41	20.4	47.4	— 6.6	22	25.0	52.0	Spr	9	26.7	53.7	9	26.7	53.7	0.3
Amyl	24.9	33	20.9	45.8	— 4.0	9	24.6	49.5	Spr							
Butyl	22.8	25	20.7	43.5	— 2.1	Spr			Spr							
Propyl	20.5	8	20.3	40.8	— 0.2	Spr			Spr							
Ethyl	17.0	Spr														
Miscellaneous																
Water	72.8	100	— 12.7	60.1	— 85.5	94	— 5.1	67.7	Spr	90	— 0	72.8	Spr	93	— 3.8	— 70.6
Glycerol	63.4	96	— 6.7	56.7	— 70.1	87	3.2	66.6	Spr	82	8.8	— 64.6	Spr	85	5.5	— 57.9
Formamide	58.2	91	— 1.0	57.2	— 59.2	75	15.1	73.3	Spr	82	8.1	— 60.1	Spr	79	11.1	— 47.1
Methylene iodide	50.8	84	5.3	56.1	— 45.5	76	12.3	63.1	Spr	64	22.3	— 28.5	Spr	69	18.2	— 32.6
α -Brom naphthalene	44.6	67	17.4	62.0	— 27.2	63	20.3	64.9	Spr	48	23.8	— 14.8	Spr	50	22.3	— 22.3
Tricresyl phosphate	40.9	67	16.0	56.9	— 21.2	56	22.9	63.8	Spr	44	29.4	— 11.5	Spr	55	23.5	— 17.4
Tricresyl phenylundecanoate	37.7	64	16.5	54.2	— 24.9	54	22.2	59.9	Spr	37	30.1	— 7.6	Spr	58	23.2	— 12.5
<i>tert</i> -Butyl naphthalene	33.7	55	19.3	53.0	— 14.4	45	23.8	57.5	Spr	18	32.1	— 1.6	Spr	39	26.2	— 7.5
di(2-Ethylhexyl)phthalate	31.2	54	18.3	49.5	— 12.9	39	24.2	56.4	Spr	6	31.0	— 0.2	Spr	32	26.5	— 4.7
Benzene	28.8	45	20.4	49.2	— 8.4	25	26.1	54.9	Spr				Spr	20	27.1	— 1.7
Polymonochlorotrifluoroethylene ^a	25.0	Spr							Spr				Spr			
Perfluorinated hydrocarbon ^b	20.2	Spr							Spr				Spr			
Polymethylsiloxane (35 cst.)	19.9	20	18.7	38.6	— 1.2				Spr				Spr			
Perfluorinated hydrocarbon ^c	18.3	Spr							Spr				Spr			
Perfluorodimethylcyclohexane	16.0	Spr							Spr				Spr			

Spr = Spreads.

^a 86.9 centistokes at 100°F. (Hooker Electrochemical Co.).^b Boiling range 60–130°C. at 10 mm. (Du Pont Co.).^c Boiling range 130–180°C. at 760 mm. (Du Pont Co.).

10–90. For the sake of brevity only the results for the 80–20 and 60–40 copolymers and Kel-F in this series will be given here. The values obtained for the intermediate copolymers formed a regular series with those presented here and can be obtained by interpolation if desired. An alternative way of describing the composition of the polymers involves consideration of the mole percent of halogen substitution, e.g., TFE contains 100 mole % fluorine and no chlorine. The 80–20 and 60–40 copolymers contain, respectively, 95.6 and 4.4 mole % fluorine and chlorine and 90.9 and 9.1 mole % fluorine and chlorine. Kel-F contains 75 and 25 mole % fluorine and chlorine, respectively. The TFE-E was a light brown, hard solid containing 50 mole % fluorine substituent, the other 50% substitution being hydrogen.

EXPERIMENTAL RESULTS

The Perhalogenated Polymers

Table I contains the measured values of the contact angle (θ_E) and also the values of $\gamma_{LV} \cos \theta_E$ (or f_{SL}), the work of adhesion (W_A), and the final spreading coefficient S_{LV}/SV calculated as indicated in Eqs. [ii], [iv], and [viii]. In each of the three groups given, the liquids have been arranged in order of decreasing surface tensions. As in the study of TFE (1), it is evident that as the liquid surface tension decreases, the contact angle on a given surface decreases and the spreading coefficient increases.

Figures 1 and 2 give the curves for cosine θ_E (and θ_E) vs. γ_{LV} and S_{LV}/SV vs. γ_{LV} , respectively, for these polymers. The curves derived

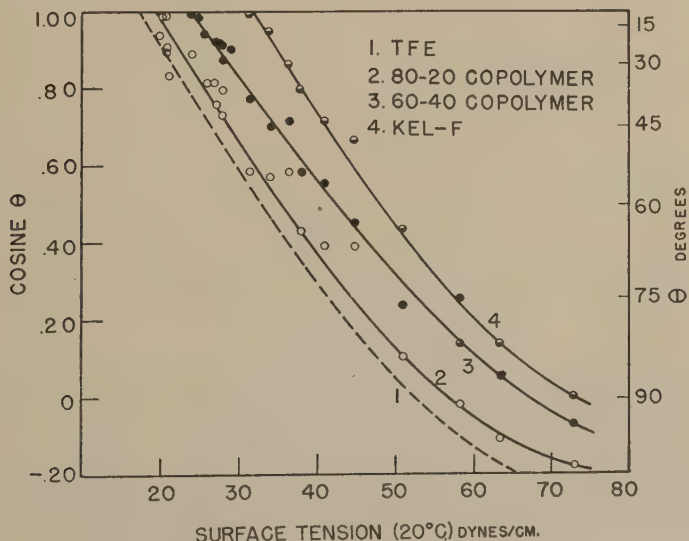


FIG. 1. Surface tension vs. cosine of the contact angle of some liquids on fluorinated polymers.

from the data on TFE (1) are included as one extreme case in this series. Although there is some scatter in the points, the individual curves are clearly delineated. In Fig. 2 the curves approach the 45° slope mentioned earlier in connection with Eq. [xii], but only in the upper portion of the curves where the points are mainly those of the *n*-alkanes and di-*n*-alkyl ethers, since f_{SL} cannot be expected to be constant for the wide variety

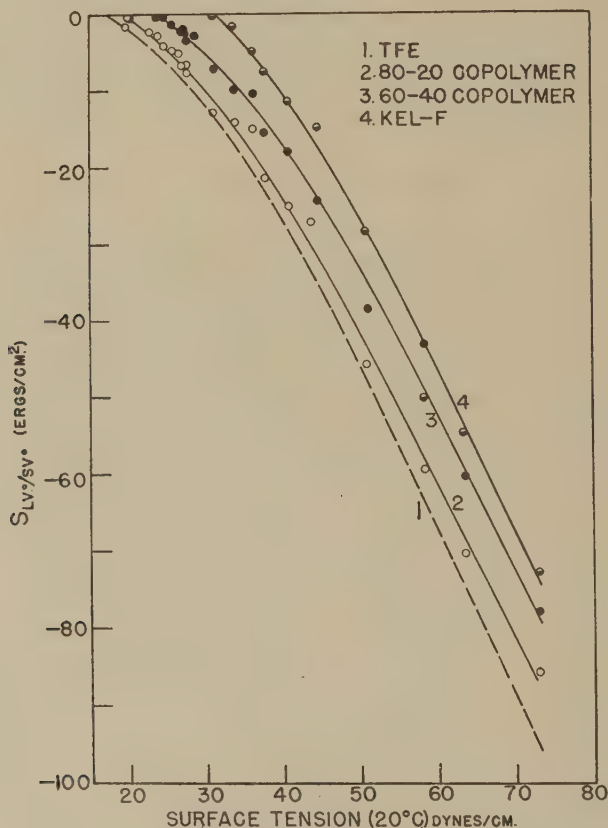


FIG. 2. Surface tension vs. spreading coefficient of some liquids on fluorinated polymers.

of liquids reported here. The intersection of each curve of Fig. 1 with the ordinate $\cos \theta_E = 1$ is equivalent to the critical surface tension (γ_c) which has been defined (1) as that value of the liquid surface tension below which liquids spread for a given polymer. Of special interest is the fact that as the chlorine content in the polymer increases, the contact angle for a given liquid decreases. A corollary to this fact is that γ_c of the polymer increases with decreasing fluorine content. Thus in the series of

polymers having increasing chlorine content: TFE, 80-20 copolymer, 60-40 copolymer, and Kel-F, the approximate values of γ_C are 18, 20, 24, and 31 dynes/cm., respectively. The intercepts of the curves of Fig. 2 with the ordinate $S_{LV^\circ}/S_V^\circ = 0$ must, of course, have the same values as γ_C . Since the S_{LV°/S_V° vs. γ_{LV° curves near the intercepts on the axis of abscissae approach straight lines having a 45° slope, it follows that the intercept on the axis of ordinates of the curves (or f_{SL}) must have the same numerical values as γ_C , at least for the alkanes. It is worth noting that a plot of f_{SL} vs. mole per cent fluorine substitution in the interpolymer

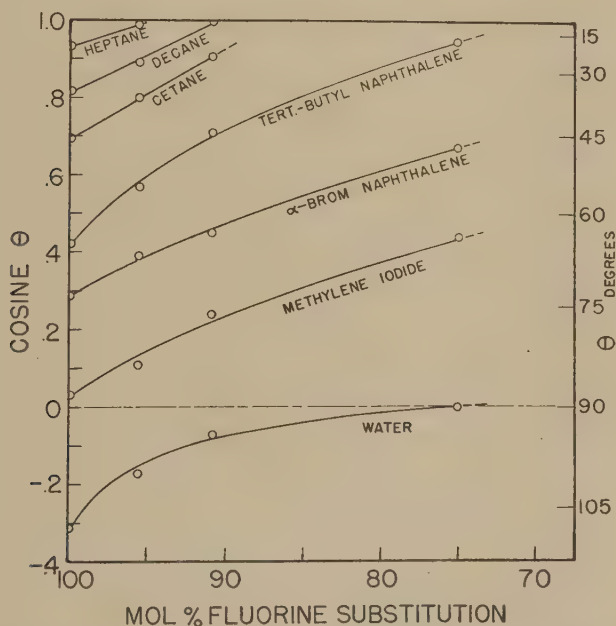


Fig. 3. Cosine of the contact angle of various liquids on fluorinated polymers vs. mole per cent fluorine substitution (remainder of substituent is chlorine).

is a straight line. Only liquid polychlorotrifluoroethylene spread on the 80-20 copolymer and 60-40 copolymer although its surface tension of 25.0 dynes/cm. was higher than the "critical" values of 20 and 24.

In Fig. 3 are plotted $\cos \theta_E$ (and θ_E) vs. mole per cent fluorine substitution in the copolymers for a number of liquids that give regular curves. With the exception of those for water and *tert*-butyl naphthalene, the graphs are approximately straight lines; the water curve appears to be nearly asymptotic at $\cos \theta_E = 0$, suggesting that the contact angle of water on these polymers will not fall much below 90° regardless of the relative proportions of fluorine and chlorine.

If the work of adhesion is plotted against the boiling point or against constitutive variables of the liquids such as molecular weight and parachor, regularities are found only in the homologous series of liquids. However, a plot of W_A for each solid against the surface tension of the liquids can be fitted approximately to one curve for all the liquids (see

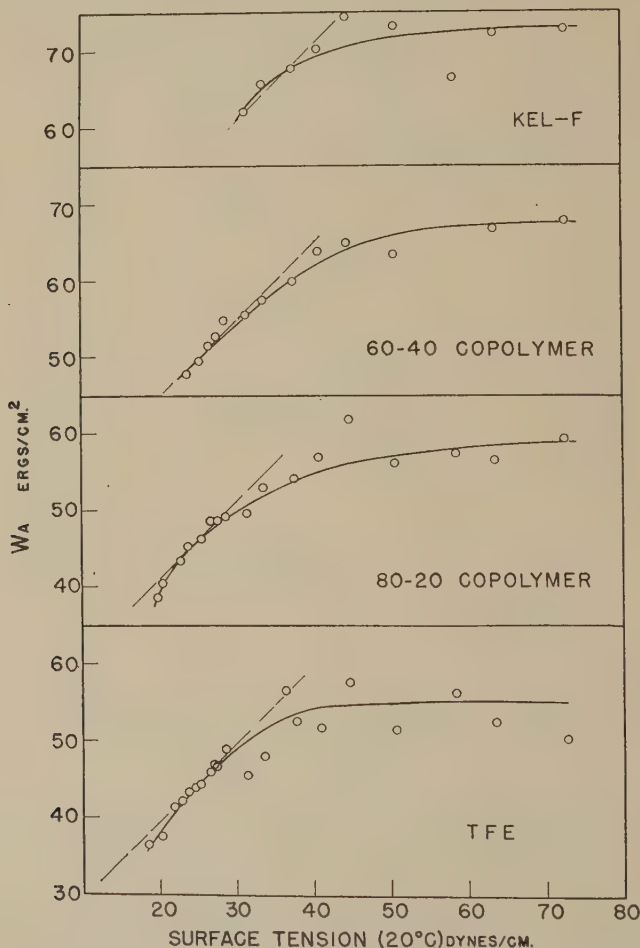


Fig. 4. Surface tension vs. work of adhesion of some liquids on fluorinated polymers.

Fig. 4). At low values of γ_{LV} the majority of the points lie on a straight line with a positive 45° slope which, according to Eq. [xi], means that f_{SL} is a constant for these liquids. In each curve there is a rise from the minimum value for each polymer, determined by γ_c (at this point $W_A = 2\gamma_{LV}$), to a fairly constant value characteristic of the polymer. The ratio of the maximum to the minimum work of adhesion for the

three polymers with the greatest fluorine content is approximately 1.5, for the TFE-E it is 1.3, and for Kel-F, it is 1.2.

When W_A is plotted against mole per cent fluorine substitution (Fig. 5), there is clearly brought out the decreased adhesion of liquids for the copolymers with increasing fluorine content. This plot also shows the effect of fluorine content on γ_c , the line connecting the W_A values corresponding to the latter for the various polymers defining the region in

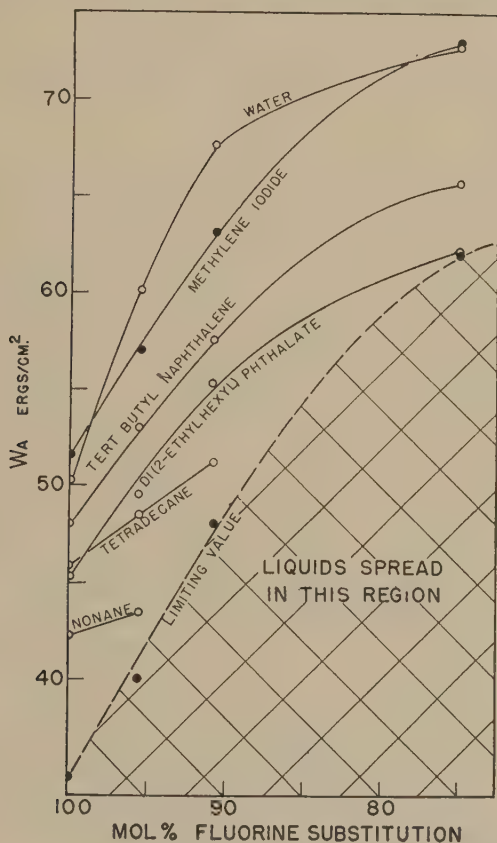


FIG. 5. Work of adhesion of some liquids on fluorinated polymers vs. mole per cent fluorine substitution in the polymers.

which liquids will or will not spread. Evidently the region for nonspreading is quite extensive at 100 mole % fluorine substitution but becomes progressively more restricted with decreasing fluorine content.

Tetrafluoroethylene-Ethylene Copolymer

The surface energy relations of TFE-E resemble closely those of the polymers containing only fluorine and chlorine substitutions. For TFE-E,

γ_C (for the *n*-alkanes) is 26–27 dynes/cm., only a little greater than the value for the 60–40 copolymer. The plot of W_A vs. γ_{LV}° for TFE-E resembles closely the curves of Fig. 4.

DISCUSSION

For the solids of this study, cosine θ_E is to a first approximation a linear function of the surface tension for each homologous series of liquids. Thus a plot of cosine θ_E vs. γ_{LV}° for the *n*-alkanes is a straight line whose slope decreases and whose intercept with the axis of ordinates increases with increasing proportion of chlorine to fluorine in the series of inter-polymers described above. At very high surface tensions the graph is concave upward.

There seems to be no important reason for all the points for a given solid to fall on a single curve when plotting the final spreading coefficient against surface tension (Fig. 2); hence these curves are useful only as empirical correlations for these solids. Equation [xii] predicts that the points for all liquids for which f_{SL} is a constant should fall on a 45° line with negative slope. This appears to be the case at low values of γ_{LV}° (*n*-alkanes and di-*n*-alkyl ethers) in Fig. 2. But f_{SL} is clearly not constant for the variety of liquids studied here so that the curves for the final spreading coefficient deviate from the 45° slope at higher surface tensions. The approximately parabolic shape of the curves of Fig. 2 are a consequence, as pointed out earlier (1), of the linear relationship of cosine θ_E and γ_{LV}° .

As chlorine increasingly replaces fluorine in the series of copolymers, the surfaces exhibit progressively a greater tendency to wet and f_{SL} increases accordingly. This is shown in Fig. 2 by the shift upward of the curves of final spreading coefficient with increasing chlorine content as predicted by Eq. [xii].

Similarly, one important feature of the curves of W_A vs. γ_{LV}° (Fig. 4) is in accordance with what could be expected from Eq. [xi]. For the homologous series of liquids it is seen that the points fall on a straight line with a 45° positive slope, the lower molecular weight members of the series deviating somewhat. As for the other liquids, the curve deviates from this line increasingly with increase in surface tension and the scatter of points from the line becomes greater. A maximum value of W_A characteristic of the polymer appears to exist which is identical with the value given by that liquid which has a 90° contact angle on the given polymer. There is no obvious explanation for this maximum value of W_A being about three times the numerical value of γ_C .

When data are available on the temperature coefficient $\frac{\partial W_A}{\partial T}$, the values of W_A given here will permit calculation of the total energy of

adhesion ϵ_A by the well known relation

$$\epsilon_A = W_A - T \frac{\partial W_A}{\partial T}. \quad [\text{xiii}]$$

When liquids are members of a homologous series, f_{SL} may be nearly constant. Thus, in the case of the n -alkanes, we have a set of liquids which are largely composed of methylene groups with a varying proportion of methyl groups. For the higher molecular weight members of this series one would expect f_{SL} to be constant since the solid is immersed in each case essentially in a polymethylene liquid. The ratio of methyl to methylene groups begins to change significantly between members of the series on going to low molecular weight homologues; hence f_{SL} can be expected to become smaller since methyl groups are more "inert" than methylene groups. In the three cases for which data are available (TFE, 80-20 copolymer, 60-40 copolymer) this is found to be the case. For liquids not in homologous series, f_{SL} will vary depending on the van der Waals forces between surface molecules of the polymer and the liquid. Other examples of the constancy of f_{SL} are found in the series of di- n -alkyl ethers where the value of f_{SL} is nearly identical with that for the n -alkanes as would be expected, and in the series of polymethylsiloxanes and TFE (1).

Attempts have been made to measure γ_{S° by means of contact angle measurements. Antonoff (5) assumed γ_{SL} to be zero for the liquid which just spreads on the solid. From Eq. [vii] this means that γ_{SV° should equal γ_C and when f_{SV° is negligible, γ_{S° should equal γ_C ; therefore, γ_C should be a constant for all types of liquid on any one solid. But in this and our previous study (1) γ_C was found to vary with the type of liquid.

Elton (6) attempted to measure γ_{S° by assuming that the interfacial tension solid/liquid equals the difference in (γ_{SA}) and (γ_{LA}) , where A refers to air. A more precise treatment shows that the relation he used should be:

$$\gamma_{S^\circ} - f_{SV^\circ} = 1/2 \gamma_{LV^\circ} (1 + \cos \theta_E). \quad [\text{xiv}]$$

Applying to [xiv] our earlier results on TFE (1) and those presented here, it appears that the right side of [xiv] varies from about 18 to 30 ergs/cm.² although for liquids within a narrow range of surface tensions only minor variations may be found. Elton obtained constant values because he did not vary sufficiently the surface tension and contact angles of his liquids. Clearly, his assumption and conclusions are not justifiable.

We have found it useful to define γ_C as that value of the liquid surface tension below which liquids will spread on the given solid. This is a

convenient concept for the solids studied here because to a rough approximation, γ_C is the same for all the liquids used. But the concept must be used with caution since, as was pointed out above, γ_C varies between liquid types. In particular, it is not valid to construe γ_C as a measure of γ_S° .

We can consider Figs. 2 and 5 plots of $(W_A - W_C) - f_{SV}^\circ$ and $W_A - f_{SV}^\circ$ against surface tension. It is interesting to consider the effect of f_{SV}° on the surface energy relations of those liquids which have low contact angles, i.e., where the assumption that $f_{SV}^\circ = 0$ is least likely to be correct. It is to be expected at any given temperature that f_{SV}° will increase as the molecular weight decreases in a homologous series of liquids which are below their critical temperatures or as the liquids come closer to spreading. Therefore, the effect to be expected from making the calculations exact by including f_{SV}° would be to straighten the curves of W_A and $W_A - W_C$ vs. γ_{LV}° near the value γ_C . But it must be noted that in this region the cosine changes so slowly with the angle that f_{SV}° would have to be unreasonably large to produce a noticeable effect on the curves.

From the linear relation of f_{SL} with mole per cent fluorine substitution, one would predict a value of about 43 ergs/cm.² for a 50 mole % fluorinated polymer of the F and Cl type. Actually, it was found that f_{SL} for the TFE-E is about 26 ergs/cm.². Hence the effect of replacing chlorine by hydrogen atoms is to decrease f_{SL} . This emphasizes the similarity of hydrogen and fluorine atoms in their contribution to the inertness or decrease in wettability of the polymers.

A point that deserves mention is that we have in this study experimental evidence of exceptions to the generalization proposed by Boyd and Livingston (3) that nonpolar liquids spread on nonpolar solids in the large contact angles observed for the *n*-alkanes, benzene, carbon tetrachloride, tetrachloroethylene, sym-tetrachloroethane, and sym-tetrabromoethane on Teflon.

SUMMARY

1. Data are presented on the equilibrium contact angles of a wide variety of liquids on specially prepared surfaces of halogenated derivatives of polyethylene. The free energy decrease of immersion (f_{SL}), the work of adhesion (W_A), and the spreading coefficients have been calculated for the liquids which do not spread. The free energy decrease on immersion of these solids in the saturated vapor of most of the liquids of this study is shown to be negligible.

2. For each solid surface the contact angle and spreading coefficient follow the relation to liquid surface tension reported previously for polytetrafluoroethylene, i.e., as the liquid surface tension increases, the contact angle increases and the spreading coefficient decreases.

3. Substitution of chlorine or hydrogen for fluorine in these polymers increases W_A , f_{SL} , and the spreading coefficient with respect to a given liquid, the increase depending on the proportion of nonfluorine substituent. Substitution of hydrogen for fluorine has a smaller effect in this respect than substitution of chlorine for fluorine.

4. It is shown that when f_{SL} for a given solid in a series of liquids is constant, the plots of W_A vs. surface tension and spreading coefficient vs. surface tension should be straight lines with positive and negative 45° slopes, respectively. The data presented for the fluorinated polymers and the liquid *n*-alkanes and di-*n*-alkyl ethers fall on such lines. The values of f_{SL} for the fluorinated polymers plot as a straight line against mole per cent fluorine substitution.

5. There appears to be a maximum value of W_A characteristic of the polymer, which is identical with the work of adhesion given by the liquid having a contact angle of 90° on the given solid.

6. It is shown experimentally that there are many exceptions to the "rule" that nonpolar liquids wet nonpolar solids.

7. From the data it is shown that recent attempts to measure the surface tension of solids by contact angle measurements alone involve unjustifiable assumptions.

REFERENCES

1. FOX, H. W., AND ZISMAN, W. A., *J. Colloid Sci.* **5**, 514 (1950).
2. BANGHAM, D. H., AND RAZOUK, R. I., *Trans. Faraday Soc.* **33**, 805, 1459 (1937).
3. BOYD, G. E., AND LIVINGSTON, H. K., *J. Am. Chem. Soc.* **64**, 2383 (1942).
4. SUMNER, C. G., *Wetting and Detergency*. Chemical Publishing Co., New York, 1937, p. 15.
5. ANTONOFF, G., *J. Phys. and Colloid Chem.* **52**, 969 (1948).
6. ELTON, G. A. H., *J. Chem. Phys.* **19**, 1066 (1951).

THE INFLUENCE OF DIFFERENCES IN MOLECULAR SIZE ON THE SURFACE TENSION OF SOLUTIONS. IV. ¹

I. Prigogine and J. Marechal ²

Faculté des Sciences, Université Libre de Bruxelles, Brussels, Belgium

Received October 26, 1951

ABSTRACT

The statistical calculation of the surface tension of solutions containing two sorts of molecules, one occupying r sites and the other one site, has been carried out for a simplified model in which only configurations of the molecules parallel to the surface are taken into account.

For this model, it is possible to deduce very simple explicit formulas, which are used for a qualitative discussion of the surface tension of polymer solutions.

INTRODUCTION

Recently statistical thermodynamics have been applied to the calculation of the surface tension of perfect (1, 2) and regular solutions (3).

The influence of differences in size of the molecules has been taken into account by I. Prigogine and his co-workers, for dimer-monomer systems (I) as well as for trimer-monomer systems (II). The generalization of these results for rigid rods of any size has also been indicated (II).

The predictions of the theory have been tested by an experimental investigation of several systems and the agreement has been found to be very satisfactory (III). However, for the different models used until now, it has proved impossible to obtain theoretical results in the form of explicit algebraic formulas. To facilitate the qualitative discussion of the surface tension of polymer solutions, we, therefore, shall examine a simplified model in which only configurations of the r -mer, parallel to the vapor-solution interface have been taken into account. We shall show in the next section that this model gives qualitatively the same results as those obtained previously (I, II).

THEORY

Consider a solution containing N_A molecules, each occupying one site, and N_B molecules, each occupying r sites of the quasi-crystalline lattice

¹ The previous papers of this series are: I. PRIGOGINE, I., *J. chim. phys.* **47**, 33 (1950); II. PRIGOGINE, I. AND SAROLEA, L. *J. chim. phys.* **47**, 807 (1950); III. MARECHAL, J., submitted for publication to the Faraday Society.

² Titulaire d'une Bourse de spécialisation de l'Institut pour l'Encouragement de la Recherche Scientifique.

($N_A + N_B = N$). Following the procedure outlined in previous papers, the solution is divided in successive layers. In the present treatment, we shall only consider configurations for which the molecules B are parallel to the vapor-solution interface. It is assumed that only the first layer has a composition different from that of the bulk phase (for the justification of this assumption cf. I, sec. 4). Molecules situated in the first layer are denoted by an index, 1. The number of first neighbors of each molecule is z in the bulk phase, lz in the same layer, and mz in each adjacent layer ($l + 2m = 1$). The partition function Z of the system may then be evaluated by the well-known Flory-Huggins' method. If f_A and f_B denote the partition functions per segment of pure components A and B , and N^c the number of sites in each layer, we obtain for the first layer

$$Z^{(1)} = \frac{(lz)^{N_B^{(1)}}}{(N^c)^{N_B^{(1)}}} \cdot \frac{1}{2^{N_B^{(1)}}} \cdot \frac{N^c!}{N_A^{(1)}! N_B^{(1)}!} \cdot f_A^{N_A^{(1)}} \cdot f_B^{rN_B^{(1)}} \quad [1]$$

and for the bulk phase

$$Z = \frac{(lz)^{N_B}}{(N^c)^{N_B}} \cdot \frac{1}{2^{N_B}} \cdot \frac{N!}{N_A! N_B!} \cdot f_A^{N_A} \cdot f_B^{rN_B} \quad [2]$$

In the first layer, the thermodynamic potential, $G^{(1)}$, corresponding to the variables T , p , σ , and the number of moles³ is given by

$$G^{(1)} = F^{(1)} + pV - \sigma\Omega \approx F^{(1)} - \sigma\Omega = -kT \ln Z^{(1)} - \sigma\Omega, \quad [3]$$

where Ω is the surface area and σ the surface tension. For the bulk phase, we have

$$G = F + pV \approx F = -kT \ln Z. \quad [4]$$

By derivation of the free energies we obtain

$$\begin{aligned} \mu_A^{(1)} = \left(\frac{\partial G^{(1)}}{\partial N_A^{(1)}} \right)_{T, p, \sigma} &= kT \ln \frac{N_A^{(1)}}{N_A^{(1)} + rN_B^{(1)}} \\ &+ kT (r-1) \frac{N_B^{(1)}}{N_A^{(1)} + rN_B^{(1)}} - kT \ln f_A^{(1)} - \sigma\omega \end{aligned} \quad [5]$$

$$\begin{aligned} \mu_A = \left(\frac{\partial G}{\partial N_A} \right)_{T, p} &= kT \ln \frac{N_A}{N_A + rN_B} \\ &+ kT (r-1) \frac{N_B}{N_A + rN_B} - kT \ln f_A \end{aligned} \quad [6]$$

$$\begin{aligned} \mu_B^{(1)} = \left(\frac{\partial G^{(1)}}{\partial N_B^{(1)}} \right)_{T, p, \sigma} &= -kT \ln lz + kT \ln \frac{N_B^{(1)}}{N_A^{(1)} + rN_B^{(1)}} \\ &+ kT (r-1) \frac{rN_B^{(1)}}{N_A^{(1)} + rN_B^{(1)}} - rkT \ln f_B^{(1)} - r\sigma\omega \end{aligned} \quad [7]$$

³ For a discussion of the thermodynamic potential G^1 corresponding to the variables p , T , σ , and the number of moles, see R. Defay and I. Prigogine (4).

$$\mu_B = \left(\frac{\partial G}{\partial N_B} \right)_{T,p} = -kT \ln lz + kT \ln \frac{N_B}{N_A + rN_B} + kT(r-1) \frac{rN_B}{N_A + rN_B} - rkT \ln f_B, \quad [8]$$

where ω denotes the area per segment at the surface.

Henceforth the volume fractions appearing in Eqs. 5-9, will be expressed by $\varphi_A^{(1)}$ and $\varphi_B^{(1)}$ for the first layer and by φ_A and φ_B when referring to the bulk phase, according to

$$\varphi_A^{(1)} = \frac{N_A^{(1)}}{N_A^{(1)} + rN_B^{(1)}}, \quad \varphi_B^{(1)} = \frac{rN_B^{(1)}}{N_A^{(1)} + rN_B^{(1)}} \\ \varphi_A = \frac{N_A}{N_A + rN_B}, \quad \varphi_B = \frac{rN_B}{N_A + rN_B}.$$

At the adsorption equilibrium,

$$\mu_A^{(1)} = \mu_A \quad \text{and} \quad \mu_B^{(1)} = \mu_B. \quad [9]$$

From the equality of chemical potentials, we obtain two equations for the surface tension and for the composition of the monolayer (Eqs. 10 and 11)

$$\sigma\omega = kT \ln \frac{\varphi_A^{(1)}}{\varphi_A} + kT(r-1) \frac{\varphi_B^{(1)} - \varphi_B}{r} - kT \ln \frac{f_A^{(1)}}{f_A} \quad [10]$$

$$\sigma\omega = \frac{kT}{r} \ln \frac{\varphi_B^{(1)}}{\varphi_B} + kT(r-1) \frac{\varphi_B^{(1)} - \varphi_B}{r} - kT \ln \frac{f_B^{(1)}}{f_B}. \quad [11]$$

By applying [10] and [11] to pure components *A* and *B*, respectively, we get

$$\sigma_A\omega = -kT \ln \frac{f_A^{(1)}}{f_A} \quad \text{and} \quad \sigma_B\omega = -kT \ln \frac{f_B^{(1)}}{f_B}.$$

The equation for the composition of the monolayer may be written in the form

$$e^{\frac{\omega(\sigma_A - \sigma_B)}{kT}} \cdot \frac{(\varphi_B)^{1/r}}{(1 - \varphi_B)} = \frac{(\varphi_B^{(1)})^{1/r}}{(1 - \varphi_B^{(1)})}. \quad [12]$$

If r is sufficiently large, we have

$$(\varphi_B)^{1/r} = (\varphi_B^{(1)})^{1/r} = 1 \quad (\text{if } \varphi_A \text{ and } \varphi_B \neq 0)$$

and hence for the surface tension

$$(\sigma - \sigma_A)\omega = -(\sigma_A - \sigma_B)\omega + kT \frac{r-1}{r} (1 - e^{-\frac{\omega(\sigma_A - \sigma_B)}{kT}}) \varphi_A. \quad [13]$$

Furthermore, is $\left[\frac{\omega(\sigma_A - \sigma_B)}{kT} \right] \ll 1$, Eq. [13] becomes

$$\sigma = \sigma_A \varphi_A + \sigma_B \varphi_B. \quad [14]$$

We thus see that for the first approximation, there is additivity with respect to the volume fractions, whereas for perfect solutions there is additivity with respect to the mole fractions. An approximation in which terms of the order of $1/r$ are retained has also been worked out, but, as the correction terms are very small, even for $r = 10$, the calculations will be omitted. Furthermore we have worked out a series of computations which clearly demonstrate that for given values of σ_B , σ_A , and r , the surface tensions σ are almost identical, whatever the model used for the evaluation. As an example, the diagram represents the results for a 10-1

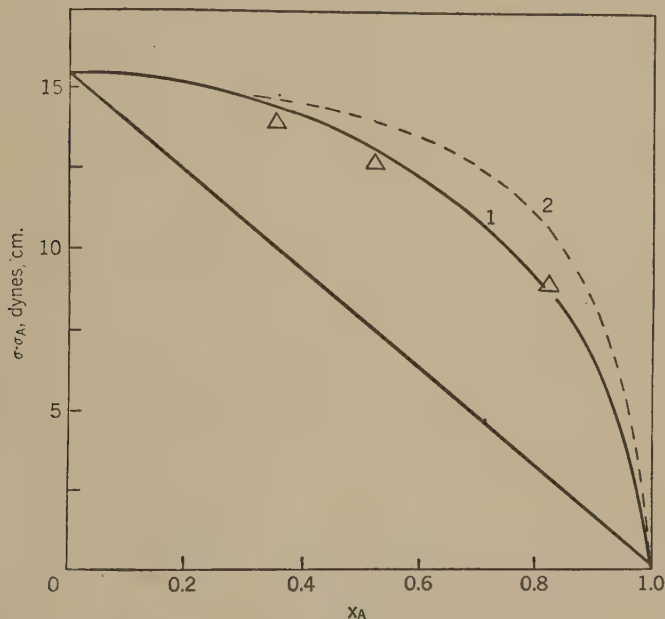


FIG. 1. For a 10-1 system: Curve 1: Calculated by considering molecules as rigid rods (cf. II). Δ : points calculated from [12] (graphic resolution) and [10]. Curve 2: Calculated from [14]. Values of the parameters used are (cf. II):

$$\sigma_B - \sigma_A = 15.29 \text{ dynes/cm.}; \quad \omega = 27.3 \text{ \AA}^2 \quad T = 343^\circ\text{K.}$$

system, calculated by means of the new model and by the model in which the molecules are considered as rigid rods. The curve calculated by the law of additivity [14] is also given (Fig 1). It is seen that this last equation gives results which agree for the first approximation.

DISCUSSION

The use of the model described in this paper leads to a simple explicit expression for the surface tension,

$$\sigma = \sigma_A \varphi_A + \sigma_B \varphi_B \quad [14]$$

valid as a first approximation. This is very similar to the law for perfect solutions

$$\sigma = \sigma_A x_A + \sigma_B x_B, \quad [15]$$

where x_A and x_B are the mole fractions.

As we do not know of any experimental determinations of surface tensions for polymer solutions which would permit a test of Eq. [14], we shall limit ourselves to a short qualitative discussion. It is seen immediately from [14] that when the surface tension of the polymer is greater than that of the solvent, $\sigma_B - \sigma_A > 0$, there is an increase of the surface tension with respect to the linear law [15] in mole fractions. If however the surface tension of the solvent is greater, $\sigma_B - \sigma_A < 0$, the surface tension of the solution is lowered in comparison with the linear law. When the difference between the surface tensions of pure A and B becomes appreciable $\left(\left[\frac{\omega(\sigma_A - \sigma_B)}{kT} \right] \text{ not negligible with respect to } 1 \right)$, the first layer is enriched in the component with lower surface tension, and consequently the surface tension of the solution is lowered with respect to the additive law in volume fractions [14]. This is very similar to the behaviour of the perfect solutions.

An interesting extreme case is that of aqueous solutions. As for these systems the difference between the surface tension of the pure component is large, $\sigma_A \gg \sigma_B$, the lowering with respect to the linear law [15] in mole fraction will be appreciable. Also, the effect of the heat of mixing is to lower the surface tension for solutions which mix with absorption of heat (II), although this effect becomes relatively less important with increasing r as shown in (II). Another point concerns the parallelism between deviations of the surface tension from additivity [15] and deviations of vapor pressure from Raoult's law. Several authors⁴ have directed attention to the existence of a rule which indicates that the deviations with respect to the linear law have opposite signs for surface tension and for vapor pressure. This rule is verified for almost all known systems. The present work shows one case where this rule is certainly not valid. Indeed, solutions of molecules, sufficiently different in size, will show at the same time negative deviations from Raoult's law for the vapor pressure (a result of the high positive excess entropy of mixing), and negative deviations for surface tension, when the surface tension of the r -mer is lower than that of the solvent ($\sigma_B < \sigma_A$).

We have found an example of this case during preliminary investigation of the surface tension of solutions of liquid methyl silicones in

⁴ See R. Defay and I. Prigogine (4). Original papers are: YAJNIK, N. A., *et al.*, *J. Indian Chem. Soc.* **3**, 63 (1926); DEFAY, R., AND PRIGOGINE, I., *Bull. soc. chim. Belges* **53**, 115 (1944).

benzene ($\sigma_B - \sigma_A < 0$). The surface tension of these systems is considerably smaller than that predicted by the linear law [15] in mole fractions.

REFERENCES

1. SCHUCHOWITSKY, A., *Acta physicochim. U.R.S.S.* **19**, 176 (1944).
2. BELTON, J. W., AND EVANS, M. G., *Trans. Faraday Soc.* **41**, 1 (1945).
3. GUGGENHEIM, E. A., *Trans. Faraday Soc.* **41**, 150 (1945).
4. DEFAY, R., AND PRIGOGINE, I. Tension superficielle et adsorption. Desoer, Liège, 1951.

EFFECT OF ELECTROLYTES ON THE VISCOSITY OF POTATO STARCH PASTES

G. C. Nutting

Eastern Regional Research Laboratory,¹ Philadelphia, Pennsylvania

Received November 19, 1951

INTRODUCTION

A most important property of all starches is their ability to swell in hot water to form viscous liquids, or pastes. This property is utilized whenever starch is used as a thickening or gelling agent, a coating or sizing material, or an adhesive. Among the commercial starches potato starch swells the most, thereby giving the most viscous and unstable pastes, and is also the most variable. It is now evident that these distinctive qualities arise largely because potato starch is a polyelectrolyte. Its electrolyte properties are conferred by dihydrogen-orthophosphate groups in ester combination with the branched amylopectin fraction of the starch. Thus combined, the phosphate groups have substantially the same dissociation properties as the first and second hydrogens of ordinary phosphoric acid (1).

The phosphorus content of native potato starch is variable, but usually lies in the range 0.06–0.10%. This corresponds to one phosphate group to roughly 400 glucose residues in the whole starch, or to 300 residues in the amylopectin. At the normal potato starch pH of around 6.5, three-fourths of the phosphoric acid hydrogens are replaced by metal ions, principally potassium. When the starch is pasted its electrolyte groups ionize, leaving the carbohydrate with a negative charge. Repulsion of the negative amylophosphate ions greatly opens up the branched amylopectin molecules and increases their solvation. Compared with an electrically neutral starch this has the result that the pasted granules are larger and the starch paste viscosity is higher but sensitive to small concentrations of added electrolyte. Forty years ago Samec (2) noted that potato starch sols and pastes are electroviscous, and correctly associated the electroviscosity with the starch-phosphoric acid. Other notable reports on potato starch-electrolyte interaction have been made by Bungenberg de Jong (3), Ripperton (4), and Wiegel (5).

The cations of potato starch are easily exchangeable by others (6,7). In the experiments described here a series of such modified starches was

¹ One of the laboratories of the Bureau of Agricultural and Industrial Chemistry, Agricultural Research Administration, United States Department of Agriculture.

prepared, with sodium, potassium, ammonium, hydrogen, and calcium as cations. The viscosity of pastes made from these starches was measured, and effects of pH and added electrolyte were observed. Viscosity and starch granule swelling were related by means of photomicrographs.

EXPERIMENTAL

Preparation of Modified Starches

Starting material was a high grade commercial potato starch (Aroos-toocrat Brand). In this, as in commercial potato starches generally, the original potassium had been largely replaced by calcium during manufacture. Exploratory experiments, in which the natural potassium starch was prepared from potatoes in the laboratory, indicated no advantage over the commercial starch. To make the cation modified starches, kilogram portions of the parent starch were soaked 2 hours in 0.5 *N* solutions of either sodium, potassium, ammonium, calcium, and hydrogen chlorides, or in 3.8% "sodium hexametaphosphate" (Calgon, used as the grade, Medi-Calgon). The starches were washed repeatedly with distilled water, then with 95% ethanol, absolute methanol, and were dried at room temperature in a current of filtered air. For all but the hydrogen starch the conductivity of 1% pastes was equivalent to that of 1 to 3×10^{-4} *N* KCl. This magnitude is appropriate for the starch-phosphoric acid and associated cations, and suggests that any residue of uncombined electrolyte was negligible in amount. For the hydrogen starch, owing doubtless to the extraordinary mobility of hydrogen ion, the paste conductivity was equivalent to 8×10^{-4} *N* KCl. From the phosphorus content of the hydrogen starch, 0.09%, it may be computed that the (combined) phosphoric acid concentration in the 1% paste was 3×10^{-4} molar. The paste pH was 3.6, corresponding to a hydrogen ion concentration of 2.5×10^{-4} *N*. The hydrogen starch, then, likewise seemed free from appreciable amounts of foreign electrolyte. It was considered that potato starch could not be electrodialed free from electrolytic contaminants without spoiling it for the intended application. For as the metal ions are replaced by hydrogen ions during the necessarily prolonged electro dialysis the pH drops to about 3.5, so hydrolysis or at least damage to granule structure is to be anticipated.

Preparation of Starch Pastes

For viscosity measurements pastes were prepared at two concentrations, 0.4% and 1%. To make a 0.4% paste, 4.5 g. of distilled water was added to a 0.4 g. starch sample, and to this slurry 95 g. of distilled water at 100° was added almost instantaneously. The paste was swirled, kept at 100° without further agitation for 30 min., then transferred to a water bath at 30° for at least $\frac{1}{2}$ hour before filling the capillary viscosimeter,

which was kept and used in the same 30° bath. The 1% pastes were made analogously, with slurries composed of 1 g. of starch and 4 ml. of water. After addition of the boiling water the paste was put in a 90° bath for about 5 min. The viscosimeter was then filled and viscosities at 90° measured over periods of 2 to 4 hours.

Viscosity Measurement

Starch pastes are non-Newtonian fluids. So marked is their structural viscosity that Ostwald type viscosimeters even of the same ASTM series—and thus with about the same capillary diameter—cannot be used interchangeably as they can for ordinary liquids. To further illustrate how sensitive starch pastes are to rate of shear, the apparent viscosity of both potato and corn starch pastes was roughly ten times higher when measured with a Brookfield (torsional) viscosimeter, using the most appropriate rotor and rotational speed, than with a capillary viscosimeter. All the viscosities reported here were measured in a single ASTM series 300 pyrex viscosimeter, whose calibration constant was 0.1887. Flow times ranged from 6 sec. to almost half an hour. Over-all reproducibility of paste viscosity observations was ordinarily $\pm 5\%$ or better. Viscosity lowering by electrolyte dissolved from the viscosimeter was apparently unimportant for freshly made pastes, since decreases in flow time with less than 10^{-4} *N* added electrolyte were easily measured both with the Ostwald viscosimeter and with the Brookfield viscosimeter, whose parts in contact with the starch paste were made of stainless steel. An effect possibly assignable to electrolyte dissolved from the glass capillary was the viscosity decrease on standing at 90° shown by pastes made from several of the regenerated potato starches. This decrease was considerably greater than Wiegel (5,8) observed with a silica viscosimeter and more like that observed with a viscosimeter made from Thuringia glass. Alternatively, the pronounced viscosity decrease may simply be an expression of the conditions of pasting, since Wiegel also noted high initial but unstable viscosity when pasting was done rapidly (5).

RESULTS

Figure 1 shows the variation of viscosity with duration of pasting at 90° for four 1% pastes. Viscosity is expressed as "apparent centistokes," computed as the product of flow time and viscosimeter constant for normal fluids. The parent commercial potato starch (Curve 3) had a low paste viscosity which fell only slightly during three hours. The derived sodium starch (Curve 2) had an initial viscosity over ten times as high. The viscosity fell rapidly, from 280 to 60 in an hour and a half, but during the period of observation was always more than three times that of the parent starch. "Calgon starch" (Curve 1) had an even higher viscosity

than the sodium starch, and was similarly unstable. Pasting the Calgon starch in 0.00125 *N* CaCl₂ reduced the viscosity to a very low constant value (Curve 4) not much greater than that for water. Other starches and other electrolytes at equivalent concentration gave comparably short flow times (10 sec.). A distilled water paste of the Calgon starch, initially clear and viscous, was made 0.0025 *N* in Na⁺. Instantly the paste became cloudy and its viscosity dropped to a stable value of 3. The granule sacs of the original paste were shrunk in the electrolyte, but because of their

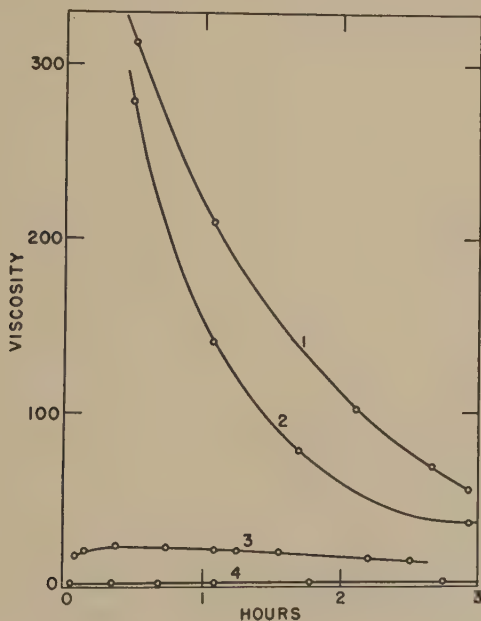


FIG. 1. Viscosity of 1% potato starch pastes at 90°C. 1. Calgon-treated starch. 2. Sodium starch. 3. Parent commercial starch. 4. Calgon-treated starch pasted in 0.00125 *N* calcium chloride. Viscosity is expressed as "apparent centistokes."

irregular form a quantitative estimate of the magnitude of the shrinkage was not attempted (9).

The 0.4% pastes at 30° were much more stable with respect to time, and the single viscosity values given in Table I are characteristic for the particular samples of modified starches. The hydrogen starch paste was measured at its natural pH, 4.2, whereas the pH of the other starches was adjusted when necessary to 6.7 by means of 0.01 *N* KOH, thereby increasing the electrolyte concentration by a maximum of 4×10^{-5} *N*. The Calgon starch paste viscosity was more than twice as high as that of any other starch. A pure calcium starch gave a higher viscosity than the parent commercial starch, presumably because the commercial starch

was contaminated with a small amount of soluble electrolyte and this depressed the viscosity. Potassium chloride at 10^{-4} *N* concentration reduced the potassium starch viscosity from 25.7 to 7.0. Borax, which at higher starch concentrations increases viscosity (10), lowered the viscosity of dilute potato starch pastes just as any other electrolyte. Microscopic examination showed that the hydrogen starch granules were largely destroyed in the pasting at pH 4. This leads to the inference that the major reason for the low paste viscosity was the diminished size of the flowing units due to solution or granule breakup rather than granule swelling hindered by electrolyte.

TABLE I
Viscosity of Starch Pastes at 30°C.

	pH	Viscosity "apparent centistokes"
Potato starches, 0.4%		
"Calgon"	6.7	100.3
Ammonium	6.7	38.7
Sodium	6.7	31.5
Potassium	6.7	25.7
Calcium	6.7	12.5
Parent commercial	6.7	8.5
Hydrogen	4.2	3.0
Potassium, in 10^{-4} <i>N</i> KCl	6.7	7.0
Potassium, in 10^{-4} <i>N</i> CaCl ₂	6.5	5.9
Potassium, in 10^{-3} <i>N</i> KCl	6.5	2.5
Sodium, in 10^{-3} <i>N</i> Na ₂ B ₄ O ₇	9.5	2.5
Sodium, in 2×10^{-3} <i>N</i> NaCl	9.5	2.1
Waxy maize starch, 1%	5.7	6.6
Waxy maize starch, 1%	10.0	16.0
Waxy maize starch, 1%, in 10^{-3} <i>N</i> NaCl	6.2	8.3
Tapioca starch, 1%	6.0	7.3
Tapioca starch, 1%	10.0	13.2
Tapioca starch, 1%, in 10^{-3} <i>N</i> NaCl	5.4	6.9

Figure 2 shows the large effect of pH on the viscosity of sodium starch pastes. The pH was changed by adding KOH or HCl to the pastes after cooling to 30° in order to minimize granule damage and hydrolysis. The pH-viscosity curve rises almost symmetrically from values near 4 at pH 4 and 12 to a maximum viscosity of 40 at pH 8.4. At pH 2 the starch is practically unionized and the paste viscosity is nearly as low as that of water. As the pH rises, starch ionization increases, and with it the viscosity. According to Briggs and Hanig (1) the second hydrogen of amylophosphoric acid is neutralized at pH 8.75, but at higher pH alkali continues to react with starch, possibly by combining with the slightly acidic glucoside hydroxyls. Further development of charge by this mechanism

could conceivably increase the potato starch electroviscosity still more. Experience showed instead that the viscosity decreased markedly above pH 8.4. To raise the paste pH from its normal value to 10, the additional cation introduced as KOH amounted to roughly $5 \times 10^{-4} N$, and this induced the viscosity decrease expected of $5 \times 10^{-4} N$ NaCl or other electrolyte.

Negative ionization of glucoside hydroxyls and correspondingly increased viscosity apparently was realized with 1% pastes of waxy maize and tapioca starches. At normal pH these are nonelectrolytes and have nearly the same viscosity in $10^{-3} N$ NaCl as in water, but the viscosity

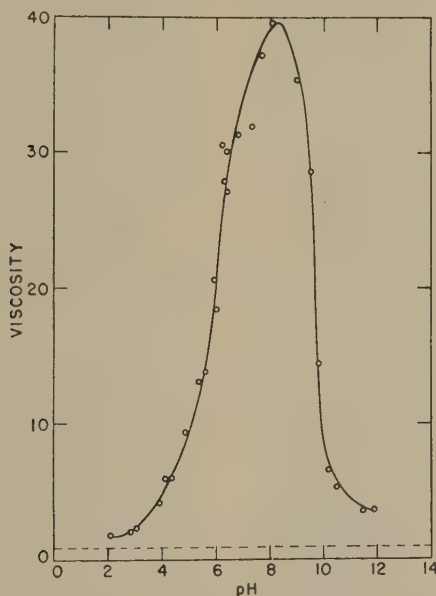


FIG. 2. Effect of pH on the viscosity of 0.4% sodium starch pastes at 30°. The dotted line represents the viscosity of water. Viscosity is expressed as "apparent centistokes."

of both starches doubled as the pH was raised from 6 to 10 (Table I). Equivalent behavior expected of potato starch pastes was masked by the predominant electroviscous effect of the phosphate ions.

Changes in granule appearance on pasting in water and in dilute electrolytes are shown in the photomicrographs of Figs. 3 and 4. Figure 3a is unpasted commercial potato starch. All the unpasted potato starches had a similar appearance. Figures 3b, c, and d, made at the same magnification, are, respectively, sodium starch pasted in distilled water, sodium starch pasted in $0.001 N$ CaCl_2 , and ammonium starch pasted in distilled water. All were pasted $\frac{1}{2}$ hour in a boiling water bath at 0.4% concentration, and were then diluted to a concentration suitable for micrography

with 8 volumes of a saturated solution of iodine in distilled water. Iodine stains preferentially the amylose component of the starch. It stains the granule sacs, the liquid contents and the suspending liquid, showing the presence of amylose in all, and reveals much more detail in the structure than is possible without the stain. Iodine has the important disadvantage, however, that while it stains it also partially de-swells the pasted gran-

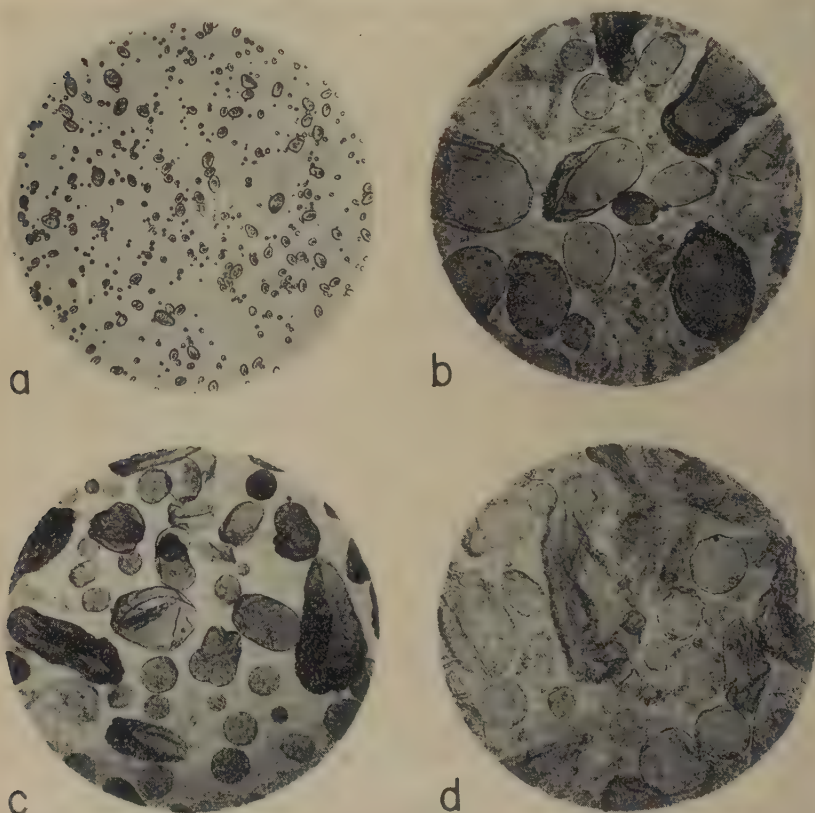


FIG. 3. Photomicrographs of potato starches. (a) Commercial starch, not pasted. (b) Sodium starch pasted in water, diluted with I₂ solution. (c) Sodium starch, pasted in 0.001 *N* CaCl₂, diluted with I₂ solution. (d) Ammonium starch, pasted in water, diluted with I₂ solutions. Magnification 36 \times .

ules; the viscosity of pastes diluted with iodine solution is considerably less than the viscosity of pastes diluted with water alone, and the average granule size is smaller. It may be surmised that the action of the iodine solution is twofold: action of electrolyte in the iodine solution on the amylopectin, and action of the iodine itself in forming the helical complex with amylose (11). Both would have the effect of shrinking the carbo-

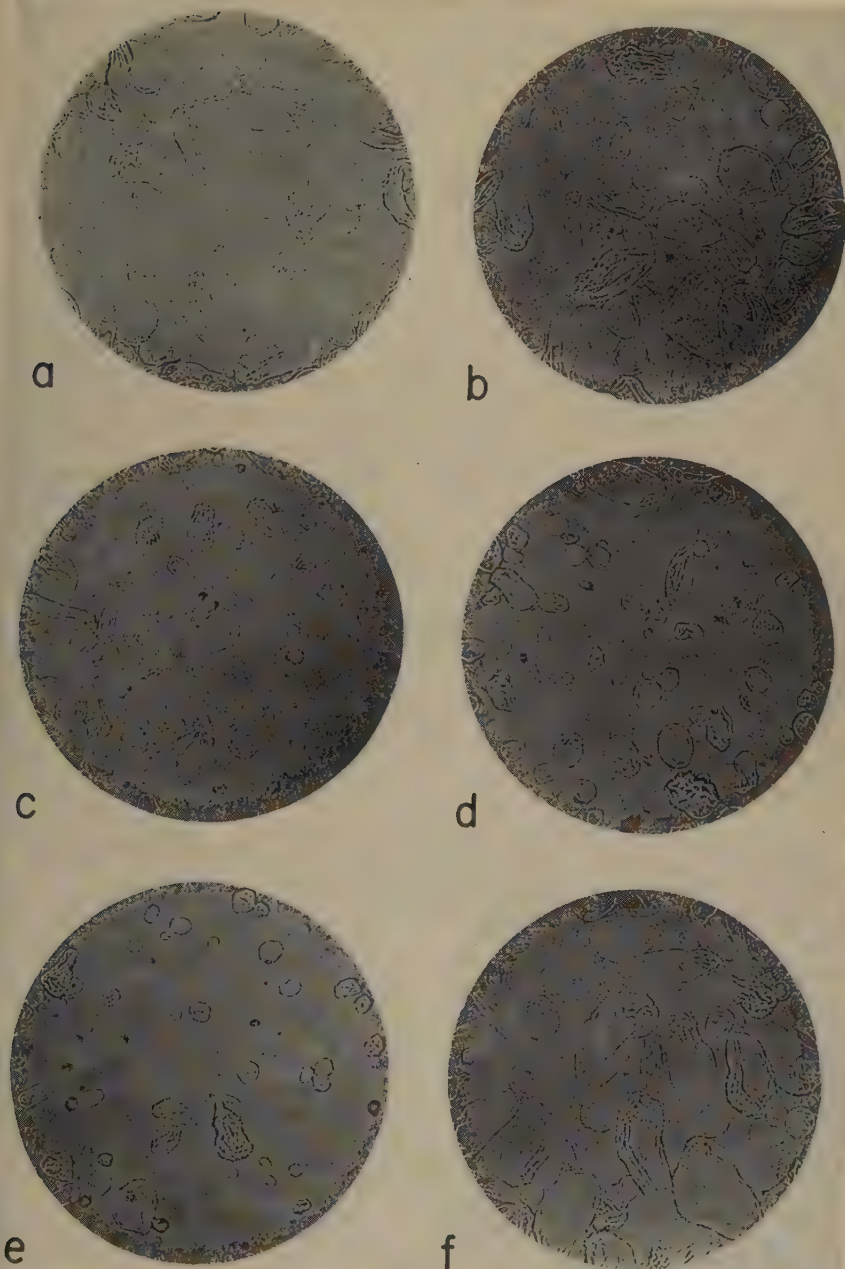


FIG. 4. Photomicrographs of pasted potato starches; 0.008% concentration; not stained. (a) Sodium starch. (b) Calcium starch. (c) Sodium starch pasted in 0.001 *N* NaCl. (d) Sodium starch pasted in water, then made 0.001 *N* in NaCl. (e) Sodium starch pasted in 0.001 *N* $\text{Pb}(\text{NO}_3)_2$ at pH 6.1. (f) Calgon starch. Magnification 29 \times .

hydrate. For photomicrography the stained pastes were contained in a cell $220\ \mu$ thick. A comparison of Fig. 3*b*, *c*, and *d* with *a* shows the large increase, amounting to five- or tenfold, in linear dimensions of the granules on pasting. The smaller pasted granules are approximately circular in cross-section, whereas the larger granules are progressively irregular, and at the onset of collapse the sacs develop a system of wrinkles or folds. It is obvious that the extent of swelling in CaCl_2 solution is considerably less than in water.

In Fig. 4 the photomicrographs were made at 0.008% concentration. Since many swollen granules are 100 to $200\ \mu$ or more in at least one dimension, a cell 2 mm. thick was used to avoid distortion or artifact formation due to confining the granules. The starch was not stained, with the result that at sharpest focus the contrast in the images was so slight

TABLE II
Analytical Data on the Potato Starches

Starch	Na	K	Ca	P	SiO_2	Ash	pH of 1% paste
	%	%	%	%	%	%	
1. Commercial (parent)	0.007	0.01	0.063	0.108	0.012	0.36	6.5
2. Sodium	0.07	0.002	0.01	0.104	0.013	.32	6.6
3. Calgon	0.06	—	0.005	0.088	0.02	—	5.8
4. Potassium	—	0.11	—	—	—	—	6.6
5. Calcium	—	—	0.09	—	—	—	6.9
6. Hydrogen	0.001	0.001	0.002	0.090	0.014	0.04 ^a	3.7
7. Laboratory ^b	0.003	0.07	0.006	0.096	0.007	0.29	6.1

^a Ash with magnesium acetate, 0.19%.

^b Contained also 0.04% R_2O_3 ; several other starches contained 0.03 to 0.04%; hydrogen starch contained 0.01%. Laboratory starch prepared from potatoes using only distilled water, and air dried at room temperature.

as to be unuseable. The photomicrographs were purposely made slightly out-of-focus. They thus show only the granule outlines and the major folds. Sodium and Calgon starches pasted in distilled water (4*a* and *f*) swell greatly, calcium starch (4*b*) somewhat less, and sodium starch pasted in 0.001 *N* NaCl (4*c*) very much less. The sodium starch of Fig. 4*d* was first pasted in distilled water, so that the granule swelling was comparable with 4*a*. Sodium chloride then added to a final concentration of 0.001 *N* instantly shrunk the granules, as is shown in 4*d*. Pasting the sodium starch in 0.001 *N* $\text{Pb}(\text{NO}_3)_2$ produced the least granule swelling of all (4*e*). It may be noted from Fig. 4 that smooth spherical granules are decidedly the exception.

Analytical data on some of the starches are given in Table II. In general the data agree rather well with the much more extensive analyses of Tryller (6). The principal differences are in the SiO_2 and R_2O_3 contents.

Tryller found 0.04 to 0.09% SiO_2 , whereas we found 0.007 to 0.02%; and Tryller found 0.01% R_2O_3 whereas our analyses showed about 0.04%. Noteworthy is the small total content of metal ions and ash in the hydrogen starch. The intrinsic metal and ash content of potato starch is of course variable with pH, owing to different extent of neutralization of the two replaceable hydrogens of the starch phosphoric acid. The Calgon starch contained no unusual amount of either sodium or phosphorus on which an explanation of its abnormal paste viscosity could be based.

DISCUSSION

In a starch grain the linear amylose molecules and even the branches of the globular amylopectin molecules have a generally radial arrangement extending from the hilum to the surface. This arrangement, in effect, places the three hydroxyls of each glucose residue perpendicular to the radii. When starch is heated in water, hydration of the hydroxyl groups produces enormous tangential expansion. As a rule the granule expansion is so rapid and so great that most of the starch substance goes into the balloon-like envelope or sac (often momentarily hollow) filled with water that seeps through between molecules or lamellae, or cracks or breaks (12). In this interior water there must be a greater or lesser amount of dissolved amylopectin and amylose. For a $20\ \mu$ granule which on pasting becomes $200\ \mu$ in diameter, the computed sac thickness is only 330 Å., even if it is assumed that all the starch substance goes into the sac. Owing to hydration and change in molecular shape the actual thickness is doubtless greater, but it is still very thin, correspondingly fragile and liable to be broken by simple dissolving away of the hydrated starch molecules if not by shear or other mechanical shock.

Paste viscosity correlates with the size of the flowing units that appear in photomicrographs to the extent that the more viscous pastes have the larger granules. It must be recognized, however, that the granules are considerably swollen, even in pastes whose viscosity is not much greater than the viscosity of water: such pastes as 0.4% sodium starch at pH 2, and 0.4% sodium starch in $10^{-3}\ N\ \text{Pb}^{++}$. In order that the granules might be separately visible, the photomicrographs in Figs. 3 and 4 were made at a concentration much lower than that used for the viscosity measurements. In the 0.4% and the 1% pastes the granules were presumably somewhat smaller than in the photomicrographs simply for lack of enough water to produce the maximum swelling. This is especially likely among the more viscous pastes, in which the swollen granules occupy practically the whole volume.

It is usually thought that the high viscosity of dilute potato starch pastes originates principally in the intact swollen granules, for when these are broken by vigorous stirring the viscosity drops abruptly. There may be, however, a substantial contribution to the paste viscosity by the dis-

solved starch substance. To illustrate, in one experiment the intact granules and the broken sacs were separated from a sodium starch paste by vacuum filtration through a Corning medium porosity sintered glass filter. About two-thirds of the volume was recovered in the filtrate before the filter clogged. Flow time for the original paste was 180 sec., for the filtrate, 88 sec., and for the filtrate after being made 10^{-3} *N* in KCl, 10 sec. The filtrate contained no particles visible in a microscope at 500 \times . When KCl was added to the filtrate it became much more opalescent, yet still there were no microscopically visible particles. These observations seem to indicate that starch substance dissolved from the granules and sacs occurs in units so large that by mutual hindrance as they move they develop considerable viscosity in the pastes aside from the contribution by the granules. The assumed units may be molecule aggregates or microgel particles, perhaps comparable in diameter to the wavelength of light, but invisible because they are sufficiently highly hydrated that their refractive index is almost the same as the refractive index of the medium. Dehydration by electrolyte reduces the particle size so much that mutual hindrance becomes trifling and the viscosity is correspondingly lowered. Accompanying dehydration is an increase in the refractive index difference between particle and medium, as evidenced by the heightened turbidity of the sol. The kinetic units are much larger than molecules, for solutions of potato amylopectin prepared from sodium starch are considerably less viscous and also less sensitive to the addition of electrolyte than the filtered paste at the same concentration.

In a 0.4% potato starch paste the grundmolarity of the glucose residues is only 0.025 and the concentration of esterified phosphate groups about 10^{-4} *N*. Although locally the concentration may be much higher than 10^{-4} *N*, the phosphate groups are far enough apart that there is little mutual interference with their dissociation tendency, as is shown by the titration curves for potato starch and orthophosphoric acid. Nevertheless, the phosphate ions are apparently close enough to exert appreciable electrostatic repulsion, which has the effect of expanding the amylopectin molecules and promoting their hydration. Cations from even a small concentration of added electrolyte, by clustering around the phosphate ions, neutralize their negative charge and the repulsion is no longer significant. The amylopectin molecules and larger structures of which they form a part are then dehydrated and deswelled, and the paste viscosity is reduced to a few per cent of its value in the absence of added electrolyte.

ACKNOWLEDGMENT

Thanks are expressed to C. O. Willits and associates for the starch analyses; to G. F. Oppenlander for aid in the viscosity measurements; and to R. T. Whittenberger for some of the photomicrographs.

SUMMARY

Flow times of potato starch pastes were measured in a single Ostwald viscosimeter made of pyrex glass. Concentrations were 0.4% and 1% and measurements were made at 30 and 90°C. Starches were derived by cation exchange from a high grade commercial potato starch. Under comparable conditions flow times were: "sodium hexametaphosphate" starch, 531 sec.; ammonium starch, 205 sec.; sodium starch, 167 sec.; potassium starch, 136 sec.; calcium starch, 66 sec.; parent commercial starch, 45 sec.; hydrogen starch, 16 sec.; water, 6 sec. The flow time for the potassium starch was reduced to 37 sec. in 10^{-4} *N* KCl; 31 sec. in 10^{-4} *N* CaCl₂ and 13 sec. in 10^{-4} *N* KCl. The curve of pH versus flow time has a high maximum near pH 8.5, the pH of complete ionization of the amylophosphoric acid. Pastes of tapioca and waxy maize starches, which normally are unionized and show no electroviscosity, doubled their viscosity between pH 6 and 10, possibly due to ionization of glucoside hydroxyls. A corresponding effect in potato starch pastes was apparently masked by the ordinary viscosity reduction by the cation of the base used to adjust the pH. Correlation of paste viscosity and starch granule swelling was made through photomicrographs.

Potato starch paste viscosity is related to the ionization of the small content of phosphoric acid esterified with the amylopectin component. Mutual electrostatic repulsion by the ions promotes hydration of the starch and thus increases particle volume and paste viscosity. Factors that decrease the repulsion, such as reduction of phosphoric acid dissociation at low pH, combination of phosphate ions with multivalent cations, or screening of the phosphate ions by cations of added electrolyte, diminish the hydration and paste viscosity.

REFERENCES

1. BRIGGS, D. R., AND HANIG, M., *Cereal Chem.* **23**, 277 (1946).
2. SAMEC, M., *Kolloid-Beihefte* **4**, 132 (1912).
3. BUNGENBERG DE JONG, H. G., *Rec. trav. chim.* **43**, 189 (1924).
4. RIPPERTON, J. C., *Hawaii Agr. Expt. Sta. Bulletin No. 63* (1931).
5. WIEGEL, E., *Kolloid-Z.* **67**, 47 (1934).
6. TRYLLER, H., *Chem. Ztg.* **44**, 833, 845 (1920).
7. WOLFF, O., *Chem. Ztg.* **51**, 1001 (1927).
8. WIEGEL, E., *Kolloid-Z.* **62**, 310 (1933).
9. MEYER, K. H., AND FULD, M., *Helv. Chim. Acta* **25**, 391 (1942).
10. KERR, R. W., *Chemistry and Industry of Starch*. 2nd Ed., Academic Press, New York, 1950, p. 616.
11. Reference 10, p. 170.
12. BEAR, R. S., AND SAMSA, E. G., *Ind. Eng. Chem.* **35**, 721 (1943).

THE PROCESS OF SPONTANEOUS EMULSIFICATION

M. van der Waarden

(Koninklijke/Shell-Laboratorium, Amsterdam)

Received January 2, 1952

INTRODUCTION

Some homogeneous liquid systems, consisting of hydrocarbons and interfacially-active compounds, form stable emulsions of oil in water when poured out into water and stirred very moderately. This phenomenon is called spontaneous emulsification. It should be distinguished from emulsification by addition of a solution to a liquid in which the solvent can, and the dissolved liquid cannot be molecularly dispersed; for, neither hydrocarbons nor the interfacially-active substances concerned can be molecularly mixed with water. The phenomenon under discussion should also be distinguished from emulsification by pouring out a solution of acids in hydrocarbons into an alkaline aqueous solution; such processes may be referred to as a chemical emulsification, because they involve a reaction—in this case a neutralization reaction—at the oil-water interface.

Whereas the phenomena of spontaneous emulsification can be more accurately observed in the microscope, e. g., by application of the phase contrast method (1), information on its mechanism can only be obtained by examination of the systems before and after spontaneous emulsifications. The present paper deals with the spontaneous emulsification of systems of hydrocarbons and sodium alkylarylsulfonates. In a previous paper (2) the conclusion was that the sulfonates in such systems are present as micelles strongly departing from the spherical form, possibly consisting of more or less flexible, plate-shaped, double layers of sulfonate molecules, the sulfonate groups being present between the layers.

In the present investigation it was determined to what extent, during spontaneous emulsification of these hydrocarbon sulfonate systems, the sulfonate passes into the water phase of the emulsion. Separation of the water phase from the spontaneously formed emulsion, which contains a great many, extremely small oil droplets (diameter some tens of millimicrons and larger) cannot be realized by simple means. Therefore the surface tension of the emulsion was taken as a measure of the sulfonate concentration in the water phase of the emulsion.

EXPERIMENTAL

As emulsifying, hydrocarbon-soluble substances the following were used: sodium soaps of alkyl benzenesulfonic acids (1 chain with 12, 16 and 20–22 carbon atoms, respectively) prepared¹ by alkylation of benzene with dodecene, cetene, and a narrow α -olefin fraction (b.p. 330–340°C.), respectively, and subsequent sulfonation, neutralization, and separation into fractions by recrystallization; if necessary, an alcoholic solution of the sulfonates was given an after-treatment with active carbon. The oil-soluble fractions, which will hereafter be called C₁₂-, C₁₆-, and C₂₁-sulfonates, contained, in addition to the *o*-compounds, probably a small proportion of the *p*-compounds; they were yellow to brownish yellow in color and pulverizable.

When heated to 90°C. the sulfonates are soluble to an unlimited extent in a white mineral oil (mixture of aliphatic and saturated cyclic hydrocarbons with an average mol. wt. of 320 and a viscosity of 39 cs. at 20°C.); on cooling they form clear gels or flakes in oil.

In addition, a purified sodium naphthasulfonate (chiefly a mixture of alkyl benzene (naphthalene) sulfonates), described earlier (2), was used, as well as some fractions of it, isolated by extracting them with an aromatic-free 60/80 gasoline from a solution of the naphtha sulfonate in alkaline 50% ethanol.

With the sulfonate solutions in white mineral oil, oil-in-water emulsions were prepared

a) by dropping the emulsible oil at a suitable temperature and at a steady rate into a beaker of specified dimensions, containing a given quantity of twice distilled water, while stirring mechanically at a very moderate rate and under steady conditions (spontaneous emulsification);

b) by very slowly adding twice distilled water to the emulsible oil, while stirring after each addition until homogeneous. The system then becomes, in succession, less viscous, more viscous, gelled, plastic and turbid and, after addition of a certain quantity of water, is inverted into an oil-in-water system which is thinly liquid; after this, further dilution can take place rapidly (emulsification through phase inversion).

The surface tension (γ) of sulfonate solutions in water and of emulsions was measured at room temperature (20–24°C.) with a DuNoüy interfacial tensiometer, the corrections being made according to Harkins and Jordan (3). The procedure was regularly checked by determinations in benzene and water.

The repeatability of the measurements on emulsions was very satisfactory (differences of some tenths of a dyne). The differences between

¹ By Dr. H. W. Huyser of this laboratory.

measurements on emulsions each time freshly made from one and the same emulsible oil were somewhat greater. For sulfonate solutions in water the repeatability of measurements was very satisfactory if $\gamma < 40$ dynes/cm., poor if $\gamma > 47$ dynes/cm., and fairly satisfactory in the intermediate range.

RESULTS

1. The Surface Tension of Emulsions as a Measure of the Sulfonate Concentration in the Water Phase

The surface tension of sulfonate solutions in water and of emulsions can only be used as a measure of the sulfonate concentration in the water phase in the range of concentrations where there is a distinct relation between sulfonate concentration and surface tension, i.e., at not too high and not too low concentrations.

If the surface tension of an emulsion is determined only by that of its water phase and we mix (1) an emulsion prepared with a given simple sulfonate with (2) an aqueous solution of the same sulfonate having a surface tension equal to that of the emulsion, then the surface tension of the mixture will be the same as that of the original emulsion and the aqueous solution. According to Table I this is actually true for C_{16} - or C_{21} -sulfonate.

However, if similar observations are made with mixtures of sulfonates of widely different surface activities (C_{12} - and C_{21} -sulfonates), or with natural mixtures (naphthasulfonates), then, when emulsions and sulfonate solutions in water of equal surface tension are mixed, an increase in surface tension is found (Table I). This effect is characteristic of the presence of a mixture of surface-active substances and also of the presence of an oil-water interface; for, if the latter is absent a decrease in surface tension is observed (see Table II).

A change in surface tension after mixing emulsions with sulfonate solutions in water of the same surface tension points to a difference in composition between the water phase of the emulsion and the sulfonate solution in water. The fact that only increases are found suggests that a portion of the sulfonates showing the highest interfacial activity finds its way from the water phase into the oil-water interface, or, at this interface, is exchanged for less interfacially-active sulfonates, which is conceivable only if the water phase of the emulsion contains less of the last mentioned components than the solution of the original sulfonates in water. This means that on emulsification of the sulfonate-oil system preferably the constituents with the lowest interfacial activity (those of the lowest molecular weight) find their way into the water phase.

TABLE I
Surface Tensions (γ) of 1:1 Mixtures of Emulsions and Sulfonate Solutions in Water

Emulsions		Sulfonate solutions in water		Mixture 1:1
Composition		Composition	γ at 20°C. dynes/cm.	γ at 20°C. dynes/cm.
30% C ₁₅ -sulfonates in white oil; 20% C ₂₁ -sulfonates in white oil; 10% C ₂₁ +10% C ₁₂ -sulfonates in white oil; 10% Naphthasulfonates in white oil; 20% Naphthasulfonates fraction VIII ^a 30% C ₁₅ -sulfonates in white oil; 10% Naphthasulfonates in white oil;	0.05% em.	C ₁₅ -sulfonates in water	39.7	39.6
	0.10% em.	C ₂₁ -sulfonates in water	41.5	41.7
	1.0% em.	C ₂₁ +C ₁₂ -sulfonates 1:1 in water	39.2	43.8
	1.0% em.	Naphthasulfonates in water	41.4	44.4
	1.0% em.	Naphthasulfonates fraction VIII ^b	38.4	41.8
	0.05% em.	Naphthasulfonates in water	39.7	40.9
	1.0% em.	C ₁₅ -sulfonates in water	39.7	41.9
	1.0% em.	C ₁₅ -sulfonates in water	39.7	41.9

^a In white oil.^b In water.

TABLE II
Surface Tensions (γ) of Mixtures of Solutions of Sulfonates in Water

Sulfonate 1 dissolved in water	Sulfonate 2 dissolved in water	1:1 mixture of solutions 1 and 2		Sulfonate 1 dissolved in water	Sulfonate 2 dissolved in water	1:1 mixture of solutions 1 and 2	
		γ at 20°C. dynes/cm.	$\Delta \gamma$			γ at 20°C. dynes/cm.	$\Delta \gamma$
C ₁₅ -sulfonate γ = 38.2	C ₁₅ -sulfonate	38.2	0	C ₁₅ -sulfonate γ = 38.3	C ₂₁ -sulfonate	38.3	0
C ₁₅ -sulfonate γ = 38.2	C ₁₂ + C ₂₁ -sulfonate 8:2	γ = 38.1	-1.0	C ₁₅ -sulfonate γ = 38.3	C ₂₁ + C ₁₂ -sulfonate 8:2	37.2	-1.0
C ₁₅ -sulfonate γ = 38.2	C ₁₂ + C ₂₁ -sulfonate 5:5	γ = 38.3	-3.3	C ₁₅ -sulfonate γ = 38.3	C ₂₁ + C ₁₂ -sulfonate 5:5	36.2	-2.1
C ₁₅ -sulfonate γ = 38.2	C ₁₂ + C ₂₁ -sulfonate 2:8	γ = 38.0	-4.8	C ₁₅ -sulfonate γ = 38.3	C ₂₁ + C ₁₂ -sulfonate 2:8	34.4	-3.8
C ₁₅ -sulfonate γ = 38.2	C ₂₁ -sulfonate	γ = 38.3	-5.2	C ₁₅ -sulfonate γ = 38.3	C ₁₅ -sulfonate	33.0	-5.2

TABLE III

Surface Tensions (γ) in dynes/cm. of Sulfonate Solutions in Water

Sulfonate concentration % wt.	C ₁₂ - sulfonate	C ₁₆ - sulfonate	C ₂₁ - sulfonate
0.100	33.7	—	—
0.045	—	33.6	—
0.025	37.2	34.5	34.0
0.015	41.9	35.2	35.0
0.005	52.8	37.3	36.9
0.0025	—	44.7	38.5
0.0010	—	55.1	41.6

1% wt. C₁₂-sulfonate = 28.7 mmols/liter.1% wt. C₁₆-sulfonate = 24.7 mmols/liter.1% wt. C₂₁-sulfonate = 21.1 mmols/liter.*2. The Distribution of Sulfonate over Oil Droplets and Water Phase*

A solution of 25% wt. C₁₆-sulfonate in white mineral oil was emulsified at 90°C. in water to concentrations of 0.1–30% oil on emulsion (initial concentration) and then at once cooled to room temperature. The spontaneously formed emulsions contain a fair amount of microscopically visible droplets (1 to 5 μ). These emulsions were diluted with water to final concentrations varying between 0.02 and 5%, after which the sur-

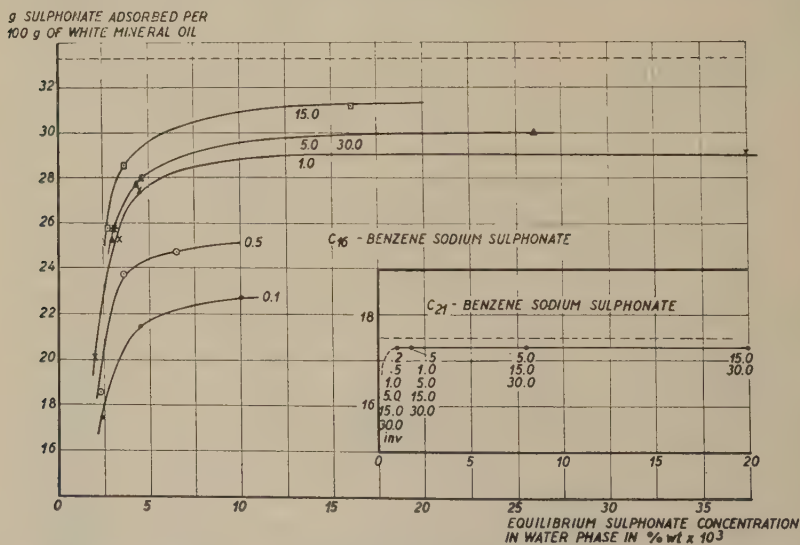


FIG. 1. Adsorption of sodium alkylbenzene sulfonates on the interface between white mineral oil and water in emulsions at room temperature (20–24°C.). The figures at the curves or the points indicate the concentration of the emulsions from which the emulsions measured are prepared by dilution. ---- = total amount of sulfonate present in the emulsion per 100 g. white mineral oil. Inv. = emulsions made by means of phase inversion.

face tensions were determined. From these surface tensions (of the water phase of the emulsion) the sulfonate concentrations in the water phases of the emulsions were derived, using the surface tension/concentration curves of the sulfonate in water (data in Table III). From these figures and from the total quantities of sulfonate in the system we calculated the quantity of sulfonate that had remained bound per 100 g. of emulsified oil, presumably almost entirely on the interface.

Similar experiments were carried out with emulsions prepared by emulsifying a 15% solution of C_{21} -sulfonate in white mineral oil in water at 70°C., to 0.2–30% (initial concentrations). The emulsions, which contain only few microscopically visible particles, were then diluted to final

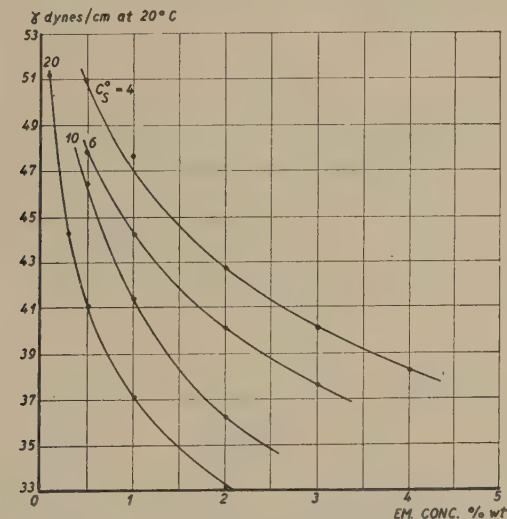


FIG. 2. Relation between surface tension and emulsible oil concentration of emulsions made by means of phase inversion, using different naphthasulfonate concentrations (C_S^0) in white mineral oil.

concentrations, varying between 0.2 and 5%. The lowest final concentration was now 0.2%, against 0.02% for the C_{16} -sulfonate, because the C_{21} -sulfonate concentrations in the water phases of the emulsions were much lower than for emulsions made with C_{16} -sulfonate. Errors of measurement made calculations at very low sulfonate concentrations in the water phase inaccurate.

In Fig. 1 the quantity of sulfonate that remains bound to 100 g. emulsified oil (adsorbed on the interface of the oil droplets), after emulsification to a given concentration and subsequent dilution, has been plotted against the sulfonate concentration of the water phase; for emulsions made with C_{21} -sulfonate the graph includes the results obtained

with emulsions prepared by phase inversion. In the case of C_{16} -sulfonate the maximum quantity adsorbed is dependent on the initial concentration of the oil in the emulsion and also on the final concentration; however, in the range measured the quantity of adsorbed C_{21} -sulfonate remains the same under these conditions.

If, instead of simple sulfonates, mixtures are employed (a sodium naphthasulfonate), then, for emulsions obtained by dilution of 0.3–10% emulsions, the surface tension shows the same trend as for C_{16} -sulfonate, and for emulsions obtained by dilution of 15–35% emulsions it is the same as when using C_{21} -sulfonate. Since we are dealing here with mixtures of sulfonates, the sulfonate concentrations of the water phases cannot be derived with certainty from the surface tension. It seems, however, that the behavior of this mixture is intermediate between that of C_{16} - and C_{21} -sulfonate.

TABLE IV
*The Concentrations of Oils with Various Sulfonate Contents
in Emulsions at Given Surface Tensions*
(Derived from Fig. 2)

Surface tension of emulsions in dynes/cm. at 20°C.	Emulsion concentration for sulfonate contents (% wt.) of the oil of			
	20	10	6	4
47	1	2.3	3.3	5.2
42	1	2.1	3.4	5.1
38	1	1.9	3.4	4.9
Average	1	2.1	3.4	5.1

From 4, 6, 10, and 20% solutions of the sodium naphthasulfonate in white mineral oil 0.3–4% oil-in-water emulsions were made by phase inversion. The relation between surface tension of these emulsions and emulsion concentration is shown in Fig. 2.

Table IV gives the concentration of the emulsions (based on those with 20% of sulfonate in oil as 1) having the same surface tension.

These ratios are found to be almost constant for the whole of each curve and inversely proportional to the sulfonate content of the emulsible oil $\left(1: \frac{1}{2.0}: \frac{1}{3.33}: \frac{1}{5.0}\right)$. This means that if the sulfonate content of the emulsible oil becomes a times larger, the emulsion obtained by phase inversion can be diluted a times more strongly to produce the same surface tension.

DISCUSSION

As regards the emulsions formed spontaneously on addition of a C_{16} -sulfonate-oil system to water, measurements of light transmittance and

the number of microscopically visible particles after dilution to one and the same final concentration have shown that the average particle size decreases with rising oil concentrations. With decreasing particle size the area of oil-water interface per gram of emulsified oil (the specific surface area of the oil droplets) increases. Therefore, at a given equilibrium concentration of the sulfonate in the water phase, the quantity of sulfonate adsorbed on the oil-water interface will increase as the particle size decreases.

The adsorption of C_{16} -sulfonate on the oil-water interface (Fig. 1) shows that this is actually true, the saturation value of the adsorption rising as the initial concentration of the emulsion rises. As appears from these saturation values, the specific surface area increases rapidly on spontaneous emulsification of 0.1–5% of oil in water; above this concentration it increases slowly, probably up to a limiting value.

If C_{21} -sulfonate is used, the adsorption curves in the range measured coincide and 97 to 98% of the total quantity of sulfonate remains adsorbed on the oil droplets (Fig. 1). It further appears that in the whole range of emulsion concentrations examined the saturation value is reached, so that on dilution no sulfonate is withdrawn from the oil drops (only the water phase being diluted). The data of emulsions obtained by phase inversion coincide with the others. All this suggests that the fineness of the emulsions obtained with C_{21} -sulfonate is the same under all these conditions.

Maximum adsorption of C_{21} -sulfonate on the oil-water interface occurs at equilibrium concentrations lower than $1 \times 10^{-3}\%$ wt. (0.25×10^{-4} N) in the water phase; for C_{16} -sulfonate it occurs at 5 to $10 \times 10^{-3}\%$ wt. ($1.05 - 2.1 \times 10^{-4}$ N).

The C_{21} -sulfonate therefore shows much greater interfacial activity; in view of its longer alkyl chain this need not surprise us. The difference in surface-activity in water is much smaller.

The question as to why the fineness of the emulsions depends on the quantity of spontaneously emulsified oil in a given quantity of water can only be answered if we have some idea of how spontaneous emulsification actually takes place.

When a dispersion of non-spherical—say, plate-shaped—sulfonate micelles in hydrocarbons (see *Introduction*) comes into contact with water, we may assume that the water very rapidly penetrates into the micelles, via the sulfonate groups. This process begins with the micelles that happen to be present at the emulsible-oil water interface, and subsequently progresses towards the other micelles in the oil (see Fig. 3). The oil is thus divided into a number of smaller volumes, the size of which is determined by the number and size of the micelles present. Thus the double layers of the micelles are split and in the first stage of the

process, the simple sulfonate layers as a whole form the oil-water interface of the oil particles A in the water phase. During this formation of the interface, i.e., while no equilibrium has yet been reached and the size of the interface is not yet fixed, sulfonate molecules may find their way into the water phase, by (1) expulsion of sulfonate molecules from the interface as a result of a decrease of the interfacial area originally formed, this decrease being due to the fact that the oil particles originally formed need not be spherical; (2) the establishment of an adsorption equilibrium at the oil-water interface.

Expulsion of sulfonate molecules from the interface will take place in any case and thus a fixed percentage of the sulfonate originally present in the emulsible oil will always pass into the water phase. It was actually found that this percentage is never lower than 2 to 3%, both after

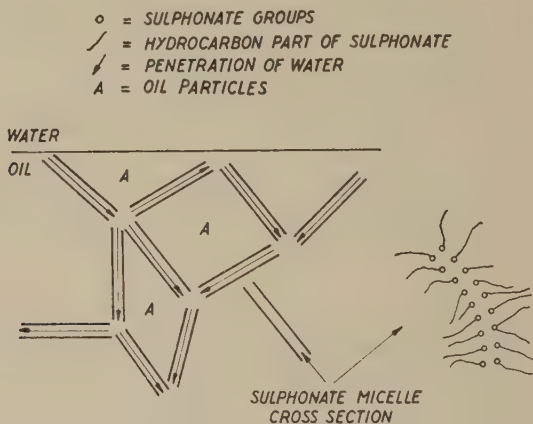


FIG. 3. Schematic presentation of the first stage of the process of spontaneous emulsification.

spontaneous emulsification and after emulsification by phase inversion. Subsequently an adsorption equilibrium with the water phase will be established. If small quantities of oil have been emulsified, then, in view of the high ratio between volume of medium and area of interface, a relatively large quantity of sulfonate will be withdrawn from the oil. The result may be that the interface becomes so sparsely occupied with sulfonate molecules that the oil droplets originally formed are no longer stable. They will then coalesce and consequently reduce the interface until the interface is sufficiently occupied to stabilize the particles. This conception of the process of spontaneous emulsification was confirmed by experiments in which the emulsible oil was emulsified in water as well as in dilute sulfonate solutions in water. The number of large droplets decreased strongly in the latter experiments.

If more oil is emulsified the ratio between volume of medium and area of interface decreases; consequently, on re-establishment of the adsorption equilibrium a smaller percentage of sulfonate will be withdrawn from the newly formed oil drop interfaces. If the instability of the drops persists, this can be eliminated by less coalescence. Finally, on emulsification of more oil, the sulfonate molecules given up to the water phase through expulsion will supply the quantity required for the adsorption equilibrium and eventually even exceed this quantity. Then the drops no longer increase in size.

This course of things may explain why the quantities of oil first emulsified supply the largest drops, while the number of these drops increases less and less rapidly as more oil is emulsified, and therefore relatively continues to decrease. Thus the emulsion as a whole will become increasingly finer, the fineness increasing asymptotically to a limit.

The fact that in the case of C_{21} -sulfonate, in the same range of emulsion concentrations, these phenomena are not observed may be ascribed to a very strong interfacial activity of this sulfonate, as a result of which the tendency to withdraw sulfonate from the oil-water interface will be very weak.

If sulfonate is withdrawn from the oil droplets only due to factor (1), the finest possible and most homogeneous emulsions should be formed. This condition is fulfilled in emulsification by phase inversion.

The results obtained with emulsions made by phase inversion, using sodium naphtha sulfonate, can also be regarded from the above point of view. It has been found that when the sulfonate concentration of the emulsible oil is a times higher, the emulsion can be diluted a times more strongly to reach the same surface tension. This too, suggests, that on emulsification through phase inversion a fixed percentage of the sulfonate (the interfacially least active) is expelled towards the water phase (factor 1) and that on further dilution to emulsion concentrations of some tenths per cent no more sulfonate is withdrawn from the oil droplets. Just what percentage of the sulfonate is expelled cannot be calculated with certainty from the surface tension of the emulsion in this case, because a mixture of sulfonates is present.

SUMMARY

1. The distribution of some sodium alkyl benzene sulfonates over oil droplets and water phase in emulsions was determined by measuring the surface tensions of the emulsions. The emulsions were formed from white mineral oil/sulfonate systems either by spontaneous emulsification or by phase inversion.

2. The results show that with spontaneous emulsification part of the sulfonate originally present in the oil passes into the water phase and that

at the interface of the oil droplets subsequently formed an adsorption equilibrium is established between the sulfonate in the interfacial layer and that in the water phase.

3. In spontaneous emulsification the quantities of emulsible oil that first come into contact with water give off a higher percentage of their sulfonate to the water than the quantities of oil subsequently emulsified. It seems that in any case a low minimum percentage of the sulfonate finds its way into the water phase, also in emulsification by phase inversion.

4. Based on data previously obtained on the structure of sulfonate solutions in hydrocarbons and on the above data, a picture is given of the possible mechanism of spontaneous emulsification.

REFERENCES

1. REUMUTH, H., *Kolloid-Z.* **115** (1950). Sonderausgabe (Verhandlungsberichte der Kolloid-Gesellschaft, Band 14).
2. VAN DER WAARDEN, M., *J. Colloid Sci.* **5**, 448 (1950).
3. HARKINS, W. D., AND JORDAN, H. F., *J. Am. Chem. Soc.* **52**, 1751 (1930).

AN APPLICATION OF THE GIBBS' ADSORPTION THEORY TO FILMS AT OIL-WATER INTERFACES ^{1,2}

E. Hutchinson and D. Randall

Chemistry Department, Stanford University, California, and E. I. duPont de Nemours Inc., Knolls Laboratory, Schenectady, New York

Received January 8, 1952

From interfacial tension measurements of the system water-benzene + third component, viz., an alcohol, fatty acid, or ester, together with the necessary freezing point depression data, calculations have been made of the surface concentrations of the third component. It is shown that the assumptions necessary to calculate these concentrations, depending on the extra-thermodynamic interpretation of surface film structure, affect very considerably the numerical values of the surface concentrations.

INTRODUCTION

Due to the solubilities of paraffin chain, and other, derivatives in the oil-phase it is difficult to study the force-area curves of films at oil-water interfaces by the methods applicable to the air-water surface (1), and recourse must generally be had to studies of the properties of adsorbed films. In this case the surface pressure of the film is readily obtained by the equation

$$F = \sigma_0 = \sigma, \quad [1]$$

where σ_0 = interfacial tension between the pure phases,

σ = interfacial tension in presence of a third (solute) component.

The area per molecule of the film material must be obtained by calculation, using the Gibbs adsorption theory. Due to the comparatively low surface activity of alcohols, acids, and esters at the benzene-water interface concentrated solutions are required to reduce the interfacial tension by, say, 10–15 dynes/cm. Guggenheim and Adam (2) proposed a number of ways of calculating surface concentrations, Γ , for concentrated solutions; in particular they showed how Γ may be evaluated on the assumption that the adsorbed film is monomolecular. Starting with the "Gibbs" convention, which places the reference plane so that $\Gamma^{(1)}_{\text{solvent}}$

¹ Taken from a dissertation submitted by D. Randall in partial fulfillment of the requirements for the Ph.D. degree, Fordham University.

² Presented at the Colloid Chemistry Division, Diamond Jubilee meeting of the American Chemical Society, New York 1951.

$\neq 0$, they deduced other conventions, the v , and u , conventions. Putting $\Gamma_{\text{solvent}}^{(1)} = 0$

$$\Gamma_2^{(1)} = \frac{-d\sigma}{d \ln a_2}, \quad [2]$$

where σ = interfacial tension,

a_2 = activity of solute.

Then $\Gamma_2^{(1)}$ = surface concentration of solute (2) on the Gibbs convention and

$$\Gamma_2^{(1)} = \Gamma_2^{(v)} \left\{ 1 + \frac{N_2 \bar{V}_2}{N_1 \bar{V}_1} \right\} = \frac{\Gamma_2^{(u)} \{N_1 a_1 + N_2 a_2\} - N_2}{N_1 a_1}$$

where $\Gamma_2^{(v)}$ = surface concentration of 2 on the v convention,

$\Gamma_2^{(u)}$ = surface concentration of 2 on the u convention,

a_1 = cross section of the solvent molecules ($\text{cm.}^2/\text{mole}$)

a_2 = cross section of the solvent molecules ($\text{cm.}^2/\text{mole}$)

N_1, N_2 = mole fractions of components 1 and 2.

The v convention places the Gibbs plane very close to the physical boundary between the two bulk phases and the u convention assumes that the interfacial film is monomolecular.

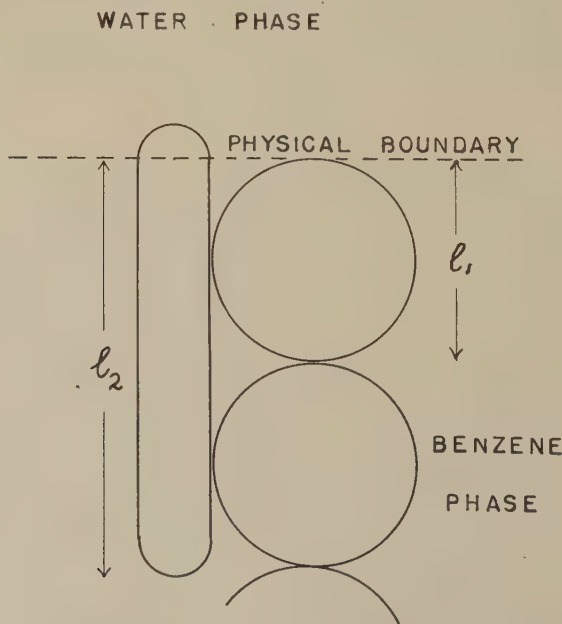


FIG. 1. Assumed model for film structure.

The application of the Guggenheim and Adam treatment to the present experiments involves a number of problems. First, the question arises as to how sharp the physical boundary is between benzene and water bulk phases. In terms of the geometry of the molecules the boundary can probably be represented by a plane which is definable within \pm ca. 2 Å. Hence the position of the Gibbs plane in the v convention is definable to this order of precision. Second, it was implicitly assumed by Guggenheim and Adam that the solvent and solute molecules in the monomolecular film are of identical size and this is certainly untrue in the present experiments. The treatment proposed below for systems where the molecules are of different sizes may be understood from Fig. 1. The Gibbs plane is placed at the lower end of the longer molecule: even assuming random rotation and coiling of the chain of this molecule a statistical average for this plane will be definite to within 1 Å. or so. The surface film thus defined is then monomolecular with respect to the longer molecule, and not all of the shorter molecules will make a contribution to the area of the monomolecular film. Thus,

$$\Gamma_1^{(u')} \cdot a_1 \frac{l_1}{l_2} + \Gamma_2^{(u')} \cdot a_2 = 1, \quad [4]$$

whereas in the Guggenheim and Adam treatment

$$\Gamma_1^{(u)} \cdot a_1 + \Gamma_2^{(u)} \cdot a_2 = 1. \quad [5]$$

It may be shown that:

$$\Gamma_2^{(u')} = \frac{N_2 + \frac{l_1}{l_2} a_1 \Gamma_2^{(1)} N_1}{N_1 \frac{l_1}{l_2} \cdot a_1 \sim N_2 a_2} = \frac{l_2 N_2 + l_1 a_1 \Gamma_2^{(1)} N_1}{N_1 l_1 a_1 + N_2 l_2 a_2}.$$

But $l_1 a_1 \cong \bar{V}_1$ = partial molal volume of solvent; $l_2 a_2 \cong \bar{V}_2$ = partial molal volume of solute, if the chain is not markedly curled. Thus

$$\Gamma_2^{(u')} \cong \frac{l_2 N_2 + N_1 \bar{V}_1 \Gamma_2^{(1)}}{N_1 \bar{V}_1 + N_2 \bar{V}_2}$$

and from Eq. [3]

$$\Gamma_2^{(u')} = \Gamma_2^{(v)} + \frac{l_2 N_2}{N_1 \bar{V}_1 \sim N_2 \bar{V}_2}. \quad [6]$$

Now the concentration of the solute (in moles/cm.³) c_2 is given by

$$c_2 = \frac{\rho_s N_2}{\bar{V}_1 \rho_1 N_1 + \bar{V}_2 \rho_2 N_2},$$

where ρ_s = density of the solution,

ρ_1 = density of the solvent,

ρ_2 = density of the solute.

For many organic materials $\rho_s \approx \rho_1 \approx \rho_2 \approx 1$ so that

$$\Gamma_2^{(u')} = \Gamma_2^{(v)} + l_2 c_2. \quad [7]$$

By the same argument

$$\Gamma_2^{(u)} = \Gamma_2^{(v)} + l_{12} c_2, \quad [8]$$

where $l_{12} = l_1 = l_2$. Thus both the u and u' conventions amount simply to moving the Gibbs plane through a distance l_2 from the physical boundary and both equations are derivable from the familiar equation,

$$\Gamma_x = \Gamma_0 + c_2 x. \quad [9]$$

The importance of Eq. [7] is that in the present experiments c_2 assumes values of ca. 10^{-3} moles/cm.³, so that for $l_2 = 10 \text{ \AA}$, $c_2 l_2 = 10^{-10}$ moles/cm.², which is not negligible compared to Γ . The area per molecule A_2 of the solute in the surface film is given by $A_2 = \frac{1}{N \Gamma_2^{(u')}}$ where N = Avogadro's number, and clearly A_2 depends on the value assigned to l_2 , which in turn depends on the detailed model chosen for the film. Values of $\Gamma_2^{(1)}$ are obtained from the equation,

$$\Gamma_2^{(1)} = \frac{N_2}{N_1} \cdot \frac{L}{RT_0^2} \cdot \frac{d\sigma}{d\theta}, \quad [10]$$

where θ = freezing point depression of the solution (6). This equation eliminates g , the osmotic coefficient of the solvent, which is determined at the freezing point of the solution, and for more concentrated solutions ($c_2 \approx 0.5$ molar) errors may result from using such g values at temperatures some 20–30°C. higher. The temperature coefficient of g depends on the differential heat of dilution of the solution (9). No data are at present available for these heats, but it is to be noted, from the solubility data given by Ralston and Hoerr (3), that the integral heat of dilution is small and hence the differential heat is also probably small. $\Gamma_2^{(1)}$ values may be in error by ca. 5% in concentrated solutions from this approximation. In determining the value of $\Gamma_2^{(1)}$ the errors involved are: (a) errors of measurement, which are probably less than 1%, (b) errors in assuming temperature independence of g , and (c) errors in obtaining values of $\frac{d\sigma}{d\theta}$. For concentrated solutions (b) may cause 5% errors whereas $\frac{d\sigma}{d\theta}$ is determinable to an accuracy well within ca. 5%. For dilute solutions (b) is probably not a serious source of error, but the rapid change of σ with θ makes the determination of the value of $\frac{d\rho}{d\theta}$ uncertain to about $\pm 5\%$. In deriving force-area curves for the adsorbed films two simple models may be adopted.

(a) The solute molecule is assumed to be oriented normal to the interface so that l_2 = length of the uncurled molecule.

TABLE I

n-Octyl Alcohol in Benzene at 25°C.

Mole fraction of alcohol, N_2	Density of solution	Freezing point depression °C.	Interfacial tension dynes/cm.
0.006627	0.8720(7)	0.469	28.8
0.01206	0.8717(1)	0.727	25.7
0.02479	0.8698(3)	1.170	21.9
0.03728	0.8685(4)	1.491	20.2
0.05055	0.8675(1)	1.788	19.2
0.06062	0.8660(7)	2.003	18.5
0.07083	0.8651(6)	2.218	18.0
0.08093	0.8640(9)	2.428	17.5
0.1005	0.8623(9)	2.834	16.6
0.1006	0.8634(1)	2.834	16.6
0.1260	0.8603(8)	3.363	16.0
0.1600	0.8572(5)	4.068	15.3
0.2008	0.8545(5)	4.913	14.5

TABLE II

n-Decyl Alcohol in Benzene at 25°C.

Mole fraction of alcohol, N_2	Density of solution	Freezing point depression °C.	Interfacial tension dynes/cm.
0.005012	0.8722(5)	0.362	29.8
0.01105	0.8714(6)	0.668	27.2
0.02015	0.8702(4)	0.991	24.4
0.03025	0.8689(8)	1.264	22.3
0.04015	0.8678(1)	1.498	20.9
0.05020	0.8665(9)	1.724	19.9
0.07537	0.8639(8)	2.274	19.1
0.09693	0.8620(3)	2.743	18.1
0.1308	0.8590(3)	3.482	17.2
0.1604	0.8566(5)	4.123	16.4
0.1992	0.8538(9)	4.996	15.5

TABLE III

n-Dodecyl Alcohol in Benzene at 25°C.

Mole fraction of alcohol, N_2	Density of solution	Freezing point depression °C.	Interfacial tension dynes/cm.
0.005011	0.8721(2)	0.357	30.6
0.01005	0.8713(3)	0.630	27.7
0.02006	0.8698(0)	1.025	24.6
0.03009	0.8684(0)	1.319	22.9
0.04103	0.8670(1)	1.590	21.5
0.04782	0.8662(5)	1.749	20.8
0.06976	0.8638(5)	2.230	19.7
0.08689	0.8619(9)	2.600	19.4
0.1004	0.8606(2)	2.891	18.8
0.1201	0.8589(3)	3.315	18.2
0.1638	0.8545(6)	4.255	17.3
0.1999	0.8525(3)	5.031	16.7

TABLE IV
n-Tetradecyl Alcohol in Benzene at 25°C.

Mole fraction of alcohol, N_2	Density of solution	Freezing point depression °C.	Interfacial tension dynes/cm.
0.005024	0.8720(5)	0.309	30.2
0.01063	0.8710(6)	0.618	28.3
0.02015	0.8696(1)	0.997	25.4
0.03008	0.8681(7)	1.289	23.3
0.04058	0.8667(2)	(1.554)	22.4
0.04999	0.8655(2)	(1.764)	21.4
0.06018	0.8643(1)	(1.984)	20.8
0.0800	0.8618(2)	(2.406)	20.0
0.1010	0.8600(8)	(2.851)	19.2
0.1308	0.8573(0)	(3.484)	18.6
0.1606	0.8592(2)	(4.114)	17.1
0.2009	0.8526(5)	(4.969)	16.1

 TABLE V
Cetyl Alcohol in Benzene at 25°C.

Mole fraction of alcohol, N_2	Density of solution	Freezing point depression °C.	Interfacial tension dynes/cm.
0.005056	0.8719(3)	0.370	30.0
0.01015	0.8708(7)	0.645	27.9
0.02021		1.027	25.2
0.02029	0.8694(9)	1.030	24.6
0.02959			23.4
0.03005	0.8680(7)	1.303	23.4
0.04024	0.8665(8)	1.546	22.1
0.05069	0.8653(1)	(1.779)	20.0
0.06019	0.8643(0)	(1.984)	19.3
0.08005		(2.408)	17.4
0.08080	0.8619(4)	(2.424)	16.6
0.1008	0.8600(2)	(2.848)	14.8
0.1308	0.8575(3)	(3.483)	12.5
0.1606	0.8555(4)	(4.114)	10.6

 TABLE VI
Octadecyl Alcohol in Benzene at 40°C.

Mole fraction of alcohol, N_2	Density of solution	Freezing point depression °C.	Interfacial tension dynes/cm.
0.004953	0.8559(0)	(0.246)	31.6
0.01010	0.8549(3)	(0.642)	29.5
0.02022	0.8537(3)	(1.028)	27.2
0.03026	0.8520(0)	(1.308)	25.7
0.04026	0.8505(6)	(1.547)	24.7
0.05021	0.8494(7)	(1.768)	23.7
0.06040	0.8483(8)	(1.989)	23.0
0.08140	0.8462(7)	(2.436)	22.4
0.1004	0.8445(7)	(2.840)	21.7
0.1331	0.8400(9)	(3.531)	20.5
0.1597	0.8400(9)	(4.097)	17.6

TABLE VII
n-Caprylic Acid in Benzene at 25°C.

Mole fraction of acid, N_2	Density of solution	Freezing point depression °C.	Interfacial tension dynes/cm.
0.00505	0.8731(4)	0.199	29.8
0.01005	0.8734(3)	0.358	27.7
0.02011	0.8741(1)	0.734	25.9
0.03001	0.8741(1)	1.080	24.6
0.05045	0.8748(6)	1.800	22.9
0.08034	0.8760(1)	2.953	21.0
0.1000	0.8767(9)	3.710	20.0
0.1195	0.8776(0)	4.500	19.2
0.1403	0.8785(1)	5.324	18.4
0.1611	0.8793(1)	6.277	18.0
0.2015	0.8808(9)	8.169	16.8
0.2411		10.241	
0.2520	0.8837(9)	10.456	16.0
0.3096	0.8853(2)	(13.41)	14.8

TABLE VIII
n-Capric Acid in Benzene at 25°C.

Mole fraction of acid, N_2	Density of solution	Freezing point depression °C.	Interfacial tension dynes/cm.
0.00504	0.8730(8)	0.197	29.6
0.00998	0.8731(7)	0.371	28.1
0.02012	0.8734(5)	0.736	26.2
0.04018	0.8739(0)	1.431	23.9
0.06005	0.8743(6)	2.186	22.4
0.08017	0.8747(8)	2.940	21.9
0.1000	0.8748(9)	3.800	21.1
0.1211	0.8759(0)	4.605	20.2
0.1594	0.8770(3)	6.284	18.7

TABLE IX
Lauric Acid in Benzene at 25°C.

Mole fraction of acid, N_2	Density of solution	Freezing point depression °C.	Interfacial tension dynes/cm.
0.00505	0.8730(5)	0.203	29.9
0.00970	0.8730(5)	0.370	28.5
0.02017	0.8730(4)	0.752	26.8
0.04007	0.8731(3)	1.450	24.5
0.06031	0.8733(5)	2.191	23.0
0.08052	0.8736(4)	2.798	22.4
0.1004	0.8738(7)	(3.641)	21.7
0.1224	0.8742(1)	(4.502)	20.9
0.1413	0.8747(7)	(5.262)	19.9
0.1602	0.8749(4)	(6.049)	19.6
0.1988	0.8758(8)	(7.719)	18.5

TABLE X
Myristic Acid in Benzene at 25°C.

Mole fraction of acid, N_2	Density of solution	Freezing point depression °C.	Interfacial tension dynes/cm.
0.00502	0.8730(1)	0.237	30.5
0.01005	0.8729(0)	0.409	28.9
0.02009	0.8727(4)	0.787	26.9
0.04028	0.8726(9)	(1.535)	25.1
0.06013	0.8725(7)	(2.297)	24.1
0.07971	0.8726(7)	(3.052)	22.9
0.1001	0.8726(8)	(3.843)	22.2
0.1196	0.8728(2)	(4.601)	21.6
0.1390	0.8730(0)	(5.359)	21.0
0.1605	0.8732(8)	(6.204)	20.4

TABLE XI
Palmitic Acid in Benzene at 40°C.

Mole fraction of acid, N_2	Density of solution	Freezing point depression °C.	Interfacial tension dynes/cm.
0.00504	0.8569(7)	(0.192)	29.4
0.01012	0.8568(8)	(0.386)	27.7
0.02020	0.8567(7)	(0.768)	25.5
0.04038	0.8568(8)	(1.565)	22.6
0.06040	0.8569(8)	(2.308)	22.0
0.07942	0.8570(8)	(3.040)	21.7
0.09722	0.8571(7)	(3.730)	21.0
0.1467	0.8574(3)	(5.661)	19.0

(b) The solute molecule is assumed to be uncurled, and l_2 chosen to vary with Γ , i.e., the angle of tilt is proportional to the area per molecule in the film.

Values corresponding to model (a) have been calculated, from which appropriate values of the area per molecule have been derived. Values corresponding to model (b) have been determined, for a few cases, as follows. From the $\Gamma_2^{(1)}$ values, obtained by using Eq. [10], an approximate area per molecule A_2 was calculated. Assuming that the product of the area per molecule and the effective thickness of the monomolecular film is constant, the latter was then calculated, and finally $\Gamma_2^{(u)}$ values were obtained using Eq. [7], from which areas per molecule were calculated. Owing to the sources of possible error outlined above, the final precision is such that we have not considered it worthwhile to postulate more complex models than these two.

EXPERIMENTAL

The principal method used for interfacial tension measurements was the sessile bubble method (4). Less accurate check determinations were

made by Gaddum's modification of the drop volume method (5). In the first method the bubble was formed on a tube dipping into a fused Pyrex cell immersed in a thermostat provided with a Pyrex optically flat window. The whole apparatus was mounted on a heavy stone bench and the travelling microscope used to measure the bubble was placed on a heavy glass plate cemented to the same stone bench. Errors due to non-parallelism of the cell windows (6) were negligible. Density data were obtained by use of a 25 ml. pycnometer, with a reproducibility of ca. ± 0.00005 g./cm.³. Freezing point data were obtained by means of a conventional Beckmann apparatus. For freezing point depressions greater than 5°C. a second Beckmann thermometer set for a lower range was used, extending the measurements to about 10°C. Results agree with available data (4,7) to within 1% or better. The water used in these experiments was air-free conductivity water, and the benzene was the middle fraction of a reagent grade sample distilled in a three-foot heated column. The various solutes, obtained from Eastman Kodak and Humphrey Wilkinson, Inc., were used as supplied except in the case of palmitic acid which required three recryst-

TABLE XII

Ethyl Caprylate in Benzene at 25°C.

Mole fraction of ester, N_2	Density of solution	Freezing point depression °C.	Interfacial tension dynes/cm.
0.01008	0.8727(1)	0.769	33.9
0.02517	0.8722(8)	1.803	33.1
0.05017	0.8715(3)	3.600	31.9
0.0751(5)	0.8709(0)	5.385	30.9
0.1006	0.8703(1)	7.229	30.5
0.1248	0.8697(9)	9.115	30.0
0.1511	0.8693(6)	(10.96)	29.4
0.1755	0.8589(0)	(12.75)	28.9
0.1999	0.8685(1)	(14.55)	28.2
0.2503	0.8678(3)	(18.30)	27.4
0.3019	0.8672(9)	(22.18)	26.9

TABLE XIII

Methyl Stearate in Benzene at 40°C.

Mole fraction of ester, N_2	Density of solution	Freezing point depression °C.	Interfacial tension dynes/cm.
0.01006	0.8562(8)	0.754	32.7
0.02508	0.8553(9)	1.790	31.1
0.05054	0.8543(8)	3.565	30.3
0.07435	0.8534(9)	(5.369)	29.3
0.09989	0.8528(5)	(7.223)	29.0
0.1250	0.8523(6)	(9.049)	28.5
0.1499	0.8520(4)	(10.87)	28.6
0.1749	0.8515(9)	(12.70)	28.1
0.2000	0.8515(1)	(14.56)	27.9

tallizations from acetone to reduce ageing. The values of $\frac{d\sigma}{d\theta}$ needed for the calculation of $\Gamma_2^{(1)}$ were obtained by fitting analytical expressions to the $\sigma - \theta$ curves and differentiating. For some of the higher homologues freezing point data were not obtainable over a sufficient range due to low solubility at the freezing point. Extrapolated values of θ were used for these with some confidence because all of the homologues appear to fall on the same $\theta \sim N_2$ curve very closely within their solubility limits.

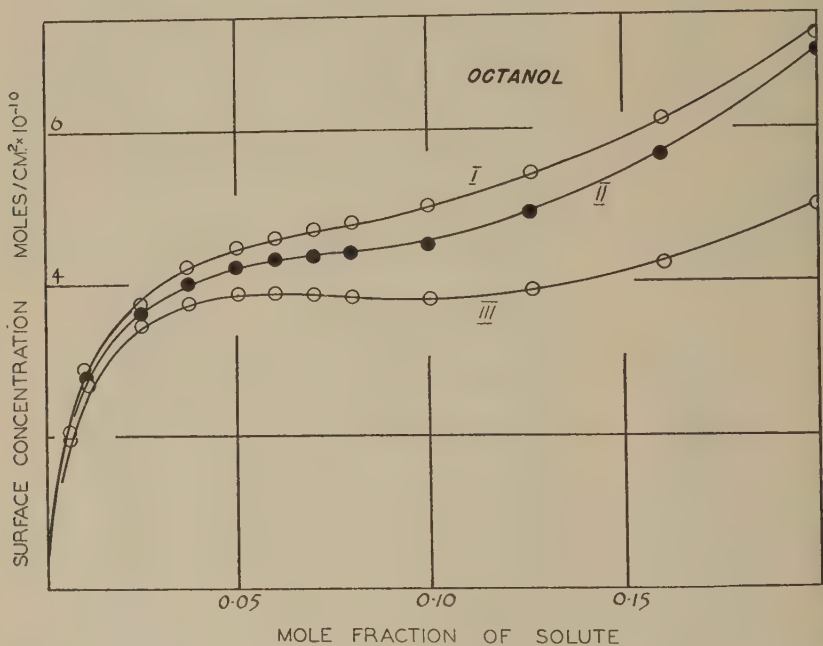


FIG. 2. Surface concentration *vs.* mole fraction curves for octanol at 25°C. Curve I: U' convention. Curve II: 1 convention. Curve III: V convention.

Partial molal volumes \bar{V}_1 , \bar{V}_2 were calculated from the equations

$$\bar{V}_1 = \frac{M_1}{\rho_s - c_2 \frac{d\rho_s}{dc_2}}, \quad \bar{V}_2 = \frac{M_2 - 1000 \frac{d\rho_s}{dc_2}}{\rho_s - c_2 \frac{d\rho_s}{dc_2}}.$$

where M_1 = molecular weight of solvent,
 M_2 = molecular weight of solute,
 ρ_s = density of the solution,
 c_2 = molarity of solute.

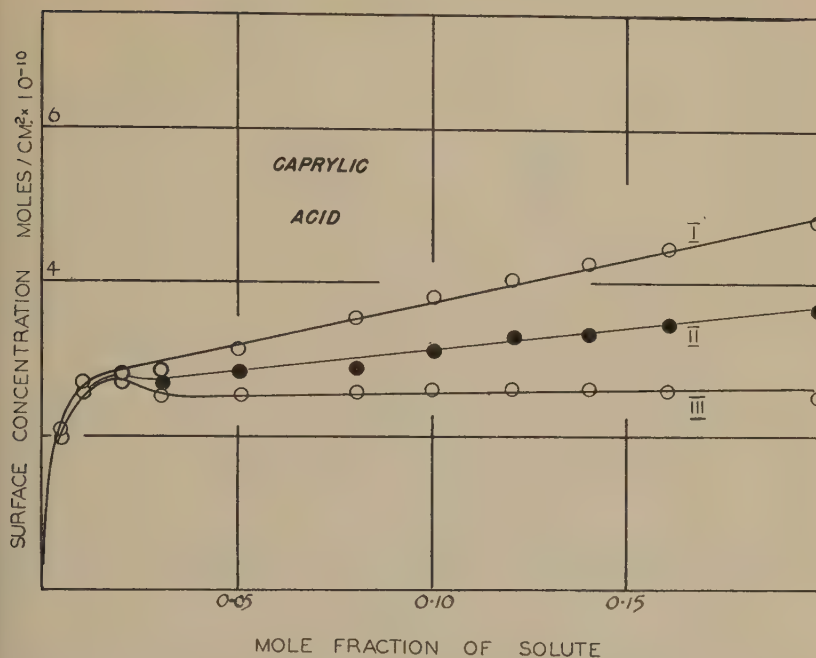


FIG. 3. Surface concentration *vs.* mole fraction curves for caprylic acid at 25°C. Curve I: U' convention. Curve II: 1 convention. Curve III: V convention.

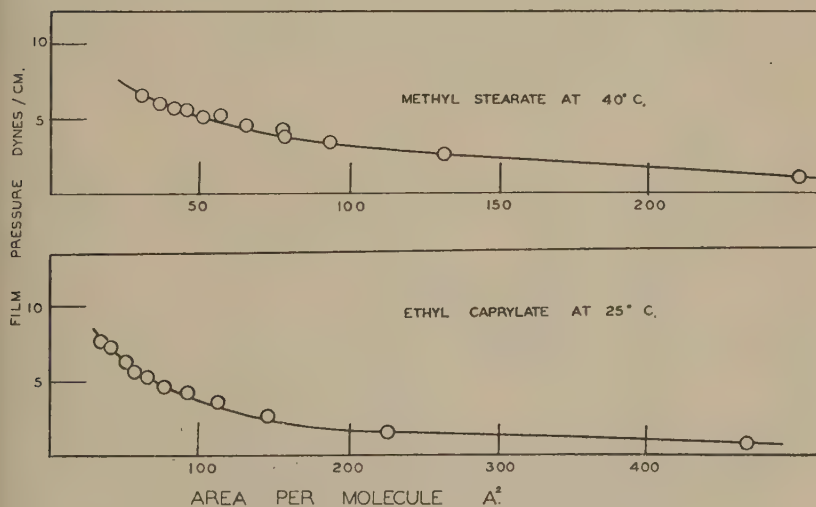


FIG. 4. Force-area curves of ester films.

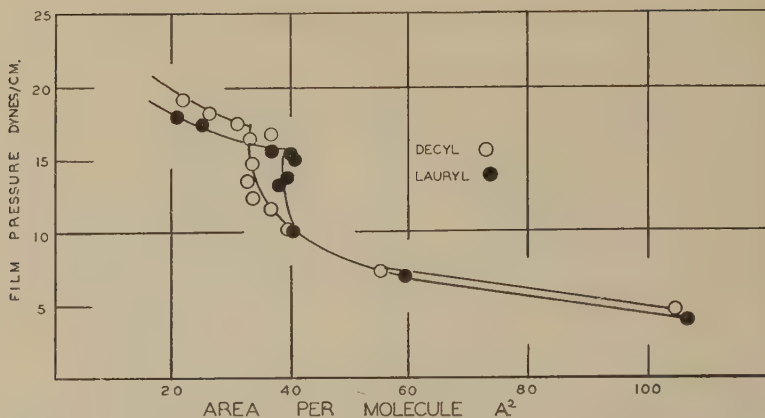


FIG. 5. Force-area curves of alcohol films. Open circles, decyl alcohol at 25°C. Solid circles, lauryl alcohol at 25°C.

ρ_s was found to follow accurately an equation $\rho_s = \rho_s^0 + ac_2 + [bc_2^2]$ from which values of $\frac{d\rho_s}{dc_2}$ were obtained. c_2 was calculated from the equation

$$c_2 = \frac{1000 \rho N_2}{M_1 N_1 + M_2 N_2}.$$

RESULTS

Data for the freezing points, densities, and interfacial tensions of the various systems are given in Tables I-XIII. Typical plots of surface

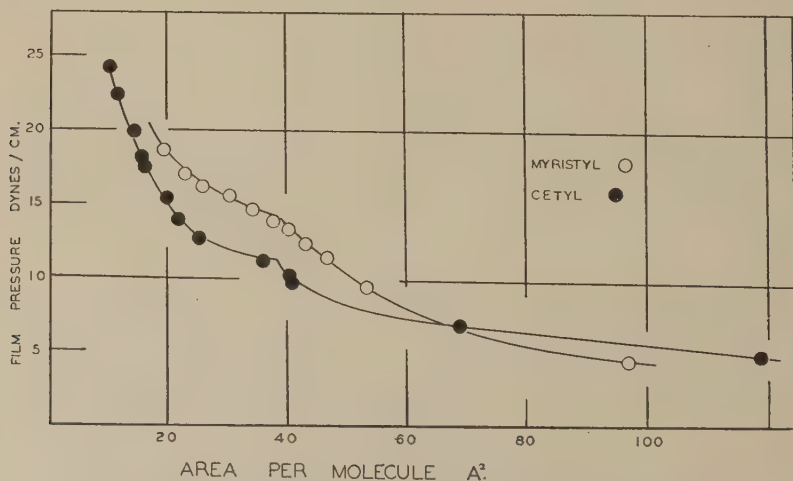


FIG. 6. Force-area curves of alcohol films. Open circles, myristyl alcohol at 25°C. Solid circles, cetyl alcohol at 25°C.

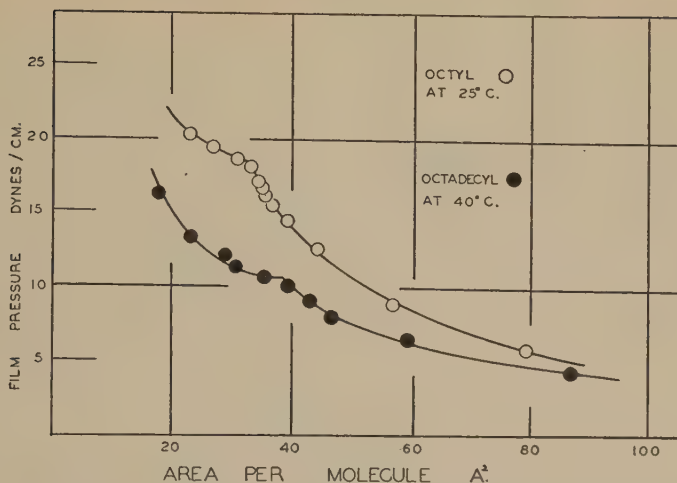


FIG. 7. Force-area curves of alcohol films. Open circles, octyl alcohol at 25°C. Solid circles, octadecyl alcohol at 40°C.

concentrations of solute as a function of bulk concentration are given in Figs. 2 and 3, and force-area curves of the adsorbed films based on the vertically oriented U' convention are given in Figs. 4-10.

DISCUSSION

The interfacial tensions, and the necessary density determinations, obtained in this study are as accurate as can readily be obtained by methods presently available. Nevertheless the calculated values of Γ may be seriously in error, for reasons outlined earlier. In view of this the propriety

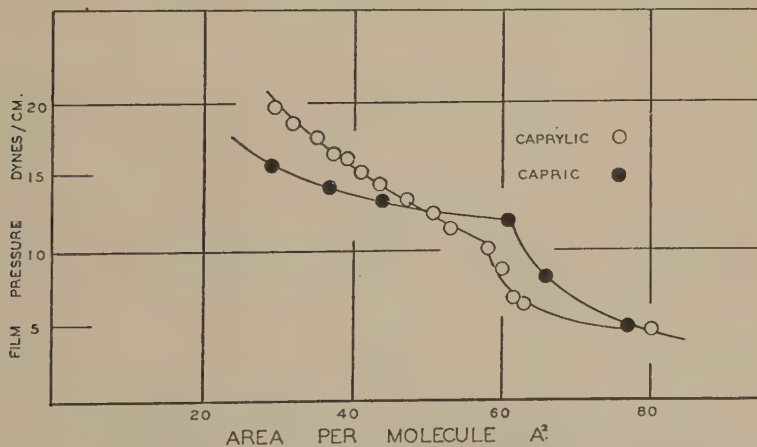


FIG. 8. Force-area curves of acid films. Open circles, caprylic acid at 25°C. Closed circles, capric acid at 25°C.

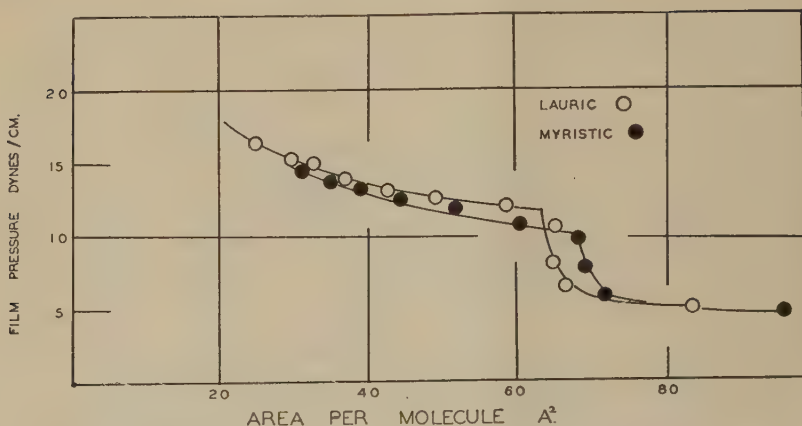


FIG. 9. Force-area curves of acid films. Open circles, lauric acid at 25°C. Solid circles, myristic acid at 25°C.

of calculating force-area curves for the adsorbed films may be seriously challenged. However, despite the large possible errors, it does appear that, whether one uses a v or a u convention, the force-area curves for fatty acids and alcohols exhibit discontinuities, and that while the curves would be affected in scale by the errors, the existence of these discontinuities seems real. Thus whatever the detailed nature of the force-area curve may be, and it would be unjustifiable to be specific on this point, the results confirm and extend the earlier observations (4) that films of fatty acids and alcohols at a benzene-water surface are not gaseous, but expanded films showing signs of condensation. Further, this study shows how much more difficult it is to obtain data for films adsorbed at oil-

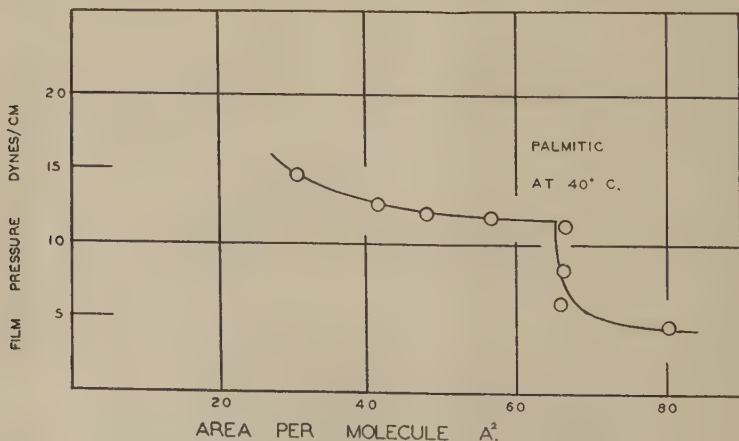


FIG. 10. Force-area curve of palmitic acid at 40°C.

water interfaces than it is for insoluble monolayers at the air-water surface, and raises the question as to whether this approach is sufficiently profitable. Recent studies of adsorbed films using radioactive tracers (8,10) indicate that a direct approach may be easier. Even here, however, it is still necessary, as in every other case of adsorption, to postulate a convention to interpret the data, and the present study shows how critically the results depend on the particular convention adopted, owing to the relatively high values of concentration of solute generally encountered in oil-water systems. Since many phenomena in biological systems are related to film behavior at oil-water interfaces it is clearly desirable that a more complete knowledge of these films be attained.

REFERENCES

1. ADAM, N. K., *The Physics and Chemistry of Surfaces*. Oxford University Press, London, 1943.
2. GUGGENHEIM, E. A., AND ADAM, N. K., *Proc. Roy. Soc., London* **A155**, 695 (1935).
3. RALSTON, A. W., AND HOERR, C. W., *J. Organic Chem.* **7**, 546 (1942).
4. HUTCHINSON, E., *J. Colloid Sci.* **3**, 219 (1948).
5. GADDUM, J. H., *Proc. Roy. Soc., London* **B109**, 114 (1931).
6. KEMBALL, C., *Trans. Faraday Soc.* **42**, 526 (1946).
7. GIACALONE, A., *Gazz. chim. ital.* **72**, 348, 429 (1942).
8. HUTCHINSON, E., *J. Colloid Sci.* **4**, 599 (1949).
9. GUGGENHEIM, E. A., *Thermodynamics*. North Holland Publishing Company, Amsterdam, 1949.
10. SALLEY, D. J., WEITH, A. J., ARGYLE, A. A., AND DIXON, J. K., *Proc. Roy. Soc., London* **A203**, 42 (1950).

THE SPREADING OF LIQUIDS ON LOW-ENERGY SURFACES.

IV. MONOLAYER COATINGS ON PLATINUM

Elaine G. Shafrin and William A. Zisman

Naval Research Laboratory, Washington, D. C.

Received June 14, 1951; revised January 18, 1952

INTRODUCTION

A monomolecular film of oriented amphipathic molecules adsorbed on a smooth solid such as glass or metal causes remarkable changes in the wetting properties of the surface. The recent investigations of the oleophobic (1, 2) and hydrophobic properties (3, 4) of such films have permitted for the first time the quantitative study of their wettability. The use of such adsorbed monolayers provides an unparalleled opportunity for studying wettability phenomena on surfaces for which the molecular orientation and packing are known and readily reproduced. This is a report on the wetting properties of these films and their comparison with the results recently reported (5) for the wettability of smooth, low-energy hydrocarbon surfaces of *n*-hexatriacontane, paraffin, and polyethylene.

EXPERIMENTAL METHODS

For the purpose of this investigation it was preferable to study oleophobic films of *pri-n*-octadecylamine adsorbed from nonaqueous solution in *n*-hexadecane, thus avoiding the possibility of salt formation or inclusion of molecularly dispersed water in the interstices of the film. The monolayers were prepared from solutions of sufficiently high concentrations to ensure the rapid and complete coverage of the adsorbing surface. The majority of the experiments were performed using freshly-flamed, rolled platinum foil as the adsorbing surface. Some measurements were also made on benzene-refluxed, freshly fire-polished, blown glass, the latter representing an extremely smooth surface. Details concerning the sources, methods of purification, tests for purity, and the surface tensions γ_{LV}° of each liquid studied have been reported (6).

Contact angle measurements were made as before (6), using the same improved goniometer, with room temperature held to $20.0 \pm 0.2^{\circ}\text{C}$. and relative humidity at 50%. Each contact angle reported represented the average of measurements on at least three independently prepared specimens of the oleophobic surface; the reproducibility of the measurements ranged from ± 1 to $\pm 2^{\circ}$. In all, three different methods were employed

to form and measure the sessile drops. For the first, measurements were made immediately after placing the sessile drop of pure liquid on the monolayer in order to minimize effects due to volatility of the liquids and solubility of the oleophobic films in the liquids; these initial angles did not represent equilibrium advancing contact angles but were readily repeatable. In the other two methods, the size of the sessile drop was increased by the addition of successive small increments of liquid until the contact angle remained unaffected by subsequent increases. This procedure resulted in a reproducible measurement of the advancing angle practically under conditions of mechanical equilibrium (7). Since this drop-build-up method required prolonged contact of the sessile drop with the oleophobic surface, a significant proportion of the adsorbed monolayer might be expected to dissolve in the drop. Measurements were therefore made both on drops of each pure liquid and on drops of nearly saturated solutions of the octadecylamine in the liquid. Possible effects of the dissolved surface-active amine in depressing the surface tension of the liquid in the test drop will be discussed later.

In the vacuum experiment, a monolayer-coated surface and a liquid reservoir were mounted independently on movable stages within a vacuum chamber equipped with plane windows. Transfer of the liquid was accomplished by lowering the shorter limb of a thin-walled, pyrex, capillary siphon into the reservoir, allowing the tube to fill by capillary action, and siphoning off a single drop by contacting the tip of the longer limb of the siphon to the surface under study. Particular care was taken to form and detach the drop extremely slowly in order to minimize effects due to receding contact angles. The illuminated profile of the drop was measured through the transparent vacuum wall by means of an externally mounted goniometer telescope.

EXPERIMENTAL RESULTS

Table I presents the results of advancing contact angle measurements for several amine-saturated *n*-alkanes against octadecylamine monolayers adsorbed on rolled platinum foil and on smooth blown glass. As previously reported (1, 2), identical equilibrium contact angles are to be expected for monolayers of a given long-chain compound adsorbed on different substrates, providing the surfaces are smooth and the adsorbed molecules of the monolayers are close-packed, as in the present case. Any differences in contact angles observed experimentally for different substrates should, therefore, be indications of differences in the roughness of the surface of the underlying solid. Comparison of the data obtained using both glass and platinum substrates revealed only slight differences in the equilibrium contact angles. Such differences significantly exceeded the reported reproducibility of the measurements only for the lower

alkanes. The roughness factor R (see Table I) was calculated using Wenzel's relation (8)

$$R = \frac{\cos \theta}{\cos \theta'}$$

assuming that the contact angle observed on unetched glass is a good approximation to that on an ideal smooth surface of contact angle θ' . The difference in the values of R so obtained did not exceed $2\frac{1}{2}\%$. Undoubtedly, R for the platinum foil uncoated by octadecylamine is greater than 1.013; hence, the low value observed reflects the extent to which monolayers of these long-chain compounds adsorbed on rolled platinum foil were able to bridge surface asperities. Consistent with this conclusion is the experimental fact that the difference in $\cos \theta$ for glass and platinum substrates becomes greater the lower the chain length and the greater

TABLE I

Comparison of the Equilibrium Contact Angles of the Normal Alkanes Exhibited on Different Oleophobic Surfaces at 20°C.

Liquid	Advancing contact angle (θ) for amine-saturated liquids on octadecylamine monolayers adsorbed on:		Roughness factor calculated from $R = \frac{\cos (\theta \text{ for platinum})}{\cos (\theta \text{ for glass})}$
	Rolled platinum foil	Blown glass plate	
<i>n</i> -Hexadecane	39°	39°	1.000
<i>n</i> -Tetradecane	34	34	1.000
<i>n</i> -Dodecane	30	32	1.021
<i>n</i> -Undecane	26	28	1.018
<i>n</i> -Decane	21	24	1.022
<i>n</i> -Nonane	13	18	1.024
<i>n</i> -Octane	6	9	1.007

1.013 = Average

the ability of the *n*-alkane sessile drop to attack the adsorbed film of amine. Presumably solvent attack occurs wherever CH_3 (and perhaps CH_2) groups project out above the exposed surface of the monolayer.

Contact angle data for some sixty liquids have been listed in Tables II and III, the compounds first being grouped according to structural similarities and then arranged in order of decreasing surface tension within each group. Despite the wide variety of structural types reported, there was a strong correlation of θ_E to γ_{LV}° . In general, the lower members of the homologous series exhibited zero contact angles, while the contact angles of the higher members increased with increasing surface tension. Although spreading was observed for the series of polymethylsiloxanes ranging from 5 to 27 silicone monomers per molecule, a polyethylsiloxane fluid (of relatively high surface tension) exhibited an appreciable contact angle.

An equilibrium contact angle of 102° was obtained for water, in agreement with the previously reported value for the advancing angle on films prepared in the absence of water (4). This compares with the value of 108° for bulk paraffin and 111° for single crystals of *n*-hexatriacontane reported by Fox and Zisman (5). As before (1, 3, 4), a contact angle of 90° was obtained on an oriented monolayer whose interstices had been

TABLE II

Surface Energy Relations of Some Homologous Series of Liquids on an Octadecylamine Monolayer (at $20^\circ\text{C}.$)

Liquid	γ_{LV}°	Initial θ (pure liquid)	Advancing θ (pure liquid)	Advancing θ (amine-sat. liquid)	$\gamma_{LV}^\circ \cos \theta_E$	$\gamma_{LV}^\circ (1 + \cos \theta_E)$	S_{LV}° / S_V°
	dyne/cm.	degree	degree	degree	erg/cm. ²	erg/cm. ²	erg/cm. ²
<i>n</i> -Alkanes							
Hexadecane	27.6	36	38	39	21.4	49.0	-6.2
Tetradecane	26.7	30	34	34	22.1	48.8	-4.6
Dodecane	25.4	23	30	30	22.0	47.4	-3.4
Undecane	24.7	16	26	26	22.2	46.9	-2.6
Decane	23.9	13	18	21	22.3	46.2	-1.6
Nonane	22.9	11	13	13	22.3	45.2	-0.6
Octane	21.8	ca. 0		6	21.7	43.5	-0.1
Heptane	20.3	Spread		Spread			
Hexane	18.4	Spread		Spread			
Cycloalkanes							
Cyclohexane	25.0	>15		16	24.0	49.0	-1.0
Cyclopentane	22.4	> 5		7	22.3	44.7	-0.1
<i>n</i> -Alkylbenzenes							
Decylbenzene	31.2	41	44	45	22.0	53.2	-9.2
Hexylbenzene	30.0	32	39	40	23.0	53.0	-7.0
Butylbenzene	29.2	30	32	37	23.3	52.5	-5.9
Propylbenzene	29.0	25	29	34	24.0	53.0	-5.0
Ethylbenzene	29.0	26	31	34	24.0	53.0	-5.0
Toluene	28.5	>20	31	32	24.2	52.7	-4.3
Benzene	28.9	>15	33	33	24.2	53.1	-4.7
di(Alkyl) ethers							
di(<i>n</i> -Decyl) ether	28.4	33	37	36	22.7	51.1	-5.7
di(<i>n</i> -Octyl) ether	27.7	32	36	36	22.4	50.1	-5.4
di(<i>n</i> -Heptyl) ether	27.0	28	34	34	22.4	49.4	-4.6
di(<i>n</i> -Amyl) ether	24.9	17	22	24	22.7	47.6	-2.2
di(<i>n</i> -Butyl) ether	22.8	8	9	9	22.5	45.3	-0.3
di(<i>n</i> -Propyl) ether	20.5	Spread		Spread			
di(iso-Amyl) ether	23.0	9		9	22.7	45.7	-0.3
di(iso-Propyl) ether	17.8	Spread		Spread			
Linear polyalkylsiloxanes							
Polyethylsiloxane (13 cstk. at $25^\circ\text{C}.$)	23.3	15		21	21.7	45.0	-1.7
Polymethylsiloxane (approx. 27 monomers/molecule) (35 cstk. at $25^\circ\text{C}.$)	19.9	Spread		Spread			
Heptadecamer	19.9	Spread					
Dodecamer	19.6	Spread					
Nonamer	19.2	Spread					
Octamer	18.8	Spread					
Heptamer	18.6	Spread					

saturated with molecularly dispersed water. This is not surprising in view of the porosity of such films to molecules as small as water (9).

The possibility was recognized that the inability of these liquids to wet completely the film-coated solid was due to the presence of a thin layer of air or water vapor between the sessile drop and the octadecylamine monolayer; this led to observations of the wettability of an oleo-

phobic film on platinum after it had been maintained in a vacuum of 10^{-4} mm. Hg for 20 minutes prior to contact with the test drop. The angles exhibited by drops of *n*-hexadecane toward such surfaces before, during, and after evacuation agreed with each other within the limits of error ($\pm 1^\circ$) of the contact angle measurements, indicating either that the adsorbed vapor was not responsible for the nonwetting property or

TABLE III
Surface Energy Relations of Some Miscellaneous Fluids on an Octadecylamine Monolayer (at 20°C.)

Liquid	γ_{LV}°	Initial θ (pure liquid)	Advancing θ (pure liquid)	Advancing θ (amine-sat. liquid)	$\gamma_{LV}^\circ \cos \theta_E$	$\gamma_{LV}^\circ (1 + \cos \theta_E)$	S_{LV}° / S_V°
	dyne/cm.	degree	degree	degree	erg/cm. ²	erg/cm. ²	erg/cm. ²
Fluorocarbons							
Polymonochlorotrifluoroethylene (86.9 cstk. at 100°F.)	25.0	40	40	37	19.2	44.2	- 5.8
Perfluorinated hydrocarbon FCD-330 (B. R. 60-130°C. at 10 mm.)	20.2	25	30	30	17.5	37.7	- 2.7
Perfluorinated hydrocarbon FCD-329 (B. R. 130-180°C. at 760 mm.)	18.3	16	17	18	17.4	35.7	- 0.9
Perfluorodimethylcyclohexane FCD-328	16.0	Spread		Spread			
Nonfluorinated halocarbons							
Methylene iodide	50.8	60	65	66	20.7	71.5	-30.1
Arachlor 1242	45.3	53	59	61	22.0	67.3	-23.3
α -Bromonaphthalene	44.6	51	58	58	23.6	68.2	-21.0
Arachlor 1248	44.2	60	60	61	21.4	65.6	-22.8
Perchlorocyclopentadiene	37.5	40	45	49	24.6	62.1	-12.9
Hexachlorobutadiene	36.0	30	32	38	28.4	64.4	- 7.7
Chloroform	27.1	10		20	25.5	52.6	- 1.6
Carbon tetrachloride	26.7	12		18	25.4	52.1	- 1.2
Esters							
Tricresyl phosphate	40.9	56	65	61	17.3	58.2	-23.6
Benzyl phenylundecanoate	37.7	54	58	56	20.0	57.7	-17.7
di(2-Ethylhexyl) phthalate	31.2	48	49	45	20.5	51.7	-10.7
di(2-Ethylhexyl) sebacate	31.1	42	46	44	21.6	52.7	- 9.5
Pentaerythritol tetracaprate	30.4	45	43	42	21.5	51.9	- 8.9
1,6-Hexamethylene glycol di-2-ethylhexanoate	30.2	41	44	41	21.7	51.9	- 8.5
di(2-Ethylhexyl) adipate	30.2	40	45	42	21.4	51.6	- 8.8
tri(2-Ethylhexyl) tricarallylate	29.6	37	45	42	20.9	50.5	- 8.7
Miscellaneous							
Mercury	485.	146			-402	73	-897
Water	72.8	90	102	102	-15.1	57.7	-87.9
Glycerine	63.4	90	90	94	- 5.5	57.9	-68.9
Formamide	58.2	79	81	81	9.1	67.3	-49.1
Ethylene glycol	47.7	73	73	78	9.9	57.6	-37.8
α -Methyl naphthalene	36.4	44	55	54	20.9	57.3	-15.5
<i>tert</i> -Butyl naphthalene	33.7	41	47	47	23.0	56.7	-10.7
Carbon disulfide	31.4	19		25	28.5	59.9	- 2.9

that it had not been successfully removed by vacuum treatment. The latter was considered less probable in view of the low affinity shown by the close-packed surfaces of methyl groups for such a wide variety of liquids of different chemical types.

It was recognized that conditions of thermodynamic equilibrium did not obtain completely for contact angle measurements made in the open

air; therefore, some measurements were made in an enclosed system allowed to equilibrate at 20.0°C. Under these conditions, conclusive measurements could not be made for *n*-octane (10.5 mm. Hg vapor pressure at 20°C.) because of excessive condensation. Repeated observations over 15-minute periods, under experimental conditions precluding the creepage of bulk liquid, established that condensation occurred from the vapor phase to form small, wet areas of zero contact angle. No significant differences were obtained in open air or in saturated air for the contact angle of dibutyl ether which has a vapor pressure of 4.8 mm. Hg at 20°C. With liquids having lower vapor pressures, the equilibrium contact angle was found to be equal, for all practical purposes, to that obtained with an unenclosed system. This conclusion would therefore apply to all the liquids except those homologues below *n*-nonane, butyl ether and propylbenzene, to the two cycloalkanes and to an occasional low member of the halocarbons.

Included in Tables II and III are the calculated values of several quantities of thermodynamic interest, each based on the maximum value of θ reported for a given liquid. These derived values have been calculated neglecting f_{SV}° , the free energy decrease on immersion of the solid in the saturated vapor. This seems justified in view of the equality of the contact angle observed with the dibutyl ether in a saturated vapor with that obtained in an unenclosed system.

DISCUSSION

In Fig. 1, the cosines of the contact angles corresponding to the three different methods of sessile drop formation have been plotted against γ_{LV}° for the homologous *n*-alkanes and *n*-alkylbenzenes; comparable plots for the di(*n*-alkyl) ethers were analogous to those for the alkanes. Parabolic curves best fitted the data for the initial angles of the homologous alkanes (and ethers), while linear relations were found for both types of advancing angles; data for the three types of angles observed for the alkylbenzenes fell along three straight lines. In similar plots for the several groups of miscellaneous liquids, essentially rectilinear relations are also found corresponding to each method of sessile drop formation.

There is evident in Fig. 1 a general downward displacement of each line in going from initial to advancing contact angle measurements for the pure liquids, the effect of establishing conditions of mechanical equilibrium being to increase the contact angle. Measurements made using sessile drops of amine-saturated liquid resulted in some slight further increase in the contact angle, the effect being more pronounced for those lower members of each series having the higher solvent powers for the amine. Similar results were obtained for many of the miscellaneous liquids. For the esters and one of the fluorocarbons, however, the use of

amine-saturated liquid resulted in a small, but definite decrease in the advancing angle. The possibility that amine adsorption at the liquid/air interface appreciably alters the liquid surface tension and thus decreases θ can be discounted, since the surface tension of the organic liquid is already low and the effective amine concentration is restricted owing to limited solubility. For the esters there exists the possibility that the dissolved amine interacts with free acid present in the ester to form an insoluble compound which collects at the solid/liquid interface. In general, solubility effects due to action of sessile drops on octadecylamine monolayers were relatively minor.

The $\cos \theta_E$ -vs.- γ_{LV}° data for all sixty liquids studied have been plotted in Fig. 2 using as the equilibrium contact angle (θ_E) the maximum value

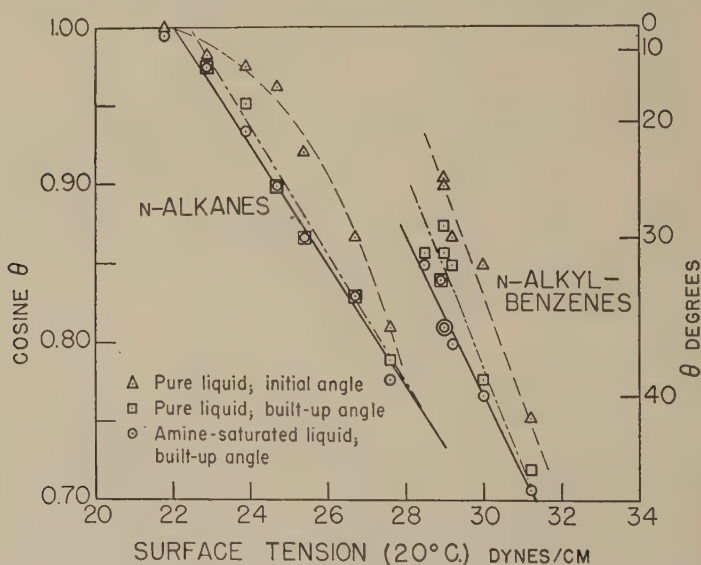


FIG. 1. Surface tension vs. cosine of the contact angle for two homologous series of liquids on octadecylamine-coated platinum.

of θ observed with the drop—build-up method. Linear relations were obtained for each homologous series, for the group of esters, and for the limited group of fluorocarbons. Even the data for the nonfluorinated halocarbons and miscellaneous liquids were best represented (with considerable scatter) by straight lines. In a similar treatment of data for the wetting of bulk paraffin surfaces and single crystals of *n*-hexatriacontane, Fox and Zisman (5) also reported linear relations for many of the same liquids, the positions and slopes of the lines approximating those reported here.

Extrapolation of the $\cos \theta_E$ -vs.- γ_{LV}° lines in Fig. 2 to the $\cos \theta_E = 1.0$

axis reveals as in (5) the existence of several different values for the characteristic "critical" surface tension (γ_c) which must be exceeded for members of a given homologous series to be nonspreading on the surfaces studied. The order of increasing γ_c for the various series of liquids approximates the order of solvent power of these liquids with respect to hydrocarbon derivatives like octadecylamine.

When homology is disregarded, the data points of Fig. 2 can be considered as falling on or between two limiting, approximately parallel, straight lines: along line *A* lie the data for the fluorocarbons, ethylene glycol, formamide, glycerine, and water; along line *C* lie the data for the various nonfluorinated halocarbons and carbon disulfide. Data for the

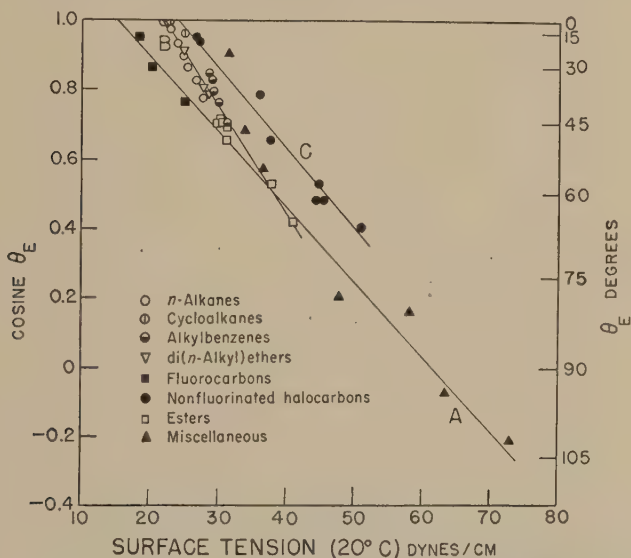


FIG. 2. Surface tension *vs.* cosine of the equilibrium contact angle of some liquids on octadecylamine-coated monolayers.

remainder of the liquids lie between these two lines, approximating an intersecting straight line *B*. As in (5), the general correspondence of γ_c to solvent power and to the solid/liquid interfacial tension can well account for the separation of the present data onto the discrete lines indicated in Fig. 2.

In Fig. 3 there have been plotted on equal scales the surface tension (γ_{LV}°) and the work of adhesion (W_A) for each of the liquids studied. As before (5, 6, 10), W_A has been calculated (7th column, Tables II and III) from the corrected Young-Dupré relation, assuming f_{SV}° to be negligible for these highly-repellent, low-energy surfaces. The data group onto three curves, the segregation of the liquids corresponding to that observed

in Fig. 2. Fox and Zisman have shown (5) that the observed linear relations between γ_{LV}° and $\cos \theta_E$ must necessarily result in parabolic relations between γ_{LV}° and W_A . Thus, from the analytic data for each line in Fig. 2, it becomes possible to derive the entire parabola without being restricted to that segment of the curve defined by experimental data; such calculated curves are indicated in Fig. 3 where the good correlation with the experimental points is evident. Completely analogous behavior was observed for surfaces of long-chain hydrocarbons (5).

It has been shown (10) that for equiscalar plots of W_A vs. γ_{LV}° , data points for all liquids producing the same free energy decrease on immer-

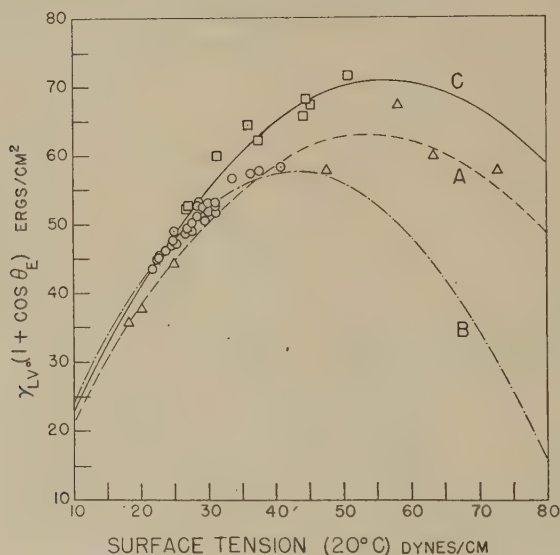


FIG. 3. Surface tension vs. work of adhesion for some liquids on octadecylamine-coated platinum. Curve A: Fluorocarbons, glycol, glycerine, formamide, water. Curve B: Normal and cyclic alkanes, alkylbenzenes, naphthalene derivatives, di(alkyl)ethers, esters. Curve C: Nonfluorinated halocarbons and carbon disulfide.

sion (f_{SL}) must fall on the same straight line of +1 slope, the intercept of this line with the axes of coordinates giving the value of f_{SL} . From Fig. 3 it is seen that this constancy requirement is met by the data for the homologous series of alkanes and ethers and for the two analogous perfluorinated hydrocarbons. Data for the alkylbenzenes, however, exhibited no such constancy, which is not surprising since this is not strictly a homologous series. When the calculated values of f_{SL} (i.e., $\gamma_{LV}^\circ \cos \theta_E$) are plotted against the liquid surface tension, essentially horizontal straight lines characterize the data for the alkanes and the two analogous fluorocarbons. Alkylbenzenes, however, have a linear decrease in f_{SL} with increasing γ_{LV}° .

The magnitudes of f_{SL} for the various liquids on amine-coated platinum surfaces were approximately the same as those reported for surfaces of bulk paraffin and single crystals of *n*-hexatriacontane. From the relation

$$f_{SL} = \gamma_{S^\circ} - \gamma_{SL}$$

it is seen that at its maximum value f_{SL} for any solid is equal to the free surface energy (γ_{S°). As in (5), it is concluded that the small range and low experimental values of f_{SL} observed on the monolayers indicate that

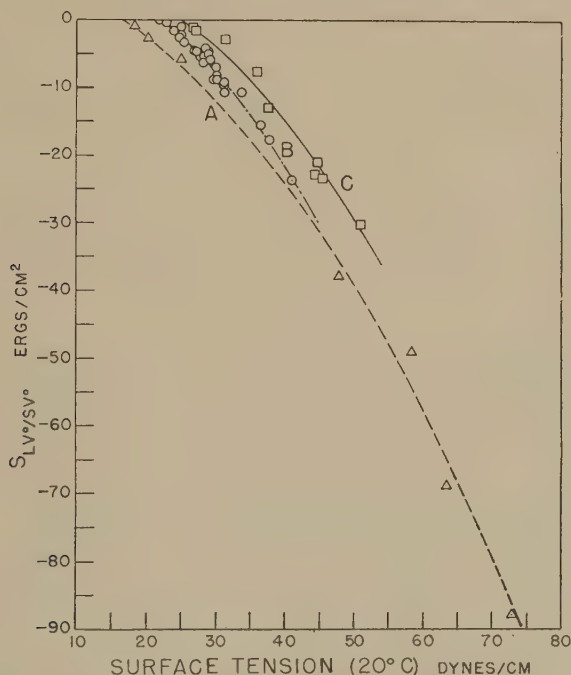


FIG. 4. Surface tension vs. spreading coefficient of some liquids on octadecylamine-coated platinum. Curve A: Fluorocarbons, glycol, glycerine, formamide, water. Curve B: Normal and cyclic alkanes, alkylbenzenes, naphthalene derivatives, di(alkyl)ethers, esters. Curve C: Nonfluorinated halocarbons and carbon disulfide.

γ_{S° , too, is probably not much more than 28.5 ergs/cm². The comparable figure inferred for single crystals of hexatriacontane was about 21.5; that for paraffin, about 30.5 (5).

A plot of γ_{LV° against the final spreading coefficient S_{LV°/S_{V° for liquids spreading on a solid is shown in Fig. 4. Since f_{SV° is considered negligible, the final spreading coefficients in Fig. 4 are equivalent to initial spreading coefficients, S_{LV°/S° . The data for the liquids again separate into three curves having the same constituents as the corre-

sponding curves in Figs. 2 and 3. As a consequence of the essential constancy of f_{SL} within the homologous alkane and ether series, the data for these series lie along lines with -1 slopes.

A comparison of the various wetting properties reported here and in (5) indicates that the amine-coated platinum represents a surface approximately intermediate between that of a single-crystal of *n*-hexatriacontane and that of bulk paraffin. The surface of bulk paraffin is composed of both methyl and methylene groups, while the surface of the single crystal is comprised solely of methyl groups in closest possible packing. In the case of the monolayer, each amphipathic molecule adsorbs with the polar group at the platinum surface and the nonpolar portion of the molecule directed away from the metal to form an external surface rich in methyl groups. The increased wettability of the monolayer over that of the single crystal is a reflection of the lower degree of molecular packing of the adsorbed monolayer.

The complete correspondence of the nonwetting behavior of the monolayers with that observed for bulk paraffin and hexatriacontane (5) attests to the capacity of a single layer of organic molecules to modify a metal surface to such an extent that behavior characteristic of a typical low-energy solid results.

The wetting data for hexatriacontane and for the monolayers provide reference points which are fundamental in any attempt to calculate from contact angle data the degree of packing of adsorbed films. Although much is known about the relation of the properties of monolayers at the water/air interface with respect to the degree of packing and orientation of the molecules, the analogous information is not yet available for adsorbed films at the solid/air interface. An approach on this problem has been described by us recently (11).

SUMMARY

The equilibrium contact angle (θ_E) has been measured for some sixty diverse liquids with respect to a smooth platinum surface coated with an adsorbed oriented monolayer of *n*-octadecylamine. Linear relations were found between cosine θ_E and the liquid surface tension (γ_{LV}°) for every homologous series. When homology was disregarded, the $\cos \theta_E$ -vs.- γ_{LV}° data for all the liquids collected on three straight lines, two of which were approximately parallel. Simple curvilinear relations obtained between the work of adhesion (W_A) and γ_{LV}° and between the final spreading coefficient (S_{LV}°/S_V°) and γ_{LV}° , the constituents of each set of three curves being the same as before. The grouping onto multiple lines corresponds to differences in the solid/liquid interfacial tension, γ_{SL} , and to the relative solvent power of the liquids for the adsorbed octadecylamine. The same

correlation obtained for the critical surface tension (γ_c), which was shown to be specific both to the homologous series and to the solid surface.

Constant values of the free energy decrease on immersion (f_{SL}) were observed for the homologous series of *n*-alkanes and *n*-alkyl ethers, while the alkylbenzene series showed a linear decrease with increasing γ_{LV}° . From the small range and low experimental values of f_{SL} observed for many unrelated liquids, it is concluded that the free surface energy of the monolayer-coated solid is probably not much more than 28.5 erg/cm².

The striking similarity observed for the wetting properties of the monolayer-coated surfaces compared with those reported previously for surfaces of single crystals of *n*-hexatriacontane and bulk paraffin (5) demonstrates that the wetting behavior of a surface is essentially controlled by the nature and packing of the outermost group of atoms in the molecules. Intercomparison of wetting data for the monolayer with reference data obtained for a surface of methyl groups in closest packing (i.e., *n*-hexatriacontane single crystals) is proposed as an approach for determining, from contact angle measurements, the packing of adsorbed films at the solid/air interface.

REFERENCES

1. BIGELOW, W. C., PICKETT, D. L., AND ZISMAN, W. A., *J. Colloid Sci.* **1**, 513 (1946).
2. BIGELOW, W. C., GLASS, E., AND ZISMAN, W. A., *J. Colloid Sci.* **2**, 563 (1947).
3. SHAFRIN, ELAINE G., AND ZISMAN, W. A., *J. Colloid Sci.* **4**, 571 (1949).
4. BAKER, H. R., SHAFRIN, ELAINE G., AND ZISMAN, W. A., *J. Phys. Chem.* **56**, 405 (1952).
5. FOX, H. W., AND ZISMAN, W. A., Part III, submitted to this journal.
6. FOX, H. W., AND ZISMAN, W. A., *J. Colloid Sci.* **5**, 514 (1950).
7. SUMNER, C. G., *Wetting and Detergency*. Chemical Publishing Co., New York, 1937, p. 15.
8. WENZEL, R. N., *Ind. Eng. Chem.* **28**, 988 (1936).
9. BAKER, H. R., AND ZISMAN, W. A., *Ind. Eng. Chem.* **40**, 2338 (1948).
10. FOX, H. W., AND ZISMAN, W. A., *J. Colloid Sci.* **7**, 109 (1952).
11. SHAFRIN, ELAINE G., AND ZISMAN, W. A. *Hydrophobic Monolayers and Their Adsorption from Aqueous Solution*. Presented at the Symposium on Monomolecular Layers, American Association for the Advancement of Science, Dec. 26, 1951.

LIGHT SCATTERING BY SOME THIXOTROPIC GELS

Mata Prasad, K. E. Subramanian, R. L. Desai and C. R. Kanekar

Chemistry Department, Institute of Science, Bombay, India

Received April 16, 1951; revised January 15, 1952

INTRODUCTION

Various investigators assume that the particles in a thixotropic system must be essentially non-spherical, that is, anisotropic in shape. Dube (1), Engelhardt (2), and Russel and Rideal (3) have attributed the thixotropic behavior to the ultimate disc-like or rod-like strongly anisometric or anisotropic colloidal particles. This view is supported by the fact that the particles are rod-shaped in thixotropic sols of V_2O_5 (4), benzopurpurin (5), barium malonate (6), and in thixotropic pastes of bentonite (7), and are plate-like in the thixotropic sol of iron oxide and in the thixotropic paste of clay (8). Although Freundlich (9) states that in the case of soln-hofen slate the particles do not show a marked deviation from an isometric shape, still he (10) considers that it would be rash to say that thixotropy is not bound to a nonspherical shape of the particles.

It has been observed by Freundlich (10) that the size of the particles in a thixotropic system must be below a certain limit. In the case of soln-hofen slate he found that the system is thixotropic only when the diameters of a certain percentage of the particles are $1\ \mu$ and less; if the diameters of all the particles are $10\ \mu$ or more the system is nonthixotropic. According to Freundlich this is due to the fact that large particles, being heavier, tend to get closely packed and the amount of liquid between them does not suffice for thixotropic behavior.

It has been shown by several workers (11,12) that the intensity of the scattered light and the depolarization factors ρ_u , ρ_v and ρ_h measured on using the incident light unpolarized and vertically and horizontally polarized, respectively, undergo a change during the process of gel-formation. Subbaramaiya (13) and Krishnan (14) have shown that the changes in the values of ρ_h and ρ_v indicate, respectively, the changes in the size and the anisotropy of the particles taking part in gelation. Therefore, a systematic study of the values of ρ_h and ρ_v could be reliably used to examine the validity of the conclusions arrived at by Freundlich and others regarding the anisotropy and the size of the particles in a thixotropic system.

The present paper gives the results of systematic investigation on the effect of mechanical shaking on the changes in values of the depolarization factors and intensity of the light scattered by the thixotropic gels of aluminum and thorium molybdates. Prasad and Doss (12) are the only workers to investigate the effect of mechanical shaking on the scattering of light by thixotropic gels. They have observed in the case of ceric phosphate gels that the values of the depolarization factors do not alter on shaking the set gel. The effect of addition of some electrolytes on the depolarization values was also studied since it is well-known that electrolytes alter the time of setting of gels and hence probably alter the size and shape of the particles and the ultimate structure of the gels.

EXPERIMENTAL

Measurement of the Depolarization Factors

The depolarization factors were measured by the well-known Cornu's method which is fully described by Prasad and Doss (12). For taking the depolarization measurements accurately the following precautions were taken:

The images seen through the double-image prism were just separated without overlapping. The images were neither too bright nor too dim. The required amount of brightness was obtained by adjusting the iris diaphragm attached to the condensing lens. All parasitic light was cut off with suitable screens. In order to achieve a perfect dark background the glass cell containing the gel-forming systems was wrapped completely with black paper with only three openings, two for the passage of the incident light and the third, at right angles to these two, for observing the scattered light. Since with limited background enhanced values of depolarization factors are obtained, only the natural background method was used throughout the investigation. The effect due to the secondary scattering was reduced to a minimum by using a very narrow pencil of the incident light. All the observations were confined to the focal plane of the condensing lens so that the beam of light was practically parallel in the medium. The depolarization values are given in percentages.

Measurement of Intensity of Scattered Light

The intensity of scattered light was measured by a new photoelectric method based on the one given by Ananthakrishnan (15). The circuit diagram is given in Fig. 1.

In practice, it is found that a steady state is reached about half an hour after switching on the various connections. Balance is first obtained with the photocell in the dark by adjusting the potentiometer r_1 when the double way switch is in position connecting terminals a and b with c

and d , putting the photocell out of the circuit, and then finally by adjusting the rheostat r_2 when the double way switch is in position connecting terminals a and b with e and f . Both r_1 and r_2 control the grid of one of the vacuum tubes. The photocell is mounted at one of the ends of the metal chassis so that the scattered light falls on the sensitive vane of the photocell. When the cell is illuminated, the photoelectric current developed produces a small change in the grid potential of one of the vacuum tubes and thus disturbs the balance. The deflection of the galvanometer due to this resultant current is a measure of the light falling on the photocell.

In order to prevent the effect of any stray electrical disturbance all wiring of the circuit was done with shielded wires and the photocell was

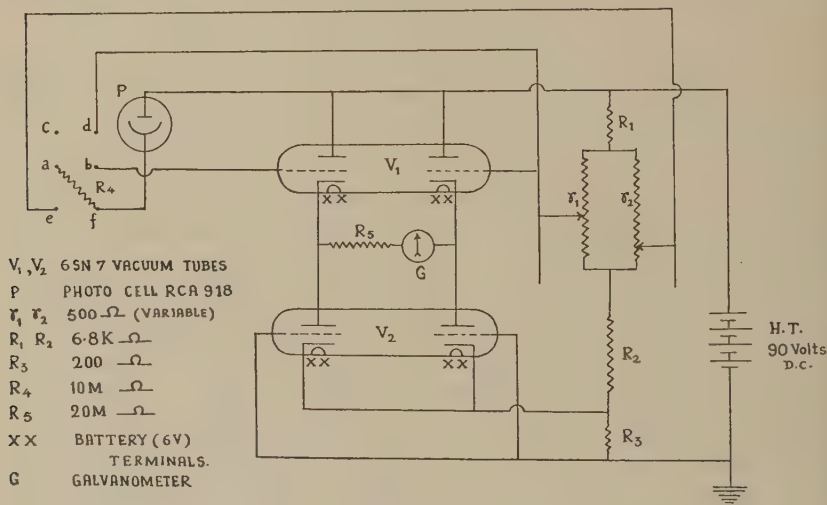


FIG. 1.

covered with a metallic cover having a window in front of the sensitive vane of the photocell. The window was provided with a sliding door. The secondary scattering was reduced in the same manner as with depolarization measurements. To eliminate error due to the divergent nature of the scattered beam and to measure the scattering exactly at right angles to the incident track, the window on the metal cover of the photocell was made the same size as the slit on the solution cell. Perfect collimation was obtained by inserting one more slit similar to the above two slits in between the solution cell and the photocell unit. When there was no glass cell in the path of the incident light, the galvanometer showed zero deflection with or without the incident light, thereby showing that the galvanometer deflections were exclusively due to light scattered by the gel-forming mixtures contained in the solution cell. The intensity readings

are given in terms of galvanometer deflection in centimeters, and are purely relative.

All the experiments were carried out in a dark room in which the entry of all stray light was avoided.

As the presence of dust particles in the solution greatly affects the values of intensity and depolarization factors of the scattered light, the solutions were made completely free from dust particles by filtering repeatedly through sintered glass filters.

Preparation of the Gels

Aluminum Molybdate Gels. These gels were first prepared by Mushran (16) by mixing suitable amounts of 11.5% solution of aluminum chloride with 20% solution of sodium molybdate. The authors prepared these gels by a new method by mixing suitable volumes of 20% solutions of aluminum nitrate (A_1) and potassium molybdate (B_1) with and without the addition of $N/3$ solutions of KCl (C_1), KNO_3 (D_1) and K_2SO_4 (E_1); the total volume was made up to 27 cc. for all mixtures. A precipitate was thrown off immediately on mixing the two gel-forming solutions which got peptized in a few minutes and a clear sol was obtained, finally setting to a translucent gel.

Thorium Molybdate Gels. These gels were prepared by mixing suitable volume of 6% solution of thorium nitrate (A_2) and 10% solution of potassium molybdate (B_2), with and without the addition of 1 N solutions of HCl (C_2), HNO_3 (D_2) and H_2SO_4 (E_2); the total volume was made up to 10 cc. for all mixtures. A precipitation was obtained immediately on mixing the two gel-forming mixtures, which became peptized within a few seconds. The result was an opaque sol that ultimately set to a transparent gel.

Procedure

In order to take the readings the gel-forming mixture in the sol state was placed in a rectangular optical glass cell and the depolarization factors and the intensity of the scattered light were immediately measured in the usual manner. The readings were then taken after the gels had set. To find the effect of thixotropic setting on these values, the set gels were liquefied by shaking the optical cell, the liquefied contents were transferred quickly to a beaker and thoroughly shaken for half a minute. They were then transferred back to the optical glass cell and the depolarization factors and the intensity of the scattered light were immediately measured. These readings were taken again after the gels had re-set.

RESULTS

The results obtained are given in the following tables in which t_1 denotes the reading for the sol, t_2 the readings of the systems when they

had just set, t_3 the readings immediately on shaking the set gel, and t_4 the reading after the gels have re-set. T denotes the time of setting of the gels, and $T.T.$ the thixotropic time of setting. For the sake of brevity the values of T , $T.T.$, ρh , and I are given only in Tables I and IV. The values of A_1 , B_1 , C_1 , D_1 , and E_1 and A_2 , B_2 , C_2 , D_2 , and E_2 are given in cc. Tables II, III, and V bring out the effect of the addition of electrolytes on the values of ρu and ρv .

TABLE I

Light Scattering by Aluminum Molybdate Gels

	$A_1 = 13.5; B_1 = 6.0; T = 63'15'';$ $T.T. = 4'45''$				$A_1 = 13.5; B = 6.9; T = 60'45'';$ $T.T. = 4'30''$			
	ρu	ρv	ρh	I	ρu	ρv	ρh	I
t_1	0.32	0.23	90	0.20	0.49	0.28	88	0.30
t_2	5.33	2.37	35	16.70	9.65	3.78	45	28.50
t_3	5.33	2.37	35	16.20	9.65	3.78	45	28.10
t_4	5.33	2.37	35	16.75	9.65	3.78	45	28.60

TABLE II

Effect of Electrolytes on Light Scattering by Aluminum Molybdate Gels $A_1 = 13.5; B_1 = 6.0$

	C_1				D_1				E_1			
	1.0		2.0		1.0		2.0		1.0		2.0	
	ρu	ρv	ρu	ρv	ρu	ρv	ρu	ρv	ρu	ρv	ρu	ρv
t_1	0.28	0.09	0.23	0.07	0.28	0.07	0.19	0.12	0.19	0.07	0.19	0.07
t_2	2.95	1.11	2.23	0.93	3.43	1.30	2.65	1.20	4.10	1.66	4.92	1.85
t_3	2.95	1.11	2.23	0.93	3.43	1.30	2.65	1.20	4.10	1.66	4.92	1.85
t_4	2.95	1.11	2.23	0.93	3.43	1.30	2.65	1.20	4.10	1.66	4.92	1.85

TABLE III

Effect of Electrolytes on Light Scattering by Aluminum Molybdate Gels $A_1 = 13.5; B_1 = 6.9$

	C_1				D_1				E_1			
	1.0		2.0		1.0		2.0		1.0		2.0	
	ρu	ρv	ρu	ρv	ρu	ρv	ρu	ρv	ρu	ρv	ρu	ρv
t_1	0.49	0.15	0.38	0.07	0.49	0.09	0.38	0.07	0.49	0.09	0.38	0.07
t_2	2.37	1.30	2.10	1.11	3.78	1.40	3.11	1.20	6.93	2.23	7.69	2.10
t_3	2.37	1.30	2.10	1.11	3.78	1.40	3.11	1.20	6.93	2.23	7.69	2.10
t_4	2.37	1.30	2.10	1.11	3.78	1.40	3.11	1.20	6.93	2.23	7.69	2.10

TABLE IV

Light Scattering by Thorium Molybdate Gels $A_2 = 5.0; B_2 = 0.4; T = 152'36'';$
 $T.T. = 128'17''$ $A_2 = 5.0; B_2 = 0.6; T = 52'12'';$
 $T.T. = 42'6''$

	ρu	ρv	ρh	I	ρu	ρv	ρh	I
t_1	3.96	2.50	90.06	10.1	6.45	3.60	90.06	11.2
t_2	1.85	0.84	82.50	1.0	2.23	0.93	75.57	1.3
t_3	1.85	0.84	82.50	1.0	2.23	0.93	75.57	1.3
t_4	1.85	0.84	82.50	1.0	2.23	0.93	75.57	1.3

TABLE V

Effect of Addition of Acids on Light Scattering by Thorium Molybdate Gels

	$A_2 = 5.0; B_2 = 0.4$						$A_2 = 5.0; B_2 = 0.6$					
	$C_2 = 0.25$		$D_2 = 0.25$		$E_2 = 0.25$		$C_2 = 0.50$		$D_2 = 0.50$		$E_2 = 0.50$	
	ρu	ρv	ρu	ρv	ρu	ρv	ρu	ρv	ρu	ρv	ρu	ρv
t_1	0.77	0.49	2.10	1.02	2.37	1.20	0.93	0.62	2.37	1.02	6.69	2.51
t_2	0.69	0.37	1.40	0.62	2.10	1.01	0.77	0.32	1.30	0.62	3.11	1.30
t_3	0.69	0.37	1.40	0.62	2.10	1.01	0.77	0.32	1.30	0.62	3.11	1.30
t_4	0.69	0.37	1.40	0.62	2.10	1.01	0.77	0.32	1.30	0.62	3.11	1.30

DISCUSSION OF RESULTS

It will be seen from the above tables that generally there is no perceptible change in the values of the depolarization factors on shaking the set gels. Prasad and Doss (12) have also made similar observations with ceric phosphate gels. From these observations it is established on the basis of Krishnan's theory that the particles of a set thixotropic gel do not undergo any change in size and shape when the gel is liquefied by mechanical shaking.

The final values of ρv obtained in this investigation are quite small, indicating that the particles are nearly isotropic in shape. Hence it can be inferred that the particles of a thixotropic gel need not necessarily be strongly anisotropic. These observations are in conformity with those of Pryce-Jones (17) who observed that the particles in thixotropic wax globules were spherical.

The depolarization factors obtained in the present investigation show that although the particles in the sols of thorium and aluminum molybdates are very nearly of the same size, the particles in thorium molybdate gels are much smaller than those in the aluminum molybdate gels (cf. the values of ρh in Tables I and IV).

It can be seen from the values of ρv in Tables I and IV that the addition of increasing amounts of potassium molybdate causes the formation of less isotropic particles whereas the reverse is the case with the addition

of increasing amounts of aluminum nitrate or thorium nitrate, respectively. Tables I, II, and III show that the addition of KCl and KNO_3 to the gel-forming mixtures of aluminum molybdate decreases the final values of ρu and ρv whereas the addition of K_2SO_4 increases these values. These effects are probably due to (i) the peptizing action of the chloride and the nitrate ions, since the gels are formed only in the presence of excess of aluminum nitrate or aluminum chloride (Mushran's method) over potassium or sodium molybdate and (ii) the coagulating effect of the sulfate ions. The effect of the addition of acids on thorium molybdate gels (cf. Tables IV and V) can also be explained in the same manner.

Freundlich (18), Ostwald (19), Hauser (20) and Kistler (21) have shown that the lysospheres of the gel particles are destroyed on shaking and re-formed on allowing them to stand. Prakash and Biswas (22) have also assumed that the liquefaction of thixotropic systems by mechanical shaking liberates the structurally imbibed liquid which provides the dispersion medium for the jelly-forming substances. The observations given in this paper, namely, the constancy of the values of the depolarization factors of the gel systems during thixotropic gelation, give a very important and fairly conclusive experimental evidence that the mechanical shaking of a thixotropic gel only breaks its ultimate structure and does not cause any disintegration of the ultimate gel particles.

It is observed in the case of aluminum molybdate gels that there is a slight but definite decrease in the intensity of scattered light when the gel is mechanically shaken and liquefied and a subsequent rise when it re-sets. As no changes in the size and shape of the particles take place during these processes the observed changes in the intensity may be attributed to the destruction of the gel structure on shaking and re-formation on re-setting. Similar behavior was not observed with thorium molybdate gels due to the fact that the final intensity of the scattered light is very small in these gels.

The authors feel grateful to Shri V. Sundaram for his assistance during the writing of this paper.

SUMMARY

The measurements of depolarization factors and intensity of transversely scattered light have been made during the thixotropic gelation of aluminum molybdate and thorium molybdate gels. It has been observed that mechanical shaking of a thixotropic gel does not affect the size and the shape of the particles. The low values of ρv indicate that the particles in the gels are isotropic.

REFERENCES

1. DUBE, G. P., *Indian J. Phys.* **17**, 189 (1943).
2. ENGELHARDT, W., *Kolloid Z.* **102**, 217 (1943).
3. RUSSEL, J. L., AND RIDEAL, E. K., *Proc. Roy. Soc. London* **154A**, 540 (1936).

4. FREUNDLICH, H., AND SCHALEK, E., *Z. physik. Chem.* **108**, 153 (1924).
5. PAPKOVA-KUITZEL, T. P., *Kolloid-Z.* **69**, 57 (1934).
6. ZOCHER, H., AND ALBU, H. W., *Kolloid-Z.* **46**, 33 (1928).
7. BUZAGH, A., *Kolloid-Z.* **47**, 223 (1929).
8. JEPPESEN, A., *Kolloid-Z.* **57**, 175 (1931).
9. FREUNDLICH, H., Thixotropy. Herman & Cie., Paris, 1935 edn., p. 19.
10. FREUNDLICH, H., Thixotropy. Herman & Cie., Paris, 1935 edn., p. 21.
11. MARDLES, E. W., *Trans. Faraday Soc.* **18**, 318 (1923); KRAMER, E. O., AND CO-WORKERS, *J. Phys. Chem.* **29**, 1169 (1925); **31**, 764 (1927); HOLWERDA, B. J., *Rec. trav. chim.* **50**, 601 (1931); KRISHNAMURTHI, K., *Proc. Roy. Soc. London* **122A**, 76 (1929); **129A**, 490 (1930); RAMAIAH, D. S., *Proc. Indian Acad. Sci.* **5A**, 128, 138 (1937); PRASAD, M., AND GURUSWAMY, S., *Proc. Indian Acad. Sci.* **19A**, 47, 66, 77 (1944).
12. PRASAD, M., AND DOSS, K. D. V., *J. Colloid Sci.* **4**, 349 (1949).
13. SUBBARAMAIIYA, D. S., *Proc. Indian Acad. Sci.* **1A**, 709 (1935).
14. KRISHNAN, R. S., *Proc. Indian Acad. Sci.* **1A**, 717, 782 (1935).
15. ANANTHAKRISHNAN, R., *Proc. Indian Acad. Sci.* **1A**, 201 (1934).
16. MUSHRAN, S. P., *Current Sci. (India)* **18**, 48 (1949).
17. PRYCE-JONES, J., Experiments in Colloid Chemistry. By Hauser and Lynn, McGraw-Hill, New York, p. 113.
18. FREUNDLICH, H., *Kapillarchemie*. 1932 edn., Vol. II, 624.
19. OSTWALD, W. O., *Kolloid-Z.* **46**, 263 (1928).
20. HAUSER, E. A., *J. Rheology* **2**, 5 (1931).
21. KISTLER, S. S., *J. Phys. Chem.* **35**, 815 (1931).
22. PRAKASH, S., AND BISWAS, N. N., *J. Indian Chem. Soc.* **8**, 549 (1931).

THE DISTRIBUTION OF IONS BETWEEN CELLULOSE AND SOLUTIONS OF ELECTROLYTE

J. Farrar and S. M. Neale *

Faculty of Technology, University of Manchester, England

Received January 14, 1952

INTRODUCTION

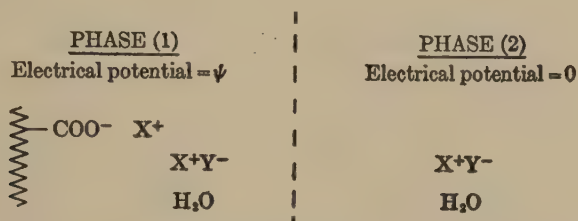
Although the interactions between electrolytes and hydrophilic macromolecular substances such as cellulose, gelatin and keratin play an important part in many technical processes, and in the behavior of living cells, their mechanism is by no means fully understood. In the treatment of equilibria in such systems, the classical thermodynamics of Willard Gibbs, and in particular the Donnan theory of membrane equilibrium, have been usefully employed. In the process of dyeing, for instance, the color ion usually has some specific affinity for the fiber and is therefore adsorbed, whereas the distribution of the other ions is commonly supposed to be governed merely by the variations of electrical potential within the system.

In the equipotential surface theory of Gilbert and Rideal (1), the color ions and their gegen-ions are adsorbed in equivalent amounts upon an interface (Model I). In the equipotential volume theory of Hanson, Neale, and Stringfellow (2), followed by Willis *et al.* (3), the fiber with its imbibed water is regarded as a homogeneous bulk phase separate from the external solution (Model II). The application of the classical thermodynamics to these models leads to very similar predictions as to the effects of temperature and of dye and salt concentration upon the equilibrium adsorption of the color ions. Dye adsorption measurements alone, therefore, cannot be used to discriminate between these two models, of the equipotential surface and of the equipotential bulk phase, respectively.

Now it is an experimental fact that cellulose and other hydrophilic fibers adsorb large quantities of water from saturated vapor and similar amounts from pure water and dilute aqueous solutions. This imbibed water with its dissolved ions can be fairly sharply separated from the external solution by means of the centrifuge and the composition of the internal solution can then be determined by analysis.

* One of us (J. F.) wishes to acknowledge his indebtedness to the British Rayon Research Association for a research scholarship, during the tenure of which this work was done.

Model I with its extended surface offers no information as to the electrical potential or composition of the enclosed solution. Only the second model enables us to predict the composition of the internal solution, and this may be done by the use of the principle of the Donnan membrane equilibrium. Suppose, for example, the system to be one of cellulose in aqueous salt solution, the ion exchange properties of the cellulose being determined solely by the presence of carboxylic acid groups. (It will appear later that such an explanation is not wholly adequate.) The system can then be represented as follows on the basis of Model II:



The conditions of equilibrium for the cations and anions of the salt are:

$$\mu_1^{0+} + RT \ln a_1^+ + \psi F = \mu_2^{0+} + RT \ln a_2^+ \quad [1]$$

and

$$\mu_1^{0-} + RT \ln a_1^- - \psi F = \mu_2^{0-} + RT \ln a_2^- \quad [2]$$

if the effect of the hydrostatic pressure difference between the two phases be neglected (4, 5). Addition of eqs. [1] and [2] gives:

$$\begin{aligned}
 \Delta\mu^{0+} + \Delta\mu^{0-} &= RT \ln a_1^{\pm} - RT \ln a_2^{\pm} \\
 &= RT \ln m_1^+ + RT \ln m_1^- + 2RT \ln f_1^{\pm} \\
 &\quad - RT \ln m_2^+ - RT \ln m_2^- - 2RT \ln f_2^{\pm} \\
 &= RT \ln \left[\frac{m_1^+}{m_2^+} \cdot \frac{m_1^-}{m_2^-} \cdot \left(\frac{f_1^{\pm}}{f_2^{\pm}} \right)^2 \right] \\
 &= RT \ln \left[\lambda^+ \cdot \lambda^- \cdot \left(\frac{f_1^{\pm}}{f_2^{\pm}} \right)^2 \right]
 \end{aligned} \quad [3]$$

The experimental determination over a sufficient concentration range of the "internal" and "external" ionic concentrations m_1^+ , m_1^- , m_2^+ and m_2^- , as has been done in the present work, will afford a check on the possibility of describing the system in terms of Model II, although since the activity coefficients f are unknown, absolute verification is at present not possible.

The validity of the assumptions commonly made, either explicitly or implicitly, in dealing with such a system, namely: (a) that $\Delta\mu^0$ is zero for the ions of simple electrolytes and (b) that the differences in activity coefficients between the internal and external phases can be neglected,

can also be checked if the measurements are sufficiently accurate and extensive. It will be noted that if these two assumptions are in fact made, equation (3) reduces to:

$$m_1^+ \cdot m_1^- = m_2^2 \quad \text{or} \quad \lambda^+ \cdot \lambda^- = 1 \quad (\lambda = \text{ion distribution ratio}),$$

which is the Donnan expression in its simplest form.

Usher and Wahbi (6) were the first to attempt to determine by direct chemical analysis, the validity of such assumptions in the distribution of ammonium chloride between water and cellulose sheet both with and without adsorbed anionic dyes. They concluded "that a Donnan equilibrium exists in 0.1 *M*, but not in 0.5 *M* solution," and it will now appear that this contradiction arises through a cancellation at high concentrations of the Donnan effect (depressing the chloride ion concentration in the internal phase) against some slight specific affinity between ammonium chloride and cellulose ($\Delta\mu^0$ is not zero). A careful examination of their results, moreover, shows them to be hardly extensive or accurate enough for an adequate solution of the problem (7). In the present work an attempt has been made, following careful refinement of the analytical methods employed, to measure the distribution of both cations and anions of a small number of uni-univalent salts between cellulose and water, over as wide a range of concentrations as possible.

EXPERIMENTAL METHODS

In order to obtain the highest possible accuracy, it was decided to separate the two phases as far as possible before analysis of each, rather than to measure the change in concentration of a solution upon contact with cellulose.

Removal of the External Solution from the Sample

At the outset of this work the external solution was removed from the Cellophane by the usual method of "blotting" between sheets of dry filter paper or moistened cotton cloth. Such samples showed, on analysis, higher internal salt concentrations than did samples prepared by centrifuging for 5 minutes at 2000 r.p.m. on a non-adsorbent plate.

When an experiment was performed in which the sample of cellophane was compressed under direct pressure between clean cotton pads, the results indicated that the equilibrium condition was disturbed owing to the too rapid removal of water. Centrifugal separation at 1400 *g* for 5 minutes was therefore adopted as the standard procedure. It was found that the quantity of water (*W*) retained by many textile fibers (including cellulose) could be expressed by the following relationship:

$$W = A + B\gamma$$

where γ = surface tension (in dynes/cm.) of the air-water interface, B = proportionality constant (ca. 0.3 for many hydrophilic fibers), and A appears to correspond to the regain from saturated water vapor. Figure 1 illustrates these facts. It is based upon experiments in which

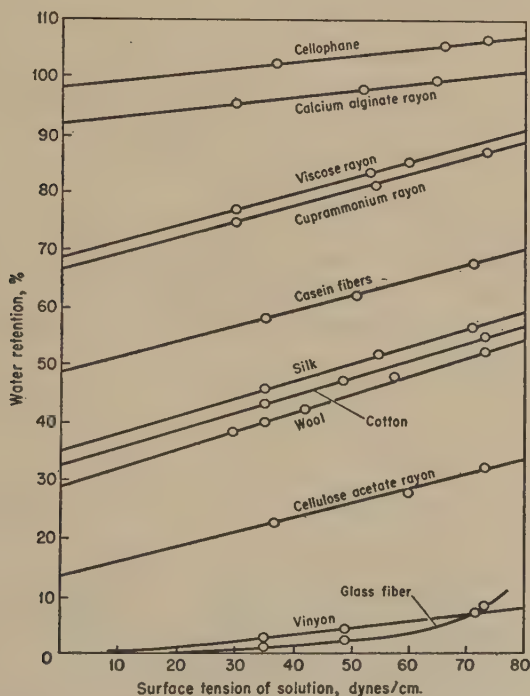


FIG. 1. Variation of the water retention of several fibers with the surface tension of the air/water interface.

traces of commercial wetting agents (Lissapol and Teepol) were added to the water in which the fibers were soaked. It will be seen that sufficient external solution remains on the Cellophane to justify the assumption that the centrifuging does not express any of the internal solution.

Analysis

The electrolytes were extracted from the cellulose samples with hot water or dilute acetic acid in a Soxhlet apparatus. Acetic acid was employed to supply hydrogen ions which are particularly effective in replacing the bound cations on account of the low dissociation of the cellulose carboxylic acid groups. The ammonium ions were estimated by making the extract alkaline with caustic soda and then distilling off the ammonia into boric acid. Completion of ammonia distillation was checked by examining the conductivity of the distillate continuously, as it emerged

from the condenser. The boric acid solution was then titrated with 0.01 *M* hydrochloric acid using a screened indicator (8).

The halide ions present in a portion of the extract were estimated by potentiometric titration with silver nitrate using silver electrodes or mercurous nitrate using mercury electrodes.

EXPERIMENTAL MATERIALS

(1) *Cellophane*. The "600" grade (produced by the British Cellophane Co. Ltd., Bridgewater) was used when washed free from glycerol with water. The material had the following properties:

Weight = ca. 6 mg./cm².

Fluidity (0.5% solution) = 10

Copper number (Heyes' micromethod) = 1.28

Carboxyl content (Neale's titration method) = 0.048 milliequivs./g. Cellophane.

(2) *Cotton*. Commercially produced bleached cotton yarn was used having the following characteristics:

Fluidity = 4.5

Copper number = 0.04

Carboxyl content = 0.005 milliequivs./g. cotton.

(3) *Oxycelluloses*. Prepared from the above materials by periodate-chlorite oxidation (9, 10).

(4) *Dyed Cellophane*. Cellophane sheets were dyed for 5 hours at 60°C. from 0.1 *M* ammonium chloride solution containing Benzopurpurine 4B. They were allowed to stand at room temperature (18°C.) in this solution for several weeks before analysis. The dyestuff was estimated colorimetrically in the solution after stripping from the sample by means of aqueous pyridine.

(5) *Esterified Cellophane*. The Cellophane sheets were treated with very dilute acid to remove cations, they were then washed in water and immersed for several days at room temperature in a 1% aqueous solution of ethylene oxide (11). Since the product gave no acid reaction in salt solution, it was presumed that the carboxylic acid groups had been fully esterified.

(6) *Solutions*. The salts used were of A.R. grade and since the cellulose samples were immersed in large volumes of salt solution, the pH of these solutions remained constant at about 5.6.

RESULTS

The distribution of various anions and cations between cellulose and water and between cellulose and alcohols were examined as described above and the results given in the following tables are the means of several experiments in close agreement.

m_2 = external (bulk) concentration of ions expressed in g. moles/1000 g. water,

$\frac{W}{C}$ = g. imbibed water/g. cellulose,

m_1^+ and m_1^- = internal concentration of cations and anions respectively,

$\lambda^+ = \frac{m_1^+}{m_2^+}$ and $\lambda^- = \frac{m_1^-}{m_2^-}$ are the distribution ratios for cations and anions respectively,

$\lambda^+ \cdot \lambda^- = \lambda^2$, which equals unity for the ideal case of the Donnan theory.

DISCUSSION OF THE RESULTS

In Table I it is clearly seen that λ^- decreases with decreasing concentration, as predicted by the Donnan theory, while λ^+ increases as it must if the NH_4^+ ion forms a salt linkage with COO^- groups. The internal concentration of COO^- groups should be equal to $(m_1^+ - m_1^-)$. It will be noted that this quantity decreases with decreasing salt concentration,

TABLE I

Distribution of Ions between Cellophane and Solutions of Electrolyte

Salt	m_2	$\frac{W}{C}$	m_1^+	λ^+	m_1^-	λ^-	λ^2
NH_4Cl	6.275	1.038	6.480	1.033	6.470	1.030	1.064
NH_4Cl	2.164	1.168	—	—	2.220	1.025	—
NH_4Cl	1.041	1.177	1.085	1.043	1.034	0.993	1.034
NH_4Cl	0.510	1.190	0.533	1.041	0.484	0.949	0.993
NH_4Cl	0.100	1.201	0.123	1.23	0.0811	0.811	0.997
NH_4Cl	0.05	1.205	0.0751	1.50	0.0338	0.675	1.013
NH_4Cl	0.02	1.24	0.0485	2.42	0.00868	0.434	1.050
NH_4Cl	0.01	1.23	0.0321	3.21	0.00175	0.350	1.124
NH_4Cl	0.005	1.24	0.0205	4.09	0.00160	0.320	1.310
LiCl	18.56	1.089	—	—	21.64	1.166	—
LiCl	9.780	1.108	—	—	10.20	1.044	—
LiCl	0.100	1.204	0.125	1.25	0.0778	0.78	0.975
KI	8.150	1.159	—	—	9.005	1.105	—
KCl	3.930	1.117	—	—	4.113	1.046	—
KCl	0.100	1.205	0.121	1.21	0.082	0.82	0.997
KCl	0.05	1.222	—	—	0.0388	0.675	—
KCl	0.02	1.214	—	—	0.00824	0.412	—
KCl	0.01	1.210	—	—	0.00338	0.338	—
KCl	0.005	1.200	—	—	0.00141	0.282	—

although the total number of carboxylic acid groups in the cellulose must remain constant. This effect is to be attributed to a lowering of internal pH as λ^+ increases for, according to the Donnan theory, this distribution ratio applies to all univalent cations.

As already pointed out, if the activity coefficients in the Donnan expression cancel and if $\Delta\mu^0$ is zero, λ^2 should always be equal to unity.

TABLE II

Distribution of Ions between Cotton and Solutions of Electrolyte

Salt	m_s	$\frac{W}{C}$	m_1^+	λ^+	m_1^-	λ^-	λ^2
NH ₄ Cl	5.400	0.457	5.550	1.028	5.304	0.982	1.010
NH ₄ Cl	3.484	0.460	3.570	1.023	3.405	0.978	1.002
NH ₄ Cl	1.041	0.488	1.080	1.036	0.981	0.942	0.978
NH ₄ Cl	0.510	0.496	0.536	1.051	0.481	0.943	0.991
NH ₄ Cl	0.100	0.500	0.106	1.06	0.092	0.92	0.975
NH ₄ Cl	0.05	0.500	0.0574	1.15	0.0435	0.87	1.00
NH ₄ Cl	0.01	0.507	0.0134	1.34	0.0078	0.78	1.045
LiCl	7.390	0.484	—	—	8.310	1.125	—
KCl	3.793	0.470	—	—	4.137	1.091	—
Na ₂ S ₂ O ₃	2.859	0.497	—	—	2.660	0.930	—
Na ₂ S ₂ O ₃	1.641	0.473	—	—	1.436	0.875	—
Na ₂ S ₂ O ₃	0.540	0.523	—	—	0.460	0.851	—

It appears, however, that λ^2 tends to be greater than one, especially in dilute solutions. The reason for this may be that the NH₄⁺ ions that play the part of counter ions to the COO⁻ groups in the macromolecular network do not have the same escaping tendency or activity as if they were in fact in true solution.

High values of λ^2 could also arise from some specific affinity of the electrolyte for cellulose, so that $\Delta\mu^0$ is not zero (eq. [3]). This is suggested by the fact that at high concentrations λ^2 and even λ^- are greater than one, especially for lithium or iodide ions that have the power of swelling cellulose. The good agreement between the λ^- values for potassium and ammonium chlorides over the whole concentration range down to 0.01 *M* shows that the experimental accuracy was adequate.

Table II refers to bleached cotton in which the carboxylic acid content is only about one-tenth that of the Cellophane. The water uptake however is less than half, so that the expected value of the carboxyl ion concentration is about a quarter of that for Cellophane. The smaller differences between m_1^+ and m_1^- , and the rather higher values of λ^- in dilute solutions, agree with this expectation. The variations in λ^2 are similar to those already encountered in Table I.

TABLE III

Distribution of Ions between Oxycelluloses and 0.1 M Ammonium Chloride Solutions

$\frac{A}{C}$	$\frac{W}{C}$	m_1^+	λ^+	m_1^-	λ^-	λ^2
0.112	1.17	0.166	1.66	0.067	0.67	1.112
0.192	1.10	0.211	2.11	0.061	0.61	1.287
0.357	1.09	0.307	3.07	0.050	0.50	1.535
0.808	1.05	0.413	4.13	0.042	0.42	1.735

$\frac{A}{C}$ = meq. carboxylic acid groups/g. oxycellulose

The materials to which Tables III and IV refer were prepared in an attempt to increase the cationic binding power of the cellulose, in the first case by the formation of extra carboxylic acid groups by oxidation, and in the second by the adsorption of an anion-active dye. Here very high values of λ^2 are encountered, increasing with increase of λ^- . This may be ascribed to decreased activity of the cations in the internal phases. The general pattern of the Donnan distribution $\lambda^+ > 1 > \lambda^-$ is, however, still maintained.

TABLE IV

Distribution of Ions between Benzopurpurine 4B Dyed Cellophane and 0.1 M Ammonium Chloride Solutions

$\frac{D}{C}$	$\frac{A}{C}$	$\frac{W}{C}$	m_1^+	λ^+	m_1^-	λ^-	λ^2
0.329	0.373	1.06	0.401	4.01	0.052	0.52	2.084
0.174	0.221	1.14	0.250	2.50	0.060	0.60	1.500
0.0684	0.1184	1.15	0.169	1.69	0.065	0.65	1.096

$\frac{D}{C}$ = meq. SO_3H groups in adsorbed dye/g. dyed Cellophane

$\frac{A}{C}$ = total meq. anionic exchange groups/g. dyed Cellophane

$\frac{W}{C}$ = g. imbibed water/g. dyed Cellophane

TABLE V

Distribution of Ions between Esterified Cellophane and Ammonium Chloride Solutions

m_2	$\frac{W}{C}$	m_1^-	λ^+	m_1^-	λ^-	λ^2
0.10	1.318	0.111	1.11	0.090	0.90	1.00
0.05	1.305	0.0625	1.25	0.043	0.86	1.075
0.02	1.300	—	—	0.0152	0.76	—
0.01	1.292	0.0155	1.55	0.00785	0.785	1.217

TABLE VI

Distribution of Hydrochloric Acid and Nitric Acid between Cellulose and Aqueous Solutions

Cellulose	Acid	m_2	$\frac{W}{C}$	m_1^-	λ^-
Cotton	HCl	2.103	0.449	2.070	0.984
Cotton	HCl	0.507	0.50	0.486	0.959
Cotton	HCl	0.1032	0.50	0.0949	0.920
Cotton	HNO_3	0.100	0.519	0.0925	0.925
Cotton	HCl	0.0346	0.496	0.0306	0.886
Cotton	HCl	0.0176	0.560	0.0151	0.856
Cotton	HNO_3	0.010	0.50	0.0083	0.830
Cellophane	HNO_3	1.733	1.15	1.705	0.984
Cellophane	HNO_3	0.217	1.14	0.200	0.921
Cellophane	HCl	0.1035	1.12	0.0937	0.905
Cellophane	HCl	0.0208	1.10	0.0167	0.806
Cellophane	HCl	0.0103	1.12	0.0073	0.720

Table V shows the ionic distribution for a material believed to be free from active carboxylic acid groups. It is rather surprising to find that here the Donnan effect still persists, though in a much smaller measure. Similarly in Table VI where the dissociation of the carboxylic acid groups was repressed by the use of hydrochloric acid as the electrolyte, low values of λ^- were again obtained. The explanation of these peculiarities is not altogether clear, but it may be noted that Neale and Peters (12) found the negative electrical charge of cellulose could not be repressed, save by the adsorption of large amounts of cation-active dyes. It appeared in this earlier work that the prevalent negative charge arose from the use of water as the solvent. In the present work, therefore, experiments using alcohols as solvents for chlorides were carried out. The results are given in Table VII. It will be seen that very high values of λ were obtained,

TABLE VII

Distribution of Ions between Cellophane and Alcoholic Solutions of Electrolytes

Alcohol	Salt	Solubility (molalities)	$\frac{S}{C}$	m_2	m_1^+	λ^+	m_1^-	λ^-
Propyl	NH ₄ Cl	0.0438	0.566	0.0438	0.615	14.1	0.591	13.5
Ethyl	NH ₄ Cl	0.227	0.738	0.227	1.196	5.27	1.158	5.10
Methyl	NH ₄ Cl	0.603	0.816	0.603	1.482	2.46	1.435	2.38
Ethyl	LiCl	2.125	0.787	2.058	—	—	3.320	1.61
Ethyl	NaCl	0.040	0.690	0.0368	—	—	0.629	16.7
Ethyl	KCl	0.0127	0.898	0.0111	—	—	0.310	27.9
Ethyl	RbCl	0.0248	0.758	0.0228	—	—	0.746	32.7
Ethyl	CsCl	0.0480	0.684	0.0239	—	—	0.732	31.7

$\frac{S}{C}$ = g. alcohol taken up/g. Cellophane

increasing with decreasing solubility in the alcohol. This could be interpreted as evidence of a certain "solubility" of the salt in cellulose, as indeed was indicated by the fact that λ^2 was greater than one at high concentrations in aqueous solutions. The increase in λ with decreasing solubility of the salt in alcohol is to be anticipated because in these saturated solutions the chemical potential of the salt is constant.

SUMMARY

The cationic and anionic distribution ratios for some simple salts between cellulose and water have been measured by chemical analysis. In an attempt to throw light on the origin of the cation binding power of cellulose, oxycelluloses and dyed celluloses have also been employed. The ionic distribution is in general agreement with the Donnan theory if water is regarded as the solvent in both phases. In concentrated solutions it may however be necessary to take account of a specific affinity between the salt and cellulose, and when large numbers of anionic groups

are present in the cellulose there is evidence of reduced activity of the counter ions.

REFERENCES

1. GILBERT, G. A., AND RIDEAL, E. K., *Proc. Roy. Soc. (London)* **A182**, 335 (1944).
2. HANSON, J., NEALE, S. M., AND STRINGFELLOW, W. A., *Trans. Faraday Soc.* **31**, 1718 (1935).
3. WILLIS, H. F., WARWICKER, J. O., STANDING, H. A., AND URQUHART, A. R., *Trans. Faraday Soc.* **41**, 506 (1945).
4. DONNAN, F. G., AND GUGGENHEIM, E. A., *Z. physik. Chem.* **A162**, 346 (1932).
5. ADAIR, G. S., *Trans. Faraday Soc.* **33**, 1106 (1937).
6. USHER, F. L., AND WAHBI, A. K., *J. Soc. Dyers and Colourists* **58**, 221 (1942).
7. NEALE, S. M., *J. Soc. Dyers and Colourists* **59**, 148 (1943).
8. MA, T. S., AND ZUAZAGA, G., *Ind. Eng. Chem., Anal. Ed.* **14**, 280 (1942).
9. DAVIDSON, G. F., *J. Textile Inst.* **32**, T109 (1941).
10. RUTHERFORD, H. A., MINOR, F. W., MARTIN, A. R., AND HARRIS, M., *J. Research Natl. Bureau Standards U. S.* **29**, 131 (1942).
11. DEUEL, H., *Helv. Chim. Acta* **30**, 1523 (1947).
12. NEALE, S. M., AND PETERS, R. H., *Trans. Faraday Soc.* **42**, 478 (1946).

LETTER TO THE EDITORS

MOLECULAR CROSS SECTIONS IN FILMS OF FATTY ACIDS ON WATER

During the last several years the classical work of Adam and associates, Langmuir and others on the structure of surface films has come under review and extension. Much of this work has been discussed recently by Epstein (1). The purpose of this note is to point out the possible significance of the lack of cylindrical symmetry of hydrocarbon chain molecules, a factor which seems not to have been considered hitherto.

For stearic acid films on dilute HCl, molecular cross sections of 25.1 or 20.5 sq Å. can be obtained depending on the surface pressure. It is here suggested that in the less compact film the molecules, which are effectively elliptical in cross section, rotate freely, while in the more compact film such rotation is inhibited. Although direct experimental verification of this speculation has not been attempted, it seems intuitively more plausible than any of the previously suggested explanations which include tipping the chains with respect to the normal to the substrate to obtain the larger area, varying the degree of hydration of the

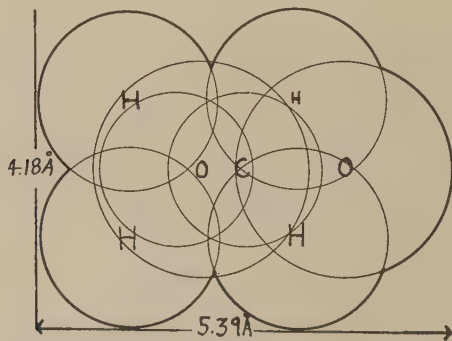


FIG. 1. Projection of a *n*-fatty acid molecule on a plane perpendicular to the chain axis.

Atomic radii: C = 1.00 Å. H = 1.20 Å. O = 1.40 Å.

Bond angles: H—C—H, C—C—C, C—C—H = 109° 30'

O—C—O = 125°; C—C—O = 117° 30'

Bond lengths: C—C = 1.54 Å.; C—H = 1.09 Å.; C—O = 1.28 Å.

The oxygen atoms and carbon atoms are coplanar.

carboxyl group, or displacing the chains parallel to the molecular axis to obtain alternatively close-packed "heads" or close-packed "tails."

The present speculation can be shown to be consistent with the geometry of the fatty acid molecule. The atomic radii and bond angles given by Pauling (2) lead to the projection of the fatty acid molecule on a plane perpendicular to its axis given by Fig. 1. The most efficient packing of such molecules seems to be that given by Fig. 2 and leads to an area per molecule of 20.5 sq. A. Cylindrical close packing of the molecules but allowing free rotation leads to an area per molecule of $5.39^2 \times \sqrt{3}/2 = 25.2$ sq. A. in good agreement with experimental results.

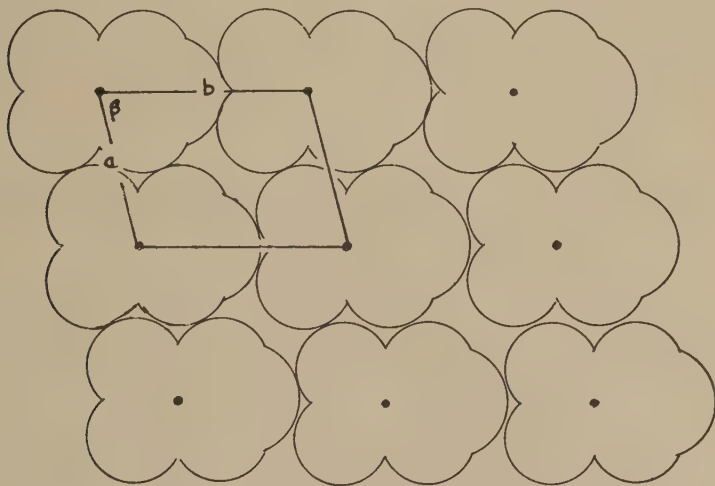


FIG. 2. Efficient packing of vertically oriented *n*-fatty acids.

$$a = 4.18 \text{ A.}; \quad b = 5.24 \text{ A.}; \quad \beta = 69^\circ 20'.$$

$$\text{Area per molecule} = ab \sin \beta = 20.5 \text{ sq. A.}$$

There are a number of moderately direct experimental tests of the present hypothesis. For example, self-diffusion of fatty acids in the films, measured by the radioactive isotope technique, should be more rapid in the less compact film, and the surface viscosity should be lower. Measurement of the thermal effects at the transition from one type of film to the other could be compared with those reasonable for transition from free rotation to hindered rotation. Conductance or dielectric data would also be pertinent. However, inasmuch as it is not currently feasible to undertake these tests in the writer's laboratory, it seems desirable merely to make note of the idea for what use it may be to others working more actively in the field.

REFERENCES

1. EPSTEIN, H. T., *J. Phys. & Colloid Chem.* **54**, 1053 (1950).
2. PAULING, L., *Nature of the Chemical Bond*. Cornell Univ. Press, Ithaca, New York, 1939.

*Department of Chemistry,
The University of Southern California,
Los Angeles, California*

MARJORIE J. VOLD

Received December 5, 1951

BINGHAM AWARD TO P. W. BRIDGMAN¹

The Committee for the Award for 1951, as reported in the Fall Issue of the Bulletin of the Society of Rheology, by unanimous vote decided to honor Dr. P. W. Bridgman. The Medal, awarded yearly since 1948 in the memory of Professor Bingham, is given to workers who have made outstanding contributions to the field of rheology. The ceremony took place as usual at the Social Evening Session of the Society's Annual Meeting. Professor Slater delivered the introductory speech and made the award. His talk and Dr. Bridgman's acceptance are given in full below.

PRESENTATION OF BINGHAM MEDAL TO P. W. BRIDGMAN²

J. C. Slater

Massachusetts Institute of Technology, Cambridge, Massachusetts

It is not often in the history of science that a field of investigation is as closely tied up with a single investigator as is the field of high pressures with Bridgman. He started into this line of research at the very beginning of his scientific career. He got his education at Harvard, and proposed as a thesis the effect of pressure on the index of refraction; it is well known that the elementary theory of refractive index predicts a dependence on volume, and Bridgman set about to measure that. As so often happens, he tried to do more than one can on a doctor's thesis; for he found that the techniques of handling high pressures were so difficult that by the time he had explored ways of reaching pressures of a number of thousand atmospheres he had enough for a doctor's degree, without ever putting windows in his pressure chamber and making optical measurements; it was, in fact, many years before he was able to return to his first problem and measure index of refraction under pressure.

What he did do, right at the beginning, however, was to make several inventions of technique which opened up the whole field of very high pressures. Others had worked before him; but always they had the rather obvious problem of keeping their pressure chambers from leaking.

¹ Presented at the Annual Meeting of the Society of Rheology, Chicago, Illinois, October 24, 1951.

² Presented at the Annual Meeting of the Society of Rheology, Chicago, Illinois, October 24-27, 1951.

Bridgman invented a way of making a rubber packing with an unsupported area, which automatically developed a higher pressure in the packing than in the fluid that was trying to leak through, and hence made leaks less and less likely, the higher the pressure. This principle, applied in a variety of ways, led to methods which he has extended to continually higher pressures. Other extremely ingenious experimental methods have followed all through his career, so that, where a few thousand atmospheres were an achievement in the early days, he can now make measurements at 100,000 atmospheres.

In our ordinary experimentation, we are inclined to think of temperature as the most important variable at our disposal in working on properties of solids; for most of us, the change in properties which we can make by pressure is small compared to the change produced by temperature. In Bridgman's pressure range, however, this is no longer true: the pressure effects are much greater than the maximum temperature effects resulting on the one hand from going to the absolute zero, on the other from going to the melting or boiling point. All the physical properties of solids, then, become important to measure as a function of pressure: their compressibility and other elastic properties, their electrical resistance, and a variety of other things, and Bridgman has made very extensive series of measurements of many different sorts. The measurements which would most concern a group of rheologists are naturally those of change of viscous and plastic properties under high pressure. Bridgman has made many of these, showing that viscosity changes with pressure more than any other physical property, as we should expect from the way in which molecules can be squeezed toward each other, and will get in each other's way in a compressed state when they try to flow. Some of the measurements of such properties were the result of direct experiment; but other observations interesting to rheologists have come more or less incidentally. Obviously the principal limiting condition on the pressure that can be reached is the strength of materials and Bridgman has had unequalled chances to observe the plastic deformation and other types of failure of materials under extreme pressure conditions. These observations by no means always fit in with the preconceptions of classical theories, and they point the way to new concepts of mechanical failure.

In this short presentation, I want to do more than just describe Bridgman's field of research. I should like to give a little idea of the sort of person he is; and I have had a good chance to observe, having assisted him and taken my degree under his direction years ago, having been a colleague for a few years after that, and having lived near him ever since. In the first place, in these days of great cooperative research projects, he has remained an old-fashioned physicist. He has always realized

that the most difficult part of his task was the design and construction of the apparatus; and in the days when I used to assist him, he would spend most of his time in the shop or laboratory personally making part of his equipment or designing the rest, leaving the taking of observations mostly to assistants. He has never built up a great group of technicians and collaborators; even now his laboratory has much the same quiet, intimate atmosphere that it had 30 years ago, and it is still true that when you visit him he will show off the results of something he tried out a few days before. It is still possible to do good physics with relatively simple equipment; for, in spite of the great pressures he reaches, the high pressure apparatus is simplicity itself compared to some of the equipment of modern nuclear physics. It is even still possible to get Nobel prizes for this kind of work, and in fields other than nuclear physics.

One cannot do all this, however, just as an empirical experimenter; one has to have theoretical insight and good judgment as to what should be worked on, and Bridgman has been conspicuous for these qualities. The best theoretical courses I took at Harvard were from him, in electromagnetic theory and thermodynamics. And the reason they were so good was that he knew how to use them in his business. He learned thermodynamics in a sense because he wanted to get out of work. It is very hard to make thermal measurements at high pressure; and he wanted to know to what extent one can really be confident in calculating the results of hypothetical specific heat and latent heat experiments at high pressure, by using thermodynamics applied to other measurements that are easier to carry out. He found one really could be confident in these methods; but in the process he learned how to use thermodynamics, and has become one of the best experts in the field. Similarly his electromagnetic theory was vitalized by the uses he made of it in connection with electrical and magnetic measurements at high pressures.

Just the application of theoretical physics to high pressures by no means has satisfied Bridgman, however. He has always been of an inquiring and practical turn of mind, and has always wanted to extend the methods that prove useful in a restricted range, to wider problems. The general scientific method, the operational definitions of concepts, are things that he has thought a great deal about, and about which he has written extensively; and leading on from this, he has thought deeply and written much about the application of scientific methods and ideas to problems of society in general. Probably the traits that have characterized him most in these thoughts have been honesty and straightforwardness. There is nothing devious or fuzzy about his thinking. If something is true and makes sense, it is true, and that is the end of it. There are altogether too few people like that in the world.

This, then is a brief sketch of your medalist. He is a life-long product

of New England, and a living proof that the old New England virtues of ingenuity, honesty, straightforwardness, and clearheadedness have not died out. I am honored to make the presentation of the Bingham medal to him, as I am honored to count him among my oldest friends.

ACCEPTANCE OF THE BINGHAM MEDAL¹

P. W. Bridgman

Harvard University, Cambridge, Massachusetts

It is needless to say that I am most appreciative of the honor done me by the officers and members of the Society of Rheology in conferring on me the Bingham Medal. I am especially appreciative because my work on flow under hydrostatic pressure has not been one of my major activities and has been treated in a comparatively small number of papers. I am also most grateful to Professor Slater for the kind remarks which he was able to make. It must have demanded considerable effort to think up so much to say, and I am sure that he made a much more convincing case for the award than I would have been able to myself.

As far as I am concerned this award came at a strategic time, because I was beginning to feel that some of this work of mine on flow was not sufficiently known, and in fact I had felt so low in my mind about it that I have written a book, which is called *Large Plastic Flow and Fracture* which is due to come out in a couple of months, in which I have endeavored to correlate my experiments on plastic flow and to give them a wider circulation. Perhaps if I had known a little earlier that you were going to make this award I would not have felt it necessary to write the book, and so could have spared myself much labor.

Professor Slater alluded to the fact that the effect of pressure on viscosity is greater than on any other physical property and varies through a wider range of numerical values. In this connection it is worth calling attention to some recent experiments on the effect of pressure on the viscosity of a series of silicones, in which enormous effects occur, reaching increases of viscosity of as much as 10^7 for increases of pressure of less than 10,000 kg./cm.². Since the increase with pressure is much more rapid than exponential it is to be anticipated that at pressures of 30,000 kg./cm.², which are attainable in the laboratory, these substances become effectively glasses. Here is an inviting field for future inquiry, both theoretical in understanding the mechanism responsible for such enormous increases, and experimental in devising methods for measuring

¹ Presented at the Annual Meeting of the Society of Rheology, Chicago, Illinois, October 24-27, 1951.

the relaxation times and similar properties of the glasses formed by pressure.

Not only does pressure have enormous effects on the viscosity of liquids, but it may also have enormous effects on the plasticity of solids. The most striking effect is on ductility, that is, the elongation which a rod of solid will tolerate without fracture. At sufficiently high pressures metals like steel become literally incapable of fracturing under elongation, any incipient fractures being pushed back into contact by the external pressure, so that indefinitely great elongations become possible.

The whole field of the plasticity of solids is unfamiliar to the average physicist, and he has no intuitive feeling for what to expect. He is all too likely to think of a plastic solid as sort of a glorified viscous liquid, with perhaps the modification that viscous flow does not begin until stress reaches a critical value. In dealing with plastic solids we are of course dealing with properties which are themselves altered by the very forces which call the properties into play. It makes no sense to ask what is the plasticity of a solid under zero stress. All the phenomena of plasticity are out of the linear range of conventional physics—effects no longer are additive: twice the force does not produce twice the effect—all of which makes difficulty for intuition. But I think that even the professional “plastician” who is thoroughly familiar with all this elementary analysis, is also too likely to think of plasticity in terms of the idealized plastic body to which so much mathematical analysis has been devoted. Such a body is either in the elastic state (if the stresses are not too high), or in the plastic state, if a certain function of the stresses reaches a critical value. This critical value may not be exceeded; if the experimenter attempts to exceed it the body responds by indefinite and infinitely rapid yielding.

Of course, no body is capable of infinitely rapid yield, and beyond the critical stress there is a region in which the body is in a state of flow or yield, and in which the parameters which describe the state of the body are strain, stress, and rate of yield. This whole domain in which the body is in a state of flow is usually lost sight of in the analyses of plasticity. For a non-idealized body, the domain of flow is the entire domain beyond the conventional strain hardening curve. Within this domain there is a world of effects waiting for study. These effects get increasingly complicated at high strains and stresses. For their elucidation we shall eventually be driven into the microscopic domain or, what is the same thing, be compelled to take into account the past history of the substance. Among the unusual effects in this domain are unconventional time effects, such as regeneration of flow after apparent subsidence or spasmodic and capricious yield. These may be of practical importance, as in the seismic yielding of the crust of the earth.

A GENERALIZED FLUIDITY POWER LAW AND LAWS OF EXTRUSION¹

M. Mooney and S. A. Black

General Laboratories of the United States Rubber Company,² Passaic, New Jersey

Received February 11, 1952

ABSTRACT

Raw rubbers are assumed to obey the fluidity power law, $\varphi = f\tau^{n-1}$, φ = fluidity, τ = shearing stress, $n > 1$. For three-dimensional flow the generalized law is assumed to be $\varphi = gW^{(n-1)/(n+1)}$, where W = rate of energy dissipation. It is shown that this law is equivalent to Nadai's three-dimensional law of steady creep, expressed in terms of the octahedral shearing stress and octahedral rate of shear. On the basis of the fluidity power law, laws of extrusion are derived for circular and slit tubes and orifices, surface slip also being included in the analysis. By dimensional analysis a general theorem is established concerning the effects of stress (or pressure) and apparatus dimension on deformation and flow rates. Experimental data, obtained with circular tubes of various lengths and diameters and covering a 100-fold range in extrusion rates, agree roughly with the power form of the derived extrusion laws, but do not give the expected values of the exponent n in some cases. Surface slip was too small to measure in the present experiments.

INTRODUCTION

Extrusion operations are quite common in the rubber industry. They are performed not only in the ubiquitous continuous extruder, with the rubber pressed through by a rotating worm, but also in piston-operated devices, such as the extrusion plastometer and the piston injector for injection molding.

The present paper deals with the rheological theory of extrusion and the empirical laws of extrusion as observed with raw rubber stocks. According to an empirical law in the rheological literature (1,2), the extrusion through a cylindrical tube is proportional to a power of the extrusion pressure. Such a power law of extrusion can be theoretically derived for the cylindrical tube (2) if it is assumed that the fluidity of the material extruded is proportional to a power of the shearing stress, in accordance with the Porter-Rao (3) fluidity power law.

In the theoretical sections of the present paper the rheological theory will be extended to include a three-dimensional generalization of the fluidity power law. On the basis of the original two-dimensional law and

¹ Presented at the Annual Meeting of the Society of Rheology, Chicago, Illinois, October 24-27, 1951.

² Contribution No. 117.

the three-dimensional generalization of it, various theoretical extrusion power laws are developed. The effect of surface slip is included in some of the analyses.

In the experimental section of the paper extrusion rates are reported for a range of pressures and a series of circular tubes of various radii and lengths, the shortest length being only $\frac{1}{32}$ in. The experimental work is designed so as to distinguish between the entrance pressure drop and the pressure drop along the length of a tube, and so as to permit a calculation of surface slip.

MATHEMATICAL DERIVATIONS

Two-Dimensional Flow

The fluidity power law has the form

$$s = f\tau^n, \quad [1]$$

where s is the rate of shear in a two-dimensional flow, τ is the shearing stress, and f and n are empirical constants.

Equation [1] is equivalent to

$$\varphi = f\tau^{n-1}, \quad [2]$$

where φ is the fluidity.

While this relationship, in accordance with custom, is referred to in this paper as a fluidity "law," it is to be noted that the relationship is actually only an empirical equation which can be fitted approximately to the published two-dimensional flow data for many non-Newtonian fluids, including raw rubber in its working temperature range and within the stress range from 10^4 to 10^6 dynes/cm.² (4).

Probably the law fails completely in the limit as $\tau \rightarrow 0$, where it indicates zero fluidity; but such a failure is not important in many practical applications.

In applying this law in the derivation of an expression for the efflux through a cylindrical tube as a power of the pressure gradient, it is desirable in the case of raw rubber to take account also of surface slip. The published literature contains no reports of measured or observed slippage, but its existence can be inferred from the fact that commercial extrusion operations are normally carried out for hours at a time without any trouble due to scorching of the raw stock in contact with the hot metal surfaces of the extruder.

The general Eq. [2] for the efflux from a cylindrical tube, with slip included, as given by Mooney (5), is

$$E_c = \frac{Q_c}{\pi a^3} = \frac{1}{T^3} \int_0^T \varphi \tau^3 d\tau + \frac{V(T)}{a}, \quad [3]$$

where Q_c is the absolute efflux, a is the tube radius, φ is the fluidity at shearing stress τ , T is the value of τ at the tube wall, and $V(T)$ is the velocity of slip at shearing stress T . The characteristic efflux, E_c , has the dimension of reciprocal time and is therefore of zero dimension in length.

When φ as given by Eq. [2] is substituted in Eq. [3], we obtain

$$E_c = \frac{fT^n}{n+3} + \frac{V(T)}{a}. \quad [4]$$

For the case $V = 0$ this equation is the same as that recently published by Eccher (2).

Let us now consider a delivery tube having a rectangular section large in width, W , in comparison with the breadth, $2b$. If we neglect end effects in this narrow slit section and follow the same mathematical procedure as that in Ref. (5), we are led to the following general expression for the efflux from a slit tube,

$$E_s = \frac{Q_s}{2Wb^2} = \frac{1}{T} \int_0^T \varphi \tau^2 d\tau + \frac{V(T)}{b}. \quad [5]$$

The notation corresponds to that in Eq. [1]. Now substituting from Eq. [2], we are led to

$$E_s = \frac{fT^n}{n+2} + \frac{V(T)}{b}. \quad [6]$$

Three-Dimensional Flow

The problems we have treated so far are two-dimensional problems. When we come to consider three-dimensional flow, such as the flow within an extrusion chamber toward the exit hole or tube, the Porter-Rao law requires generalization. Probably the general fluidity is, strictly speaking, a tensor and has the same complexity as the elasticity of a rhombic crystal. However, in the absence of definite knowledge on the point, we shall assume that the fluidity is approximately a simple scalar.

The problem that remains is to express the fluidity as a function of some invariant of the rate of strain tensor that will reduce to the power law of Eq. [1] or [2] for the two-dimensional case. We choose

$$\varphi = gW^{(n-1)/(n+1)}, \quad [7]$$

where W is the local rate of energy dissipation by the viscosity, and g and n are constants.

When the dilatation is zero, W has the form, in Cartesian coordinates

$$W = \sum e_i \sigma_i + \sum s_{jk} \tau_{jk}, \quad [8]$$

where e_i and s_{jk} are the rates of elongation and shear, respectively, the τ_{jk} are the shearing stresses, and the σ_i are the normal stress deviations from the mean normal stress.

On the assumption that the fluidity is a scalar,

$$\begin{cases} \sigma_i = 2e_i/\varphi, & [9a] \\ \tau_{jk} = s_{jk}/\varphi. & [9b] \end{cases}$$

From Eqs. [7], [8], and [9], it easily follows that the fluidity can be expressed in either of the two forms,

$$\begin{cases} \varphi = g^{(n+1)/2n} [\Sigma 2e_i^2 + \Sigma s_{jk}^2]^{(n-1)/2n}, & [10a] \end{cases}$$

or,

$$\begin{cases} \varphi = g^{(n+1)/2} [\Sigma \sigma_i^2/2 + \Sigma \tau_{jk}^2]^{(n-1)/2}. & [10b] \end{cases}$$

The invariant functions in the brackets of Eqs. [10] are, except for a numerical factor, the octahedral rate of shear and the octahedral shearing stress, respectively. The fluidity power law expressed by Eq. [7] in terms of W is therefore equivalent to the power law of steady creep for metals, proposed by A. Nadai (6) and expressed in terms of the octahedral shearing stress and shearing rate.

For simple shear referred to the j, k axes, Eq. [10b] reduces to

$$\varphi = g^{(n+1)/2} \tau_{jk}^{n-1}, \quad [11]$$

while Eq. [9b] then gives

$$s_{jk} = g^{(n+1)/2} \tau_{jk}^n. \quad [12]$$

These two equations are equivalent to [1] and [2], respectively, with

$$f = g^{(n+1)/2}. \quad [13]$$

Let us now consider an elongation in the i -direction, combined with a uniform contraction in the jk -plane, produced by a unidirectional stress σ operating in the i -direction.

$$\begin{cases} \sigma_i = 2\sigma/3, \\ \sigma_j = \sigma_k = -\sigma/3, \\ \tau_{jk} = \tau_{ki} = \tau_{ij} = 0. \end{cases} \quad [14]$$

Equations [9a] and [10b] then yield

$$e_i = \left(\frac{g}{3}\right)^{(n+1)/2} \sigma^n. \quad [15]$$

If Eqs. [12] and [15], with the appropriate experimental data, are found to give the same values of n and g , then the assumed scalar character of the fluidity would be, to that extent, proved valid.

The general field equation for the three-dimensional flow of a non-Newtonian, incompressible liquid with a scalar fluidity can be written, in vector notation,

$$\nabla p = \nabla \cdot \left[\frac{2}{\varphi} \Sigma e_i \mathbf{ii} + \frac{1}{\varphi} \Sigma s_{jk} (\mathbf{jk} + \mathbf{kj}) \right], \quad [16]$$

where

$$\nabla = \Sigma i \frac{\partial}{\partial x}, \quad [17]$$

and p is the pressure. Equation [16] may be derived from Weatherburn, for example, Eq. (36') Chap. VIII and previous equations. The factor $1/\varphi$ must be brought under the operator ∇ because φ is not in our work a constant.

In problems in which the flow lines cannot be determined except by solving Eq. [16] the complete solution will be quite difficult. However, some further advance in the general theory can be made by a dimensional analysis of Eq. [16].

Let us suppose that this equation with a particular set of boundary conditions has a solution; and then let us consider a similar problem in which the geometry, the boundary stresses, and velocities are magnified by certain factors. We shall prove the following:

Theorem: If the fluidity of a liquid is proportional to the $(n-1)/(n+1)$ power of the instantaneous local rate of work, and if in any deformation or flow process all dimensions are multiplied by a factor μ and all boundary stresses by a factor α , then the flow pattern will be magnified by the factor μ but remain similar in form, all stresses will be multiplied by the factor α , all velocities by the factor $\mu\alpha^n$, and all deformation rates by the factor α^n .

To prove this theorem let us denote the variables in the transformed problem by an asterisk, and let us try the transformation of variables,

$$\begin{aligned} x^*, y^*, z^* &= \mu(x, y, z), \\ u^*, v^*, w^* &= \mu\beta(u, v, w), \\ e_i^* &= \beta e_i, \\ s_{jk}^* &= \beta s_{jk}, \\ \sigma_i^* &= \alpha \sigma_i, \\ \tau_{jk}^* &= \tau_{jk}, \\ p^* &= \alpha p. \end{aligned} \quad [18]$$

The new parameter, β , is adjustable; u, v , and w are the velocity components of the flow.

According to [18] the transformed differential operator will be

$$\nabla^* = \frac{1}{\mu} \nabla. \quad [19]$$

From Eqs. [10b] and [18] it follows that

$$\frac{\varphi^*}{\varphi} = \frac{[\Sigma \sigma_i^{*2}/2 + \Sigma \tau_{jk}^{*2}]^{(n-1)/2}}{[\Sigma \sigma_i^2/2 + \Sigma \tau_{jk}^2]^{(n-1)/2}} = \alpha^{n-1}. \quad [20]$$

If we now write Eq. [16] for the transformed problem in terms of the transformed variables and then make the substitutions indicated by Eqs. [18], [19], and [20], we find that μ cancels and the equation reduces to

$$\frac{\alpha^n}{\beta} \nabla p = \nabla \cdot \left[\frac{2}{\varphi} \Sigma e_i \mathbf{i} \mathbf{i} + \frac{1}{\varphi} \Sigma s_{jk} (\mathbf{j} \mathbf{k} + \mathbf{k} \mathbf{j}) \right]. \quad [21]$$

Since by hypothesis p , e_i , etc. are a solution of Eq. [16], if we now set

$$\beta = \alpha^n, \quad [22]$$

Eq. [21] is satisfied; and furthermore the transformations [17] involving β now satisfy the requirements of the theorem. The theorem is therefore proved.

It is to be noted that the postulates of this theorem concerning the boundary conditions require one of three conditions with regard to surface slippage: (a) there is no slippage; (b) there is free slippage, that is, zero friction; or (c) velocity of slip is proportional to μT^n , T being the tangential shear stress at the surface.

Since the third condition involves the scale factor, μ , accurate predictions of injection performance based on small-scale models can only be made for the first two conditions, no slippage or free slippage. The third condition can be covered when some experimentalist is clever enough to control a finite, non-zero slip velocity and make it proportional to the scale factor.

For the case $\mu = 1$ this theorem is analogous to the theory published by Ilyushin (7), in a study of plastic deformation. The present authors are indebted to Professor W. Prager for knowledge of Ilyushin's work and a translation of its essential features.

Extrusion through a Hole

Consider a cylinder from which a liquid, such as raw rubber, is being extruded under pressure through a hole in a thin plate. If the cylinder is large in comparison with the dimensions of the hole, we may treat it as infinitely large. Then by applying the above theorem we can derive a formula for the variation in extrusion rate with the pressure and with the dimensions of the hole. Let the hole lie in the x , y -plane. Then with the previous notation we have for the efflux

$$Q_e^* = \iint w^* dx^* dy^* = \mu^3 \alpha^n \iint w \, dx \, dy = \mu^3 \alpha^n E_c, \quad [23]$$

$$Q_e^* = C \mu^3 (p^*)^n,$$

where the constant C is Q_e/p^n .

For a circular hole of radius a this equation reduces to

$$E_c^* = \frac{Q_c^*}{\pi a^3} = C_c p^{*n}. \quad [24]$$

For a slit hole of width $2b$ and length W , the corresponding equation is

$$\frac{Q_s^*}{2Wb^2} = C_s p^{*n}. \quad [25]$$

Effect of a Change in the Liquid

This dimensional analysis so far has proceeded on the assumption that the liquid, or rubber, being extruded is the same in all cases. If the rubber is different, with different values of f and n , the flow lines will be altered and the solution is no longer subject to dimensional analysis. However, in the special case where only f changes while n remains constant, a dimensional analysis can be made. If the expression for φ in Eq. [10a] is substituted in Eq. [16], the result is

$$\nabla p = \frac{-1}{g^{(n+1)/2n}} \nabla \cdot \left\{ \frac{2\Sigma e_i \mathbf{i} \mathbf{i} + \Sigma s_{jk} (\mathbf{j} \mathbf{k} + \mathbf{k} \mathbf{j})}{[\Sigma 2e_i^2 + \Sigma s_{jk}^2]^{(n-1)/2n}} \right\}. \quad [26]$$

From this it is clear that if a solution exists for a given value of g and n , a solution will also exist for the same n and for any other g , say g^* ; and in the new solution the e_i and s_{jk} will be invariant, and p^* will vary inversely as $(g^*)^{(n+1)/2n}$ according to the relation

$$p^* = p \left(\frac{g}{g^*} \right)^{(n+1)/2n}.$$

It is assumed here that the exit pressure, or the reference pressure where $\sigma_i = \tau_{jk} = 0$, is taken to be zero. Otherwise, we merely substitute $p^* - p_0$ for p^* , etc.

By virtue of Eq. [13], Eq. [26] may be written

$$p^* = p \left(\frac{f}{f^*} \right)^{1/n}. \quad [27]$$

Similar equations can be established for the general stresses σ_i and τ_{jk} , by making use of Eqs. [9] and [10a].

We have therefore now proved the following:

Corollary: If the fluidities of two liquids are, respectively,

$$f^{2/(n+1)} W^{(n-1)/(n+1)} \text{ and } (f^*)^{2/(n+1)} W^{(n-1)/(n+1)},$$

where W is the local rate of work, and if in any deformation or flow process all dimensions in the second case are multiplied by a factor μ and all boundary stresses by a factor $\alpha (f/f^*)^{1/n}$, then the flow pattern in the

second case will be magnified by the factor $\alpha (f/f^*)^{1/n}$, all velocities by the factor $\mu\alpha^n$, and all deformation rates by the factor α^n .

Suppose that the viscosities of two rubber stocks characterized by the same n have been measured at the same rate of shear. By definition, the viscosity is

$$\eta = 1/\varphi = \tau/s. \quad [28]$$

Then, by combining this with Eq. [1], it is found that

$$\eta = \frac{1}{(fs^{n-1})^{1/n}}. \quad [29]$$

Hence, for constant s and n , the ratio of the two viscosities will be

$$\frac{\eta^*}{\eta} = \left(\frac{f}{f^*}\right)^{1/n}. \quad [30]$$

From this it follows that in the statement of the above corollary $\alpha\eta^*/\eta$ may be substituted for $\alpha (f/f^*)^{1/n}$. Also Eq. [27] may be written

$$\frac{p^*}{p} = \frac{\eta^*}{\eta}. \quad [31]$$

If desired, the viscosity ratings by any test may be substituted for η^* and η , provided still that the two stocks considered have the same value of n , and provided that the viscosity test is one in which the rates of shear at all points will be the same for both samples. The Mooney viscosity test, incidentally, meets this condition very closely.

EXPERIMENTAL

Equipment

The experimental work has been carried out with the aid of a modified Elmes laboratory press³ equipped with a 6-in. diameter pneumatic cylinder operating a $\frac{3}{4}$ -in. diameter plunger in the extrusion chamber. The maximum air pressure reliably available to operate the pneumatic cylinder was 75 lb./in.² Because of the area ratio of 64:1 this corresponds to a maximum rubber pressure of 4800 lb./in.² The plunger works with 0.003 in. clearance in a cavity $2\frac{3}{16}$ in. long which is temperature controlled and which can be equipped with interchangeable cylindrical sprues or orifices of various lengths and hole diameters. The diameters used were $\frac{1}{16}$, $\frac{1}{8}$, and $\frac{3}{16}$ in.; the lengths were $\frac{1}{32}$, $\frac{1}{2}$, 1, 3, and 6 in.

³ The major modifications of the press were designed by H. F. Jurgeleit of U. S. Rubber Central Engineering. Further changes of detail were carried out by U. S. Rubber General Laboratories.

Program

The samples used consisted of blended Hevea smoked sheet broken down to appropriate viscosity levels. Experiments were performed on rubber with the following values of Mooney viscosity as measured at the indicated temperatures:

Stock A	{	200°F. (93°C.)	50 ML-4
	{	212°F. (100°C.)	48 ML-4
	{	250°F. (121°C.)	43 ML-4
Stock B	{	212°F. (100°C.)	18 ML-4
	{	250°F. (121°C.)	14 ML-4

Procedure

The injection cylinder is loaded by an indirect process in order to reduce spurious results due to trapped air in the sample. An auxiliary chamber with a $\frac{3}{4}$ -in. diameter cavity, open at both ends, is placed in a special loading jig where it is filled with rubber. The rubber is then compressed by a piston loaded by a weight and lever arrangement that compacts the rubber under a pressure of roughly 200 lb./in.² The sample is compressed for 10 min. or more, depending on the duration of injection operations on the previously formed sample. The auxiliary cylinder is then placed over the cavity of the injection press and the piston is lowered through the cylinder to transfer the rubber into the injection chamber. The piston is raised, the cylinder removed, and the piston is again lowered until it just touches the top of the rubber sample. The sample is heat conditioned for 10 min. in the injection chamber.

Air is fed to the pneumatic cylinder through a pressure regulator that is manually adjusted to give the desired gage reading during the injection stroke. If the time for the stroke is too small to permit regulation at the prescribed pressure, dummy runs are made during which the pressure regulator is adjusted to give the proper value for the speed of piston movement attained.

The press is equipped with two microswitches that are actuated in succession by the descending piston. These switches start and stop an electrical clock counting to 0.1 sec. The timer records the time necessary for extrusion of a fixed volume of rubber, except for a negligible flash which extrudes backward past the piston. During operation of the press the setting of the microswitches is checked daily by means of a carefully weighed test extrusion. This, since it is performed with the compound under test, tends to compensate for the previously mentioned flash.

In the analysis of the experimental data for comparison with Eq. [4], allowance must be made for the entrance pressure drop. Hence, the pressure gradient is always calculated from the difference between the interpolated extrusion pressures required for a given efflux through two sprues of the same diameter but different lengths.

RESULTS

Figure 1 shows typical curves (full) of absolute efflux for short and long $\frac{1}{16}$ -in. sprues, and also curves (dashed) of the pressure difference. This pressure difference, divided by the length difference, gives the pressure gradient required for the corresponding efflux. The relationship between characteristic efflux and shear stress at the wall is shown in Fig. 2, in which the various pairs of sprues that were used are identified. Three plots such as Fig. 1 were used in the development of Fig. 2.

According to Eq. [3], wall slippage will be indicated by an increase in characteristic efflux, at a given wall stress, as the sprue diameter is decreased. This effect occurs only over limited portions of the curves, and the validity of the effect is open to some question because of the irregularities apparent in the curves. It can be stated, however, that data have been obtained which lack the irregularities of this particular series of experiments and do indicate in a significant manner the existence of wall slippage. The slip velocity increases with the shearing stress at the wall.

Curve 1 of Fig. 3 is an average of the 200°F. curves of Fig. 2. Included for comparison are averaged curves on the same stock at 250°F., curve 3. Each of these curves is approximately linear, indicating a rough check with the extrusion power law and the two-dimensional fluidity power law. If the slip is negligible, as seems to be indicated by these data, the characteristic efflux E_c is given by

$$E_c = \frac{fT^n}{n+3}$$

The departures from constancy of the exponent n are indicated in the tables at the lower part of the figure, where values of n for each of the

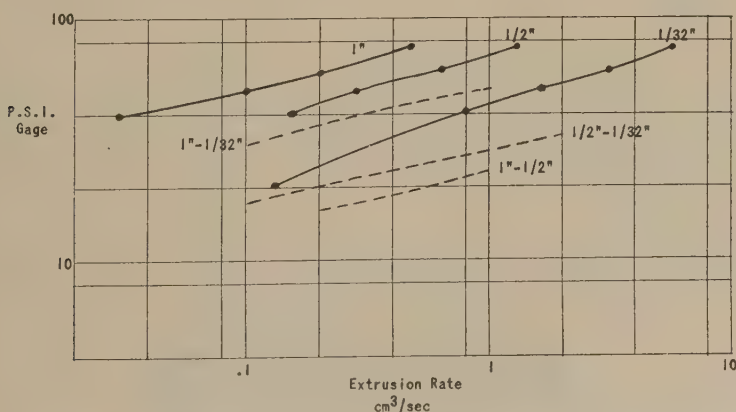


FIG. 1. Typical results, absolute extrusion rate vs. gage pressure; $\frac{1}{16}$ in. diameter sprues; smoked sheet; 48 ML-4, 212°F.; 50 ML-4, 200°F.

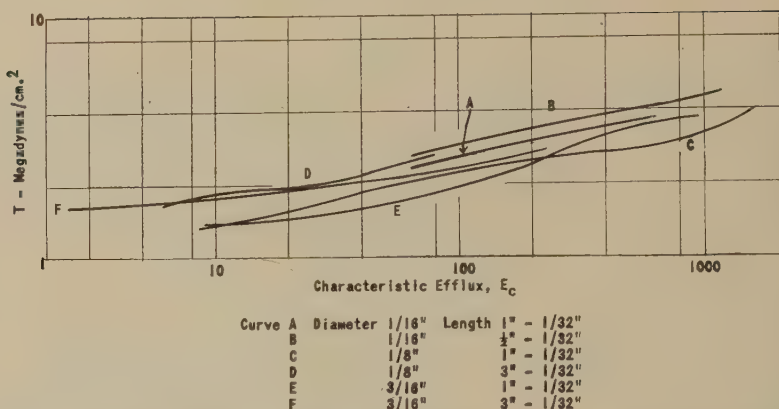


FIG. 2. Characteristic efflux vs. shear stress at wall. Extrusion temperature, 200°F.; smoked sheet; 48 ML-4, 212°F.; 50 ML-4, 200°F.

curves are given as obtained by an averaging of characteristic efflux values over each logarithmic cycle. Also given are the values of the constant f in the equation for characteristic efflux. It is to be observed that in most cases n increases with increasing efflux, and consequently with increasing shearing stress. This trend seems to be beyond experimental error. A similar trend can be observed in Eccher's (2) published data, even though Eccher did not comment on it.

The fluidity φ can be obtained for any set of conditions in the range of the curves from the equation:

$$\varphi = f\tau^{n-1}.$$

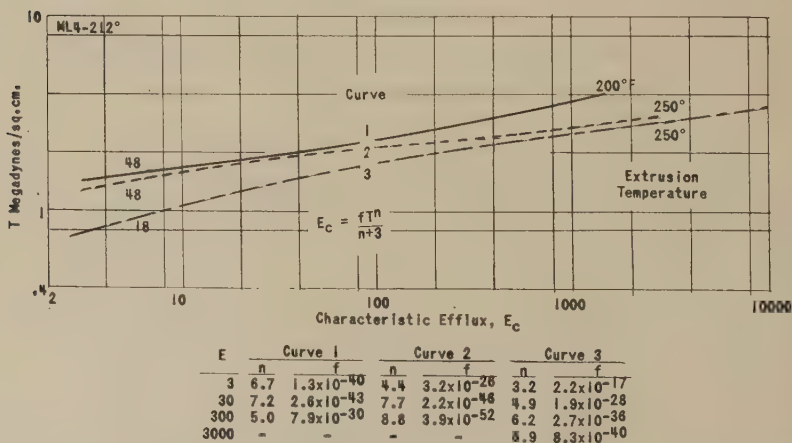


FIG. 3. Characteristic efflux vs. shear stress at wall. Averaged data for smoked sheet.

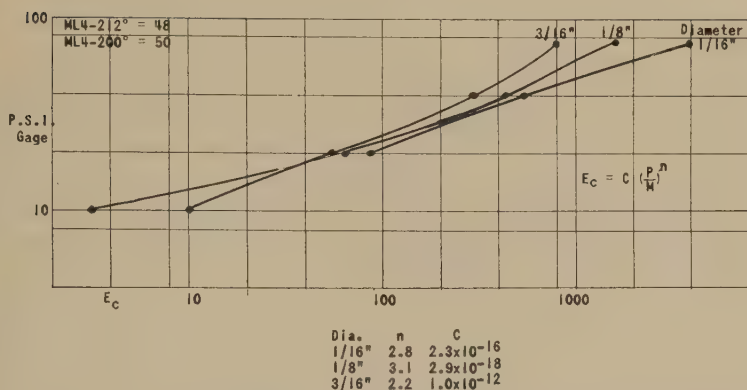


FIG. 4. Characteristic efflux vs. gage pressure. Smoked sheet; die length, $\frac{1}{32}$ in.; extrusion temperature, 200°F.

If the slip were indicated to be other than zero, the component of efflux due to slip would have to be determined and subtracted from the total before determination of f and n and before determination of ϕ .

Equation [24] describes the expected flow through a circular hole in a plate. The data of this series of experiments lend itself to a check of this equation. Values of $Q/\pi a^3$ were computed for the $\frac{1}{32}$ -in. long sprues. A plot of these against gage pressure in Fig. 4 indicates a separation of the $\frac{3}{16}$ -in. and $\frac{1}{8}$ -in. curves which, by analogy with the cylindrical case, suggests slippage. The effect shown by the $\frac{1}{16}$ -in. curve of crossing over the others is not a typical effect; other data for different viscosity rubber and for other temperatures do not show it. The tabulated values of C and n refer to straight-line approximations to the curves. According to the

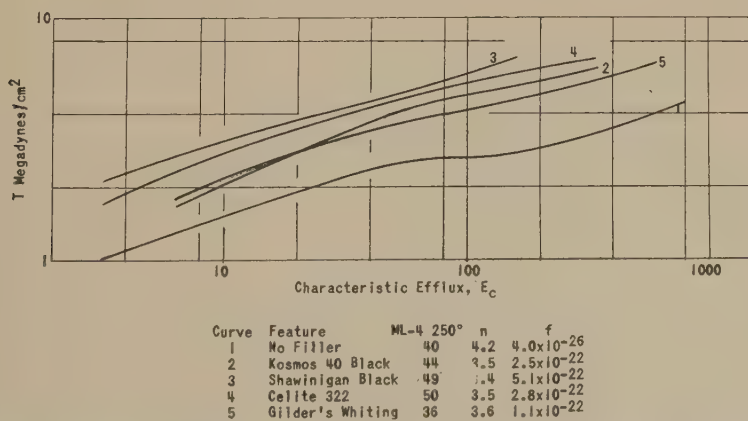


FIG. 5. Characteristic efflux vs. shear stress at wall. Comparison of fillers at 20 cc. loading in standard GR-S.

theory, n found here should equal n previously found for cylinders, but the values actually differ by a factor of two or more.

The separation of the curves, which the theory predicts should coincide, suggests either a failure of the experimental technique or an oversimplification in deriving the equation for efflux.

Figure 5 presents the effect of 20 ml. of filler per 100 g. of standard GR-S rubber. The fillers used represent extremes in shape in both black and mineral classes; it is interesting that the tabulated values of the exponent n agree so well among the fillers.

DISCUSSION

The theoretical section of this paper includes a number of equations not tested by the experimental work. Nevertheless, the experimental data serve to test several crucial points in the theory.

It was known before this work that extrusion of rubbers through circular tubes and holes varied roughly as a power of the extrusion pressure, the power being usually in the range from 2 to 5. A new point brought out in this work is the relatively large entrance pressure drop. For example, for a cylindrical tube of a length eight times its diameter, the entrance pressure drop is, in a particular case, 0.7 of the total extrusion pressure. For a Newtonian liquid the same ratio would be roughly 0.1. Another point of interest in the present data concerns surface slip, which apparently is too small for easy detection or measurement, in spite of its practical importance in preventing scorching in commercial extrusion. The situation apparently calls for higher precision in extrusion measurements.

The greatest departure from theory in the data reported lies in the smaller value of n for extrusion through a circular hole, as compared with extrusion of the same rubber through a tube. This discrepancy may possibly arise from a combination of two facts: first, that the rubbers do not obey the fluidity power law exactly, but show an increasing n at the higher stresses; and second that the mean effective shearing stress in extrusion through a hole is considerably less than the wall stress in a tube for the same value of E_c . Thixotropic effects, if important, would probably be in the wrong direction to explain the discrepancy.

Local variations in temperature have not been considered in the present theories of extrusion. Certainly they exist; but their effects are considerably mitigated by the fact that the heat development due to viscosity occurs mostly near the walls of the delivery tube, where the temperature is most effectively controlled by the wall temperature itself.

It will be observed in Fig. 5 that the various curves do not lie in the same sequence as the Mooney viscosities. This is contrary to what would be expected according to any reasonable theory. Thixotropic effects may be responsible. The conclusion is indicated that for any precise rheological

measurements on raw rubber, care must be taken to have the rubber in the same state of thixotropic structure or lack of structure in the tests and the processing operations to be compared.

When the necessary precautions are taken, the above theory may lead to reliable approximate predictions of the pressure drop in the various flow channels involved in the injection molding operation. In such rough calculations, slippage can apparently be neglected. It should be noted, however, that viscosity measurements should be made at a rate of shear comparable with those attained in the operation considered; and two or more testing rates must be used if both the parameters of the fluidity power law are to be determined.

ACKNOWLEDGMENT

The authors wish to thank Mr. J. M. Taliaferro for his careful execution of the experimental work.

REFERENCES

1. MARZETTI, B., *Rubber Age* (N. Y.) **15**, 454 (1924).
2. ECCHER, S., *Ind. Eng. Chem.* **43**, 479 (1951).
3. PORTER, A. W., AND RAO, P. A. M., *Trans. Faraday Soc.* **23**, 311 (1926).
4. MOONEY, M., *Physics* **7**, 413 (1936).
5. MOONEY, M., *J. Rheol.* **2**, 210 (1931).
6. NADAI, A., *J. Applied Phys.* **8**, 418 (1937); NADAI, A., *Theory of Flow and Fracture of Solids*, McGraw-Hill Book Co., New York, 1950.
7. ILYUSHIN, A. A., *Prikl. Mat. Mekh.* **10**, 347 (1947).

EFFECT OF SHEAR TEMPERATURE ON VISCOSITY IN A ROTATIONAL VISCOMETER MEASUREMENT¹

Ruth N. Weltmann^{2,3} and Perry W. Kuhns³

N. A. C. A. Lewis Flight Propulsion Laboratory, Cleveland, Ohio

Received January 28, 1952

ABSTRACT

A method is described which permits determination of the approximate temperature distribution over the cross-sectional area of a Newtonian material which is subjected to shearing forces in a rotational viscometer. By correlating the change of viscosity to temperature increases, and by determining the actual viscosity value as found in the rotational viscometer, the effect of thixotropy can be studied.

Temperature calculations with regard to an Oronite polybutylene oil and a silicone fluid have been made, in each case for various operational conditions of a rotational viscometer. It appears that in some instances where previously the presence of thixotropy was suspected, temperature increases might be responsible for viscosity breakdown. In other instances thixotropic behavior must still be postulated to explain the experimental results.

INTRODUCTION

There has been some discussion in the past with regard to what part thixotropy and what part temperature increases play in the decrease of viscosity when a material is subjected to shearing forces in a rotational viscometer. Some literature references pertaining to this subject may be found in a paper by Blok (1). Since heat is generated in viscometric measurements, a temperature increase of the material must be taken into consideration.

The careful experimenter will attempt to maintain a constant temperature by submerging the cup into an appropriate bath; nevertheless, experiments have shown that the wall of the bob generally increases in temperature during the measurement. The assumption has frequently been advanced that the highest temperature of the material is found at the bob wall. For this case temperature calculations were reported (2) for lubricating oils in bearings, where the highest temperature is found at the journal surface. In rotational viscometers, however, when dealing

¹ Presented at the Annual Meeting of the Society of Rheology, Chicago, Illinois, October 24-27, 1951.

² Consultant in Rheology to The Research Laboratories, Interchemical Corp., New York, N. Y.

³ Staff Members of N.A.C.A. Lewis Flight Propulsion Laboratory.

with greater separations than in bearings, such assumption is not always correct.

Therefore, in this presentation, an attempt is made to obtain a distribution pattern of the temperature in the material over the distance from cup to bob for conditions as would exist in actual viscometric applications. This information, which is arrived at by calculation, and employs the measured cup and bob temperatures as boundary conditions, is then used to establish an effective viscosity value, which is subsequently related to the experimental viscosity value. It is then assumed that if the viscosity found by measurement is substantially lower than the effective viscosity thus calculated, thixotropic breakdown must be responsible for the difference.

TEMPERATURE DISTRIBUTION

To simplify the calculation, transient conditions have been disregarded and temperature equilibrium for all operating conditions of the rotational viscometer has been hypothesized. Under this condition, all the heat which is generated in the material must be conducted away. This assumption leads to the following equation:

$$\nabla \times \mu(\nabla \mathbf{v}) \times \mathbf{v} = -k\nabla^2 T \quad [1]$$

where μ is the viscosity, \mathbf{v} is the velocity, k is the heat conductivity, and T is the temperature. For a rotational viscometer $\mathbf{v} = \mathbf{r} \times \boldsymbol{\omega}$, and Eq. [1] becomes:

$$\nabla \times \{\mu[(\nabla \boldsymbol{\omega}) \times \mathbf{r}] \times \boldsymbol{\omega} \times \mathbf{r} - \mu[(\nabla \mathbf{r}) \times \boldsymbol{\omega}] \times \boldsymbol{\omega} \times \mathbf{r}\} = -k\nabla^2 T \quad [2]$$

where $\mu[(\nabla \mathbf{r}) \times \boldsymbol{\omega}] \times \boldsymbol{\omega} \times \mathbf{r}$ is set equal to zero, because it does not contribute to the heat process. In Eq. [2], r is the radius and $\boldsymbol{\omega}$ is the angular velocity. For a Newtonian material:

$$r \, d\omega/dr = \theta/2\pi r^2 h \mu = A/\mu r^2 \quad [3]$$

where θ is the torque, h is the height of the bob, and A is used for later convenience. Equation [3] is also employed for non-Newtonian materials, in which case μ is called the apparent viscosity. Substituting Eq. [3] into Eq. [1] yields:

$$T - T_c = -\frac{A^2}{k} \int_{R_B}^r \left[\frac{1}{r} \int_{R_B}^r \frac{dr}{\mu r^3} \right] dr + K' \ln(r/R_B) + K'' \quad [4]$$

This equation is solved in the subsequent parts of the paper by a graphical method using the principle of successive approximation.

As a starting point the simplified but obviously incorrect assumption is made that the material under test has a constant viscosity. This assumption leads to the following solution of Eq. [4]:

$$T - T_c = \frac{A^2}{4\mu k} \left[\frac{1}{r^2} - \frac{1}{R_B^2} + K_1 \ln(r/R_B) + K_2 \right] \quad [5]$$

For the given boundary conditions, $T = T_c$ at $r = R_c$ and $T = T_B$ at $r = R_B$, $K_1 = \frac{1/R_B^2 - 1/R_c^2 - K_2}{\ln(R_c/R_B)}$ and $K_2 = \frac{T_B - T_c}{A^2/4\mu k}$, where R_B is the radius of the bob, the stationary cylinder; R_c is the radius of the cup, the rotating cylinder; and T_B and T_c are the temperatures measured at the bob and cup surfaces. To give a better physical picture, Eq. [5] can be rewritten as follows:

$$T - T_c = [T_B - T_c] \frac{\ln(R_c/r)}{\ln(R_c/R_B)} + \frac{A^2}{4\mu k} \left[(1/R_B^2 - 1/r^2) - (1/R_B^2 - 1/R_c^2) \frac{\ln(r/R_B)}{\ln(R_c/R_B)} \right] \quad [6]$$

The first term of the right side of Eq. [6] represents a logarithmic temperature pattern between bob and cup which is typical of heat conduction between two cylindrical surfaces of different temperature. The second term indicates the heat generated by the shearing forces. Only when the second term is negligible compared to the first one can an average temperature be approximated by $\frac{1}{2} (T_B + T_c)$. This condition exists when the heat conduction of the system is large in relation to the heat generated. The heat generation term can be seen from Eq. [6] to increase with increasing values of A , with decreasing values of μ and k , and with increasing cup-bob separations.

To obtain a first approximation of the temperature profile along the radius between cup and bob, Eq. [5] is solved for a constant viscosity such as the mean value between cup and bob, $\frac{1}{2} (\mu_c + \mu_B)$. The equation for the successive approximations follows from Eq. [4]:

$$(T - T_c)_n = \frac{A_{n-1}}{k} \int_{R_B}^r \left[\frac{1}{r} \int_{R_B}^r \frac{dr}{\mu_{n-1} r^3} \right] dr + K' \ln(r/R_B) + K'' \quad [7]$$

where $A_n = \frac{v_c}{R_c \int_{R_B}^{R_c} \frac{dr}{\mu_{n-1} r^3}}$. The integration constants K' and K'' are

solved by introducing the boundary conditions, $T = T_B$ at $r = R_B$ and $T = T_c$ at $r = R_c$. A temperature profile can thus be obtained by a graphical method which is a close approximation to the solution of Eq. [4]. In each of Figs. 1, 2, and 3, two series of curves are shown. One family of curves is a plot of the temperature distribution for the assumed constant viscosity $\frac{1}{2} (\mu_B + \mu_c)$ (Eq. [5]), while the second series of curves shows the temperature distribution making allowance for changes of viscosity as function of temperature (Eq. [5]). All curves are bounded by given temperatures at the cup and bob surfaces. While the cup wall temperature was assumed constant in all cases, experimental bob wall temperatures, previously reported (3) for a water cooled stainless steel,

a solid stainless steel and a copper sleeved Lucite bob were employed for all but the smallest cup-bob combinations. The employed viscosity temperature relationship, Fig. 4, is that found for extremely low rates of shear, at which the materials exhibit Newtonian behavior.

COMPARISON OF RESULTS

For the purpose of being able to compare experimental and calculated results, two materials, an Oronite polybutene oil and a silicone fluid, have been studied since experimental data had previously been reported. For the Oronite oil the cup speeds were selected to give the same mean shearing stress for varying cup-bob separations.

It is noteworthy that for small distances between cup and bob the temperature distribution of the constant viscosity family of curves almost coincides with the temperature pattern of the series of curves which takes cognizance of the viscosity dependence upon temperature.

From the information contained in each curve in Figs. 1-3 and from the viscosity temperature relationship shown in Fig. 4, it is possible to extract a viscosity which corresponds to that which the rotational viscometer would have measured for a Newtonian material for the respective temperature distribution. At this point it seems to be in order to analyze briefly what in this presentation has been called experimental viscosity.

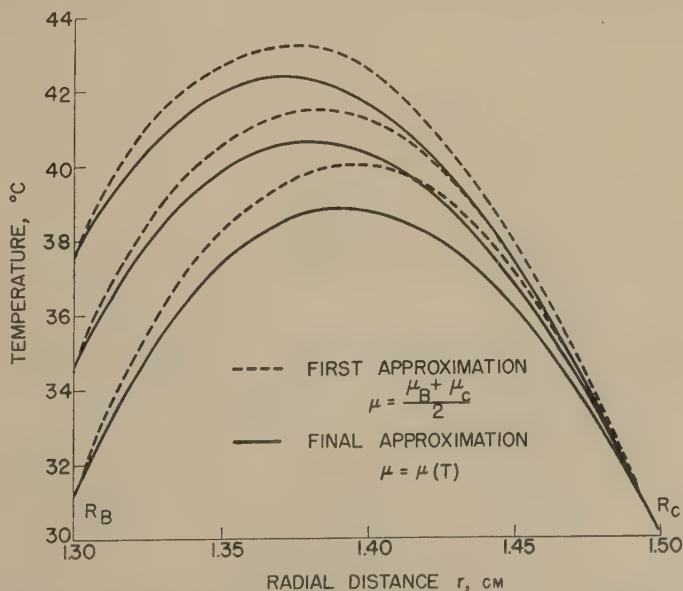


FIG. 1. Temperature distribution along the radial distance between cup and bob of silicone fluid No. 5101C for three bob temperatures.

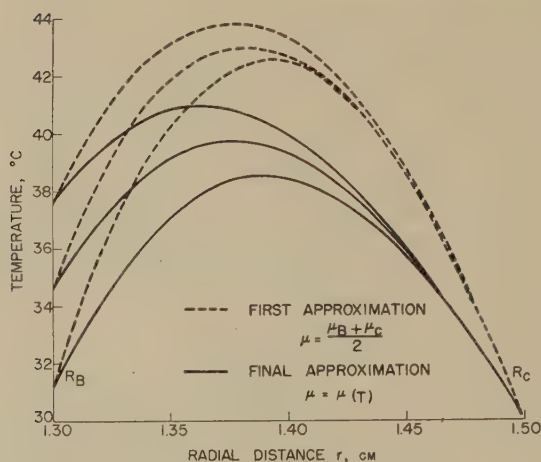


FIG. 2. Temperature distribution along the radial distance between cup and bob of Oronite polybutene oil No. 32 for three bob temperatures.

This experimental viscosity represents a quantity which is given by the ratio of measured torque to cup speed multiplied by an appropriate instrumental constant. This relationship is derived from Eq. [3] under the assumption that the viscosity μ is of constant value. Although this assumption has not always been justified, data given in the literature on experimental viscosity do not take heat distribution and thus resulting

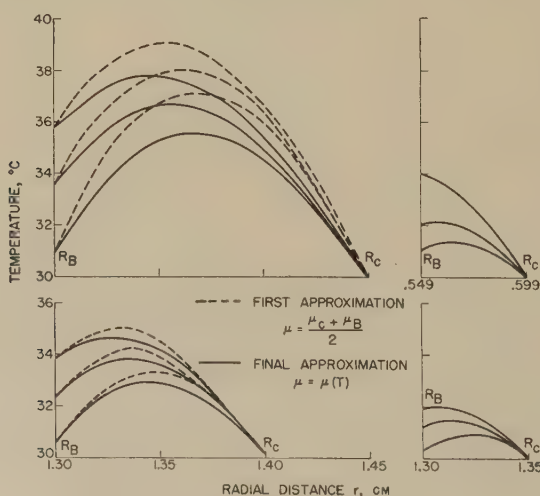


FIG. 3. Temperature distribution along the radial distance between cup and bob of Oronite polybutene oil No. 32 for three bob temperatures and different cup-bob dimensions.

viscosity changes over the sheared cross section specifically into consideration. When temperature variations between concentric layers from cup to bob are present, this experimental viscosity, as determined from measured torque values and the given cup speed, might be considered as composed of the following summation:

$$\mu_{\text{exp}} \simeq \left[\frac{1}{\sum_i x_i} \sum_i \frac{x_i}{\mu_i} \right]^{-1} \quad [8]$$

For small separations, x can be approximated by the thickness of the individual concentric layers over which the viscosity μ is assumed constant, then $\sum_i x_i$ represents the cup-bob separation.

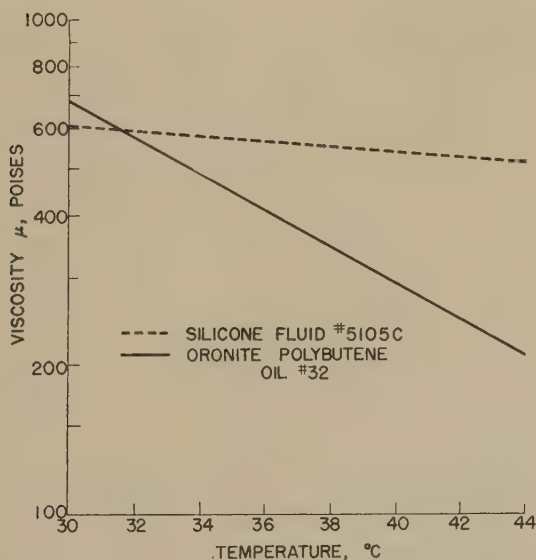


FIG. 4. The viscosity temperature relationship for silicone fluid No. 5101C and Oronite polybutene oil No. 32 as reported previously (3) for extremely low rates of shear.

The viscosity as a function of radial position between cup and bob as obtained from Eq. [4] must be appropriately weighted so as to establish a calculated effective viscosity which represents a comparable quantity to the experimental viscosity. This is done by calculating the effective viscosity as follows:

$$\mu_{\text{calc. eff.}} = \int_{R_B}^{R_C} \frac{dr}{r^3} / \int_{R_B}^{R_C} \frac{dr}{\mu_{n-1} r^3} = \frac{A_n}{A/\mu} \quad [9]$$

where A/μ is obtained from Eq. [3] upon integration under the assumption that μ is of constant value and A_n is determined as described in Eq. [7].

In Table I the calculated effective viscosities are listed in the last vertical column for the various given operating conditions for an Oronite polybutene oil and a silicone fluid. The adjacent column gives the experimental viscosity values which have been taken from the literature (3). There are a series of other physical quantities shown, as for example the temperature difference between cup and bob wall, the average tempera-

TABLE I

Physical Constants, Experimental and Calculated Data for Two Materials When Sheared in a Rotational Viscometer Under Various Operating Conditions

Mean rate of shear = 218 sec.^{-1} for $\mu = \mu_c$.

Height of bob, $h = 5.2 \text{ cm.}$

Cup temperature, $T_c = 30.0^\circ\text{C.}$

Oronite Oil No. 32: Heat conductivity, $k = 1.28 \times 10^4 \text{ dynes/sec./cm. for } 1^\circ\text{C./cm.}^a$

Cup temperature viscosity, $\mu_c = 675 \text{ poises}^b$

Silicone fluid No. 5101C: Heat conductivity, $k = 1.55 \times 10^4 \text{ dynes/sec./cm. for } 1^\circ\text{C./cm.}$

Cup temperature viscosity, $\mu_c = 605 \text{ poises}^b$

Material	R_B	R_c	v_c	$T_B - T_c$	$(T_B - T_c)_{\text{eff.}}$	$\frac{\mu_c + \mu_B}{2}$	$\mu_{\text{exp.}}^b$	$\mu_{\text{calc. eff.}}$
	cm.	cm.	cm./sec.	$^\circ\text{C.}$	$^\circ\text{C.}$	poises	poises	poises
Silicone Fluid No. 5105C	1.30 ^c	1.50 ^c	47.1	7.65	9.5	578	255	540
	1.30 ^c	1.50 ^c	47.1	4.70	7.8	588	255	550
	1.30 ^c	1.50 ^c	47.1	1.18	6.5	601	255	565
Oronite Polybutene Oil No. 32	1.30 ^c	1.50 ^c	47.1	7.65	8.5	515	365	330
	1.30 ^c	1.50 ^c	47.1	4.70	7.3	565	365	365
	1.30 ^c	1.50 ^c	47.1	1.18	6.0	642	365	410
	1.30 ^b	1.45 ^b	34.6	5.73	5.9	546	365	410
	1.30 ^b	1.45 ^b	34.6	3.53	5.0	589	—	445
	1.30 ^b	1.45 ^b	34.6	0.89	3.8	650	365	490
	1.30 ^b	1.40 ^b	22.6	3.82	3.6	583	—	500
	1.30 ^b	1.40 ^b	22.6	2.35	2.8	615	—	530
	1.30 ^b	1.40 ^b	22.6	0.59	2.0	655	—	570
	1.30 ^b	1.35 ^b	11.1	1.91	1.4	625	—	600
	1.30 ^b	1.35 ^b	11.1	1.18	1.1	643	—	620
	1.30 ^b	1.35 ^b	11.1	0.30	0.7	668	—	640
	0.549 ^{d*}	0.599 ^{d*}	11.4	4.0	2.7	579	—	540
	0.549 ^{d*}	0.599 ^{d*}	11.4	2.0	1.6	623	—	590
	0.549 ^{d*}	0.599 ^{d*}	11.4	1.0	1.1	648	—	615

^a See Ref. (4).

^b See Ref. (3).

^c See Ref. (5).

^d See Ref. (6).

* This viscometer had been used to establish empirical temperature corrections. The authors (7) suggested to keep either cup, bob or the mean temperature at 30°C. depending on the energy input range. As can be seen from Fig. 3, such temperature corrections might be feasible only for the smallest cup-bob separations.

ture increase which would need to be hypothesized to establish proper correlation to the calculated effective viscosity value, the viscosity which the material has at the cup wall at 30°C., and the physical and instrumental constants required for solving Eq. [4].

In comparing the experimental and calculated effective viscosities for the silicone fluid the difference is so substantial that thixotropic breakdown must be assumed. On the other hand, for the Oronite polybutene oil the differences between the experimental and calculated effective viscosities are small with the possible exception of the value for the cup-bob separation of 1.5 mm. at $T_B - T_C = 0.89^\circ\text{C}$. No explanation for this difference is advanced, since there were no more experimental data available for a similar set of operational conditions. The small differences in experimental and calculated effective viscosity shown for the Oronite polybutene oil suggest that temperature effects might fully account for the measured viscosity decreases. Attention is called to the two vertical temperature columns. In most instances the average effective temperature increase, $(T_B - T_C)_{\text{eff.}}$, necessary to satisfy the calculated effective viscosity is higher than the temperature measured at the bob wall. It is also interesting to note that the effective viscosities, calculated for a given cup-bob separation, do not change as much as one might have expected for the appreciable differences in bob wall temperature.

CONCLUDING REMARKS

In concluding, one might take issue with the assumption that the temperature pattern is entirely controlled by the heat energy arising from local friction and by heat conductivity. Although laminar flow can well be assumed, it appears likely that there will be a continuous exchange of the material over the distance between cup and bob. This mechanism of heat exchange will tend to suppress the maximum of the temperature pattern. Such temperature reduction, if it could be taken into consideration, would cause the calculated effective viscosity to be of somewhat higher value than has been reported here.

Another point which might require further analysis is that the experimental viscosity values, which were available from previously published data, were obtained from measurements performed without giving the material a chance to attain heat equilibrium, a condition which has been assumed to exist for purposes of simplifying calculation of the effective viscosity values.

It is hoped that this presentation might stimulate further work in the direction of providing better tools for separating the effect of heat and that of thixotropy upon the viscosity decrease of materials, when sheared in a rotational viscometer.

REFERENCES

1. BLOK, H., *Ingenieur (Utrecht)* **60**, 58 (1948).
2. HAGG, A. C., *J. Applied Mechanics* **2**, 72 (1944).
3. WELTMANN, R. N., *Ind. Eng. Chem.* **40**, 272 (1948).
4. Miscellaneous Publications of the Bureau of Standards No. **97** (Nov. 9), (1929).
5. GREEN, H., *Ind. & Eng. Chem., Anal. Ed.* **14**, 576 (1942).
6. BUCHDAHL, R., CURADO, J. G., AND BRADDIKS, R., JR., *Rev. Sci. Instruments* **18**, 168 (1947).
7. LOWER, G. W., WALKER, W. C., AND ZETTMLOYER, A. C., Program of the Chem. Soc. Meeting, Sept. 1951, Div. of Paint, Varnish and Plastic Chem.

IMPLICATIONS OF PHILIPPOFF FLOW CURVES FOR THE DETERMINATION OF INTRINSIC VISCOSITY OF HIGH POLYMER NITROCELLULOSES¹

Carl M. Conrad and Hilda M. Ziifle

*Southern Regional Research Laboratory,²
New Orleans, Louisiana*

Received January 28, 1952

INTRODUCTION

Recently, a study was undertaken (1) in which the technique of Krieble and Whitwell (3,4) for intrinsic viscosity of high polymer, non-Newtonian solutions was to be applied to a series of raw cotton samples. However, it was found that when the logarithms of the reduced viscosity counterparts³ were plotted against the concentrations, the results all lay on curves. This finding was contrary to the experience of Krieble and Whitwell, for whom these plots had proven to be linear within the range of concentration studied. A second, though less noticeable deviation was found in the behavior of the z vs. concentration plots which differed in curvature from those observed by Krieble and Whitwell.

After a careful examination of the techniques failed to disclose any obvious experimental sources of error, recourse was taken to an independent source of data for comparison. For this purpose, the extensive and very complete set of flow curves, published by Philippoff and Hess (6) seemed appropriate. These curves were obtained by them from a high-molecular-weight ($[\eta] = 40$) cellulose nitrate in butyl acetate. As can be seen from their Fig. 2, they covered a range of stresses from 1 to over 10,000 dynes/sq. cm.; a range of rates of flow from 0.01 to 100,000 sec.⁻¹; and concentrations of 0.05, 0.10, 0.25, 0.50, and 1.00 g./dl. The present report deals with the results of the study of these curves and their relation to certain types of viscosity treatments.

MATERIAL AND METHODS

Unfortunately, for the purpose of the present study, none of the original data had been published by Philippoff and Hess, but only the

¹ Condensed from a paper of the same title presented at the Annual Meeting of the Society of Rheology, Chicago, Illinois, October 24-27, 1951.

² One of the laboratories of the Bureau of Agricultural and Industrial Chemistry, Agricultural Research Administration, U. S. Department of Agriculture.

³ The "reduced viscosity counterpart" is defined by $(\zeta/\eta_0 - 1)/c$; cf. Ref. (3).

chart. In order to obtain necessary data to compute viscosities, a photographic negative of the figure was placed on the stage of a micro comparator; the points of intersection of the curves with the grid lines were then read off and evaluated in relation to the logarithmic scale. From the known values of the logarithmic scales the quotients of the shearing stresses, P , to the rates of shear, V , were determined. It is estimated that the precision of the viscosities, based on the curves and on a series of replicate readings with the comparator, was of the order of 0.2%.

It can be easily shown that the slopes of the logarithmic flow curves of Philippoff and Hess are equivalent to the z of Krieble and Whitwell (3). In order to apply the Krieble and Whitwell technique it is necessary to know the z values corresponding to the viscosities. For this purpose a fivefold photostatic enlargement of Philippoff and Hess's flow curves was prepared. This was carefully examined by applying a straightedge at the outer grid lines and found to be free from detectable spherical curvature. The slopes were read off the curves at one-eighth intervals of the abscissal grid spaces with the aid of a prismatic tangent meter similar to that described by Richards and Roope (7). The precision, based upon repeated readings, was determined at high and low slopes, and on the basis of three readings each was found to be of the order of 3.5 and 1.7%, respectively.

In the presentation of shear-sensitive data, both constant rate of shear (velocity gradient) and constant shearing stress were used as reference points.

RESULTS

The Derived Data

The solvent viscosity, based on 12 separate readings distributed along the entire curve, averaged 0.00740 poise, with a standard deviation of 2.8%.

The mean measured values of z are shown in Fig. 1, as a function of the shearing stress, P , and in Fig. 2 as a function of the rate of shear, V , in both cases on logarithmic coordinates.

In Fig. 1 it is seen that the z values lie moderately uniformly about their individual modal points, the curve for 0.05 g./dl. being the most skew. One important feature of the curves is that as the concentration increases the modes are displaced in the direction of increasing shearing stresses. As will be evident later this leads to seemingly erratic curvature in functions depending on the value of z . Although it is not certain that the differences are outside the limits of experimental error, it is evident that the curves fail to return to the shearing stress axis at the higher stress values.

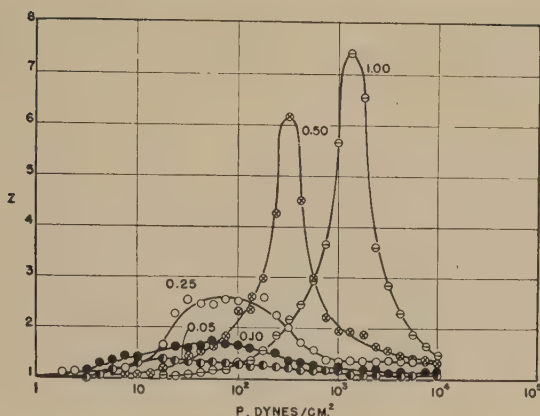


FIG. 1. Slope, z , for the different concentration curves, represented as a function of P . The circles show the mean of three observations; some circles at low z values were omitted in order to avoid overlapping and confusion.

In Fig. 2, curves similar to those of Fig. 1 are observed, except that here they all appear to have a common mode. The apparent failure at low concentrations may or may not be within the limits of experimental error. This more nearly common modality of the z curves leads to more nearly linear curves when based on constant rates of shear.

Relation of Z to Concentration

Figure 3 shows the relation of z , derived from Figs. 1 and 2, to concentration. The large variability of slope in each of these sets of curves is

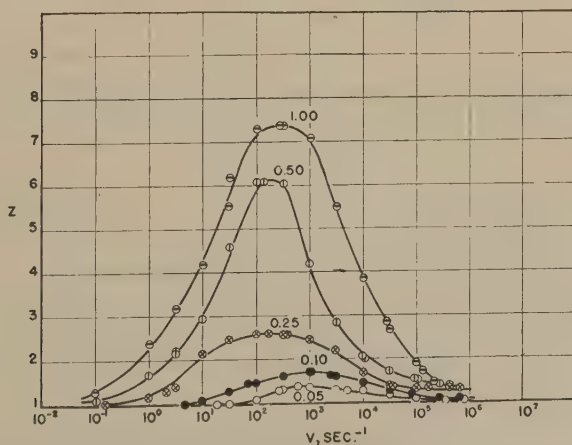


FIG. 2. Slope, z , for the different concentrations (indicated by the numbers), represented as a function of V . The circles show the means of three observations.

immediately evident. It is seen that the curves based on shearing stress are more variable than those based on constant rate of shear; this, of course, is traced back to the greater displacement of modes in Fig. 1 than in Fig. 2.

Relation of Reduced Viscosity Counterpart to Concentration

The more important objective lay in finding an explanation for the curvature with concentration of reduced viscosity counterpart (1). Accordingly, reduced viscosity counterparts were computed from the Philippoff and Hess viscosities, using only the three lowest concentrations because it was believed these included the maximum concentrations that would be accepted in ordinary practice. The results were computed both

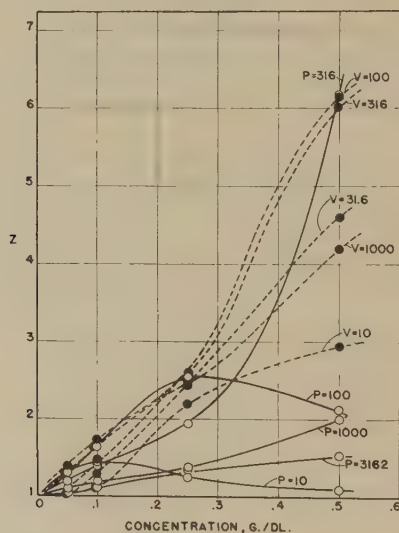


FIG. 3. Relation of z to concentration at constant shearing stresses, P , (smooth curves) and at constant rates of shear, V (broken curves), for cellulose nitrate in butyl acetate [derived from figure of Philippoff and Hess (6)].

for different constant shearing stresses, P , and for constant rates of shear, V , and are shown in Fig. 4.

It is seen that the curves of Fig. 4 display a rather wide range of position and slope. At a shearing stress of $P = 100$ and in the vicinity of constant rate of shear, $V = 100$ the curves are practically linear. Again, between $P = 316$ and 1000 a change in the sign of curvature occurs. At other positions of constant P or V the lines are distinctly curvilinear. In general, the curves at normal constant rates of shear, V , are less curvilinear than are those at normal constant shearing stresses, P . Except for the essentially linear plots it is evident that considerable uncertainty

must exist concerning the value of the intercepts on the zero-concentration axis. It is possible, though by no means certain, that all the curves would have a constant intercept if the measurements were carried to a sufficiently low concentration.

Relation of Reduced Apparent Viscosity to Concentration

It seemed of special interest in the present study to examine the type of curves that would be obtained according to more conventional methods. For this purpose reduced apparent viscosities were computed at both constant shearing stresses and constant rates of shear, without reference to the z value. The data were plotted both according to Martin's and

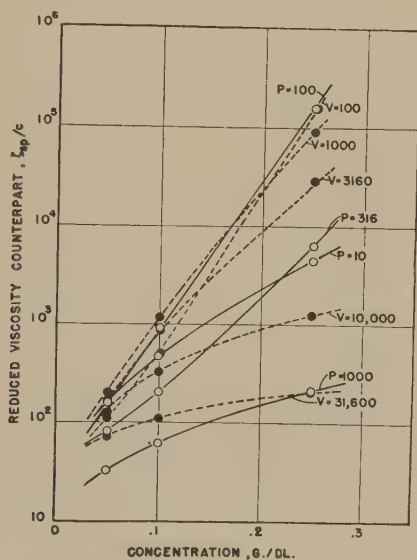


FIG. 4. Relation of reduced viscosity counterpart (log scale) to concentration at different constant shearing stresses, P (smooth curves), and at constant rates of shear, V (broken curves) [derived from figure of Philippoff and Hess (6)].

Huggins' procedures. To conserve space only those plotted according to the Huggins' procedure are reproduced here, as Fig. 5.

These curves at constant shearing stresses are the typical Philippoff eighth-power ones, used by him for concentration extrapolations (5). Intercepts could not be reliably determined from the limited data available until the stresses exceed 100 dynes/sq. cm., or the rates of shear several hundred reciprocal seconds. The plots at constant rate of shear are similar to those at constant shearing stress, though displaying less prominent changes of curvature. There is considerable evidence that the lower limbs, i.e., at the lower concentrations, of these curves are linear

for both constant shearing stresses and constant rates of shear. Again, the wide divergence of intercepts indicates the failure of the technique as ordinarily employed, if applied to very high-polymer celluloses showing pronounced shear effects.

According to Martin's plot, the curves at shearing stresses of $P = 100$ or more showed quite linear limbs at concentrations of 0.25 g./dl. or less, but curved limbs at lower stresses. At constant rates of shear, linear limbs did not appear below 1000 sec.⁻¹. For both constant shearing stresses and constant rates of shear the intercepts apparently differed widely depending on the particular values of P or V chosen. Based on

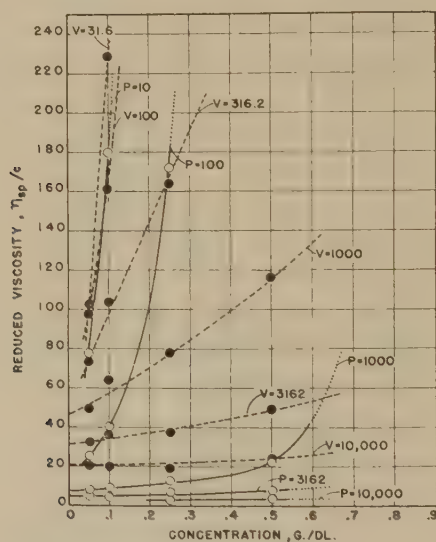


FIG. 5. Relation of reduced apparent viscosity to concentration at different constant shearing stresses, P (smooth curves), and constant rates of shear, V (broken curves), for cellulose nitrate in butyl acetate [derived from figure of Philippoff and Hess (6)].

recent findings from several different sources (8,9) including our own observations with cellulose nitrate in ethyl acetate, it is believed that the apparent linearity of some of these curves at the lower concentrations is an artifact, which can be disclosed by observations at still lower concentrations where the curves near the zero concentration axis suddenly turn down.

DISCUSSION

One of the interesting features of the present study is the relation of the slopes of the logarithmic flow curves to rate of shear, shearing stress, and concentration of polymer. These slopes derived from sigmoid-type flow curves, rise from a minimum of 1, reach a maximum, and then recede

again to, or near 1. The curves appear to be essentially symmetrical, the small amount of skewness observed, for instance, in the 0.05 g./dl. concentration, and the failure to return to 1 at the highest stress values being, perhaps, within the observational errors.

It is clearly evident from Fig. 1 that the z curves do not have a common mode with log shearing stress. The mode shifts progressively toward the higher stress values as the concentration increases. To the non-coincidence of modes on this basis can be ascribed entirely the peculiar behavior of both the relation of z to concentration and the relation of reduced viscosity counterpart to concentration. From Fig. 2 it is apparent that the z curves are much more nearly unimodal when plotted against log rate of shear (velocity gradient). For this reason, in the present study at least, the relations of z and of the derived viscosity functions to concentration are much less influenced by the particular value chosen. In both constant shearing stress and constant rate of shear there appear to be unique combinations which give straight-line plots, but such combinations seem to be the exception rather than the rule.

While Philippoff has shown the wide conformity among different high-polymer substances to the type of flow curves displayed by cellulose nitrate in butyl acetate, it is by no means certain that the results observed in the present study can be carried over bodily to cellulose dissolved in cupriethylenediamine or other solvents. There is evidence that the non-Newtonian behavior of cellulose nitrate is approximately twice as great for the same shearing stresses and concentrations as of cellulose in cupriethylenediamine solutions. A series of curves of a high degree of polymerization (D.P.) cellulose in this solvent and in cuprammonium similar to those supplied by Philippoff and Hess for cellulose nitrate in butyl acetate would be needed.

A very interesting result of the present study is the lack of common intercepts at zero concentration of the reduced viscosity, already noted for cuprammonium and cupriethylenediamine solvents (2). A common intercept might be found if observations were made at still lower concentrations, but observational errors do not make it appear promising to strive in this direction. On the other hand, consideration of plausible rotatory diffusion constants shows that a true shear dependence of the intrinsic viscosities for the systems investigated might well become measurable.

While the present data may indicate a moderate advantage of rate of shear as a basis for common reference of non-Newtonian viscosity data, much more work is needed to show how far the relationships shown by cellulose nitrate in butyl acetate can be extended to other systems.

SUMMARY AND CONCLUSIONS

As a result of an analytical study of flow curves of cellulose nitrate in butyl acetate at different concentrations, published by Philippoff and Hess, it is concluded that:

1. The value of the slope, z , of the logarithmic flow curves, representing the relation of log rate of shear to log shearing stress, increases with increasing log shearing stress or log rate of shear from approximately 1, which is normal for Newtonian solutions, to a maximum and then recedes again nearly symmetrically to or near 1 at the higher stresses or rates of shear.

2. When the z slopes are plotted against log shearing stress the modes of the curves for the different concentrations are not coincident, but progress with increasing concentration to higher shear stresses and with increasing amplitude. On the other hand when the z slopes are plotted against log rate of shear the modes are more nearly coincident, the deviations being perhaps within the limits of experimental error; the amplitudes increase with concentration in this case also.

3. Insofar as the z modes do not coincide for different concentrations, the relation of z and of derived viscosity quantities to concentration assumes widely different curvilinear configurations, depending on the experimental conditions of stress and rate of shear under which observations are made.

4. In conformity with earlier studies of cuprammonium and cupriethylenediamine solutions of cellulose, it is found for cellulose nitrate in butyl acetate, also, that the intercepts of reduced viscosity at zero concentration (intrinsic viscosities) vary widely with the constant velocity gradient used, and in the present series also with the constant shearing stress employed. This follows regardless of whether the data are plotted according to Martin's or the Huggins' scheme.

5. While it has been shown by Philippoff that the type of flow curves here considered are quite general among solutions of different types of high-polymer substances, there are many details to be verified concerning degree of conformity and magnitude before the present results can be carried over to other systems.

REFERENCES

1. CONRAD, C. M. AND RUSCA, R. A., Some Viscometric Studies of Cellulose in Cotton in Relation to Mechanical Processing. Paper presented before Sec. 15 of the XIIth International Congress of Pure and Applied Chemistry, New York, N. Y., Sept. 10-13, 1951.
2. CONRAD, C. M., TRIPP, V. W., AND MARES, T. J. *Phys. & Colloid Chem.* **55**, 1474-91 (1951).

3. KRIEBLE, J. G., AND WHITWELL, J. C., *Textile Research J.* **19**, 253-8 (1949).
4. KRIEBLE, J. G. AND WHITWELL, J. C., *Textile Research J.* **19**, 556-62 (1949).
5. PHILIPPOFF, W., *Viskosität der Kolloide*, T. Steinkopff, Dresden and Leipzig, 1942.
6. PHILIPPOFF, W. AND HESS, K., *Z. physik. Chem.* **B31**, 237-55 (1935).
7. RICHARDS, O. W., AND ROOPE, P. M., *Science* **71**, 290-1 (1930).
8. STREETER, D. J., AND BOYER, R. F., *Ind. Eng. Chem.* **43**, 1790-97 (1951).
9. WEISSBERG, S. G., SIMHA, R., AND ROTHMAN, S., *J. Research Natl. Bur. Standards* **47**, 298-314 (1951).

THE FLOW OF POLYSTYRENE THROUGH RECTANGULAR CHANNELS¹

C. E. Beyer and F. E. Towsley

The Dow Chemical Company, Midland, Michigan

Received February 11, 1952

INTRODUCTION

The equation of flow of a viscous liquid through a circular channel can easily be used in engineering calculations. On the other hand, the equation of flow through a rectangular channel is much more difficult, and in all practical cases an approximate form must be used. To further add to the difficulties, polystyrene, like many other high polymers, is a non-Newtonian material, where the rate of shear is not proportional to the shearing stress.

The present paper is an attempt to present a simplified method of determining the flow of polystyrene through rectangular channels that can be used for practical engineering calculations.

DISCUSSION

The streamline flow of a viscous liquid through a circular channel is given by Poiseuille's law:

$$Q = \frac{\pi R^4 P}{8\eta l} \quad [1]$$

where Q = volume rate of flow,

R = radius of channel,

η = viscosity,

P = pressure drop, and

l = length of channel.

It may be shown by dimensional analysis (2) (Appendix I) that the flow of a liquid through any shape channel can be expressed by

$$Q = \frac{C_1 P D^4}{\eta l}, \quad [2]$$

provided the cross-sectional shape is constant along its length. In this expression D is some representative dimension of the cross section and C_1

¹ Presented at the Annual Meeting of the Society of Rheology, Chicago, Illinois, October 24-27, 1951.

is a dimensionless constant depending only on the shape of the cross-sectional area. For example, in the circular channel, if D is the radius, then $C_1 = \pi/8$. For other shapes of channels (rectangular, triangular, elliptical, etc.), the degree of approximation of Eq. [2] is almost entirely dependent upon the degree of approximation used in calculating the constant C_1 . Several approximate methods of calculating the constant C_1 can be found in the literature, (3,4,6,11), and a few of these are listed in Table I. The expression for the rectangular channel listed in Table I is used for the calculations in this paper.

TABLE I

No. of parameters	Shape	Size parameter D	Shape parameter	C_1	Ref.
(1)	Circle	Radius	—	$\frac{\pi}{8} = 0.393$	
(2)	Rectangle	Semi-side (shorter)	$R = \frac{\text{long side}}{\text{short side}}$	$\frac{4}{3} \left[R - 0.6274 \left(\tanh \frac{\pi R}{2} + 0.0045 \right) \right]$	(4)
(1)	Square	Semi-side	—	$\frac{4}{3} (0.4128) = 0.561$	(4)
(2)	Ellipse	Semi-axis (shorter)	$R = \frac{\text{long axis}}{\text{short axis}}$	$\frac{\pi R^3}{4} (1 + R^2)$	(3)
(1)	Equilateral triangle	Semi-side	—	$\frac{\sqrt{3}}{20} = 0.0866$	(11)
(2)	Circular annulus	Semi-spacing	$R = \frac{\text{outer radius}}{\text{inner radius}}$	$\frac{2\pi}{(R-1)^4} \left[(R^4 - 1) - \frac{(R^2 - 1)^2}{\log_{10} R} \right]$	(4)
(2)	Circular annulus	Outer radius	$R = \frac{\text{outer radius}}{\text{inner radius}}$	$\frac{\pi}{8R^4} \left[(R^4 - 1) - \frac{(R^2 - 1)^2}{\log_{10} R} \right]$	(4)

The flow of many of the common high polymers is not completely given by the preceding expression. The output rate does not increase proportionally with the pressure gradient but increases as some function of this variable. The functional relations for a rectangular channel can be determined by dimensional analysis (Appendix II). The resulting expression is

$$Q = \frac{C_1 P D^4}{\eta_0 l} F \left\{ C_2 K \tau_w, \frac{b}{a} \right\} \quad [3]$$

where a and b are the sides of the rectangular cross section, τ_w is the average shear stress at the wall, and K is a material constant having the di-

mensions of the reciprocal shear modulus. C_2 is a dimensionless constant depending on the ratio of the sides.

One way to visualize nonlinear flow is to consider the viscosity as a variable, and to express the viscosity as its reciprocal, fluidity, as a function of the shearing stress. Spencer and Dillon (9) have used this approach to determine an empirical fluidity function that fits the experimental data for circular channels.

$$\phi_A = \phi_0 \left\{ 1 + K\tau + \frac{K^2\tau^2}{2!} + \frac{K^3\tau^3}{3!} + \frac{K^4\tau^4}{4!} \right\} \quad [4]$$

with ϕ_A as the "apparent fluidity" and ϕ_0 as the Newtonian or zero shear stress fluidity. Then flow in the circular channel or tube is described by

$$Q = \frac{\pi}{8} \frac{PR^4}{l} \phi_A. \quad [5]$$

From this expression Wiley and Pierce have developed a similar expression for the flow between infinite parallel plates (10), for application to annular channels of small gap. The apparent fluidity function obtained for this type of flow is for practical purposes identical with expression [4]. The ratio ϕ_A/ϕ_0 which contains all of the nonlinear part of the flow be-

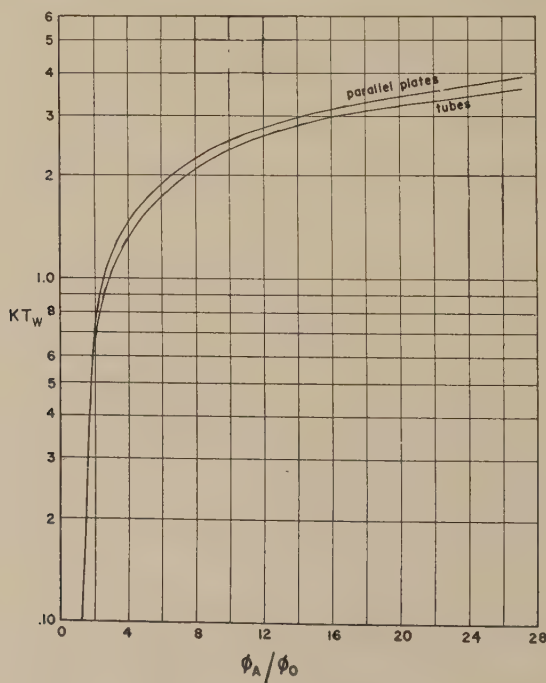


FIG. 1. Nonlinear flow of polystyrene.

havior is shown in Fig. 1 as a function of $K\tau_w$ for these two cases. These curves were calculated from the data of Wiley and Pierce.

Since only one expression is needed for practical engineering calculations in these two quite different extrusion situations (circular and annular channels), a simple combination of the dimensional analysis and the Spencer-Dillon equation has been tried and found useful in expressing the nonlinear flow through rectangular channels.

$$\phi_A = \phi_0 \left\{ 1 + C_2 K \tau_w + \frac{(C_2 K \tau_w)^2}{2!} + \frac{(C_2 K \tau_w)^3}{3!} + \frac{(C_2 K \tau_w)^4}{4!} \right\} \quad [6]$$

where ϕ_A is a general "apparent fluidity" and C_2 is a dimensionless parameter depending on the cross-sectional shape of the channel. The argument

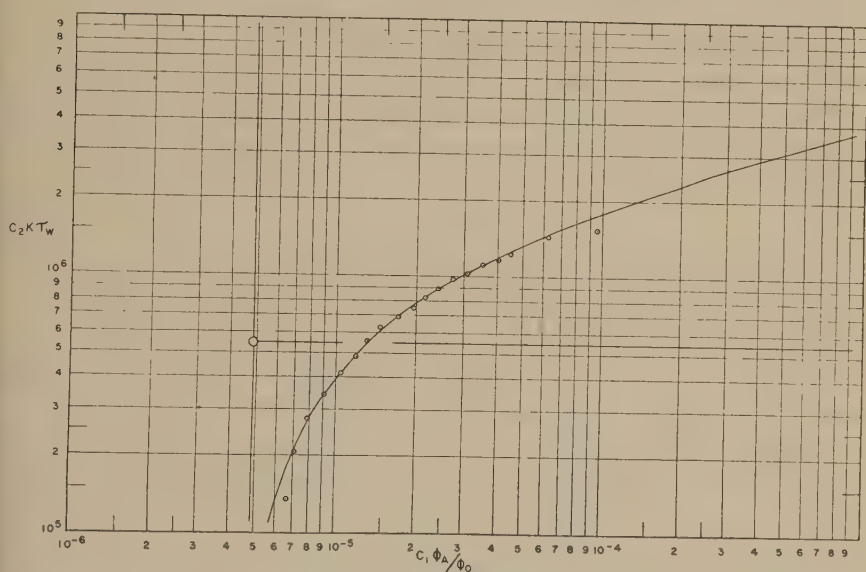


FIG. 2. Apparent fluidity function versus shear stress at wall for square channel.

b/a has been dropped from the dimensional analysis expression [3], for rectangular channels. The experimental curves for rectangular channels fit formula [6] sufficiently well to allow this convenient simplification, with C_2 as an empirical function of b/a .

The Celluloid prototype curve method as described by Spencer (7) is used in the evaluation of the constants for the rectangular channels. In this method a plot of $\log_{10} \phi_A/\phi_0$ against $\log_{10} C_2 K \tau_w$ is made on a Celluloid sheet with reference axes located at $C_2 K \tau_w = 1$, and $\phi_A/\phi_0 = 1$ (Fig. 2). Then the experimental points are plotted on the same type of graph paper and the Celluloid prototype is laid over the graph paper with its curve

fitted to the experimental points by translation along both axes. The coordinate on the ϕ_A axis gives $C_1\phi_0$ or C_1/η , and that on the τ_w axis gives $1/C_2K$. Since the values of the constants C_1 and C_2 are known for circular channels ($C_1 = \pi/8$; $C_2 = 1$), the values of η_0 and K can be determined. Using the same material and temperature in the rectangular die and knowing η_0 and K , the constants C_1 and C_2 can be calculated.

EXPERIMENTAL METHODS

A capillary viscometer similar to that described by Nason (5) was used to force the polymer through the channel. The apparatus consisted of a vertical cylinder immersed in an oil bath. A nitrogen tank was connected to the top of the cylinder and the pressure forced the polymer through the vertical channel attached to the bottom of the cylinder. The pressure was controlled by a Victor Gas-O-Dome regulator and measured by a calibrated Bourdon pressure gauge. The temperature of the oil bath was controlled to about $\pm 0.1^\circ\text{C}$. with a Precision "Micro-set" thermoregulator. To maintain the temperature in the capillary, it was jacketed with a small electrical heater and the voltage regulated to maintain the temperature to within $\pm 0.5^\circ\text{C}$. of the desired value.

TABLE II

Channel Dimensions

Rectangular channels

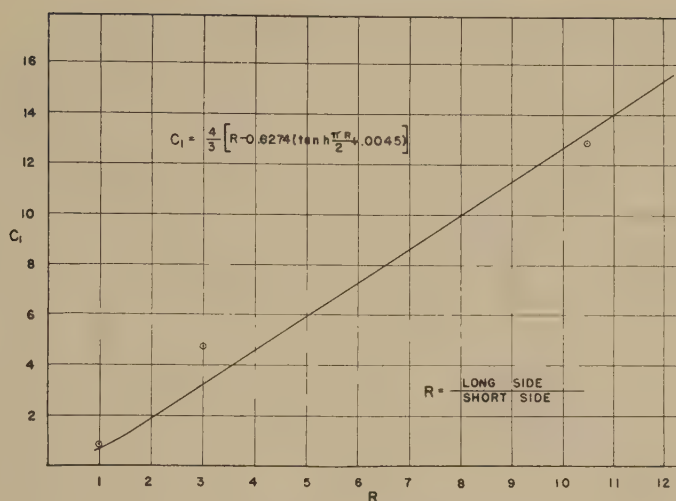
No.	R	a cm.	b cm.	Length cm.
1	1	0.102	0.102	2.540
2	2.86	0.203	0.0711	2.540
3	10.58	0.323	0.0305	2.540
Circular channel				
4	radius:	0.0529 cm.	length:	2.9870 cm.

The dimensions of the various channels used are listed in Table II. The length of the channels were made much larger than the cross-sectional dimensions so that end corrections would be small and could be neglected for practical purposes.

The flow rates were measured by cutting off the sections of the filament extruded during a measured interval of time, and weighing. This was then connected to volume rate, using the specific volume data of Spencer and Boyer (8). The polystyrene used in this work was the same

TABLE III

	R	C_2	C_1	Calculated C_1
Square channel	1	2.09	0.621	0.561
Rectangular channel	3	1.78	4.70	3.15
Rectangular channel	10	1.21	12.8	13.27
Infinite planes	∞	1.07		

FIG. 3. C_1 versus R for rectangular channels.

as that used by Spencer and Dillon (9). The polymer was an unfractionated material having a weight average (light-scattering) molecular weight of 360,000.

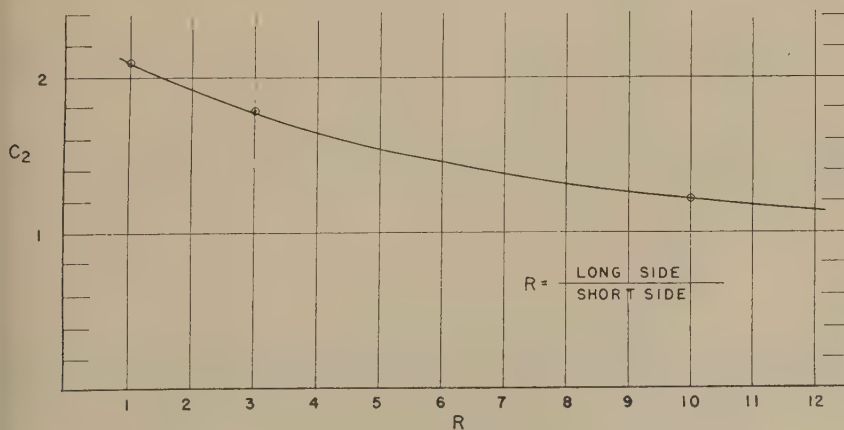
The values of η_0 and K as determined by the circular channel for polystyrene at 225°C. are

$$\eta_0 = 1.32 \times 10^5 \text{ poises,}$$

and

$$K = 3.64 \times 10^{-6} \text{ cm.}^2 - \text{dyne}^{-1}.$$

The results of the experimental data for the rectangular channels are listed in Table III. Figure 3 shows the relationship between the constant

FIG. 4. C_2 versus R for rectangular channels.

C_1 and the side ratio R . The curve is calculated from the expression of Table I and the points represent the experimental data. The large amount of error in the data for the channel $R = 3$ is probably due to the end effects. The cross-sectional area was made larger with respect to the length than the other channels. Figure 4 shows the variation in the experimental value of C_2 with the side ratio. The value of C_2 decreases to 1.07 for flow between infinite planes. It was found that with the size channels used the flow rate could be predicted to within $\pm 10\%$. When a channel having a ratio of short side to length greater than 0.05 the error in calculating the flow rate was greater than $\pm 10\%$.

SUMMARY

For ϕ_A/ϕ_0 ratios up to 10, the flow of polystyrene in rectangular channels may be predicted by the expression

$$Q = \frac{C_1 P D^4}{\eta_0 l} \left\{ 1 + (C_2 K \tau_w) + \frac{(C_2 K \tau_w)^2}{2!} + \frac{(C_2 K \tau_w)^3}{3!} + \frac{(C_2 K \tau_w)^4}{4!} \right\} \quad [7]$$

where C_1 and C_2 are dimensionless parameters depending upon the ratio of the sides of the channel. One approximate equation for calculating the constant C_1 is given, and experimental values of both constants have been determined experimentally. This expression can be used to predict the rate of flow of polystyrene in rectangular channels to within $\pm 10\%$ if the ratio of the short side to length is less than 0.05.

REFERENCES

1. BRIDGMAN, P. W., *Dimensional Analysis*. Yale University Press, New Haven, 1932.
2. HERSEY, M. D., AND SNYDER, G. H., *J. Rheol.* **3**, 298-317 (1932).
3. LAMB, H., *Hydrodynamics*, p. 587. Dover Publications, Inc., New York, 1945.
4. LEA, F. C., AND TADROS, A. C., *Phil. Mag.* **11**, 1235-47 (1931).
5. NASON, H. K., *J. Applied Phys.* **16**, 338 (1945).
6. PURDAY, H. F. P., *An Introduction to the Mechanics of Viscous Flow*. Dover Publications, Inc., New York, 1949.
7. SPENCER, R. S., *J. Polymer Sci.* **5**, 591-608 (1950).
8. SPENCER, R. S., AND BOYER, R. F., *J. Applied Phys.* **17**, 398 (1946).
9. SPENCER, R. S., AND DILLON, R. E., *J. Colloid Sci.* **4**, 241-8 (1949).
10. WILEY, R. M., AND PIERCE, J. E., *Chem. Eng. Progress* **47**, 432-5 (1951).
11. YADOFF, O., *Compt. rend.* **223**, 192-3 (1946).

APPENDIX I

Dimensional Analysis For Linear Flow

The array of quantities relevant for flow of viscous material in channels of constant cross section, and the application of the Buckingham II-theorem (1) are shown below (for our purposes here it is convenient to take, as fundamental dimension, force F , length L , and time T):

Quantity	Symbol	Dimensions
Volume rate of flow	Q	L^3T^{-1}
Pressure gradient	G	FL^{-3}
Representative cross section dimension	D	L
Viscosity	η	$FL^{-2}T$

By the Buckingham theorem, with four quantities and three fundamental dimensions there is one dimensionless group of variables in the problem, that is:

$$Q^\alpha G^\beta D^\gamma \eta^\delta = \text{a dimensionless constant, } C_1.$$

Inserting quantity dimensions in this equation, and arbitrarily setting $\alpha = 1$, one obtains

$$\beta = -1, \quad \gamma = -4, \quad \delta = 1.$$

Then $Q = C_1 G D^4 / \eta = C_1 P D^4 / \eta l$, where pressure gradient G is given by pressure drop P over channel length l . C_1 here is a form factor. That is, it changes only when the channel cross section shape is changed.

APPENDIX II

Dimensional Analysis for Nonlinear Flow in Rectangular Channels

In this case one makes use of previous experience with nonlinear flow of polystyrene. Spencer and Dillon found that the flow in circular channels is characterized by two material constants: K , a constant having the dimensions of a reciprocal shear modulus; and η_0 , the zero-shear stress viscosity. In nonlinear flow in rectangular channels we can then expect the physical situation will involve the following quantities:

Quantity	Symbol	Dimensions
Volume rate of flow	Q	L^3T^{-1}
Pressure gradient	G	FL^{-3}
Long rectangle side	a	L
Short rectangle side	b	L
Viscosity at zero shear stress	η_0	$FL^{-2}T$
Non-Newtonian material constant	K	$F^{-1}L^2$

With six quantities and three fundamental dimensions we will have three dimensionless groups and arbitrary choice of three exponents in each of these.

$$\text{General equation } Q^{\alpha_1} G^{\beta_1} a^{\gamma_1} b^{\delta_1} \eta_0^{\epsilon_1} K^{\lambda_1}$$

Choosing the arbitrary exponent judiciously, one has the three dimensionless groups,

$$Q^1 G^{\beta_1} a^0 b^{\delta_1} \eta_0^{\epsilon_1} K^0 = \text{a dimensionless constant.}$$

$$Q^0 G^{\beta_2} a^{\gamma_2} b^{\delta_2} \eta_0^0 K^0 = \text{a dimensionless constant.}$$

$$Q^0 G^{\beta_3} a^0 b^{\delta_3} \eta_0^{\epsilon_1} K^1 = \text{a dimensionless constant.}$$

Inserting dimensions, solving for exponents, and combining results one obtains $Q = CGb^4/\eta_0$ times a function of two arguments, GKb and b/a . Substituting P/L for G ,

$$Q = \frac{CPb^4}{\eta_0 l} F \left\{ \frac{KPb}{l}, \frac{b}{a} \right\}.$$

Now average shear stress at the wall, τ_w , is given by

$$\frac{Pb}{l} \frac{1}{2 \left(\frac{b}{a} + 1 \right)}.$$

Then the equation can be written as

$$Q = \frac{C_0 P D^4}{\eta_0 l} F \left\{ C_2 K \tau_w, \frac{b}{a} \right\}$$

where C_2 is a dimensionless function of b/a .

RESIDUAL STRESSES AND STRAINS IN MOLDED PLASTICS¹

W. H. Markwood, Jr. and H. M. Spurlin

Hercules Powder Company, Wilmington, Delaware

Received January 28, 1952

INTRODUCTION

A great many objects encountered in everyday life give evidence of localized strains. For example, unless the glass of a thermometer is well annealed, it will change its calibration with time. Unless a welded boiler is stress-relieved, it may fail in service or show high localized corrosion. These defects, changes of dimensions, liability to failure in service, and optical imperfections, can be even more noticeable in plastic articles than in other materials. But just as tempering can protect a tumbler from breakage, articles made from high polymers can have improved properties in certain respects if they have been subjected to a process giving controlled strains. It has been obvious for a long time that a study of the causes and effects of strains would be valuable for plastics technology.

It is well known that the rheologic behavior of thermoplastic materials generally follows a superposition principle. That is, the deformations due to elastic, delayed elastic, and viscous motion while a piece is under stress are additive and phenomenologically separable. The cellulose derivatives are not exceptions, but the various species respond quite differently to the application of deforming stresses. This discussion is primarily aimed at illustrations of the molding behavior of ethyl cellulose, for which little fundamental information has been reported. The purpose is to present certain of the reasons why this tough, resilient polymer behaves as it does and why some difficulties have arisen when it has been injection molded.

Discussion and Experimental

In accordance with the superposition principle, when ethyl cellulose or cellulose acetate is compressed and then allowed to relax at a fixed temperature, a familiar type of curve is obtained (Fig. 1). It is seen that the application of a fixed load produces a first deformation which for all practical purposes is time independent. This is followed by an

¹ Presented at the Annual Meeting of the Society of Rheology, Chicago, Illinois, October 24-27, 1951.

ever-increasing strain until the load is removed, whereupon a rapid recovery occurs, which again is instantaneous from a practical point of view and is of the same magnitude as the first deformation. Then follows a slow recovery until, for all practical purposes, recovery ceases, leaving a permanent deformation.

The practice of dividing these strains into three classes: the elastic part, the delayed elastic part, and the viscous part, is of course familiar. One way of describing their behavior is to represent them with a series of mechanical models: an instantaneously recoverable spring having an elastic modulus E ; a time-dependent, slowly recoverable parallel spring and dashpot of modulus E' and viscosity η' ; and a time-dependent, nonrecoverable viscosity η . The delayed elastic element is also character-

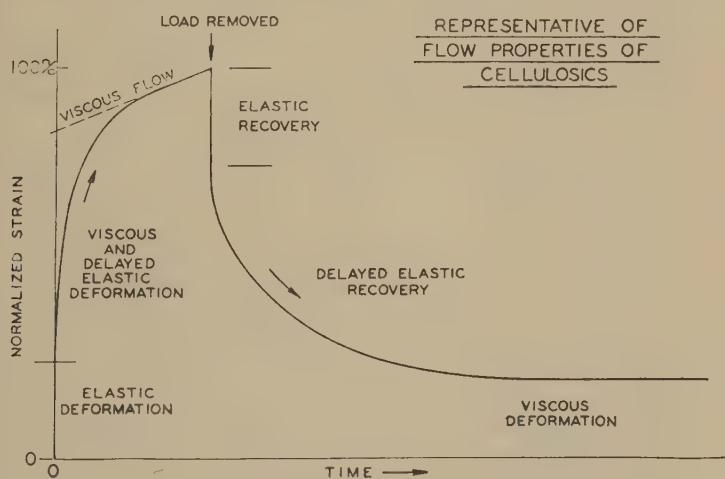


Fig. 1. Strain and relaxation of a thermoplastic.

ized by a relaxation time defined as the time required for it to recover one e^{th} of its deformation after stress is removed. The time is numerically equal to the ratio η' over E' . Furthermore, considerations of the delayed elasticity as consisting of a spectrum of deformations described by a spectrum of retardation or relaxation times is well known. However, due to the limitations of experimental techniques it is usually acceptable to cut the spectrum into regions of only a few "average" relaxation times which can be measured with not too much difficulty. It so happens that three of these retardation times seem adequate to describe the creep and relaxation of both ethyl cellulose and cellulose acetate. The times are of about the same order of magnitude for both polymers, roughly 20, 200, and 1000 sec., and, somewhat surprisingly, they seem to be little influenced by temperature or plasticizer concentration.

On the other hand, the permanent deformation and the Hookean elasticity of both plastics are temperature dependent, as might be expected, but to different degrees (Fig. 2). On this graph the log viscosities and the log moduli are plotted against reciprocal temperatures. The plastics are commonly used injection-molding types of cellulose acetate and ethyl cellulose, although the ethyl cellulose contains about twice as much plasticizer as usual. The viscosities lie between 10^9 and 10^{12} poises,

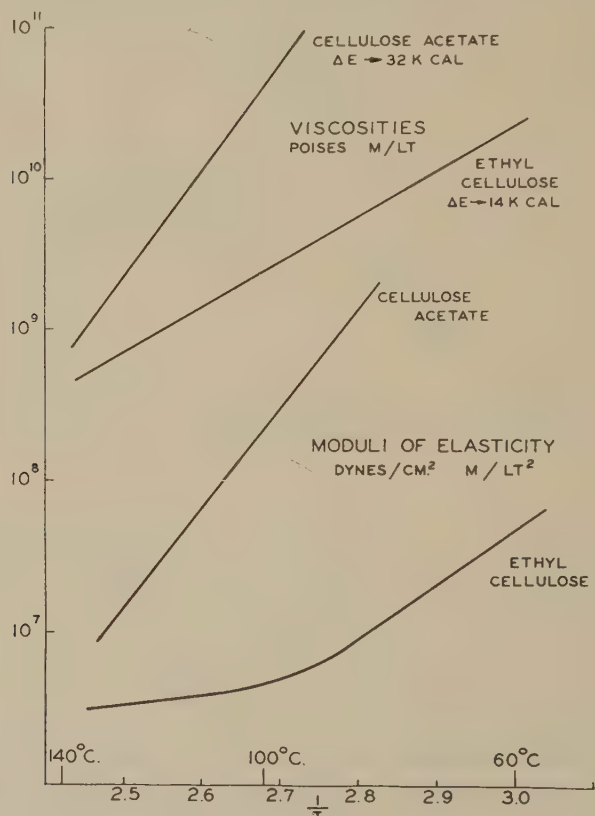


Fig. 2. Temperature variation of viscosity and elasticity in two plastics.

and the activation energy for cellulose acetate is about double that of ethyl cellulose; cellulose acetate is much more temperature sensitive. Although the range of the elasticities is somewhat lower, 10^6 – 10^9 dynes/sq. cm., the activation energies are about the same except at the higher temperatures where that for ethyl cellulose begins to decrease. This indicates an important difference between the polymers which is further illustrated by the role their three kinds of deformation play when plastic objects are stressed at different temperatures (Fig. 3). This chart shows

the percentage of the total deformation that is due to each kind when plotted against $1/T$.

It is seen that as temperature is raised, deformation due to viscous flow in cellulose acetate increases, while that due to elastic and delayed elastic decreases. The opposite is true for ethyl cellulose. Although it would probably be unsafe to extrapolate these curves linearly to injection-molding conditions, it seems valid to conclude that while an increase of molding temperature would tend to reduce frozen-in stresses in cellulose acetate, it would have much less effect in the molding behavior of ethyl cellulose, which tends to retain its tough, rubbery character.

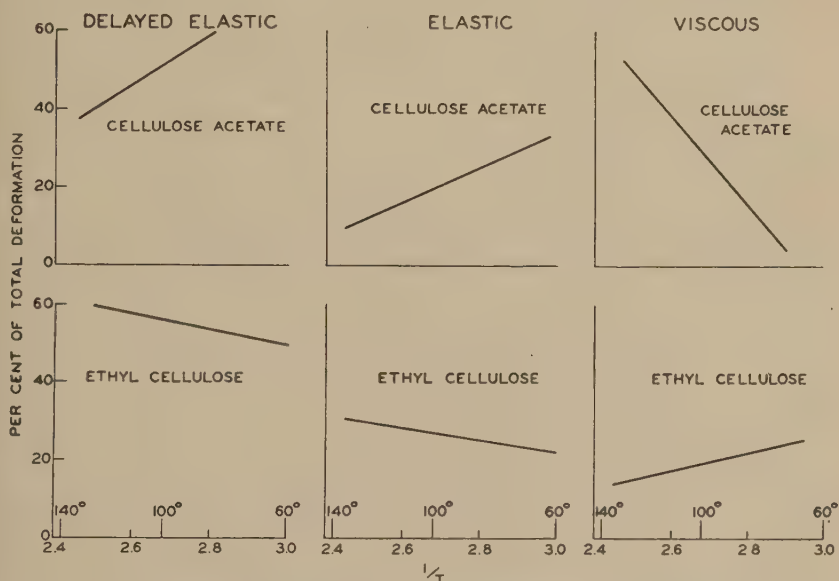


Fig. 3. Effect of temperature on the various types of deformation occurring during compression of two plastics.

So far we have observed the behavior of ethyl cellulose when stressed and relaxed at constant temperatures. Further interesting observations may be made if ethyl cellulose is molded at one temperature, quickly cooled, then reheated to successively increasing temperatures and its relaxation observed after each successive temperature. Such flow and relaxation behavior of plasticized ethyl cellulose is markedly influenced by its degree of ethylation (Fig. 4). This curve is typical of its flow in capillaries. The ordinate is the relative time required to flow a predetermined distance under a constant load, and the abscissa is ethoxyl content.

The ethyl cellulose most often used for injection molding contains approximately 46% ethoxyl. If this type, with 12% plasticizer added

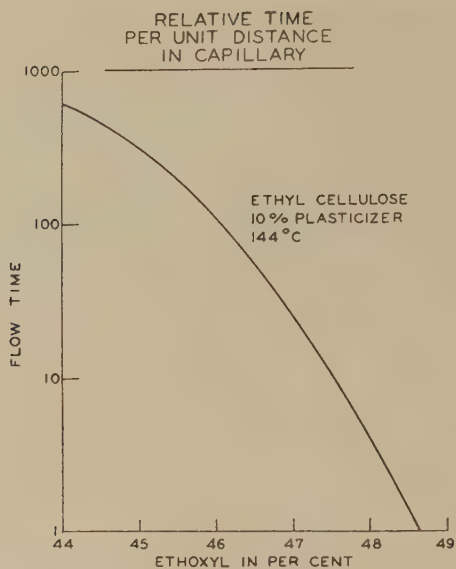


FIG. 4. Influence of composition on flow of plasticized ethyl cellulose in a capillary.

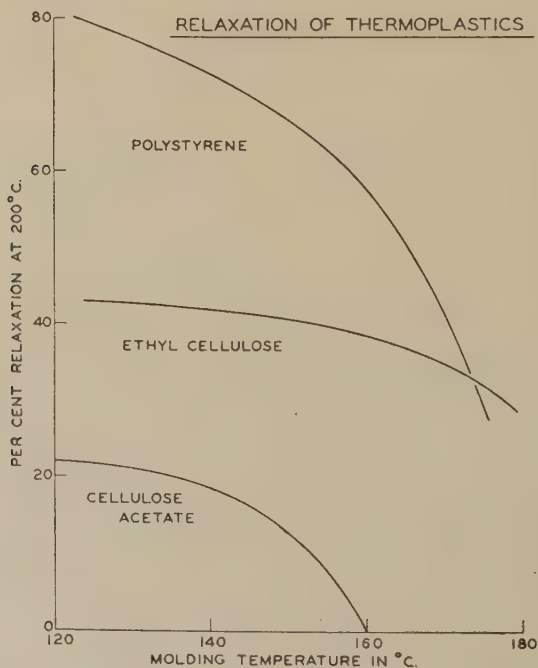


FIG. 5. Effect of molding temperature on frozen-in strains.

(as is commonly used), is forced into a Rossi-Peakes Flow Tester capillary, quickly cooled, and then relaxed above the molding temperature, the curve on Fig. 5 is obtained in substantiation of the foregoing remarks about elasticity. Cellulose acetate and polystyrene are shown for comparison; they are standard molding types, the cellulose acetate containing about 30% plasticizer. It is seen that in this range the molding temperature has relatively little effect on the ethyl cellulose elasticity, but a pronounced one on polystyrene and cellulose acetate. Indeed, above 160°C. all the cellulose acetate deformation is viscous flow.

Just as substitution affects flow, it also influences relaxation (Fig. 6).

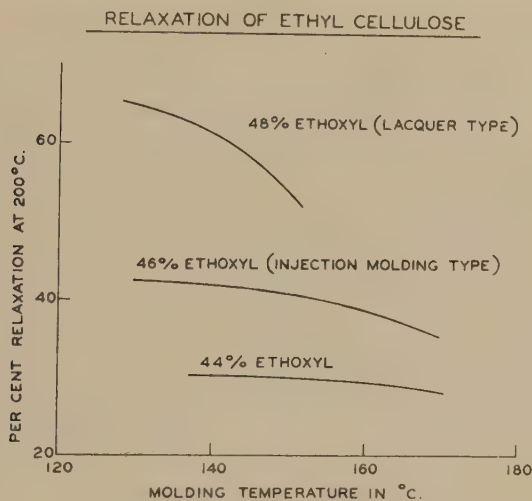


FIG. 6. Effect of composition on frozen-in strains.

Furthermore, by special treatment, the amount of frozen-in stress can be varied (Fig. 7). This shows two ethyl celluloses that have the same degree of substitution, but the one showing fewer internal, recoverable strains was made from a flake that had a particular treatment prior to the preparation of the molding powder used. This treatment probably exerts an influence by decreasing the formation of intramolecular hydrogen bond networks.

It is to be noted that not only are stresses frozen in during molding, but they show relatively little relaxation when heated to temperatures below molding temperature, and recover rapidly as it is passed. The fact that a plastic has been allowed to relax partially does not necessarily affect the total amount it is capable of relaxing. In fact, experiments with polystyrene, cellulose acetate, and ethyl cellulose have shown that relaxations of these materials at successively higher temperatures add up to the same relaxation as obtained if heated at once to the highest

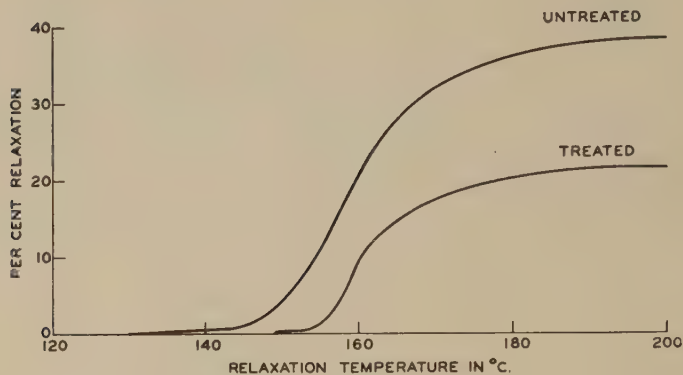
ETHYL CELLULOSE MOLDED AT 160°C.

FIG. 7. Effect of chemical treatment on frozen-in strains.

temperature employed (200°C.). That is, reheating to 200°C. any piece represented by a point on the Fig. 7 curves produces a total relaxation equal to that of a piece heated at 200°C. only.

It should also be pointed out that the recoverable strains in a molded object are not equally distributed and respond differently and to different extents to the frozen-in stresses "surrounding" them when the piece is reheated. The relative magnitude of these strains can be readily observed by a microscopic, birefringence technique. Observations have been made

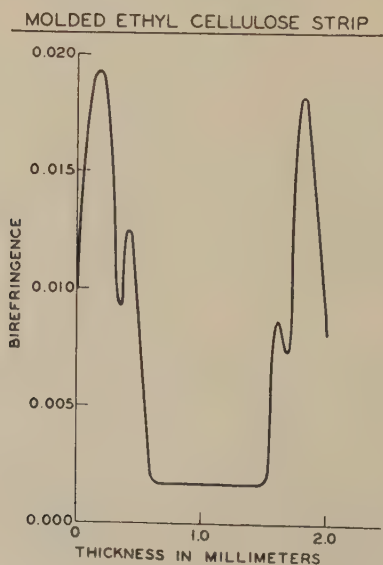


FIG. 8. Birefringence from strains induced by injection molding.

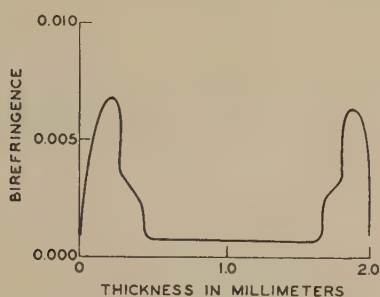
MOLDED ETHYL CELLULOSE STRIP AFTER RELAXATION

FIG. 9. Birefringence after relaxing injection molded strains.

on wedge-shaped sections cut from the center of injection-molded strips and extending from surface to surface through the thin dimension of the strip. On such a sample the retardation of light passing in one plane of polarization behind that in the other plane is measured by the color which results. From the retardation and thickness, the birefringence can be

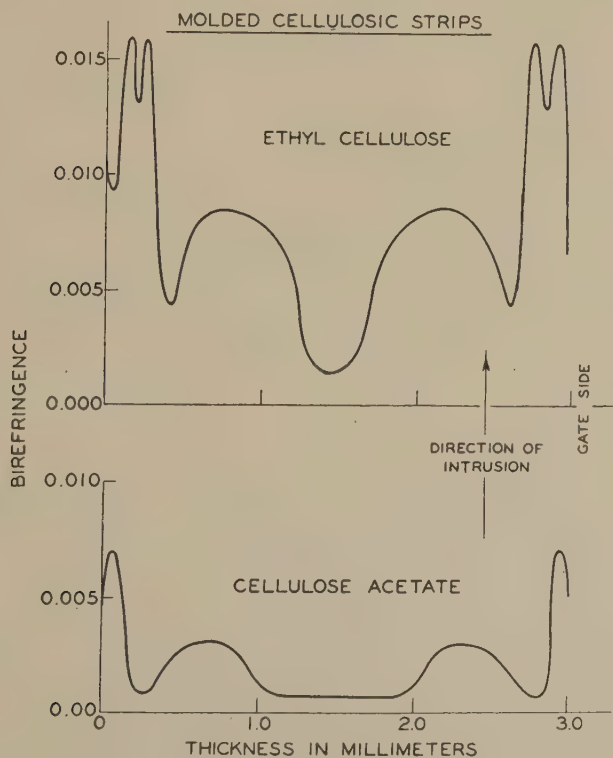


FIG. 10. Birefringence comparison of injection molded strains in ethyl cellulose and cellulose acetate.

determined directly. Figure 8 shows the birefringence from surface to surface through the thin dimension of the strip.

The birefringence observed is due to strain frozen into the plastic. However, a question arises whether the birefringence is proportional to the amount of strain. Figure 9 shows the birefringence through the same piece after relaxation at 150°C. for 10 min. The pattern shows the regions of high and low birefringence to be in the same relationship as before. It would seem that, in comparing different samples of the same plastic, the amount of birefringence is directly related to degree of strain.

To compare the amount of strain in two different plastics by comparing their birefringences would be speculative. However, the fact that the nature of the strains is different is readily seen in Fig. 10 where similar plots for unrelaxed ethyl cellulose and cellulose acetate are shown.

SUMMARY

In recapitulation, this paper has attempted to show that: (a) the flow of cellulose can be described rather simply by a phenomenologically observable superposition principle; (b) ethyl cellulose and cellulose acetate differ markedly in their response to molding temperature, ethyl cellulose tending to be more rubberlike; (c) their flow is influenced by internal chemical structure; and (d) when molded, they exhibit local frozen-in stresses that, on reheating, produce different degrees of relaxation in different parts of injection-molded objects.

If we consider the above facts, it is obvious that we may make specimens that will have a given amount of total frozen-in strain and yet be different in over-all properties. To be specific, let us consider strips of ethyl cellulose that have been stretched 100% at 130°C. in one case and at 160°C. in another case. These strips will further be supposed to have been held extended at their stretching temperatures for a time and then quenched, the time of holding being so adjusted that the strips would recover half of the 100% elongation if they were reheated. Now it is clear that both these specimens have a total frozen-in strain of 50%. Yet since the one stretched at 130° required more work to deform it in the first place, it would tend to recover against a greater opposing force, and it would therefore recover at a lower temperature. In fact, it acts as if it has stronger springs tending to bring it to its equilibrium shape.

It seems entirely logical to use the term "frozen-in stress" to describe the force per unit area required to hold the specimens extended the moment before they were quenched. This stress was there before quenching. It cannot be demonstrated at room temperature. It will be there again if the specimen is rapidly warmed while being held extended. Obviously, the magnitude of this frozen-in stress will be important in determining the tendency of a molded specimen to deform at moderate service temperatures.

CONSTANT STRESS ELONGATION OF SOFT POLYMERS: TIME AND TEMPERATURE STUDIES¹

C. A. Dahlquist and M. R. Hatfield

*Central Research Department,² Minnesota Mining and Manufacturing Company,
St. Paul, Minnesota*

Received January 28, 1952

INTRODUCTION

The effect of time and temperature on the viscoelastic behavior of rubbery materials is of great practical significance and has long been the subject of extensive investigation and theoretical interpretation. It has been shown that time and temperature have an equivalent effect on the elastic modulus of linear rubbery polymers (2). A quantitative relationship between time and temperature can be derived from the apparent activation energy for viscous flow (6) or for elastic deformation (3). The temperature dependence of the modulus can then be reduced to an equivalent time dependence, and data covering a wide range of time and temperature can be represented by a single "master curve" of reduced variables.

The constant-stress method (5) used in this laboratory for characterization of soft polymers is well-suited for study of the time and temperature dependence of viscoelastic properties. The data are similar in many respects to the stress relaxation data of Andrews *et al.* (2,3,4). It was of interest to investigate the treatment of creep data by reduced variables and to compare the two methods cited above. It was also of interest to extend the treatment to polymers other than polyisobutylene, preferably to one which can be subjected to high elongation without undergoing crystallization.

THEORY

The modulus of elasticity, as used in this paper, is defined as the stress per unit elongation. A discussion of the applicability of such a property to constant-stress measurements on soft polymers has been given in an earlier paper (5).

Reduced modulus is calculated by multiplying the experimental value by the factor $298/T$, where T is the absolute temperature. This factor reduces all modulus contributions associated with entropy change to the

¹ Presented at the Annual Meeting of the Society of Rheology, Chicago, Illinois, October 24-27, 1951.

² Contribution No. 39.

same reference temperature, 298°K., as predicted by the kinetic theory of rubberlike elasticity.

If all retardation processes contributing to the total creep have the same temperature dependence, they can be characterized by a single activation energy. This activation energy can be calculated by use of the Arrhenius equation in which the reciprocal of the reaction rate at temperature T is replaced by the time, t , required to attain a given modulus. Thus

$$t = A' e^{E/RT} \quad [1]$$

where A' is a constant, E the activation energy, and R the gas constant. A plot of the natural logarithm of time versus the reciprocal temperature yields a straight line of slope E/R . The correction factor, K , which reduces the time corresponding to a given modulus at one temperature to that corresponding to the same modulus at another temperature, is given by Eq. [1] written for two temperatures

$$K = \frac{t_0}{t} = \frac{e^{E/RT_0}}{e^{E/RT}} \quad [2]$$

A master curve of reduced modulus versus reduced time can be obtained by use of Eq. [2]. (Andrews, Hofman-Bang, and Tobolsky in Ref. (3) give a more detailed discussion of the theory presented here.)

Creep curves may be shifted along the log time axis to form a single master curve which, if the activation energy is constant, will coincide with that described above. The temperature dependence of the time correction factor, as calculated from the actual shift, is given by the Arrhenius equation

$$K = A e^{-E/RT} \quad [3]$$

It should be noted that Eq. [3], which gives the temperature dependence of K , becomes identical with Eq. [2] if A is evaluated for the reference temperature at which K is equal to unity.

A treatment based on steady-flow viscosity allows a similar reduction of time to arrive at a master curve of reduced modulus and reduced time. Recently, Ferry (6) derived the relationships which apply to dynamic properties, and the treatment for creep measurements is quite similar to that presented by Ferry.

The polymeric substance is assumed to behave like a group of Voigt units in which each elasticity mechanism is represented by a modulus G_i and each flow process by $\tau_i G_i$. Under the restriction of constant stress, the elongation at time t is given by the well-known relationship

$$\sigma_t = S \sum_i (1/G_i) (1 - e^{-t/\tau_i}), \quad [4]$$

where S is the applied stress. If modulus is defined as stress per unit strain, Eq. [4] becomes

$$1/G_t = \sum_i (1/G_i) (1 - e^{-t/\tau_i}). \quad [5]$$

The temperature dependence of all retardation mechanisms is assumed to be given by a single factor A_T dependent only upon the polymer material and temperature. The modulus G_i of rubberlike springs is proportional to the absolute temperature so that

$$G_i = (T/T_0)G_{i0}, \quad [6]$$

where the subscript zero designates a reference temperature. Equation [5] at temperature T is then

$$1/G_t = \sum_i (T_0/T) (1/G_{i0}) (1 - e^{-t/A_T \tau_i}). \quad [7]$$

It follows that

$$G_t = (T/T_0)G_{0t/A_T}. \quad [8]$$

Ferry (6) has shown that the steady-flow viscosity η at temperature T is given by

$$\eta = A_T \frac{\rho T \eta_0}{\rho_0 T_0}, \quad [9]$$

where ρ is the density.

Marvin (8) has calculated A_T values for polyisobutylene from precise viscosity (7) and linear expansion (11) data. These data were used in this paper.

EXPERIMENTAL

The constant-stress apparatus was recently described by Dahlquist, Hendricks, and Taylor (5). A strip of polymer cut from a thin sheet or film is loaded with a weight which sinks into a liquid as the film stretches. By suitable design of the weight, which incidentally, takes the form of a hyperboloid, the load can be reduced in proportion to the change in cross-sectional area of the stretching film. The same technique has been used by Andrade (1) to study viscous flow in metallic wires.

The apparatus has recently been modified to the extent that the thread release has been replaced by a magnetic release. The technique of supporting the tension weight by a thread and subsequently transferring the load to the test strip by burning the thread proved to be rather cumbersome, and a release mechanism was developed wherein the load is initially supported by an electromagnet. A soft iron rod, $1\frac{1}{4}$ in. long \times $\frac{3}{8}$ in. diameter, inserted in the tab attached to the lower end of the vertically mounted test strip serves as an armature for the magnet, and supports the hyperbolic weight which is suspended by a fine wire. The load is transferred to the test strip when the armature is released by breaking the field circuit of the magnet.

The tab attached to the upper end of the test strip is held in a movable clamp to permit taking up of slack in the specimen after it has been positioned in the tester.

Temperature control was accomplished by enclosing the test specimen in a chamber, $5 \times 4 \times 14$ in., with an opening at the top leading into a Dry Ice container. Air was forced through the Dry Ice and down into the test chamber, an inverted funnel just below the cold air inlet serving as a baffle to break up the air stream and distribute it uni-

formly throughout the chamber. The temperature was adjusted by regulating the volume of incoming air. Temperatures above 25°C. were obtained by replacing the Dry Ice container with a preheating unit.

The test strips were cut from sheets approximately 0.020 in. thick cast from solution on amalgamated tin panels. Polyisobutylene was dissolved in *n*-heptane without preliminary treatment, while GR-S rubber received a brief cold milling. The drying schedule was as follows: (a) 24 hr. slow drying under cover, (b) 24 hr. uncovered, and (c) 16 hr. vacuum drying at 50°C. Further details of the film-casting technique are described in the earlier publication (5).

The stress conditions were controlled by regulating the initial cross-sectional area of the test specimen. Had the same stress been used in all of the experiments, the deformations would have been very small at the lowest temperatures, or excessively large, leading to rupture of the specimens, at the highest temperatures. To avoid this an attempt was made to control the stress to give approximately the same 10-min. elongation at all temperatures. However, it was difficult to prepare specimens of sufficiently small cross section to fulfill the stress requirements for the -20, -35, and -50°C. tests. Since polyisobutylene tends to crystallize when extended beyond 150%, its deformations were held below 100%. The deformation of GR-S, which does not crystallize, was permitted to exceed 200% in only one instance.

At the higher temperatures, polyisobutylene exhibited a small degree of permanent set. This was subtracted from the total deformation to give the purely elastic deformation, and the modulus values were based upon the elastic component. GR-S showed no permanent set in these experiments.

The modulus values were calculated according to the conventional "stress over strain" formula:

$$G = \frac{\text{stress} \times \text{initial length}}{\text{deformation}}.$$

The polyisobutylene (Vistanex) was furnished by R. S. Marvin of the National Bureau of Standards. It had been carefully selected as a reference standard for comparative dynamic testing by a number of laboratories and has been described very completely by Marvin (8). It has a viscosity average molecular weight of 1.35×10^6 , a density³ of 0.913 g. cc. at 25°C., and a coefficient of linear expansion of $0.58 \times 10^{-3}/^\circ\text{C}$.

GR-S X-274 was taken from a bale of commercial gum rubber. It was characterized as follows: intrinsic viscosity in benzene, 2.41; viscosity average molecular weight, 306,000 (9); Mooney viscosity, 66; gel content, zero. The measured density was 0.935. To determine the change in density with temperature the linear coefficient of expansion was taken as $1.85 \times 10^{-4}/^\circ\text{C}$., the value reported by Vieweg and Schneider (10) for Buna S-I.

RESULTS AND DISCUSSION

Abridged experimental data are presented in Tables I and II. Fig. 1 and 5, which contain all of the data, show plots of "reduced modulus" as a function of the logarithm of time at the various temperatures considered. The "reduced modulus" was determined by multiplying the experimental modulus by the factor $298/T$, where T is the absolute temperature. If all retardation processes have the same temperature dependence, a master curve of reduced modulus vs. time may be obtained

³ Private communication from Dr. Marvin.

by merely shifting the creep curves along the log time axis. This implies that all time values at a given temperature are multiplied by a single correction factor. Andrews *et al.* (3) have shown that this correction factor is related to an apparent activation energy.

Activation energy values were calculated from a plot of log time at constant reduced modulus vs. reciprocal temperature. Figs. 2 and 6

TABLE I
Polyisobutylene Creep Data^a

Log time min.	Total elongation %	Viscous flow %	Elastic elongation %	Log $(T_0/T)G$ (G in megadynes/sq. cm.)
1. Temp = 40°C. Stress = 2200 g./sq. cm.				
-1.778	31.5	—	31.5	0.824
-0.699	38.6	—	38.6	0.726
-0.301	43.6	—	43.6	0.673
0.000	49.4	0.3	49.1	0.621
0.699	70.2	2.7	67.5	0.483
1.000	86.5	7.3	79.2	0.413
2. Temp = 10°C. Stress = 3710 g./sq. cm.				
-1.778	43.6	—	43.9	0.943
-0.699	51.7	—	52.0	0.869
-0.301	56.0	—	56.4	0.835
0.000	60.5	—	60.8	0.802
0.699	75.4	0.3	75.1	0.708
1.000	85.3	0.7	84.6	0.657
3. Temp = -20°C. Stress = 4240 g./sq. cm.				
-1.778	19.2	—	19.2	1.408
-1.177	34.1	—	34.1	1.158
-0.699	41.2	—	41.2	1.075
-0.301	45.9	—	45.9	1.029
0.000	49.0	—	49.0	0.999
0.699	58.4	—	58.4	0.924
1.000	61.5	—	61.5	0.900
4. Temp = -50°C. Stress = 7190 g./sq. cm.				
0.301	24.5	—	24.5	1.581
0.699	44.7	—	44.7	1.324
1.000	60.3	—	60.3	1.193

^a Abridged table.

represent these plots for the two polymers under investigation. The activation energy derived from the polyisobutylene data (see Table IV) appears to be reasonably constant over the entire range, and the average value of 20.1 kcal. is in substantial agreement with the value 19.5 obtained by Brown and Tobolsky from stress relaxation measurements in the temperature range 0 to -45°C. (4).

A master curve for polyisobutylene based on a constant activation energy of 20.1 kcal. is shown in Fig. 3. The translated data superpose nicely except for some scattering at the very low temperatures (short reduced time).

A second master curve based on steady-flow viscosities is presented in Fig. 4. The data show more scatter than in Fig. 3. The two curves are in

TABLE II
GR-S X274 Creep Data^a

Log time <i>min.</i>	Total elongation ^b %	Log $(T_0/T)G$ (G in megadynes/sq. cm.)
1. Temp = 40°C. Stress = 1306 g./sq. cm.		
-2.000	29.6	0.615
-1.778	34.1	0.554
-1.000	52.5	0.365
-0.699	63.5	0.283
-0.301	81.8	0.176
-0.000	100.7	0.083
0.699	166.0	-0.136
1.000	208.5	-0.233
2. Temp = 10°C. Stress = 2008 g./sq. cm.		
-2.000	24.7	0.924
-1.000	40.3	0.712
-0.699	45.7	0.634
-0.301	60.0	0.516
0.000	74.0	0.425
0.699	120.	0.215
1.000	146.	0.130
3. Temp = -20°C. Stress = 5300 g./sq. cm.		
-2.000	35.2	1.241
-1.778	37.1	1.218
-1.000	46.1	1.123
-0.699	52.5	1.067
-0.301	63.4	0.985
0.000	74.8	0.913
0.699	118.0	0.715
1.000	150.7	0.609
4. Temp = -50°C. Stress = 9470 g./sq. cm.		
-2.000	8.0	2.190
-1.000	24.2	1.712
-0.699	31.3	1.599
-0.301	42.7	1.461
0.000	48.7	1.408
0.699	62.7	1.297
1.000	68.7	1.255

^a Abridged table.

^b GR-S had no permanent set.

TABLE III

Polyisobutylene and GR-S Time Correction Factors

Temp. °C.	Log K, polyisobutylene		Log K, GR-S	
	Constant <i>E</i> (20.1 kcal.)	Viscosity data	Constant <i>E</i> (20.0 kcal.)	Shifting of creep curves
40	0.708	0.541	0.705	0.592
25	0.000	0.000	0.000	0.000
10	-0.783	-0.628	-0.779	-0.698
-5	-1.649	-1.361	-1.640	-1.468
-20	-2.625	-2.234	-2.610	-2.578
-35	-3.720	-3.271	-3.700	-3.934
-50	-4.960	-4.514	-4.940	-5.344

TABLE IV

Polyisobutylene: Apparent Activation Energy at Constant Reduced Modulus

Log (T_0/T) <i>G</i>	1.400	1.191	0.976	0.900	0.792	0.656
<i>E</i> (kcal./mole)	19.8	19.8	20.2	22.9	21.1	16.6

TABLE V

GR-S: Apparent Activation Energy at Constant Reduced Modulus

Log (T_0/T) <i>G</i>	1.24	0.99	0.80	0.61	0.47	0.34	0.13
<i>E</i> (kcal./mole)	28.0	25.3	19.6	17.7	16.7	16.4	15.5

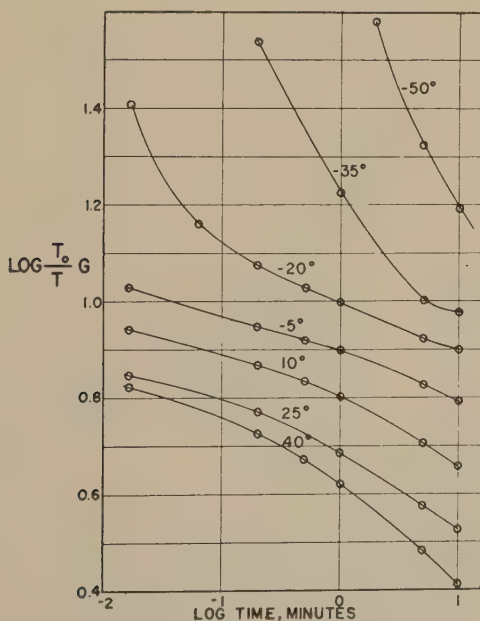


FIG. 1. Polyisobutylene creep curves.

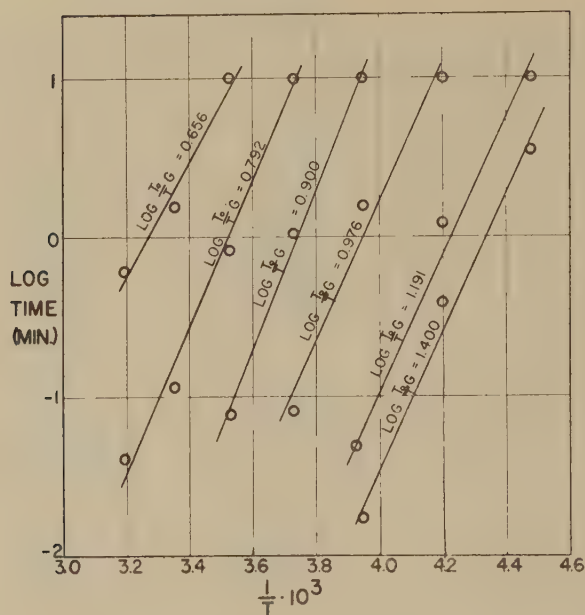


FIG. 2. Polyisobutylene: log time vs. reciprocal of temperature at constant reduced modulus.

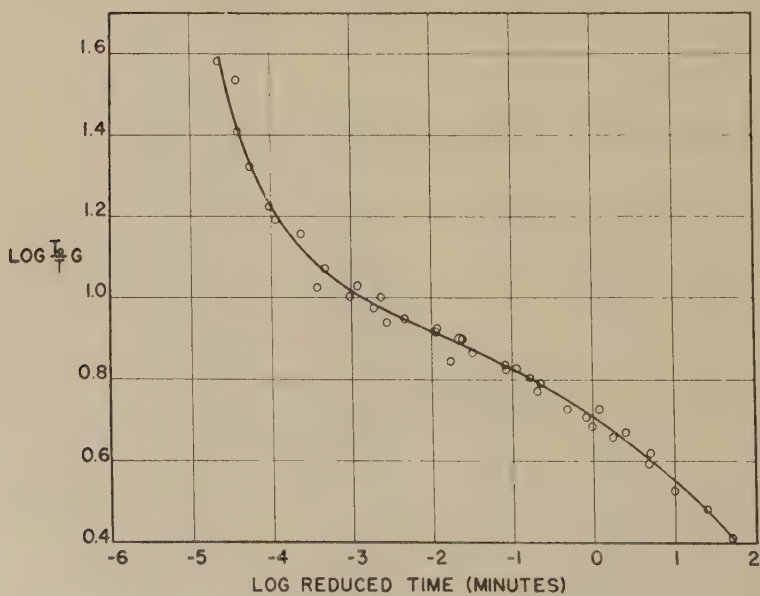


FIG. 3. Polyisobutylene "master curve." Time reduction based on constant activation energy.

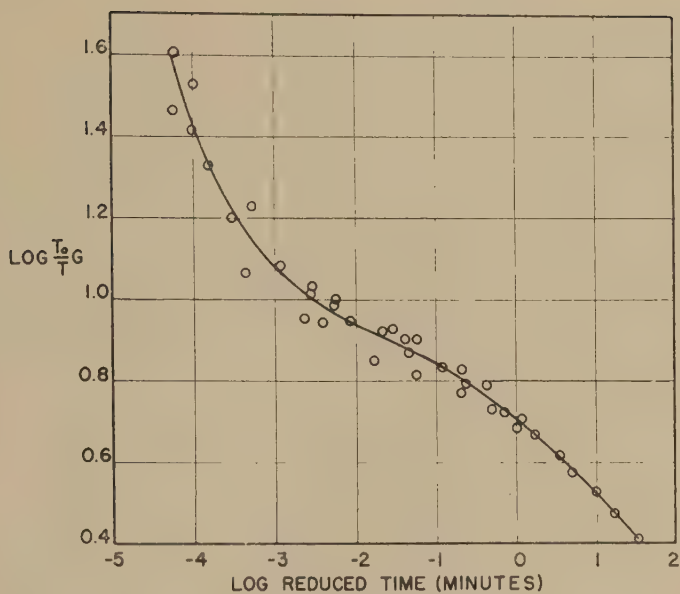


FIG. 4. Polyisobutylene "master curve." Time reduction calculated from steady-flow viscosities.

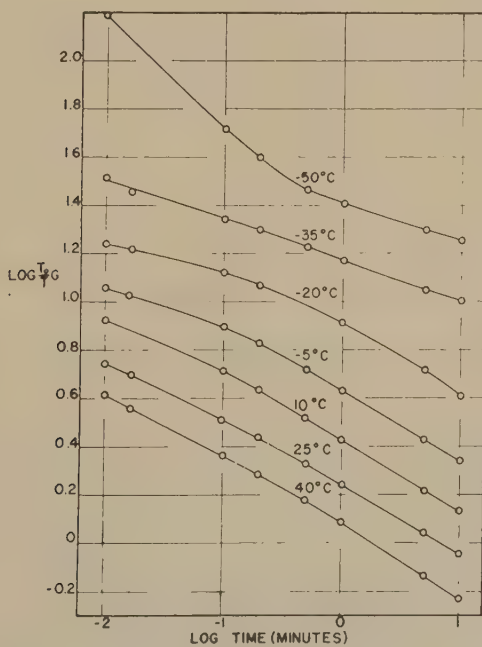


FIG. 5. GR-S creep curves.

good agreement in the longer time region but diverge somewhat at times shorter than 10^{-4} min.

Actual time correction values for the two methods are not equal at any point along the curves except, of course, at the reference temperature where the correction is zero. The methods of calculation are not equivalent because the method based on steady-flow viscosity involves a continuous change in viscous flow activation energy.

Brown and Tobolsky noted a change in apparent activation energy taking place at temperatures around -45°C . for a high-molecular-weight polyisobutylene. No such variation was observed in this investigation but it might have become apparent had the measurements been extended to lower temperatures.

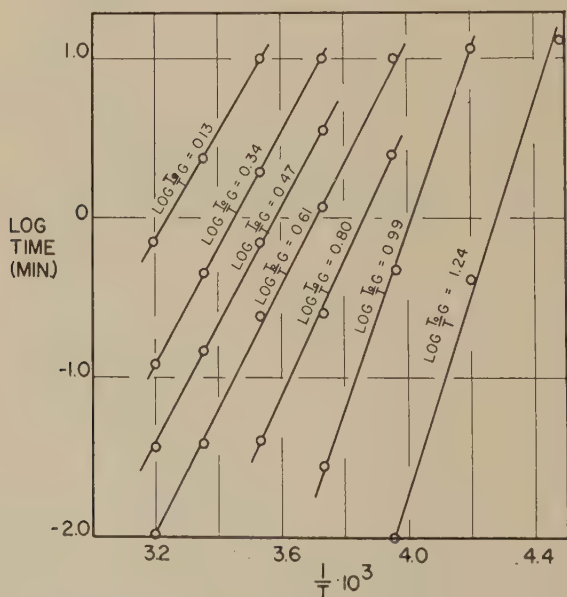


FIG. 6. GR-S: log time vs. reciprocal of temperature at constant reduced modulus.

In contrast to polyisobutylene, GR-S rubber does not display a constant apparent activation energy as determined by the slopes of the log time vs. reciprocal temperature curves (Fig. 6). Nevertheless, a master curve based on a constant average activation energy (Fig. 7) shows a reasonably good superposition of data, though not as good as that obtained by shifting the reduced modulus-log time curves along the log time axis (Fig. 8). Time factors calculated from the shifting process are

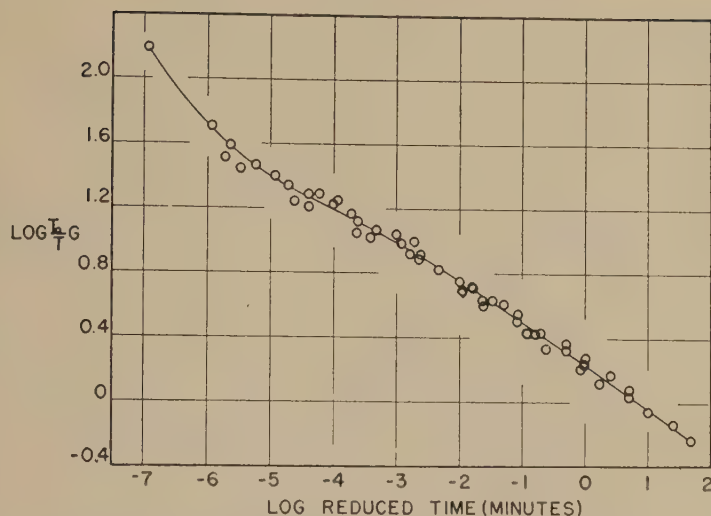


FIG. 7. GR-S "master curve." Time reduction based on constant activation energy.

plotted against reciprocal temperature in Fig. 9. The activation energy appears to change abruptly with temperature at -10°C .

If the apparent activation energies obtained from the log time-reciprocal temperature curves are plotted against reduced modulus, it is seen that the activation energy increases in a roughly linear manner

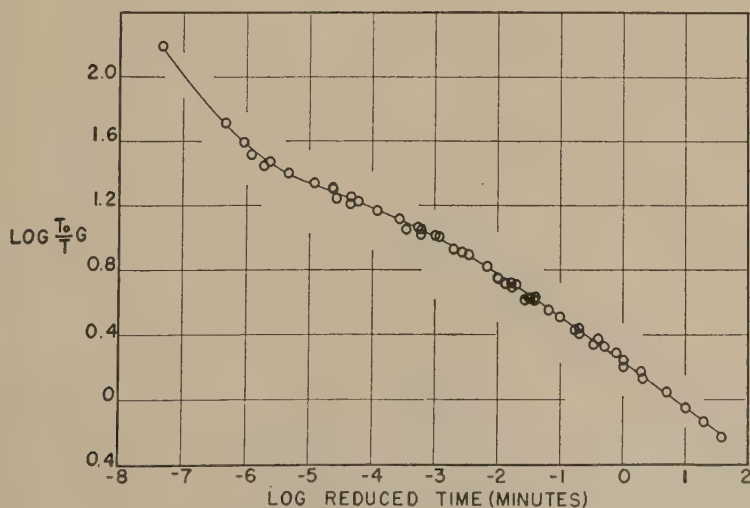


FIG. 8. GR-S "master curve" obtained by shifting creep curves along time axis.

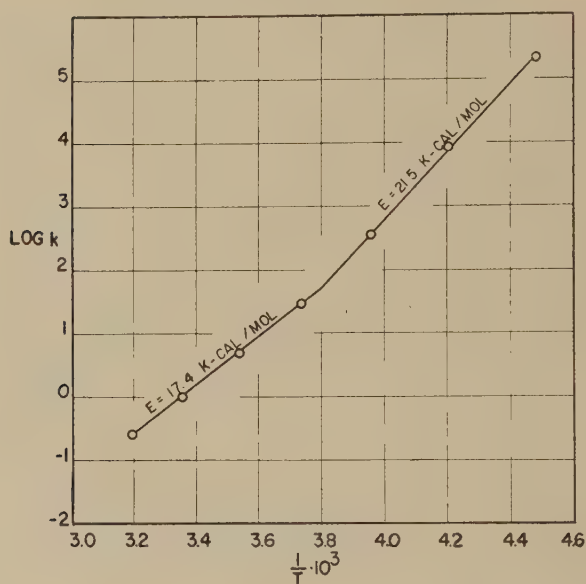


FIG. 9. Temperature dependence of creep curve translation factors (GR-S).

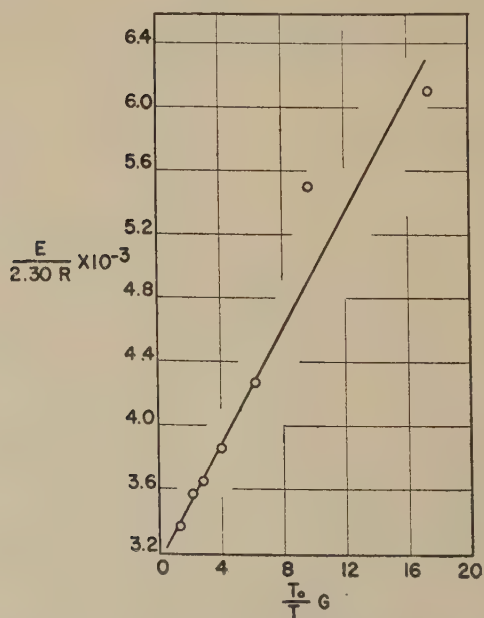


FIG. 10. Variation in apparent activation energy with reduced modulus.

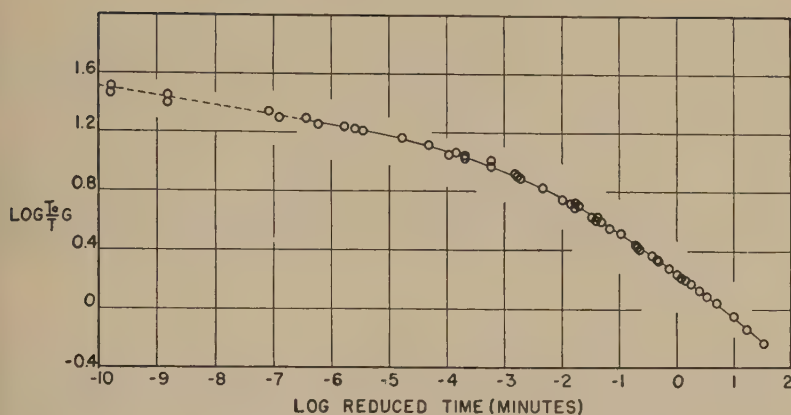


FIG. 11. GR-S "master curve." Time reduction based on modulus-dependent activation energy.

with increasing modulus (Fig. 10). From the least squares method the equation representing this dependence was calculated as $\frac{E}{2.303R} = 183 \left(\frac{T_0}{T} G \right) + 3145$.

This implies that the activation energy for the elastic deformation is dependent upon the particular process, i.e., processes characterized by short retardation times have higher activation energies than those of long retardation times. This is not necessarily justified from a theoretical point of view, but modulus-time data reduced on this basis fall very nicely on a master curve with practically no scatter (see Fig. 11). This

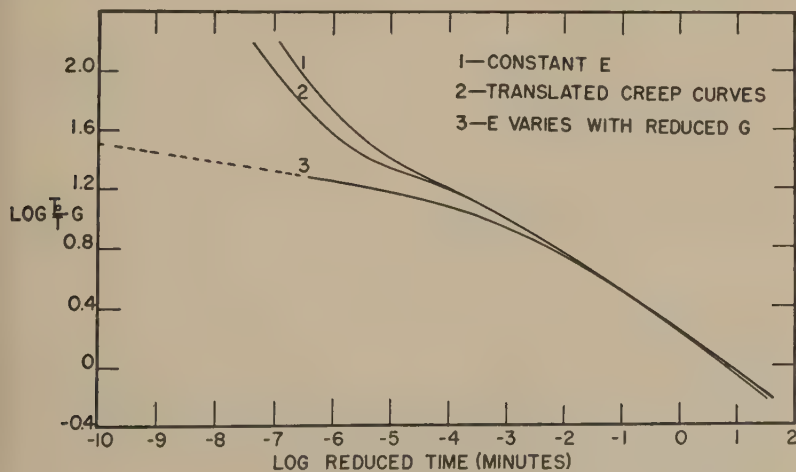


FIG. 12. Comparison of GR-S master curves.

curve coincides with the other two in the long time region from 10^2 to 10^{-2} min., but at times shorter than 10^{-2} min., log modulus increases at a much slower rate (Fig. 12). The portion of the curve represented by the broken line is based on extrapolated activation energies.

ACKNOWLEDGMENTS

The authors wish to express their appreciation to R. S. Marvin for supplying the standard polyisobutylene, and to W. E. Luedke for conducting the experimental measurements.

SUMMARY

The constant-stress method recently described by Dahlquist *et al.* is well-suited for the study of the time and temperature dependence of viscoelastic properties. Creep data are given for polyisobutylene and GR-S rubber in the time range of 0.01 to 10 min. and the temperature range of 40 to -50°C . The data were transferred into master curves of log reduced modulus vs. log reduced time.

The polyisobutylene data superposed satisfactorily using either (a) a time reduction method based on a constant apparent activation energy for elastic deformation, or (b) a time reduction method based on steady-flow viscosities. The two master curves coincide except in the short time range.

In contrast to polyisobutylene, GR-S showed a considerable variation in activation energy with modulus. Three master curves are presented, the first calculated on the basis of a constant average activation energy, the second obtained by shifting individual modulus curves along the log time axis, and the third derived by assuming a linear dependence of activation energy on modulus.

The scattering of the data decreases in order from the first to the third. The first and second curves coincide completely within experimental error. The third curve coincides with the first and second in the time range of 10^{-2} to $10^{1.5}$ min. but diverges considerably at time intervals less than 10^{-2} min.

As yet the concept of a modulus-dependent activation energy must be considered of doubtful theoretical significance.

REFERENCES

1. ANDRADE, E. N. DA C., *Proc. Roy. Soc. (London)* **84**, 1 (1910).
2. ANDREWS, R. D., AND TOBOLSKY, A. V., *J. Chem. Phys.* **13**, 3 (1945).
3. ANDREWS, R. D., HOFMAN-BANG, N., AND TOBOLSKY, A. V., *J. Polymer Sci.* **3**, 669 (1948).
4. BROWN, G. M., AND TOBOLSKY, A. V., *J. Polymer Sci.* **6**, 165 (1951).
5. DAHLQUIST, C. A., HENDRICKS, J. O., AND TAYLOR, N. W., *Ind. Eng. Chem.* **43**, 1404 (1951).

6. FERRY, J. D., *J. Am. Chem. Soc.* **72**, 3746 (1950).
7. FOX, T. G., JR., AND FLORY, P. J., *J. Am. Chem. Soc.* **70**, 2384 (1948).
8. MARVIN, R. S., Interim Report on Coop. Program on Dynamic Testing. *Natl. Bureau Standards* (U. S.), April 25, 1951.
9. SCOTT, R. L., CARTER, W. C., AND MAGAT, M., *J. Am. Chem. Soc.* **71**, 220 (1949).
10. VIEWEG, VON R., AND SCHNEIDER, W., *Kunststoffe* **31**, 215 (1941).
11. WORK, R. N., Tech. Rept. to Office Naval Research, Proj. No. ONR(QMC), NR-033-314, October 30, 1950.

APPLICATION OF EYRING'S RATE EQUATION TO VISCOMETRIC DATA ON PARAPLEX¹

H. B. Whitfield² and Thomas Baron³

University of Illinois, Urbana, Illinois

Received March 27, 1952

INTRODUCTION

Eyring's theory of viscosity (1) is a very attractive one, both from the point of view of the physical chemist and the chemical engineer. The theory of absolute reaction rates used by Eyring in developing his equation reduces the less familiar rate problem of molecular motion to a more familiar problem in thermodynamics.

In comparing theory with experiment, one can obtain the energy of activation for the molecular motion as well as the volume of the unit of flow. The energy of activation is usually found to be around 10,000 cal./mole which appears to be a very reasonable figure in the light of the known heats of vaporization of the molecules. Results concerning the volume of flow are less satisfactory. For example, Smallwood (6), analyzing the data of Mooney (5), on the flow of rubber, found a volume for the unit of flow less by several orders of magnitude than expected from considerations of molecular magnitudes calculated from bond distances. A similar discrepancy between calculated and expected values for volume of flow is reported below.

In view of these results, and because of the simplifying assumptions involved in the theory, it is best to employ Eyring's hyperbolic sine equation as essentially an empirical one. The results reported below indicate that it does have usable empirical validity.

EXPERIMENTAL

The rotational viscometer employed in these experiments was a modification of the apparatus described by H. Green (2,3). The viscometer was constructed with the purpose of measuring thermal conductivities as well as viscosities of non-Newtonian liquids.

In choosing the dimensions of the viscometer, care was taken to avoid heat convection and turbulence. In order to prevent convection, the gap opening between the cylinders was designed to make the product of the Prandtl number and Grashof number for

¹ Presented at the Annual Meeting of the Society of Rheology, Chicago, Illinois, October 24-27, 1951.

² Present address: E. I. du Pont de Nemours and Company, Wilmington, Delaware.

³ Present address: Shell Development Company, Emeryville, California.

the particular liquid not greater than 600, as proposed by Milverton and Schmidt (4). Care was also taken to avoid turbulence.

While the special features of this viscometer were chosen to permit measurements of thermal conductivity under shear, they were also found of advantage in connection with viscosity measurement. In particular, it was found that with this arrangement end effects are minimized.

THEORY

For a derivation of the Eyring equation and consistent nomenclature used throughout this paper, the reader is referred to Ref. (1). The equation is:

$$\mu = \frac{A\tau \exp(a/T)}{2 \sinh\left(\frac{b}{T}\tau\right)}, \quad [1]$$

where

$$a = \frac{\epsilon_0}{k}, \quad b = \frac{\lambda_2\lambda_3\lambda}{2k}, \quad \text{and} \quad A = \frac{\lambda_1 h F}{\lambda k T F^{+}}.$$

Thus, a is related to energy of activation, A to the entropy of activation, and b to the volume of the unit of flow. At very small shear stress, the limiting form of Eq. [1] is:

$$\mu_0 = \frac{A}{2} \left(\frac{T}{b}\right) \exp\left(\frac{a}{T}\right), \quad [2]$$

whereas at high shear stresses, the limiting form is:

$$\mu_\infty = A\tau \exp\left(\frac{a}{T}\right) \exp\left(-\frac{b}{T}\tau\right). \quad [3]$$

Equation [1] may be put into a somewhat more convenient form with the aid of Eq. [2]:

$$\mu = \mu_0 \frac{(\tau/\tau_c)}{\sinh(\tau/\tau_c)}, \quad \text{where} \quad \tau_c = \frac{T}{b}. \quad [4]$$

Reference to the original derivation of Eyring shows that τ_c which we choose to call the critical shear stress is the shear stress necessary to insure a rate of forward jump of molecules e (base of natural logarithm) times the number of forward jumps when no shear stress is applied. The viscosity at any given value of the shear stress is thus seen to be determined by the viscosity in the limit of zero shear stress and the ratio of the shear stress to the critical shear stress.

RESULTS

Figure 1 illustrates the trend of the data obtained on 100% Paraplex (G-40) supplied by Rohm and Haas Company. The curvature of the lines indicates the non-Newtonian nature of the fluid.

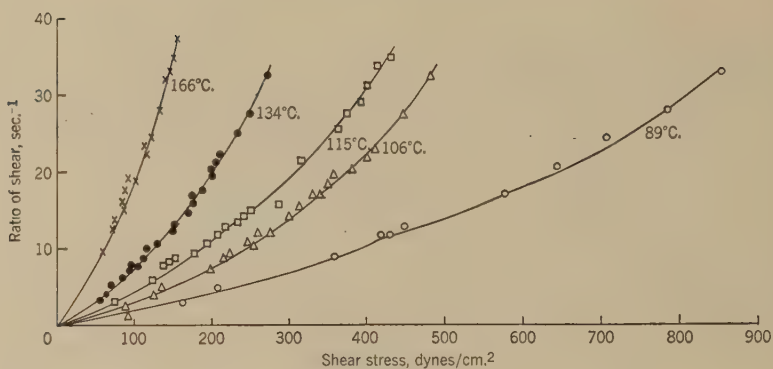


FIG. 1. Effect of shear stress on the rate of shear.

According to Eq. [2] the plot of the logarithm of the viscosity divided by the shear stress versus the reciprocal of the temperature should give a straight line with a slope $a - b\tau$. This relationship is shown in Fig. 2. The relationship would seem to be satisfactory; however, there is a tendency for the high temperature points to drop below the lines. An analysis of the experimental accuracy shows that this cannot be accounted

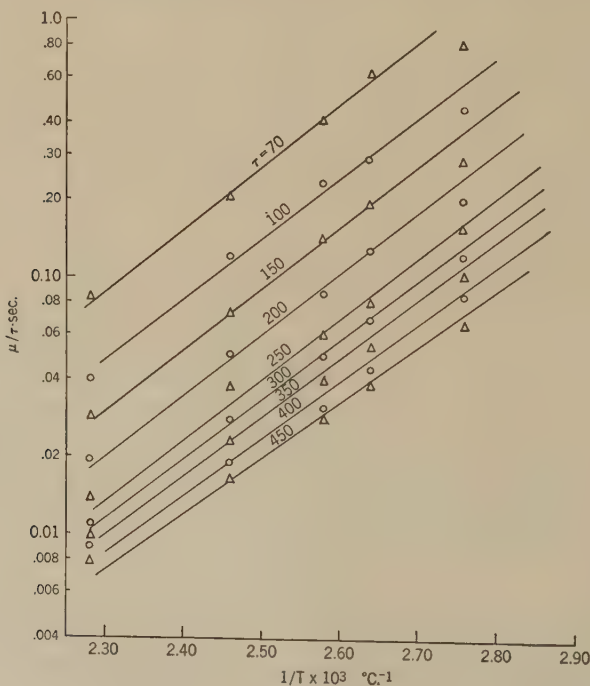


FIG. 2. Effect of temperature and shear stress on viscosity.

for by experimental errors. We feel, therefore, that at least as far as this one liquid is concerned, the Eyring equation is only an approximate one. Because of scatter of some of the high temperature points, there was some uncertainty in the choice of slopes for some of the sets of points, especially those at the shear stress corresponding to 100, 250, 350, and 400 dynes/cm.² The slopes shown were chosen as follows: First, the lines for $\tau = 70$ and 450 were drawn in as shown using the method of least squares. It was then assumed that the slopes indeed satisfied the relationship,

$$\text{Slope} = a - b\tau$$

and the slopes for the other shear stresses were calculated from this equation. It is seen that apart from the high temperature points the experiments are consistent with Eyring's equation.

The energy of activation was found to be 11,500 cal./mole. This is in the expected range. However, the volume of the unit of flow was found to be only 10^{-16} cm.³ which is again many orders of magnitude smaller than that expected from molecular sizes.

It is felt that the measurements reported in this paper as well as other measurements of similar nature do not offer conclusive evidence of the correctness of the assumptions underlying Eyring's theory. However, the dependence of the viscosity on shear stress and temperature as arrived at by Eyring appears to be representative for a large number of non-Newtonian fluids and certainly for the 100% Paraplex used in the present experiments. Certainly the equation is useful for engineering purposes since it permits ready evaluation of the constants and integration of the equations of motion for simple symmetries.

REFERENCES

1. EYRING, H., GLASSTONE, S., AND LAIDLER, K. L., *The Theory of Rate Processes*. McGraw-Hill Book Company, New York, 1941.
2. GREEN, H., *Ind. Eng. Chem., Anal. Ed.* **14**, 569 (1944).
3. GREEN, H., AND WELTMAN, R. N., *J. Applied Phys.* **14**, 576 (1942).
4. MILVERTON, S. W. AND SCHMIDT, R. J., *Proc. Roy. Soc. (London)* **A134**, 288 (1935).
5. MOONEY, M., *Physics* **7**, 413 (1936).
6. SMALLWOOD, H. M., *J. Applied Phys.* **8**, 505 (1937).

THE RHEOLOGY OF A LUBRICATING OIL AT TEMPERATURES BELOW THE POUR POINT¹

S. P. Jones and J. K. Tyson

Armour Research Foundation of Illinois Institute of Technology, Chicago, Illinois

Received March 10, 1952

INTRODUCTION

Many petroleum-base lubricating oils become rigid solids or semi-solids at temperatures below their cloud points. A widely used test for evaluating the low-temperature usefulness of an oil, devised by the American Society for Testing Materials, defines the pour point as that temperature below which the oil will not pour from a standard vessel under rigidly specified conditions of cooling and manipulation.² Previous investigations of the rheology of petroleum oils in the temperature region below the pour point have been reviewed by Bondi (1), who comments that the field of low-temperature viscometry of lubricating oils is in an exploratory stage in which each investigator has devised a flow-measuring apparatus for his own particular aims. For the most part the instruments used have been viscometers of a capillary type. This paper presents observations on the behavior of a lubricating oil below the pour point in a rotational, concentric-cylinder viscometer, and some aspects of the rheology of a suspension of a normal paraffin hydrocarbon in a petroleum oil.

EXPERIMENTAL METHODS

The low-temperature studies in this investigation have been made with a rotational viscometer patterned after that described by Green (2). The oil is situated in an annular space between coaxial cylinders, the outer of which (the cup) rotates at a number of constant velocities in 40 equal increments to 400 r.p.m. The inner cylinder (the bob) is attached to a torsion spring which permits measurement of the torque imparted to it. The measurements are expressed in absolute units of shearing stress, S , in dynes/cm.², and rate of shear, e , in sec.⁻¹.

In order that the shear rate attainable might be extended, two cups having radii of 1.40 and 1.50 cm., giving cup-to-bob clearances of 1.0 and 2.0 mm., respectively, have been employed. In the data presented the cup used is indicated by the use of solid symbols for the former and open symbols for the latter.

The low-temperature measurements were made at -25 and $-30^{\circ}\text{C}.$, such temperatures being maintained by means of a special bath surrounding the viscometer cup and

¹ This work was sponsored by the Wright Air Development Center, under contract A.F. 33(038)-1644.

² A.S.T.M. Standards on Petroleum Products and Lubricants, Test D97-47.

an external cooling system. The viscometer cup was situated in a steel bath 5.5 in. in diameter and 9.5 in. high, insulated with 2 in. of glass wool. Through the bath was circulated a coolant, isopropyl alcohol, continuously pumped through coils in a cryostat containing an alcohol-water mixture freezing about 10°C. below the temperature of the experiment, and cooled with dry ice. Variations in temperature were opposed by a 125-w. electric heater in the pumping system transferring heat to the bath liquid. The heater was operated intermittently by the control circuits of a Micromax recording potentiometer which recorded the output of a three-junction thermopile in the viscometer bath. Under steady-state conditions temperature control of $\pm 0.25^\circ\text{C}$. was obtained; however, in the initial stages of shearing at high rates there was observed a slight rise in temperature, the degree of control being estimated at $\pm 0.5^\circ\text{C}$. A plastic frost shield extending from the bath cover to the bob bearing sleeve was flooded with precooled dry nitrogen, preventing moisture condensation on the sample and excessive heat loss through the bob shaft.

Since the thermal history of an oil is known to affect its low-temperature rheology (3), the rate of cooling the sample to the temperature of the experiment was controlled by the rate of addition of dry ice to the cryostat, and, unless otherwise noted, the samples were cooled at a rate of $1^\circ\text{C}/\text{min}$. and maintained at the temperature of the experiment for 30 min. before shearing.

This investigation was made on one oil, designated Pennsylvania 150 neutral, dewaxed to a pour point of -15°C . All samples were obtained from a single 50 gallon lot, being withdrawn in quantities of about 1 l. and heated to 100°C . before use.

A high-pour-point oil was prepared by the addition of Eastman white label grade *n*-octacosane to the above oil. This system was studied with a Stormer viscometer with cylindrical cup and bob, modified according to Fischer (4). The sample was heated to solution of the wax at 60°C ., placed in the viscometer cup and, with the bob in place, cooled to 30°C ., at which temperature it was quite solid.

RESULTS AND DISCUSSION

1. General Characteristics

To observe the decrease in apparent viscosity with time of shearing, the change in shearing stress with time while shearing the oil at a constant rate was recorded. Typical stress-time curves for a number of shear rates at -30°C . are shown in Fig. 1. At the higher rates of shear the stress-time curves may be approximately represented as an exponential relaxation equation,

$$S_t = (S_0 - S_\infty)e^{-t/t_r} + S_\infty, \quad [1]$$

where the shearing stress, S_t , decreases as a function of time, t , from an initial value, S_0 , to an equilibrium value, S_∞ , at a rate determined by the time constant, t_r , which will be referred to as the relaxation time.

At very low rates of shear, however, such as curve 5, Fig. 1, the stress-time curves exhibit a marked deviation from Eq. [1], and it becomes necessary to add higher order terms to approximate the form of the curves. Two exponential terms of a series are a reasonably good approximation of the data, thus:

$$S_t = (S_0 - S_\infty)e^{-t/t_r} + (S_0' - S_0)e^{-t/t_r'} + S_\infty. \quad [2]$$

In Fig. 2 the stress-time data at a number of constant rates of shear have been used to construct the consistency curves for the oil initially, i.e., at zero time, and when the rigid structure is completely reduced, S_∞ . This reveals that the initial stress at low shear rates, S_0' , is disproportionately higher than for high shear rates, S_0 . The explanation becomes apparent from the calculated values of relaxation times, t_r and t_r' , in Fig. 3, showing that the higher order terms become rapidly transient with increasing rates of shear and would not be observed experimentally. Thus,

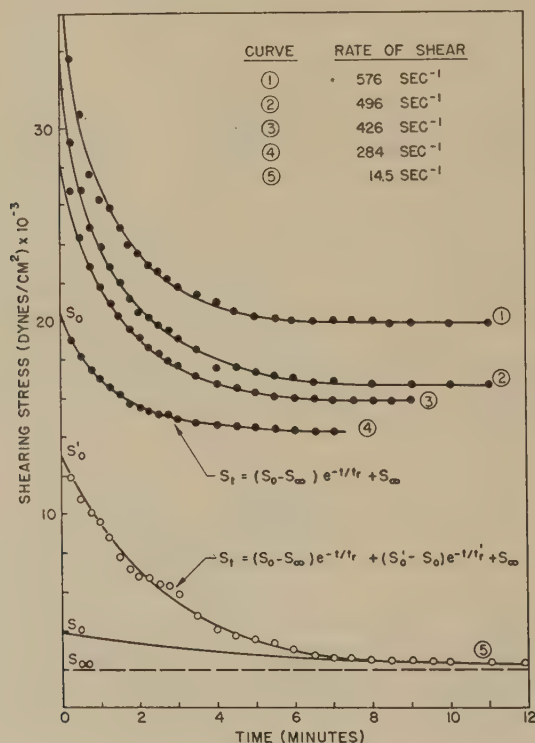


FIG. 1. Stress relaxation curves at constant rates of shear for Pennsylvania 150 neutral oil at -30°C .

while the consistency of the unsheared oil would appear to correspond with the S_0 curve in Fig. 2 on the basis of experiments at high rates of shear, it must at least be as high as S_0' , which curve is largely undetermined, the breakdown in the initial structure being very rapid at high shear rates.

Stress relaxation curves from experiments employing a much lower cooling rate permitting a higher degree of crystallinity are shown in Fig. 4. Here it is quite evident that a rapid degeneration of structure occurs in

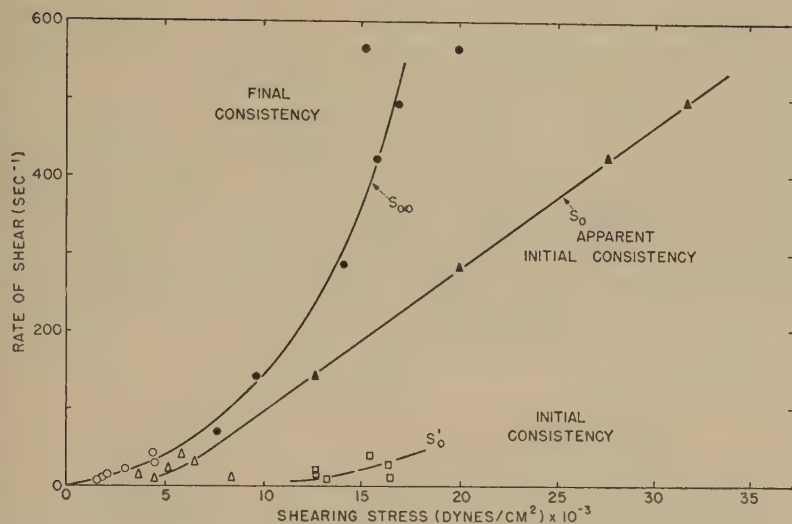


FIG. 2. Consistency curves for Pennsylvania 150 neutral oil constructed from stress relaxation data. Temperature, -30°C .

the first seconds of shearing and that the initial stress is quite high and impossible to determine by extrapolation. Cooling rate was observed to have no effect on equilibrium stress, as may be seen in Fig. 9 to be presented later in the text.

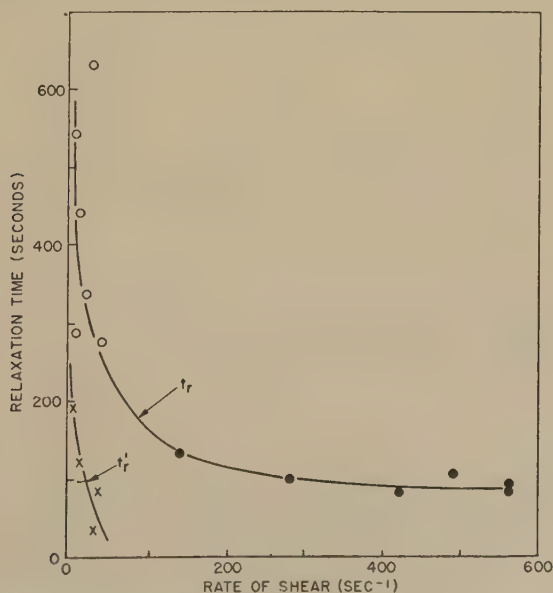


FIG. 3. Relaxation times as a function of rate of shear. Temperature, -30°C .

At equilibrium the shearing stress for corresponding rates of shear describes the S_∞ curve in Fig. 2; however, this curve is not uniquely defined, and the experiment depicted in Fig. 5 demonstrates that the oil in this state behaves as if it were a Newtonian liquid for periods of time short compared with the relaxation time, t_r . This equilibrium Newtonian viscosity decreases with increasing rates of shear. If the oil is sheared until equilibrium is attained at some constant shear rate, e_1 , a consistency curve then determined in a time short compared to the relaxation time, t_r , is linear through the origin. Increasing the rate of shear to a higher

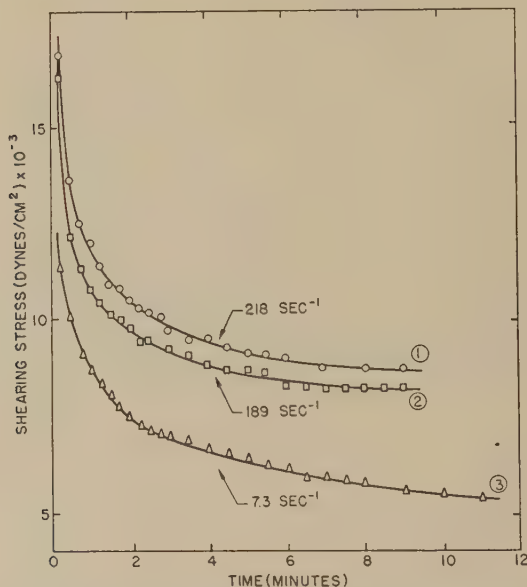


FIG. 4. Stress relaxation curves for a low rate of cooling. Temperature, -30°C . Cooling rate = 0.3°C./min .

level, e_2 , results in an initial stress, S_2 , followed by a relaxation to S_3 , corresponding to an equilibrium Newtonian viscosity for the higher rate of shear. The departure from linearity of the curves from higher rates of shear may be attributed to relaxation during the time required for the determination.

In the matter of a recovery in viscosity when the oil is allowed to "rest" after shearing to equilibrium, the behaviors at high and low rates of shear are in marked contrast. Viscosities computed from rapidly determined consistency curves after successive 5-min. intervals of no shearing, following shearing to equilibrium at 496 sec^{-1} , show a rapid increase (Fig. 6). On the other hand, no increase in viscosity was observed after

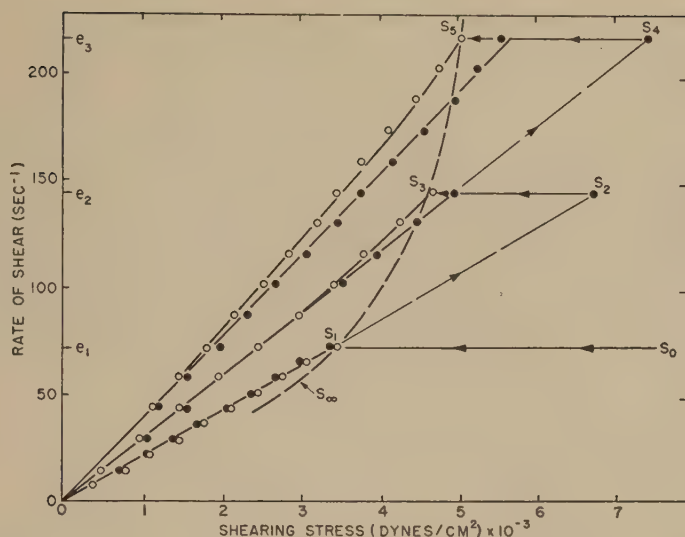


FIG. 5. Consistency curves determined after reaching equilibrium at successively higher rates of shear. Temperature, -25°C . Open symbols: decreasing rates of shear. Solid symbols: increasing rates of shear. Arrows indicate succession of measurements.

2 hr. rest when a sample had been sheared to equilibrium at 14.5 sec.^{-1} (Fig. 7).

The differences in behavior observed at low and high shear rates may be reconciled if it is concluded that two different phenomena are involved,

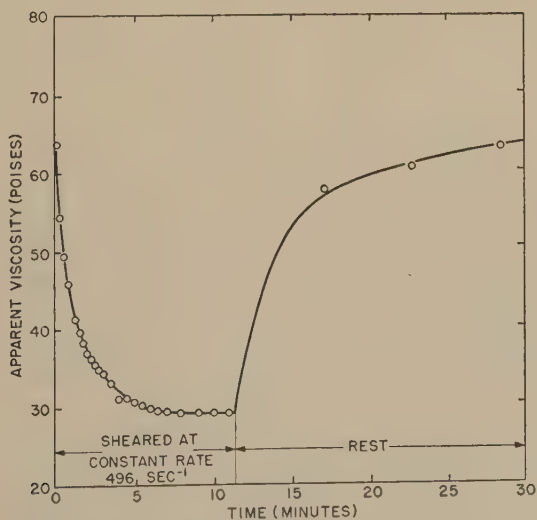


FIG. 6. Recovery of viscosity on standing after shearing to equilibrium at a high rate of shear. Temperature, -30°C .

namely, (a) an irreversible (within the time scale of the experiment) breakdown in the initial rigid structure of the oil, which is predominant at low shear rates and rapidly transient at high rates of shear; and (b) a reversible apparent thixotropy predominant at high rates of shear and similar to the behavior of high viscosity oils at room temperature reported by Weltmann (5,6).

Weltmann attributed the apparent thixotropy of high viscosity oils in a rotational viscometer to molecular orientation in the main; however, temperature effects due to heat generated in shearing are known to play some part in the decrease in viscosity as evidenced by recorded rises in temperature at the bob wall. The temperature rise was found to be pro-

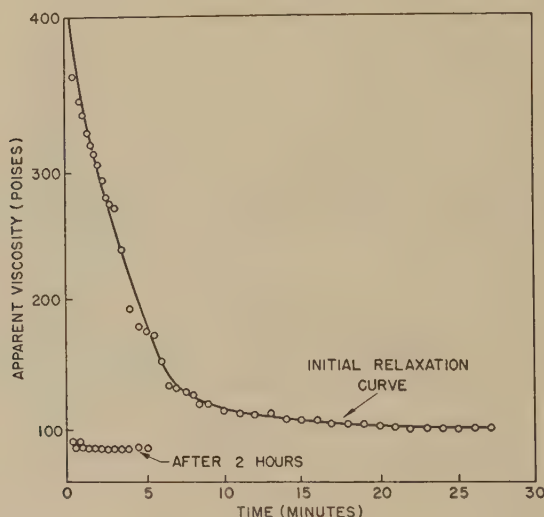


FIG. 7. Relaxation curves determined at a low rate of shear, 14.5 sec.^{-1} , initially and after 2 hrs. standing. Temperature, -25°C .

portional to the cup-to-bob clearance (6). If temperature effects contribute to the observed decrease in viscosity with increased rate of shear, the equilibrium viscosity should show a dependence on cup-to-bob clearance. Such a dependence was observed, the equilibrium viscosities being consistently higher when measured with a 1.4-cm. cup than with a 1.5-cm. cup, giving clearances of 1.0 and 2.0 mm., respectively.

2. Temperature Effects

The effect of frictional heating on the measured value of the equilibrium viscosity can be calculated from the equations of heat flow and mechanical equilibrium if the flow is assumed to be Newtonian. This has been done by Hagg (7) for a number of cases corresponding to assumed

temperatures at the cup and bob. The temperature dependence of the viscosity was assumed to have the form:

$$\eta(T) = \eta_0 e^{-\alpha T}, \quad [3]$$

where η_0 is the viscosity at the reference temperature (the cup temperature in the present case), T is the temperature rise, and α the temperature coefficient of viscosity. For the case at hand it is assumed that the cup temperature is maintained at the temperature of the bath and that the bob is thermally insulated. The calculations then give for the temperature rise of the bob at thermal equilibrium the result:

$$T_{\text{bob}} = (1/\alpha) \ln (1 + \beta/2), \quad [4]$$

where β is a dimensionless parameter given by the alternative forms:

$$\beta = \frac{\alpha \eta_0 R_c \omega^2}{\kappa} = \frac{\alpha \eta_0 d^2}{\kappa} \left(1 + \frac{d}{R_b}\right) e^2 \quad [5]$$

the other symbols being defined as follows:

R_b = radius of the bob,

R_c = radius of the cup,

$d = R_c - R_b$ = cup-to-bob clearance,

ω = angular velocity of the cup,

e = rate of shear,

κ = thermal conductivity of the oil.

Calculation of the apparent viscosity at thermal equilibrium yields the result:

$$\eta = \eta_0 \sqrt{\frac{2}{\beta}} \frac{\sinh^{-1} \sqrt{\beta/2}}{\sqrt{1 + \beta/2}}. \quad [6]$$

In order to estimate the possible magnitude of the viscosity change due to the rise in temperature of the oil, it is assumed that the completely sheared oil is a Newtonian liquid and that the dependence of equilibrium viscosity on rate of shear is due entirely to heating effects. The true viscosity, η_0 , can then be estimated from the slope at the origin of the S_∞ curve (Fig. 8). This gives 90 poises and 220 poises for η_0 at -25 and -30°C ., respectively, from which the viscosity temperature coefficient, α , at -30°C . is found to be $0.18 (^\circ\text{C})^{-1}$. The thermal conductivity is taken to be $0.00035 \text{ cal./cm. sec. } ^\circ\text{C}$. At a rate of shear of 600 sec.^{-1} the temperature rise of the bob is calculated to be 10 and 17°C . for the 1.4 - and 1.5 -cm. cups, respectively. With such high temperature rises it appears unlikely that the assumption that the bob is thermally insulated is a good approximation. If account were taken of the heat loss of the bob to

the surroundings the calculated equilibrium viscosities would not fall off as rapidly with increasing rate of shear.

A comparison of the calculated and observed equilibrium viscosities appears in Fig. 9. Heating effects are of the correct order of magnitude and in qualitative agreement with the observations, although the viscosity falls off much more rapidly than predicted from the calculations. A possible source of discrepancy is the uncertainty in the choice of the initial viscosity, η_0 , and likewise in the determination of the temperature coefficient, α , used in the theoretical formula. In any event, it appears that heating effects do not explain the entire relaxation of viscosity to the equilibrium value.

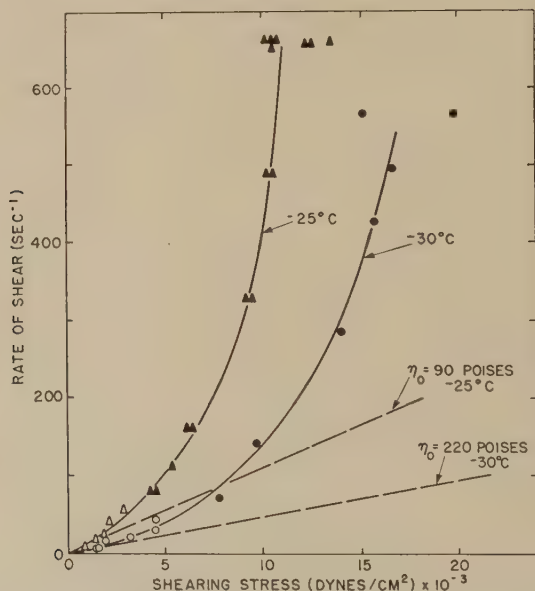


FIG. 8. Estimated equilibrium viscosities in the limit of low rates of shear at -25°C. and -30°C.

3. Wax-Oil Suspensions

The existence of a network of solid wax crystals in natural petroleum oils below their pour points has been reported by Erk (8), who suggests that this structure is responsible for the rigidity. In order to determine the effect of suspended wax in an oil under such conditions that temperature effects may be neglected, a study was made of the rheology of Pennsylvania 150 neutral oil containing 7% *n*-octacosane. Observations were made at $+30^{\circ}\text{C.}$ using a modified Stormer viscometer with which very low rates of shear may be obtained.

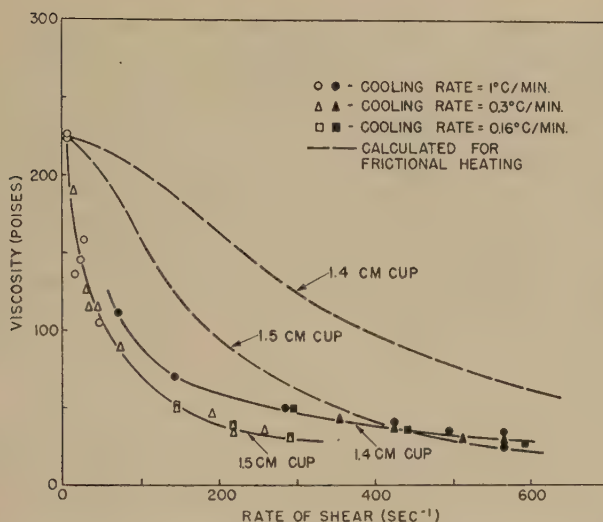


Fig. 9. Calculated and observed equilibrium viscosities for two cup-to-bob clearances. Temperature, -30°C . The 1.5- and 1.4-cm. cups give cup-to-bob clearances of 2 and 1 mm., respectively. The effect of cooling rate on equilibrium viscosity is also shown.

With the Stormer viscometer the amount of continuous shearing possible without rewinding the line to which the load is attached is about 100 revolutions. When the sample is sheared to this extent repeatedly at constant load, the breakdown is additive and with the same result as if the sample had been sheared continuously for the same number of revolutions. Furthermore, when different loads are used the increase in fluidity of

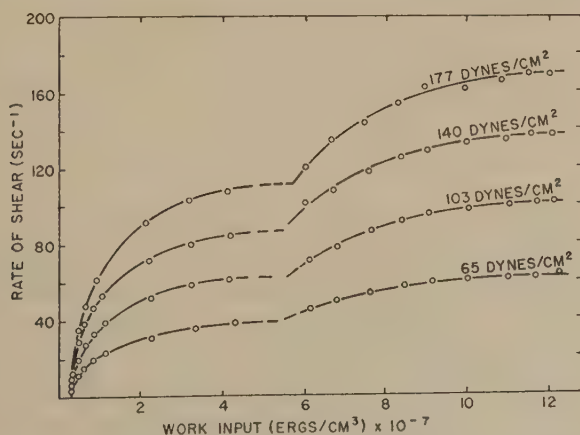


Fig. 10. Thixotropy of a suspension of *n*-octacosane in Pennsylvania 150 neutral oil at constant shearing stresses. Temperature, 30°C .

the sample is a function of the total work which has gone into shearing, i.e., the sum of the products of the load and the number of revolutions of the viscometer at that load. Data obtained from a single experiment are shown in Fig. 10, where the rate of shear at constant loads is plotted against the total work of shearing. The shearing was not continuous and was with shearing stresses varying from 65 to 177 dynes/cm.² The same data are used to plot the consistency curves for the suspension at different degrees of breakdown in Fig. 11, which shows a progression from plastic flow to Newtonian flow with a decreasing viscosity toward a minimum. The discontinuity appearing in the curves in Fig. 10 is not clearly under-

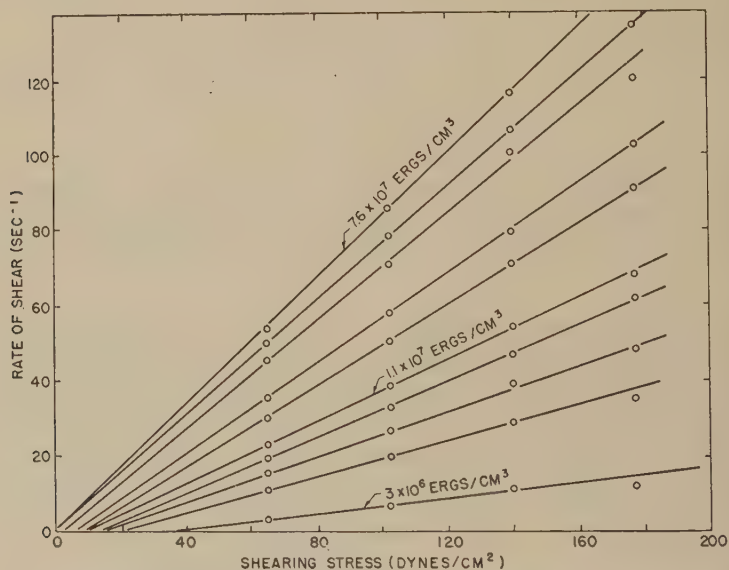


FIG. 11. Consistency curves for a suspension of *n*-octacosane in Pennsylvania 150 neutral oil with increasing work of shearing. Temperature, 30°C.

stood, but is attributed to changes due to fluctuations in temperature of the sample.

Since the degree of breakdown is determined by the work done in shearing, the rate of relaxation at constant rates of shear should be determined by the rate of energy input to the system. Thus, as a first approximation, the relaxation times should be inversely proportional to the square of the rate of shear, which is in accord with the rapid decrease in relaxation times observed for the natural oil at low temperatures.

In the case of Pennsylvania 150 neutral oil and the high-pour-point mixture containing suspended *n*-octacosane, the failure to exhibit recovery of rigidity after shearing, and the Newtonian flow characteristics

(for short time intervals) of the sheared samples in all but the very early stages of breakdown, suggest that the forces of adhesion between the wax crystals are not the electrical forces attributed to normal gels. The observed properties may be explained by assuming that the adhesion is through lattice forces, i.e., that the crystals are grown together, and that the decreasing viscosity is due to the mechanical degradation of this rigid network into progressively smaller units due to shearing.

ACKNOWLEDGMENTS

The authors are indebted to G. B. Costa, operator of the viscometer, and to G. Gavlin for his many helpful suggestions.

CONCLUSIONS

The thixotropy exhibited by Pennsylvania 150 neutral oil below its pour point in a rotational, concentric-cylinder viscometer may be resolved into two processes occurring simultaneously:

1. A degeneration of the rigid structure, predominantly observed at low rates of shear and occurring very rapidly at high rates of shear.
2. A reversible apparent thixotropy occurring predominantly at high rates of shear.

A calculation of the form and magnitude of temperature effects due to frictional heating accounts for a large part but not all of the latter effect.

A suspension of a pure normal paraffin hydrocarbon precipitated in a petroleum oil produces a high-pour-point system which has been studied in the absence of heating effects. This system exhibits a progressive increase in fluidity as a function of the work done in shearing, and a transition from plastic to Newtonian flow.

An explanation proposed is that the wax crystals existing in the saturated solution are grown together at the points of contact and that this matrix is mechanically degraded due to shearing.

REFERENCES

1. BONDI, A., *Physical Chemistry of Lubricating Oils*, pp. 68-90. Reinhold Publishing Corp., New York, 1951.
2. GREEN, H., *Ind. Eng. Chem.* **14**, 576-85 (1942).
3. JORDACHESCU, M. *Bull. assoc. franç. techniciens pétrole* **36**, 51-8 (1936).
4. FISCHER, E. K., *Colloidal Dispersions*, p. 160. John Wiley and Sons, Inc., New York, 1950.
5. WELTMANN, R. N., *Ind. Eng. Chem., Anal. Ed.* **15**, 424-9 (1943).
6. WELTMANN, R. N., *Ind. Eng. Chem.* **40**, 272 (1948).
7. HAGG, A. C., *J. Applied Mechanics* **11**, A72 (1944).
8. ERK, S., *Congr. mondial pétrole, 2me Congr., Paris 1937*, **II**, Sec. 2, *Phys. Chem. Raffinage*, 917-23.

FINE STRUCTURE AND RHEOLOGICAL PROPERTIES OF LITHIUM SOAP-OIL DISPERSIONS¹

B. W. Hotten and D. H. Birdsall

California Research Corporation, Richmond, California

Received February 11, 1952

INTRODUCTION

Semisolid dispersions of lithium soaps in oils are becoming increasingly important for application as lubricants. Lithium soaps have several desirable properties for such application. They are dispersible in a greater variety of petroleum and synthetic oils than are most other soaps. They also yield lubricating greases which have better water resistance than do greases made from sodium soaps, and higher melting points than greases made from calcium or aluminum soaps. Lithium soap greases have been widely used for aircraft lubrication and, more recently, for automotive lubrication.

Disadvantages of lithium soaps include their high cost, their high proöxidative action in oils, and in some cases the high shear-softening rates which they impart to greases.

This paper describes the effects of soap anion composition, oil composition, and dispersion procedure on soap particle structure and on certain rheological properties of lithium soap-oil dispersions of the types used for lubricating greases. The knowledge of this structure is of general interest from crystallographic and colloidal viewpoints; it is also of practical interest from the functional viewpoint, for the size and shape of these particles determine the texture and flow properties of the bulk grease and thus its behavior in service.

SAMPLE PREPARATION AND ELECTRON-MICROSCOPIC EXAMINATION

Greases were prepared by formation of the soaps *in situ*. Lithium hydroxide dissolved in water was added to a suspension of a fatty acid in oil and the resulting mixture was stirred and heated in a beaker until its temperature reached 200°C. At this temperature a clear fluid solution was present. It was poured into an evaporating dish whereupon it formed a solid gel as the temperature dropped 5–10°C. After cooling to room temperature the gel was forced through a 200-mesh screen. Samples were

¹ Presented at the Annual Meeting of the Society of Rheology, West Coast Section, Berkeley, California, November 16, 1951.

prepared in 100-g. quantities with 12% soap concentration. A "pale oil" having a viscosity of 360 Saybolt standard units (S.S.U.) at 37.8°C. (100°F.) and containing about 40% alkyl, 37% naphthenic, and 23% aromatic carbon atoms was used as the dispersion medium except where otherwise noted.

For examination of dispersed soap particles or micelles in the electron microscope (RCA model B), about 1 mg. grease was placed on a collodion film which was supported on a wire screen. The oil phase was then washed out with hexane as described by Birdsall and Farrington (1). The residual soap particles were shadowed with chromium according to the procedure of Williams and Wyckoff (7). Electron micrographs were made at 8000 power magnification.

ANION VARIATION

Unsubstituted Carboxylates

Most commercial lithium soap greases contain a mixture of palmitate and stearate soap anions.

The effect on micelle structure of molecular weight variation among saturated acids was determined with the aid of five pure acids (Eastman White Label except for the margaric which was obtained from A. D. Mackay Co.) containing from 12 (lauric) to 18 (stearic) carbon atoms per molecule. Electron micrographs obtained are shown in Fig. 1.

Lithium laurate formed relatively large, straight-sided micelles, and the dispersion was very soft and mushy. The myristate, palmitate, margarate, and stearate soaps assumed in general a rodlike form, the rods being about 0.1μ wide and about 1μ long. The greases containing these soaps were smooth in texture and moderately stiff (230–250 A.S.T.M. penetration). The presence of an odd number of carbon atoms in the margarate did not lead to a crystal form noticeably different from those of the even-atom carboxylates.

Soaps made with two unsaturated fatty acids were examined. The oleate gave micelles having a plump, swollen appearance in comparison with the saturated acid soaps. The linoleate micelles also appear plump. They taper down at the ends and appear to be intertwined to some extent. Both of the greases containing these unsaturated soaps were less smooth and were softer than the saturated soap greases. Anion double bonds may cause micelle modification either directly by an effect on intermolecular attraction or arrangement in crystal lattices or indirectly by promoting oil absorption.

Substituted Carboxylic Acids

Lithium 12-hydroxystearate forms double, intertwined, fibrillar micelles (Fig. 2) which previously have been observed only in hydrated calcium soaps. All of the fibrils twist by the same hand. This behavior



FIG. 1. Effect of soap anion variation on Fiber structure in lithium soap greases. Unsubstituted carboxylates. $\times 8000$.

- A. Laurate $\text{LiO}_2\text{CC}_{11}\text{H}_{23}$
- B. Myristate $\text{LiO}_2\text{CC}_{13}\text{H}_{27}$
- C. Palmitate $\text{LiO}_2\text{CC}_{15}\text{H}_{31}$
- D. Margarate $\text{LiO}_2\text{CC}_{16}\text{H}_{33}$
- E. Oleate $\text{LiO}_2\text{CC}_{17}\text{H}_{33}$
- F. Linoleate $\text{LiO}_2\text{CC}_{17}\text{H}_{31}$

is explained by the fact that the hydroxystearic acid used was a single stereoisomer. Thus, uniform orientation of the hydroxyl groups occurred in all micelles. The hydroxystearate grease was smooth and moderately stiff.

The 9,10-dihydroxystearate [acid made by oxidation of oleic acid (6)] was harder to disperse in oil than the 12-hydroxystearate was. The



FIG. 2. Effect of soap anion variation on fiber structure in lithium soap greases. Substituted carboxylates. $\times 8000$.

- A. 12-Hydroxystearate $\text{LiO}_2\text{C}(\text{CH}_2)_{10}\text{CHOHC}_6\text{H}_{13}$
- B. Ricinoleate $\text{LiO}_2\text{C}(\text{CH}_2)_7\text{CH}:\text{CHCH}_2\text{CHOHC}_6\text{H}_{13}$
- C. 9,10-Dihydroxystearate $\text{LiO}_2\text{C}(\text{CH}_2)_7(\text{CHOH})_2\text{C}_8\text{H}_{17}$
- D. 12-Ketostearate $\text{LiO}_2\text{C}(\text{CH}_2)_{10}\text{C}:\text{OC}_6\text{H}_{13}$

micelles are roughly hexagonal platelets which resemble true crystals more closely than the usual dispersed soap particles do. The grease was soft and granular.

The ricinoleate (from hydrolyzed castor oil), which contains both a double bond and a hydroxyl group, formed micelles which have the plump

appearance of the oleate and also to some extent the twisted structure of the 12-hydroxystearate.

Because ketone groups on soap anions cannot form a chain of lateral hydrogen bonds as the hydroxyl groups can, they would not be expected to have so profound an effect on particle structure as the latter groups. Actually, the micelles of lithium 12-ketostearate [acid made by oxidation of 12-hydroxystearic acid (4)] were found to resemble lithium stearate in shape, but they are considerably larger in diameter.

Several lithium alkanephosphonates and alkane- and alkylbenzene-sulfonates were examined, but no satisfactory greases could be obtained.

Mixed Anions

Mixed-anion soaps have considerable crystallographic interest. The degree of interchangeability of anions in micellar lattices is important in the determination of the shape and uniformity of the micelles. Electron micrographs of two mixed-anion soaps appear in Fig. 3.

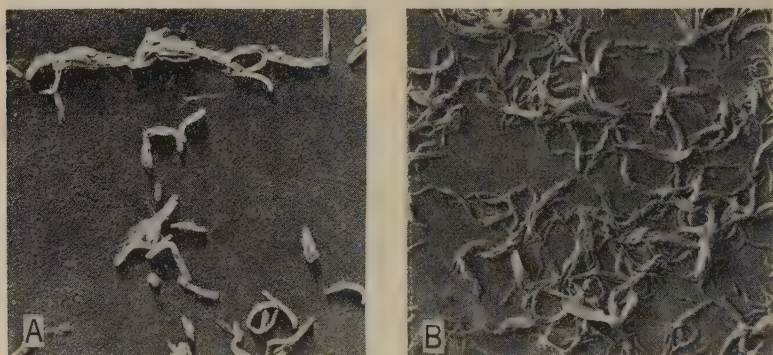


FIG. 3. Effect of soap anion variation on fiber structure in lithium soap greases.
Mixed anions. $\times 8000$.

A. Palmitate-stearate

B. Stearate-hydroxystearate (1:1)

The palmitate-stearate micelles are quite uniform, and they are intermediate in form between the individual single anion soaps.

The stearate-hydroxystearate micelles are less uniform. A few of them have the distinctive twist of lithium hydroxystearate, but most of them more closely resemble the stearate. There is thus probably a small portion of anion fractionation in this case.

Both mixed-anion greases were smooth in texture and moderately stiff in consistency.

OIL VARIATION

Oils present in commercial lithium soap greases include naphthenic and paraffinic mineral oils, diesters, polyethers, and polysiloxanes.

Micelle structures of lithium stearate dispersed under the same conditions in three of these oils appear in Fig. 4.

The finest structure is present in the naphthenic oil grease. This may be correlated with the high optical clarity, very smooth texture, and relative stiffness for a given soap content which are usually associated with lithium soap-naphthenic oil greases.

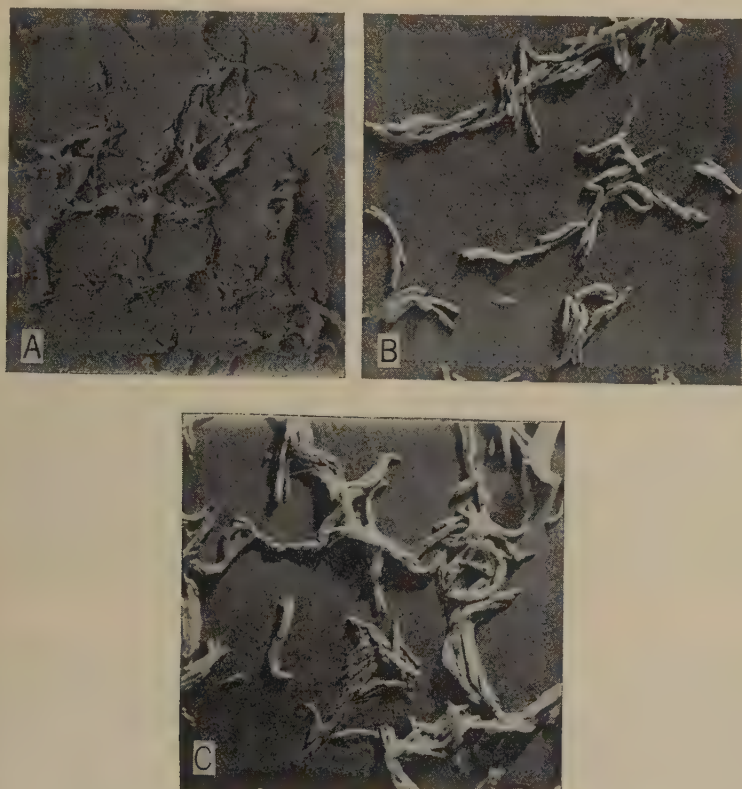


FIG. 4. Effect of oil type on fiber structure of lithium stearate greases. $\times 8000$.

- A. Naphthenic oil
- B. Paraffinic oil
- C. Diester oil

The paraffinic oil grease micelles are of similar form but slightly larger and more uniform in appearance than the naphthenic oil micelles. The paraffinic oil greases have less optical clarity than naphthenic oil greases, but they are only slightly less smooth in texture and somewhat softer.

The lithium stearate micelles from the ester oil are about twice as thick as, and generally longer than, those from mineral oils. The ester

grease has considerably less optical clarity and a coarser, softer structure than corresponding mineral oil greases.

Numerical consistencies of these three 12% lithium stearate greases were as follows, the highest penetration (5) representing the softest grease:

Oil	Naphthenic	Paraffinic	Ester
A.S.T.M. penetration, unworked, 25°C. (77°F.)	302	307	340

COOLING RATE

Cooling rates from the melt were varied over wide limits for two soap-oil compositions (12% soap in a naphthenic oil), and the effect on micelle structure was observed. Each mixture was heated to 200°C. so that the soap was completely dissolved. One portion was then poured out to a depth of 2 mm. in a metal dish at Dry Ice temperature so that it cooled during a few seconds. A second portion was poured into a 5½ in. diameter evaporating dish so that it cooled to room temperature during about 1 hr. A third portion was placed in an oven at 200°C. and the oven turned off so that the grease cooled to room temperature during about 4 hr.

Electron micrographs of the micelles formed are shown in Fig. 5. The most rapidly cooled lithium stearate formed globular, partially agglomerated micelles; that cooled at a medium rate formed small rods; and that cooled slowly formed appreciably larger rods with deep longitudinal striations.

Lithium oleate exhibits similar variations with cooling rate.

GENERAL CORRELATION OF MICELLE STRUCTURE WITH RHEOLOGICAL PROPERTIES

The texture, consistency, and behavior during flow of greases are directly related to the size and shape of the dispersed solid particles.

Texture

The lithium soap greases described are smooth, nonfibrous, and translucent when the micelles are rodlike and about 0.1 by 1 μ in dimension. An increase in these dimensions causes increasing granularity and opacity in the grease.

Consistency

A previous attempt to correlate micelle shape with grease consistency was made by Bondi *et al.* (2) with the aid of length:diameter ratio. Because there was not much variation in this ratio among these lithium soaps, a more sensitive parameter was sought.

Average surface areas and volumes were calculated for the micelles observed in the electron microscope. Values obtained are shown in

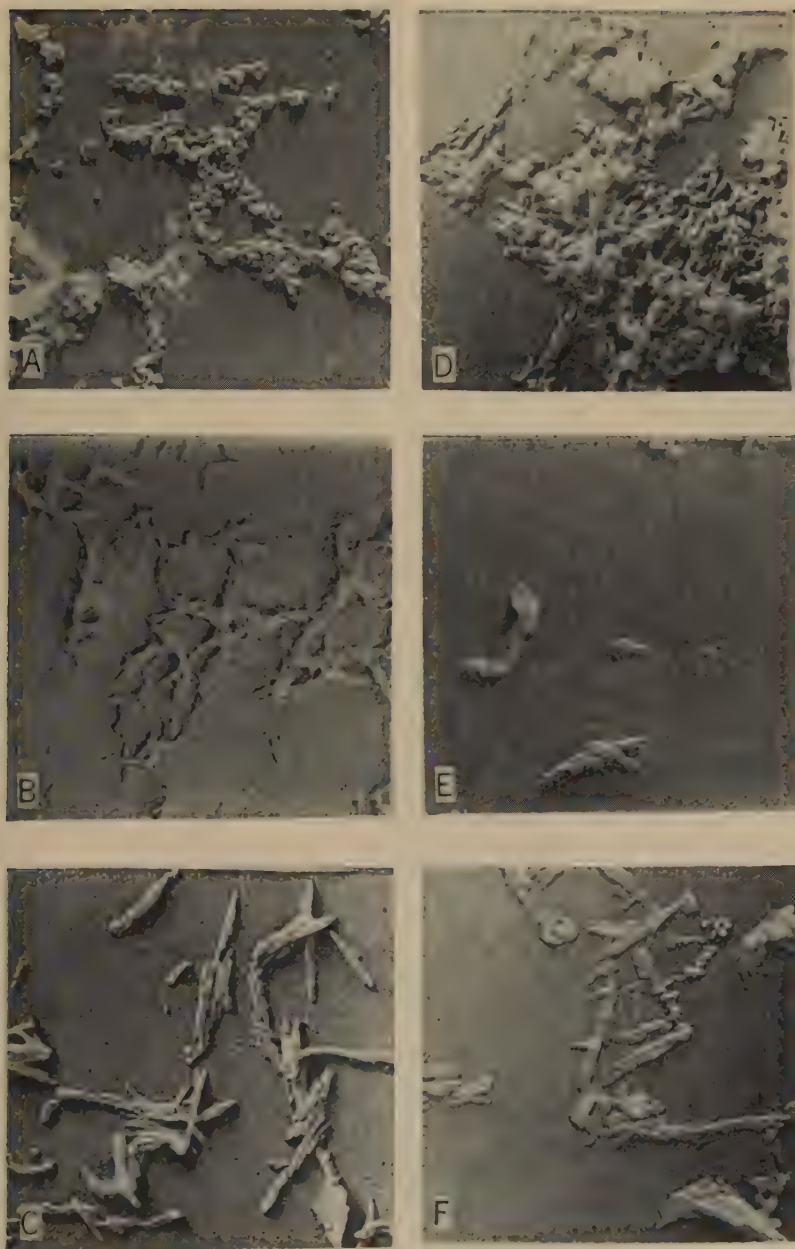


Fig. 5. Effect of cooling rate on fiber structure of lithium soap greases. $\times 8000$.

Lithium stearate

- A. Fast
- B. Medium
- C. Slow

Lithium oleate

- D. Fast
- E. Medium
- F. Slow

TABLE I

Effect of Anion Variation on the Fiber Dimensions and Consistency of 12% Lithium Soap Greases

Anion	Estimated average soap fiber dimensions					Area/ volume	Grease consistency ^a
	Thickness	Width	Length	Surface area	Volume		
	μ	μ	μ	μ^2	μ^3		
Laurate	0.1	0.3	3.0	2.5	0.09	27	Soft mush
Myristate	0.08	0.1	0.9	0.34	0.0072	47	230
Palmitate	0.06	0.12	0.7	0.27	0.0049	53	240
Margarate	0.1	0.1	0.9	0.3	0.0071	42	250
Stearate	0.08	0.08	0.5	0.14	0.0025	54	230
Oleate	0.1	0.25	1.5	1.1	0.037	30	280
Linoleate	0.2	0.3	0.7	0.71	0.0042	17	348
12-Hydroxystearate	—	0.009 diam.	0.8	0.24	0.0051	47	235
Ricinoleate	0.1	0.2	1.5	0.94	0.03	31	250
9,10-Dihydroxystearate	0.2	0.5	1.1	1.74	0.11	16	Soft mush
12-Ketostearate	—	0.3 diam.	1.6	1.65	0.11	15	370
Eocenephosphonate	—	0.6 diam.	—	4.5	0.9	5	Fluid
Stearate-hydroxystearate	—	0.1 diam.	1.2	0.39	0.0094	42	219
Single molecules of lithium stearate as in solution		0.0005 diam.	0.0025	4×10^{-6}	5×10^{-10}	8000	Fluid

^a Consistencies are in the usual A.S.T.M. D 217-48 units of decimillimeters penetration, obtained by conversion of penetrations made with the halfscale cone described by Hotten and Kibler (5).

Table I. Consistencies as measured by A.S.T.M. penetrations were then plotted against surface area per unit micelle volume, and the curve shown in Fig. 6 was obtained. It indicates a rather sharp increase in gelling power as surface area/volume (S/V) increases to about 30 reciprocal microns. At S/V values between 30 and 60 the increase is less sharp. The curve

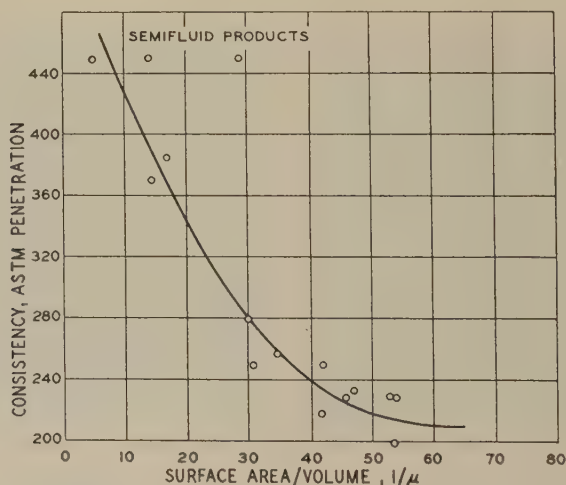


FIG. 6. Effect of soap fiber surface area/volume on consistency of 12% lithium soap greases.

should reach a minimum and then rise again as S/V approaches the value of a true solution of soap molecules (8000 for lithium stearate).

Flow Orientation

Streaming birefringence has been demonstrated by Gallay and Puddington (3) for the rodlike sodium stearate micelles and shown by them to be absent for threadlike sodium oleate micelles. The lithium palmitate grease, which has the most uniformly dimensioned micelles of the lithium soaps examined, was selected for examination under polarized light as a means of determining the extent of fiber orientation during flow. Examination was made through crossed Polaroid screens with the grease at first still in a glass capillary and then flowing at a velocity of about 30 cm./sec. A marked birefringence appeared with commencement of flow but a dark line remained along the center of the tube. This demonstrates a high degree of fiber orientation near the walls and plug flow at the center. The good pumpability shown by lithium soap greases, even at very low temperatures, may be related to the ease of orienting their fine rodlike micelles on shearing.

ACKNOWLEDGMENTS

The authors wish to express their thanks to Mr. B. B. Farrington and Dr. R. T. Macdonald for their interest and advice concerning this research, and to the University of California at Berkeley for the use of their electron microscope.

CONCLUSIONS

1. Lithium soaps of saturated carboxylic acids containing 14-18 carbon atoms per molecule form fine rodlike micelles (about 0.1 by 1μ) on being dispersed in oil, and the dispersions at 12% concentration take the form of smooth greases. Lithium laurate forms larger micelles and a coarse, mushy dispersion.

2. Lithium soaps of unsaturated fatty acids form plump, fusiform micelles with lower gelling power than the saturated soap micelles.

3. Lithium 12-hydroxystearate forms distinctive intertwined fibrils with high gelling power, and the 9,10-dihydroxystearate forms hexagonal platelets with weak gelling power in oil.

4. Lithium stearate forms very finely dispersed micelles in a naphthenic oil, coarser micelles in a paraffinic oil, and still coarser micelles in an ester oil.

5. Micelle size increases with increasing cooling time of hot soap solutions.

6. Micelle surface area per unit volume is a direct determinant of gelling power.

7. When the grease flows through a tube, the rodlike micelles of dispersed lithium soap, such as the palmitate, are highly oriented at the walls parallel with the line of flow and unoriented at the center of the tube.

REFERENCES

1. BIRDSALL, D. H., AND FARRINGTON, B. B., *J. Phys. & Colloid Chem.* **52**, 1415-23 (1948).
2. BONDI, A., *et al.*, *Inst. Spokesman (Natl. Lubricating Grease Inst.)* **13**, No. **12**, 12-18 (1950).
3. GALLAY, W., AND PUDDINGTON, I. E., *Can. J. Research* **22B**, 173-81 (1944).
4. GRUMMITT, O., AND SIEDSCHLAG, K. G., *J. Am. Oil Chemists' Soc.* **26**, 690-91 (1949).
5. HOTTEN, B. W., AND KIBLER, G. M., *Anal. Chem.* **22**, 1574-5 (1950).
6. ROBINSON, G. M., AND ROBINSON, R., *J. Chem. Soc.* **127**, 175-80 (1925).
7. WILLIAMS, R. C., AND WYCKOFF, R. W. G., *J. Applied Phys.* **17**, 23 (1946).
8. FARRINGTON, B., *Ann. N. Y. Acad. Sci.* **52**, 979 (1951).

SIZE DETERMINATIONS OF CLAY PARTICLES IN WATER SUSPENSIONS BY USE OF LOW-ANGLE X-RAY DIFFRACTION^{1,2}

W. J. West

California Research Corporation, La Habra, California

Received January 28, 1952

ABSTRACT

Low-angle x-ray diffraction permits studies of sizes of clay particles as they exist in clay-water suspensions. Change in the state of the suspension can be made, and sizes of the particles can be determined again as they exist in the new state. Particle-size determinations by other methods do not share this advantage. Supercentrifugal size analysis must be made with sample at high dilutions, and electron microscope size analysis must be made with sample in the dry state. The two-crystal x-ray spectrometer designed and built by Professor J. W. M. DuMond at the California Institute of Technology was used to measure the low-angle x-ray diffraction from clay-water suspensions. From these measurements, particle sizes were determined. Particle size determinations on several clays that are used as drilling fluids in the petroleum industry showed:

(a) The size of hydrated clay particles in water suspension was larger than the size of the particles in the original dry powdered clay (approx. 0.3μ). The increase in size was proportional to the clays' swelling abilities. This observation contradicts the common belief that highly swelling clays have smaller particles in water suspensions than poorly swelling clays.

(b) Sizes of the hydrated particles in water suspensions were independent of dilution for concentrations less than 8%.

(c) Viscosity lowering by agents such as tetrasodium pyrophosphate involved size reduction of hydrated particles.

INTRODUCTION

Size of particles has been considered an important factor affecting the properties of swelling, viscosity, and gel strength, of clay-water suspensions. However, most methods of measuring particle size have been unable to determine size of particles as they exist in clay-water suspensions. The method of low-angle x-ray diffraction is unique in that the size of the particle can be measured as it exists in the water suspension. The sample studied is large, 2-3 cc., and is not disturbed in the sampling or measuring process. Change in the state of the suspension can be made and sizes of

¹ Results reported here were obtained in a cooperative research project between the California Institute of Technology and the California Research Corporation. The experiments were performed in the laboratories of, and through the courtesy of, Professor J. W. M. DuMond of the Institute.

² Presented at the Annual Meeting of the Society of Rheology, Chicago, Illinois, October 24-27, 1951.

the particles can be determined again as they exist in the new state. Particle-size determinations by other methods do not share this advantage. Supercentrifugal size analysis must be made with sample at high dilutions, and electron microscope size analysis must be made with sample in the dry state.

This paper presents the results of an investigation of the use of low-angle x-ray diffraction as a tool for studying sizes of particles in clay-water suspensions. The method of using low-angle x-ray scattering for measuring particle size is discussed in detail. Results of size determinations on clay-water suspensions are presented and briefly discussed. This paper does not present a complete report on the subject, but presents results of initial investigations.

LOW-ANGLE X-RAY DIFFRACTION FROM SPHERES

During the past few years, several articles (1-5) have been published describing low-angle x-ray diffraction from small particles. In these articles have been considered the problems of shapes of particles, particle-size distribution, and multiple scattering as well as the problems of measuring low-angle x-ray diffraction. In this paper, only the simple case of diffraction from spheres will be considered, and the investigation of the usefulness of the low-angle x-ray method for studying sizes of particles in clay-water suspensions will be presented.

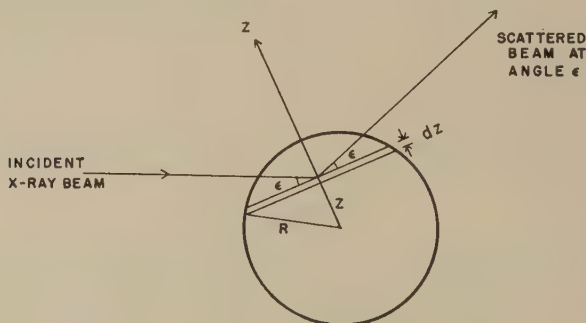


FIG. 1. Geometrical construction for calculating the diffraction of x-rays by spherical particles.

In Fig. 1, a spherical particle is shown being radiated by x-rays. Let a disk of thickness dz be cut in the sphere so that the surface of the disk makes equal angles with the incident and scattered beam. The phase of the scattered wave from all parts of the disk is the same but changes as the disk is moved along z . The fraction of the incident x-ray beam scattered by disk and observed in direction ϵ is given by:

$$dA_s = A_e \pi (R^2 - z^2) n e^{-2\pi i e z / \lambda} dz \quad [1]$$

where A_e is the fraction of the total beam scattered by one electron; n is the electron density of the particle (if particle is surrounded by a liquid, then n is the difference between the electron density of the particle and the liquid); λ is wavelength of incident x-rays; and R , z , and ϵ are defined by Fig. 1. Integrating Eq. [1] over the sphere and squaring the result gives the intensity of the diffracted beam observed in direction ϵ .

$$\frac{I_s}{I_e} = \left[\frac{A_s}{A_e} \right]^2 = \left[\pi n \int_{-R}^R (R^2 - z^2) e^{-2\pi i \epsilon z / \lambda} dz \right]^2$$

$$= N^2 \left[\frac{\sin (2\pi \epsilon R / \lambda) - (2\pi \epsilon R / \lambda) \cos (2\pi \epsilon R / \lambda)}{(2\pi \epsilon R / \lambda)^3} \right]^2 \quad [2]$$

where $N = 4/3\pi R^3 n$ and is equal to total number of electrons per particle. The intensity of the scattering from many particles in a sample is just the algebraic sum of the intensity of the scattering from each of the particles, provided interaction can be neglected as will be the case for dilute suspensions.

Equation [2] can be approximated very closely by the Gaussian function of Eq. [3].

$$\frac{I_s}{I_e} = N^2 e^{-4\pi^2 R^2 \epsilon^2 / 3\lambda^2} \quad [3]$$

Taking the logarithm of Eq. [3] gives:

$$\ln \frac{I_s}{I_e N^2} = - \left[\frac{4\pi^2 R^2}{3\lambda^2} \right] \epsilon^2 \quad [4]$$

If the logarithm of the diffracted intensity, I_s , is plotted as a function of the square of the scattering angle, ϵ^2 ; then the slope of this plot is proportional to the square of the radius of the particles, R^2 . In this investigation, particle sizes were determined from the slopes of the measured $\ln I_s$ vs. ϵ^2 curves.

To illustrate why the term "low angle" is applied to this type of x-ray diffraction, an example is given. If the radius of the sphere is 1000 Å. (0.1 μ), and the wavelength of the x-rays radiating the sphere is 1 Å., then the "half width" of the diffraction pattern is 56 sec. of arc. Observations of the details of such a narrow diffraction pattern require special type instruments. Guinier (1), who first analyzed the details of low-angle x-ray diffraction, used a curved crystal x-ray spectrometer.

The two-crystal spectrometer (6) designed and built by Professor J. W. M. DuMond of the California Institute of Technology was used in this investigation to measure the x-ray diffraction from the clay-water suspensions. The instrument is described in the reference cited. Precision of the spectrometer is very good. Angular settings of the crystal holders can be made to within a quarter of a second of arc throughout 360 deg. of rotation.

In Fig. 2, a schematic diagram is shown of the low-angle x-ray diffraction apparatus. The target of the x-ray tube was molybdenum. Crystal *A* was set so that only the $K\alpha_1, \alpha_2$ lines ($\lambda = 0.710$ A.) of molybdenum were reflected by the crystal. All other wavelengths did not satisfy Bragg's law of reflection and so were rejected from the reflected beam. Crystal *A* served as a monochromator. The reflected beam incident on the sample was geometrically defined by the slit at *S*. Without a sample in place, the reflected beam from crystal *A* was reflected again from crystal *B* when

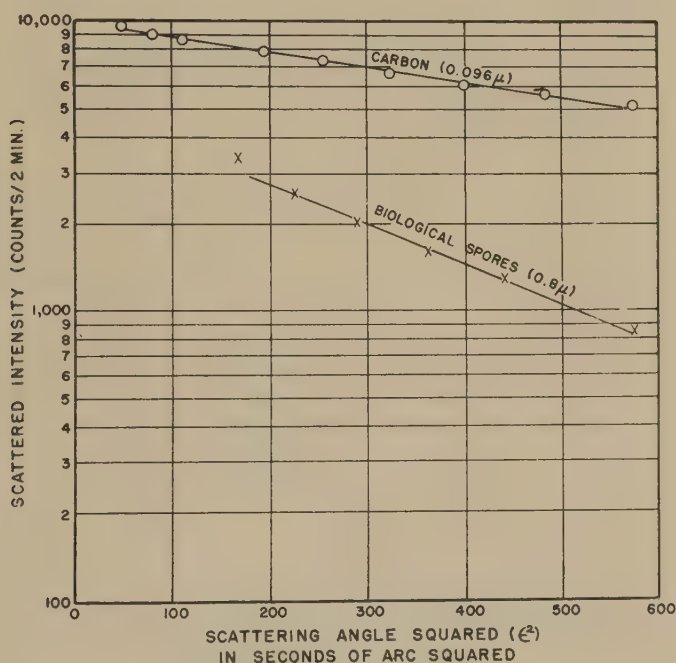


FIG. 4. Calibration of two-crystal spectrometer for particle-size determinations. Calibration particle-size measurements were made by electron microscope for carbon sample and optical microscope for biological spore sample. Particles of both samples were spheres.

crystal *B* was parallel to crystal *A*. As crystal *B* was turned away from parallelism with crystal *A*, the reflected intensity dropped quickly to zero, i.e., within a few seconds of arc. The intensity of the reflected beam was measured by a xenon-filled Geiger counter at *C*. With the sample in place, part of the x-ray beam was diffracted in passing through the sample. Because the wavelength remains unchanged in this diffraction, crystal *B* could be rotated away from parallelism with crystal *A*, where Bragg's law was satisfied for central beam, to positions where Bragg's law was satisfied by the diffracted beam. Consequently, the intensity of the dif-

fraction from the sample could be measured at several scattering angles by setting crystal *B* at these angles.

The procedure used for determining the size of the particles in a sample was as follows: The spectrometer was aligned so that crystals *A* and *B* were parallel and their axis of rotation vertical. The optimum thickness of the sample was determined so that the x-ray intensity was reduced by $1/e$ in passing through the sample. When this condition was satisfied, the maximum scattering was obtained from the sample. This optimum thickness was about 1 cm. After these adjustments were made,

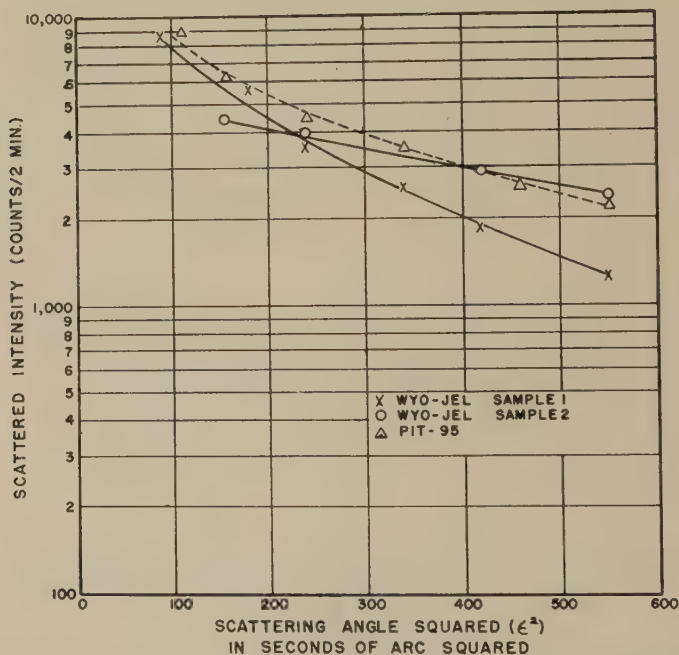


FIG. 5. Low-angle x-ray diffraction from small particles of powdered dry clay samples. Sizes lie between 0.3μ and 0.7μ .

the instrument was ready to be used in measuring low-angle diffraction from particles of clay-water suspensions. For each setting of crystal *B*, the intensity was recorded with the sample behind slit *S* and then with the sample placed in front of crystal *A*. The difference between the two readings was proportional to the diffracted beam from the sample observed at a diffraction angle ϵ . The angle ϵ was the difference in angular readings for crystal *B* when set parallel to crystal *A* and when set away from parallelism with crystal *A* for a diffraction measurement. The diffraction curve was obtained by repeating the readings for several settings of crystal *B*.

In Fig. 3 is shown two plots of intensity of the diffracted beam as a

function of the setting of crystal *B*. One plot is for no sample in place, and the other plot is for a sample of colloidal carbon in place. The extremely narrow curve of Fig. 3 for no sample in place is the feature that makes this instrument useful for measuring certain types of low-angle diffraction. The dashed curve is the diffraction from a sample of colloidal carbon. The diameter of the carbon particles was approximately 1000 Å. ($0.1\ \mu$).

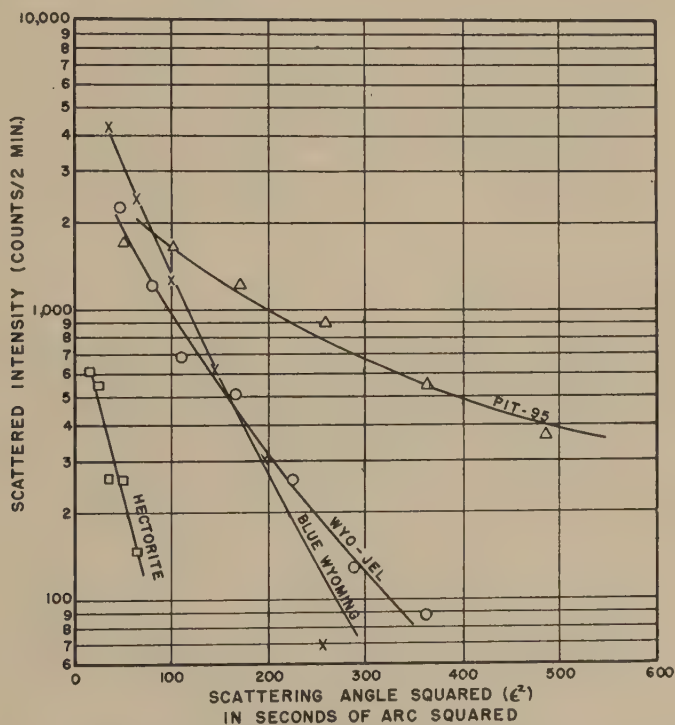


Fig. 6. Low-angle x-ray diffraction from hydrated particles of four 8% clay-water suspensions. Increasing particle size corresponds to increasing slopes of these curves. Particle size of the Pit-95 sample remained same on forming suspension. Particles of other samples increased roughly proportionate to their swelling abilities.

In Fig. 4, the logarithm of the diffracted intensity from the carbon sample is plotted as a function of the square of the diffraction angle. This curve is a straight line as predicted by the theory. For particles larger than 1000 Å., the theory ceases to hold exactly because of refraction effects. However, by calibrating the instrument with particles of known size, unknown sizes can be determined in the range of calibration. The plot of the diffracted intensity from biological spores shown in Fig. 4 was for calibration.

LOW-ANGLE X-RAY STUDIES OF CLAY-WATER SUSPENSIONS

Five clays were selected for this low x-ray investigation, some of which are used in drilling fluids in the petroleum industry. Four of the clays are of the montmorillonite type and cover a wide range of swelling abilities. These four clays have the trade names of Pit-95, Blue Wyoming, Wyo-Jel, and Hectorite, whose swelling abilities measured by the American Colloid Company test³ are 4, 9, 16, and 22, respectively. The fifth clay has the trade name Otay. This clay is a good example of a group of

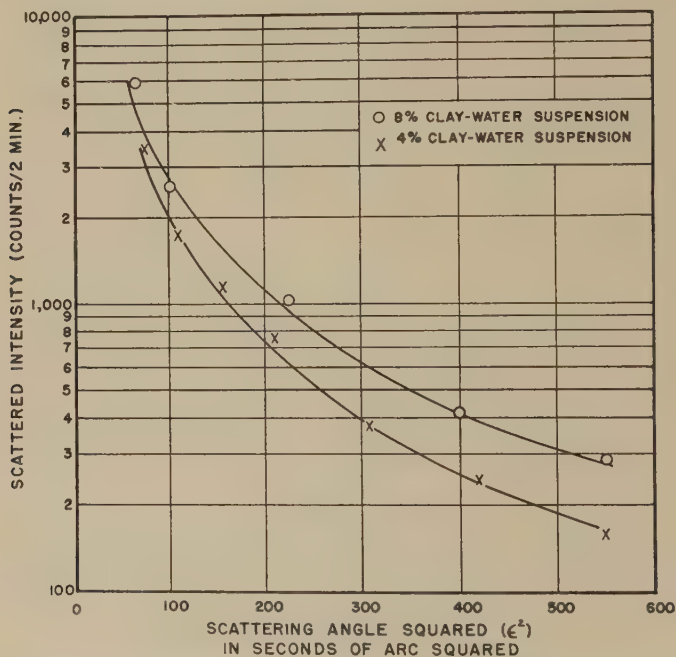


FIG. 7. Low-angle x-ray diffraction from 8% and 4% Wyo-Jel clay-water suspensions. These two curves are essentially the same, except for reduction in intensity, showing that particle size remained constant on dilution.

clays called bentonites; however, this particular clay is a poorly swelling clay. The Otay sample was selected because when tetrasodium pyrophosphate was added to Otay clay-water suspension essentially no viscosity change occurred, whereas the same additive caused a viscosity reduction to water suspension of the first four clays selected.

The first set of measurements on clay particles was made to determine the particle size of the powdered dry clay samples. In Fig. 5 is shown the

³ The swelling test used was the one publicized by the American Colloid Company, 363 West Superior Street, Chicago 10, Illinois, "Data No. 251."

low-angle x-ray diffraction from three powdered clays. Two of the curves are for two different grinds of the Wyo-Jel sample, and the other curve is for the Pit-95 sample. The particle size was determined by comparing the slopes of the curves of Fig. 5 with the calibration curves of Fig. 4. The particle size of these samples was found to be between 0.3 and 0.7 μ .

Eight per cent clay-water suspensions were made from the clay samples. The low-angle x-ray diffraction measured by the two-crystal

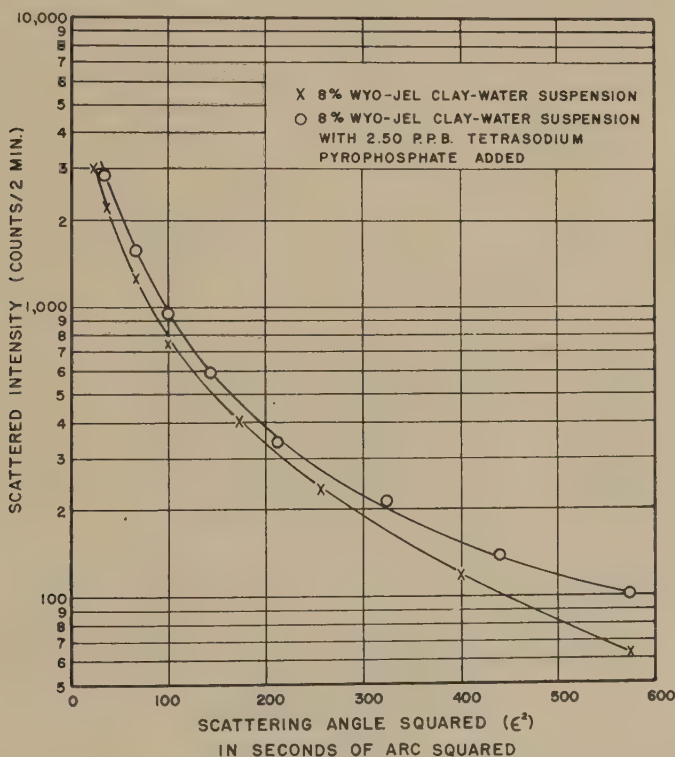


FIG. 8. Low-angle x-ray diffraction from two 8% Wyo-Jel clay-water suspensions. Addition of tetrasodium pyrophosphate reduced the viscosity of suspension. The scattered intensity falls off less rapidly with scattering angle for the treated sample than for the untreated sample, indicating smaller particle size for treated sample.

spectrometer is shown in Fig. 6. The slopes of these curves are widely different. The increase in the slopes of the curves of Fig. 6 over those of Fig. 5 is greatest for Hectorite, next for Blue Wyoming and Wyo-Jel, and least for Pit-95. The slope of the curve for Pit-95 in clay-water suspension increased very little over the curve for Pit-95 in dry powdered state. Comparing the curves of Fig. 6 with the calibration curves of Fig. 6 shows that particle-size increase in forming a clay-water suspension was

greatest for Hectorite, and particle-size increase was least for Pit-95. This same trend is found in the swelling ability, viscosity, and gel strength of these clays. The swelling ability, viscosity, and gel strength were greatest for the Hectorite clay-water suspension and least for the Pit-95 clay-water suspension. This experiment shows that the sizes of clay particles increase in forming water suspensions and the increase is proportional to the swelling ability of the clay.

An absolute particle-size determination could not be made because the diffraction curves for the clay-water suspensions fell outside the cali-

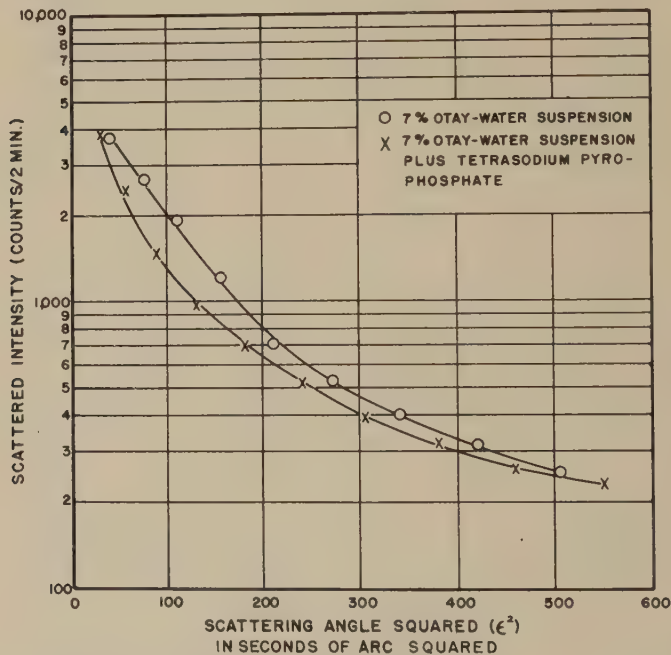


FIG. 9. Low-angle x-ray diffraction from two 7% Otay clay-water suspensions. Addition of tetrasodium pyrophosphate did not reduce viscosity of suspension. These two curves show no appreciable change in particle size between treated and untreated suspensions.

brated range of the instrument. Further calibration of the instrument will be made when larger particles of known sizes can be obtained. The data obtained are useful because they show relative changes in particle size when water suspensions are formed.

In the next experiment, the results of which are shown in Fig. 7, an 8% Wyo-Jel suspension was diluted to a 4% suspension. No appreciable change in particle size was observed. This experiment indicates that the size of the hydrated particles is essentially independent of further dilution.

In the concluding set of experiments, changes in particle sizes were measured when tetrasodium pyrophosphate was added to clay-water suspensions. Figure 8 shows that the size of particles of the Wyo-Jel sample decreased when tetrasodium pyrophosphate was added. The decrease in size is indicated by the decrease in the slope of the logarithmic plot of the diffraction curve. Figure 9 shows that the size of the particles of the Otay suspension changed very little. Viscosity measurements show that the decrease in viscosity of the Wyo-Jel suspensions is greater than the decrease in the viscosity of the Otay suspensions with the addition of tetrasodium pyrophosphate. This experiment shows that viscosity lowering by adding tetrasodium pyrophosphate is accompanied by size reduction of the hydrated particles.

CONCLUSIONS

This study has shown that low-angle x-ray diffraction can be used to measure sizes of particles in clay-water suspensions. The principal advantage of the method is that the sample studied is relatively large and it is not disturbed in the sampling or measuring process.

From these measurements of size of particles in clay-water suspensions a better picture of the physical nature of the clay-water system has been obtained. These experiments show that the clay particle size increases in forming the water suspension. The increase in size is proportional to the swelling ability of the clay. The best swelling clays had the largest particle size in the clay-water suspension. This is contrary to the theory that particles in a water suspension are smaller for a highly swelling clay than for a poorly swelling clay. The clay-water systems with the largest particles were found to have the largest viscosity and the largest gel strength. The experiments also showed that viscosity lowering by additives is accompanied by size reduction of the particles.

REFERENCES

1. GUINIER, A., *Ann. phys.* **12**, 161 (1939).
2. WARREN, B. E., *J. Applied Phys.* **20**, 96 (1949).
3. BOLDUAN, O. E. A., AND BEAR, R. S., *J. Applied Phys.* **20**, 983 (1949).
4. KAESBERG, P., *Phys. Rev.* **74**, 71 (1948); RITLAND, H. N., KAESBERG, P., AND BEEMAN, W. W., *J. Chem. Phys.* **18**, 1237 (1950); *J. Applied Phys.* **21**, 838 (1950).
5. FANKUCHEN, I., AND JELLINEK, M. H., *Phys. Rev.* **67**, 201 (1945); *Ind. Eng. Chem.* **41**, 2259 (1949); JELLINEK, M. H., SOLOMON, E., AND FANKUCHEN, I., *Ind. Eng. Chem., Anal. Ed.* **18**, 172 (1946); BARTON H. M., AND BRILL, R., *J. Applied Phys.* **21**, 783 (1950).
6. DUMOND, J. W. M., AND MARLOW, D., *Rev. Sci. Instruments* **8**, 112 (1937).

A HIGH SHEAR METHOD OF RATING BRUSHABILITY OF PAINTS¹

W. K. Asbeck, D. D. Laiderman and M. Van Loo

The Sherwin-Williams Company, Chicago, Illinois

Received January 28, 1952

ABSTRACT

A rotational viscometer is described which operates in the range of high shear velocities encountered in the brushing of paints. Because the centering of the inner cylinder is handled automatically, the construction is rather simple, and clearances of 100 μ are maintained easily. At these clearances, shear velocities in the order of 20,000 reciprocal seconds are attainable, while at smaller clearances these values may be increased substantially without excessive temperature rise.

Good correlation of brushability of paints was found between qualified painter opinion and ratings based on viscosity characteristics determined at the high shear velocities of about 12,000 to 35,000 reciprocal seconds established during brushing application. Corroboration of practical experience was obtained that painters have different standards of acceptable brushing qualities for different types of paints. Temperature also strongly affects relative ease of brushing.

A one-point method of rating brushability of paints on an absolute basis is feasible through proper design of a viscometer which measures within the shear velocity range of brush application.

INTRODUCTION

There has been a long standing need for a simple, practical method for measuring the brushability of paints. The common method is to obtain the opinion of a competent and experienced painter after a practical brushing test. A practical instrument which could define the brushability of paints independently of personal opinion, and preferably on an absolute basis, would fill a definite need in the field of testing in the paint industry.

Failures of previous attempts to correlate viscosity data, obtained with current instrumentation, with actual brushing qualities undoubtedly is due to the difficulty of duplicating the very high shear velocities to which a paint is subjected during brush application. These shear velocities are in the order of 12,000–35,000 reciprocal seconds if a film thickness of 1–3 mils (about 2.5×10^{-3} to 7.5×10^{-3} cm.) is laid down at a brushing rate of about 3 ft./sec. (about 90 cm./sec.), as applied by the average painter. Most technical viscometers currently available for paint testing,

¹ Presented at the Annual Meeting of the Society of Rheology, Chicago, Illinois, October 24–27, 1951.

even the best of the so-called high shear type, are capable of measuring at a maximum of about 1000 reciprocal seconds so that the normal brushing range is not even approximated. The viscosity of most paints as considered in relation to brushability exhibits a decided dependence on shear velocities. Therefore, it is necessary to either determine the viscosity of these materials at the shear velocities encountered in brushing, or to devise some reliable method for extrapolation to such values. Of the two, the former is, of course, preferable.

ROTATIONAL VISCOMETERS

Numerous attempts have been made to construct viscometers with high shear velocity gradients, but, as has been said, values of more than 1000 reciprocal seconds have seldom been surpassed in rotational type apparatus. Because of the uniformity of shear velocity across the entire annular space, this type of instrument is superior to the capillary type, although high shear velocities are more readily obtainable in capillary viscometers.

In most rotational viscometers, high shearing rates are obtained by increasing the rotational velocities as far as it is possible while keeping the annular space between the internal and external shearing surfaces as small as practicable. It is necessary to maintain an exact concentricity of the two surfaces in order to obtain definable shear velocities. Therefore, either the thickness of the annulus must be kept relatively large or excessively complicated centering devices must be employed to maintain a precise clearance between the two shearing surfaces. A consistent and accurate concentric clearance of less than 0.5 mm. has seldom been maintained with any degree of satisfaction.

The heat conductivity of many of the test materials with which we are concerned is relatively low. Therefore, an increase in rotational speeds with relatively thick films is limited. This restriction stems from the temperature rise encountered in the test material due to the increased shearing stress required for the increased shear velocity. The dissipation of this heat through a thick film is relatively slow, so that excessive and uncontrollable temperature rise in the test material results. The centrifugal action at very high rotational speeds also presents problems. There is a tendency to expel material from the test cup if special precautions are not taken to prevent this action.

DESIGN OF AN IMPROVED INSTRUMENT

It would seem, then, that the most rewarding direction for the design of viscometers of the rotational type capable of shear velocities higher than those presently available would be one in which the clearance between the internal and external shearing surfaces could be maintained

concentrically at the lowest clearances commensurate with the material to be tested. For most paints, including those containing relatively coarse extended pigments, this would be about $100\ \mu$. For materials of the colloidal type, where the maximum particle size is considerably smaller, this clearance could be reduced to perhaps the order of magnitude of several microns.

In order to be practical, clearances of this magnitude must be maintained to within several per cent, and the apparatus for obtaining concentricity should be relatively simple. Fortunately, a physical principle exists which makes the achievement of these ends relatively easy. Clearances may be obtained automatically within the desired tolerances through the tangential forces produced during the process of measuring viscosities. This is the principle underlying the bearing and the sliding wedge. Tremendous carrying forces are evolved in a shaft rotating in a bearing surrounded by a viscous medium or by a slightly tipped plate sliding over another with a wedge of viscous material separating them. These forces can be employed conveniently to center exactly the inner and outer cylinders of a rotational viscometer (2).

A very simple and inexpensive instrument, the Band Viscometer (1), has been built on the principle of the sliding wedge. Its practical maximum shear velocity, at a film thickness of $50\ \mu$ and a maximum linear velocity of about 20 cm./sec., is about 4000 reciprocal seconds. This is still below the range required for brushability tests. Furthermore, with fluids having viscosities of 5 down to 2 poises or less, the operation becomes cumbersome and untidy. Consequently an apparatus of the concentric cylinder type was constructed, making use of the principle of the bearing. It was expected that much higher linear velocities of the shearing surfaces could be obtained at about the same clearances as the band viscometer. This would provide proportionally higher shear velocities in the order of 10,000 reciprocal seconds and higher.

The instrument is illustrated in cross section in Fig. 1. It consists of a water-jacketed cylindrical container within which a cylindrical bob of diameter about $200\ \mu$ less than the outer cylinder is suspended on two universal joints. One joint is in the approximate geometrical center of the inner cylinder. The other joint is placed at some distance above the top of the bob, its upper member being clamped into one of the standard rotational viscometer stands such as the Stormer or Wolff-Hoepke type, replacing the regular paddle. As an alternative, a motor-driven stand with an auxiliary torque-measuring equipment also could be used.

The two universal joints allow the bob to swing freely and to align itself concentrically within the outer cylinder as soon as sufficient torque is applied to the upper universal to cause the bob to rotate. It should be noted that exact alignment of the instrument is not necessary, because this action takes place automatically from the design of the apparatus.

The mathematical derivation for the forces causing exact centering of the inner cylinder upon rotation are entirely similar to those causing centering of the band in the band viscometer and have been described in the previous paper. Because of the curvature of the cylindrical surfaces and their infinite measuring length, the final differential equation

for the centering force differs from that of the band instrument (3). It now becomes:

$$\frac{dp}{d\xi} = \frac{6\eta w}{\psi^2} \times \frac{(1 + x \cos \xi) - \alpha(1 - x)}{(1 + x \cos \xi)^3}.$$

The symbols correspond to those used in Fig. 2. They are: a , the eccentricity; ξ , the angle from greatest film thickness; q , the quantity of viscous material flowing; η , the viscosity; w , the rotational velocity; b , the width of the annular slot; and h , its thickness. Alpha (α) equals

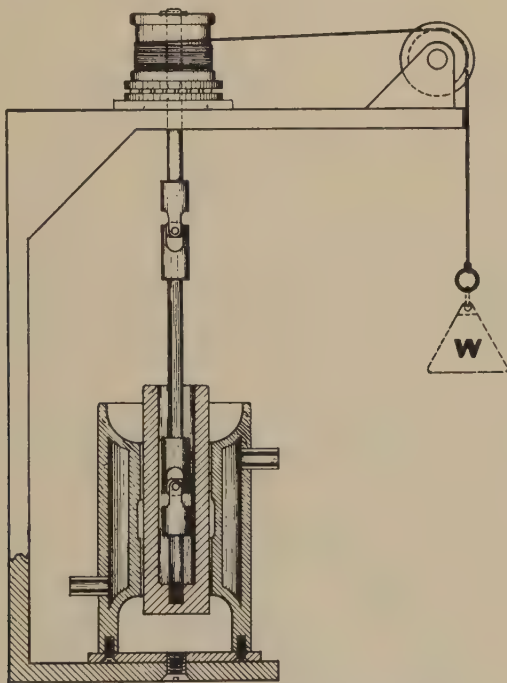


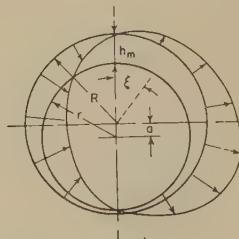
FIG. 1. High shear self-centering rotational viscometer.

$h_m/(R - r - a)$, where h_m = maximum thickness of the annulus between the cylinder; ψ equals $(R - r)/r$; and $x = a/(R - r)$. It will be seen that the force causing centering of the bob is proportional to the viscosity of the material being measured and the angular velocity of rotation of the bob, and that it is a function of the radii of outer and inner cylinders and their degree of eccentricity.

The vectorial forces applied to an eccentric bob are illustrated schematically in Fig. 2 for an instrument with an uninterrupted annular space. It must be noted that there exists some practical lower limit of velocity of rotation and viscosity below which the centering forces will

not function sufficiently to be effective. However, these limits are relatively low, and with the present instrument are equivalent to a shearing stress of less than 5 g./cm.².

For the contemplated study of the brushability/viscosity relationships of paints, a slight modification was made in the instrument. This



$$\frac{dp}{d\xi} = \frac{6\eta\omega \cdot (1 + x \cos \xi) - \alpha(1-x)}{\psi^2 (1 + x \cos \xi)^3}$$

FIG. 2. Forces causing centering of viscometer bob.

was the inclusion of two wells which introduce discontinuity into the annulus at the two ends of a diameter of the external cylindrical surface. This is illustrated in a top view of the apparatus in Fig. 3. This was done to achieve a closer approximation of the physical action of brushing. A brush has finite dimensions. Therefore, a viscometer in which the shearing stress is maintained on the test material for considerable periods or time, such as would be the case for the apparatus with unbroken

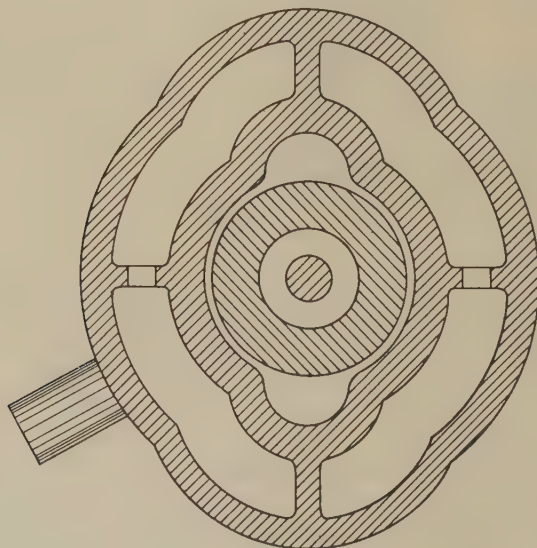


FIG. 3. Concentric cylinder viscometer with wells.

annulus, possibly would not provide the desired correlation with brushing, even if the appropriate high shear velocities were achieved. The centering forces for producing concentricity are not affected in a major way in the modified instrument, except that they correspond more closely to those existent in the band viscometer (1).

The rheological measuring system produced by the introduction of the wells differs considerably from that in a normal rotational device. Whereas in the latter the shearing stress is maintained on the test material throughout the time of measurement, in the present instrument the stress is substantially relieved twice for every revolution, corresponding to the two wells.

Although no extended attempts were made to substantiate the fact, no thixotropic hysteresis curves were observed for the paints tested. This was true even for materials which displayed a decided "puffiness" upon examination. The same apparent viscosity was obtained for a given test paint at a given shear velocity, whether the shear velocity gradient was approached from above or below. Repeated measurements of the same material at the same shear velocity also showed no decrease in viscosity of the test mass within the limits of error of the instrument. This is undoubtedly due to the fact that the shearing stress is momentarily relieved at the positions of the wells, allowing the rebuilding of viscous structure at these points.

Three oils, an SAE No. 10, an SAE No. 30, and a calibration oil for the Gardner Mobilometer having standardized viscosities of 0.595, 0.92, and 6.3 poises, respectively, were run on the instrument to test its linearity, and the theoretical clearance between the inner and outer cylinders was calculated. For the SAE No. 10 oil this calculated clearance was 3.50 mils; for the SAE No. 30, 3.54 mils; and for the calibration oil, 3.50 mils. The machined clearance of the apparatus was specified as 4 mils. The variations which were found between theoretical and specified clearances are probably due to the difficulty of actually measuring the very small differences in diameter of inner and outer cylindrical shearing surfaces.² There was excellent linearity between shearing

² The following considerations will show that these differences are not caused by the forces required to center the bob when the apparatus is not too far misaligned. It will be found that by application of simple force analysis a static force of less than 7 g. applied vertically to the bob will be required to center it if it weighs 100 g., when the distance between the centers of the universal joints is 15 cm. and the misalignment amounts to 1 cm. For 2 mm. misalignment this force is equal to about 1 g. The force will be manifested during measurement as extra weight required to produce a given shear velocity. At the high rates of shear used in the present study large forces are required to produce the desired rotational velocities. Therefore, this loss is relatively negligible, and becomes of the order of magnitude of the reproducibility of the measurements for even such serious misalignment as 1 cm.

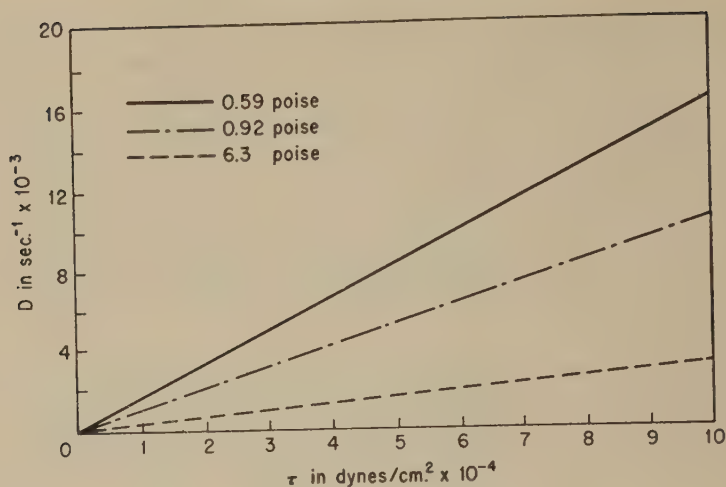


FIG. 4. Viscosity relationships for oils.

stress and shearing strain for these oils, as shown in Fig. 4, indicating laminar flow up to the highest shear velocity, which was 16,700 reciprocal seconds for the SAE No. 10 oil.³ These results were obtained even after the apparatus was deliberately thrown out of alignment by more than a centimeter, no differences in the measurements being observed. Were the bob eccentric, higher apparent viscosity measurements would have been observed, in accordance with the equations described previously for causing centering of the bob.

EVALUATION OF BRUSHING QUALITIES OF PAINTS

A series of four typical oil type house paints was submitted to two competent painters for rating of brushing qualities. These tests were performed in a constant temperature room at 77°F. The results are tabulated in Table I.

It is obvious that painter II is more critical of "stickiness" in brushing house paints than painter I. Painter II might have rejected all four

TABLE I
Rating of Brushing Qualities

Paint	Painter I	Painter II
A	Slightly sticky	Sticky
B	Sticky	Stickiest of lot
C	Good	Slightly sticky but best of lot
D	Slightly sticky	Sticky

³ The authors feel that this linearity obviates an analysis by Reynolds numbers which, in view of the design and of the nature of the systems measured, would be impractical.

paints on this ground, while painter I would have rated at least one paint, paint *C*, as entirely acceptable from the standpoint of brushing. However, it is interesting to note that in spite of the difference in opinion as to whether the brushability was good or poor both painters rated the paints in the same order. Both rated paint *C* as best of the series, *D* and *A* intermediate, and *B* poorest.

Following the practical brushing tests, the viscosities of the house paints were determined on the new high shear viscometer. The determinations again were made at 25°C. (77°F.), the temperature used in the practical brushing tests. The shearing stress which could be applied on the bob of the instrument was limited by the fact that the dimensions of the current model were chosen on the large side, and at the moment only a standard Stormer frame was available. As a result the shear velocities obtained with paints having relatively high viscosities were somewhat below those desired for best correlation with painter opinion of brushability.

Shear velocities of 10,000 reciprocal seconds and higher are obtained readily with paints of lower viscosity. Higher shear velocities may also be obtained using paints having higher viscosities, either by reducing the dimensions of the cylinder or by modifying the frame to accommodate heavier weights.

In the earlier paper on the band viscometer (1) an apparently reliable empirical method was developed for extrapolation to high shear velocities. A straight-line relationship is obtained when the logarithm of the apparent viscosity as measured on the instrument is plotted against the reciprocal square root of the shear velocity. The viscosity of the material up to infinite shear velocity may be obtained graphically by extrapolating the reciprocal function of the shear velocity to zero. It should be pointed out that this "viscosity at infinite shear velocity" is a convenient mathematical point which cannot be attained in practical measurements. Figure 5 shows such a plot for the paints *A*, *B*, *C*, and *D* rated previously by the two painters. Two more curves are included for paints identified as *E* and *F* which were brushed out by painter I only and rated "sticky" for paint *E* and "very good" for paint *F*. The brushing range shear velocities are indicated by the shaded areas. Here, too, no sudden break occurs in the graphs up to the highest shear velocities measured, indicating that these measurements were still carried out under laminar conditions.

It will be noted that, besides their position relative to each other with respect to viscosity, the structural breakdown of the various paints with increasing shear velocities varies considerably. Structural breakdown seems to be least rapid with paint *E*, while *B*, *C*, and *F* show considerable decrease in viscosity with increased shear velocity. *A* and *D* are intermediate.

The empirical equation for these curves is:

$$\eta = \eta_{\infty} e^{SD^{-\frac{1}{2}}}$$

where η is the apparent viscosity at any given shear velocity D ; η_{∞} is the apparent viscosity at infinite shear velocity; and S is a function of the structure of the rheological system. Values of $S = 0$ designate a Newtonian liquid, while increased S denotes increasing structure.

The curves demonstrate that the instrument classifies the paints in an order which corresponds very well with the brushability ratings made by the painters. The danger of determining brushing viscosities by means of viscometers at any other than the brushing shear velocities also becomes apparent. This is shown most convincingly in curve C . Were

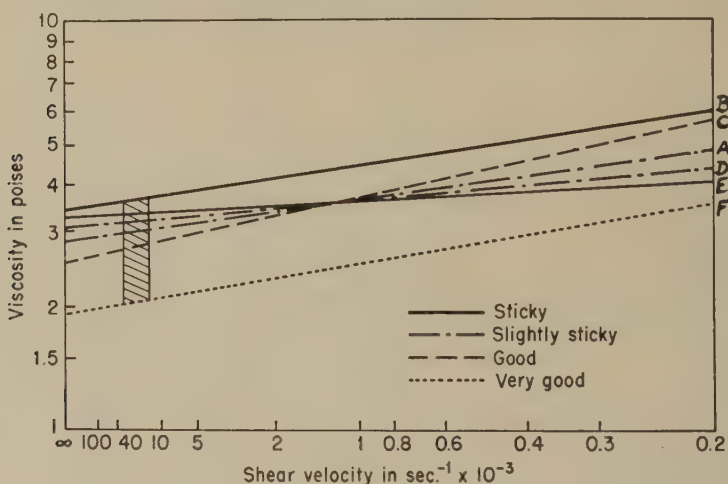


FIG. 5. Viscosity characteristics of house paints.

the viscosity of the paint measured at the low shear velocities obtainable in most commercial rotational viscometers, at the right hand limit of Fig. 5, this paint would have been classified as being almost as poor as paint B . Actually it is the second best of the series, being better than even A and D in brushing characteristics. Paints E and F also fall in very well with their painting ratings. The relatively low viscosity of F in the brushing range shear velocity indicates very good brushing qualities, while E corresponds closely to A and C in this characteristic.

Similar tests were conducted using oil-type flat wall paints, porch and floor enamels, and household enamels. Again the correlation between painter rating and instrument rating was good. The instrument can separate two paints which are relatively close in viscosities, where the painter would have considerable difficulty in differentiating as to brusha-

bility. As might be expected, the acceptable brushing ranges of viscosity are somewhat different for the various types of paint.

The viscosity/temperature characteristics were found to correspond closely to the classical oil viscosity/temperature relationships. The graphical representation of logarithm of viscosity plotted against the reciprocal of the absolute temperature gives a straight line. Paints about double in viscosity in the high shear range when their temperature falls from 105°F. to the 65–70°F. range, resulting in considerable change in brushing characteristics.

FLOW PROPERTIES

It may appear that paint application problems could be solved very simply by keeping the viscosity below certain maximum values. However, there are other properties which are involved. A wall paint, for example, should not sag or curtain due to too free flow on the one hand, nor retain too pronounced brush marks due to poor leveling qualities or too little flow on the other. In some cases a compromise must be made in ease of brushing to obtain a paint having most acceptable all-around properties. Flow properties of paints seem to be related to the slope S of the rheological curves. It is conceivable that a relationship will be established between the structure of paints at low shear velocities and their viscosities at high shear velocities.

There are certain addition agents available to the paint industry which are capable of altering the leveling characteristics of some paints. In some cases this is accomplished by reducing the degree of rheological structure to improve flow. In other cases they increase the structure to reduce sagging or curtaining. The brushing properties often remain substantially unaltered. The effects of additions of such agents may be studied using the high shear viscometer. It is often found that the slopes of the viscosity/shear velocity curves with agents added differ significantly from those of the same paints with no agent added. At the same time the viscosities in the brushing shear velocity range may be very similar. This will correlate very well with the brushing properties.

The slopes of the curves again are proportional to the rheological structure of the paints. Further work is being done to determine the physical meaning of this difference in slope as well as the theoretical treatment of the rheology of paints and paintlike materials as revealed with the high shear viscometer.

REFERENCES

1. WACHHOLTZ, F., AND ASBECK, W. K., *Kolloid-Z.* **93**, 280 (1940); *ibid.* **94**, 66 (1941).
2. NEEDS, S. J., Symposium on Methods of Measuring Viscosity at High Rates of Shear. A.S.T.M. Special Technical Publication No. 111, 24.
3. GÜMBEL, L., AND EVERLING, E., *Reibung und Schmierung im Maschinenbau*, 1st Ed. 110–116. Berlin, 1925.

THE BAND VISCOMETER¹

Harry H. Hull

R. R. Donnelley & Sons Co., Chicago, Illinois

Received January 28, 1952

INTRODUCTION

Deviations from Newtonian flow may be expressed as functions of two primary variables: total displacement in shear and rate of displacement in shear. When the deviations from Newtonian flow are studied primarily in terms of the total displacement in shear, the result is a study of elasticity, thixotropy, and possibly dilatancy. When the deviations are studied in terms of rate of shear, the result is a study of plasticity or pseudoplasticity. The rotational cup viscometer and the band viscometer are designed for the second type of study and the effects of elasticity and thixotropy are minimized by keeping displacement in shear large and hence beyond that required to attain a steady state.

The band viscometer, first described by Wachholtz and Asbeck, is not well known and has not been applied by others to rheological studies at high rates of shear. This is unfortunate for the band viscometer has four important advantages: the sample is subjected to a uniform shearing force throughout; the heat energy formed in the sample during testing is dissipated efficiently; it operates effectively at rates of shear to 10,000 reciprocal seconds, which is higher than the more commonly used rotational cup viscometers; and it is a quick test and the instrument is easy to clean.

A band viscometer modeled after that of Wachholtz and Asbeck was constructed for the study of inks. It was found necessary to increase the clearance between the tape and the block to minimize errors caused by variations in tape thickness. This in turn made it necessary to install an automatic timing device which measures time intervals to 0.01 sec. This viscometer is now being used to study the rheology of inks and other similar materials.

APPARATUS

The viscometer is shown in the photograph, Fig. 1. The various parts of the apparatus are:

1. Shear blocks as shown in Figs. 2 and 3 are made of stainless steel and hardened. These blocks must be carefully made in two respects: the first is that the contour of the

¹ Presented at the Annual Meeting of the Society of Rheology, Chicago, Illinois, October 24-27, 1951.

inlet must be precisely made and the second is that the shearing surfaces be flat. A good lapped surface will be flat to within 0.00001 in. This can be conveniently tested by light interference methods.

These shear blocks (*a*) are held apart by 0.006 in. brass shims (*b*) $\frac{3}{4}$ in. wide. The blocks are held together by nuts tightened with a torque wrench. It is necessary to



FIG. 1. Band viscometer.

thermally insulate these shear blocks from the mounting structure. This is done by placing the following in the mounting: a section of glass cloth (*c*), a $\frac{3}{4}$ -in. brass block through which water (*d*) is circulated, and then a block of $\frac{1}{2}$ -in. fiber board (*e*).

The design of these shear blocks can be improved by making them longer to eliminate the front plate, by making the well deeper by adding $\frac{1}{4}$ in. to the blocks, and possibly by building in the shims minimizing cleaning time.

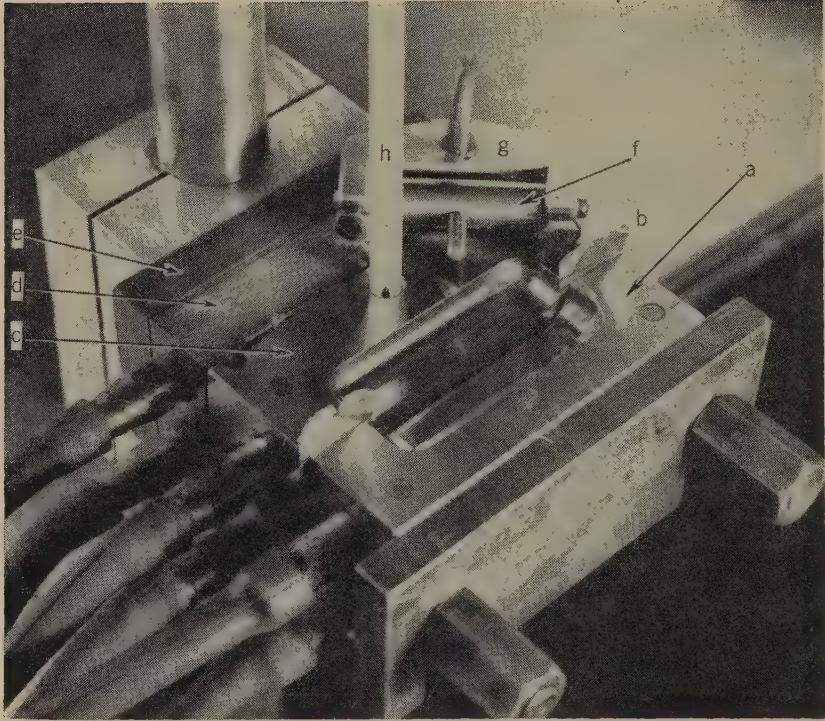


FIG. 2. Shear blocks for band viscometer.

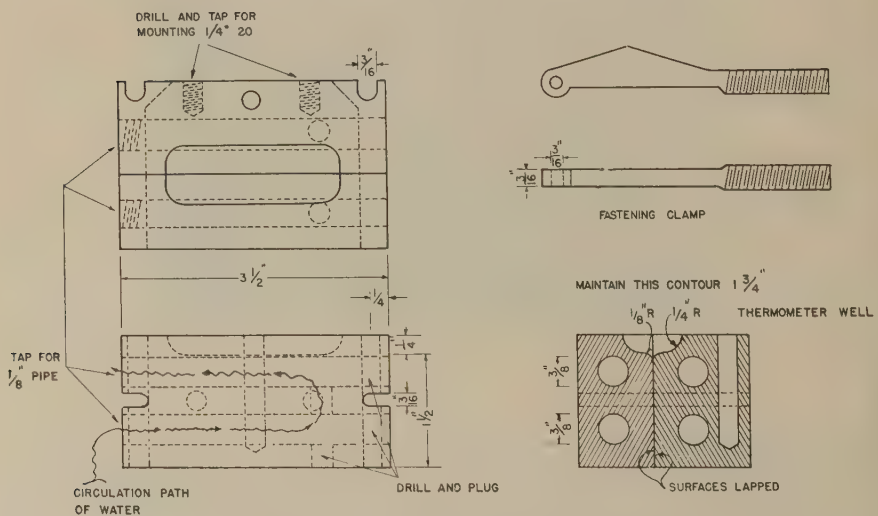


FIG. 3. Shear blocks for band viscometer.

2. Constant temperature water bath with circulating pump such that the temperature of the shear block is controlled within $\pm 0.05^\circ\text{C}$. is necessary (thermometer *L*, Fig. 3).

3. The timing unit consists of a clock (S-1 Standard Electric Time Co.) operated by the circuit shown in Fig. 4. This times to within 0.01 sec. The starting and stopping mechanism is a small metal bead mounted on a linen fish line. This passes over two split metal pulleys (*W1* and *W2*), the two halves of which are electrically insulated from each other. Shorting these halves operates the relays (*R1* and *R2*) which start and stop the clock.

4. The tape (Kodapak No. 200 rigid formula 120, manufactured by Eastman Kodak Co.) is 1- $\frac{1}{2}$ in. wide and 0.002 in. thick and is made of cellulose acetate. This tape is not of uniform thickness, and it would be very desirable to obtain better tape. However, it is sufficiently uniform to give reproducible results when there is a clearance of 0.002 in. between each side of the tape and the shearing blocks.

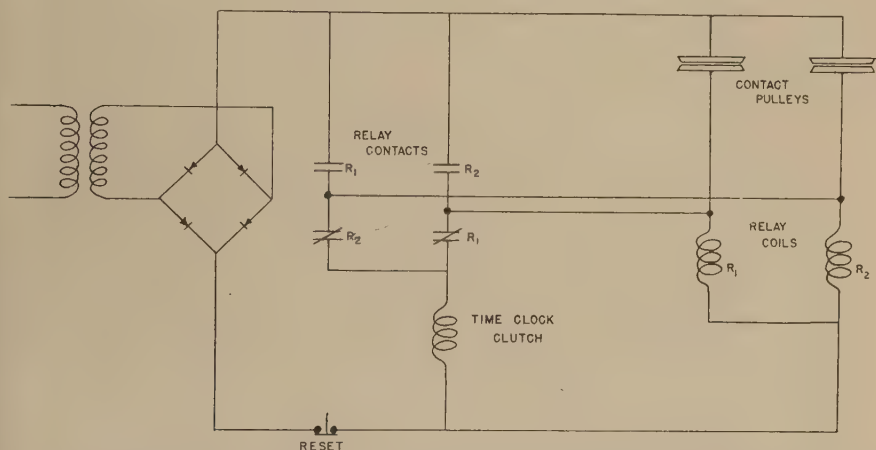


FIG. 4. Timing circuit for band viscometer. A small metal bead placed on the string which passes over the two pulleys shorts the two halves operating the relays.

The tape is fastened at the top to the previously mentioned fish line by an ordinary photographic film clamp and at the bottom by a specially made clamp on which various weights are hung. The latter clamp is shown in Fig. 3, and consists of a small eccentric (*f*) which on turning will force the film against a flat side (*g*), holding the tape by a wedging action.

RESULTS

Figure 5 shows the force rate of shear curve obtained with two near-Newtonian fluids, oil OB-4 from the National Bureau of Standards, and polybutene No. 24 from the Oronite Chemical Co., San Francisco. Rate of shear is a straight-line function of force for the lower portion of the curve; however there is a slight curvature upward at the higher rates of shear. It is not known whether this is a characteristic of the fluids or of the instrument. If the upward curve is caused by frictional heating, decreasing the thickness of the fluid film by using thinner shims should straighten out the curve.

Figure 5 also shows the curve obtained with Silicone 200 fluid, viscosity 30,000 centistokes at 25°C. This is much more non-Newtonian than the previous materials and none of the curve is linear.² Unusual difficulty was experienced in checking results particularly at the higher rates of shear. Normal spread between four readings is about 2% while

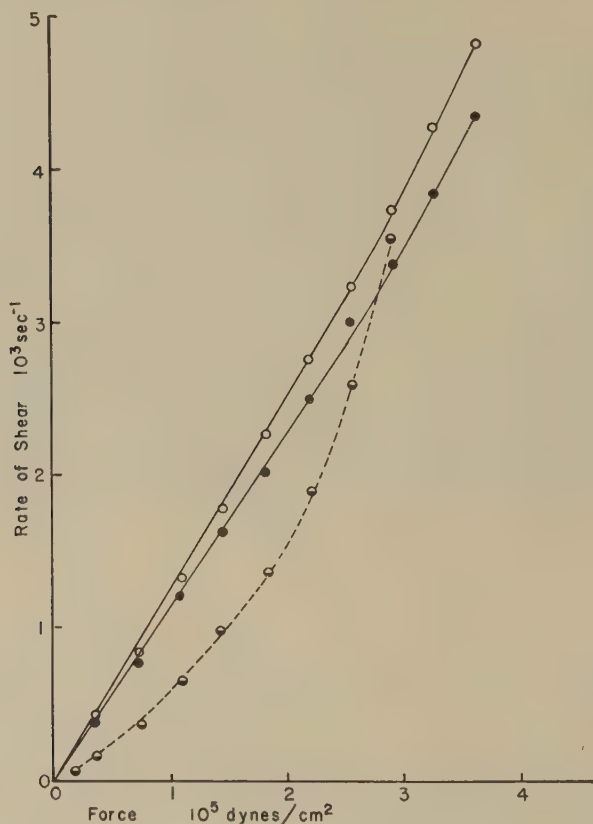


FIG. 5. Band viscometer curves of near-Newtonian and non-Newtonian liquids. Temperature 35°C. —○— Polybutene.
—●— Bureau of Standards oil OB-4.
---●--- Silicone 200 fluid.

these showed a spread of 10%. A possible explanation of this is that a longer time is needed to reach equilibrium velocity than normal, and hence it was not reached in the space allowed.

² A similar result was obtained by Lower, Walker, and Zettlemoyer, as reported at the Amer. Chem. Soc. Fall Meeting, New York, 1951; see also Weltmann and Kuhns, this volume.

Figure 6 shows the curves from a set of four color oil inks. Since these are printed over each other without drying between, their consistencies must be from heaviest to lightest in the order of printing. This order of yellow, red, blue, black is clearly shown by these curves.

This instrument has been used to study materials with a consistency range of 5 to 1000 poises satisfactorily. The maximum rate of shear reached

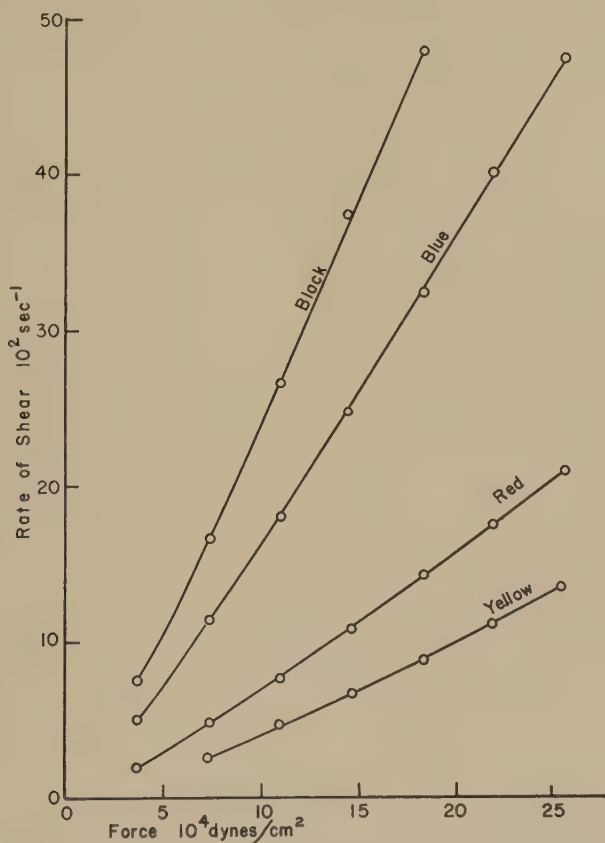


FIG. 6. Consistency curves: drying oil inks, process colors for "wet" printing. Temperature 35°C.

is limited by the strength of the tape for the more viscous materials. The tape will support approximately 12 kg. (a force of 4.3×10^5 dynes/cm 2). For the less viscous materials the rate of shear is limited by the physical dimensions of the apparatus, for allowance must be made for distance to reach equilibrium velocity and increased distance must be allowed to give precision to the timing device. There are a few materials which do not feed into the viscometer properly. This is evident on inspection of the

tape for there will be areas which are not covered. The greases are an example of a material which gave this trouble. Some mechanical feeding device should aid in the study of these materials.

CONCLUSION

A band viscometer similar to that of Wachholtz and Asbeck has been constructed. It has been found useful in evaluating the consistencies of non-Newtonian materials particularly at the higher rates of shear and where large numbers of tests must be run. The tests are not time consuming and the instrument is easily cleaned.

REFERENCE

- WACHHOLTZ, F. V., AND ASBECK, W. K., *Kolloid-Z.* **93**, 280-97 (1940); *ibid.* **94**, 66-81 (1941).

THE RHEOLOGY OF BLOOD. A SURVEY

Alfred L. Copley^{1,2}

*Department of Medicine, New York Medical College, New York, New York
and Marine Biological Laboratory, Woods Hole, Mass.*

Received January 28, 1952

Blood is a very special organ, consisting of a complex of cellular elements suspended in a fluid phase, plasma. In both its cellular and plasmatic components, blood constitutes an assortment of vehicles of transport, and in its behavior is anomalous as compared to other organs. The cellular elements and the plasma circulate at various velocities. Physiologically, the cellular components are not cemented to each other, but move as single, separate bodies. The complexity of blood as a rheological system is augmented by the great variety in the size, shape, and functions of pathways through which it flows, after continuously being pumped through this intricate system of endothelial-lined channels by the action of the heart.³

Papers on the rheology of blood are scarce and have not been properly connected in textbooks or manuals dealing with blood or the blood circulation. Rheological phenomena have been described mainly in connection with some other investigation. Reviews on the viscosity of blood deal largely with data on apparent viscosities. The relative paucity of rheological treatments of blood is contrasted by the large number of observations of rheological phenomena of this humor. In a recent survey of biorheological problems a brief summary of the rheology of blood was given (1).

THE ANOMALOUS FLOW PROPERTIES OF BLOOD

Van Leeuwenhoek (2) was the first to describe, in 1699, the circulation in capillary blood vessels and found apparently "clotted" red cells in stagnated tadpole blood. After the flow of blood resumed, the "clotted"

¹ Recent studies performed under Contract No. AT(30-1)-780 of the Atomic Energy Commission and Contract No. N7onr-40102 of the Office of Naval Research, Department of the Navy.

² Presented at the Annual Meeting of the Society of Rheology, Chicago, Illinois, October 24-27, 1951.

³ Blood rheology or "hemorheology" is concerned with deformation and flow properties of cellular and plasmatic components of blood in macroscopic, microscopic, and submicroscopic dimensions, and with the rheological properties of vessel structure with which blood comes in direct contact.

red cell masses were seen to break into smaller particles and appeared to be clusters or aggregations of red cells. This phenomenon has been observed ever since by many students of the capillary circulation in different animals.

In 1846, fundamental investigations by the physiologist and physician Poiseuille laid the foundation of rheology. Poiseuille (3a) was concerned with the causes of the flow of blood in capillary vessels and realized that great differences exist in the composition of blood capillary systems with regard to the extent and diameter of these minute vessels. He noted that the intensity of the contraction of the heart varies, causing variations in blood pressure, and that parts of the body are subjected to different temperatures because of their positions. His search for an understanding of the flow of blood through living vessels of very small diameter led Poiseuille to his famous study of the effects of capillary pressure, length, diameter, and temperature.

In our studies on the flow of blood in 1941 (4), we applied Bingham's concepts of pseudoviscosity and yield value. We established, by the use of a modified falling-ball viscometer at several stresses, that the flow of blood does not conform to the Newtonian equation, and concluded that, in general, the Bingham treatment characterizes the anomalous flow properties of blood. We further found that the physiological anticoagulant heparin tends to increase the fluidity of blood and plasma, although no satisfactory explanation can be offered. Our findings of thixotropy in heparinized blood (4,5) emphasize the complexity of this phase of the problem.

THE FLUIDITY OF BLOOD

Bingham (6,7), following earlier work by Hess and others (1,8), introduced an empirical relation for the fluidity of blood, based mainly on observations by several investigators in the beginning of the century, which he expressed as $\Phi = 53 - 0.24 H$, where Φ is the reciprocal viscosity and H is the amount of hemoglobin. His formula needs further experimental proof because the hemoglobin determinations are open to criticism (1).

Bingham and Roepke (6) believed that single red blood cells must possess a rather high mobility in their interior. With Hatschek, (8) they regarded red cells rheologically not as solid particles but rather as an emulsion with a high fluidity of the internal phase. Many observers have watched the deformation of a red cell as it actually squeezes its way through very narrow lumina of certain capillary vessels or even through interendothelial spaces in the capillary wall.

Denning and Watson (9) observed that the fluidity of the blood is decreased in narrow capillary tubes, but Fahraeus and Lindquist (10) found it to be increased in capillary tubes of about 0.3 mm. diameter.

Fahraeus (11a) noted that a suspension of blood corpuscles becomes diluted in streaming through a capillary tube of small diameter. These differences were already explained by Duncan and Gamgee in 1871 (12) who found the rate of flow of freshly drawn noncoagulated blood through tubes of narrow diameter to be much greater than that of defibrinated blood. In the latter system the corpuscles tend to aggregate and thus hinder the flow of blood, as first observed by Poiseuille in 1847 (3b).

Blood is generally considered to flow in the body in streamlines; however, turbulence can arise in the large blood vessels and in the heart. Lampport (13) considered blood at high flow rates to behave as though "slippage" occurs, the central streaming red cells, with their longer dimension oriented axially, being distinct from the surrounding plasma sheath.

BLOOD VESSEL SYSTEMS AND HEMODYNAMICS

The study of hemodynamics concerns the interrelationship of blood flow and pressure through blood vessels, and the effect of various agents which produce changes in the circulation. Thus it is concerned also with rheological properties of vascular walls, the lumina and length of vessels, and the way they are interconnected. The development of pressure and surface recorders has contributed to the knowledge of the arterial pulse. The varying elasticity coefficient of the arterial wall makes even carefully obtained surface records an inadequate representation of the actual pressure changes. Venous constriction can increase resistance to flow toward the heart, as demonstrated by Hooker (14) in nervous reflex responses, or according to Fleisch (15) following chemical stimuli. Findings by Pappenheimer and Soto-Rivera (16) indicate that stretching of a vein by internal pressure does not reduce venous resistance considerably. Bazett (17) contends that, upon maintaining an average capillary pressure of about 20 mm. Hg, the rate of blood flow from the arteries to the capillaries varies according to the excess of arterial pressure above the capillary pressure. Reuterwall (18) considered the elasticity of human arteries to be dependent upon passively elastic structures and the active contractility of smooth muscles. We showed that under certain stresses capillary vessels may have a high degree of elasticity, while in others the same stresses may result in deformation or bulging of the vessel wall which form so-called microaneurysms,⁴ which also occur in human pathology in certain diseases.

SHAPE CHANGES OF RED CELLS

The classic controversy about two prototypes of the mammalian red cell, the balloon-like structure with a fluid interior and a body with a structure in its interior, has now been superseded by a new approach

⁴ Unpublished data.

concerning shape transformation from disk to sphere which often is reversible. A remarkable phenomenon was described in 1897 by Hamburger (19) who observed under the microscope that the mammalian red cell in the absence of serum or plasma, but suspended in sodium chloride solutions, appears as a perfect sphere, and that the addition of plasma or serum reconverts the sphere into its original biconcave discoid shape. Numerous developments following Hamburger's discovery have been reviewed by Ponder (20). He distinguishes tentatively between a surface and an interior ultrastructure where the intimacy in which the hemoglobin molecules are situated with respect to one another, constitutes the most striking feature.

In certain individuals, e.g., American Negroes, the red cells undergo reversible changes, from the normal biconcave discoid form to shapes like crescent moons or sickles, in sickle-cell anemia. This sickling phenomenon may occur *in vitro* without an associated pathology (sickle-cell trait) by lowering the oxygen tension, and has been observed in deer and elks (20). Pauling *et al.* (21) termed sickle-cell anemia a "molecular disease," associated with the state and nature of the hemoglobin within the erythrocyte. Other investigations point to solubility changes in the presence of excess glutathione (53). In the patient, the sickling increases the blood viscosity and causes a clogging of capillaries, followed by a breaking up of the fragile sickled cells.

THE SEDIMENTATION OF RED CELLS

Fahraeus (11b) studied the occurrence of increased sedimentation rate of red cells, a phenomenon known in ancient medicine, and developed the erythrocyte sedimentation test. He applied Stokes's law to the sedimentation rate of red cells; although the sinking velocity of the single particle would be sufficiently small, he neglected the fact that the suspension fluid should be of infinite extension in relation to the moving particle. In applying this law, he thus could obtain only an approximate idea either of the individual sedimentation velocity, or of the corpuscle aggregates in different cases, viz. of the degree of "agglutination" which he considers to be identical with rouleaux formation of erythrocytes. Fahraeus found that strong "agglutination" is produced by the globulins of the plasma, that fibrinogen has an even stronger effect, and that albumin aggregates the corpuscles only to a small extent.

INTRAVASCULAR CELLULAR AGGREGATION AND AGGLUTINATION

Since van Leeuwenhoek's (2) observations, the phenomenon of intravascular red cell masses has been reported by numerous investigators. According to Flexner (23), the *in vivo* agglutination of red cells is not uncommon in infectious diseases in man and animals. Various kinds of

circulating or embolizing red cell masses were observed by Knisely *et al.* (24) which were of different sizes and appeared to undergo various deformations when passing through the different-sized vessels of the capillary bed. They also appeared to produce considerable lowering in the fluidity of blood.

Lutz (25) does not consider the findings of Knisely *et al.* as acceptable evidence for the existence of true red cell agglutination emboli. Lutz, Fulton, and Akers (26) found that, when a mass of so-called "sludged"⁵ blood approaches a capillary, individual red cells peel off from the mass and pass through the capillary separately. Sufficiently high magnification was used to distinguish the individual cellular elements.

MIGRATION AND SHAPE CHANGES OF WHITE CELLS

As a result of slowing of the blood stream, white cells are long known to move out of the central core to the vessel walls, preceding their emigration, and that their active penetration through the wall is dependent upon ameboid movement. New light on these properties of the white cells has been shed by electron microscopic studies which are summarized by Bessis (22).

BLOOD CLOTTING

The most striking and longest known property of blood occurs both *in vivo* and *in vitro*. It demonstrates the difficult problem nature had to solve in supplying a medium for a highly organized animal that would circulate through the body while remaining fluid, and that would clot promptly after the vessels were injured.

(a) Cellular Clotting and Platelet Agglutination

The blood of the horseshoe crab does not contain coagulable protein or fibrinogen. We have confirmed Leo Loeb's descriptions (27, 28a) of two phases of the clotting of amebocytes, the only blood cell of this primitive animal. After agglutination of these cells, gelation of the whole blood sample occurs. A peculiar process in crustacean blood clotting is associated with Hardy's "explosive corpuscles" which break suddenly into pieces, releasing granules and initiating a coagulation process of several observable steps (29, 30).

In mammals the phenomenon of platelet agglutination is closely associated with the arrest of hemorrhage or hemostasis and with thrombosis. Copley and Houlihan (31) demonstrated in 1945 that the process of platelet agglutination is independent of fibrin formation and is brought about by agglutinant agents which reside in plasma globulins.

⁵ The term "sludge," introduced by Knisely *et al.* (24) for red cell agglutinates, is not particularly useful, unless it does not distinguish between reversible aggregation and irreversible agglutination.

(b) *Fibrin Formation and Plasma Gelation*

Numerous observations have been made in the process of fibrin gel formation. Newer observations by Ferry and Morrison (32a) led them to postulate that the fibrinogen rodlets unite end to end to form strands with lateral associations forming bundles to varying degrees. These authors consider the fibrin formation as a polymerization process in which the polymer fibrin is usually cross-linked, because of a rigid gel formation, even though a solution may contain as little as 20–40 mg. fibrinogen/l. The monomer molecule is of a very large size, about 35 A. in diameter and 700 A. long, and has a molecular weight of about 500,000 (33). Thus the size of the monomer molecule is extremely large compared to any chemical group on its surface which may be responsible for intermolecular linkages during fibrin formation.

Ferry and Morrison differentiate two independent problems in the fibrin polymerization process: the nature of the chemical bonds producing linkage of the fibrinogen units and the geometrical arrangement of these units in the fibrin structure. The latter arrangement is considered to determine largely the physical properties of the clot. They classified fibrin clots which range in properties between a fine clot which is clear, gelatinous, elastic, friable, and nonsynergetic, and a coarse clot which is opaque, plastic, nonfriable, and synergetic. The differences in rheological and other physical properties between "fine" and "coarse" clots studied by Ferry and Morrison (32b) suggest structural differences at a molecular level.

Very striking electron microscopic studies of clots, prepared from fibrinogen and thrombin, were made by Hawn and Porter (34) who concluded that fibrinogen molecules were polymerized by the action of thrombin to crystal-like protofibrils of needle shape, which become aligned by lateral association into fiber strands. Of interest are the conclusions of Morrison and Scudder (35), from their studies on very thin fibrin clots with the electron microscope, that such preparations do not represent a suitable measure of clot structure formed in bulk solution, under the same conditions.

Edsall reviewed the recent literature on plasma proteins and their fractionation (36). Estimation of molecular weights and axial ratios for many of the plasma fractions involved have been made on the basis of studies of viscosity, sedimentation constant, osmotic pressure, and partial specific volume of plasma fractions by Oncley *et al.* (37). The shapes of the molecules vary from the very large, practically spherical β_1 -lipoprotein to the thin molecule of fibrinogen.

In 1879 Hammersten (38) and recently Laki and Mommaerts (39) considered the fibrinogen-fibrin transition as a two-stage process, in which, according to Laki (40), in the first step thrombin acts enzymatically

and modifies the fibrinogen molecules, which polymerize to the fibrin clot in the second step. He contends that the polymerization is not an end-to-end association of the altered fibrinogen molecules, but that the latter polymerize to a unit with a particle weight of about 1.5 million and then build up the primary fibrils from these units, probably connected by electrostatic forces. That thrombin is not involved in the polymerization process is supported by the findings of Mihalyi (41), since fibrin and fibrinogen dissolved in 30% urea exhibit the same relative viscosity. Waugh and Livingstone (42) found that at the time when a solution containing fibrinogen and thrombin gellates and the first fibrin strands become visible, only a part of the total fibrin has been incorporated into the clot-structure, while the remainder exists as unattached fibrin strands or activated fibrinogen.

The transformation of the sol fibrinogen into a precipitate of fibrin particles is generally considered the second phase of blood coagulation, the first one being the thrombin activation phase. A third phase of blood coagulation, the gelation phase of plasma, was recently postulated by Copley (28*b*) and is based on observations that fibrin particles in plasma do not necessarily form a gel. Such gel formation may not occur in hemophilic or heparinized plasma, although fibrin particles are present. The formation of a plasma gel or whole gel is enhanced by an accelerating factor, termed "geloplastin," in tissue juice,⁶ as well as by minute amounts of calcium ions (28*c, f*). Heparin, which is an inhibitor in the first and second phases of blood coagulation, also inhibits the third or gelation phase.

These new findings do not fit in the generally accepted concept that the gelation of plasma is due solely to the conversion of fibrinogen to fibrin. There appears to be a difference in the formation of a fibrin gel prepared from (*a*) isolated fibrinogen with the addition of thrombin and (*b*) from the gelation of whole blood or plasma. Therefore some doubt may be raised as to whether or not the thrombin and the fibrinogen as they occur normally in native blood are identical to the fibrinogen and thrombin preparations available today.

ADHESION, SYNERESIS AND FIRMNESS OF BLOOD CLOTS

Coagulation thrombi, produced by Copley and Stefko (43) in arterial and venous segments in the living dog, were nonadherent to the vessel wall and exhibited syneresis. These observations offer evidence that a non-adherent, syneretic coagulum which forms within a noninfected artery or vein is significant because of the potential danger for the genesis of thromboembolism.

⁶ Unpublished data.

Studies⁴ on clot firmness of the blood of the dogfish shark (*Mustelis canis*) and of three invertebrates, the horseshoe crab (*Limulus polyphemus*), the spider crab (*Libinia*), and the lobster (*Homarus americanus*), have been made in special viscometer tubes (28*d*). The positive air pressure needed to deform and to force blood gels, plasma gels, or cell agglutinates through narrow portions of these tubes was taken as an index of clot firmness. In scrupulously cleaned glass tubes, gelation times of dogfish blood or plasma have been as long as 2 days, a phenomenon which has not been observed with other animals in whole blood or plasma contacting glass surfaces. Dogfish blood gels which were adhesive to glass and cork exhibited very low firmness. Addition of calcium ions tended to increase their firmness. Higher values for firmness were obtained in synergetic gels. Homologous muscle tissue extracts produced a very great shortening of gelation time with marked increase in gel firmness. The firmness of the blood cellular agglutinates from all three invertebrates is much greater than that of their whole blood gels.

Mammalian blood was treated with large amounts of heparin, used as a platelet agglutination-promoting agent as well as a plasma gelation inhibitor. Platelet agglutinates produced in this manner exhibited a very high degree of firmness.⁴ These findings are in striking contrast to our earlier studies of firmness of blood gels which formed when minute amounts of heparin were used. The extreme increase found in clot firmness of dog blood gels following major abdominal surgical operations we consider to indicate increased hemostatic function of the blood (44).

Comparative studies of clot firmness and syneresis contacting foreign surfaces in dog blood were made by Copley (28*d*). No syneresis occurred in lusteroid-lined tubes, and various degrees of syneresis were obtained in tubes lined with paraffin. Nonsyneretic blood gels often showed higher degrees of clot firmness than syneretic gels. The general contention, as found in the biological and medical literature, that strengthening of the blood coagulum is always produced by syneresis, could not be corroborated.

Studies by Burstein (45) on the compressibility of citrate plasma gels showed variations in different mammalian species. The rate of gelation and the amount of fibrinogen are important factors, while platelets are not involved. In his studies on the effect of ultrasonic waves on platelet-free citrate plasma gels, Burstein (45) found different types of syneresis. They were transparent upon the addition of thrombin, while thrombin with calcium made them more opaque, more dense (with regard to filament formation), and more syneretic. Calcium alone, which also gives a delayed gelation, resulted in a less syneretic and more densely appearing gel. Controls of spontaneous syneresis of platelet-free citrate plasma gels show no retraction.

Morrison and Seiler (46) described two procedures for the quantitative determination of adhesion in fibrin clots. In studies of the influence of various surfaces they found good adhesion to metals, suggesting that electrostatic forces were important in the binding. They interpreted their findings of good adhesion to substances such as Lucite as showing that nonpolar interaction can be effective.

A new procedure for the quantitative measure of syneresis in fibrin clots has been developed by Morrison (47a). He interpreted his findings on the retardation of syneresis by cryoglobulin, by citrate, and by small amounts of calcium, in terms of greater or lesser crosslinking of adjacent fibrin strands. He pointed out (47b) that "spontaneous syneresis" and "syneresis under pressure" are different phenomena.

BLEEDING AND HEMOSTASIS

A number of rheological factors are involved in hemostasis which may be summarized under platelet agglutinability, blood coagulation, vasomotion, as well as adhesiveness and firmness of such minute blood plugs which seal breaks in the injured vessel wall. The bleeding in capillary hemorrhagic diathesis is considered to be due to increased fragility of blood capillaries and impairment of hemostasis (48a).

The fragility of blood capillaries is mainly tested by physical methods using negative and positive pressures (49). We found⁷ by applying special minute suction cups to capillary vessels that their walls are stretched beyond their elastic limit, resulting in extravasation of blood into the supporting structures surrounding the blood vessels. The degree of breaking strain necessary to produce capillary hemorrhage differed widely in human beings and animals.

A number of rheological phenomena, described by Copley and Lalich (50, 51), can be readily observed as the blood emerges from the inflicted wounds into the saline bath. A rheological *in vivo* test, named "clot resistance," estimates both the firmness of the clot and its ability to adhere to the vessel wounds, and is a clinical measure for hemostasis. We applied this test to various mammals which were exposed to high ionizing radiation in the lethal range (28e) and found impaired hemostasis as early as 3 hr. following exposure. Thus far, this test appears to be the only one which may detect at an early date radiation injury. Prolonged bleeding times, also indicative of impaired hemostasis, were rarely found before the fifth post-radiation day (48b).

In visceral and cutaneous capillary beds of various mammals, numerous rheological observations have been made with a new method permitting clear visualization of circulating platelets, by employing a microscopic method of oblique illumination (52) hitherto not applied to biological

⁷ Unpublished data.

systems. During the first few days following exposure of various mammals to high ionizing radiation, platelets appeared to agglutinate readily, contributing to their diminution commonly found in radiation injury. Around the ninth post-radiation day, platelets tended not to agglutinate. Aggregated platelets were seen to be washed away one at a time by the passing blood stream (48b).

REFERENCES

1. COPLEY, A. L., *Proc. Intern. Cong. Rheology, Holland* **1**, 47; **3**, 8 (1948).
2. LEEUWENHOEK, A. v., *Phil. Trans.* **22**, 447 (1700). (Spelled Lewenhoeck in the original paper).
3. POISEUILLE, J. L. M., (a) *Sci. math. et phys.* **9**, 433 (1846); (b) *Ann. chim. phys., 3e série* **28**, 76 (1847).
4. COPLEY, A. L., KRCMA, L. C., AND WHITNEY, M. E., *J. Gen. Physiol.* **26**, 49 (1942).
5. COPLEY, A. L., *Science* **94**, 543 (1941).
6. BINGHAM, E. C., AND ROEPKE, R. R., (a) *J. Gen. Physiol.* **28**, 79, 131 (1944-45); (b) *J. Am. Chem. Soc.* **64**, 1204 (1942).
7. BINGHAM, E. C., (a) *J. Gen. Physiol.* **28**, 605 (1945); (b) Personal Communications (1943-44).
8. HATSCHKE, E., *Die Viskosität des Flüssigkeiten*, Th. Steinkopff, Dresden, 1929.
9. DENNING, A. D. P., AND WATSON, J. H., *Proc. Roy. Soc. (London)* **B78**, 328 (1906).
10. FAHRAEUS, R., AND LINDQUIST, T., *Am. J. Physiol.* **96**, 562 (1931).
11. FAHRAEUS, R., (a) *Physiol. Revs.*, **9**, 241 (1929); (b) *Acta Med. Scand.* **55**, 1 (1921).
12. DUNCAN, J. M., AND GAMGEE, A., *J. Anat. Physiol.* **5**, 150 (1871).
13. LAMPORT, H., *Federation Proc.* **8**, 90 (1949).
14. HOOKER, D. R., *Am. J. Physiol.* **28**, 235 (1911).
15. FLEISCH, A., *Arch. ges. Physiol. (Pflügers)* **228**, 399 (1931).
16. PAPPENHEIMER, J. R., AND SOTO-RIVERA, A., *Am. J. Physiol.* **152**, 471 (1948).
17. BAZETT, H. C., *Am. J. Physiol.* **149**, 389 (1947).
18. REUTERWALL, O. P., *Acta Med. Scand., Suppl. II* (1921).
19. HAMBURGER, H. J., *Arch. Anat. Physiol., Physiol. Abt., Arch. f. Physiol.* 137 (1897).
20. PONDER, E., *Hemolysis and Related Phenomena*. Grune & Stratton, New York, 1948.
21. PAULING, L., ITANO, H. A., SINGER, S. J., AND WELLS, I. C., *Science* **110**, 543 (1949).
22. BESSIS, M., *Blood* **5**, 1083 (1950).
23. FLEXNER, S., *Univ. Penn. Med. Bull.* **15**, 324 (1902).
24. KNISELY, M. H., BLOCH, E. H., ELIOT, T. S., AND WARNER, L., *Science* **106**, 431 (1947).
25. LUTZ, B. R., *Physiol. Revs.* **31**, 107 (1951).
26. LUTZ, B. R., FULTON, G. P., AND AKERS, R. P., *Circulation* **3**, 339 (1951).
27. LOEB, L., *Univ. Penn. Med. Bull.* **16**, 441 (1904); *Protoplasma* **2**, 512 (1927).
28. COPLEY, A. L., (a) *Federation Proc.* **6**, 90 (1947); (b) *Abstr. 18th Intern. Physiol. Cong. Copenhagen*, p. 165 (1950), *Federation Proc.* **10**, 29 (1951); (c) *Am. J. Physiol.* **167**, 775 (1951); (d) *Federation Proc.* **3**, 7 (1944); (e) *ibid.* **11**, 27 (1952); (f) *Abstr. 2nd Intern. Biochem. Cong. Paris*, 1952 (in press).
29. GRÉGOIRE, C., AND FLORKIN, M., *Physiol. comp. et oecol.* **2**, 126 (1950).
30. TAIT, J., *Quart. J. Exptl. Physiol.* **12**, 1 (1918).
31. COPLEY, A. L., AND HOULIHAN, R. B., *Federation Proc.* **4**, 173 (1945).
32. FERRY, J. D., AND MORRISON, P. R., (a) *J. Am. Chem. Soc.* **69**, 388 (1947); (b) *ibid.* **69**, 400 (1947).
33. EDSALL, J. T., FOSTER, J. F., AND SCHEINBERG, H., *J. Am. Chem. Soc.* **69**, 2731 (1947).

34. HAWN, C. v. Z., AND PORTER, K. R., *J. Exptl. Med.* **86**, 286 (1947); *ibid.* **90**, 225 (1949).
35. MORRISON, P. R., AND SCUDDER, C. L., to be published, 1951.
36. EDSALL, J. T., *Advances in Protein Chem.* **3**, 383 (1947); *Ergeb. Physiol., bio. Chem. exptl. Pharmacol.* **46**, 308 (1950).
37. ONCLEY, J. L., SCATCHARD, G., AND BROWN, A., *J. Phys. & Colloid Chem.* **51**, 184 (1947).
38. HAMMERSTEN, O., *Arch. ges. Physiol. (Pflügers)* **19**, 563 (1879).
39. LAKI, K. L., AND MOMMAERTS, W. F. H. M., *Nature* **156**, 664 (1946).
40. LAKI, K. L., *Federation Proc.* **8**, 90 (1949).
41. MIHALYI, E., *Acta Chem. Scand.* **4**, 334, 344 (1950).
42. WAUGH, D. F., AND LIVINGSTONE, B. J., *Federation Proc.* **10**, 143 (1951).
43. COPLEY, A. L., AND STEFKO, P. L., *Surg. Gynecol. Obstet.* **84**, 451 (1947).
44. COPLEY, A. L., STEFKO, P. L., AND NAYLOR, J., *Surg. Gynecol. Obstet.* **85**, 646 (1947).
45. BURSTEIN, M., personal communications, Paris, Aug. 1-11, 1951.
46. MORRISON, P. R., AND SEILER, A., to be published, 1951.
47. MORRISON, P. R., (a) personal communication, Oct. 17, 1951; (b) personal communication, Oct. 12, 1951.
48. COPLEY, A. L., (a) *Proc. Third Intern. Cong. of Intern. Soc. Hematology, Cambridge, England*, 1950. New York, Grune & Stratton, 1951, p. 541; (b) *Congress Handbook, Fourth Intern. Cong. of Intern. Soc. Hematology, Mar del Plata, Argentine*, 1952 (in press).
49. COPLEY, A. L., AND KOZAM, G., *J. Applied Physiol.* **4**, 311 (1951).
50. COPLEY, A. L., AND LALICH, J. J., (a) *J. Clin. Invest.* **21**, 145 (1942); (b) *Am. J. Physiol.* **135**, 547 (1942).
51. LALICH, J. J., AND COPLEY, A. L., *Arch. Surg.* **46**, 224 (1943).
52. SAYLOR, C. P., *J. Research Natl. Bur. Standards* **15**, 277 (1935).
53. KASS, E. H., communication, Meeting Soc. Clin. Invest., Atlantic City, April 1951.

VISCOSITY OF GLASS¹

Webster Capps

National Bureau of Standards, Washington, D. C.

Received January 28, 1952

ABSTRACT

A review is presented of some methods for measuring viscosity and of some of the work of various authors in relating their data to the structure of glass and to the size of the units participating in the flow process.

The range of measurements covers from about 10^2 poises to about 10^{15} poises at temperatures up to 1400°C .

An outline is presented of some attempts which have been made to extend the kinetic theory of gases and solid-state theories to the liquid state.

The relative importance of ionic size and interionic binding forces in various temperature ranges is discussed for some binary alkali silicates.

Evidence is given that many glasses are Newtonian liquids in both high and low viscosity ranges.

The study of viscosity of liquids has increased in importance because of its usefulness in many industries which handle and process liquids and because it has led to advances in the understanding of the liquid state and of various rheological properties. The glass industry is particularly interested in viscosity because the manufacture of glass products involves careful control of this property during many steps covering a range of several hundred poises to about 10^{15} poises. To a great extent, the modern manufacturer depends on high-speed automatic machines. These require that the viscosity of the glass be quickly and accurately controlled. Formerly, the glass manufacturer had to learn by actual trial what temperatures to use for a particular glass composition for various processes. A tremendous advance was made when it was proved that these critical temperatures were related to definite viscosities or viscosity ranges.

Accurate viscosity measurements of glass are difficult to make because of the wide range of viscosity which is encountered and because of the many restrictions imposed by the high temperatures to which the glass must be heated. Because most commercial glass is high in silica, the melts are highly viscous. A typical container glass has a viscosity of nearly 10^{14} poises at 500°C . and as much as several hundred poises at

¹ Presented at the Annual Meeting of the Society of Rheology, Chicago, Illinois, October 24-27, 1951.

1300°C. No one apparatus can measure this range of values, and hence several types of apparatus must be used.

The low-viscosity range has been covered by using rotating, concentric cylinders, free-falling spheres, and restrained spheres. The rotating cylinder method has been the most commonly used. Lillie (1), Shartsis and Spinner (2), Heidtkamp and Endell (3), Robinson and Peterson (4), English (5), Babcock (6), Proctor and Douglas (7), and others have used this method. The measurements were put on an absolute basis by Lillie (1,8) who evaluated the effect of the end of the inner cylinder on the measurements. Lillie (9) later found that a spindle having two cone-shaped ends need not be kept at a constant distance from the bottom of the outer cylinder. The range of measurements can be extended in the direction of higher viscosity by using an aperiodic method. Lillie (10), Heidtkamp and Endell (3), and Robinson and Peterson (4) have made use of this method.

Wood (11) used free-falling spheres and timed their passage through the glass melt by taking periodic radiographs. Stott, Irvine, and Turner (12) and Shartsis and Spinner (2) have used the restrained sphere apparatus. The velocity is measured that is attained by a sphere moving through the liquid in response to a known force. The change of velocity per change of load is a function of the viscosity. This is not an absolute method, but with proper calibration yields excellent results on comparing with other methods. An advantage of this method is that the data obtained can yield density values and thermal expansivities.

Littleton (13,14) defined the strain, annealing, and softening points in terms of the rate of deformation of glass fibers or rods. This led to the development of the fiber elongation method for measuring viscosities between 10^7 and 10^{15} poises, cf. Lillie (15), Robinson and Peterson (4), and Poole (16).

In order to obtain high quality data from experiments conducted at temperatures as high as 1400–1500°C. the investigator must overcome a number of serious difficulties. Among these are: contamination of the glass by reaction with the walls of the container, selective volatilization, temperature control, lack of good analytical methods, and the duration of the experiments. As a result of these limitations there has been a relatively meager output of good data.

Increasing interest in the structure of glass has stimulated careful research and considerable speculation about the size of flow units, the binding forces between these units, and the binding forces between the various atoms or ions composing the units.

Commercial glass compositions are usually very complex from a chemical point of view. They may have been made from as many as ten different chemical compounds, which, on melting together, do not

remain independent. A viscosity-composition-temperature study becomes extremely complicated and the interpretation of the results is very difficult. A more rewarding task is the study of simpler glass-forming systems. Because silica is the major component of most commercial glasses, much of the work on simple systems has been done with silica plus varying percentages of one or two other oxides. Great emphasis has been placed on soda-lime-silica glasses because of their industrial importance. This has resulted in much work on the viscosity of glasses containing only these three components. However, interpretation of results is perhaps even more profitable if binary systems can be used. The use of binary systems has been limited because of the strong tendency of these systems to devitrify either wholly or partially or to separate into two liquid phases. Nevertheless, a program has been established in the Glass Section of the National Bureau of Standards to study various physical properties of as many binary glasses as possible. The properties studied to date include viscosity, surface tension, density, thermal expansivity, and electrical conductivity in a relatively high temperature range. Viscosity data have been obtained for sodium, potassium, and lithium silicates (17) and for sodium, potassium, and lithium borates (18). The alkaline-earth borates will be studied next.

Early investigators of glass-forming systems looked for evidence of compound formation at compositions having simple oxide ratios. If they found maxima or minima in the viscosity at these compositions they considered it evidence of compound formation. In substituting boric oxide for silica in a sodium silicate glass, a definite maximum occurs in the viscosity-composition curve at 15 mole per cent of B_2O_3 at $700^\circ C$. and below. According to English (5) this indicates compound formation, but he also suggests that the compound is unstable, showing complete dissociation at $800^\circ C$. and above, at which temperatures no maximum occurs. E. Preston (19) investigated the soda-silica system and reported viscosity minima at about 25 and 33 mole per cent of soda. These compositions have the molar ratios $Na_2O \cdot 3SiO_2$ and $Na_2O \cdot 2SiO_2$. According to the phase equilibrium diagram for that system (20), $Na_2O \cdot 2SiO_2$ forms a stable crystalline compound below its liquidus; $Na_2O \cdot 3SiO_2$, on the other hand, has never been identified as a crystalline compound but instead is a eutectic mixture at the liquidus temperature which is the lowest liquidus in the entire system. Obviously the idea that maxima or minima in the viscosity-composition curve prove compound formation in the liquid state is erroneous. Other investigators (3,6,9,17) of the sodium silicates failed to find such minima, but these examples indicate the trend in structure speculation for glass in the fluid range.

The behavior of liquids has been partially explained by considering the similarity between liquids and gases. Andrade, van der Waals, and

others have tried to extend the kinetic theory of gases to apply to liquids including glasses. Andrade (21) related the viscosity at the freezing point of the liquid to the molecular weight, molar volume, and temperature. According to Mark and Tobolsky (22), van der Waals related viscosity to the number, size, and mass of the molecules, the temperature and the difference between the average energy of a molecule, and its energy at the moment of collision. Sheppard and Houck (23) derived several expressions relating molecular weight, density, specific heat, and the change in viscosity with temperature. Several people have applied these equations to glass in an effort to determine "molecular weights" or aggregate sizes, believing that discrete clusters, which move among each other, increase in size as the glass cools. Lillie (15) applied these equations to glass and calculated the molecular weight to vary from 15,000 at about 1100°C. to 112,000 at about 500°C., the latter of which would correspond to an aggregate diameter of 5×10^{-7} cm. Admittedly, these values may be considerably in error. F. W. Preston (24), by considering the fluidity of liquids to be a direct analogy with the vapor pressure of gases, related the change of viscosity with changing temperature to the heat of fusion, just as Boltzmann related the change in vapor pressure with changing temperature to the heat of vaporization. He estimated the "molecular weight" of glass to be about 3000 at 500°C. Douglas (25) has recently developed a theory of the viscosity of glass based on the structure of the glass as determined by means of x-ray diffraction work. He derived an expression relating viscosity to temperature and to the glass structure. The estimated values of some of the constants agree fairly well with those calculated from viscosity data of a soda-lime-silica glass, but he has not yet been able to calculate the viscosity from the atomic arrangement and interatomic distances.

Stanworth (28) writes that the activation energy of boric oxide glass at low temperature is 78 kcal./mole; at high temperature it is 13.7 kcal./mole. The difference, 64.3 is in remarkably close agreement with the heat of vaporization of boric oxide, 65.6 kcal./mole at 1200°C. He explains that at low temperature, hole formation is more difficult, and that the energy required to make a hole is the same as the energy of vaporization, but that at high temperature the liquid is in an expanded state full of holes, and this energy term drops out of the activation energy expression. This seems to agree with the conclusions drawn from the Eyring (26) and Frenkel (27) theories that the flow unit is very small and in the order of size of one molecule of B_2O_3 , or that the boric oxide is not polymerized even at low temperature (annealing range).

N. W. Taylor and co-workers (29,30) show that at about 740°C. $K_2O \cdot 4SiO_2$ has a lower viscosity than $Na_2O \cdot 4SiO_2$. Heidtkamp and Endell (3) show that between 1000° and 1500°C. $Li_2O \cdot 2SiO_2$ has the

lowest viscosity, $\text{Na}_2\text{O} \cdot 2\text{SiO}_2$ has an intermediate value, and $\text{K}_2\text{O} \cdot 2\text{SiO}_2$ has the highest value at any one temperature. The activation energies (defined by Taylor) at low temperatures are greater for the sodium silicate than for the potassium silicate. At high temperatures the activation energies are proportional to the size of the alkali ion or that $\text{K} > \text{Na} > \text{Li}$. According to Stanworth (31), in the low-temperature range or high-energy-of-hole-formation range the alkali ion to oxygen bond strength is the important factor. The greater the binding energy the more difficult is hole formation. At high temperature the glass structure is expanded and the size of the ion controls the fluidity; the lithium silicates flow more easily than sodium or potassium silicates.

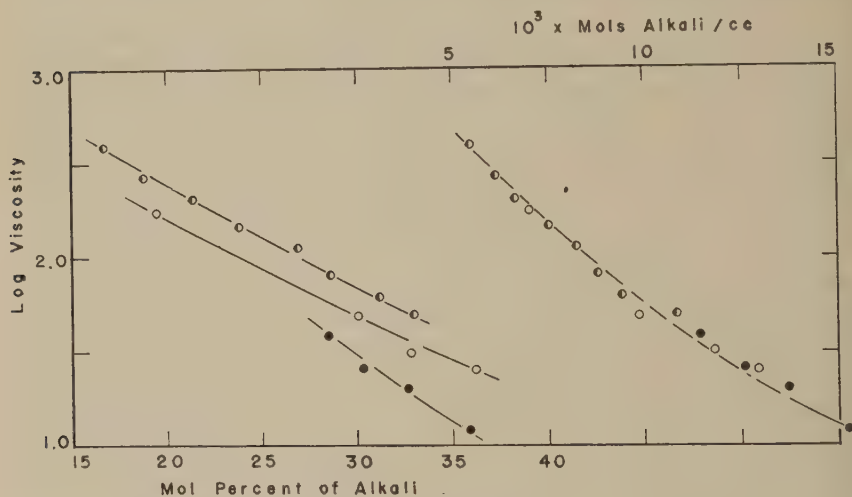


Fig. 1. Log viscosity versus alkali concentration of alkali silicates at 1400° C. [See Ref. (17).]

Half-filled circles represent potash-silicates, open circles represent soda-silicates and filled circles represent lithia-silicates.

Shartsis, Spinner, and Capps (17) also find the high-temperature viscosity, compared on an equal mole per cent basis, to increase with the size of the alkali ion (see Fig. 1).

In studies of the effect on some physical property of the replacement of one kind of ion with another, the expression of composition on a mole per cent basis has become accepted practice. Presumably, when a replacement is made on an equal mole per cent basis, any variation of the physical property being studied is due only to the change of the kind of ions. This is generally accepted as true. However, some question has been raised as to the validity of using a mole per cent basis for viscosity measurements (17). In order to measure viscosity, flow must take place

in the liquid. This has been pictured as a movement of atoms or ions or groups thereof with respect to each other. For such movement to occur, the electrostatic binding forces between the flow units must be overcome by an externally applied force. The magnitude of the inter-ionic attraction depends on the species of ions. If the liquid is homogeneous with respect to the flow units, the viscosity is a measure of the average attraction between these units. However, if some of the units are strongly attracted to each other while different units are only weakly attracted to the surroundings, the viscosity is more a measure of these weaker forces. This suggests that viscosity, a bulk property, depends not only on the magnitude of the weak forces, but on the number of places where they exist in a unit volume of liquid. In speculating on the flow process, it was proposed that the viscosity of the expanded glasses at high temperatures should depend on the number of "weak bonds" in a unit volume of liquid, as well as on the type of weak bond. Because the alkali-oxygen bond was considered to be the weakest link in the liquid structure, the number of weak bonds per cubic centimeter was considered to be equal to the number of alkali ions per cubic centimeter. Therefore, viscosities were compared for lithium, sodium, and potassium silicates on the basis of moles of alkali per cubic centimeter of glass using high temperature density values in the calculations (see Fig. 1).

The viscosity-composition curves for the three kinds of silicates coincided remarkably well when plotted on a mols/cc. basis. Apparently in the viscosity range of 10 to 10,000 poises, at least, the viscosity of these liquids is a function of the number of weak bonds in a unit volume of liquid rather than of the particular kind of weak bond present. This suggests that the structure is in such an expanded state that the potassium to oxygen bond is not very different in strength from the sodium to oxygen or lithium to oxygen bonds. Perhaps these different kinds of weak bonds are all so much weaker than the oxygen to silicon bonds that their differences are negligible. At lower temperatures, as the structure tightens, these differences become greater or at least they exert more influence on the viscosity.

It would be very interesting to make a systematic study of the viscosity of the same alkali silicates in a lower temperature region, and it is hoped that this study can be made in the near future.

There has been speculation as to whether or not glasses show Newtonian behavior. Many workers (e.g., 2,10) using the rotating, concentric cylinder method of measuring viscosity have found that the deflection of the suspended cylinder is proportional to the velocity of the cylinder to which external power is applied. This holds for all speeds

which do not cause turbulence. This indicates that the rate of shear in the liquid is proportional to the stress applied.

Harrison, Stephens, and Shelton (32), using a rotating-cylinder-type viscometer, found that various ground-coat enamel frits are Newtonian liquids; whereas cover-coat enamels containing dispersed crystalline phases are non-Newtonian liquids (see Fig. 2).

The restrained sphere apparatus yields results for glasses similar to the concentric cylinder method. The velocity of the ball is proportional to the load applied for velocities low enough so that the inertia of the restraining system is negligible (18) (see Fig. 3).

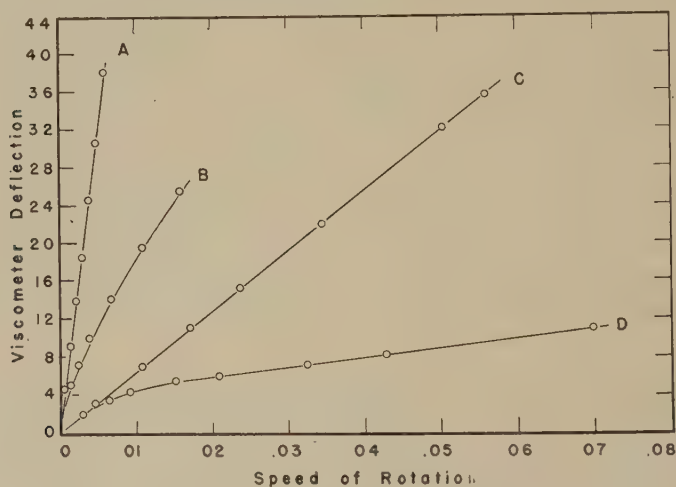


FIG. 2. Rotating-cylinder viscometer deflection versus speed of rotation for four different enamel frits. [See Ref. (32).]

Curve A: A hard, ground-coat enamel frit.

Curve B: A soft, ground-coat enamel frit.

Curve C: An opaque, enamel frit for sheet iron.

Curve D: A leadless, dry-process enamel frit.

Curves A and C are straight lines showing Newtonian behavior, but curves B and D are not straight showing non-Newtonian behavior.

Taylor and Doran (30) showed, on loading and unloading glass fibers in the high viscosity or "solid" range, both instantaneous and delayed elastic effects superimposed on the viscous flow (see Fig. 4). For a typical curve depicting the progress of flow, the fiber was first heat treated at the test temperature until a constant rate of flow *AB* was attained. Upon application of an additional load to this stabilized fiber, an instantaneous (or very rapid) elastic elongation *BC* occurred. The rate of elongation then gradually slowed down to constant values shown by section *CDE*. This changing rate is due to a combination of a delayed elastic process and a viscous flow, the rate of the latter part being given

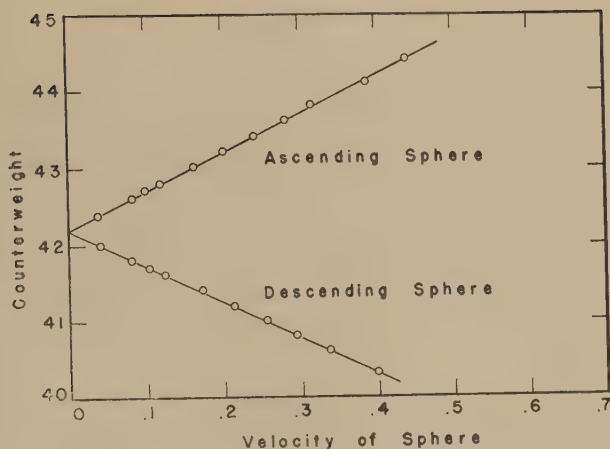


FIG. 3. Restrained sphere counterweight versus sphere velocity for a lithium borate glass at 603°C . [See Ref. (18).]

The weight-velocity curves are straight lines indicating Newtonian behavior of the glass.

by the slope KDE . When the additional load was removed, an instantaneous elastic contraction EF occurred, equal in amount to BC . This was followed by a period FG during which the delayed elastic contraction opposed the viscous flow. The curve FGH shows that the rate of elongation fell to zero and then increased to the constant rate, indicated by the slope LGH , which is parallel to and therefore equal in magnitude to the slope AB . The elastic effects appear to be completely reversible. Because the entire elongation during a determination is only a small percentage of the original fiber length, changes in diameter are negligible.

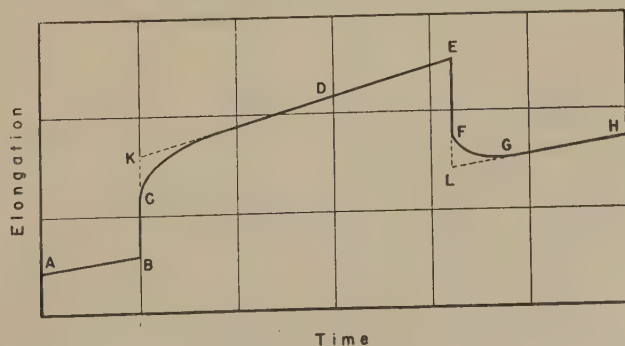


FIG. 4. Elongation of a glass fiber versus time, in the annealing range of temperature. [See Ref. (30).]

Loading and unloading of the fiber cause the instantaneous and delayed elastic changes in length; these effects are superimposed on continuous change caused by viscous flow.

CONCLUSION

At the present time the consensus is that glass is a continuous, unoriented, three-dimensional dynamic network, and that no particular aggregates or molecules exist. The viscous flow of glass therefore can not be explained on the basis of the motion of discrete molecular groups which change in size according to the temperature. The units of flow may be the atoms or ions themselves, and the viscosity be a measure of the resistance to the motion of the moving ions, controlled partly by the size of the ions and partly by the binding forces exerted on them. None of the theories proposed to date adequately explains the flow properties of glass in general.

REFERENCES

1. LILLIE, H. R., *J. Am. Ceram. Soc.* **12**, 505 (1929).
2. SHARTSIS, L., AND SPINNER, S., *J. Research Natl. Bur. Standards* **46**, 176 (1951).
3. HEIDTKAMP, G., AND ENDELL, K., *Glastech. Ber.* **14**, 89 (1936).
4. ROBINSON, H. A., AND PETERSON, C. A., *J. Am. Ceram. Soc.* **27**, 129 (1944).
5. ENGLISH, S., *J. Soc. Glass Technol.*, **8**, 205 (1924).
6. BABCOCK, C. L., *J. Am. Ceram. Soc.* **17**, 329 (1934).
7. PROCTOR, R. F., AND DOUGLAS, R. W., *Proc. Phys. Soc. (London)* **41**, 500 (1929).
8. LILLIE, H. R., *Phys. Rev.* **36**, 347 (1930).
9. LILLIE, H. R., *J. Am. Ceram. Soc.* **22**, 367 (1939).
10. LILLIE, H. R., *J. Am. Ceram. Soc.* **12**, 516 (1929).
11. WOOD, A. R., *J. Soc. Glass Technol.* **16**, 43 (1932).
12. STOTT, V. H., IRVINE, E., AND TURNER, D., *Proc. Roy. Soc. (London)* **108**, 154 (1925).
13. LITTLETON, J. T., JR., AND ROBERTS, E. H., *J. Optical Soc. Am.* **4**, 224 (1920).
14. LITTLETON, J. T., JR., *J. Am. Ceram. Soc.* **10**, 259 (1927).
15. LILLIE, H. R., *J. Am. Ceram. Soc.* **14**, 502 (1931).
16. POOLE, J. P., *J. Am. Ceram. Soc.* **32**, 215 (1949).
17. SHARTSIS, L., SPINNER, S., AND CAPPS, W., "Viscosity, Density and Thermal Expansivity of Binary Alkali Silicates." Paper presented at the 53rd Annual Meeting of the Am. Ceram. Soc., Chicago, Ill., 1951.
18. SHARTSIS, L., SPINNER, S., AND CAPPS, W., unpublished data.
19. PRESTON, E., *J. Soc. Glass Technol.* **22**, 45 (1938).
20. HALL, F. P., AND INSLEY, H., *J. Am. Ceram. Soc.* **30**, 22 (1947).
21. ANDRADE, E. N. DAC., *Phil. Mag.* **17**, 497 (1934).
22. MARK, H., AND TOBOLSKY, A. V., *Physical Chemistry of High Polymeric Systems*. Interscience Publ., Inc., N. Y., 1950.
23. SHEPPARD, S. E., AND HOUCK, R. C., *J. Rheol.* **1**, 349 (1930).
24. PRESTON, F. W., *J. Am. Ceram. Soc.* **15**, 365 (1932).
25. DOUGLAS, R. W., *J. Soc. Glass Technol.* **31**, 85 (1947).
26. EYRING, H., *J. Chem. Phys.* **4**, 283 (1936).
27. FRENKEL, J., *Kinetic Theory of Liquids*. Oxford Univ. Press, London, 1946.
28. STANWORTH, J. E., *J. Soc. Glass Technol.* **32**, 20 (1948).
29. TAYLOR, N. W., AND DEAR, P. S., *J. Am. Ceram. Soc.* **20**, 296 (1937).
30. TAYLOR, N. W., AND DORAN, R. F., *J. Am. Ceram. Soc.* **24**, 103 (1941).
31. STANWORTH, J. E., *Physical Properties of Glass*. Oxford Univ. Press, London, 1946.
32. HARRISON, W. N., STEPHENS, R. E., AND SHELTON, S. M., *J. Research Natl. Bur. Standards* **20**, 39 (1938).

LETTER TO THE EDITORS

EXPERIMENTS ON LONG-RANGE ATTRACTIVE FORCES BETWEEN MACROSCOPIC OBJECTS

INTRODUCTION

In order to investigate the existence of long-range attractive forces, proposed by Kallmann and Willstätter (1), and worked out by Hamaker (2) and by Verwey and Overbeek (3) in the theory of the stability of hydrophobic colloids, experiments on direct measurements of these forces have been undertaken. Flat, highly polished glass and quartz plates were chosen as objects.

Starting from London's (4) basic equation, de Boer (5) and Hamaker (2) obtained for the force per square centimeter between two parallel flat plates at a distance d ,

$$F = - \frac{A}{6\pi d^3}, \quad [1]$$

where F = attractive force in dynes/cm.², d = distance in cm., and $A = \pi^2 q^2 \lambda$, in which q = number of atoms/cm.³ and λ is the London constant for the dispersion force between a pair of atoms.

The constant A is expected to be of the order of 10^{-13} – 10^{-11} dyne-cm. but due to the complicated structure of glass and quartz an accurate calculation is impossible. If only the polarizability of the oxygen ions is taken into account, A is calculated at very near to 10^{-12} .

Casimir and Polder (6) have calculated that due to retardation effects the inverse third power law of Eq. [1] should change to an inverse fourth power at distances much larger than the wavelength to be associated with the dispersion forces.

EXPERIMENTS¹

The two plates were carefully adjusted over an area of the order of 1 cm.². Newton interference colors were used to estimate the parallelism and the distance. One of the plates was attached to a fairly stiff spring. The force F was obtained by measuring the bending of this spring, using an electric capacity method, capable of measuring the bending with an accuracy of about 10 A.

The air pressure in the system was lowered to 0.04 mm. Hg. At this pressure the viscosity of the air was low enough to permit establishment of the equilibrium at the distances required (5000–15,000 A.) within a

¹ A preliminary note on the first experiments has been published in *Proc. Koninkl. Nederland. Akad. Wetenschap.* **54**, 387 (1951).

few seconds and high enough to damp vibrations of the plate. Water vapor was removed by flushing the system with dry air. In order to avoid spurious electrostatic effects the air inside the apparatus was made conducting by the presence of a radioactive preparation or by ionizing.

The major difficulties in the measurements were formed by obstacles between the plates, probably dust particles or small pieces of the gel-like surface layer of glass.

In all the experiments mentioned below, the two plates were free from each other except in the experiments at a distance of about 200 Å., which could only be obtained by forcing the plates together by crushing or by pushing away the dust particles between them.

A full description of the experimental setup will be given in a future publication.

RESULTS

Results of the measurements with one set of glass plates ($n_D = 1.5209$; $d_{15} = 2.556$) are assembled in Fig. 1. In the double logarithmic plot the best straight line leads to the force-distance relation

$$F = \frac{2.5 \times 10^{-12}}{6\pi d^{2.64}} \text{ dynes/cm.}^2 \quad [2]$$

but the scattering of the points is so large, that an exponent of 3 cannot be ruled out. With this exponent the most probable value of A would be 3×10^{-11} . An exponent of 4 would not agree with our measurements.

Replacing of one of these glass plates by a crown glass plate of different origin ($n_D = 1.515$; $d_{15} = 2.55$) led to forces which were about two times larger.

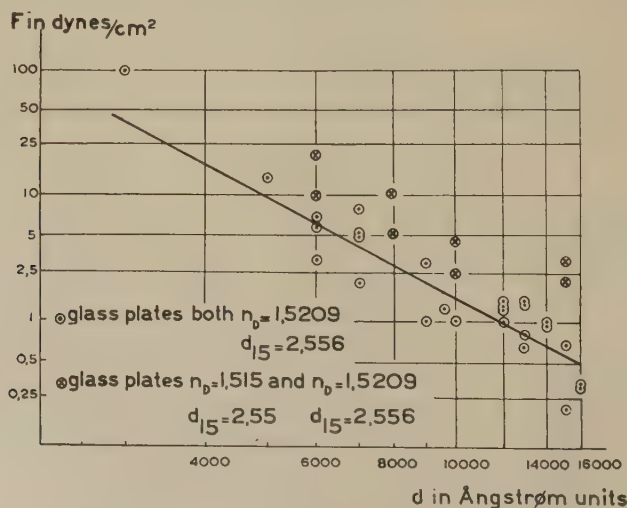


FIG. 1. Graph of force vs. distance. The force value at 3000 Å. is not included in the line drawn in the figure.

A few measurements with two quartz plates gave the following results from which a value of A of about 3×10^{-11} is calculated, assuming the exponent to have the value of 3.

$\frac{d}{A}$	$\frac{F}{\text{dynes/cm.}^2}$
12,000	0.7-2
16,000	0.2

Evaporating a thin layer of silver (100-200 Å.) upon the plates did not materially change the attractive force at distances of about 6000 Å. It has not yet been possible to obtain satisfactory measurements with thicker silver layers due to comparatively large obstacles between the plates in those cases.

With all the glass plates attractive forces of more than 10^5 dynes/cm.² at a distance of about 200 Å. have been found. In these experiments the force was measured which was just large enough to tear the plates apart. In these cases both the measuring of the force and that of the distance was relatively inaccurate, but the values obtained are in agreement with those found by Lord Rayleigh (7), and assuming again the inverse third-power law an A value of about 2×10^{-11} is found.

CONCLUSIONS

Attractive forces do exist between macroscopic objects. An origin by spurious electrostatic charges can be ruled out by the conductivity of the air, by the experiments with the silver layer, and by the reproducibility of the values. The dependence of the force on the distance is in accordance with the inverse third-power law following for the London forces although there is a tendency to a somewhat smaller power than three. An inverse fourth power predicted by Casimir and Polder for the retarded London force is not found in our experiments.

The absolute value of the forces measured is somewhat larger than that predicted on the most simple assumptions, but still within the range possible for London forces.

The experiments are being continued.

REFERENCES

1. KALLMANN, H., AND WILLSTÄTTER, M., *Naturwissenschaften* **20**, 952 (1932).
2. HAMAKER, H. C., *Physica* **4**, 1058 (1937).
3. VERWEY, E. J. W., AND OVERBEEK, J. TH. G., Theory of the Stability of Lyophobic Colloids, Chap. 6. Elsevier, Amsterdam, 1948.
4. LONDON, F., *Z. physik. Chem.* **B11**, 222 (1931).
5. DE BOER, J. H., *Trans. Faraday Soc.* **32**, 21 (1936).
6. CASIMIR, H. B. G., AND POLDER, D., *Nature* **158**, 787 (1946); *Phys. Rev.* **73**, 360 (1948).
7. RAYLEIGH, J. W. S., *Proc. Roy. Soc. (London)* **A156**, 326 (1936).

van't Hoff Laboratory,
University of Utrecht, Holland
Received April 21, 1952

J. TH. G. OVERBEEK
M. J. SPARNAAY

SECOND APPROXIMATION METHODS FOR DETERMINING THE RELAXATION TIME SPECTRUM OF A VISCOELASTIC MATERIAL¹

John D. Ferry and Malcolm L. Williams

Department of Chemistry, University of Wisconsin, Madison, Wisconsin

Received March 10, 1952

INTRODUCTION

Of the various methods which may be employed to specify the time-dependent mechanical properties of a viscoelastic material (1), the distribution function of relaxation times has proved to be particularly useful because other functions such as stress relaxation and the real and imaginary parts of the complex dynamic rigidity, and quantities such as the steady-flow viscosity and the modulus of delayed elasticity, can be easily derived from it. The versatility of the distribution function has stimulated interest in methods for obtaining it from experimental data.

First-approximation procedures for evaluating the distribution function from graphical differentiation of experimental data on stress relaxation (2,3) and dynamic rigidity (4,5,6) or viscosity (6) have been used by various authors. These methods depend upon replacing $e^{-t/\tau}$ by zero or unity accordingly as $t/\tau > 1$ or < 1 , or correspondingly on replacing the fraction $\omega^2\tau^2/(1 + \omega^2\tau^2)$ by zero or unity, and the fraction $1/(1 + \omega^2\tau^2)$ by unity or zero, accordingly as $\omega\tau < 1$ or > 1 . (Here t is time, τ a relaxation time, and ω circular frequency.)

Stress relaxation measurements provide no inherent test of the validity of the above approximations, but dynamic measurements do, since the calculation of the distribution function from the real part of the rigidity may be compared with the calculation from the imaginary part (or the dynamic viscosity). In studies on concentrated polyvinyl acetate solutions (6), these two calculations were found to differ by a constant factor of 1.3. They could be made to agree by changing the critical "cutoff" value of $\omega\tau$ from 1, as ordinarily used in the first-approximation method, to 1.3; but there is no obvious justification for such a change. Moreover, in later studies on polyisobutylene (7,8), good agreement was found with the usual cutoff value of 1. Until recently, experimental precision did not

¹ This work was supported in part by the Research Committee of the Graduate School of the University of Wisconsin from funds supplied by the Wisconsin Alumni Research Foundation, and in part by a grant from Research Corporation.

warrant further investigation of these discrepancies; but improved precision has created a need for better procedures for obtaining the distribution function. Second-approximation methods, which provide corrections to the first approximations in the form of sets of numerical factors, are outlined here.

DERIVATION OF SECOND APPROXIMATION METHOD

The distribution function $\Phi d \ln \tau$ used here is the differential contribution to the shear modulus associated with relaxation times whose natural logarithms lie between $\ln \tau$ and $\ln \tau + d \ln \tau$. It is identical with the functions which are called K by Alfrey (2) and Δ by Zener (9). We prefer to consider shear rather than elongation because it is more simply related to viscosity. The corresponding function for Young's modulus, denoted W by Nolle (4), is for rubberlike materials under most conditions larger than Φ by a factor of 3; and the function for Young's modulus defined in terms of a range $d \log_{10} \tau$ rather than $d \ln \tau$, as used by Andrews (3), is under most conditions larger than Φ by a factor of $3 \times 2.303 = 6.91$.

The commonly used first-approximation equations for calculating Φ are as follows:

From stress relaxation at constant strain following sudden strain (2,3):

$$\Phi(\tau = t) = - (1/\gamma) d\mathfrak{T}/d \ln t. \quad [1a]$$

From stress relaxation at constant strain following cessation of steady flow (10):

$$\Phi(\tau = t) = - (1/\dot{\gamma}t) d\mathfrak{T}/d \ln t \quad [1b]$$

(this is subject to a non-Newtonian correction (10) even at relatively small stresses).

From the real part of the dynamic rigidity, G' (4,5,6):

$$\Phi(\tau = 1/\omega) = G'(d \log G'/d \log \omega). \quad [1c]$$

From the imaginary part of the dynamic rigidity, G'' (7):

$$\Phi(\tau = 1/\omega) = G''(1 - d \log G''/d \log \omega). \quad [1d]$$

From the real part of the dynamic viscosity, η' (6,7):

$$\Phi(\tau = 1/\omega) = - \omega \eta'(d \log \eta'/d \log \omega). \quad [1e]$$

Here \mathfrak{T} is shear stress, γ strain, $\dot{\gamma}$ rate of strain (during steady flow), t time elapsed following sudden strain or cessation of flow, respectively, and ω the circular frequency. The derivatives in Eqs. [1c], [1d], and [1e] may, of course, be written with either natural or common logarithms.

It is found experimentally that a plot of $\log \Phi$ against $\log \tau$ shows little curvature over ranges of several decades. For example, a flat region where Φ is nearly constant has been identified by several authors (3,11) in rubber and polyisobutylene. At shorter times, in polyisobutylene, the above plot curves rather sharply and then has a slope of about -0.6 over several decades (7). Similar linear regions are found for polymer solutions (see Fig. 1 below). Thus, in the immediate vicinity of any particular point (unless it happens to be at a sharp bend) Φ can be approximated by an exponential form, $k\tau^{-m}$, where m is usually positive since Φ is in general a decreasing function of τ .

This behavior affords an opportunity of checking the first-approximation equations for Φ . The form $\Phi = k\tau^{-m}$ is assumed, and the functions $\mathfrak{T}(t)$, G' , G'' , and η' are calculated from it by well-known exact equations [summarized in (8)]. Then the first-approximation Eqs. [1] are applied to these functions, and the resulting expressions for Φ are compared with the originally assumed form.

For example, the relaxation of stress following sudden strain is exactly given (1) by $\mathfrak{T}(t) = \gamma \int_{-\infty}^{\infty} \Phi e^{-t/\tau} d \ln \tau$. Substituting $\Phi = k\tau^{-m}$, we obtain $\mathfrak{T}(t) = \gamma k \Gamma(m) t^{-m}$. Operating on this with Eq. [1a] gives $\Phi = \Gamma(m+1) k \tau^{-m}$, which is in error by the factor $\Gamma(m+1)$. If it can be assumed that this same error will occur in the application of Eq. [1a] to experimental data, a second-approximation equation can be written as $\Phi(\tau = t) = -[1/\Gamma(m+1)](1/\gamma) d\mathfrak{T}/d \ln t$.

Similarly, the real part of the dynamic rigidity is exactly given (1,11) by $G'(\omega) = \int_{-\infty}^{\infty} \Phi \omega^2 \tau^2 / (1 + \omega^2 \tau^2) d \ln \tau$. Substituting $\Phi = k\tau^{-m}$, we obtain

$G'(\omega) = \Gamma\left(1 - \frac{m}{2}\right) \Gamma\left(\frac{m}{2}\right) k \omega^m / 2$. Operating on this with Eq. [1c] gives

$$\Phi = \frac{2}{2-m} \Gamma\left(2 - \frac{m}{2}\right) \Gamma\left(1 + \frac{m}{2}\right) k \tau^{-m},$$

which is again in error by a numerical factor involving gamma functions of m .

The remaining Eqs. [1] can be treated similarly, leading to the following second-approximation formulas for calculating Φ :

From stress relaxation following sudden strain:

$$\Phi(\tau = t) = -M(1/\gamma) d\mathfrak{T}/d \ln t. \quad [2a]$$

From stress relaxation following cessation of steady flow:

$$\Phi(\tau = t) = -N(1/\gamma t) d\mathfrak{T}/d \ln t. \quad [2b]$$

From dynamic properties:

$$\Phi(\tau = 1/\omega) = AG'(d \log G'/d \log \omega) \quad [2c]$$

$$\Phi(\tau = 1/\omega) = BG''(1 - d \log G''/d \log \omega) \quad [2d]$$

$$\Phi(\tau = 1/\omega) = -C\omega\eta'(d \log \eta'/d \log \omega) \quad [2e]$$

with numerical factors defined thus:

$$M = 1/\Gamma(m+1), m \geq 0$$

$$N = 1/\Gamma(m), m \geq 1$$

$$A = (2-m)/2\Gamma\left(2 - \frac{m}{2}\right)\Gamma\left(1 + \frac{m}{2}\right), 0 \leq m \leq 2$$

$$B = C = (1+m)/2\Gamma\left(\frac{3}{2} - \frac{m}{2}\right)\Gamma\left(\frac{3}{2} + \frac{m}{2}\right), -1 \leq m \leq 1.$$

The limitations imposed on the values of m are not serious, since the observed values usually fall within the allowed ranges for the respective methods.

Numerical values for the factors are given in Table I.

TABLE I

Values of Numerical Factors for Second-Approximation Formulas for Calculating Φ

m	M	N	A	B
-1.0				0
-0.8				0.109
-0.6				0.234
-0.4				0.368
-0.2				0.505
0	1.000		1.000	0.637
0.1	1.051		0.996	0.699
0.2	1.089		0.984	0.757
0.3	1.114		0.963	0.810
0.4	1.127		0.936	0.858
0.5	1.128		0.900	0.900
0.6	1.119		0.858	0.936
0.7	1.101		0.810	0.963
0.8	1.074		0.757	0.984
0.9	1.040		0.699	0.996
1.0	1.000	1.000	0.637	1.000
1.2	0.908	1.089	0.505	
1.4	0.805	1.127	0.368	
1.6	0.700	1.119	0.234	
1.8	0.597	1.074	0.109	
2.0	0.500	1.000	0	

APPLICATIONS TO EXPERIMENTAL DATA

In using these methods, Φ is first obtained from the appropriate first-approximation Eqs. [1] and plotted logarithmically against τ , and the slope m is measured at various points. The numerical factors from Table I are then employed to shift the curve to the second approximation.

Figure 1 shows the results of such a calculation on reduced dynamic data on solutions of three samples of polyvinyl acetate in 1,2,3-trichloro-

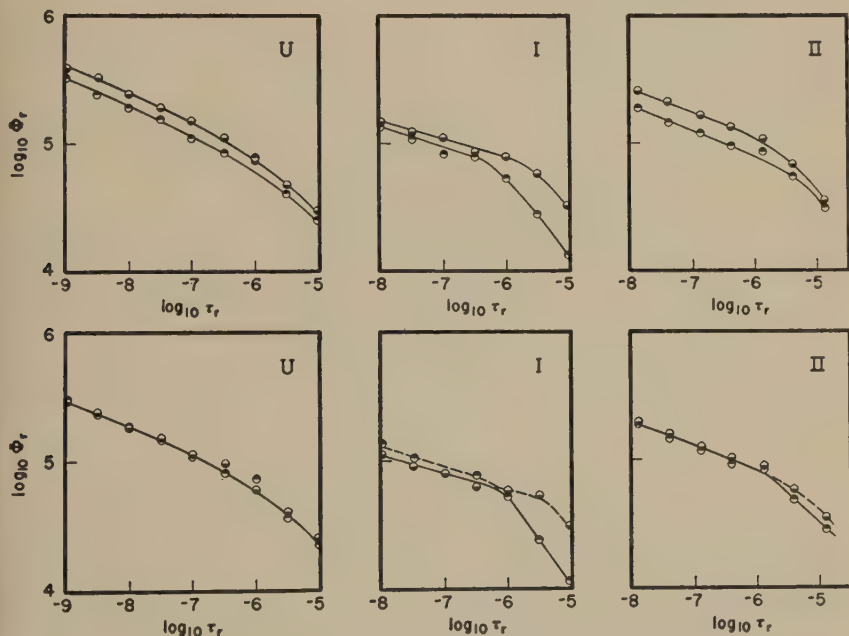


FIG. 1. Logarithmic plots of Φ against τ for solutions of three samples of polyvinyl acetate in 1,2,3-trichloropropane. Upper graphs: first-approximation calculation; lower graphs: second-approximation calculation. Key to points: top shaded, calculation from G' ; bottom shaded, calculation from η' . U = unfractionated, $M_n = 140,000$; I = fraction I, $M_n = 840,000$; II = fraction II, $M_n = 280,000$. All data reduced to unit viscosity at 25°C.

propane. The data for the unfractionated sample and fraction I are taken from a previous paper (6), and those for fraction II from an unpublished report (12). Values of Φ calculated from both G' and η' are compared in all cases. In the first approximation, these values differ, but in the second approximation they are brought into quite satisfactory agreement except for fraction I below a rather sharp bend.

In treating previously published data on polyisobutylene (7), the values of Φ calculated by the first approximation from G' were found to

be only about 6% higher than those calculated from η' . This rather close agreement would be expected from Table I, since the factors A and B are nearly equal in this range ($m = 0.6$). By the second approximation, the values from G' were about 5% lower than those from η' —a slightly better concurrence. In other cases, dynamic mechanical data on solutions of polystyrene in decalin (13) and on gels of polyvinyl chloride in dimethylthianthrene (14) have been used for calculation of Φ , and the application of the second approximation has improved the agreement between values from G' and η' here also.

When the calculation is made for a point on the low τ side of a bend such as appears in the plot of Φ for fraction I in Fig. 1, the function $k\tau^{-m}$, using the measured slope at that point, is invalid on the other side of the bend. On the other side, the contributions of Φ to G' are large but those to η' are small, as determined by the exact integral expressions for G' and η' in terms of Φ (1,11). Hence, the second-approximation formula based on η' , Eq. [2e], will be more nearly correct than that based on G' , Eq. [2c]. Similarly, for a point on the high τ side of a bend, Eq. [2c] will be more reliable than [2e] or [2d]. In Fig. 1, the more reliable calculation is shown by a solid line and the other by a dashed line in each case.

It may be remarked that an entirely analogous treatment may be applied to the calculation of distribution functions of electrical relaxation times from dielectric constant measurements (14).

THE APPROXIMATION FORMULAS OF TER HAAR

In a recent series of papers (15,16), ter Haar has proposed another type of approximate method which is claimed to be superior because it does not involve the uncertainty of measuring the slope of an experimental curve. Comparison of his method with others is complicated by his use of a distribution function, N , of relaxation *frequencies* instead of time; his $N = \tau\Phi$. In terms of Φ his approximate expressions are

$$\Phi(\tau = t) = (1/\gamma)\mathfrak{I}(t), \quad [3a]$$

$$\Phi(\tau = 1/\omega) = G'(\omega). \quad [3b]$$

It is to be expected that these approximations are much rougher even than the first approximations given by Eqs. [1], because each is based on only a single experimental point. When they are tested by application to a function of the form $\Phi = k\tau^{-m}$, exactly as Eqs. [1] were tested above, it is found that they are approximately valid only when $m = 1$. In this case (which happens to be the particular case chosen by ter Haar for illustration) Eqs. [3a] and [3b] give the same results as the first-approximation Eqs. [1a] and [1c], respectively; the first is exact and the second is too high by a factor of 1.57. But when $m = 1/2$, Eqs. [3]

are both too high by a factor of 2.22—far worse than Eqs. [1]; and when $m = 0$, Eqs. [3] do not even give the right functional form for Φ . The method of ter Haar is, therefore, not recommended.

SUMMARY

Second-approximation methods are given for deriving the distribution function of relaxation times of a viscoelastic material from experimental measurements of stress relaxation after sudden strain, stress relaxation after cessation of steady-state flow, the real and imaginary parts of the complex dynamic rigidity, and the real part of the complex dynamic viscosity. The numerical coefficients required for the calculations are tabulated, and the methods are illustrated by application to experimental data on solutions of polyvinyl acetate.

REFERENCES

1. ALFREY, T., AND DOTY, P., *J. Applied Phys.* **16**, 700 (1945).
2. ALFREY, T., *Mechanical Behavior of High Polymers*. Interscience Publishers, New York, 1948.
3. ANDREWS, R. D., *Ind. Eng. Chem.* **44**, 707 (1952).
4. NOLLE, A. W., *J. Polymer Sci.* **5**, 1 (1950).
5. IVEY, D. G., MROWCA, B. A., AND GUTH, E., *J. Applied Phys.* **20**, 486 (1949).
6. FERRY, J. D., SAWYER, W. M., BROWNING, G. V., AND GROTH, A. H., JR., *J. Applied Phys.* **21**, 513 (1950).
7. FERRY, J. D., FITZGERALD, E. R., JOHNSON, M. F., AND GRANDINE, L. D., JR., *J. Applied Phys.* **22**, 717 (1951).
8. FERRY, J. D., FITZGERALD, E. R., GRANDINE, L. D., JR., AND WILLIAMS, M. L., *Ind. Eng. Chem.* **44**, 703 (1952).
9. ZENER, C., *Elasticity and Anelasticity of Metals*. University of Chicago Press, Chicago, 1948.
10. SCHREMP, F. W., FERRY, J. D., AND EVANS, W. W., *J. Applied Phys.* **22**, 711 (1951).
11. KUHN, W., KÜNZLE, O., AND PREISSMANN, A., *Helv. Chim. Acta* **30**, 307 (1947).
12. GROTH, A. H., JR., Senior Thesis, University of Wisconsin, 1950.
13. GRANDINE, L. D., JR., AND FERRY, J. D., unpublished experiments.
14. FITZGERALD, E. R., AND FERRY, J. D., unpublished experiments.
15. TER HAAR, D., *Physica* **16**, 719, 738, 839 (1950).
16. TER HAAR, D., *J. Polymer Sci.* **6**, 247 (1951).

PARTICLE MOTIONS IN SHEARED SUSPENSIONS. II. COLLISIONS OF UNIFORM SPHERES

R. St. J. Manley¹ and S. G. Mason

Pulp and Paper Research Institute of Canada, McGill University, Montreal, Canada

Received January 30, 1952

LIST OF SYMBOLS

- a = diameter of sphere.
- A = YZ projection area of "collision" sphere.
- c = volume fraction of particles in suspension.
- f = collisions per particle in unit time.
- F = two-body collision frequency per unit volume of suspension.
- G = rate of shear.
- n = number of particles per unit volume.
- N = number of collisions observed.
- $p(\xi)$ = differential distribution function, i.e., $p(\xi) \cdot d\xi$ is fraction of assembly having modes between ξ and $\xi + d\xi$.
- $P(\xi)$ = integral distribution function = $\int_0^\xi p(\xi) d\xi$.
- t = time.
- T = period of rotation.
- u, v, w = respective velocity components along X -, Y -, Z -axis.
- θ, Φ = colatitudinal and azimuthal spherical polar coordinates of initial point of contact (Z = polar axis).
- Φ' = azimuthal coordinate of line joining centers of doublet.
- τ = life of a doublet.
- ω = $d\Phi'/dt$.

INTRODUCTION

In an earlier paper (1), the rotations executed by rigid spheres and cylinders in suspensions subjected to velocity gradients were described. This communication deals with two-body collisions of rigid spheres using the same experimental technique. The precision of the method made it possible to follow particle interactions in considerable detail.

Apart from their intrinsic interest, shear-induced collisions are believed to be important in particle aggregation phenomena (2-5). Several authors have speculated on the mechanism of collision (6,7,8), but no experimental observations are reported.

Consider a suspension containing n rigid spheres per unit volume, uniformly dispersed and of equal diameter a . The particles are neutral, non-sedimenting and without Brownian motion. Let the suspension undergo laminar motion defined by $u = -Gy$, $v = 0$, and $w = 0$.

¹ Holder of a Studentship from the National Research Council of Canada.

Each free sphere (singlet) has the translational velocity of the fluid at the same y -coordinate (1). Let us assume that this holds until the centers of two spheres approach within a distance a . A disturbance of the motion of each particle must then occur; we define this disturbance as a collision. This simple assumption and this definition enable us to calculate the collision frequency. For purposes of analysis, we shall consider the colliding particles to be in physical contact.

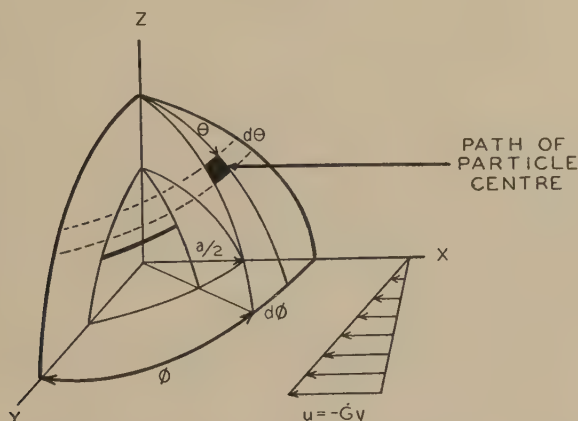


FIG. 1. Spherical polar coordinate system for describing the collisions of spheres.

If a "collision" sphere of diameter $2a$ is described about a reference sphere placed at the origin, as in Fig. 1, all particles whose centers are carried to the surface of the circumscribed sphere will collide with the reference particle. Let dA be the area, projected on the YZ -plane, of the surface element contained in the interval $d\theta$, $d\Phi$ at θ , Φ on the collision sphere. The number of particles whose centers pass through this area in unit time is $-n u dA = n G y dA$. Using the transformation equations

$$dA = a^2 \sin^2 \theta \sin \Phi d\theta d\Phi$$

and

$$y = a \sin \theta \cos \Phi,$$

the number of collisions per unit time with the reference sphere is

$$df(\theta, \Phi) = a^3 n G \sin^3 \theta \sin \Phi \cos \Phi d\theta d\Phi. \quad [1]$$

The total number of collisions per unit time with the reference sphere is given by integrating over the first octant and multiplying by 4, viz.,

$$\begin{aligned} f &= 4a^3 n G \int_0^{\pi/2} \int_0^{\pi/2} \sin^3 \theta \sin \Phi \cos \Phi d\theta d\Phi \\ &= \frac{4}{3} a^3 n G. \end{aligned} \quad [2]$$

The two-body collision frequency per unit volume (F) is $fn/2$, whence

$$F = \frac{2}{3} a^3 n^2 G. \quad [3]$$

If c is the volume concentration of particles in the suspension, $\pi a^3 n/G = c$, and [2] and [3] can be written in the alternative forms

$$f = \frac{8cG}{\pi} \quad [4]$$

and

$$F = \frac{24c^2G}{\pi^2 a^3}. \quad [5]$$

It should be noted from [4] that, for particles of uniform size, f is determined by c and is independent of a .

Equation [2] has been derived before (2,3) using a simpler set of coordinates. The reasons for adopting the form used here will become apparent later.

The fraction of collisions in the interval $d\theta, d\Phi$, taking the limits of θ and Φ for convenience to be between 0 and $\pi/2$, is, from Eqs. [1] and [2],

$$p(\theta, \Phi) d\theta d\Phi = 3 \sin^3 \theta \sin \Phi \cos \Phi d\theta d\Phi. \quad [6]$$

The fraction of collisions having initial values less than θ and Φ is therefore

$$\begin{aligned} P(\theta, \Phi) &= \int_0^\theta \int_0^\Phi p(\theta, \Phi) d\theta d\Phi \\ &= 1/2 [2 - \cos \theta (\sin^2 \theta + 2)] \sin^2 \Phi. \end{aligned} \quad [7]$$

Let $\tau(\theta, \Phi)$ be the life of a doublet, i.e., the time interval between (a) initial contact of two spheres at θ, Φ to form a doublet and (b) separation into singlets. The mean doublet life is then given by

$$\bar{\tau} = \int_0^{\pi/2} \int_0^{\pi/2} \tau(\theta, \Phi) p(\theta, \Phi) d\theta d\Phi. \quad [8]$$

Thus if $\tau(\theta, \Phi)$ is known, the differential and integral distribution functions of doublet lives $p(\tau)$ and $P(\tau)$, respectively, and the mean doublet life can in principle be calculated from Eqs. [6], [7], and [8].

In the experiments which we describe below, measurements of the collision frequency f were made in suspensions of glass spheres at low shear rates to confirm Eq. [4]. Detailed observations were made of the history of a doublet which, combined with measurements of the rotational velocity of single particles between and during collisions, leads to a simple relation for $\tau(\theta, \Phi)$ and to an explicit evaluation of $p(\tau)$, $P(\tau)$, and the maximum life of a collision (τ_{\max}). These relationships were confirmed by direct measurements of doublet lives.

The bulk of the experimental evidence strongly suggests that the collisions are real, i.e., the particles of a doublet actually are in contact; however, one set of experiments considered in the "Discussion" casts some doubt upon this conclusion.

EXPERIMENTAL

Suspensions were introduced into the double Couette apparatus (1) and the cylinders were set in motion in opposite directions. A sphere was singled out for observation in the microscope field and located in a surface of zero fluid velocity, i.e., at $y = 0$, by adjusting the speeds of the inner and outer cylinders. The interaction between the stationary reference sphere and other spheres was observed by viewing along the Y -axis (Fig. 1).

A supply of glass spheres having a narrow size distribution was prepared by screen fractionation of a bulk sample obtained from the Flex-O-Lite Manufacturing Company. The size spectrum is given in Table I.

TABLE I
Size Distribution of Spheres

Diameter a μ	Weight percent of diameter $< a$
125	15
135	63
145	98
155	100
Number average diameter	= 137 μ .
Standard deviation	= 7.2 μ .
Volume average diameter	= 138 μ .
Standard deviation	= 7.2 μ .
Number of particles/cc. glass	= 7.35×10^5 .

Suspensions of known concentration were prepared by adding the particles to high-viscosity corn sirup, stirring thoroughly to assure uniform dispersion, and finally by deaerating under vacuum.

RESULTS

1. Collision Frequency

Each collision was found to be sharply defined. On approaching one another, there was an abrupt change in the motion of the participating spheres, and the contact between them appeared to the eye to be real. The change in particle velocity is shown in Fig. 2 where the distance of separation Δx of the centers of two colliding spheres is shown as a function of time. With experience, a collision could be predicted in advance by judging the velocity and vertical position of the moving sphere and the extent to which it was in focus; this greatly facilitated the observations.

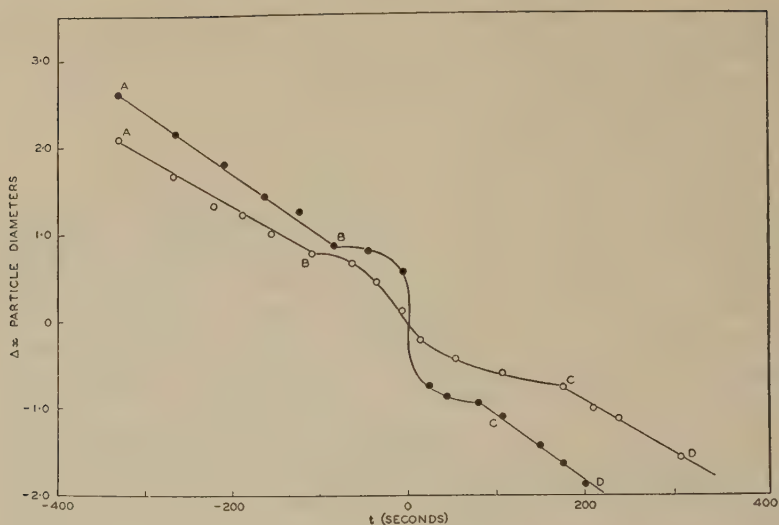


FIG. 2. Distance along X -axis between two spheres during approach (AB), collision (BC), and separation (CD) for two collisions at a low (unmeasured) G . Note the apparent discontinuities in $d\Delta x/dt$ at B and C . These serve to define a collision sharply. For the significance of this, see "Discussion."

All collisions with the reference sphere were counted over a measured time until the particle was lost to the observer.

Since the intervals between collisions presumably obey random statistics, the standard deviation of the observed collision frequency is f/\sqrt{N} where N is the observed number of collisions.

Values of f vs. G for several concentrations, showing the calculated spread in f , are compared in Fig. 3 with values calculated from Eq. [4]. The agreement is within the estimated standard deviation.

A condensed summary of $f_{\text{obs}}/f_{\text{calc}}$ for a total of 1437 collisions is given in Table II, where the ratios have been weighted in proportion to N at each value of c and G . The agreement is seen to be excellent, notwith-

TABLE II

Comparison of Observed and Calculated Frequencies for Various Suspensions

Volume fraction $c/10^3$	Range of G sec.^{-1}	N	Weighted mean, $f_{\text{obs}}/f_{\text{calc}}$	Estimated stand. dev. of $f_{\text{obs}}/f_{\text{calc}}$
3.98	0.4-0.8	94	1.06	0.103
7.94	0.4-0.8	190	1.01	0.073
11.9	0.4-0.8	216	1.01	0.068
15.8	0.5-1.9	731	1.02	0.037
19.6	0.4-0.6	172	0.975	0.076
23.4	0.4	34	0.80	0.171
	Total	1437	1.01	0.026

standing the fact that the spheres are not strictly uniform. It is evident that the rectilinear path of a particle is disturbed only when it projects into the collision sphere of another particle, as was assumed in the "Introduction"; otherwise $f_{\text{obs}}/f_{\text{calc}}$ would exceed unity.

2. The History of a Doublet

Detailed observations of the behavior of doublets may be summarized as follows:

1. When two spheres collide, each particle after separating returns to the y -coordinate existing before collision.

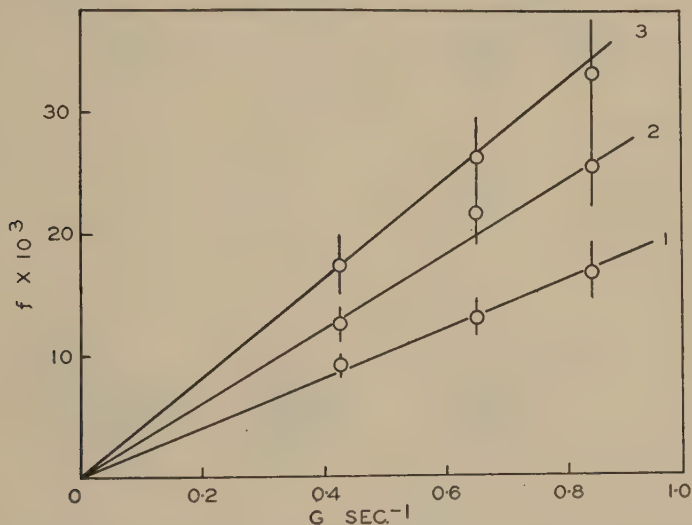


FIG. 3. Measured values of f at various shear rates for c 's of 7.9×10^{-3} (curve 1), 11.9×10^{-3} (curve 2) and 15.8×10^{-3} (curve 3). The total spread in f is shown as twice the estimated standard deviation. The lines are calculated from Eq. [4].

2. The z -coordinate of each particle is the same before, during, and after collision; i.e., the locus of contact is a minor circle at constant θ . This is shown as the heavy line in Fig. 1.

3. There is no rotation of either singlets or doublets about the X -axis during a collision or over a long sequence of collisions.

4. During its life, the doublet rotates as a rigid dumbbell.

The conservation of y -coordinates, in fact, made it possible to measure collision frequencies, since otherwise a collision would have caused the reference particle to move out of the microscope field; instead it remained in the field for long periods of time except for slow migration due to gravitational and centrifugal sedimentation. During collision, the y -coordinate of each particle was disturbed and the doublet rotated as a whole; but

the separating particles returned to their starting velocities, thus exhibiting a striking "memory" effect, first observed by Trevelyan (9).

This was shown by measuring the translational velocity u of spheres colliding with the reference sphere before and after collision. A scale having 100 divisions was placed horizontally (i.e., parallel to the X -axis) in the ocular of the microscope, and velocities were measured for a number of particles which, in the course of their traverse of the field, collided with the reference particle located near the midpoint of the scale. These measurements were difficult to make because of the relatively high speed of the spheres in the field and because of parallax; thus the accuracy was not high. (The measurements shown in Fig. 2 were carried out in a similar manner.) The results (Table III) for 13 collisions selected at random show that the particle velocity remains unchanged.

TABLE III

Particle Velocities Before and After Collision with the Stationary Reference Particle

Sphere No.	Velocity before collision, u_1 divisions/sec.	Velocity after collision, u_2 divisions/sec.	u_1/u_2
1	3.7	3.84	0.96
2	10.0	10.0	1.00
3	2.94	3.12	0.94
4	14.3	12.5	1.16
5	2.5	2.5	1.00
6	3.7	3.33	1.10
7	5.55	5.90	0.94
8	7.7	7.7	1.00
9	5.26	5.26	1.00
10	5.9	5.9	1.00
11	3.12	3.12	1.00
12	3.45	4.17	0.83
13	8.35	7.70	1.07
		Mean	1.00

The rotation of the doublet as a rigid dumbbell, i.e., without sliding or rolling motion, but with points of osculation fixed during the life of the doublet, was established in a number of ways. The most convincing of these was the following. A sphere with a dyed circular spot on its surface was selected for observation. After an extended period, a "bull's-eye" hit was scored. During the life of this collision the point of contact (which could be seen through the transparent spheres) remained in a fixed position within the dyed circle.

The remaining details of doublet behavior were established by a direct, although lengthy, series of observations which we omit.

One collision was observed in which θ did not remain constant. This occurred at Φ close to $\pi/2$. In this case there was a vertical separation of the particle centers during the collision, but the y - and z -coordinates

appeared to be restored. A nearly "head-on" collision was never observed again, as might be expected since $p(\theta, \pi/2) = 0$ (Eq. [6]).

The behavior of the doublet is shown in the projections on the XY - and YZ -planes (Fig. 4) for the beginning, midpoint and end of a collision. The doublet rotates as a right-angled cone of apex angle 2θ with an angle of departure of $-\Phi$.

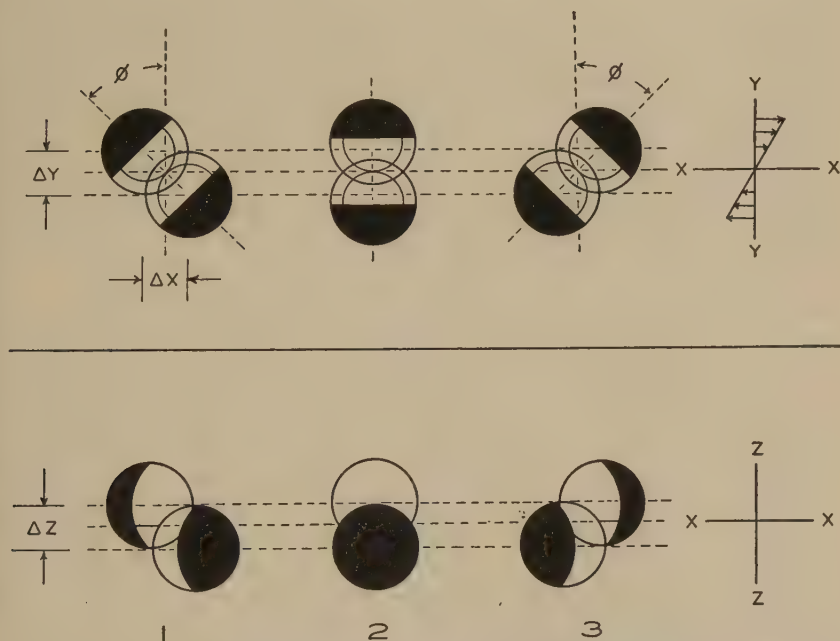


FIG. 4. Projections of doublet on XY and XZ planes for beginning (1), mid-point (2) and end (3) of a collision. For convenience the point of contact is shown in the lamina where $u = 0$.

3. The Doublet Life

Since the doublet executes a rigid rotation at constant θ , each particle rotates about its Z -axis through the same angle 2Φ as the doublet itself, as is evident from Fig. 4. This basic relationship, together with a series of measurements of the period of rotation of individual spheres in singlet and doublet form, led to an unexpectedly simple expression for the life of a doublet (τ).

We have shown (1) that a single sphere rotates about Z with a constant angular velocity $\omega = d\phi'/dt$ given by

$$\omega = -G/2 \quad [9]$$

and therefore with a period

$$T = 4\pi/G. \quad [10]$$

By selecting spheres having optical imperfections on the surface or in the interior, which served as points of reference, T could be measured over intervals during which the particle was either free, or suffered collisions.

Periods were measured over a range of concentrations and shear rates, the last being determined with an accuracy of about 0.5%. The results showed no significant departure from Eq. [10]; the effects of hydrodynamic interaction and of collision on T were, if anything, small and, to be revealed, required precise measurements of T and G .

Since G was calculated from the dimensions and angular velocities of the Couette cylinders (1), it was first necessary to check the accuracy of this calculation. This was done by timing a number of rotations of single spheres and a number of rotations of the Couette cylinders. The results (which we do not reproduce here) showed agreement with Eq. [10] within several parts per thousand.

TABLE IV
Periods of Rotation of Single Particles Undergoing Collisions
 $c = 15.8 \times 10^{-3}$

G sec. ⁻¹	Number of particle rotations	N	T , calculated from Eq. [10] sec.	Total time in rotation Observed sec.	Calculated ^b sec.	Total time spent in collision sec.
0.09183	8	4	136.9	1093	1095	91.0
0.1090	6	3	115.3	692	692	64.8
1.092	100	51	11.50	1149	1150	152.0
0.5370	81	44	23.40	1896	1895	198.0
1.112	57	27	11.31	643.4	644.6	(77.0) ^a

^a Estimated.

^b For single undisturbed sphere.

Similar measurements on free (i.e., noncolliding) particles in suspensions showed similar agreement, thus indicating no significant hydrodynamic interaction.

A series of measurements in which the particles underwent collisions was then made. The number of rotations, the number of collisions, and the total time spent by the particle in collisions were recorded. The results for a range of shear rates (Table IV) show that the average period of rotation of the individual spheres, which at the concentration used in these experiments exist for about 12% of the time in doublet form, is unaffected by collision.

The simplest measurements to perform were with large numbers of collisions at relatively high values of G . Since the possibility could not be excluded that T of the reference particle might be increased by a collision in which Φ lay in the 1st quadrant (Fig. 1) and decreased for Φ in the third quadrant, or vice versa, with no change in \bar{T} , it was considered desirable to measure T for a small number of collisions. This was done at low G with the same result (Table IV).

It may be concluded from these experiments that the time taken by a doublet to describe its orbital angle 2Φ (Fig. 4) is the same as that required by a single particle to describe the same angle. Thus we have from Eq. [9] the following simple relation for the life of a doublet:

$$\tau(\theta, \Phi) = 4\Phi/G. \quad [11]$$

4. Angular Velocity of Doublets

The angular velocity $d\Phi'/dt$ of the doublet throughout its life was measured in the following manner. Using the ocular scale, it was possible

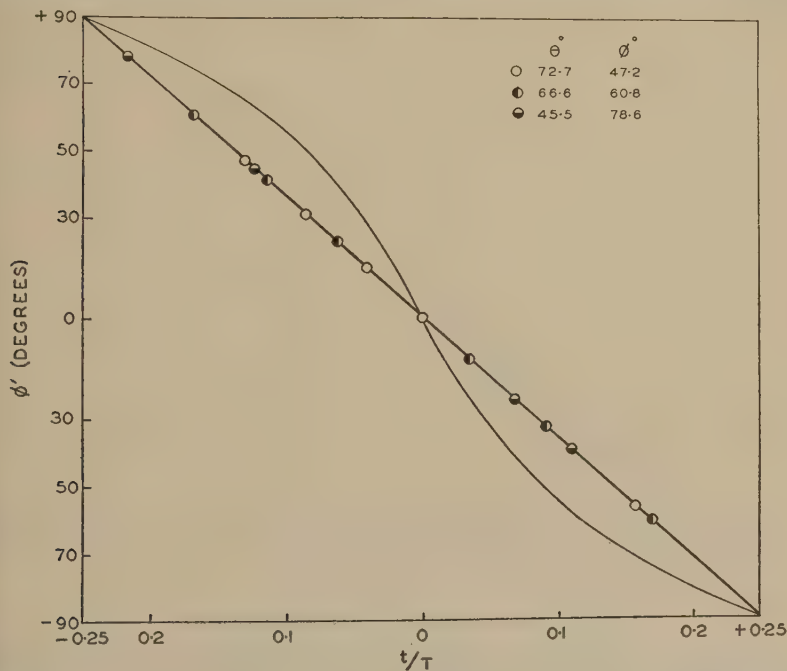


FIG. 5. Variation of Φ' for various doublets as calculated from measurements of Δx and Δz . Coincident points have been omitted for clarity. The curve is calculated for a rigid ellipsoid of axis ratio 2 from Jeffery's equation (10) in the form $\tan \Phi' = 2 \tan (2\pi t/T)$.

to determine the distance along the X -axis between the outermost points of the two spheres. Knowing the size of the particles in units of scale divisions, the distance Δx between centers (Fig. 4) could be determined throughout the life of the doublet. The distance Δz (which remained constant) was also measured. Since (see Fig. 1) $\Delta x = a \sin \theta \sin \Phi'$ and $\Delta z = a \cos \theta$, it is therefore possible to calculate θ and Φ' .

In Fig. 5, Φ' is plotted against t/T for several doublets. The data are in remarkably close agreement despite the difficulty of the measurements,

and indicate that the angular velocity of the doublet is constant throughout its life.

Values of Φ' for a rigid ellipsoid of rotation of axis ratio 2 calculated from Jeffery's equations (10), which we have previously confirmed (1), are shown for comparison. Such a particle has a minimum ω at $\Phi = \pi/2$ and a maximum when $\Phi' = 0$, and undergoes a change in θ during rotation. Clearly the orbits of the doublet and the rigid ellipsoid are different.

The data shown in Fig. 2 were obtained by a similar method except that the measurements were extended to cover a period before and after collision.

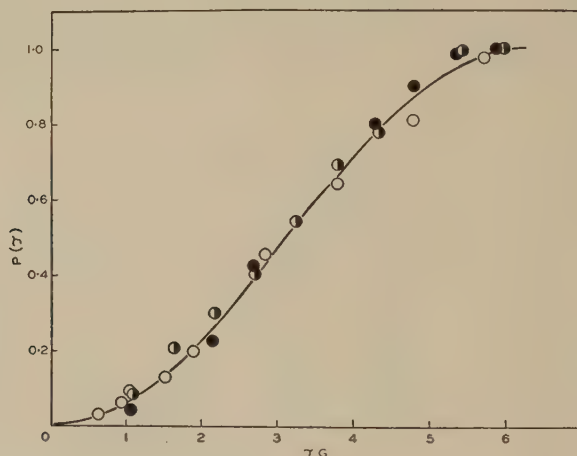


FIG. 6. Measured values of the doublet life distribution function $P(\tau)$ for the three sets of G and N given in Table VI. The curve is calculated from Eq. [15].

5. The Distribution of Doublet Lives

We can now calculate the functions describing the distribution of doublet lives. Since τ depends only upon Φ (Eq. [11]), we can insert the limits of θ in Eqs. [6] and [7] and consider only

$$\begin{aligned} p(\Phi)d\Phi &= \int_0^{\pi/2} 3 \sin^3\theta \sin \Phi \cos \Phi d\theta \\ &= 2 \sin \Phi \cos \Phi d\Phi \end{aligned} \quad [12]$$

and

$$P(\Phi) = \sin^2\Phi. \quad [13]$$

Substituting for $\tau(\Phi)$ from Eq. [11] we obtain

$$p(\tau) d\tau = \frac{G}{2} \sin \frac{\tau G}{4} \cos \frac{\tau G}{4} d\tau \quad [14]$$

and

$$P(\tau) = \sin^2(\tau G/4) \quad [15]$$

where $P(\tau)$ is the fraction of collisions having lives less than τ .

Experiments were carried out at three different shear rates in a suspension of $c = 15.8 \times 10^{-3}$ to test Eq. [15]. The time interval between initial contact and separation was measured with the aid of an integrating timer for as large a number of successive collisions of one particle as possible.

The results (Fig. 6) show good agreement with Eq. [15] despite the scatter due to the limited size of the three populations. When the three populations are combined, as in Table V, the agreement becomes remarkably good.

TABLE V
Distribution of Doublet Lives

τG	Collisions having values $< \tau G$	Observed $P(\tau)$	$\sin^2\left(\frac{\tau G}{4}\right)$
1	26	0.06	0.06
2	105	0.23	0.23
3	215	0.48	0.46
4	322	0.72	0.71
5	408	0.91	0.90
6	449	1.00	0.995

6. Mean and Maximum Doublet Lives

Combining Eqs. [8], [11], and [12] we obtain for the mean life

$$\begin{aligned} \bar{\tau} &= \int_0^{\pi/2} 2\tau(\Phi) \sin \Phi \cos \Phi d\Phi \\ &= \int_0^{\pi/2} \frac{8\Phi}{G} \sin \Phi \cos \Phi d\Phi. \end{aligned}$$

On integrating by parts this yields

$$\bar{\tau} = \pi/G. \quad [16]$$

Since $\Phi_{\max} = \pi/2$, it follows from Eq. [11] that

$$\tau_{\max} = 2\pi/G. \quad [17]$$

TABLE VI
Mean and Maximum Doublet Lives

G sec.^{-1}	N	$\bar{\tau}$ sec.	$\bar{\tau}G/\pi$	τ_{\max} sec.	$\tau_{\max} G/2\pi$
0.54	136	5.7	0.98	11.0	0.94
1.09	153	3.0	1.04	5.5	0.96
1.91	160	1.68	1.02	3.1	0.94
		Mean	1.01		

Table VI shows $\bar{\tau}$ and τ_{\max} for the three sets of data in Fig. 6. The low observed values of $\tau_{\max}G/2\pi$ are to be expected since $p(\tau_{\max}) = 0$ (Eq. [12]).

The results confirm Eqs. [16] and [17].

DISCUSSION

The principles described above have a number of important applications to particle aggregation phenomena in sols and suspensions where velocity gradients exist from stirring, flow, etc. These will be considered in a separate communication. We restrict our remaining remarks to the immediate results and to the question of whether or not the spheres of a doublet are in true contact.

It should be emphasized that the simple theoretical treatment presented here involves geometrical, and not hydrodynamical, principles. The relations describing doublet lives are based upon these principles and the observed mechanism of collision. The close agreement between $P(\tau)$, $\bar{\tau}$ and τ_{\max} and the predicted values confirms the validity of doublet behavior shown in Fig. 3.

Bingham (6) postulated that the spheres of a doublet become locked, as has been found, but that they separate when $\Phi = 0$, i.e., at point 2, Fig. 4.

On the other hand, Vand (7) considered the two particles to roll over one another along an orbit which is a portion of a great circle passing through the X - X axis, until they separate at $\Phi = 0$. This mechanism leads to $\bar{\tau} = \pi/2G$, $\tau_{\max} = \infty$, and functions $p(\tau)$, $P(\tau)$ differing considerably from Eqs. [14] and [15].

This assumption introduces a minor error into Vand's theoretical equation for the relative viscosity of suspensions of spheres. Using Eq. [16], the coefficient of the quadratic concentration term is increased from 7.349 to 10.049. The latter value is in better agreement with our experimental value of 11.9 (11). It compares less favorably with Vand's value of 7.17 (12). We have reason to believe, however, that Vand's results are in error because of questionable corrections for changes in concentration in the viscometer reservoirs and capillaries.

Mooney (8) states (without elaboration) that the paths of approach and recession of colliding spheres are curvilinear and are mirror images of one another. While the latter prediction has been borne out, we have found no evidence to suggest that the paths are not rectilinear.

There is one interesting aspect of the collision process to which we call attention. It is readily shown from Eq. [9] that the relative velocities in the XY -plane of the two points of contact of the rolling spheres

immediately before collision are

$$u' = \frac{Ga}{2} \sin \theta \cos 2\Phi$$

$$v' = \frac{Ga}{2} \sin \theta \sin 2\Phi$$

along the normal to, and parallel to, the line joining particle centers, respectively. Immediately after collision, the relative velocities are zero. There is therefore a discontinuity in the motion of each particle at the instant of impact and the instant of separation.

This is illustrated alternatively by considering the relative velocities of the particle centers in the X -direction. Before collision

$$d\Delta x/dt = -Gy = -Ga \sin \theta \cos \Phi.$$

During collision, from the mechanism described,

$$\begin{aligned} \frac{d\Delta x}{dt} &= \frac{d}{dt} (a \sin \theta \sin \Phi') \\ &= -\frac{Ga}{2} \sin \theta \cos \Phi'. \end{aligned}$$

Thus at impact and separation, $d\Delta x/dt$ is halved. This discontinuity is indicated in Fig. 2, but the experimental points are not sufficiently detailed to evaluate the apparent discontinuity quantitatively.

A rigorous hydrodynamic treatment of the interaction of colliding spheres can, in principle, be made by applying the equation of continuity and the Stokes-Navier equation, restricting the treatment to low G 's where inertia terms can be neglected, as an extension of Vand's method (7) for calculating interaction at large distances of separation. The method, however, involves difficulties which have not been resolved, one of which is the discontinuity mentioned above.

If the spheres of a doublet come into true contact, there must exist a force holding them together. This would arise from a nonvanishing integral of the pressure distribution established on the surface of the doublet by distortion of the fluid motion. If this force exists, it must act along the line joining particle centers.

This type of stress distribution would account, in part, for the difference (Fig. 5) between the orbit of a doublet and that of a rigid ellipsoid which can support bending stresses. The remaining difference would be due to particle shape.

Assuming the existence of an interaction force, the memory effect may be explained as follows. As the doublet rotates, each

particle suffers a displacement in the fluid field from (see Fig. 4) $\Delta y_{\min} = a \sin \theta \cos \Phi$, at point 1, to $\Delta y_{\max} = a \sin \theta$, at point 2.

The interaction force, proportional to G and the viscosity of the medium, will grow from zero at Φ to a maximum at the midpoint, and then decline symmetrically to zero at $-\Phi$ where the particles separate.

This explanation fails to account for one important fact not previously mentioned. If a doublet rotates to an angle Φ' and the fluid motion is brought to rest and then restored, we would expect that (a) when $\Phi' > 0$, the doublet would continue to rotate and then separate at $-\Phi'$, and (b) if $\Phi' < 0$, the doublet would immediately separate. To our surprise, this did not occur. In all cases, even when the doublet was at rest for as long as 1 hr., separation did not occur until $-\Phi$.

This suggests that the interaction force is zero, and that the spheres are not in physical contact but are separated by distances which depend upon the path of approach. This, however, would not be expected to lead to discontinuous behavior but rather to vaguely defined collision effects.

The visual observations and the experimental results indicate true contact, but owing to the last mentioned exception the evidence is not unequivocal. This is an interesting point; we believe that it can best be resolved by theoretical analysis of interaction forces.

SUMMARY

The interaction of model glass spheres in suspensions subjected to velocity gradients has been studied in detail.

Absolute "inelastic" collision frequencies have been measured and found to be in excellent accord with a theory based upon simple geometrical considerations.

A doublet so formed rotates as a rigid dumbbell at a known constant angular velocity, and separates at a point which is a mirror image of the initial point of contact. This memory effect persists through interruptions of motion of the suspension, a phenomenon which casts some doubt on the otherwise definite evidence of true contact of the spheres.

The details of doublet rotation which have been established experimentally make it possible to calculate the mean and the maximum values of the life of a doublet, and the frequency distribution of doublet lives. Good agreement between various measured and calculated values of doublet lives has been found.

Up to the instant of doublet formation, there is no measurable interaction effect upon the translational or rotational velocity of singlets at volume fractions of as high as 1.6%.

REFERENCES

1. MASON, S. G., AND TREVELYAN, B. J., *J. Colloid Sci.* **6**, 354 (1951).
2. SMOLUCHOWSKI, M. VON, *Physik. Z.* **17**, 557, 583 (1916); *Z. physik. Chem.* **92**, 129 (1917).
3. MASON, S. G., *Pulp & Paper Mag. Can.* **51**, No. 5, 93 (Apr., 1950).
4. HUBLEY, C. E., ROBERTSON, A. A., AND MASON, S. G., *Can. J. Research* **B28**, 770 (1950).
5. CAMP, T. R., AND STEIN, P. C., *J. Boston Soc. Civil Engrs.* **30**, 219 (1943).
6. BINGHAM, E. C., *Fluidity and Plasticity*. McGraw-Hill, New York, 1922.
7. VAND, V., *J. Phys. & Colloid Chem.* **52**, 277 (1948).
8. MOONEY, M., *J. Colloid Sci.* **6**, 162 (1951).
9. TREVELYAN, B. J., Thesis, McGill University, 1951.
10. JEFFERY, G. B., *Proc. Roy Soc. (London)* **A102**, 161 (1922).
11. MANLEY, R. ST. J., AND MASON, S. G., to be published.
12. VAND, V., *J. Phys. & Colloid Chem.* **52**, 300 (1948).

STABILITY OF MONODISPERSED SULFUR HYDROSOLS

Robert H. Dinegar¹ and Robert H. Smellie²

*The Departments of Chemistry, Columbia University, New York City,
and Trinity College, Hartford, Connecticut*

Received February 18, 1952

INTRODUCTION

The production of a colloid whose particles do not differ in radii by an appreciable amount makes possible a precise study of several colloidal properties that heretofore either could not be measured at all or at best only approximated. These properties include coagulation, electrophoresis, and the stability of the particles to changes in the ionic environment. In addition, the applicability of such absorption equations as Beer's law to the scattering of light, may be investigated.

It is our purpose to report and discuss the results of the investigation of these colloidal properties in a series of three papers. Part I will consist of the applicability of Beer's law to light scattering by colloidal sulfur particles and the stability of dilute sodium thiosulfate-hydrochloric acid sulfur hydrosols. Part II will deal with the electrokinetic phenomena associated with the stability of colloidal sulfur. Part III will comprise the results of coagulation and particle-interaction studies.

PART I

APPLICABILITY OF BEER'S LAW TO THE SCATTERING OF LIGHT BY MONODISPERSED COLLOIDAL SULFUR

When monochromatic light enters an absorbing medium its intensity decreases exponentially in accordance with the law of Lambert, i.e., $I = I_0 e^{-kl}$ where k is a constant for a given wavelength, l is the thickness of the absorbing medium, and I_0 and I refer to the original and transmitted intensities at a given wavelength.

If, in addition to the above, the absorbing medium is a solution, the intensity decreases exponentially in accordance with the Beer-Lambert law, $I = I_0 e^{-kcl}$, where c is the concentration of absorbing solute. Thus for a given tube length, Beer's law predicts a linear dependence of the optical density ($\log I_0/I$) of an absorbing solution on the concentration of the solute.

¹ Present address: Los Alamos Scientific Laboratory, Los Alamos, New Mexico.

² Present address: Department of Chemistry, Trinity College, Hartford, Conn.

The Beer-Lambert law is found to apply in all cases where no alteration of the solute molecules has occurred, but does not hold if the molecules dissociate, ionize, associate, or in any way change their absorbing properties.

If the absorbing particles increase in size until they are no longer of molecular dimensions, the total amount of light abstracted from the incident beam will no longer depend only on the concentration but also on the size since now an appreciable amount of light is scattered as well as absorbed.

This is the situation for spherical particles of colloidal sulfur in aqueous solution, subjected to illumination of wavelength less than 3900 Å. (in the air) (1). For wavelengths greater than 3900 Å. the total dissipation of light is that due to scattering only, for sulfur is transparent to wavelengths above this value.

The equation relating the intensity of the incident and transmitted light to the area of the particles of radius r and number n is: $\log I_0/I = Kr^2nl/2.3$, where K is a constant describing the total dissipation of radiant energy/unit area/particle.

If no change in the size and shape of the particles occurs and if there is a negligible amount of secondary scattering of light, Beer's law of absorption should apply to the scattering and to the scattering plus absorption of light by colloidal particles.

EXPERIMENTAL

Monodispersed sulfur sols were made with minor variations according to the method of La Mer and Barnes (2) using 0.0015 M $Na_2S_2O_3$ and 0.0020 M HCl .

At the desired time the growth of the sol was arrested by the addition of I_2 in KI . The optical density of the sol was measured for two selected wavelengths with a Beckman quartz spectrophotometer (model DU) in 10-cm. quartz cells. Aliquots of the same sol were diluted with varying amounts of solution and the optical density of these portions measured. The diluting solutions chosen were: (a) 0.0015 M $Na_2S_2O_3$; (b) 0.002 M HCl ; (c) 0.002 M HCl and 0.0015 M $Na_2S_2O_3$, plus the same concentration of I_2 in KI used to arrest sol growth; and (c) distilled water.

All measurements were made as rapidly as possible ($< \frac{1}{2}$ hr.) so as to eliminate any effects of settling, coagulation, and general instability due to the change in medium.

DISCUSSION OF RESULTS

The results are shown in Figs. 1 and 2 where the optical density is plotted as a function of the fraction of the diluting medium. It is seen that the sols follow Beer's law of dilution and that no large discrepancies are noted.

Since Beer's law holds and secondary scattering is absent, the optical density of a mixture of hydrosols of various sizes and number, should be the sum of that fraction taken of the individual components. Experiments run on mixtures of hydrosols showed this to be true (3). A complete

treatment of the analysis of mixtures of hydrosols by this method has been given by Kerker and La Mer (3).

STABILITY OF MONODISPERSED SULFUR HYDROSOLS WITH RELATION TO CHANGES IN IONIC ENVIRONMENT

The stability of colloidal systems is usually considered only from the standpoint of their resistance to coagulation and the effect of ionic environment on the rate of flocculation. This aspect will be discussed more fully in Part III of this series of papers. Dilute sulfur sols prepared by the dilute acid decomposition of dilute sodium thiosulfate show

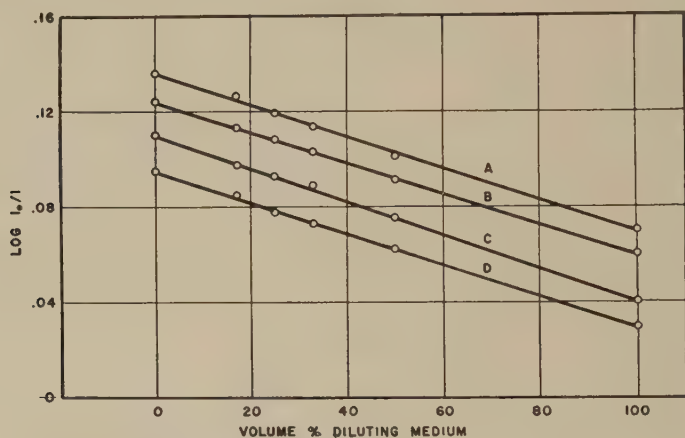


FIG. 1. Curve A: Sol diluted with equivalent concentration of hydrogen ion. Plotting increment = $+.07$; $\lambda = 4500$ A.

Curve B: Sol diluted with equivalent concentration of hydrogen ion, thiosulfate ion, and iodine in potassium iodide. Plotting increment = $+.06$; $\lambda = 4500$ A.

Curve C: Sol diluted with equivalent concentration of thiosulfate ion. Plotting increment = $+.04$; $\lambda = 4500$ A.

Curve D: Sol diluted with distilled water. Plotting increment = $+.03$; $\lambda = 4500$ A.

Curve E: Sol diluted with distilled water. Plotting increment = $+.05$; $\lambda = 4500$ A.

Curve F: Sol diluted with distilled water. $\lambda = 3500$ A.

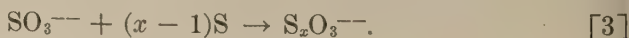
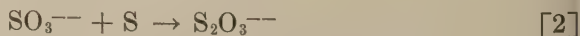
(Curves E, F see page 373.)

instability in an entirely different manner. In these sols the reaction products are capable of reacting together and forming not only the original reactants, but also higher polythionates; i.e.:

forward reaction:



reverse reaction:



For bulk sulfur, reaction [2] is quite slow (4). This need not hold, however, when the sulfur is in the finely divided or colloidal state. In fact, it will be demonstrated that the reverse reaction is much faster than the forward reaction. Stable products, formed by reaction [3], with $x > 2$ are quite unlikely. In addition, higher polythionates ($S_4O_6^{--}$, $S_5O_6^{--}$) have been tested for (5) and were found either to be completely absent or in concentrations very much smaller than SO_3^{--} . Consequently, Eq. [2] will be considered as the complete reverse reaction. In moderate to strong acid solutions, the concentration of SO_3^{--} is so low that reaction [2] is negligible with respect to reaction [1]. Under these conditions, the production of sulfur goes practically to completion.

The position of equilibrium and the rate of the reverse reaction may be determined in the following manner. After the same length of time of

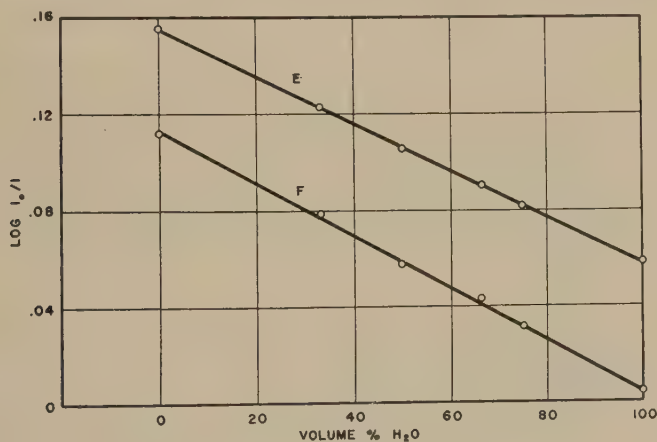


FIG. 2. See Fig. 1 for details.

growth, all solutions of the same initial concentration of reactants have the same value of total sulfite and unreacted thiosulfate. By adjustment of the pH of the solution the position of equilibrium may be found. If the pH is too high, the particles will dissolve; if it is too low, the particles will grow. The rate of change of particle size is then a measure of the rates of the two processes. Since the rate of growth has been previously measured (6), it will not be discussed here, and attention will be focused on the rate of dissolving at high pH and the position of equilibrium.

EXPERIMENTAL

Monodispersed sulfur sols were made by mixing 0.0020 *M* $Na_2S_2O_3$ and 0.0020 *M* HCl and allowing the reaction to proceed for a period of 8 hr. at 25°C. At this time the value of the hydrogen ion was adjusted by neutralization with NaOH and addition of small (<0.001 *M*) amounts of phosphate or acetic acid-acetate buffers. The pH of the

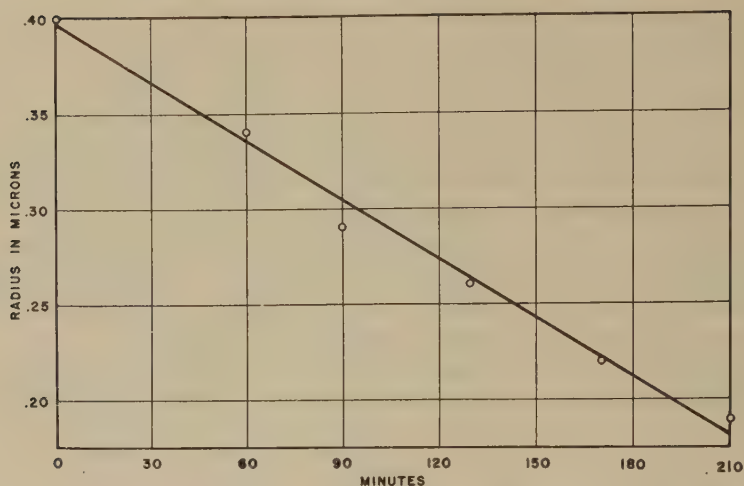


FIG. 3. Radius of sulfur particle in microns as a function of time in minutes.

solution was then measured by a glass-electrode pH meter, standardized against Clark and Lubs' buffer at pH 7.00 and 6.00, periodically, and was constant to ± 0.02 pH units. The amount of thiosulfate unreacted and the amount of total sulfite generated up to this point was determined by titration of an aliquot with standard I_2 in KI, the molarity of which was approximately $\frac{1}{2}$ that of the original thiosulfate. One ml. of a 1% starch solution was the indicator.

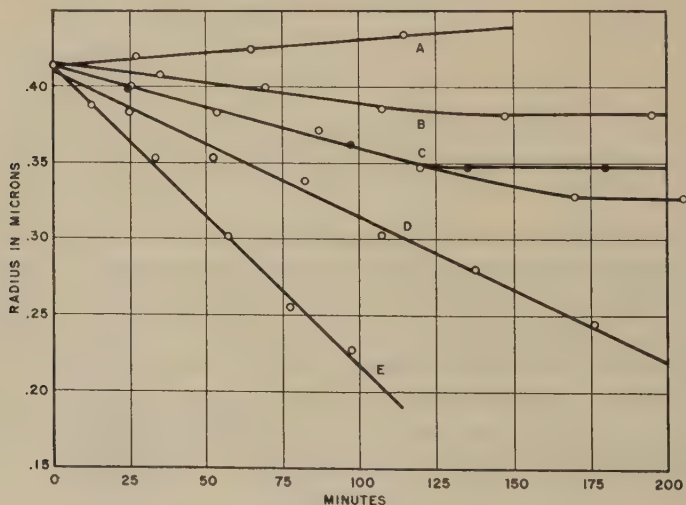


FIG. 4. Variation of radius of particle with time for various values of the pH.

Curve A: pH = 3.08; curve B: pH = 4.88; curve C: pH = 5.50 open circles, pH = 5.49 plus $\sim 0.002 M S_2O_3^{2-}$ solid circles; curve D: pH = 5.92; curve E: pH = 5.92 plus $\sim 7 \times 10^{-6} M SO_3^{2-}$ added.

The particle size was determined according to the method of angular scattering described by Johnson and La Mer (7). The particle number was determined by the transmission method of La Mer and Barnes (2).

DISCUSSION OF RESULTS

The rate of change of particle size with time at constant pH involves a linear relationship between the radius of the particle and time. A representative run is shown in Fig. 3, where the radius in microns is plotted against time in minutes over the extent of the reaction observed.

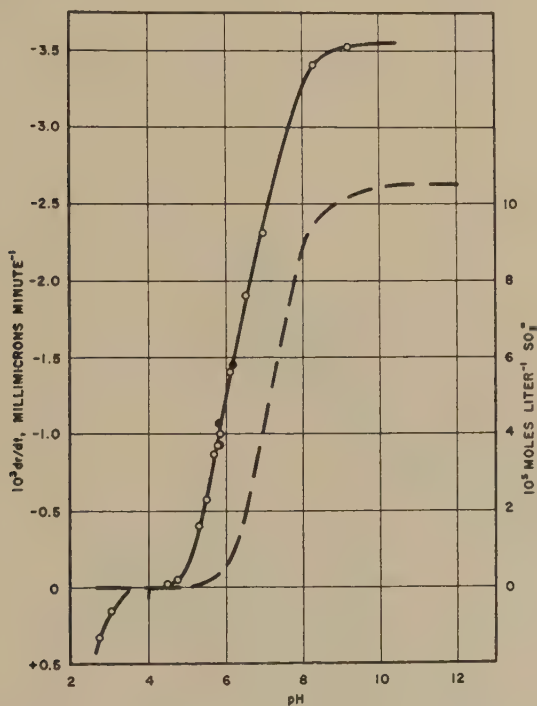


FIG. 5. Variation of dr/dt with pH (solid curve).

Solid circles = all solutions purged with N_2 , before and during runs. Variation of SO_3^{--} concentration with pH (dashed curve).

The rate of change of radius is plotted in Fig. 4 for various values of the pH. For values of hydrogen ion greater than the equilibrium value (curve A), the particle size increases with time. For pH values close to equilibrium, only a small decrease in size occurs, with the resulting radius being constant (curve B).

Figure 5 shows the variation of the rate of change of radius, dr/dt , as a function of pH. The parallel dotted curve represents the concentration

of SO_3^{--} as a function of pH. The rate of dissolving is seen to reach a constant value as the concentration of SO_3^{--} reaches its maximum value, indicating a direct proportionality between SO_3^{--} and the rate.

Figure 4 shows the effect of added Na_2SO_3 at constant pH (curve *E*). Curve *D* is for no added sulfite. Curve *C* shows the effect of added $\text{S}_2\text{O}_3^{--}$ over the normal curve (0). The large increase in rate with added sulfite further identifies sulfite as the reacting species of ion. Addition of $\text{S}_2\text{O}_3^{--}$ made no change in the rate of dissolving but caused the extent of reaction to be lessened.

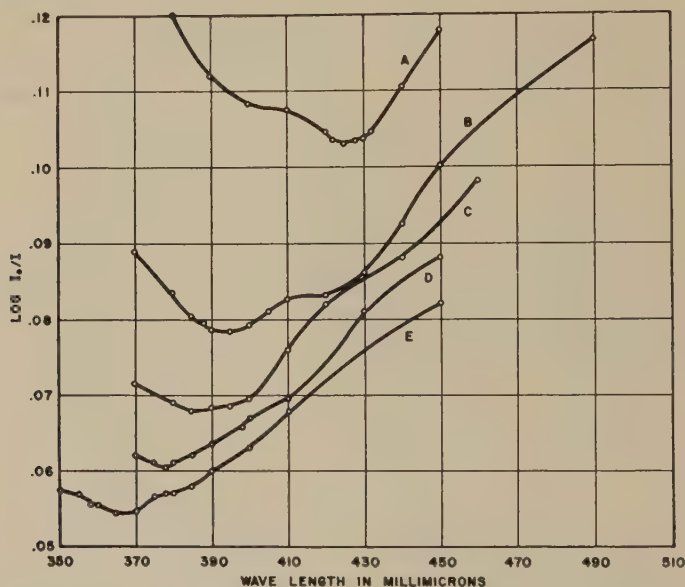


FIG. 6. Transmission curve of monodispersed hydrosol process; pH far from equilibrium value.

Figure 6 shows several typical transmission curves during the dissolving process. The "minimum" is preserved as additional evidence of the monodispersed character of the reverse reaction. The lack of a large variation of particle number with time is shown by three measurements giving the particle number ($\times 10^6/\text{cm}^3$) over 4 hr. of dissolving as $3.4 \pm .2$; $2.4 \pm .1$; $2.8 \pm .03$. A transmission curve near the equilibrium is shown in Fig. 7. The average initial radius of 20 runs was $0.41 \pm .004 \mu$ measured by angular scattering methods and a sol prepared under the same conditions gave a radius of $0.41 \pm .02 \mu$ by transmission methods. The concentration of total sulfite was measured as 10.5×10^{-5} moles/l. of sol for seven runs which checked with the value obtained by Zaiser and La Mer (10.2×10^{-5} moles/l.) (5).

KINETICS OF THE REVERSE REACTION

The reaction between sulfur and SO_3^{--} in the system under discussion might be thought of as occurring in several different ways. The first is essentially a homogeneous reaction between sulfite ion and molecularly dissolved sulfur throughout the entire body of the solution—the removal of which causes sulfur atoms to leave the surface of the particle and go into solution thereby maintaining the $\text{S (dissolved)} \rightleftharpoons \text{S (solid)}$ equilibrium. Depending upon whether the rate of reaction of SO_3^{--} with S or the rate of detachment of sulfur atoms is the slower, the rate-controlling step will differ. Attempts to formulate the problem along these lines gave no significant correlation between theory and experiment.

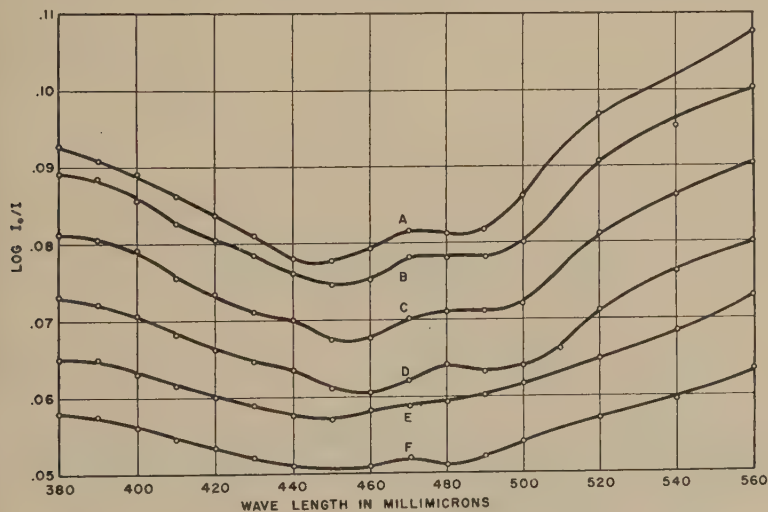


FIG. 7. Same as Fig. 6 except pH is near the equilibrium value.

A second possible mechanism involves the reaction of SO_3^{--} with S either directly attached to the sulfur particle or in a thin layer of sulfur-saturated solution around each particle. Again two possible rate-controlling steps arise in each case, depending upon the relative rates of diffusion of SO_3^{--} to the particle surface and rate of $\text{SO}_3^{--} + \text{S}$ reaction. The following development will assume that the rate-controlling step is the diffusion process. Although this assumption is sufficient to derive equations that predict the experimental results quite well, it will not be possible to say precisely whether the reaction occurs at the particle surface or in a thin saturated film around the micelle; the latter, however, is quite probably more nearly correct.

The total flux onto a spherical particle of radius r is given by Collins (8)

$$\Phi = 4\pi DC_0 r \frac{(\alpha r)}{\rho}, \quad [1]$$

where D = diffusion coefficient,

α = probability factor,

ρ = jump length ratio, and

C_0 = initial concentration of diffusing species.

The rate of transport of (SO_3^{--}) to the particle surface is then given by Φ , and if the rate of reaction of (SO_3^{--}) with the sulfur is more rapid than Φ , the flux of (SO_3^{--}) to the surface then measures the rate of disappearance of (SO_3^{--}) , i.e.:

$$k\Phi = \frac{-d(\text{SO}_3^{--})}{dt} \quad [2]$$

and
$$\frac{-d(\text{SO}_3^{--})}{dt} = k4\pi DC_0 r^2 (\alpha/\rho). \quad [3]$$

Since the total sulfite $(\text{SO}_3^{--} + \text{HSO}_3^-)$ concentration, T , is proportional to the volume of sulfur suspended in the colloidal form, we may write

$$Br^3 = T = B'v, \quad [4]$$

where: B and B' are constants of proportionality, with v being the volume of colloidal sulfur.

To calculate the concentration of SO_3^{--} , given a total sulfite ion concentration T , and acidity (H^+) , we may proceed as follows:

First dissociation equilibrium,

$$\frac{(\text{H}^+)(\text{HSO}_3^-)}{(\text{H}_2\text{SO}_3)} = K_1.$$

Second dissociation equilibrium,

$$\frac{(\text{H}^+)(\text{SO}_3^{--})}{(\text{HSO}_3^-)} = K_2 = 6.2 \times 10^{-8}.$$

For $\text{H}^+ < 10^{-4}M$, the first equilibrium is insignificant.

Since $T = (\text{SO}_3^{--}) + (\text{HSO}_3^-)$,

$$T = (\text{SO}_3^{--}) + \frac{(\text{H}^+)(\text{SO}_3^{--})}{K_2},$$

from which it follows that:

$$(\text{SO}_3^{--}) = \frac{T}{1 + \frac{(\text{H}^+)}{K_2}};$$

$$\therefore (\text{SO}_3^{--}) = \frac{T}{K}, \text{ where } K = \frac{1}{1 + \frac{(\text{H}^+)}{K_2}}; \quad [5]$$

$$\therefore (\text{SO}_3^{--}) = \frac{Br^3}{K} \quad [6]$$

and

$$(\text{SO}_3^{--})^{\frac{3}{2}} = \frac{B^{\frac{3}{2}}r^2}{K^{\frac{3}{2}}}. \quad [7]$$

Substituting [7] in [3]:

$$\frac{-d(\text{SO}_3^{--})}{dt} = k4\pi DC_0(\alpha/\rho) \left[\frac{K^{\frac{3}{2}}(\text{SO}_3^{--})^{\frac{3}{2}}}{B^{\frac{3}{2}}} \right]. \quad [8]$$

Defining C_0 , the initial concentration of SO_3^{--} as $\frac{T_0}{K}$, Eq. [8] becomes:

$$\frac{-d(\text{SO}_3^{--})}{dt} = 4\pi Dk\alpha/\rho T_0 B^{-\frac{3}{2}} K^{-\frac{1}{2}} (\text{SO}_3^{--})^{\frac{3}{2}}, \quad [9]$$

or

$$\frac{-d(\text{SO}_3^{--})}{(\text{SO}_3^{--})^{\frac{3}{2}}} = GK^{-\frac{1}{2}} dt, \text{ where } G = 4\pi DK\alpha/\rho T_0 B^{-\frac{3}{2}}, \quad [10]$$

which, when integrated becomes:

$$-3(\text{SO}_3^{--})^{\frac{1}{2}} = GK^{-\frac{1}{2}}t - 3(\text{SO}_3^{--})_0^{\frac{1}{2}}. \quad [11]$$

The concentration of sulfur (S), given in terms of the individual particle radius (r) and their number (n) is $4/3\pi r^3\rho n/m$, with ρ and m being the density and molecular weight of sulfur, respectively.

Since

$$r = \left[\frac{(\text{S})m}{4/3\pi\rho n} \right]^{\frac{1}{3}}$$

or

$$r = A(\text{S})^{\frac{1}{3}}, \quad \text{where} \quad A = \left(\frac{m}{4/3\pi\rho n} \right)^{\frac{1}{3}} \quad [12]$$

$$\therefore \frac{dr}{dt} = \frac{A d(\text{S})^{\frac{1}{3}}}{dt}. \quad [13]$$

Assuming that the product formed by the reverse reaction is $\text{S}_2\text{O}_3^{--}$, one concentration unit of sulfur is equal to one concentration unit of SO_3^{--} .

Substitution in Eq. [13] gives

$$\frac{1}{A} \frac{dr}{dt} = \frac{d(\text{SO}_3^{--})^{\frac{1}{2}}}{dt} \quad [14]$$

Equating the time derivative of Eq. [11] with the left-hand side of Eq. [14] gives:

$$\frac{dr}{dt} = G^1 K^{-\frac{1}{3}} \quad [15]$$

Thus a plot of dr/dt vs. $K^{-\frac{1}{3}}$ should be a straight line with a slope of G^1 . The result of such a plot using our experimental data is shown in Fig. 8. An excellent straight line is obtained over the entire range of concentrations studied.

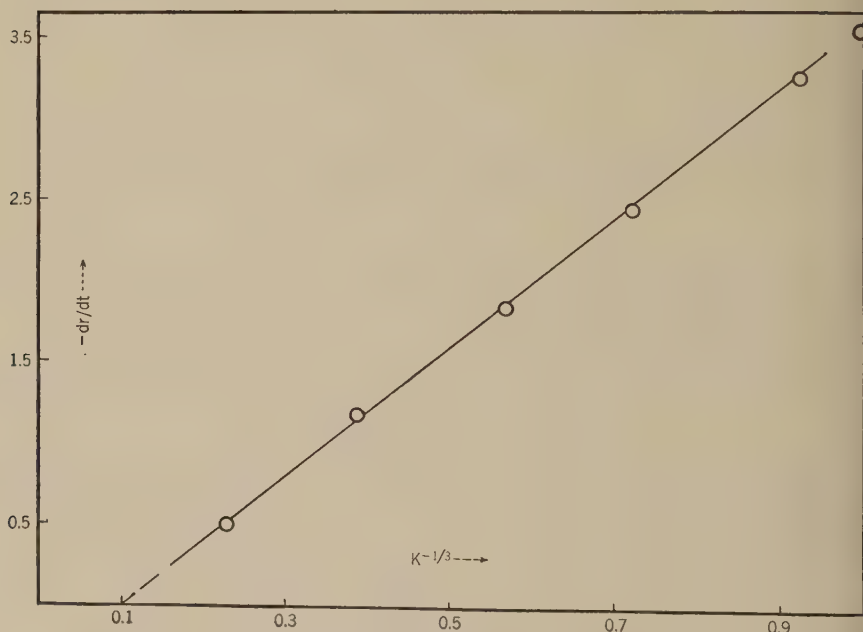


FIG. 8. Plot of $-10^3(dr/dt)$ versus $K^{-\frac{1}{3}}$.

The point of intersection of the straight line with the $K^{-\frac{1}{3}}$ axis is the value of $K^{-\frac{1}{3}}$ at equilibrium, $dr/dt = 0$. This value corresponds to a pH of 4.2 in excellent agreement with Fig. 5 which showed no growth or shrinkage of the particles when the pH was initially made 4.2.

ACKNOWLEDGMENTS

This paper has been constructed in part from a dissertation by R. H. Dinegar submitted in December, 1950, in partial fulfillment for the Ph.D. degree to the Faculty of Pure Science of Columbia University. We wish to acknowledge the encouragement of and frequent discussions with Professor V. K. La Mer on this problem during the development of our individual dissertations under his direction.

SUMMARY AND CONCLUSIONS

1. Monodispersed dilute acid-thiosulfate sulfur hydrosols obey Beer's law with respect to the scattering and scattering plus absorption of light.

2. Sulfur particles prepared by this chemical reaction method are unstable with respect to a change in ionic environment, the instability being due to a reversal of the decomposition reaction in neutral or alkaline solution.

3. The reversal of the decomposition reaction has been found to be due to reaction of sulfur with SO_3^{--} , forming $\text{S}_2\text{O}_3^{--}$. The rate of this reaction is strongly dependent upon the pH of the solution, occurring predominantly in alkaline solution.

4. The kinetics of the $\text{SO}_3^{--} + \text{S}$ reaction is adequately described theoretically by the assumption of a diffusion mechanism whereby the rate-controlling step is the diffusion of SO_3^{--} to the sulfur particle with subsequent chemical reaction taking place.

REFERENCES

1. LA MER, V. K., AND KENYON, A. S., *J. Colloid Sci.* **2**, 258 (1947).
2. LA MER, V. K., AND BARNES, M. D., *J. Colloid Sci.* **1**, 71 (1946).
3. KERKER, M., AND LA MER, V. K., *J. Am. Chem. Soc.* **72**, 3516 (1950).
4. BICHOWSKY, F. R., *J. Am. Chem. Soc.* **45**, 2225 (1923).
5. DINEGAR, R. H., SMELLIE, R. H., AND LA MER, V. K., *J. Am. Chem. Soc.* **73**, 2050 (1951).
6. ZAISER, E. M., AND LA MER, V. K., *J. Colloid Sci.* **3**, 571 (1948).
7. JOHNSON, I., AND LA MER, V. K., *J. Am. Chem. Soc.* **69**, 1184 (1947).
8. COLLINS, F. C., *J. Colloid Sci.* **5**, 504 (1950).

THE ACTIVITY OF CATALASE UNFOLDED AT THE AIR-WATER INTERFACE ¹

J. Gordin Kaplan ²

*The Department of Zoology, Columbia University, New York, New York, and the
Department of Physiology, Dalhousie University, Halifax, Nova Scotia*

Received October 31, 1951; revised February 28, 1952

ABSTRACT

1. The crystalline enzyme catalase has been spread as a monomolecular film at the air-water interface, and compressed into a fiber which retained enzymatic activity.
2. The enzymatic activity of the insoluble fiber has been compared to that of the solution from which it was prepared. The activity of the former differs from that of the latter in that it may be increased by heat and is highly resistant to inactivation by heat and ultraviolet irradiation; the specific activity of the fiber is considerably lower than that of the native enzyme.
3. Both forms of the enzyme are equally sensitive to the action of a variety of chemical inhibitors.
4. An attempt is made to account for the changes in biological activity of the enzyme on the basis of the changes in physicochemical state upon adsorption and compression of the protein monolayer at the air-water interface.
5. "Denaturation," in the accepted sense of insolubilization and other concomitant physicochemical alterations of the native protein structure, does not necessarily involve a loss of biological activity.

INTRODUCTION

Mazia and Hayashi (1) have shown that the enzyme pepsin retains its activity after having been spread as a monolayer at the air-water interface followed by compression into a solid, insoluble fiber or thread. The most vexing problem in work of this kind is to determine whether the activity attributed to the enzyme molecules which have actually undergone interfacial denaturation might not rather be due to native, unspread protein which has become enfolded in the spreading film. Hayashi and Edison (2) have adduced much experimental evidence in favor of the view that the observed activity of pepsin-albumin monolayers is due to the surface-unfolded molecules themselves.

The present experiments were undertaken with catalase, the intracellular enzyme which catalyzes the decomposition of hydrogen peroxide,

¹ Most of these data are abstracted from a section of a thesis submitted in partial fulfillment of the requirements for the Ph.D. degree, Faculty of Pure Science, Columbia University.

² Some of the work reported in the section on the effect of chemical agents was supported by a grant from the National Research Council (Canada).

and were designed to permit comparison of the activities of the native and of the surface-denatured enzymes, and thus to test the generality of the conclusions of Hayashi and Edison.

METHODS

Two samples of crystalline beef liver catalase supplied by the Delta Chemical Works were used throughout. Solutions of the enzyme were prepared on the day that they were to be used. Pyrex-redistilled water and a McIlvaine's buffer at pH 6.9 were used routinely. The method of spreading at the air-water interface was that of Hayashi and Edison (2), with modifications already described (3). The experiments were not designed to yield information as to the extent of the unfolding of the catalase molecules, since this was not germane to the present study. Additional experiments were done with trough pH varying from 5.0 to 7.0, and others where spreading was done on saturated ammonium sulfate, without change in results. Fibers, formed by compression of the catalase monolayer (Devaux effect), were picked up from the surface of the trough, washed five times with buffer, and then placed directly into Warburg flasks and covered with 1 ml. of buffer. Following preparation of a group of fibers, the remaining solution was diluted with buffer such that a 1-ml. sample would show an activity of zero order with respect to substrate concentration; thus, the activity of the fibers might be compared with that of the native enzyme from which they were prepared. A 0.06% solution of hydrogen peroxide made up in buffer was used as substrate, 1 ml. being added to the side arms of the respirometer flasks; this concentration was sufficient to saturate the enzyme fibers, eliminating substrate concentration as a limiting factor in rate determination. The respirometer bath was maintained at 30°C. Thermobarometers had buffer in the vessel proper and substrate in the side arm; fibers heated for 15 min. at 100°C. were often included in the thermobarometer vessels (see preliminary observations below). Any non-enzymatic breakdown of the substrate was thus controlled.

Specific activity was defined as the rate of enzymatic activity per microgram enzyme nitrogen. Nitrogen determinations were done by digesting the enzyme fibers and solution with sulfuric acid, followed by Nesslerization; comparison with standard nitrogen solutions was made with a Klett photoelectric colorimeter.

In examining the effect of heat on the residual activity of the enzyme fibers and solutions, the following expedient was adopted in order to minimize the variability in fiber size. At the beginning of an experiment, each fiber and solution aliquot was placed in a Warburg flask and permitted to decompose its substrate, with rate k_1 , allowing time for the theoretical end point to be reached. If to this same vessel more substrate

was subsequently added, a decreased rate, k_2 , was noted, due both to the further dilution, and to previous inactivation of the enzyme by its substrate. If the difference between the two rates ($k_1 - k_2$) is Δk , $\Delta k/k_1$ is the per cent change in activity on the second run. After the first run, the Warburg vessels containing the *experimental* native and denatured enzyme preparations were capped with parafilm and placed in a constant-temperature bath for varying durations at $40-60^\circ\text{C.} \pm 0.02^\circ$; the *control* preparations remained at 25° . More substrate was then added to the side arms, and both experimentals and controls retested for activity. The difference between the factor $\Delta k/k_1$ of the experimentals and that of the controls is thus a measure of the effect of heat on the enzyme.

Ultraviolet irradiation was also used in an attempt to distinguish the activity of the fibrous from that of the native enzyme. Samples were placed in Syracuse dishes 3 cm. beneath a Westinghouse mercury vapor lamp delivering approximately 85% of its energy at $254\text{ m}\mu$, and irradiated for 4 hr. Activity was thereafter determined as described above. The rise in temperature under this source was insignificant.

RESULTS

Preliminary Observations

When washed fibers were covered with a dilute solution of hydrogen peroxide, a vigorous bubbling was seen to occur at their surface; after fibers had been heated for 15 min. at 100° all activity was lost (3). Their

TABLE I

Specific Activities of Fibers and Solutions

A: Same fibers and solution aliquots used for both activity and N determinations

Fiber	Specific activity	Solution	Specific activity
1	0.08	1	0.57
2	0.10	2	0.24
3	0.06	3	0.28
4	0.06	4	0.34
5	0.08	5	0.48
6	0.08	6	0.35
7	0.07	7	0.39
8	0.07	8	0.29
Average	$0.08 \pm .03$	Average	$0.37 \pm .11$

B: Activity and N determinations done on alternate samples

	Activity/ $\mu\text{g. N}$	
Fibers	0.09	
Solutions	0.33	
C:		
	A	G
$\frac{\text{Activity}/\mu\text{g. N solution}}{\text{Activity}/\mu\text{g. N fiber}}$	4.6	3.7

activity was pH dependent; at pH 2 all activity was gone; at pH 4 it was greatly reduced; but between pH 6 and 8 activities were high and practically identical as had been found for the enzyme in solution by Bodansky (4). The fibers were completely insoluble despite the high solubility of the crystals from which they were prepared. Heating the fibers while they were covered with buffer did not alter either their size or shape as seen with a microscope and camera lucida. Both fibers and solutions exhibited a definite lag period, such as that reported by Sizer (5), who, working

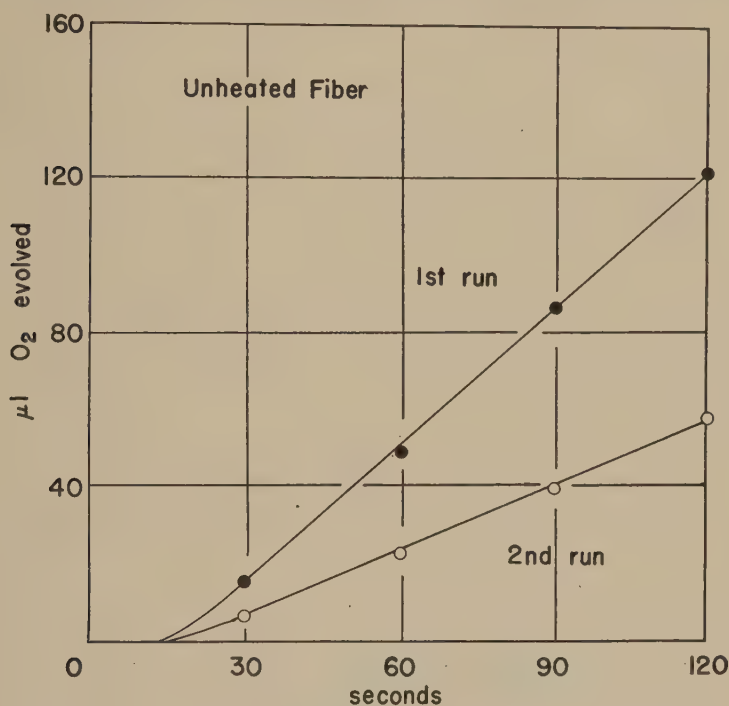


FIG. 1. Activities of fiber maintained at 25° for 60 min. between runs.

with the same general range of concentration of crystalline catalase in solution, also found kinetics described by the zero-order equation.

Specific Activities

Table I summarizes the data relating to the specific activity of native and fibrous enzymes. They indicate, as shown in part C, that the former was roughly four times as active as the latter.

Effect of Heat

If after a first run a group of fibers was heated for from 10 min. to 4 hr. at 50°C., their loss of activity on the second run was invariably less

than that of the unheated controls; in many cases, the activity of the heated fiber was greater on the second run than on the first, before heating. This is the phenomenon of "heat activation" of the surface-unfolded enzyme; it has never been observed with a solution of the native enzyme during the course of these experiments. Figure 1 represents the activity of a typical control fiber on two successive runs. In Fig. 2, another fiber has been heated at 50° between runs; its activity was greater on the second run than on the first, despite the increased dilution and inactivation by the substrate. Figures 3 and 4 represent an unheated and a heated

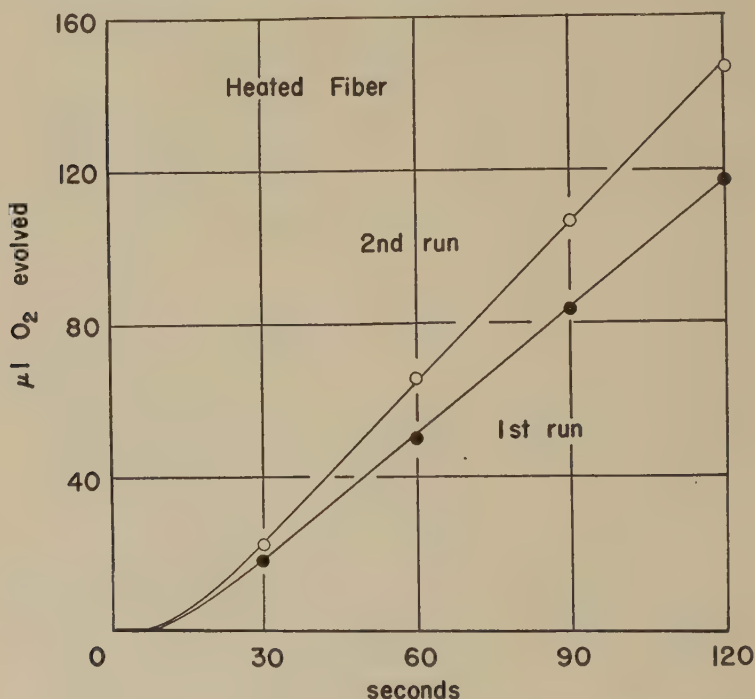


FIG. 2. Activities of fiber maintained at 50° for 60 min. between runs.

solution, respectively, the latter showing a slightly greater loss in activity on its second run than the former. Figure 5 represents the activity of fibers and solutions which were incubated between runs at 50° for durations of up to 8 hr.; each point is the average of four separate runs. Increase in activity for shorter durations of heat, as well as higher resistance to inactivation by heat of longer duration is clearly seen in the case of the fibers.

These data are summarized in Table II. The mean difference separating heated and unheated fiber populations is of extremely high signifi-

TABLE II

Activity Changes on Second Run for Fibers and Solutions

Experimentals heated at 50° for from 10 min. to 4 hr.; controls maintained at 25° for same period.

	Number of runs	$\overline{\Delta k}/k_1$	No. cases $\Delta k/k_1 \geq 0$	No. cases $\Delta k/k_1 \geq -0.10$
<i>Fibers</i>				
Experimentals	45	$-0.16 \pm .27$	15 (33.3%)	21 (47%)
Controls	67	$-0.45 \pm .16$	1 (1.5%)	2 (3%)
Difference of means		$0.29 \pm .04, t > 7^a$		

Solutions

Experimentals	12	-0.63	0	0
Controls	21	$-0.38 \pm .08$	0	0

^a For significance at .01 level, ($n = 30$), $t > 2.58$.

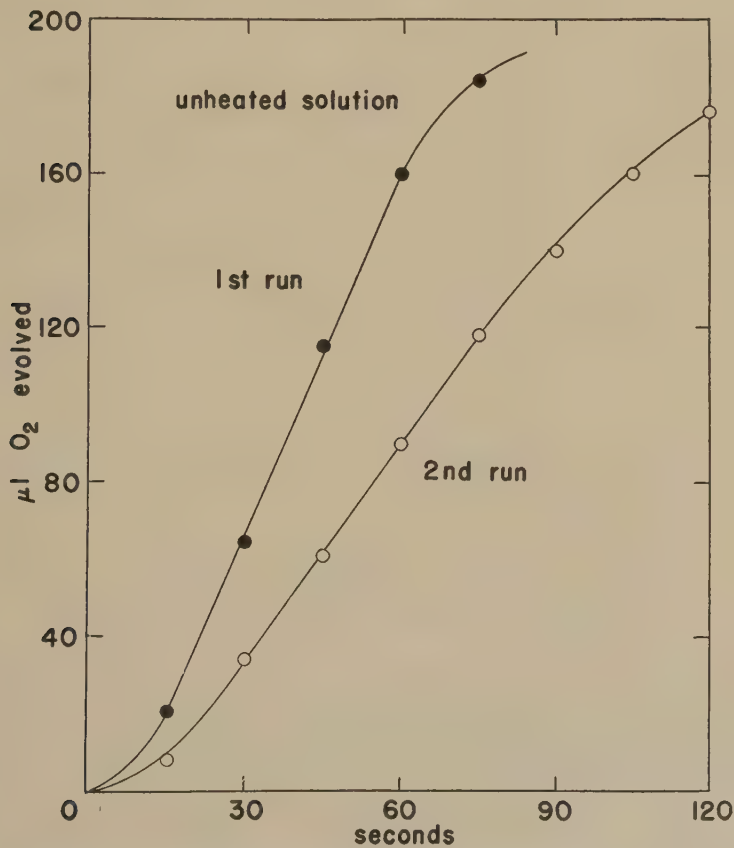


FIG. 3. Activities of solution maintained at 25° for 60 min. between runs; $\Delta k/k_1 = -0.49$.

cance, being well below the 1% level (6). Almost half the heated fibers showed less than a 10% loss ($\Delta k/k_1 \geq -0.10$) in activity on the second run. In the case of 21 control solution aliquots, and 49 experimentals, heated for varying times between 40 and 60°, the least loss of activity recorded was -0.25 . The difference between the mean activity change ($\overline{\Delta k/k_1}$) of control solutions and control fibers is not significant.

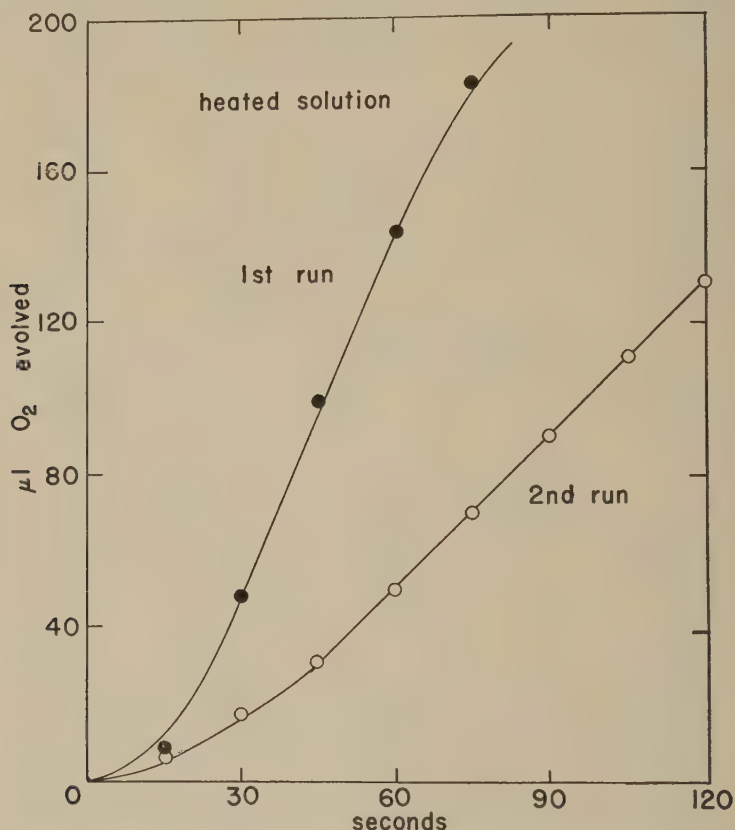


FIG. 4. Activities of solution maintained at 50° for 60 min. between runs; $\Delta k/k_1 = -0.54$.

Heating for a standard period of time at varying temperatures is illustrated in Fig. 6. Heat activation of the fibers at 50° is again seen, as well as their much greater resistance to inactivation at 55°.

In all these experiments, the $\Delta k/k_1$ of the control fibers was completely independent of the magnitude of k_1 ; the extent of the decrease on the second exposure to substrate depends on some variable factor as yet unknown, but probably connected with the method of preparation of the fibers. The observed effects of heat on the enzyme were independent of

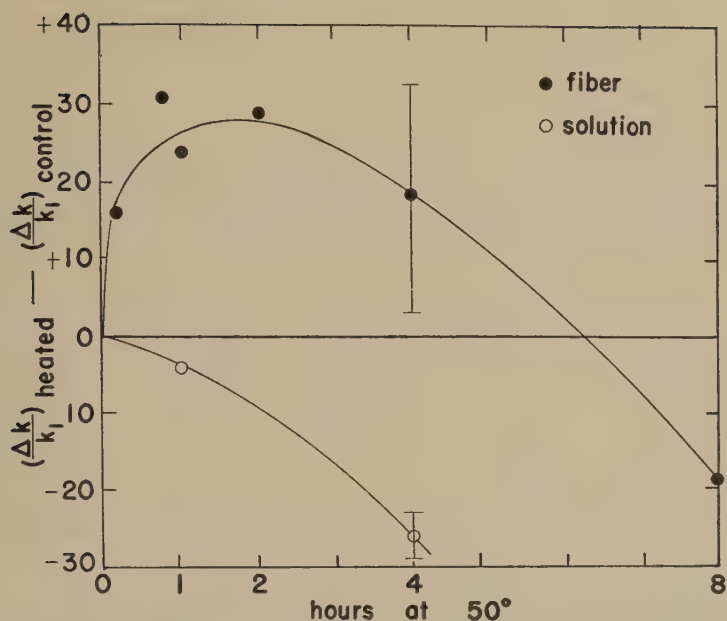


FIG. 5. Activities of fibers and solutions maintained at 50° for varying times between runs; standard deviations are shown for the 4-hr. points. Each point is the average of four individual runs.

its prior contact with substrate, as was shown by a parallel series of experiments in which fibers of approximately equal size, and aliquots of solution were heated directly without any preliminary run. Results were unchanged.

Ultraviolet Irradiation

The data on the effect of ultraviolet on the enzyme are presented in Table III. It will be noted in comparing cols. *a* and *a'* that the initial

TABLE III

Effect of Ultraviolet Irradiation on Fibers and Solutions
One of each pair of fibers and solutions irradiated for 4 hr.

Experiment	Solutions			Fibers		
	<i>a</i>	<i>b</i>	<i>c</i>	<i>a'</i>	<i>b'</i>	<i>c'</i>
	Activity	Activity irradiated	Per cent activity retained	Activity controls	Activity irradiated	Per cent activity retained
1	9.2	0.44	5	2.4	1.9	79
	7.8	0.40	5	2.5	1.2	48
	8.5	0.44	5	2.5	1.1	44
2	4.2	0.08	2	2.6	1.7	65
	4.4	0.08	2	2.3	1.3	57
	4.3	0.08	2	1.9	1.1	58
	Average		4 ± 2	Average		59 ± 13

activities of the unirradiated solutions are several times as great as those of the control fibers. Despite this, the fibers show but a 41% decrease after irradiation of intensity sufficient to eliminate virtually all the activity of the solutions.

The significance of these experiments is not entirely clear, since it is not impossible that certain of the enzyme molecules at the center of the fiber might be "shielded" by those at the periphery. While this appears unlikely, due to the low specific absorption by protein of ultraviolet

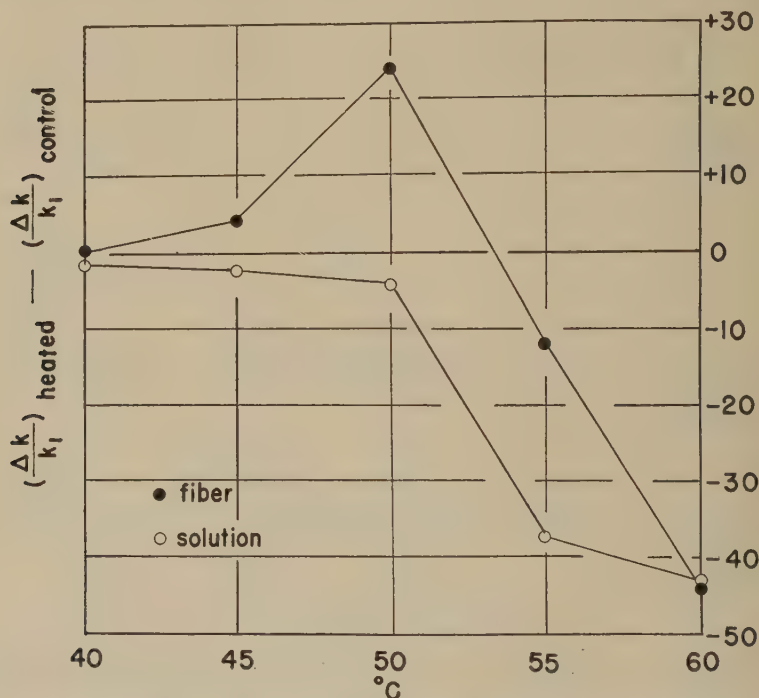


Fig. 6. Activities of fibers and solutions maintained for 60 min. at varying temperatures. Each point is the average of eight individual runs.

energy of the wavelength used, it cannot be ruled out completely on the basis of the present data. Preliminary attempts³ to measure by means of a quartz microscope and photometer the absorption by catalase fibers of monochromatic ultraviolet light (254 mμ) showed that there was never less than 1% transmission at their densest point and up to 20% elsewhere. This approach was abandoned, since it could be maintained that light was being transmitted through "interstices" in the fiber rather than through the uppermost protein layers. This question is currently being examined

³ Kindly made by Dr. Martin Flax, in the laboratory of Professor A. W. Pollister, Department of Zoology, Columbia University.

in this laboratory (Dalhousie) by the measurement of the effect of ultra-violet energy on the uncompressed films themselves.

Chemical Agents

An attempt was made to characterize fibers and solutions on the basis of a differential susceptibility to inhibition by chemical agents. This was unsuccessful; any inhibitor which would depress or eliminate the activity of the native enzyme would do the same for the fibers at identical concentrations. Specific iron enzyme poisons which were strongly effective against both were cyanide, azide, and hydroxylamine. Both were sensitive to protein denaturants and precipitants such as trichloroacetic acid and heavy metals; tin (Sn^{++}) was especially effective. Formate, one of the anions found by Agner and Theorell (7) to be most effective against catalase, was a good inhibitor of the fibers.

A series of experiments⁴ was undertaken on the effect of monoiodoacetic acid. The non-ionized acid alone was inhibitory, since at pH 6.9 no evidence of inhibition of either fibers or solutions was noted, even with final concentrations of iodoacetate as high as 0.06 *M*; this confirms the results reported by Aldous (8) on the mode of action of this inhibitor against cellular enzymes. Care must be taken to employ highly purified iodoacetic acid, as free iodine was found to be a potent inhibitor of the enzyme in both forms.

At pH 4.1, where inhibition by the undissociated acid was marked, it was found that the minimum concentration of this agent required per microgram of enzyme nitrogen to attain a given level of inhibition of enzymatic activity was, within experimental error, the same for both native and fibrous catalase. For example, in preparations containing 10 μg . enzyme N/ml. buffer, a final concentration of 10^{-3} *M* iodoacetic acid reduced the activity of both fibers and solutions to one-half that of the controls. In this series of experiments, films were spread on a substratum buffered at pH 5.7, the isoelectric point of beef liver catalase.

DISCUSSION

Reduction in Specific Activity After Interfacial Unfolding

The specific activity of the surface-unfolded catalase has been shown to be considerably lower than that of the soluble enzyme from which it was prepared. Harkins, Fourt, and Fourt (9), in what was primarily an immunochemical study, found that catalase layers adsorbed on plates from uncompressed films possessed enzymatic activity which was estimated as being between one-fifth and one-tenth of that of the native enzyme.

⁴ Performed in collaboration with Dr. J. G. Aldous and with the technical assistance of D. K. R. Stewart, of the Department of Pharmacology, Dalhousie University.

The explanation for the reduction in activity cannot be that the fibrous enzyme was localized at one restricted region of the reaction vessel, since reaction kinetics have been shown to be of zero order, and since both fibrous and soluble enzymes have been inactivated to the same extent by substrate (Table II, controls) and by iodoacetic acid. Two alternate, but not mutually exclusive, hypotheses suggest themselves:

(a) The steric rearrangement caused by the high interfacial energy at the air-water interface, which transforms the native protein into an insoluble monolayer, might result in a reduction in activity of each of the active centers of the enzyme molecule.

(b) In the process of spreading the film and compressing it into a fiber, certain of the original active centers become "buried," or inaccessible to the substrate.

On the basis of the present data, it is not possible to favor one or the other of these hypotheses.

Activation by Heat

Pretreatment of the fibrous enzyme with heat results in an increase in residual activity, as compared to the unheated controls. A theoretical heat-labile inhibitor occasionally invoked to explain this type of phenomenon (5,10) is ruled out since an activation of the soluble enzyme from which the fibers were prepared has never been observed in these experiments. Therefore, heat must in some way restore a part, but not all, of the activity lost during formation of the fibers. A rather extensive literature demonstrating a heat activation of catalase within a variety of intact cells has been discussed elsewhere (11).

Resistance to Inactivation by Heat and Ultraviolet Irradiation

When a monomolecular film of protein is compressed beyond a certain point, it collapses as a result of the formation of intermolecular linkages at high film pressures (usually between 15 and 30 dynes/cm.); when continued, the compression (in the case of most proteins) leads to the formation of completely insoluble threads or fibers, which, according to Astbury (12), "are, in a way, rough crystals of denatured protein made by pressing the polypeptide chains into parallel bundles." As a result of the strong intermolecular linkages formed during compression, the completely collapsed monolayer is no longer able to demonstrate even the slightest increase in area upon decompression. These linkages are conceived of as responsible for the great stability of the fibers to intensities of heat and ultraviolet energy sufficient to inactivate the native enzyme in solution.

Biological Activity of Surface-"Denatured" Proteins

The first work on catalase at the air-water interface was that of Langmuir and Schaefer (13), who found that films of this enzyme retained their ability to decompose hydrogen peroxide after having been transferred to conditioned plates. They concluded that further work (as yet unreported) must be done "to determine whether in the case of catalase, as with urease, the activity of the monolayer is due to unspread molecules enmeshed in the fabric of the spread monolayer." This interpretation was found by Harkins, Fourt, and Fourt (9) to be somewhat inconsistent with their own data.

In the case of the data presented above, it is not economical to attribute the activity of the surface-unfolded enzyme preparations to the presence of native molecules, since the activity of the latter was qualitatively and quantitatively different from that of the former.

Hayashi and Edison (2) have likewise, by means of a wholly different line of attack, eliminated entrapped, native molecules as an explanation of the peptic activity of fibers prepared from pepsin-albumin monolayers. The activity of pepsin and catalase fibers is, therefore, due to those enzyme molecules which have actually undergone interfacial unfolding. This is not surprising, since even the very sensitive immunological properties of protein antigens may be retained after they have been completely unfolded into monolayers one amino acid residue in thickness (14). Chambers (15) has clinched the matter by showing that the degree of specificity of the reaction between an antibody and a nucleoprotein antigen adsorbed from a monolayer to a conditioned plate depends on whether the hydrophobic or hydrophilic face of the monolayer is uppermost on the plate after adsorption; further, the magnitude of the difference in reactivity of the two faces increases as the film spreads more completely. These are matters of no concern to native protein molecules. The retention of activity of fully unfolded protein molecules suggests that the sequence of amino acids within polypeptide chains and the juxtaposition of amino acid side chains in polypeptide main chains are of importance in determining the biological and immunological specificity of protein equal to that of the final configuration, that is, the way in which the molecule is "rolled-up" into its native form.

The persistent dogma in biochemistry, stemming from Northrop's classical experiments (16), that a "denatured" (in the sense of rendered insoluble) protein loses its biological activity, can no longer be held (17). It should be noted that the protein in monomolecular films is denatured, since these films are completely insoluble, and may be repeatedly compressed to the same area, with no loss of protein to the aqueous phase beneath (13); indeed, Neurath *et al.* (17) consider that interfacial dena-

turation is the most severe of all methods of denaturation, since the structure of the native protein molecule is more radically altered by this treatment. Langmuir (18) remarked some years ago that there are cases "where, according to one definition, denaturation has occurred, while according to others it has not." This is amply illustrated by the present paper, where the biological activity of catalase has been shown to be retained despite changes of the most drastic kind in its physicochemical properties.

Experiments published elsewhere (11,19) demonstrate that the catalase of intact erythrocytes shares point for point the properties of the surface-unfolded enzyme described above, whereas, after extraction from the cell, the properties of the soluble erythrocyte catalase change to those of the native enzyme in the present studies.

ACKNOWLEDGMENTS

The author expresses his gratitude to Professor Teru Hayashi, who first interested him in this line of research, and who suggested this problem to him. He is indebted, also, to Dr. Amos Norman, Dr. Morris Foster, Professor John Gregg, Professor John Aldous, and to Sylvia Kaplan who prepared the figures. This work was made possible by support under the Servicemen's Readjustment Act ("GI Bill of Rights") which fact the author acknowledges gratefully.

CONCLUSIONS

1. Catalase, spread as a monomolecular film at the air-water interface and compressed into a fiber or thread, retains its enzymatic activity.
2. There are certain regular differences which distinguish the activity of the surface-unfolded enzyme from that of the native protein from which it was prepared. In view of this, it is not possible to ascribe the activity of the former to the presence of the latter.
3. Denaturation, in the sense of alteration of physicochemical properties, need not involve the loss of biological activity of catalase.

REFERENCES

1. MAZIA, D., AND HAYASHI, T., *Arch. Biochem. Biophys.*, in press (1952); MAZIA, D., HAYASHI, T., AND YUDOWITZ, K., *Cold Spring Harbor Symposia Quant. Biol.* **12**, 122 (1946).
2. HAYASHI, T., AND EDISON, G., *J. Colloid Sci.* **5**, 437 (1950).
3. KAPLAN, J. G., *Federation Proc.* **9**, 69 (1950).
4. BODANSKY, M., *J. Biol. Chem.* **40**, 127 (1919).
5. SIZER, I., *J. Biol. Chem.* **154**, 461 (1944).
6. FISHER, R. A., *Statistical Methods for Research Workers*, 5th Ed. Oliver and Boyd, London, 1934.
7. AGNER, K., AND THEORELL, H., *Arch. Biochem.* **10**, 321 (1946).
8. ALDOUS, J. G., *J. Biol. Chem.* **176**, 83 (1948).
9. HARKINS, W., FOURT, L., AND FOURT, P. C., *J. Biol. Chem.* **132**, 111 (1940).

10. SUMNER, J. B., AND SOMERS, G. F., *Chemistry and Methods of Enzymes*, 2nd Ed., see p. 39. Academic Press, New York, 1947.
11. KAPLAN, J. G., *Physiol. Zool.* **25**, 123 (1952).
12. ASTBURY, W. T., *Cold Spring Harbor Symposia Quant. Biol.* **6**, 148 (1938); MAZIA, D., HAYASHI T., AND YUDOWITZ, *loc. cit.*
13. LANGMUIR, I., AND SCHAEFER, V. J., *Chem. Revs.* **24**, 181 (1939).
14. BATEMAN, J. B., CALKINS, H. E., AND CHAMBERS, L. A., *J. Immunol.* **41**, 321 (1941); CHAMBERS, L. A., BATEMAN, J. B., AND CALKINS, H. E., *J. Immunol.* **40**, 483 (1941); ROTHEN, A., CHOW, B. F., GREEP, R. O., AND VAN DYCK, H. B., *Cold Spring Harbor Symposia Quant. Biol.* **9**, 272 (1941); ROTHEN, A., AND LANDSTEINER, K., *Science* **90**, 65 (1939); ROTHEN, A., AND LANDSTEINER, K., *J. Exptl. Med.* **76**, 437 (1942).
15. CHAMBERS, L. A., *J. Immunol.* **36**, 543 (1939).
16. NORTHROP, J. H., *J. Gen. Physiol.* **14**, 713 (1931).
17. NEURATH, H., GREENSTEIN, J. P., PUTNAM, F. W., AND ERICKSON, J. O., *Chem. Revs.* **34**, 157 (1944).
18. LANGMUIR, I., *Cold Spring Harbor Symposia Quant. Biol.* **6**, 161 (1938).
19. KAPLAN, J. G., *Federation Proc.* **10**, 72 (1951).

AN ELECTRON DIFFRACTION STUDY OF THE REORIENTATION OF CERTAIN ALKALI HALIDES DEPOSITED ON MICA AND ON MICA SURFACES COVERED BY ORGANIC FILMS¹

G. R. Holzman² and K. H. Moore

Physics Department, Rensselaer Polytechnic Institute, Troy, New York

Received February 22, 1952; revised April 16, 1952

ABSTRACT

In 1937, Bradley found that certain alkali halides deposited on organic films of considerable thickness covering freshly cleaved mica surfaces were capable of reorientation by mica when exposed to steam. The reorientation observed by Bradley resulted in tetrahedral forms visible optically.

We have investigated this phenomenon using electron diffraction, and have made a rather complete study of iodide layers deposited on mica, on organic films covering mica, and on organic films alone. Deposition was by evaporation in air, since iodide evaporated in vacuum penetrates thin organic films. In all cases, the reorientation was the same, and involved the presence of water vapor in limited quantity.

Diffraction studies of iodide layers freshly deposited on mica show partial tetrahedral orientation; iodide layers on organic films show no such orientation whether the film is on mica or not. Exposure to water vapor produces complete tetrahedral orientation in iodide layers on bare or covered mica; none occurs on organic films alone. The reorientation may be due either to the propagation of mica surface forces through the intermediate film or to the diffusion of iodide through organic films which are not on mica, when water vapor is used. If diffusion is basic to the process, it is due to the mica.

INTRODUCTION

The subject of surface forces has always been of interest to the physicist, chemist, and biologist because of the part these forces play in catalysis, adsorption, biological reactions, lubrication, fluid flow, suspension of colloidal particles, strength of films, oriented overgrowth, and many other special fields. In the study of surface forces, the range of propagation has been found to be a most important and amazing property.

The history of investigation concerning the effective range of surface forces has been adequately described by McBain (1). A complete review of experiments which were directly responsible for these concepts can

¹ A preliminary version of this paper, which is part of a Ph.D. thesis, was presented before a spring meeting, April, 1951, of the American Physical Society at Rensselaer Polytechnic Institute at Troy, New York, and at a Symposium on Surfaces sponsored by the Armour Research Foundation in June, 1951, at Chicago.

² Present address: Behr-Manning, Troy, New York.

also be found in a summary, "The Depth of the Surface Zone of a Liquid," by Henniker (2) who has listed some 174 papers. Included among these papers is an extremely interesting experiment by Bradley (3) on oriented overgrowth.

Bradley deposited, directly from solution, films of stearic acid, octane,

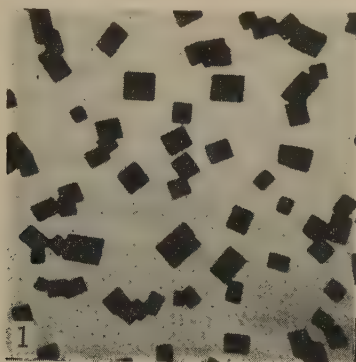


FIG. 1. Electron micrograph (5000 \times) of KI on a Formvar film after exposure to steam.

cellulose acetate, and rubber on top of freshly cleaved mica surfaces. Ammonium iodide was then sublimed in air and collected on top of these films. No external symmetry was observable under a high-power microscope. After briefly exposing the iodide layer to steam, it was found to be made up of microscopically visible, discrete tetrahedrons having $[111]$

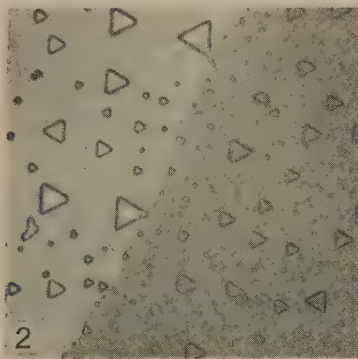


FIG. 2. Reoriented NH_4I on mica partially covered by 800-Å. cellulose acetate (500 \times).

planes face down on the film. Iodide layers deposited on most surfaces, including the cellulose acetate and other covering films mentioned above, show cubic external symmetry after exposure to steam, the basal $[100]$ plane being parallel to the underlying surface, as shown in Fig. 1. Figure 2 is a recent photograph taken at Rensselaer Polytechnic Institute showing

tetrahedral reorientation of ammonium iodide. The field to the left of the diagonal line shows iodide on bare mica; to the right, the iodide is on a film of cellulose acetate 800 Å. thick, formed on the mica before the iodide was laid down. It was found that as the thickness of the film was increased, the crystals of ammonium iodide changed in external appearance from tetrahedral and regular to cubic and irregular, with hexagonal and dendritic forms as intermediates.

This is actually a problem of oriented overgrowth, which Royer (4) has termed "epitaxy." Royer concluded that one of the most important conditions to be satisfied for an induced orientation was that the lattice spacing (or the distances between two ions) in the faces of the two crystals in contact must be almost identical or be in a simple numerical ratio. Since Royer's work in 1928, many workers have investigated epitaxy of various sorts. It has been found, for instance, that in some cases the condition of close match of lattice spacings is not so stringent as Royer supposed. Mica forms hexagons with oxygen and silicon atoms alternating, and the linking of these together gives sheets which are separated by metal atoms. The spacing between the centers of the hexagons, i.e. between the metallic atoms which separate the sheets is 5.2 Å.; this is very near the value of the edge of the smallest tetrahedron which can be cut from an ammonium iodide cubic crystal.

Bradley concluded on the basis of experiments that a mica surface force was propagated through the intervening film to influence the iodide orientation.

One objection to such a conclusion is that micropores exist in the film, and that reorientation may proceed from nuclei actually in contact with mica in the pores. Against this he reasoned:

(a) A distribution in which all the crystals are of the same type over a large area would be improbable. If the pore theory held, one would expect to find a mixture of irregularly arranged cubic crystals together with the tetrahedra.

(b) It is not clear how the pores could cause the growth of the perfectly tetrahedral forms, and at the same time the absence of pores cause the intermediate forms.

As previously stated, if the sublimed iodide layer of the Bradley experiment is examined under a microscope before exposure to steam, it is impossible to observe any external symmetry. This does not necessarily mean that the iodide is unoriented. It does mean that it is impossible to detect the orientation using a microscope. Consequently, a thorough study of Bradley's experiment was conducted using electron diffraction techniques, which would be the most sensitive means of detecting orientation via internal atomic symmetry.

EXPERIMENTAL PROCEDURES AND RESULTS

The sublimation process which has been mentioned several times is a simple process of evaporation, in air, from the solid state. A drop of iodide solution is placed on a microscope cover slip and dried over an electric hot plate. A small glass chimney approximately $\frac{3}{4}$ in. in diameter is placed over the cover slip bearing solid iodide, and the surface to be covered placed over the chimney. As heating continues, a dense white smoke appears in the chimney and is collected on the test surface. The visible smoke indicates that nuclei are formed, in air, from the vapor phase, and that the deposited layers reach the substrate in the form of crystalline aggregates. While microscopic examination shows little if any external symmetry, electron diffraction patterns³ tell another story. Figure 3 is a reflection pattern of NH_4I deposited as described on a freshly cleaved mica surface. The electron beam is parallel to the (*a*) axis of mica. The

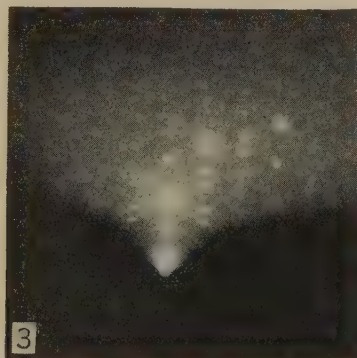


FIG. 3. Electron diffraction pattern of NH_4I on bare mica (beam parallel to (*a*) axis of mica).

pattern indicates that most of the iodide is oriented, with $[111]$ planes parallel to the mica surface, and a $[110]$ axis parallel to the (*a*) axis of mica. For brevity, this arrangement will hereafter be referred to as "tetrahedral orientation." There is evidence of some randomly oriented crystals, and some basal cubic ($[100]$ fiber axis) orientation appears.

At first it might appear that there are too many reciprocal lattice points present in Fig. 3. It should be noted, however, that the tetrahedral orientation can take two positions on the mica (twinning). The cuts through the reciprocal lattice will be different.

If the (*a*) axis of the mica is rotated 30° from the direction of the beam, Fig. 4 is obtained. Cuts through the reciprocal lattice are now the same for twinned crystals.

³ All diffraction patterns were obtained using an accelerating potential of 50 kv. and a specimen-plate spacing of approximately 40 cm.

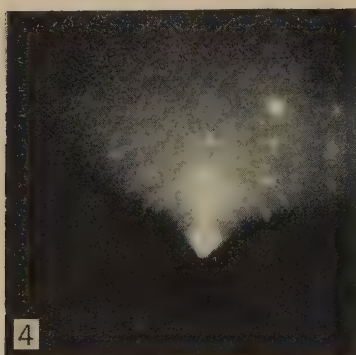


FIG. 4. Same as Fig. 3, but beam is at 30° to (*a*) axis of mica.

Complete tetrahedral reorientation of the NH_4I is achieved by momentarily holding a finger approximately 1 cm. above the mica surface which is covered with iodide. This may be seen in Fig. 5 which is the same as Fig. 4 except that it is completely void of diffraction rings and extra spots. Figure 5 is typical of a completely oriented pseudo single crystal. Figure 6 is a micrograph of such a surface, showing that reorientation has proceeded to such an extent that no twinning is evident. The crystallites are actually small visible tetrahedrons, all identically oriented.

It may, therefore, be stated that even though no visible tetrahedral orientation can be seen when looking at air-sublimed NH_4I on mica with a microscope, an electron diffraction study reveals considerable orientation. Furthermore, exposing the NH_4I layer to highly concentrated water vapor (as in the case of Bradley's steam) is unnecessary to produce orientation. It may be concluded that the mica surface forces reorient the NH_4I aggregates that are in intimate contact with the mica.

While evaporation in air resulted in only partial orientation of the iodide deposited on mica, the layers collected during *high vacuum* evapora-

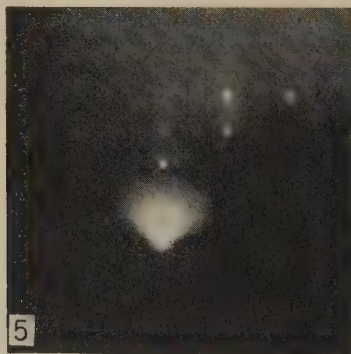


FIG. 5. Completely reoriented NH_4I on mica, beam at 30° to mica (*a*) axis.

tion showed complete tetrahedral orientation, as formed. It was, therefore, decided to investigate Bradley's work using vacuum evaporation. A thin film of the iodide was deposited by evaporation in a high vacuum, on one side of a 100-A. thick Formvar film, the other side of the film being carefully shielded. An electron diffraction reflection pattern (Fig. 7)

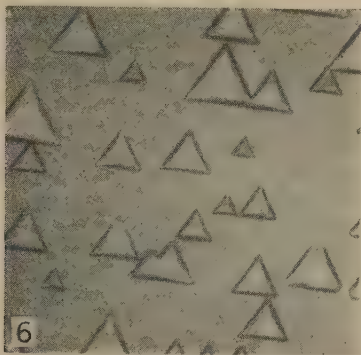


FIG. 6. Micrograph (500 \times) of completely reoriented NH_4I on mica.

of the shielded side showed the presence of iodide with some basal orientation. It seems probable that in the high-vacuum evaporating process, molecules and not crystalline aggregates arrive at the condensing surface. Because of their size and kinetic energy, they may be projected directly through the film or within a few angstroms of the farther surface. It is

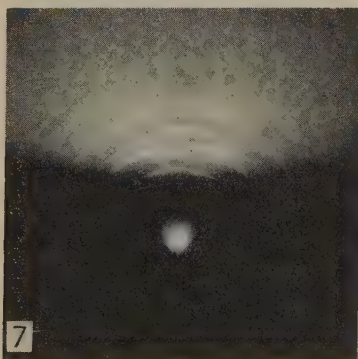


FIG. 7. Electron diffraction pattern of rear surface of 100-A. Formvar film, NH_4I vacuum-evaporated on front surface.

obviously ineffectual to perform Bradley's experiment using high-vacuum evaporation.

The very same experiment was then performed by evaporating NH_4I and KI in air (as per Bradley), and collecting it upon one face of a 100-A. thick Formvar film. The other side, face No. 2, was inspected by electron

diffraction reflection. No iodide pattern whatsoever was discernible. To make sure the iodide was actually present on face No. 1 of the film in the path of the beam, an electron diffraction *transmission* pattern was taken of the same area of the specimen. This exhibits partial basal orientation similar to that of vacuum-evaporated iodide, and is typical of cubic crys-

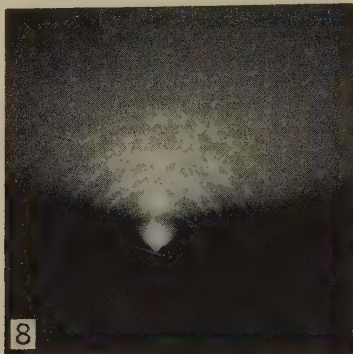


FIG. 8. NH_4I evaporated in air and collected on 800-A. cellulose acetate film on mica.

tals condensed on an amorphous surface. It was concluded, therefore, that the aggregates deposited during evaporation in air were too large to pass through the film.

The next investigation was concerned with iodide layers collected, after evaporation in air, on mica surfaces covered with thin organic films. Microscopic examination shows no observable orientation. Figure 8 is an

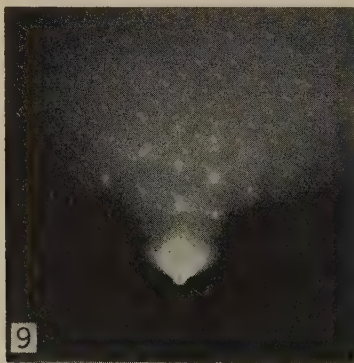


FIG. 9. Same as Fig. 8, but reoriented by "finger treatment."

electron diffraction reflection pattern of NH_4I evaporated in air and collected upon a cellulose acetate film approximately 800 Å. thick which had been formed from solution directly on a freshly cleaved mica surface. No tetrahedral orientation is evident, although basal orientation is strongly developed.

If a finger is held momentarily approximately 1 cm. above the iodide surface, complete tetrahedral reorientation results. Figure 9 is an electron diffraction reflection pattern of this result with the direction of the beam parallel to the mica (*a*) axis. This pattern indicates that all the tetrahedrons are oriented in the same direction over the area traversed by the electron beam. One may conclude that the surface force, after propagating a distance equal to the film thickness, is not of sufficient strength to cause the reorientation of large aggregates. It is possible that the finger treatment supplies enough water vapor to cause mobility on the surface and permit the mica surface forces to reorient the iodide.

The thickness of the organic film on mica that could be used and still reorient NH_4I was also investigated. The maximum thickness of Formvar that could be used was approximately 200 Å. The maximum thickness of chlorinated rubber that could be used was also about 200 Å. Chlorinated

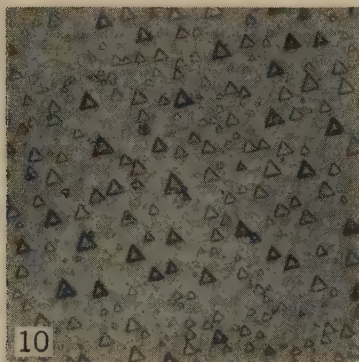


FIG. 10. Micrograph (500 \times) of RbI reoriented on 200-Å. composite film on mica.

rubber was used because it has been reported to be practically impervious to water vapor. Composite films of 100 Å. of Formvar and 100 Å. of chlorinated rubber formed on mica permitted complete orientation of NH_4I collected after being evaporated in air and passed quickly through steam. Figure 10 shows a micrograph of the reorientation in this case. The maximum thickness for cellulose acetate films is about 1500 Å.

Rubidium iodide and potassium iodide were used in place of ammonium iodide with the same results.

As a result of this work, it seems that there is a rather sharp cutoff point or critical thickness beyond which no orientation is possible. The mica surface force may cause a virtual orientation in the organic film for a specific distance, and beyond this distance there is little if any virtual orientation.

Electron diffraction reflection patterns of a mica surface covered with a 100 Å. film of Formvar only showed no specific structure. Patterns for

cellulose acetate and chlorinated rubber gave the same result. If any structure does exist in the films, it is impossible to detect it by electron diffraction so that it may be termed virtual.

It has been suggested that the reorientation of iodide collected on organic films covering mica may be the result of lateral propagation from microscopic points as projections of mica extending through the organic film. As a test of this hypothesis, a small hole was punched in a sheet of mica, and a cellulose acetate film 800 Å. thick was then formed on water and picked up by the mica so that the film covered the hole. NH_4I was deposited by evaporation in air and reoriented by holding a finger slightly over the surface. When viewed under a microscope, tetrahedral orientation prevailed up to the edge of the hole and then ceased. A similar experiment was performed by placing a very thin piece of mica 1000 Å. thick on top of a microscope slide and covering both the mica surface and the exposed glass surface with NH_4I . "Finger treatment" resulted in tetrahedral reorientation, but only on the mica surface. No fringing effects are visible at the edge of the mica. This leads to the belief that the reorientation is not propagated laterally from a reorientation center, which discourages the explanation that small mica projections protrude through the film causing orientation by lateral growth over the entire surface. As a matter of fact, mica splits in steps of the unit cell and sometimes in steps of half a unit cell, and there are always large sections which are absolutely smooth.

In connection with the experiments involving iodide deposited on mica covered by organic films, it will be noted that the presence of water vapor, even if only from a finger tip held close to the surface, was necessary for the production of tetrahedral reorientation. It was also used for *complete* (and visible) reorientation on bare mica. Some questions about the role of the water vapor inevitably arise, particularly in connection with the use of organic covering films. Since most of the films used are pervious to water vapor, with chlorinated rubber a possible exception, the question arises as to whether water may not dissolve some iodide, diffuse with its solute through micropores in the organic film, and thus allow the growth of tetrahedrally oriented crystals of iodide by direct contact with the mica.

Experience indicated that the manner of production of the organic film was immaterial, as far as orientation effects are concerned. That is, it makes no difference whether the film is produced by applying a solution of, say, Formvar or cellulose acetate to the mica and letting it dry, or whether the film is formed first on water or on glass and is then transferred to a freshly cleaved sheet of mica. Freshly cleaved mica exhibits a tremendous adhesive force for a thin film placed in contact with its surface. The 800-Å. acetate film which covers part of the field in Fig. 2 was

formed on water and transferred to mica before deposition and reorientation of the iodide layer.

Experiments were made to investigate the possible diffusion of iodide, via solution in water, through organic films which were not on mica. Ammonium iodide was evaporated in air and collected on one side of a 100-A. Formvar film. The sample was then exposed to saturated steam for several minutes. An electron diffraction reflection pattern of the other side of the film showed no sign of iodide—it had not diffused through the film. Transmission patterns showed that iodide was really present on the face originally covered. The same results were observed using KI and RbI on Formvar, and also using the three iodides on cellulose acetate films as thin as 800 Å. If diffusion does take place when the film is in contact with mica, it is due to the action of the mica and is a forced phenomenon, caused by mica surface forces.

Another experiment which suggests itself is the following: coat mica with an organic film; deposit and reorient a layer of iodide; then strip the organic film and iodide layer away from the mica and examine the back (mica side) for the presence of iodide. This was attempted, but unsuccessfully. The adhesion of the organic films on mica was too great to permit their removal without destruction. No conclusive results could be obtained.

ACKNOWLEDGMENT

The authors wish to thank the Research Committee (Rensselaer Polytechnic Institute) for a grant which enabled the improvement of the electron diffraction equipment used in this investigation.

DISCUSSION AND SUMMARY

1. The iodides used (NH_4I , KI, and RbI) condense from the vapor phase (high-vacuum evaporation) directly and completely into a tetrahedrally oriented layer upon bare, freshly cleaved mica, as would logically be expected.

2. The iodides, however, go through or are deeply imbedded in thin organic films when condensed on them during high-vacuum evaporation. When evaporated in air and collected upon thin organic films, the iodides do not pass through or deeply imbed themselves. Evaporation in air was used for all later investigation.

3. Iodides deposited on bare mica show a partial tetrahedral orientation.

4. Iodides deposited on thin organic films covering freshly cleaved mica show no tetrahedral orientation. Most of the crystals are randomly oriented, but some show basal orientation.

5. Exposure to small amounts of water vapor causes complete tetrahedral orientation of iodide, both on bare mica and on organic films covering mica.

6. There is a maximum thickness of film beyond which orientation does not take place. This ranges from about 200 Å. for Formvar to 1500 Å. in case of cellulose acetate.

7. There is no evidence of lateral propagation of the tetrahedral orientation from points or edges of mica, with or without water vapor present.

8. There is no evidence of diffusion of iodide, as solid or in solution, through organic films with no mica backing.

In view of the complexities involved in problems of interaction, it is impossible to be specific as to the actual mechanism which will explain the above experimental work. A few of the more obvious mechanisms are as follows:

(a) As has been suggested previously, the mica surface forces may be propagated through the organic film to interact specifically with the iodide and cause its reorientation. As far as electron diffraction evidence is concerned, any orientation in the film must be virtual for no unusual structure is discernible.

(b) Water vapor was a necessary adjunct to the reorientation procedure. It may play a role more extensive than merely allowing easy recrystallization of the iodide. The mica surface forces may act on the polar water on the surface of the organic film and cause it to migrate through the micropores. The mica surface forces may also be propagated through the organic film via the polar water which has diffused through the micropores. In either case the iodide might be carried through as a solute, or might be affected at the surface, by the water in the micropores.

(c) It may be possible, from a model of the mica surface and of the iodide surface, to calculate van der Waals-London forces which would be of sufficient strength and specificity to cause the reorientation.

REFERENCES

1. MCBAIN, J. W., *Colloid Science*. Reinhold, New York, 1950.
2. HENNIKER, J. C., *Revs. Modern Phys.* **21**, 322 (1949).
3. BRADLEY, R. S., *Z. Krist.* **96**, 499 (1937).
4. ROYER, L., *Bull. soc. franç. minéral.* **51**, 7 (1928).

THE EFFECT OF TEMPERATURE ON THE ELECTROPHORETIC ANALYSIS OF COTTONSEED MEAL EXTRACTS

Melvin L. Karon, Mabelle E. Adams and Seymour Newman¹

Southern Regional Research Laboratory,² New Orleans, Louisiana

Received March 3, 1952

ABSTRACT

The electrophoretic patterns of a cottonseed meal extract in the ethylamine barbital buffer (pH = 10.4 at 25°C.) have been investigated over the range of 0 to 20°C. The results indicate that there is no change in the relative concentrations of the components as a function of temperature. The application of a single viscosity correction to the solvent could not entirely compensate for the change in mobility of each component with temperature. The viscosity-mobility product displayed a decrease with increasing temperature. This trend varied irregularly for the several components present.

INTRODUCTION

Since the early work of Tiselius (1), most of the electrophoretic analyses by the moving boundary method have been conducted in the temperature range between 0 and 4°C. At these low temperatures, the density of the buffer is near its maximum and relatively high potential gradients can be applied across the protein solution-buffer boundary without producing any thermal convection. The viscosities of the protein solution and buffer are relatively high, and boundary spreading due to diffusion of protein components is much lower than at higher temperatures (2). However, some proteins, especially the plant globulins, have low solubilities at 4° in the usual buffers of ionic strength between 0.02 and 0.20. For accurate analysis, the concentration of protein should be of the order of 10. In many cases, this can be obtained by analyzing the protein at a higher temperature where its solubility is enhanced (3).

Additional advantages may also follow at elevated temperatures: thus, Johnson and Shooter (4) analyzed peanut proteins at 20°C. where it becomes possible to prepare solutions at pH values closer to the isoelectric points. For cottonseed protein extracts, it was necessary to increase the alkalinity of the buffer to values as high as pH 10 or 11 in order to effect complete solubility at low temperatures (5). Even 0.5 *N* sodium chloride extracts, if neutral, will precipitate 30% of the protein present on cooling from 20° to 0°.

¹ Resigned October 5, 1951.

² One of the laboratories of the Bureau of Agricultural and Industrial Chemistry, Agricultural Research Administration, U. S. Department of Agriculture.

Comparison of electrophoretic measurements at various temperatures may, however, be complicated by changes in the number and distribution of components resulting from (a) displacement of equilibria for association-dissociation systems, (b) increased rate of deterioration of the protein, and (c) changes in pH due to changes in temperature.

Mobility of the particles changes with temperature. This is mainly due to changes in frictional forces, which have generally been evaluated in terms of changes in the viscosity of the solvent. It is expected that if this were the only pertinent variable, the product of mobility-viscosity for any component would be a constant (1,2). However, there are probably other small, residual temperature effects. One such effect, for horse serum albumin, has been described (6) as being due to changes in particle charge.

The purpose of this work was to investigate the electrophoretic patterns of cottonseed meal extract at several temperatures in order to make possible a comparison of results under varying temperature conditions.

SAMPLE PREPARATION

Forty grams of cottonseed flakes, previously extracted with butanone to remove oil and color constituents, was further extracted with four equal volumes of ethylamine barbital buffer to yield 1 l. of clarified protein extract. The buffer solution had an ionic strength of 0.1 and a pH of 10.4 at 25°C. This solution was dialyzed against 3 l. of the same buffer at 3–5°C. on a rocking dialyzer for 48 hr., and the process repeated three times at 48-hr. intervals. The dialyzed protein liquor was cooled to slightly below 0°C. and was clarified by centrifugation at that temperature in a refrigerated centrifuge (centrifugal force of $7 \times 10^3 g$ at center of cell). This supernatant, which contained 1.06% protein (Kjeldahl analyses) and had 0.01% sodium ethylmercurithiosalicylate (merthiolate) added as a preservative, was used in all the electrophoretic measurements. There was no evidence of protein degradation in the samples treated with the preservative.

EXPERIMENTAL

The conventional Klett electrophoresis equipment (7) with only minor modifications was used. Photographic records were made by the Longworth scanning method. Mobilities were calculated from the descending patterns as recommended (7).

The thermostat was adjusted to 0, 5, 10, 15, and $20 \pm .02^\circ\text{C}$. Temperatures inside the cell, however, were somewhat higher than the temperature of the surrounding bath due to heat generated by the electric current. Measurements of the temperature rise at different current densities for each bath temperature were made with an iron-constantan thermocouple placed midway in the "ascending" leg of an 11-ml. electrophoresis cell. The current densities were chosen such that the steady-state internal

temperature would not exceed the bath temperature by more than 0.30°C.; the steady-state temperature was achieved in several minutes.

Conductivities of the protein solution and buffer were measured in a Washburn-type conductivity cell calibrated at each temperature with standard potassium chloride solutions prepared according to Parker and Parker (8). Specific conductance values used in the calculation were interpolated to the temperatures prevailing inside the cell.

Cannon-Fenske-type viscometers were calibrated with distilled water at several temperatures, and the viscosities of the protein solution and buffer determined in the standard manner. Kinetic energy corrections were found to be negligible. The viscosity data are plotted on semilogarithmic coordinates according to the following relation (9) empirically valid over small temperature intervals

$$\eta = ae^{b/T},$$

where η is the viscosity, T the absolute temperature, and a and b constants. Viscosities at required temperatures were interpolated from the smooth plot of the data (Fig. 1).

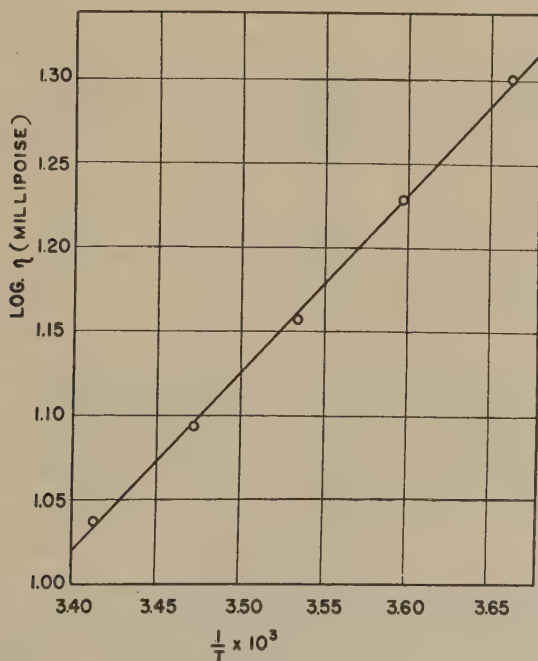


FIG. 1. Logarithm of viscosity of solvent as a function of the reciprocal of the absolute temperature.

The pH of the buffer as a function of temperature over the range 0 to 25°C. has been determined with a glass electrode against standard carbonate-bicarbonate solutions (10). The following results were obtained:

	25°	10°	0°
Ethylamine barbital buffer	10.42	10.98	11.26
Carbonate-bicarbonate buffer (standard)	10.02	10.18	10.32

In order to determine whether this change in pH value of the buffer resulting from the change in temperature could bring about any change in the mobilities of the cottonseed protein components or in their relative composition, a series of experiments was conducted at 5°C. in buffer solutions of 0.1 ionic strength and having pH values from 10.1 to 11.0 as determined at 25°C. The results indicate that over the pH range investigated there is no change in either mobility or per cent composition due to a change in pH of the buffer.

RESULTS

The electrophoretic patterns disclosed the existence of five components.³ *Measurement* of the area of each of these components indicated no apparent trend in their relative concentrations over the range of temperatures investigated. This was taken as indicating no change in protein interaction. The change in pH of the buffer with temperature

TABLE I
Areas^a of Major Components of Cottonseed Meal Extract

Com- ponent ^b	Areas at various temperatures					Mean per cent of total
	0.27°C. sq. cm.	5.24°C. sq. cm.	10.24°C. sq. cm.	15.21°C. sq. cm.	20.19°C. sq. cm.	
A	14.8	14.0	15.4	14.9	16.4	36 ± 0.9
B	19.1	19.1	18.6	17.2	18.6	44 ± 0.7

^a Areas based on photographic enlargements of schlieren diagrams of descending boundary, magnification 4X.

^b Mean percent of total for components A', C, and D was approximately 9, 7, and 4%, respectively.

did not bring about any changes in composition. The data for components A and B, which represent 80% of the material present, are summarized in Table I. Values of the electric field strength (*F*) and electrophoretic mobility (μ) are given in Table II.

DISCUSSION

Figure 2 discloses a general increase of mobility with temperature for all five components of the cottonseed meal extract. The relation is well represented by a linear function over the temperature range investigated.

³ Results obtained previously had indicated the presence of four components. Changes in the method of extraction of the oil and pigments from cottonseed meats made it possible to obtain protein solutions with improved optical transmission. Careful analysis of the electrophoretic patterns obtained with these solutions in this investigation allowed the detection of a fifth component.

TABLE II
Experimental Mobilities and Corrected Mobility \times Viscosity Products

Components	$-\mu \times 10^5$ cm./v./sec.					$-\mu\eta \times 10^{13a}$				
	0.27°C.	5.24°C.	10.24°C.	15.21°C.	20.19°C.	0°C.	5°C.	10°C.	15°C.	20°C.
A'	7.4 ₃	8.8 ₄	10.6 ₅	11.8 ₀	13.6 ₂	145. ₈	149. ₇	150. ₆	148. ₇	145. ₂
A	6.1 ₅	7.2 ₅	8.5 ₈	9.4 ₆	10.8 ₃	121. ₀	122. ₃	121. ₆	119. ₁	115. ₆
B	4.5 ₅	5.1 ₃	5.9 ₃	6.2 ₆	7.2 ₆	89. ₄	87. ₀	83. ₈	80. ₀	76. ₂
C	3.2 ₅	3.6 ₇	4.2 ₆	4.6 ₅	4.8 ₉	65. ₆	62. ₉	60. ₁	56. ₇	53. ₅
D	2.1 ₃	2.6 ₇	3.1 ₂	3.0 ₉	3.8 ₈	43. ₃	43. ₁	42. ₆	41. ₁	39. ₇
Field strength, volts/cm.	3.36	2.82	2.43	2.14	1.91					

^a Mobility in sq. cm./v./sec.; viscosity in poises.

The increase of mobility with a rise in temperature is not uniform for all components; component A' which had the highest mobility at 0°C. also had the highest increase in mobility over the temperature range of 20°. Obviously, the increase in mobility with temperature increase cannot be attributed solely to a decrease in viscosity of the solvent, which

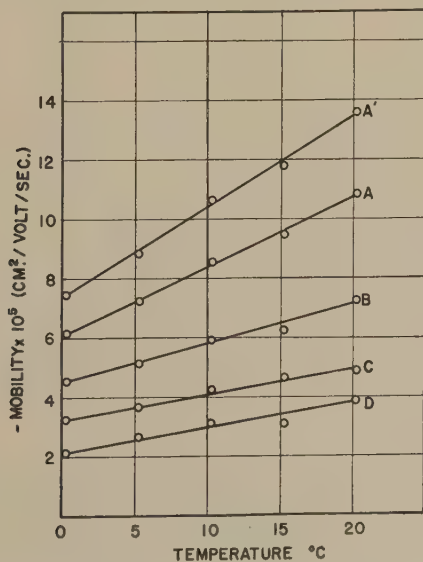


FIG. 2. Mobility of cottonseed components as a function of temperature.

would affect all components uniformly. Furthermore, the viscosity of the solvent is well represented by a logarithmic function of temperature (Fig. 1) whereas the mobilities are adequately related to temperature in a linear fashion (Fig. 2). That the mobility-viscosity products are not constant is shown in Fig. 3.

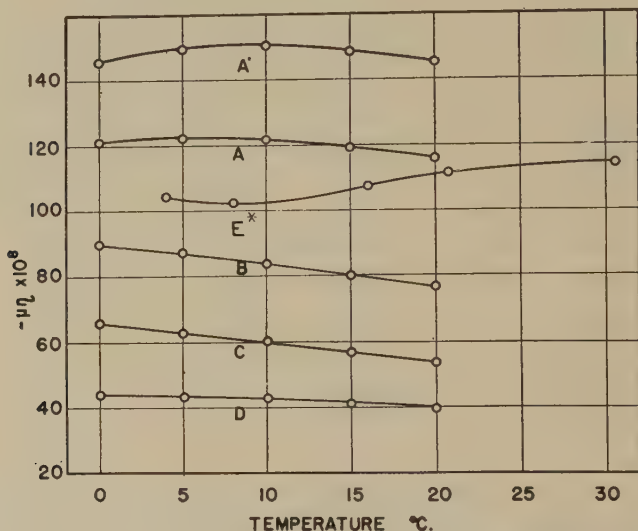


FIG. 3. Product of mobility-viscosity as a function of temperature.

* Recalculated data of Watanabe (6) on horse serum albumin.

For components *B*, *C*, and *D*, a distinct linear-like downward trend is observed. (Results for *D* are least reliable because of the small relative concentration of this component and the consequent difficulty in reading its pattern.) Components *A* and *A'*, while they similarly show a downward trend from 5 or 10°C., display an apparent rise from 0 to 5°.

The decrease in the absolute value of $-\mu\eta$ (product of mobility times viscosity) is not uniform and, in fact, is suggested by the data of Johnson and Shooter (2) on peanut protein.⁴ Included with the data for cottonseed protein in Fig. 3 are the results of Watanabe *et al.* (6) for purified horse serum albumin. These workers have attributed the increase of $-\mu\eta$ with temperature to an increase in the absolute magnitude of the charge of the protein, and supported this conclusion by concurrent information from titration data (11).

⁴ Johnson and Shooter (2), working at 4 and 20° C. found a ratio of mobilities at the two temperatures of 0.70 for peanut protein, 0.64 for human fibrinogen, and 0.61 for human serum albumin, the inverse ratio of the viscosities of water at the two temperatures being 0.64. Thus the $-\mu\eta$ factor of peanut globulin decreases, of fibrinogen remains the same, and of serum albumin increases.

In order to compare their data with those of this investigation, the logarithm of their experimental values of viscosity of the solvent was plotted against the reciprocal of the absolute temperature. The least square solution to the linear relation between $\log \eta$ and $1/T$ was used to obtain corrected values of viscosity. When these corrected values are used in calculating the product, $-\mu\eta$, the agreement of $-\mu\eta$ with temperature appears to be considerably more erratic than originally indicated. While the results from titration data paralleled the calculated changes in charge, the agreement was not satisfactory.

It is evident that a complete explanation of the effect of temperature on the electrophoretic analysis of cottonseed proteins is not possible at present. The application of both a simple viscosity correction to the solvent and an additional correction based on changes in charge is questionable.

ACKNOWLEDGMENT

We gratefully acknowledge the encouragement of Dr. A. M. Altschul of this laboratory.

SUMMARY

The electrophoretic patterns of cottonseed meal extract in ethylamine-barbital buffer have been investigated over a range of 0 to 20°C.

1. No change in the relative concentrations of the components occurred as a function of temperature.

2. The effect of temperature could not be entirely compensated for by application of a simple viscosity correction to the solvent.

3. The mobility-viscosity products displayed, in general, a decrease with increasing temperature. This trend varied irregularly for the several components present.

REFERENCES

1. TISELIUS, A., *Biochem. J.* **31**, 1464 (1937).
2. JOHNSON, P., AND SHOOTER, E. M., *J. Colloid Sci.* **3**, 539 (1948).
3. DANIELSSON, C. E., *Acta Chem. Scand.* **4**, 762-71 (1950).
4. JOHNSON, P., SHOOTER, E. M., AND RIDEAL, E. K., *Biochim. et Biophys. Acta* **5**, 376 (1950).
5. KARON, M. L., ADAMS, M. E., AND ALTSCHUL, A. M., *J. Phys. & Colloid Chem.* **54**, 56 (1950).
6. WATANABE, I., UI, N., AND NAKAMURA, M., *J. Phys. & Colloid Chem.* **54**, 1366 (1950).
7. LONGSWORTH, L. G., *Chem. Revs.* **30**, 323 (1942).
8. PARKER, H. C., AND PARKER, E. W., *J. Am. Chem. Soc.* **46**, 312 (1924).
9. PHILIPPOFF, W., *Viskosität der Kolloide*, p. 199. Verlag von Theodor Steinkopff, 1942.
10. BATES, R. G., PINCHING, G. D., AND SMITH, E. R., *J. Research Natl. Bur. Standards* **45**, 418 (1950).
11. COHN, E. S., STRONG, L. E., AND BLANCHARD, M. H., in *Proteins, Amino Acids and Peptides*, edited by COHN, E. S., AND EDSALL, J. T., p. 503. Reinhold Publishing Corp., New York, 1943.

THE ELECTROCHEMICAL PROPERTIES OF HUMIC ACID

B. Chatterjee and S. Bose

Bengal Engineering College, Howrah, India

Received March 6, 1952

INTRODUCTION

The term humic acid has been used by different investigators to designate different preparations. It was most frequently applied to that part of the organic matter which is soluble in alkali solutions. In some cases the expression "humic acid" has been used to designate only that part of this alkali solution which is precipitated by mineral acids. Oden (1) suggested that the part of the acid precipitate which is not soluble in alcohol should be called humic acid. This nomenclature is now widely used.

The electrochemical properties of humic acid have attracted the attention of quite a number of authors. Only those investigations which have a direct bearing on the present work have been discussed below.

Acid Character of Humic Acid

While Sprengel (2) and Oden (1) suggest that humic acid should be treated as a true acid, Baumann and Gully (3) are of opinion that these acids are not true acids and that acidity appears only on the addition of salts to humic acids, due to adsorption of the base by the latter. These authors looked upon humic acid as a colloidal complex with a very high power of adsorption. The two conflicting hypotheses have been bridged by Rindell (4), who believes that humic acid comprises both colloids and true acids.

Mechanism of the Interaction of Humic Acid with Neutral Salts

An acidity is developed in the interaction of humic acid with neutral salts, and the salt extract shows a greater acidity than the water extract. Eichhorn (5) was the first to show that when peats and humates are allowed to interact with salts an exchange of base takes place. König (6) explained the phenomenon by assuming that humic acid forms humates with the cations of the added salts, liberating hydrochloric acid. Daikuhara (7) considered that aluminum and iron salts adsorbed by humus are replaced by the added salts and are brought into solution, the hydrolysis of which gives rise to the observed acidity. Kappen (8) and Heinman (9) are of opinion that both humate formation and replacement of iron and aluminum take place on the addition of neutral salts to humic acids.

Trenel and Harada (10) hold that, in addition, a greater solution of the organic acids takes place in the presence of neutral salts.

Nature of the Electrometric Titration Curves of Humic Acid

Oden (1) carried out potentiometric titration of a suspension of peat with NaOH. It was observed that hydroxyl ion concentration, calculated from the observed electromotive force (e.m.f.) values, at first hardly increased with the addition of NaOH. He assumed that the OH ions are used up to form water by reaction with H ions dissociated from the humic acid, and only when this process is completed, hydroxyl ion concentration increases. Anderson (11) carried out potentiometric titration of an electrodyalyzed sample of humic acid extracted from a soil and also of an artificial humic acid prepared by the action of sulfuric acid on sucrose. He observed that the base-exchange capacity of the soil humic acid was much greater than that of the synthetic humic acid, and that humic acid showed acid properties comparable in some respects to mucic or tungstic acid, but no breaks in the titration curves were evidenced. Similar results have been obtained by Feustel (12) who studied the course of neutralization of a sample of peat as well as its humic acid fraction by titrating with $\text{Ba}(\text{OH})_2$ potentiometrically. He, however, obtained definite breaks in the curves when a much wider sample to solution ratio was used, i.e., in dilute solutions. The absence of a break in the curves in the concentrated solutions has been ascribed to the simultaneous occurrence of certain secondary reactions, such as hydrolysis of complex esters or attack of the phenolic group, in addition to simple neutralization. Zadnard (13) found that humic acid titrated with alkali hydroxides showed a much more rapid rise in pH in the titration curves than in the case with alkaline earth hydroxides. The base-exchange capacity calculated at pH 7.0 was found to be in the order: $\text{Ba}(\text{OH})_2 > \text{Ca}(\text{OH})_2 > \text{KOH} > \text{LiOH} > \text{NaOH}$. The same order was obtained when buffering of the systems was considered. Similar results were obtained by Hissink (14) while studying the pH changes of the suspensions of a humus soil on the addition of different hydroxides. Gillam (15) mentions two distinct inflexion points in the potentiometric titration curves of humic acid with NaOH.

Conductometric titration curves of humic acid with bases have been obtained by a number of investigators. The number of breaks in the curves as reported in the literature varies from one to four. In some cases good correlation has been obtained between potentiometric and conductometric data.

It will appear that in spite of considerable work carried out on the electrochemical properties of humic acid differences of opinion exist as regards (a) the acid character of humic acid, (b) the mechanism of interaction of humic acid with neutral salts, and (c) the nature of the po-

tentiometric titration curves of humic acid. The present work aims at having fuller information on these points.

For this purpose, systematic studies have been made of the free and total acids and titration curves of (a) humic acid, (b) humic acid + salt mixtures, and (c) the clear supernatant liquids above the coagula of the humic acid + salt mixtures. Merck's humic acid, as well as humic acid isolated from an acid soil from Assam, different salts, and different bases have been used in this investigation.

EXPERIMENTAL

Extraction of Humic Acid

The humic acid fraction has been extracted from an acid soil from Assam using the method of Waksman and Stevens (16) as followed by Esh and Guha-Sarker (17). Fats, waxes, and resinous matters were removed from the soil by refluxing with a benzene-ethyl alcohol (1:1) mixture, and the residue was treated with 2% hydrochloric acid at 100°C. for 1.5 hr. The acid was filtered off, washed with water, and then the soil was treated with 2% caustic potash for 10 hr., with occasional stirring. The dark colored solution was filtered off. The filtrate was then acidified with dilute hydrochloric acid and the precipitated humic acid was washed with water. The humic acid was dissolved in alkali followed by precipitation with acid. This procedure was repeated thrice. The humic acid thus obtained was again dissolved in dilute sodium carbonate solution and then reprecipitated with acid. The humic acid was then treated with ethyl alcohol, and the alcohol-soluble hymatomelanic acid was separated. Finally the humic acid was treated with acetyl bromide, washed with ether, and dried at 80–85°C.

Preparation of Humic Acid Sols

The powdered humic acid fraction was suspended in water, made just alkaline with NaOH, vigorously shaken, and allowed to settle overnight. The stable suspension was siphoned off the next day, then treated with 0.067 *M* (*N*/15) HCl and dialyzed in parchment bags against repeated changes of distilled water till the dialyzate gave no test for Cl ion. Humic acid sol thus prepared was shaken in a mechanical shaker for about 2 hr. and then allowed to stand overnight. The fraction remaining in suspension was siphoned off the next day. The sol thus obtained was very stable.

Potentiometric Measurements

A Tinsley vernier potentiometer (Type 3126), reading up to 0.01 mv., and a Hartman and Braun galvanometer, with a critical damping resistance of 22×10^4 ohms and having a sensitivity of 4.2×10^{-11} amp., have been used for e.m.f. measurements.

Conductivity Measurements

A Hartman and Braun conductivity bridge, a conductivity cell having a cell constant of 0.13, and a silenced Tinsley buzzer have been used for conductivity measurements.

Semimicro combustion methods (18) were used for the estimation of carbon and hydrogen. Semimicro-Kjeldahl method was used for the estimation of nitrogen.

A Zeiss slit ultramicroscope was used for detecting the presence of colloidal particles in the ultrafiltrates of humic acid sols.

RESULTS AND DISCUSSION

Chemical Analysis

The percentages of carbon, hydrogen, nitrogen, and ash content of oven-dried humic acid sols *A* and *B* prepared from Merck's humic acid as also of sol *C* prepared from humic acid isolated from an acid soil from Jorhat farm, Assam, are shown in Table I.

TABLE I

Chemical Analysis of Humic Acid Sols

Sol	Carbon %	Hydrogen %	Nitrogen %	Ash %
<i>A</i>	54.3	5.1	2.0	3.6
<i>B</i>	53.8	5.2	1.9	3.4
<i>C</i>	50.2	4.3	3.3	8.3

The high ash content of sol *C* prepared from the acid soil is due to the presence of inorganic impurities, e.g., Fe, Al, and Si. Similar and even higher ash contents in humic acid isolated from soils have been observed by Waksman and co-workers (19).

Intrinsic Acid Character of Colloidal Humic Acid

The free and total acids of sols *A* and *C* as also of their ultrafiltrates are shown in Table II.

TABLE II

The Free and Total Acids of Humic Acid Sols and of Their Ultrafiltrates

System	Free acid $\times 10^5 N$	Total acid, $\times 10^5 N$, calculated at inflection points with					
		NaOH		Ba(OH) ₂		Ca(OH) ₂	
		1st	2nd	1st	2nd	1st	2nd
Sol <i>A</i>	8.9	258	361	290	430	330	498
Ultrafiltrate of <i>A</i>	4.0			40			
Sol <i>C</i>	7.9	707		880		930	
Ultrafiltrate of <i>C</i>	1.6			6.6			

The potentiometric titration curves of sol *A* with bases show two inflexion points (Fig. 1) while those of sol *C* prepared from soil humic acid

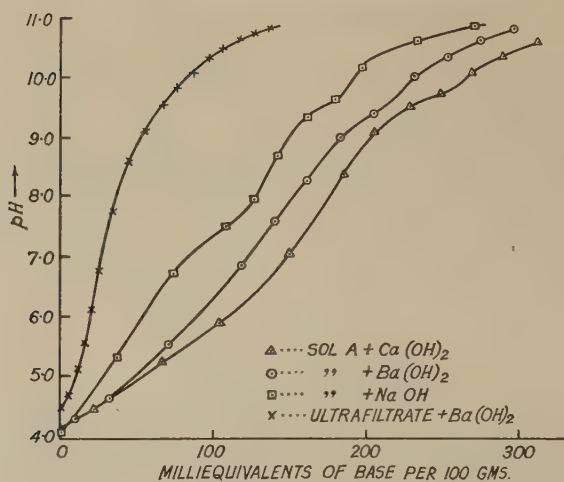


FIG. 1. Titration curves of humic acid Sol A and of its ultrafiltrate with bases.

show only one break in the curves (Fig. 2). A comparison of the total acids of the sols and of their ultrafiltrates shows beyond doubt that colloidal humic acid possesses an intrinsic acid character independent of the presence of dissolved acid in the system. The heterogeneous character of the sols is also indicated. The ultrafiltrate of sol A was distinctly colored. Examination under the ultramicroscope, however, showed the absence of colloidal particles in it. It appears, therefore, that sol A is comprised partly of an acid in true solution and partly of an acid in colloidal suspension. In this respect sol A seems to be similar to those investigated by

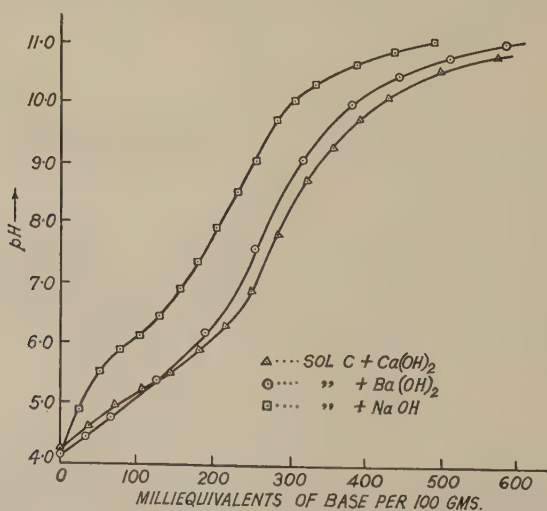


FIG. 2. Potentiometric titration curves of Sol C with bases.

Rindell (4). The ultrafiltrate of sol *C* prepared from the soil humic acid is colorless and practically does not contain any neutralizable acid. Consequently the neutralizable acidity of sol *C* is solely due to the acid present in the colloidal state. Even in the case of sol *A* the contribution of dissolved acid to the total acidity is very small.

The degree of dissociation of sols *A*, *B*, and *C* calculated as the ratio of their free acidities to total acidities has been shown in Table III.

TABLE III
Degree of Dissociation of Colloidal Humic Acid

Sol	Ratio of free acidity to total acidity with					
	NaOH		Ba(OH) ₂		Ca(OH) ₂	
	1st infect.	2nd infect.	1st infect.	2nd infect.	1st infect.	2nd infect.
<i>A</i>	0.035	0.024	0.031	0.021	0.027	0.018
<i>B</i>	0.065	0.050	0.058	0.040	0.043	0.027
<i>C</i>	0.011		0.009		0.008	

The free acidity values have been calculated from the initial pH values of the sols and the total acidity values from the inflection points in the titration curves. The data cited in Table III show that humic acid sols are dissociated to a very small extent. This would be expected of a weak acid. The potentiometric titration curves of the sols with Ba(OH)₂ and Ca(OH)₂, however, point to a moderately strong acid character of the sols. Such conflicting features would not be expected of acids in true solution.

Interaction of Humic Acid Sols with Bases: Potentiometric Titration with Bases

The total acidities of sols *A*, *B*, and *C*, calculated at pH 7.0 as also at the inflection points in the titration curves with different bases are shown in Table IV.

The data cited in Table IV show that the amounts of acid neutralized at pH 7.0 as also at the inflection points in the potentiometric titration

TABLE IV
Total Acidities of Humic Acid Sols
Acidities have been expressed in milliequivalents/100 g.
Figures within parentheses give pH at inflection.

Sol	Colloid Content g./l.		NaOH		Total acid with Ba(OH) ₂		Ca(OH) ₂	
			1st infect.	2nd infect.	1st infect.	2nd infect.	1st infect.	2nd infect.
	pH 7.0				pH 7.0		pH 7.0	
<i>A</i>	1.9	94	136 (8.4)	190 (9.8)	124 (7.9)	226 (9.8)	150 (7.9)	174 (9.8)
<i>B</i>	2.3	74	133 (9.0)	176 (10.0)	120 (8.2)	220 (10.0)	165 (8.0)	262 (10.0)
<i>C</i>	3.1	160	228 (8.3)		236 (8.2)		260 (7.9)	300

curves of humic acid sols with bases, depend on the nature of the base used. The total acid decreases in the order: $\text{Ca}(\text{OH})_2 > \text{Ba}(\text{OH})_2 > \text{NaOH}$. The same order is observed when the slopes of the potentiometric titration curves are compared.

Zadmard (13) found that the base-exchange capacity calculated at pH 7.0 is in the order: $\text{Ba}(\text{OH})_2 > \text{Ca}(\text{OH})_2 > \text{NaOH}$. However, he measured the pH of the clear supernatant liquids and not of the suspension as a whole, and plotted the observed pH values against milliequivalents of bases added. The curves thus obtained are obviously not representative of humic acid. The pH values of the supernatant liquid cannot be taken equal to those of the mixtures. In the acid region the pH of the suspension (of acidic substances) is often found (20) to be lower than that of the clear supernatant liquid, but the order is reversed in the alkaline region, viz., the pH of the suspension being higher than that of the supernatant liquid.

The greater relative effect of Ca ions compared to Ba ions may be due either to the greater insolubility of calcium humate compared with barium humate, or to the greater stability of the salt molecule formed on the surface by interaction with calcium hydroxide compared with those formed with baryta. It will be seen later (pp. 423) that in the interaction of humic acid with bases in the presence of the corresponding chlorides, Ba ion has a greater effect than Ca ion. The observed difference in the effects of Ba and Ca ions are in agreement with those previously observed by Mukherjee and co-workers, including the present authors (21,22,23), using hydrogen clays, i.e., the acid form of the inorganic colloidal constituent of the soil. The greater effect of Ca ions compared to that of Ba ions when these bases are used without the addition of salts is contrary to the usual lyotropic series and in this sense constitutes what has been termed by Mukherjee *et al.* (21,22,23) the "Irregular or Specific Cation Effect."

It appears from Table IV that the base-exchange capacity follows the same order, viz., $\text{Ca}(\text{OH})_2 > \text{Ba}(\text{OH})_2 > \text{NaOH}$, whether it is calculated at pH 7.0 or at higher pH values in the titration curves of the sols with different bases. The pH at inflection also does not appear to have a marked influence on the base-exchange capacity of humic acid sols. The pH at the first inflection point in the titration curves is highest with NaOH, but the base-exchange capacity is lowest with this base. The pH at the second inflection point is practically the same with all the bases, but the base-exchange capacity follows the order, $\text{Ca}(\text{OH})_2 > \text{Ba}(\text{OH})_2 > \text{NaOH}$. The "Cation effect" thus predominates over the "pH effect" (21).

The titration curves (Fig. 1) of Merek's humic acid show a second inflection in their titration curves with bases at pH about 9.8. With NaOH it behaves as a weak dibasic acid, while with $\text{Ba}(\text{OH})_2$ and

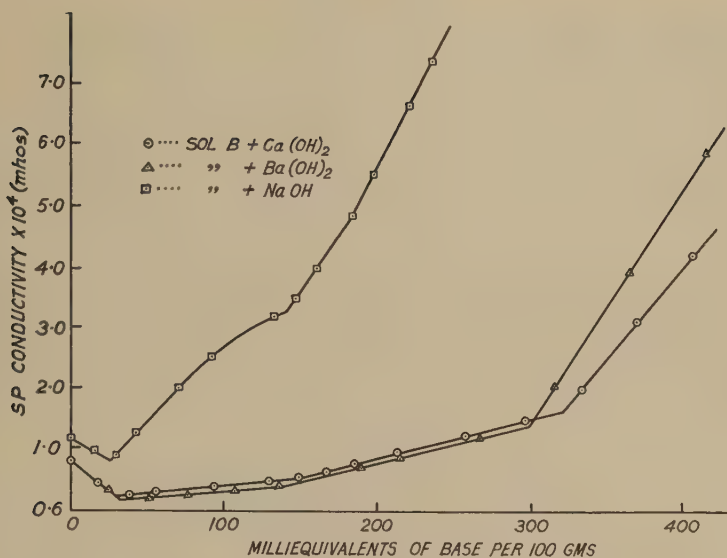


FIG. 3. Conductometric titration curves of Sol B with bases.

Ca(OH)_2 it behaves as a strong dibasic acid. On the other hand, the titration curves (Fig. 2) of sol C show that the humic acid from the soil is monobasic. The NaOH curve again shows the acid to be weak, while the Ba(OH)_2 and Ca(OH)_2 curves are typical of a strong monobasic acid. Oden (1), from a measurement of the conductivity of sodium humate with dilution, came to the conclusion that humic acid is a tribasic acid. Later, however, he considered humic acid to be tetrabasic from a consid-

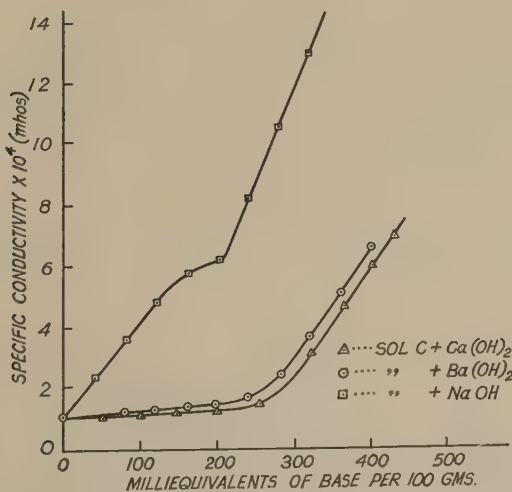


FIG. 4. Conductometric titration curves of Sol C with bases.

eration of the analytical data. Kawamura (24) is of opinion that humic acid forms aluminium trihumate with $AlCl_3$.

Conductometric Titration of Humic Acid with Bases

In contrast to the potentiometric titration curves of humic acid sols but in agreement with the previous observations of Oden (1), the conductometric titration curves (Fig. 3) of sol *B* prepared from Merck's humic acid show three breaks, indicating the acid to be tribasic. The conductometric titration curves of sol *C* prepared from soil humic acid show only one break (Fig. 4), and thus corroborate the conclusion drawn from the potentiometric titration. The total acidity values calculated at the breaks of the conductometric titration curves are shown in Table V.

TABLE V

Total Acidity of Humic Acid Sols Calculated at the Breaks in the Conductometric Titration Curves

Sol	Total acidity, mequiv./100 g. humic acid								
		NaOH			Ba(OH) ₂			Ca(OH) ₂	
	1st	2nd	3rd	1st	2nd	3rd	1st	2nd	3rd
<i>B</i>	26	140	188	31	150	302	30	160	322
<i>C</i>	208			258			280		

The data cited in Table V show that at the third and second inflection points the amounts of acid neutralized by different bases are in the order: $Ca(OH)_2 > Ba(OH)_2 > NaOH$. The amounts of neutralizable acid calculated at the first break of the conductometric titration curve with $Ba(OH)_2$ and $Ca(OH)_2$ are almost equal, but that with NaOH is slightly less.

The total acidity calculated from the inflection points in the potentiometric titration curves of sol *C* with NaOH, $Ba(OH)_2$, and $Ca(OH)_2$ are slightly greater than the values calculated from the breaks in the corresponding conductometric titration curves. The difference being 8.7, 9.1, and 6.6%, respectively.

Variations in Free and Total Acids of Sol B with Dilution

The variations with dilution in the free and total acids of sol *B* are shown in Table VI.

TABLE VI

Changes in the Total Acidity of Merck's Humic Acid with Dilution

System	Free acid $\times 10^3 N$	Total acid, mequiv./100 g. of humic acid at	
		1st inflection	2nd inflection
Sol <i>B</i>	5.8	200	316
Sol <i>B</i> /2	4.0	170	330
Sol <i>B</i> /4	2.2	150	284
Sol <i>B</i> /8	1.1	134	250

The total acidity values calculated per 100 g. of colloid at both the inflection points decrease with dilution, an exception being that at the second inflection point of the undiluted sol. This observation is rather interesting and its discussion should be deferred pending further investigation. The free acidity increases with concentration, at first linearly and then at a slower rate.

Equivalent Weight of Humic Acid

The following data (Table VII) obtained with sol *C* show that the equivalent weight of humic acid, calculated from the inflection points in the potentiometric titration curves or from the breaks in the conductometric titration curves, depends on the nature of the base used for titration.

TABLE VII

Equivalent Weight of Soil Humic Acid

Calculated from	Equivalent Weight of Soil Humic Acid With		
	NaOH	Ba(OH) ₂	Ca(OH) ₂
Potentiometric curve	439	352	333
Conductometric curve	480	387	357

The equivalent weight, with a given base, calculated from the potentiometric titration curve is slightly lower than that calculated from the conductometric curve. This is due to the total acidity calculated from the inflection point in the potentiometric titration curve being greater than that determined at the break in the corresponding conductometric titration curve (Tables IV and V). The equivalent weight of humic acid calculated from the potentiometric and conductometric titration curves with different bases follows the order: NaOH > Ba(OH)₂ > Ca(OH)₂.

Interaction of Humic Acid Sols with Neutral Salts

The lowering of pH of the humic acid sols *A* and *C* on the addition of 0.1 *N* solutions of NaCl, CaCl₂ and BaCl₂ are shown in Table VIII.

TABLE VIII

Changes of pH of Humic Acid Sols on the Addition of Salts

Sol	Lowering of pH on the addition of 0.1 <i>N</i>		
	NaCl	CaCl ₂	BaCl ₂
<i>A</i>	0.73	0.83	1.00
<i>C</i>	0.41	1.00	1.00

The results show that: (a) the pH of the sol is lowered on the addition of the salts to the sol indicating the liberation of acid; (b) the effect of Na ion is much smaller than that of the Ba or Ca ions; and (c) Ba ion has an equal, if not greater (sol *A*), effect than Ca ion. Gillespie and Wise

(25) also observed a greater lowering of pH of humic acid on the addition of BaCl_2 compared to NaCl . The greater relative effect of Ba ion compared to Ca ion becomes more pronounced when humic acid sols are titrated with bases in presence of the corresponding chlorides, as the following data with 0.1 *N* concentrations of the chlorides will show.

TABLE IX
Interaction of Humic Acid with Neutral Salts

Sol	Total acid, mequiv./100 g. humic acid at inflection points					
	NaCl + NaOH		CaCl ₂ + Ca(OH) ₂		BaCl ₂ + Ba(OH) ₂	
	1st infect.	2nd infect.	1st infect.	2nd infect.	1st infect.	2nd infect.
A	140	250	196	298	210	390
C	246		298		344	

Table IX shows that in the presence of salts the total acidities calculated at the inflection points are in the order: $[\text{BaCl}_2 + \text{Ba}(\text{OH})_2] > [\text{CaCl}_2 + \text{Ca}(\text{OH})_2] > [\text{NaCl} + \text{NaOH}]$. The relative intensities with which the different cations react are in the order: $\text{Ba} > \text{Ca} > \text{Na}$. This is in agreement with the lyotropic series and the "cation effect" is "regular" (21).

The slopes of the titration curves (Fig. 5) of sols A and C with bases in the presence of the salts of the corresponding cation indicate that the intensity with which the different cations react with humic acid sols is in the order: $\text{Ba} > \text{Ca} > \text{Na}$.

The greater relative effect of barium chloride than calcium chloride is difficult to explain from solubility considerations. In the absence of

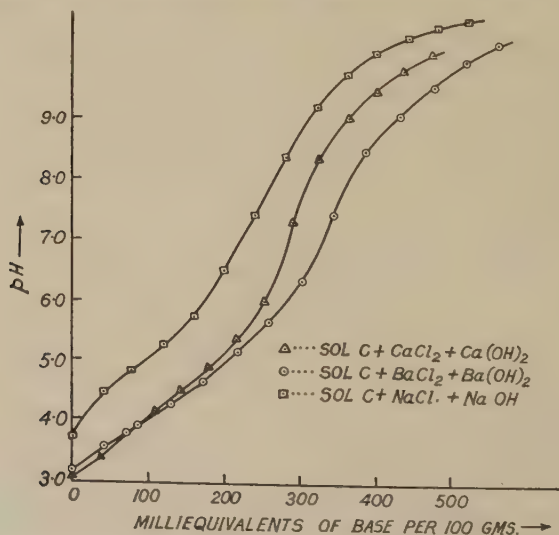


Fig. 5. Potentiometric titration curves of Sol C with bases in presence of salts.

salts (Tables IV and V) Ca ion has a greater effect, and this may be explained as due to the greater insolubility of calcium humate than barium humate; but the relative order of reactivity of the two ions is reversed in the presence of salts. Consequently, one has to assume that in the presence of the corresponding chlorides barium humate is more insoluble than calcium humate. Such *ad hoc* assumptions regarding solubility of humates are necessary to explain the mechanism of reaction from the classical theoretical point of view. Further, it is difficult to explain the development of acidity in the interaction between humic acid and sodium chloride from a purely chemical point of view. One has to believe in that case that the sodium salt of humic acid is insoluble in water. An adequate explanation can, however, be obtained in light of the theory of the electrical double layer and of secondary adsorption of ions postulated by Mukherjee (26). According to this theory the increase in total acidity on the addition of salts consists essentially in a displacement of the "bound" hydrogen ions of the double layer by the cations of the salt, which form "ionpairs" with the primary adsorbed anions of the surface. A part of the ionpair, the anionic part, is anchored to the solid surface and is definitely insoluble. The cationic part may or may not be soluble depending on the energy of adsorption of the cation as given by its valency and mobility. As a whole, the "ionpair" is neither in a state of true solution nor does it form a separate solid phase. Its solubility has no meaning.

A comparison of the data presented in Table IV with those cited in Table IX indicates that the total acidities of the sol plus salt mixtures are greater than the corresponding values of the pure sol.

*Total Amount of Acid and Al Ions Displaced from Humic Acid Sol C
on Repeated Leaching with Normal BaCl₂ Solution*

Thirty ml. of sol C was repeatedly leached with neutral solution of N BaCl₂ till the leached sol contained no titratable acidity. The total acidity of each leach is shown in Table X. The amounts of Al ions in each leach have also been determined using Berg's 8-oxyquinoline method (27). Iron ions could not be detected in the salt extract.

TABLE X

Total Amount of Acid and Al Displaced from Sol C by BaCl₂

No. of leaching	Total acidity <i>mequiv./100 g.</i>	Displaced Al <i>mequiv./100 g.</i>
1st	71.5	4.0
2nd	20.5	nil
3rd	7.5	nil
4th	0.7	nil
5th	nil	nil
Total	100.2	4.0

The amounts of titratable acidity in the leach decrease with the progress of leaching, and in the fifth leach attain a negligible value. The total amount of acid thus liberated is 100.2 mequiv./100 g. of colloid, which is only 38.8% of that calculated at the inflection point in the titration curve of sol *C* with $\text{Ba}(\text{OH})_2$. The data cited in Table X also show that Al ions are exchanged along with H ions to the extent of 4.0 mequiv. out of a total of 100.2 mequiv. of the total cation exchange. It should, however, be noted that the amount of displaced Al ions as estimated in the salt extract is a negligible fraction of the total acidity of the latter. Further, these Al ions may come from the inorganic impurities present in the humic acid. It appears, therefore, that the interaction between neutral salts and humic acid is mainly an exchange reaction between the cations of the added salts and H ions present on the surface of humic acid.

ACKNOWLEDGMENTS

The authors take this opportunity to offer their sincere thanks to Dr. S. R. SenGupta, Principal, Bengal Engineering College; and to Dr. J. N. Mukherjee, Director, Building Research Station, India, for their kind interest in the work.

CONCLUSIONS

1. Humic acid soils have hydrogen-ion activities of the order of 10^{-4} *N*. The ultrafiltrate of the sol contains a small fraction of its free and total acids. The sol, therefore, possesses an intrinsic acid character, i.e., independent of the presence of dissolved acids.

2. The great diminution in the free and total acids on ultrafiltration points to a heterogeneous character of the sol. A part of it is in a state of true solution and registers its activity on a reversible electrode, while the other part, consisting of the colloidal particle, is insoluble. Such a concept is entirely novel to the classical laws of electrochemistry.

3. Humic acid sols are weakly dissociated as shown by their ratios of free to total acids.

4. The base exchange capacity of humic acid is a variable quantity and depends on the nature of base used for titration, i.e., it depends on the "cation effect."

5. When humic acid reacts with bases alone, the "cation effect" is "irregular," i.e., it does not follow the lyotropic series, but when the reaction takes place in the presence of salts, the "cation effect" is "regular," in that it is governed by the electrical adsorbability of the cations concerned.

6. The mechanism of the interaction of humic acid with bases and salts is difficult to explain from a consideration of the classical laws of electrochemistry. A satisfactory explanation can, however, be obtained in the light of the theory of electrical double layer and of secondary adsorption of ions.

REFERENCES

1. ODEN, S., *Kolloidchem. Beihefte*, **11**, 75 (1919).
2. SPRENGEL, C., *Kastner's Arch. Ges. Naturlehre* **8**, 145 (1826).
3. BAUMANN, A., AND GULLY, E., *Mitt. K. Bayr. Moorkult.* **4**, 31 (1910).
4. RINDELL, A., *Intern. Mitt. Bodenk.* **1**, 151 (1908).
5. EICHHORN, DR., *Landw. Jahrb.* **6**, 957 (1877).
6. KÖNIG, A., *Landw. Jahrb.* **11**, 1 (1882).
7. DAIKUHARA, G., *Bull. Imp. Centr. Agr. Expt. Sta. (Japan)* **2**, 1 (1914).
8. KAPPEN, H., *Die Bodenazidität*, 1929.
9. HEINMAN, H., *Z. Pflanzenernähr., Düngung u. Bodenk.* **1**, 345 (1923).
10. TRENEL, M., AND HARADA, M., *Z. Pflanzenernähr., Düngung u. Bodenk.* **28**, 298 (1933).
11. ANDERSON, M. S., AND BYERS, H. G., *U. S. Dept. Agr. Tech. Bull. No.* **542** (1936).
12. FEUSTEL, C., *Trans. Intern. Congr. Soil Sci., Comm.* **6B**, 345 (1936).
13. ZADMARD, H., *Kolloidchem. Beihefte* **49**, 316 (1939).
14. HISSINK, D. J., AND VAN DER SPEK, J., *Trans. Intern. Congr. Soil Sci., Comm.* **2A**, 72 (1926).
15. GILLAM, W. S., *Soil Sci.* **49**, 433 (1940).
16. WAKSMAN, S. A. AND STEVENS, K. R., *Soil Sci.* **30**, 97 (1930).
17. ESH, C., AND GUHASARKAR, S. S., *J. Indian Chem. Soc.* **17**, 326 (1940).
18. PREGI, F., *Die quantitative organische Mikrochemie*, 1930.
19. WAKSMAN, S. A., AND IYER, K. R. N., *Soil Sci.* **34**, 43 (1932).
20. WIEGNER, G., *Kolloid-Z.* **35**, 433 (1926).
21. MUKHERJEE, J. N., *et al.*, *Indian J. Agr. Sci.* **12**, 86 (1942).
22. MUKHERJEE, J. N., AND MITRA, R. P., *Indian J. Agr. Sci.* **12**, 433 (1942).
23. MUKHERJEE, J. N., AND MITRA, R. P., *J. Colloid Sci.* **1**, 141 (1946).
24. KAWAMURA, K., *J. Phys. Chem.* **30**, 1364 (1930).
25. GILLESPIE, L. J., AND WISE, L. E., *J. Am. Chem. Soc.* **40**, 796 (1918).
26. MUKHERJEE, J. N., *Trans. Faraday Soc.* **16**, 103 (1920); *Phil. Mag.* **44**, 321 (1922).
27. BERG, R., *Z. anal. Chem.* **71**, 369 (1927).

THE SPREADING OF LIQUIDS ON LOW-ENERGY SURFACES.

III. HYDROCARBON SURFACES

H. W. Fox and W. A. Zisman

Naval Research Laboratory, Washington 25, D. C.

Received November 19, 1951; revised March 6, 1952

INTRODUCTION

Polyethylene, paraffin, and the flat face of a single crystal of a pure, long-chain *n*-alkane form a series of low-energy surfaces in which the proportion of methyl and methylene groups in the surface changes. Polyethylene surfaces may be considered as comprising entirely methylene groups if the molecular weight is sufficiently high; paraffin surfaces are composed of small crystals oriented at random and contain both methyl and methylene groups, the proportions of each depending on the average molecular weight of the hydrocarbons present, the size of the crystallites, and their orientation; single crystals of pure *n*-alkanes are thin, flat platelets whose major surfaces comprise methyl groups in closest possible packing. It was of interest to compare the surface energy relations of these hydrocarbon surfaces with those found earlier for the surfaces of polytetrafluoroethylene (TFE) (1), and other fluorinated polymers (2). It was expected that a decrease in adhesion to liquids would be exhibited in the order polyethylene, paraffin, single crystal. It was of interest further to compare these surfaces with the octadecylamine monolayers studied by Shafrin and Zisman (3) which have surfaces comprising methyl groups only, but with less compact packing than one obtains in single crystals.

MATERIALS AND PROCEDURES

The polyethylene used in this study was white, unplasticized material with a reported molecular weight of about 250,000. The paraffin was white, filtered material with a melting range of 68–72°C. The single crystals were extremely pure *n*-hexatriacontane platelets (for convenience these surfaces will be designated as C₃₆) prepared by Prof. R. W. Schiessler and made available through the courtesy of the American Petroleum Institute. The crystals had been grown in pure *n*-hexane and were stored under refrigeration in nitrogen until used. They were about 0.1 mm. in thickness and from about 1 × 1 mm. to about 5 × 5 mm. in area.

The polyethylene and paraffin were prepared by removing from a piece of suitable size a layer about 1 mm. thick with a grease-free microtome

blade. The resultant clean, flat surface was pressed against a piece of previously acid-cleaned plate glass, heated to the softening point of the hydrocarbon, and quenched by placing the glass on a cold stone surface. The specimens adhered strongly to the glass and were left that way until used. When pried from the glass, both the polyethylene and paraffin surfaces were flat and smooth, as evidenced by the specular reflection they gave. Static charges developed by the polyethylene by this procedure were discharged by placing the surface near an α -particle source for a minute or two. The crystals were examined in a stereoscopic microscope under 10 magnifications, and were selected for freedom from fissures and other imperfections. It was found impracticable to use crystals having the smaller surface dimension less than 3 mm. except for liquids which gave very high contact angles ($>75^\circ$). For the latter liquids it was possible to use as small a surface as 2×2 mm. Since none of the crystals had greater surface dimensions than 5×5 mm., it was not possible to study liquids having contact angles of much less than 30° . Because of the low adhesion of most of the liquids to the C_{36} surfaces it was found necessary to use a platinum wire on which sufficient liquid was collected so that the drop was about ready to fall off. The combination of the weight of the drop and the adhesion to the C_{36} surface allowed the drop to be detached from the wire. It is obvious, however, that this method did not permit the use of very small drops and therefore of small crystals.

The crystals were placed on a microscope slide which had on it a thin layer of a tacky petroleum wax and lightly pressed down along two opposite edges. This was necessary since an unattached crystal would adhere to the liquid drop when touched by the latter. For the three types of surface the following procedure was used: The specimen surface was allowed to equilibrate with the surroundings ($20 \pm 0.1^\circ\text{C}$., 50% relative humidity). A drop of liquid was carefully placed on the surface, and small additions of liquid were made to the drop until the contact angle became constant. In most cases, on the polyethylene especially, the primary drop showed the maximum angle. In other cases, it was necessary to make two or perhaps three additions. In this way frictional and other irreversible effects were minimized and the drop was made to approach mechanical equilibrium (4). Each value reported is the average of at least four determinations. The variation between determinations for a single system was generally $\pm 2^\circ$ and in many cases $\pm 1^\circ$. The pure liquids used were the same as in the previous studies (1,2).

EXPERIMENTAL RESULTS

Table I contains the measured value of the contact angle (θ), and the calculated value of the final spreading coefficient $S_{LV^\circ/SV^\circ} = \gamma_{LV^\circ} (\cos. \theta - 1)$. The values of the free energy of immersion ($f_{SL} = \gamma_{LV^\circ} \cos \theta$)

TABLE I
Surface Energy Relations of Various Liquids on Hydrocarbon Surfaces
 (All values at 20°C.)

Liquid	γ_{LV}^0 dynes/cm.	<i>n</i> -Hexatriacontane		Paraffin		Polyethylene	
		θ	SLV^0/SP^0 , ergs/cm. ²	θ	SLV^0/SP^0 , ergs/cm. ²	θ	SLV^0/SP^0 , ergs/cm. ²
<i>n</i> -Alkanes		deg.		deg.		deg.	
Hexadecane	27.6	46	-8.4	27	-3.0	Spr.	
Tetradecane	26.7	41	-6.6	23	-2.1	Spr.	
Dodecane	25.4	38	-5.4	17	-1.1	Spr.	
Decane	23.9	28	-2.8	7	-0.2	Spr.	
Nonane	22.9	25	-1.8	Spr.		Spr.	
Di(<i>n</i> -alkyl) ethers							
Decyl	28.4	54	-11.7	—		—	
Octyl	27.7	50	-9.9	23	-2.2	Spr.	
Heptyl	27.0	45	-7.9	20	-1.6	Spr.	
Amyl	24.9	41	-5.0	11	-0.5	Spr.	
<i>n</i> -Alkyl benzenes							
Hexylbenzene	30.0	47	-9.6	—		—	
Butylbenzene	29.2	45	-8.6	—		—	
Propylbenzene	29.0	45	-8.5	—		—	
Ethylbenzene	29.0	45	-8.5	—		—	
Methylbenzene	28.5	41	-7.0	—		—	
Benzene	28.9	42	-9.4	24	-2.5	Small angle	(ca.) 0

TABLE I—Continued

Liquid	γ_{LV}^0 dynes/cm.	n-Hexatriacontane		Paraffin		Polyethylene	
		θ deg.	SLV^0/SP^0 ergs/cm. ²	θ deg.	SLV^0/SP^0 ergs/cm. ²	θ deg.	SLV^0/SP^0 ergs/cm. ²
Esters							
Tricresyl phosphate	40.9	72	-28.3	62	-21.7	34	-7.0
Benzyl phenylundecanoate	37.7	62	-20.0	52	-14.5	28	-4.4
Di(2-ethylhexyl) phthalate	31.2	52	-12.0	36	-9.5	5	-0.1
Pentaerythritol tetracaproate	30.4	56	-13.4	—	—	—	—
Tri(2-ethylhexyl) tricarballoylate	29.6	56	-13.0	—	—	—	—
Halogenated liquids							
Methylene iodide	50.8	77	-39.4	66	-30.1	52	-19.5
sym-Tetrabromoethane	49.7	74	-36.0	—	—	—	—
Aroclor 1242	45.3	73	-32.1	—	—	—	—
α -Bromonaphthalene	44.6	67	-27.2	47	-14.2	35	-8.1
sym-Tetrachloroethane	36.3	60	-18.1	36	-7.0	10	-0.6
Std. fluorolube	25.1	43	-6.7	38	-5.3	Spr.	—
FCD-330 (fluorinated hydrocarbon)	20.2	45	-5.9	33	-3.2	Spr.	—
FCD-329 (fluorinated hydrocarbon)	16.0	—	—	Small angle	(ca.) 0	—	—
Miscellaneous							
Water	72.8	111	-98.9	108	-95.3	94	-77.9
Glycerol	63.4	97	-71.1	96	-70.1	79	-51.3
Formamide	58.2	92	-60.2	91	-59.2	77	-45.1
tert-Butyl naphthalene	33.7	55	-14.4	38	-7.1	7	-0.2
Carbon disulfide	31.4	53	-12.5	—	—	—	—
n-Heptylic acid	28.3	49	-9.5	—	—	—	—
Methylphenylsiloxane (102 cstokes)	26.1	49	-8.7	—	—	—	—
Polymethylsiloxane (35 cstokes)	19.9	(ca.) 20	-0.2	Spr.	—	Spr.	—

and the work of adhesion [$W_A = \gamma_{LV} (1 + \cos \theta)$] can be calculated simply from the given data if it is assumed that the free energy decrease on immersion of the solid in the saturated vapor (f_{SV}) is negligible. This assumption will be discussed below. The liquids are grouped according to structure, the members of each group being arranged in the order of decreasing surface tension.

For a given solid the contact angle, with few exceptions, decreases with decreasing surface tension of the liquid, even between nonhomologous groups. The final spreading coefficient increases with decreasing surface tension in every homologous group and also between groups, while the work of adhesion generally decreases with decrease in surface

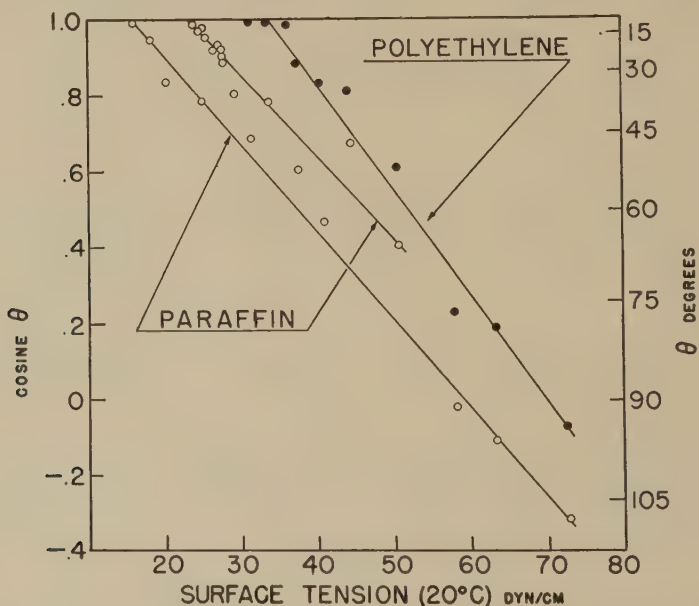


FIG. 1. Cosine of the contact angle *versus* surface tension for polyethylene and paraffin.

tension except for the miscellaneous groups of liquids. In the latter group the work of adhesion increases with decrease in surface tension, reaches a maximum value, and then decreases. For any given liquid, the contact angle decreases in going from C_{36} to paraffin to polyethylene with f_{SL} , W_A , and S_{LV}/S_V increasing in the same order.

Figure 1 is a plot of $\cos \theta$ vs. surface tension for the paraffin and polyethylene. Fewer points are available for the polyethylene than for the paraffin since most of the liquids of this study spread on the former. The points of the liquids which do not spread give a straight line intersecting the ordinate $\cos \theta = 1$ at $\gamma \sim 33$ dynes/cm. The points for paraffin with three or four exceptions appear to collect on two nearly parallel lines

intersecting the ordinate $\cos \theta = 1$ at $\gamma \sim 15$ and 22 dynes/cm., respectively. It was observed that those liquids which fell on the upper curve of Fig. 1 were soluble in paraffin on prolonged contact; i.e., the liquids either sank into the paraffin completely or, on removal of the residual drop by absorbing it in a spill of filter paper, the surface beneath was swollen and softened. The measurements on a given drop of liquid were completed within a minute after the drop was placed, but even the most powerful of the solvents for paraffin visibly showed the solubility effects only after about an hour. Thus the results reported here for liquid/solid systems which were mutually soluble on prolonged contact were reproducible and

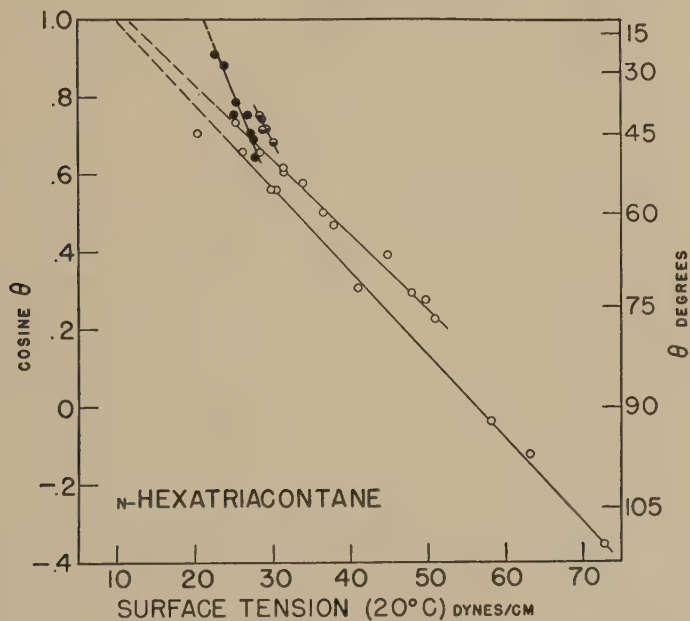


Fig. 2. Cosine of the contact angle *versus* surface tension for hexatriacontane.

○ miscellaneous liquids; ● *n*-alkanes and di-*n*-alkyl ethers;
◐ *n*-alkyl benzenes.

are believed to be significant since the rate of solution was so slow as not to affect the measurements. The liquids which fell on the lower curve were insoluble and showed no attack. The liquids which fell between the two curves showed intermediate behavior. The C_{36} crystals showed no solubility effects, while the polyethylene was attacked only slightly by some of the nonspreading liquids.

Figure 2 is a similar plot for the C_{36} crystals. Here the points collect on four lines as if the crystal surfaces have a higher "resolving power" than the other surfaces in this series of investigations. Two of the lines are roughly parallel to the lines in the paraffin plot, while the line formed

by points of the *n*-alkanes and di-*n*-alkyl ethers has a substantially different slope as does the line given by the alkyl benzenes. The intercepts in this plot can be obtained only by extrapolation since it was not possible to obtain points for liquids with angles much below 30° , as pointed out earlier. In this region, however, the cosine changes so slowly with the angle that the extrapolations probably are closely representative of the

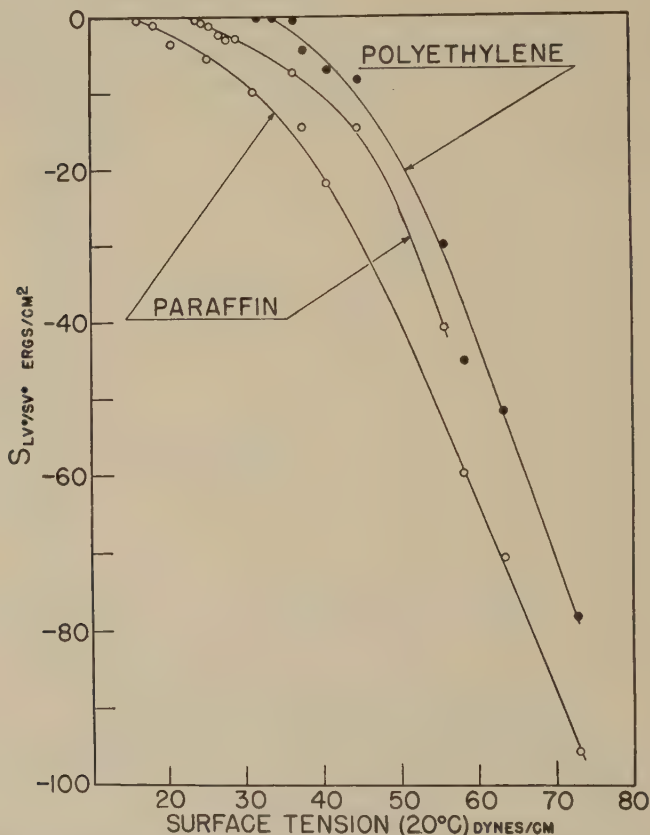


FIG. 3. Final spreading coefficient *versus* surface tension for polyethylene and paraffin.

true values. The intercepts with ordinate $\cos \theta = 1$ for the C_{36} are $\gamma \sim 10$ and 12 dynes/cm., respectively for the lower two curves and $\gamma \sim 21$ dynes/cm. for the *n*-alkanes. No extrapolation was attempted for the alkyl benzenes since the spread in surface tension for these liquids is too small to delineate an unambiguous line.

When S_{LV°/SV° is plotted against surface tension (Figs. 3, 4) the curves are parabolic in shape, a consequence as shown in Ref. (2) of the straight-

line relationships in Figs. 1 and 2. The tangents to the upper portions of the curves in Fig. 3 approximate a 45° negative slope, which, if extrapolated to the axis of abscissas, intersects the axis at the value of f_{SL} as shown previously (2). Figure 4 is a similar plot for C_{36} .

When $\gamma_{LV} \cdot (1 + \cos \theta)$ is plotted against surface tension (Figs. 5 and 6), the pair of curves for paraffin are no longer similar in shape and

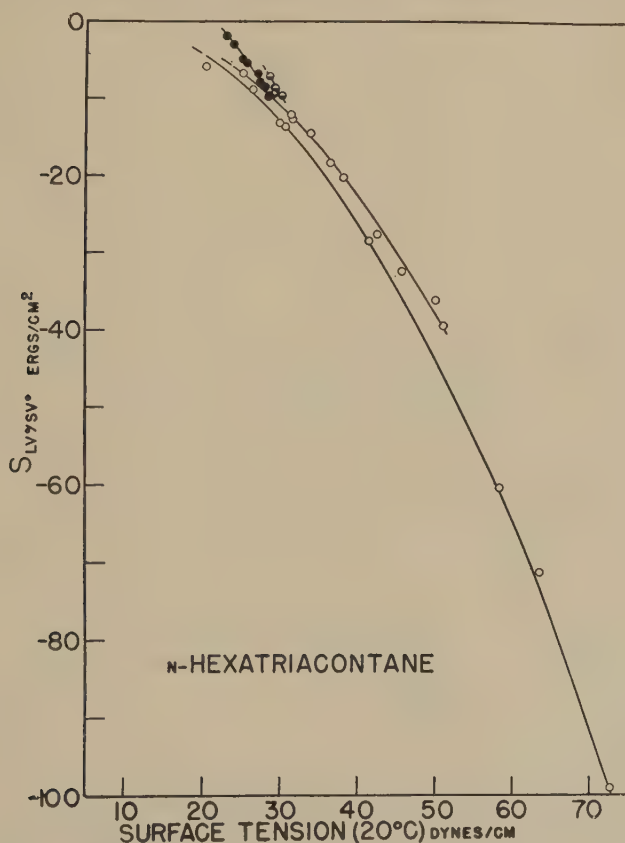


FIG. 4. Final spreading coefficient *versus* surface tension for hexatriacontane. \circ miscellaneous liquids; \bullet *n*-alkanes and di-*n*-alkyl ethers; \ominus *n*-alkyl benzenes.

orientation. The liquids of the lower paraffin curve of Fig. 1 give in Fig. 5 a curve exhibiting a maximum. The plot for polyethylene shows only one curve which is similar to the lower paraffin curve. Figure 6 is a similar plot for C_{36} , the curves resembling those of paraffin. It is noteworthy that at the lower surface tensions these curves approach straight lines with slopes of $+1$ indicating that f_{SL} is essentially constant for these liquids [see Ref. (2)].

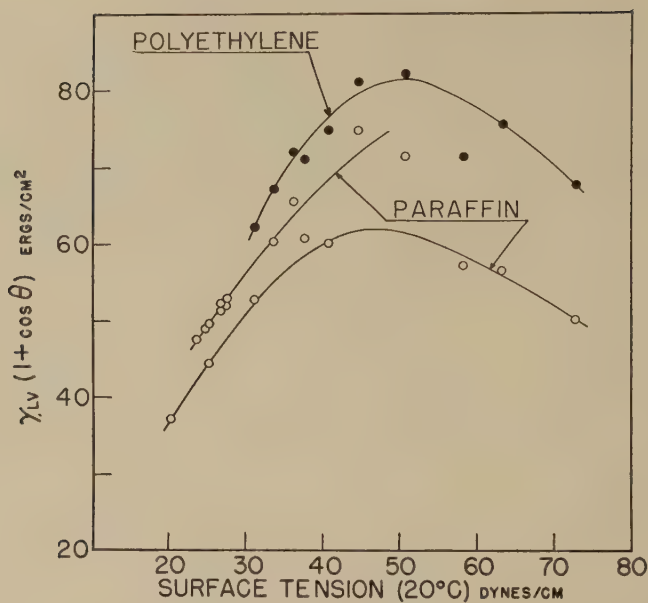


FIG. 5. $\gamma_{LV}(1 + \cos \theta)$ versus surface tension for polyethylene and paraffin.

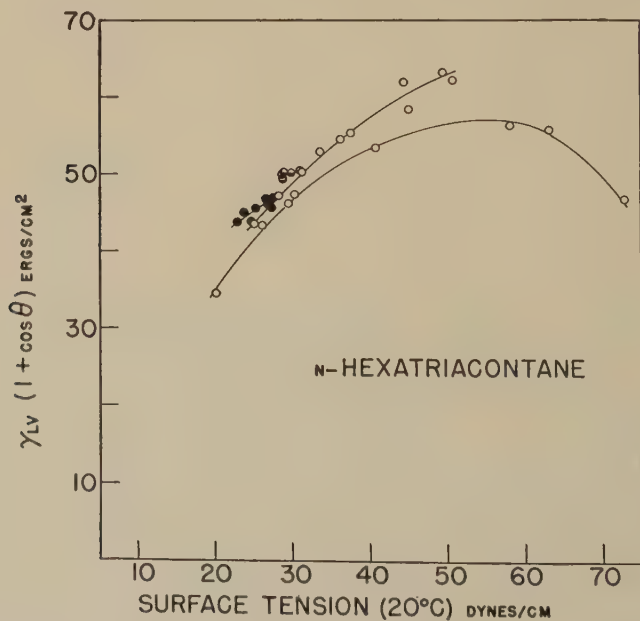


FIG. 6. $\gamma_{LV}(1 + \cos \theta)$ versus surface tension for hexatriacontane. ○ miscellaneous liquids; ● *n*-alkanes and di-*n*-alkyl ethers; ◐ *n*-alkyl benzenes.

DISCUSSION

It is evident from the data of Table I and the Figures that the wettability of these hydrocarbon surfaces decreases in the order polyethylene, paraffin, C_{36} . The reduction in wettability is attributed to the increase in the proportion of methyl groups in the surface. The surface of a C_{36} crystal is made up entirely of oriented methyl groups in the closest possible packing; this surface and surfaces of other long-chain *n*-alkanes are believed to be the least wettable of all hydrocarbon surfaces. Oleophobic monolayers (5) also have oriented methyl groups in the exterior surface but the packing is not as close as in a single crystal and therefore would be expected to be somewhat more wettable (3).

The data given here for the contact angles on C_{36} single crystals represent the highest possible contact angles for each liquid on a hydrocarbon surface. For example, water gives an angle of 111° in contrast to the frequently quoted values of 105 – 108° given in the literature for water on paraffin. The latter figures are presumably a consequence of the presence of methylene groups in the paraffin surface (note that water on polyethylene gives 94°). The variations in the contact angle of water on paraffin found in the literature may not be due entirely to variations in roughness or other topical variables but may be a consequence of variations in size and orientation of the crystallites in the surface which expose more or fewer methyl groups. It is also interesting that water gives a contact angle of 102° on a close-packed octadecylamine monolayer (3). The difference between this figure and the figure for water on C_{36} is attributable to the differences in packing of the methyl groups in the two surfaces (6). Theoretically it should be possible to calculate the packing in a monolayer from differences in hydrophobicity, using as the maximum possible hydrophobic contact angle the value of 111° . Organic liquids exhibit similar but smaller differences on C_{36} and close-packed monolayers (3). For example, hexadecane gives 46° on C_{36} and 39° on an octadecylamine monolayer. Since the packing of a monolayer of straight-chain compounds is related to the size of the polar groups and the length of the hydrocarbon chain, it may be possible to arrive at an estimate of the space occupied by a polar group by observing the differences in contact angle according to the procedures described here.

Graphs of $\cos \theta$ vs. γ for the fluorinated polymers (2) show that the points for all the liquids fall on essentially the same curve. However, the points for paraffin collect on two principal curves, and for the C_{36} crystal on two principal curves and two other shorter curves given by the alkanes and alkyl benzenes. The multiple curves of $\cos \theta$ vs. γ can be accounted for by considering the implications of the Young equation. If this equation is written

$$\frac{\gamma_{S^\circ} - \gamma_{SL}}{\gamma_{LV^\circ}} = \cos \theta \quad [1]$$

it is evident that for a given relatively large value of γ_{SL} , in order for $\cos \theta$ to become unity, γ_{LV}° must assume some small value equal to $\gamma_S^\circ - \gamma_{SL}$. But for the same solid and a liquid for which γ_{SL} is small, $\cos \theta$ will become unity at some larger value of γ_{LV}° . The magnitude of γ_{SL} relative to γ_{LV}° accounts for the multiple curves with different intercepts at $\cos \theta = 1$. It is reasonable to assume that γ_{SL} will be small when the solid tends to dissolve in the liquid (the upper paraffin curve of Fig. 1) and that γ_{SL} is significantly larger when there is no such tendency (the lower paraffin curve of Fig. 1). Since γ_{SL} may vary from zero to relatively large values for liquids with the same surface tension, there is no theoretical necessity for the existence of two curves only. For example, the points in Fig. 1 which fall on neither curve can have some intermediate relative value of γ_{SL} .

The relative values of γ_{SL} of the liquids of this study for the hydrocarbon surfaces (as determined by which of the $\cos \theta$ vs. γ curves the points lie on) correlate well with the mutual solubilities of hydrocarbons and the liquids in question. Thus, water, glycerol, formamide, tricresyl phosphate, and the fluorocarbon liquids, none of which dissolve paraffin, lie on one curve which can appropriately be designated as the curve for liquids with high γ_{SL} . Alkanes, alkyl ethers, and aromatic and halogenated hydrocarbons, all of which dissolve paraffin, lie on a second curve designated as the curve for liquids of low γ_{SL} . Esters, less polar than tricresyl phosphate and more polar than the liquids having low γ_{SL} , fall between the two main lines. The C_{36} surface is even more discriminatory in that the strongly polar liquids and the fluorocarbons fall on the line for liquids of high γ_{SL} ; the halocarbons and esters fall on a slightly displaced parallel line corresponding to a somewhat smaller γ_{SL} ; the line for alkanes and alkyl ethers indicate a still smaller γ_{SL} ; and that for the alkyl benzenes indicate the lowest γ_{SL} of all the liquids investigated. The indication is that γ_{SL} decreases and the van der Waals' forces of adhesion across the hydrocarbon-solid/liquid interface increase in the order oxygen- and fluorine-containing liquids, aliphatic hydrocarbons, aromatic hydrocarbons.

In the previous studies on fluorinated polymers (1,2), the critical surface tension, γ_C , of a solid was defined as that value of the surface tension below which liquids spread on a solid; the value of γ_C was taken to be the intercept of the plot of $\cos \theta$ vs. γ with the ordinate $\cos \theta = 1$. It is evident from the multiple curves found in this study for paraffin and for C_{36} that there can be different values of γ_C for the same solid depending on the solid-liquid interfacial tension, and that γ_C for the liquid with low γ_{SL} is from 2 to 8 dynes/cm. greater than for the liquids with high γ_{SL} . The small differences in γ_C found in the previous studies on the fluorinated polymers (1,2), and in this study for polyethylene, are a consequence of the fact that (unlike C_{36} and paraffin) no liquids could be found which had

sufficiently low interfacial tensions with these polymers and whose surface tensions were, at the same time, sufficiently great (were nonspreading).

In Figs. 5 and 6, the curves which show a maximum are those of the liquids of high γ_{SL} . These parabolic curves can be derived from the Young-Dupré equation for the work of adhesion (neglecting f_{SV})

$$W_A = \gamma_{LV}^\circ(1 + \cos \theta_E) \quad [2]$$

since $\cos \theta_E$ is a linear function of γ_{LV}° for these surfaces, thus

$$\cos \theta_E = a - b \gamma_{LV}^\circ \quad [3]$$

The maxima of the parabolas can be calculated by determining a and b from Figs. 1 and 2. For the upper curve for paraffin, W_A is found to be a maximum at $\gamma_{LV}^\circ = 59$ dynes/cm. It is now evident why the upper curve for paraffin in Fig. 5 shows no maximum. In order to make this curve turn downward again, it would be necessary to secure points for liquids of low γ_{SL} with paraffin having surface tensions of more than 59 dynes/cm. Such liquids do not appear to exist. A similar situation obtains for the C_{36} surfaces. It should be noted that the curves of W_A vs. γ_{LV}° for the fluorinated polymers of the earlier study (2) were not parabolic but rose to a maximum along which the curve continued. This was a consequence of the fact that the curves of $\cos \theta$ vs. γ were not linear.

To gain some understanding of the trends in W_A and γ_{SL} it will be useful to examine the implications of the equation for the work of adhesion quoted earlier (2), i.e.,

$$W_A = f_{SL} + \gamma_{LV}^\circ. \quad [4]$$

The curve of W_A can be regarded as the sum of two functions of γ_{LV}° , one being f_{SL} vs. γ_{LV}° and the other a straight line of slope +1. Where f_{SL} is constant, the graph of W_A vs. γ_{LV}° will be a straight line with a 45° slope and an intercept on the axis of ordinates of f_{SL} . This was shown to be the case for every homologous series in (1) and (2). It is evident from Figs. 5 and 6 that deviations of up to 15° from the +1 slope are found for the hydrocarbon surfaces. From Eq. [4], it is seen that where f_{SL} increases monotonically with γ_{LV}° , W_A will increase at a greater rate than indicated by the +1 slope; this is found to be the case with paraffin and polyethylene for the low surface tension liquids (Fig. 5). Where f_{SL} decreases monotonically with γ_{LV}° , W_A will increase at a rate smaller than that indicated by a +1 slope; this was found to be the case for the alkanes on a C_{36} surface. Where f_{SL} decreases monotonically with γ_{LV}° and, at the same time, the curve of f_{SL} vs. γ_{LV}° changes from a slope $> +1$ to $< +1$, W_A will show a maximum at the point where this change takes place. This situation is observed for the liquids of high γ_{SL} on all three hydrocarbon surfaces. Note that the horizontally asymptotic portion of

the W_A vs. γ curves of the fluorinated polymers (2) indicate that in this region f_{SL} has a slope of -1 for these surfaces.

The changes in γ_{SL} as a function of the nature of the liquid and solid can be derived from the equation defining f_{SL} and the trends in f_{SL} since

$$f_{SL} = \gamma_{S^0} - \gamma_{SL}. \quad [5]$$

Since γ_{S^0} is constant, the changes in γ_{SL} are numerically equal to the changes in f_{SL} but are of opposite sign. Thus the curves of W_A vs. γ_{LV^0} for the fluorinated polymers (2) indicate that once the asymptotic maximum is reached, thereafter γ_{SL} is a monotonically increasing function of γ_{LV^0} with a slope of $+1$ and that γ_{SL} (and hence the van der Waals' adhesive forces at the interface) is consequently dependent only on the magnitude of γ_{LV^0} and is independent of the molecular structure type of the liquid. As for the hydrocarbon surfaces, it follows that γ_{SL} increases faster than γ_{LV^0} as the liquids become more hydrophilic, indicating that the van der Waals' forces at the hydrocarbon-solid/liquid interface are decreasing as the liquids become more hydrophilic.

If f_{SL} is plotted against γ_{LV^0} for the *n*-alkane liquids, a difference in slope is noted between the graphs for the C_{36} and paraffin. For C_{36} , f_{SL} decreases about 2 ergs/cm.² with increase in chain length from nonane to hexadecane; for paraffin, f_{SL} increases about 1 erg/cm.² with increase in chain length from decane to hexadecane. This means that according to [5], γ_{SL} increases about 2 dynes/cm. for the C_{36} with increase in γ_{LV^0} from 23 to 27.6 dynes/cm., whereas for paraffin, γ_{SL} decreases about 1 dyne/cm. with increase in γ_{LV^0} from 24 to 27.6 dynes/cm. These effects are probably the resultant of two competing tendencies in the alkane liquids. As the chain length of the molecules of the liquid increases, the proportion of methyl to methylene groups decreases so that one would expect increasing adhesion to a given surface. Simultaneously, however, the surface tension of the liquid increases, thereby tending to increase the interfacial tension which means a decrease in the intensity of the van der Waals' cohesive forces at the solid-liquid interface. For the C_{36} surface, which contains only methyl groups, the latter tendency is more pronounced, whereas for a surface like paraffin which contains both methyl and methylene groups, the increase in the proportion of methylene groups overrides the effects of increasing surface tension.

In general it appears to be the case that the lower the surface energy of the solid, the more independent are f_{SL} and γ_{SL} of the constitutive properties of the liquid in contact with the surface. Consequently, the contact angle is largely determined by the surface tension of the liquid. On higher energy surfaces, the constitution of the liquid can exert profound effects which may obscure the effect of the liquid surface tension.

It is interesting to consider from Eq. [5] the maximum values that

$\gamma_{S^{\circ}}$ can assume. It appears from this equation that since $\gamma_{SL} \geq 0$, f_{SL} has $\gamma_{S^{\circ}}$ as an upper bound; and further that the maximum value of f_{SL} for a given solid will correspond to the minimum value of γ_{SL} . Thus for C_{36} , $\gamma_{S^{\circ}}$ is presumed to be not more than about 21.5 dynes/cm.; for paraffin, about 30.5 dynes/cm.; and for polyethylene, about 36.5 dynes/cm. It would be interesting to compare the value for polyethylene with the liquid surface tension of the n -alkane series extrapolated to high molecular weights. The smaller values for paraffin and C_{36} are due to the concentrations of methyl groups in the surface. Such a concentration presumably cannot occur in the liquid state because of the thermal agitation of the molecules. For TFE, $\gamma_{S^{\circ}}$ is estimated to be no more than about 24.5 dynes/cm. (1), and for polymonochlorotrifluoroethylene about 32 dynes/cm.

We have labeled the ordinate axes of Figs. 5 and 6 as $\gamma_{LV^{\circ}}(1 + \cos \theta)$ rather than W_A since the former is the exact designation of the values and points given. Strictly speaking, $W_A = f_{SV^{\circ}} + \gamma_{LV^{\circ}}(1 + \cos \theta_E)$; thus the true values of W_A for the liquid/solid systems of this investigation can be secured by adding the values of $\gamma_{LV^{\circ}}(1 + \cos \theta)$ in Table I to the appropriate values of $f_{SV^{\circ}}$ when the latter are obtainable. It is probable that the values of $\gamma_{LV^{\circ}}(1 + \cos \theta)$ given here for the liquids of high γ_{SL} are closely representative of W_A for these systems since it is believed that $f_{SV^{\circ}}$ is quite small for solids of such low adsorptivity. For the liquid of low γ_{SL} , extensive adsorption of the liquid vapors on these solid surfaces must still be considered to exert a rather minor effect on the free surface energy of the solid since the latter have such low free surface energies to begin with. Adsorption of n -alkane vapors on paraffin, for example, cannot be expected to change the free surface energy of the latter very much. Large changes could be expected to occur only when the solid has a high initial free surface energy, as for example the drastic changes which take place in the behavior of a metal surface when a monolayer of some amphipathic compound is adsorbed on it (3). It is therefore believed that for all the liquids of this investigation, the trends given in Figs. 5 and 6 are indicative of the trends of W_A for these systems.

SUMMARY

1. Contact angle measurements have been made of a wide variety of liquids on clean, smooth surfaces of polyethylene, paraffin, and surfaces of single crystals of n -hexatriacontane (C_{36}). The calculated value of the final spreading coefficient ($S_{LV^{\circ}/SV^{\circ}}$) is given and from the data there can be calculated the values of the free energy of immersion (f_{SL}), and the work of adhesion (W_A). The free energy of immersion of the solid in the liquid vapor can be neglected in these calculations since it is believed to be quite small for surfaces of low adsorptivity and low free surface energy.

It is shown that the methyl-rich surfaces of C_{36} and paraffin are not wetted by a wide variety of organic liquids, including the n -alkanes, so that the rule that nonpolar solids are wetted by nonpolar liquids is again found to be erroneous.

2. Wettability is found to decrease in the order polyethylene, paraffin, C_{36} . This is attributed to the increase in the proportion of methyl to methylene groups in the surface. The C_{36} surface, like all higher n -alkane crystals, is shown to be the least wettable of all hydrocarbon surfaces since its surface comprises only methyl groups arranged in the closest possible packing. It is shown that it should be possible to estimate the packing of adsorbed monolayers of straight-chain hydrocarbon derivatives by comparing the hydrophobic contact angle to the angle on C_{36} . Many of the variations of the hydrophobic contact angle on paraffin found in the literature are shown to be attributable to variations in the methyl/methylene ratio in the surface.

3. In contrast to the fluorinated polymers, paraffin and C_{36} are shown to have multiple curves of $\cos \theta$ vs. γ . The multiplicity of these curves is attributed to differing dependencies of γ_{SL} on γ_{LV}° due to variation in the constitution of the liquid. Increase in adhesion of hydrocarbon surfaces to liquids is found to be in the order: liquids containing oxygen or fluorine, aliphatic hydrocarbons, aromatic hydrocarbons.

4. It is shown that variation of the free energy of immersion of the n -alkane series of liquids on a given hydrocarbon surface is the resultant of two competing tendencies: i.e., increased adhesion due to increase in methylene to methyl ratio in the liquid, and decrease in adhesion due to increase in surface tension of the liquid. For the C_{36} surface, the latter tendency predominates; for the paraffin surface, the former tendency predominates. f_{SL} is shown to be the upper bound of the solid surface tension for systems where $\gamma_{SL} \geq 0$.

5. It is shown that in general there is more than one value of the critical surface tension (below which liquids spread on a given surface) for hydrocarbon surfaces, depending on the value of γ_{SL} given by a liquid of given surface tension. The fluorinated polymers are shown to be a special case where the surfaces are independent of the nature of the liquid and therefore have essentially a single value of γ_C .

REFERENCES

1. FOX, H. W., AND ZISMAN, W. A., *J. Colloid Sci.* **5**, 514 (1950).
2. FOX, H. W., AND ZISMAN, W. A., *J. Colloid Sci.* **7**, 109 (1952).
3. SHAFRIN, E. G., AND ZISMAN, W. A., *J. Colloid Sci.* **7**, 166 (1952).
4. SUMNER, C. G., *Wetting and Detergency*, p. 15. Chemical Publishing Co., New York, N. Y., 1935.
5. BIGELOW, W. C., PICKETT, D. L., AND ZISMAN, W. A., *J. Colloid Sci.* **1**, 513 (1946).
6. BAKER, H. R., SHAFRIN, E. G., AND ZISMAN, W. A., *J. Phys. Chem.* **56**, 405 (1952).

RETARDATION OF FLOW IN NARROW CAPILLARIES

John C. Henniker¹

Laboratoire de Chimie Physique, Institut Pasteur, Paris 15, France

Received January 23, 1952; revised March 21, 1952

INTRODUCTION

It is known that liquids in capillary tubes less than about $1\ \mu$ in radius often flow more slowly than predicted by Poiseuille's law. Several examples and a number of explanations have been discussed in a review on surface orientation of liquid molecules (1). There is generally some doubt as to the exact radius of the channel, and hence as to the calculated value of the viscosity. However in one significant investigation the radius was not a deciding factor (2). The rate of flow of water through a ceramic disk was found to be seven times greater after the pores had been coated with oleic acid. Two explanations were suggested: (a) There is slippage between the water and the hydrophobic layer on the wall, resulting in an effective increase in the rate of flow compared to that in untreated pores; (b) there is a wall layer that ordinarily tends to retard abnormally the passage of water, and this is removed when the pores are rendered hydrophobic. These authors expressed doubt as to the presence of slippage.

EXPERIMENTAL

In an attempt to find if slippage occurs, a sintered Pyrex disk of pore radius $7.5\text{--}20\ \mu$ has been used, and the rate of flow of liquids has been measured with and without surface-active additives. The liquids were water and paraffin oil, and the additives dodecanol, dodecylamine, and heptadecylamine. The additives effectively rendered the walls of the apparatus nonwetable, but in no case was there any change in flow rate that was not accounted for by changes in bulk viscosity. The head was 28 cm. and the precision about 0.5%. The apparatus was immersed in a water thermostat at 20° .

DISCUSSION

If slippage is present, it may be expressed as a supplement to the normal viscous flow in an extension of Poiseuille's law:

$$Q = \frac{P\pi r^3}{8\eta} (r + 4s\eta)$$

¹ Present address: R.M.D. Cowichan Station, British Columbia, Canada.

in which s may be called a "surface fluidity." One may calculate a value of s from the data of Deryagin and Krylov (2), in which the radius was $0.05\ \mu$. Application of this value to the present data indicates an increase of flow rate of 3% with water and 300% with the oil. Since no such increase was found, and in spite of the doubt introduced by substituting amines and an alcohol for oleic acid, one is led to believe that slippage is not to be expected when a Newtonian liquid flows through a nonwetable channel.

However if the results of Deryagin and Krylov are to be explained by a wall viscosity in water in untreated pores, which is removed by the oleic acid, we may picture for the moment the viscous region as a layer of rigid water. A calculation using Poiseuille's law shows that its thickness would have been 190 Å. This thickness on the walls of $10\text{-}\mu$ pores (an average radius for the pores of the Pyrex disk) would decrease the flow rate by 0.77%. Since this is hardly more than the experimental error, a wall viscosity may have been present but undetected.

Calculations show that streaming potential might equally well account for the data of Deryagin and Krylov and perhaps other observations of retardation in narrow pores. Equations for the effect of streaming potential on permeability have been developed by Onsager and Cole (3), and, more completely, by Elton (4).

There remains the problem of distinguishing the roles of streaming potential and wall viscosity experimentally. A method which has been found effective is to install identical reversible electrodes at each end of the porous element. When the electrodes are connected, the retardation of flow by streaming potential should be suppressed, and its effect should be measurable directly.

EXPERIMENTAL

A Chamberland porcelain filter candle, grade 5-L-13, of listed effective pore diameter of $0.30\ \mu$, was used as the porous element. It was cleaned by heating to redness. The Ag-AgCl electrodes were formed on spirals of silver wire fitting inside and outside the filter (5). No part of the filter surface was more than 5 mm. from an electrode. The filter was mounted in a Pyrex vessel connected to an elevated reservoir by a narrow tube. The flow rate was measured by the passage of a meniscus between two marks on a horizontal portion of this tube. The head was thus kept constant at 43.5 cm.

It has been suggested that air dissolved in the liquid may cause erratic results (5,6). All solutions were therefore boiled immediately before use, and a portion was drawn through the filter by an aspirator before each run. Plugging by bacteria is considered unlikely, since all solutions were freshly prepared and only a few milliliters were passed during each run. In addition, the sequence of solutions was such that any cumulative plugging would have diminished the observed effects. The electrodes were

tested for reversibility, and it seems certain that connecting them must have suppressed any retardation by streaming potential. No corresponding change in the flow rate was detected. Moreover, the electrokinetic retardation calculated from measured streaming potentials by Elton's method (4) amounts to only about 1% in the solutions of concentration 100, 300, and 1000 μ moles/l., and less in the others. This is of the order of the experimental error.

Runs were made with two samples of distilled water and several concentrations of KCl in the untreated porcelain, and again with water after the filter had been treated with a 10^{-4} *N* solution of dodecylamine hydrochloride to render the pores hydrophobic. No adjustment of the data had to be made for the effect of the salt on bulk viscosity, because the decrease is only 0.025% at 0.01 *N*. The temperature was held at $20 \pm 0.05^\circ$. The data are shown in Table I. The thickness of the ionic atmosphere was

TABLE I

Concentration of KCl μ moles/l.	Conductance (measured) $\Omega^{-1} \text{ cm.}^{-1} \times 10^3$	Ionic atmosphere \AA.	Streaming potential (measured) mv.	Flow time sec.	Ratio of flow times
None	4.2	550	—	48.2	1.22
None	6.0	460	—	45.6	1.15
100	19.6	254	13	42.0	1.06
300	46.8	165	13	40.6	1.03
1000	139	95	7	39.6	1.00
3000	401	55	2	39.6	1.00
10,000	1290	30.5	—	39.5	1.00
None (pores treated with amine)			—	39.7	1.01

calculated ($\alpha = 3.05/\sqrt{c}$ \AA.) from the conductance assuming all ions to be those of KCl. The ratio of flow time was based on the minimum flow time, 39.5 sec. In the first two runs with water the streaming potential was small and obscured by a variable concentration potential presumably due to ions dissolved from the filter.

RESULTS

The significant results were that the permeability to water was considerably less than to the KCl solutions, and that after the pores had been made hydrophobic the permeability to water became nearly that to 0.01 *N* KCl. Thus it is concluded that abnormally high viscosity existed in very dilute solutions in close proximity to a porcelain wall, and that this abnormal viscosity was absent in the more concentrated solutions and in the presence of an amine capable of being strongly adsorbed and of rendering the wall hydrophobic. It appears that the results of Deryagin and Krylov may be explained by the same mechanism.

A reason for this behavior may be found in the extreme potential gradients in a solution of ions near a charged surface. For example, using

an equation of Neale (7) for the potential distribution in uni-univalent electrolytes, if the surface charge is 5000 e.s.u./cm.², the gradient at the wall is found to be 234 kv./cm., diminishing to about one-tenth of this value at a distance corresponding to the thickness of the Debye-Hückel ionic atmosphere. The viscosity to be expected in regions of such gradient may be gauged from data on the flow of liquids in high electric fields (8). Preliminary calculations indicate viscosity distributions that may account for the present data on KCl solutions.

ACKNOWLEDGMENT

The author appreciates the laboratory facilities made available by Dr. D. G. Dervichian, and the stimulating discussions with him and his associates.

SUMMARY

Certain anomalies in the rate of flow of Newtonian liquids in narrow channels may be explained either by slippage (surface fluidity) under conditions of one kind, or by retardation under others. Data are presented to show that slippage is unlikely. Retardation could be due to streaming potential or to mechanical restriction. The flow rate of distilled water in pores of $0.05\ \mu$ in radius was found to be 20% less than that of a salt solution. The measured streaming potential was too small to account for the retardation. Bacteria and gas bubbles were excluded. A tentative explanation links the intense electric field existing in the electrical double layer with the augmentation of the viscosity of liquids in the presence of strong fields.

REFERENCES

1. HENNIKER, J. C., *Revs. Modern Phys.* **21**, 322 (1949).
2. DERYAGIN, B. V., AND KRYLOV, N. A., *Akad. Nauk S.S.S.R., Otdel. Tekh. Nauk, Inst. Mashinovedeniya, Soveshchanie Vyazkost, Zhidkost. i Kolloid. Rastvorov* (Conf. on Viscosity of Liquids and Colloidal Solutions) **2**, 52 (1944); see *C. A.* **40**, 3314 (1946).
3. See ABRAMSON, H. A., *J. Gen. Physiol.* **15**, 279 (1932).
4. ELTON, G. A. H., *Proc. Roy. Soc. (London)*, **A198**, 581 (1949).
5. NEALE, S. M., AND PETERS, R. H., *Trans. Faraday Soc.* **42**, 478 (1946).
6. MEYEROTT, R., AND MARGENAU, H., *Am. J. Sci.* **243**, 192 (1945).
7. NEALE, S. M., *Trans. Faraday Soc.* **42**, 473 (1946).
8. ANDRADE, Z. DA C., *Proc. Roy. Soc. (London)* **A187**, 296 (1946).

LETTERS TO THE EDITORS

THE TREATMENT OF COMPLEX ADSORBATES AS A SINGLE PHASE

According to the usual definition of a phase such as used by Gibbs (1), a phase is a homogeneous part¹ of a given mass. Therefore, it first appeared (2) that treatment of a multilayer adsorbate as a single phase, as was later done by Hill (3), was subject to doubt since matter next to the surface was not in the same physical state as matter further away from the adsorbent. For purposes of testing the thermodynamic soundness of the assumptions and model used for the Brunauer-Emmett-Teller (B.E.T.) equation, a treatment was attempted in which different layers were considered as separate phases (2). Hill (3) has objected to this on the grounds that this is a molecular picture and as such is foreign to thermodynamics. While it is not necessary to consider molecular dimensions in three-dimensional thermodynamics because the phases are large compared with molecular size, surface phases may be of molecular thickness. It, therefore, seems proper to talk of molecular dimensions in assigning surface phase boundaries.

Hill considers the adsorbate as a nonhomogeneous phase, which seems to be a contradictory term in view of the definition of Gibbs. However, if the adsorbate can in some way be split into negligibly small increments or phase units all having the same physical properties, it could be regarded as macroscopically homogeneous and thus be treated as a single phase. These phase units could comprise millions of molecules since such a unit would still be small relative to macroscopic dimensions. This appears possible in the case of most complex sorbates and, thus, the earlier treatment (4) used for two dimensional adsorbates would seem valid for adsorbates that can be regarded as macroscopically homogeneous. Figure 1 serves to illustrate in an idealized manner what is meant by negligibly small increments as applied to multilayer and capillary sorption. The phases in these idealized cases would be the sum of many of these identical units.

On the other hand, if regions of macroscopic heterogeneity such as might arise due to a nonuniform adsorbent were present, a single-phase

¹ Homogeneous part is defined by Gibbs as the part in question that is uniform throughout, both in chemical composition and physical state. It follows as a corollary that if different phases are in contact that there must be boundary surfaces or surfaces of discontinuity and that the different phases are physically distinct.

treatment would not seem adequate. Although the entropy change involved in transfer from gas phase to adsorbate at constant surface and gas-phase pressure may not depend on phase definition, to carry out such a process reversibly it appears necessary that any nonhomogeneous matter be negligible in size relative to the size of the pistons utilized in the transfer just as it is necessary to use pistons much larger than molecules to

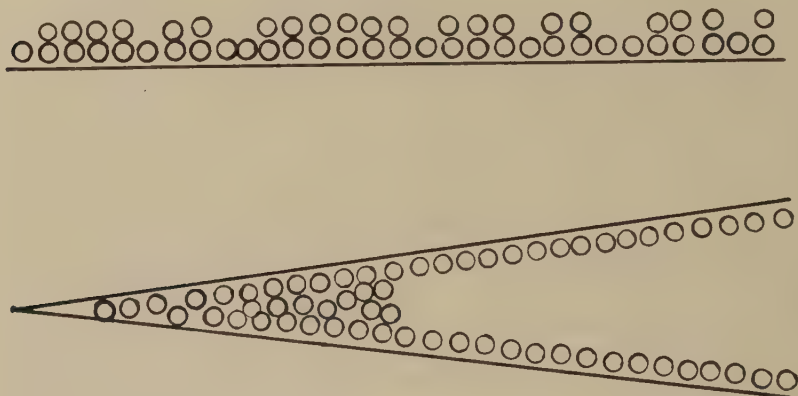


FIG. 1. Idealized phase unit cross sections for multilayer and capillary sorption.

approach reversibility in compression of a three-dimensional gas. If the surface was macroscopically heterogeneous, such a process could not be carried out reversibly at constant spreading pressure since the latter would measurably change from place to place on the surface as the pistons were moved. Or, in other words, to carry out reversible processes it seems necessary to deal with macroscopically homogeneous matter, that is, with phases.

REFERENCES

1. GIBBS, J. W., *The Scientific Papers of J. Willard Gibbs*, Vol. 1. Longmans, Green and Co., New York, 1906.
2. ROWLEY, H. H., AND INNES, W. B., *J. Phys. Chem.* **46**, 694 (1942).
3. HILL, T. L., *J. Chem. Phys.* **17**, 520, 772 (1949).
4. ROWLEY, H. H., AND INNES, W. B., *J. Phys. Chem.* **46**, 537 (1942).

W. B. INNES

*Stamford Research Laboratories,
American Cyanamid Company,
Stamford, Connecticut*

Received April 23, 1952

COMMENTS ON THE PRECEDING NOTE BY W. B. INNES

The writer's objection (1) to the treatment of Rowley and Innes (2) was specifically not to a discussion of "molecular dimensions in assigning surface phase boundaries" [which is implicit in the idea of a Gibbs dividing surface (3)], but rather to basing a thermodynamic treatment on (B.E.T.) molecular layers considered as separate "phases." First, a "molecular layer" is an explicit molecular model and not a thermodynamic concept (e.g., Gibbs avoids such concrete ideas concerning molecular organization, etc., in his treatment of interfacial regions). Secondly, because of the molecular dimensions involved and the range of intermolecular forces the properties of such a "phase" depend *explicitly* on the state of neighboring "phases." The usual criterion for equilibrium between phases breaks down in this case (4, 5). One has to treat the whole collection of "phases" as a single nonhomogeneous (on a *molecular* level) phase (5) (as Innes points out, Gibbs does not use "phase" in this way; but this is a matter of semantics, not thermodynamics).

Adsorption systems are thermodynamically very similar to solution systems with one nonvolatile component. The writer has shown (6) that, as expected, a single thermodynamic treatment can be given which includes both solution thermodynamics (sulfuric acid-water, rubber-benzene, hydrogen-palladium, etc.) and adsorption thermodynamics, and which furthermore reduces to the special case (1) of an "inert adsorbent," which is the problem Innes is concerned with. The argument (6) need not be repeated here. It shows that regardless of molecular details (swelling, heterogeneous surface, etc.), some of which seem to worry Innes, thermodynamics can still be applied—just as one can apply thermodynamics to, say, a sulfuric acid-water system without becoming concerned about the exact nature of the hydration in the neighborhood of a sulfate ion, etc.

There is, however, one troublesome point [see appendix I of Ref. (6)], at least in principle: the treatment referred to above (6) depends on being able to define the volume of the "solution" (adsorbent plus adsorbed gas) with sufficient precision. If this cannot be done, the rigorous thermodynamic procedure is then to regard the "solution" and the gas phase combined as the thermodynamic system (5,6,7). Or in some cases (e.g., Fig. 1 in Innes' note) a Gibbs dividing surface may be used (5, 6, 8) to give a rigorous treatment despite the "volume problem" mentioned above. These questions are discussed in detail elsewhere (5).

REFERENCES

1. HILL, T. L., *J. Chem. Phys.* **17**, 520 (1949).
2. ROWLEY, H. H., AND INNES, W. B., *J. Phys. Chem.* **46**, 694 (1942).

BOOK REVIEW

The Rheology of the Cross Striated Muscle Fibre. By FRITZ BUCHTHAL AND E. KAISER. *Kgl. Danske Videnskab. Selskab, Biol. Medd.* **21**, no. 7 (1951). Einar Munksgaard, Copenhagen, Denmark. 318 pp. Price D. Crs. 35/-.

This monograph is a research paper, of unusual length. About two-thirds of the paper is directly or indirectly concerned with new experimental results, and the remainder is primarily theoretical.

The experimental part represents an important and extensive contribution to biophysics. As far as the reviewer is aware, this is the most detailed application of modern rheological methods to the cross-striated muscle fiber that has been carried out. Some idea of the kind of material included may be gained from the following representative section or subsection headings: "The length-tension diagram of the resting fiber"; "Equivalent models for the description of transients"; "Spectrum of retardation times"; "Voight-model and vibration experiments"; "Isometric transient, contraction, stress-relaxation following quick changes in length"; "Shortening velocity as a function of temperature."

The theoretical section contains an excellent analysis of the rate and equilibrium properties of a chain consisting of "a large number of links occurring in two stable modifications, a short one and a long one . . . Transmutation from the one linkage to the other can be described by the transition over a potential barrier in passing from one potential minimum to another . . . The length and radius of the (transmuting) elements are assumed to be 20 and 3 A., respectively." Certain modifications of this model are also included. The theory is used rather extensively to interpret the experimental data.

A number of authors have suggested a theory of this type (long \leftrightarrow short units). It may be of interest to mention these with a few comparative remarks. The papers on this subject which the reviewer has seen are (in chronological order) by Frenkel (1), Burte and Halsey (2), Peters and Speakman (3), Gergely and Laki (4), Buchthal and Kaiser [1951], and Polissar (5). Frenkel, and Peters and Speakman discuss specifically the Astbury α - β -transition in polypeptide chains. Gergely and Laki, and Polissar apply the theory to macromolecular units, or "autones," as Szent-Györgyi calls them. Burte and Halsey, and Buchthal and Kaiser refer to units of a molecular chain of intermediate size. The treatments given by Frenkel, and Gergely and Laki include equilibrium properties only; the other authors introduce the rate problem as well. The discussions of Gergely and Laki, Buchthal and Kaiser, and Polissar are formal in the sense that these authors are noncommittal about the exact molecular nature of the fundamental units and/or the nature of the forces involved in the transmutation.

The present monograph illustrates the usefulness of interpretations of biophysical phenomena on a rather formal level. The problem of understanding on the ultimate molecular level still remains in this case (though it is being attacked actively in many laboratories). Aside from its intrinsic interest, the present type of analysis provides an extremely helpful guide to the eventual molecular interpretation.

1. FRENKEL, J., *Kinetic Theory of Liquids*, p. 485. Oxford, London, 1946.
2. BURTE, H., AND HALSEY, G., *Textile Research J.* **17**, 465 (1947).
3. PETERS, L., AND SPEAKMAN, J., *J. Textile Inst.* **39**, 253 (1948).
4. GERGELY, J., AND LAKI, K., *Enzymologia* **15**, 272 (1950).
5. POLISSAR, M., *Am. J. Physiol.* **168**, 766 (1952).

TERRELL L. HILL, Bethesda, Maryland

THE CRITICAL RANGE FOR MICELLE FORMATION BY AN OIL-DISPERSIBLE SOAP IN A HYDROCARBON SOLVENT¹

Samuel Kaufman and Curtis R. Singleterry

Naval Research Laboratory, Washington 25, D. C.

Received May 7, 1952

ABSTRACT

Micelle formation by the oil-dispersible soap, calcium xenylstearate, in moist benzene has been studied by fluorescent dye techniques, utilizing Rhodamine B and Acridine Orange. A treatment is presented for the interpretation of fluorescence depolarization data obtained from a system in which the emitting dye is present partly as a component of soap micelles and partly in true molecular solution. This method has special usefulness for identifying the onset of micelle formation in very dilute solutions. The midpoint of the critical range for the formation of micelles in this case is found to be 0.6×10^{-6} mole/l.; the size of the micelles is essentially constant over the range from 1×10^{-6} to 7×10^{-3} mole/l. The data obtained are consistent with a simple mass law equilibrium between molecularly dissolved and micellar soap. A knowledge of this equilibrium provides guidance in the development of improved rust-inhibiting oils.

INTRODUCTION

Oil-dispersible soaps, such as the petroleum mahogany sulfonates and the petroleum naphthenates, are used extensively as detergent additives for oils and as rust inhibitors in lubricants and in preservative coating materials. These practical applications have been handicapped because so little was known about the state of dispersion and the factors affecting the stability of soap dispersions in oil. Such soaps have been shown to exist in micellar form in hydrocarbon solvents (1-4). These micelles may be expected to participate in a mass-law equilibrium similar to that discussed by Jones and Bury (5) and others (6-10) although the equilibrium situation should be simpler than that found in the aqueous systems which they considered. There should then be for such oil-dispersible soaps a relatively narrow concentration range in which the system passes from one containing chiefly dissolved or molecularly dispersed soap to one containing preponderantly micellar soap in equilibrium with a small and nearly constant concentration of the molecularly dispersed material. The study of systems in or near this critical range is of interest because it defines the conditions under which micelle formation may be expected.

¹ The opinions or assertions contained in this communication are the authors', and are not to be construed as official or reflecting the views of the Navy.

3. For recent treatments, see, for example, TOLMAN, R. C., *J. Chem. Phys.* **16**, 758 (1948); KOENIG, F. O., *ibid.* **18**, 449 (1950); BUFF, F. P., *ibid.* **19**, 1591 (1951); HILL, T. L., *J. Phys. Chem.* **56**, 526 (1952).
4. HILL, T. L., *J. Am. Chem. Soc.* **72**, 5347 (1950).
5. HILL, T. L., in *Advances in Catalysis*, Vol. IV. Academic Press, New York (in press).
6. HILL, T. L., *J. Chem. Phys.* **18**, 246 (1950).
7. GUGGENHEIM, E. A., paper presented at Air Force Conference on Nucleation, Boston University, Boston, Mass., August, 1951.
8. HANSEN, R. S., *J. Phys. Chem.* **54**, 411 (1950); *ibid.* **55**, 1195 (1951).

TERRELL L. HILL

Naval Medical Research Institute,
Bethesda, Maryland

Received May 14, 1952

THE SURFACE TENSION OF SOLIDS

I have suggested recently (1) that it may be possible to obtain some estimate of the surface tension of a solid from measurements of the contact angles of various liquids upon it. Provided that all three phases (liquid, solid, and air) in a given experiment are mutually saturated, the empirical Antonoff's rule (2) may be used to calculate a value for the surface tension at the solid/air interface. If calculations are made using several reference liquids, the result obtained for the tension at the solid/air interface will only be a constant if saturation of the pure solid with the various liquids brings about no change (or the same change) in surface energy. Fox and Zisman (3) have measured contact angles of a number of liquids on solid polytetrafluoroethylene, and obtained values for γ_{SA} varying between 18 and 30 ergs/cm.². However, there is no evidence that in their experiments the phases were mutually saturated, although even if this were so, the variation in results might be real due to changes in composition of the solid. Their conclusion that the method is invalid is therefore not proved.

In this laboratory, Mr. J. W. Mitchell and I have been trying to test the equation governing the method by measuring contact angles in various

TABLE I

Validity of Antonoff's Rule for Some Organic Liquid/Water/Air Systems

	Temp. °C.	γ_{oa}^a	γ_{wa}^a	$\gamma_{wa} - \gamma_{oa}$	γ_{wo}^b
Acetophenone-water	25	36.1	49.9	13.8	13.8
Diphenyl ether-water	30	38.1	69.4	31.3	31.2
<i>n</i> -Octadecane-water	30	26.6	63.0	36.4	36.4
<i>n</i> -Hexadecane-water	25	28.1	69.0	40.9	40.6

^a γ_{oa} , γ_{wa} are the individual surface tensions against air of the mutually saturated organic liquid and water, respectively.

^b γ_{wo} is the interfacial tension between the mutually saturated liquids. All tensions are in dynes/cm.

mutually saturated organic liquid/water/air systems, where all the interfacial tensions are directly measurable. The validity of Antonoff's rule for some systems of this kind is demonstrated in Table I. We hope to publish an account of these experiments shortly.

I should like to repeat that this method cannot be regarded as a reliable one until a theoretical proof or explanation of Antonoff's rule is forthcoming. If it does prove to be a valid method, it will only measure the surface tension of the solid in an equilibrium system with all three phases mutually saturated. Confirmation of the numerical values obtained will only come from comparison with those obtained from other methods of measurement which may be devised in the future.

REFERENCES

1. ELTON, G. A. H., *J. Chem. Phys.* **19**, 1066 (1951).
2. ANTONOFF, G. N., *J. chim. phys.* **5**, 372 (1907).
3. FOX, H. W., AND ZISMAN, W. A., *J. Colloid Sci.* **7**, 109 (1952).

*Chemistry Department,
Battersea Polytechnic,
London, England*

G. A. H. ELTON

Received May 15, 1952

It also permits an estimate of the actual concentration of molecularly dispersed soap available, for example, for adsorption processes such as are responsible for rust prevention by polar additives (11,12,13). The calcium arylstearates are oil-dispersible soaps of established composition that are structurally and functionally analogous to the petroleum naphthenates. They furnish reproducible soap-hydrocarbon systems whose properties can illuminate the behavior of more widely used additives for oils.

For these arylstearates it has been shown that the micellar state persists down to soap concentrations of the order of $1 \times 10^{-6} M$ (2). This preliminary estimate of the lower concentration limit for micelle formation was considered for several reasons to be significant only as to order of magnitude. Accurate measurements on such exceedingly dilute systems are difficult because both solute and dye are lost by adsorption and because the intensity of the fluorescence is necessarily low. In addition the measurements were made before the authors had established the controlling effect of minute amounts of water on the size and type of micelles formed in such systems (13). The colloidal behavior and the practical performance of soap-oil systems depend so much on this critical range for micelle formation that it was desirable to verify the preliminary estimates of this quantity with the more precise techniques since developed. This communication reports the results of such a study in systems of controlled water content employing a dye peculiarly suited to quantitative measurements of micelle concentration in exceedingly dilute soap systems.

METHOD AND MATERIALS

A. Theory

The Rhodamine B method (3) is well suited to the determination of micelle size from depolarization data, which depend only on the relative intensities of the vertically and horizontally polarized components of the emitted fluorescence. This method, however, is less suitable for the quantitative comparison of micelle concentrations in very dilute systems because of possible losses through uncontrolled adsorption to the walls of containers and also because the equilibrium between the colored and colorless forms of the dye is shifted appreciably by traces of water or of organic acids. In the critical range for micelle formation, the amount of colorless Rhodamine B necessarily present is comparable with the stoichiometric soap concentration, and might be suspected of significantly altering the concentration at which micelle formation became dominant (1,14).

It was therefore desirable to investigate soap concentrations near the critical range by a method which ensured that species other than solvent and micelle-forming soap were present in concentrations too low to exert a major influence on micelle formation.

The use of a dye substantially insoluble in benzene alone or in the presence of molecularly dispersed soap offers such a method if the dye is solubilized by the soap micelles under study. If the dye is also fluorescent, the degree of polarization of its emission provides a positive check on the presence of micelles and on the location of the dye therein. Furthermore, useful measurements of fluorescence intensity can be made at dye concentrations too low for precise determinations of spectral absorption in cells 100 mm. or less in length.

Methylene Blue and Pinacyanol, which have been used by others for the investigation of soap systems (1,15,16), are insoluble in benzene but are freely solubilized by the arylstearate soaps, in whose presence they exhibit a brilliant red fluorescence. Methylene Blue, however, was found to be in equilibrium with a colorless and a differently colored form in nonaqueous soap systems (17), and Pinacyanol was subject to fading (18); both were therefore discarded after preliminary studies.

Acridine Orange has a finite but very slight solubility in dry or moist benzene. It is readily solubilized by calcium xenylstearate. However, xenylstearic acid, which is soluble in benzene as an equilibrium mixture of monomer and dimer, does not solubilize it appreciably. This dye can be converted to the benzene-soluble base with strong aqueous alkali, but even the free base in benzene solution is converted by arylstearate soap to a substance having the spectral properties of the salt form instead of those characteristic of the base. The possible conversion of this dye to the basic form in the presence of the mildly basic arylstearate is thus precluded. Under the conditions to which this dye was exposed, it neither faded appreciably nor was found subject to color changes. Therefore it was considered appropriate for this investigation.

The weakly polarized fluorescence of Acridine Orange in true solution and the highly polarized emission of the dye in the soap micelles are superposed to give composite polarizations and fluorescence intensities. The data, therefore, require a special treatment that differentiates between the dye in the two environments. This treatment is based upon the assumptions that (a) the dye molecules are present partially as simple molecules and partially as components of micellar soap aggregates of high molecular weight, (b) the size of the micellar aggregates does not change with the total soap concentration, and (c) in the concentration range studied the fluorescence efficiencies in the respective environments are constant although not necessarily equal. Both the large and small units are free to engage in Brownian motion.

If a small volume of such a fluorescing dye-soap dispersion at the origin of the $x y z$ system of coordinates is illuminated along the x -axis with z -polarized light and observed along the y -axis with the analyzer

oriented to pass z -polarized light, the total emission (3) is proportional to

$$I_{z \text{ av.}} = I_{z 90^\circ} \frac{3 - p}{3 + 3p}. \quad [1]$$

However,

$$I_z = I_{zm} + I_{zs} \quad [2]$$

and

$$I_x = I_{xm} + I_{xs}, \quad [3]$$

where the subscripts m and s refer to the micellar and the molecular (solution) environments, respectively. From Eqs. [1], [2], and [3], and from the definition of the degree of polarization,

$$p = \frac{I_z - I_x}{I_z + I_x}, \quad [4]$$

it can be shown that

$$\frac{RQ_m}{Q_s} = \frac{I_{zm \text{ av.}}}{I_{zs \text{ av.}}} = \frac{p_c - p_s}{p_m - p_c} \times \frac{3 - p_m}{3 - p_s}, \quad [5]$$

where the subscript c refers to the composite emission, R is the ratio of dye in the micellar environment to that in the molecular environment, and Q is the quantum fluorescence efficiency in the indicated environment. The determination of p_m can be made in a dispersion of high soap concentration, where $p_c \rightarrow p_m$.

The ratio R is effectively proportional to the concentration of micellar soap present in the system.² As compared with the quantity of dye

² Exact proportionality of R to the micelle concentration would require that the presence of a dye molecule in a soap micelle should not influence the probability of another dye molecule entering the same micelle. For systems in which the fraction x of micelles containing dye is small enough so that the number holding more than one dye molecule is negligible this equilibrium may be expressed by the relation

$$K_I = \frac{x}{D_s}, \quad (a)$$

where D_s is the concentration of dye in true solution. K_I is analogous to the familiar distribution coefficient for a monomeric species between two phases. Since $R = D_m/D_s$, where D_m is the concentration of the micellar dye; and $x = D_m/M$, where M is the concentration of micelles; then $K_I = D_m/D_s M = R/M$, and R is thus directly proportional to the micelle concentration.

The extreme departure from this simple distribution would occur if the presence of one dye molecule completely prevented the entrance of another into the same micelle. This condition is equivalent to the assumption that one dye molecule and one micelle "react" reversibly to form a 1:1 and only a 1:1 "compound". The equilibrium in this case is described by the relation

$$K_{II} = \frac{1}{1 - x} \times \frac{x}{D_s}, \quad (b)$$

in which x is not directly proportional to D_s . If, however, x is less than 0.1, the departure from strict proportionality between x and D_s will be less than 4% if D_s varies less than 50%.

solubilized, R is an especially useful indication of the micelle concentration. The ultimate amount of dye solubilized by the soap dispersion is difficult to ascertain; saturation by the dye requires many days, during which the soap undergoes oxidative deterioration. Further, the quantity of dye solubilized in a definite time interval by a given concentration of soap was not satisfactorily reproducible. Use of the function R permitted the employment of a 23-hr. solubilizing period for all but one of the concentrations studied. The resulting dispersions were not saturated with Acridine Orange, but all were found to have comparable concentrations of the molecularly dissolved dye. This dye thus not only permits measurements at lower total concentrations of dye than does Rhodamine B, but also provides positive optical evidence of the locations and amounts of all the dye present in the two states.

B. Materials

The benzene, calcium xenylstearate, and Rhodamine B were prepared and purified by methods previously reported (3).

Acridine Orange (CI 788) was twice recrystallized from the commercial product supplied by Coleman and Bell. A boiling ethanol solution of the crude substance was filtered and acidified with hydrochloric acid. Cyclohexane was added to the hot solution to incipient precipitation, and the solution was cooled gradually to 5°C. The recrystallized solid was washed with benzene and dried *in vacuo* at 65°C. In absolute ethanol (U.S.P.) previously percolated through silica gel, the molecular extinction coefficient, ϵ , at 491 m μ (the wavelength of maximum absorption) was 7.9×10^4 at $9 \times 10^{-6} M$, and 8.0×10^4 at $1.8 \times 10^{-6} M$. This conformity to Beer's law is evidence of the absence of changes of the dye with varying concentration. These extinction coefficients are somewhat higher than that deduced from data reported graphically (19,20) for the same dye in 95% ethanol. In aqueous or impure alcohol the dye dissociates somewhat into free base and hydrochloric acid to yield a diminished extinction coefficient at the hydrochloride peak (491 m μ) with an augmented coefficient at the dye base peak (426 m μ). During this investigation it was found that the coefficients depended upon the dye concentration unless the alcohol was percolated or acidified, and that the direction of variation of the two coefficients indicated the formation of the free base in the unpercolated or nonacidified solvent.

C. Instrumentation

Measurements of spectral absorption were made with a Beckman model DU spectrophotometer. Measurements of fluorescence were made with the Brice-Speiser light-scattering photometer (21) by the general procedure previously described (3), but certain modifications were neces-

sary to increase the sensitivity. The opal glass diffusor in front of the detecting element was removed, and a spherical mirror was attached to the rotating arm to reflect transmitted exciting light back through the fluorescence cell. Corrections for asymmetry of the photomultiplier were avoided by using a fixed analyzer and a rotating polarizer; this scheme is equivalent to the converse.

A fluorescent converter (a microscope slide coated with a collodion film containing the fluorescent dye) was placed immediately before the working standard in the light path. This device converted the reference stimulus to the same spectral region as that emitted by the fluorescing liquid. The secondary filter absorbed light of exciting wavelengths and transmitted the longer wavelengths of the fluorescence band; in the absence of the converter, major contributions to the reference intensity would be made by the small amount of light of nonexciting wavelengths which escapes complete absorption at the primary filter but passes freely through the secondary filter. The resulting reference energy might thus not be directly proportional to the fluorescent emission if the temperature of the light source varied. The converter also intensified reference deflections, rendering them comparable in magnitude with fluorescence deflections.

For excitation of Rhodamine B the mercury arc of the original instrument was used. The green line ($546\text{ m}\mu$) was isolated by the turret filter and a Corning Noviol Shade O filter. A Wratten 22 was used as the secondary filter. A correction was made for the slight asymmetry of polarization of this source. For excitation of Acridine Orange, a concentrated filament incandescent lamp was used. Although its output was found to be somewhat polarized, a negligible inequality remained between the intensities of the horizontally and vertically polarized components when the lamp was suitably rotated about the axis of the exciting beam. The exciting radiation was isolated by a Noviol Shade O filter and a narrow pass interference filter having its peak transmission at $500\text{ m}\mu$. With both optical arrangements, small corrections were made for residual scattered and stray light passing the secondary filters.

D. Procedure

The measurements reported here, like those of Singleterry and Weinberger (3), were made on dispersions in benzene containing 15% of the water required for saturation. This degree of saturation results in the association of slightly less than two moles of water with each mole of soap (13). Such a system is not subject to detectable changes in micelle size as a result of exposure to variable atmospheric humidities during experimental manipulations. In all of the dispersions except the final one listed in Table II, the fraction of water removed from solution by the

soap was negligible. This more concentrated final system contained 1.75 moles of extra water per mole of soap in order to maintain a comparable water concentration in the solvent phase.

Dilutions to the required concentrations were made from a stock solution of calcium xenylstearate that contained 1×10^{-3} mole of soap/l. in dry benzene. In the case of Rhodamine B the dye was introduced as a stock benzene solution; when Acridine Orange was employed, 2.0 mg. of the solid dye was added per 100 ml. of solution.

Dispersions containing Rhodamine B were allowed to stand several hours to establish adsorption equilibrium with the glass. They were then discarded, and the flasks were recharged. This procedure was repeated until no significant change in fluorescence could be observed between two successive dispersions for the same flask.

After preparation of the dispersions containing Acridine Orange, the flasks were shaken mechanically for a minimum of 23 hr. The dispersions were then decanted and discarded, leaving the solid dye in the flasks, which were recharged with fresh solutions. In this series also the procedure was repeated to establish adsorption equilibrium with the glass.

Data reported here refer to the final dispersions obtained by successive equilibrations. Before making optical measurements it was necessary to rinse the optical cells several times with the dispersion to be observed. Omission of equilibrations with any containing vessel is a serious source of errors resulting from adsorption losses. All measurements were made in a constant temperature room at $25 \pm 0.3^\circ \text{C}$.

RESULTS AND DISCUSSION

The average observed polarization was 0.293 (Table I) for the fluorescence of Rhodamine B in benzene dispersions of constant total dye concentration and varying concentration of calcium xenylstearate. The maximum deviation from the average was 0.005. This polarization corresponds closely with 0.283–0.300 found earlier (3) for dispersions of the same soap

TABLE I

Fluorescence Polarization of Rhodamine B in Benzene Solutions of Calcium Xenylstearate

Dye concentration, $1.02 \times 10^{-7} M$; benzene, 15% saturated with water

Soap concentration $M/10^{-6}$	Polarization
1.19	0.294
3.56	0.298
8.32	0.295
11.9	0.288
35.6	0.288
Average	0.293

ranging in concentration from 0.47×10^{-3} to 7.3×10^{-3} *M*. Since the fluorescence efficiency of the dye associated with micelles should be the same in all these dilute dye solutions, the constant degree of polarization indicates that the soap micelles have a constant size in this range. Such constancy is essential to the validity of the treatment applied to the data for Acridine Orange.

Observations of the fluorescence of Acridine Orange solubilized in benzene dispersions of the same soap in a 23-hr. shaking period show a varying polarization (Table II) which depends upon the stoichiometric soap concentration. This variation is predicted by Eq. [5], which permits analysis of the data to obtain the quantity RQ_m/Q_s .

Except to estimate absolute amounts of dye in the two environments, RQ_m/Q_s is as useful as *R* because the two are proportional when Q_m/Q_s is constant. A ratio of unity was computed for Q_m/Q_s from the data of

TABLE II

Behavior of Acridine Orange in Benzene Dispersions of Calcium Xenylstearate
Solubilization period, 23 hr.; benzene, 15% saturated with water

Total soap concentration <i>M</i> /10 ⁻³	Polarization	$\frac{Q_m}{Q_s}R$	Total dye concentration <i>M</i> /10 ⁻³	Total moles water Total moles soap	Moles solubilized dye Moles micellar soap	Dissolved dye concentration <i>M</i> /10 ⁻³
0	0.010	—	2.5	—	—	2.5
1.09	0.015	0.016	2.7 ₂	3540	0.9×10^{-3}	2.6 ₈
3.27	0.083	0.322	3.4	1180	3.1×10^{-3}	2.6
6.99	0.136	0.753	6.7	550	4.5×10^{-3}	3.8
11.0	0.162	1.108	4.7	350	2.4×10^{-3}	2.2
1030. ^a	0.287	—	16.7	5.5	1.6×10^{-4}	—

^a Additional water present to maintain comparable saturation; 30-min. solubilization period.

fluorescence emissions and spectral absorptions of two solutions of the dye. One contained no soap, and the other contained so large a quantity (10^{-3} *M*) that the molecularly dissolved dye would be a negligible fraction of the total dye. The estimate of unity for Q_m/Q_s is uncertain to 15% because of the error in measuring the weak absorption of the soap-free solution (0.5×10^{-8} mole dye/l.). This estimate is supported by the linear correlation (below dye concentrations of 5×10^{-7} *M*) between the spectrophotometrically determined dye concentrations and corresponding fluorescence emissions (Fig. 1) of solutions of widely varying soap content. Therefore, *R* has been taken equal to RQ_m/Q_s for computation of absolute amounts of dye in molecular solution and in soap micelles (Table II).

Since fluorescence intensities could be measured more accurately than corresponding spectral absorptions, the total dye concentrations of Table II were computed by multiplying fluorescence intensities by the factor

0.92×10^{-6} , obtained graphically from the linear portion of the curve (Fig. 1). Simultaneous determination of dye concentration and fluorescence polarization in a single operation precludes the discordancy that may result from unequal adsorption losses with separate specimens.

For the simple case of a micelle former which is not appreciably dissociated into ions (22), the mass law permits a useful interpretation of the experimental data presented here. Figure 2 is a representation of the concentrations of micellar and molecularly dissolved soap as functions of the total concentration according to the equation

$$K = \frac{S_m/n}{(S_s)^n} = \frac{(S - S_s)/n}{(S_s)^n}, \quad [6]$$

where K is the equilibrium constant, S is the total stoichiometric soap concentration, S_m and S_s are the respective concentrations of micellar

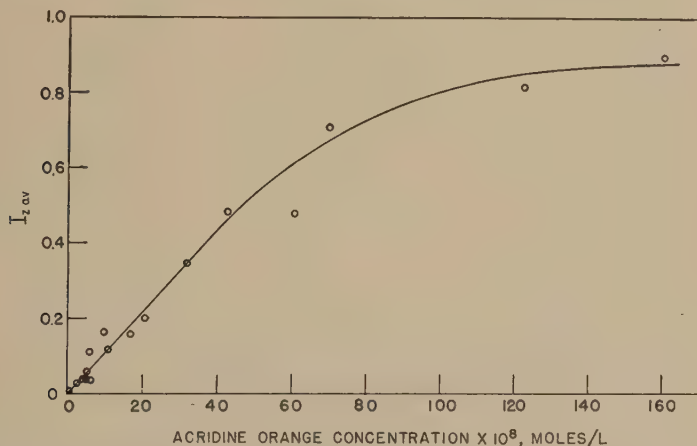


FIG. 1. Correlation between fluorescence intensity and spectrophotometric concentration.

and dissolved (molecular) soap in monomeric units, and n is the number of soap molecules aggregated in a micelle. This graph is analogous to the representation offered by Murray (8) for the more complex relation in an aqueous soap system.

The micellar trace, although almost linear, has appreciable curvature in the range S_i to $10S_i$, where S_i is the stoichiometric concentration at which the concentrations of the two species are equal; the curvature increases with decreasing values of the constant n . In this instance n was taken as 20, the approximate degree of aggregation deduced from osmotic data (3). For systems in which $n > 10$, the best straight line through points in the range S_i to $10S_i$ intersects the horizontal axis at a

point S_o , which closely approximates $S_i/2$. Now, it follows from Eq. [6] that

$$S_i/2 = \frac{1}{(K)^{1/(n-1)}} \approx S_o. \quad [7]$$

Hence, S_o , which can be obtained from suitable experimental data, is a very close approximation to a constant of the system and can be assigned definite physical significance. It falls near the midpoint of the concentration range in which the system passes from negligible micelle formation to essentially full conversion of soap increments to micelles. The quantity S_o is thus a useful numerical characterization of that range.

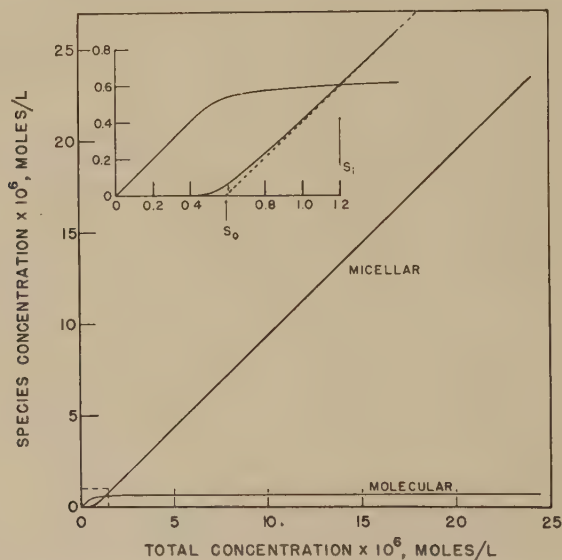


FIG. 2. Graphical representation of equilibrium for a micelle-forming soap in a hydrocarbon solvent.

The correspondence between S_o and the critical micelle concentration obtained by another method depends upon the criterion of micelle detection in the other method. The mass law requires that traces of micelles exist at even lower concentrations and the indications of micelle formation are of unequal sensitivity.

In Fig. 3 the quantity $Q_m R/Q_s$ (which is proportional to R) is plotted against S , the stoichiometric soap concentration. Within the estimated uncertainty this plot is linear within the range of 10^{-6} to 10^{-5} moles soap/l. Since R has been shown to be proportional to $S - S_o$, the micellar soap concentration, the linear extrapolation of the experimental points of Fig. 3 should intersect the horizontal axis at the same point, S_o , as the

best straight line through the micellar trace of Fig. 2, and S_0 will have identical physical significance in either case.

For the system investigated, S_0 has the value $0.6 \times 10^{-6} M$. Since above $S = S_i$ the concentration of molecularly dissolved soap, S_s , changes only very slowly with increasing stoichiometric concentrations, S_0 is a good first approximation of the non-micellar soap available for adsorption processes in dilute soap-hydrocarbon systems. If Eq. [6] defines the equilibrium, S_s in this system should increase by only 30% as S is increased 100-fold beyond S_i (from 10^{-6} to $10^{-4} M$). Thus the amount of

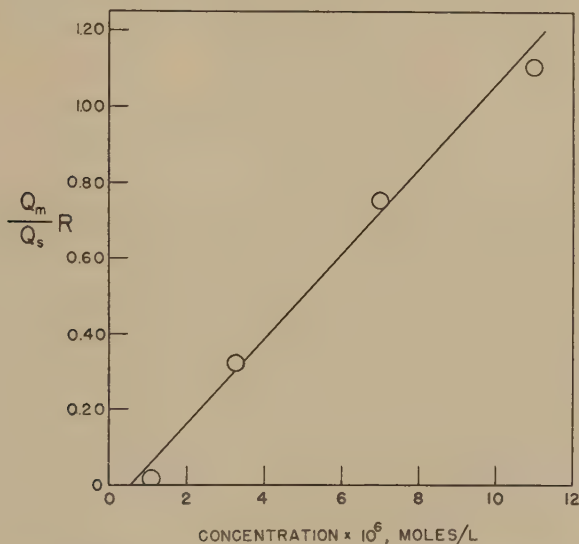


Fig. 3. Distribution of Acridine Orange between soap micelles and solvent.

soap adsorbed on a given surface will be expected to vary only slightly for equilibrium concentrations of soap lying anywhere within the practical range for oil additives.

CONCLUSIONS

1. The methods for interpreting measurements of fluorescence depolarization have been extended so that useful data may be obtained from systems in which part of the fluorescing substance is associated with a colloid and part is in molecular solution. This modified procedure leads to more reliable values than were previously attainable for the relative concentration of micelles present in extremely dilute dispersions.

2. The existence of a critical concentration for micelle formation by calcium xenylstearate in benzene has been confirmed. This concentration is approximately 0.6×10^{-6} mole soap/l.

3. The size of the soap micelles in the system studied has been shown to be very nearly constant in the concentration range between 1×10^{-6} and $7.3 \times 10^{-3} M$.

4. The experimental data are consistent with the existence of a simple mass-law equilibrium between single soap molecules and micelles in soap-hydrocarbon systems. The application of such an equilibrium leads to the conclusion that the concentration of molecularly dissolved soap available for adsorption is always very small, and that it increases less than twofold between $10^{-6} M$ and the highest soap concentrations likely to occur in rust-inhibited or detergent oils. This approximate constancy explains the negligible increase in rust inhibition resulting from a many-fold increase in soap concentration above the threshold value.

REFERENCES

1. MCBAIN, J. W., MERRILL, R. C., JR., AND VINOGRAD, J. R., *J. Am. Chem. Soc.* **62**, 2880 (1940).
2. ARKIN, L., AND SINGLETERRY, C. R., *J. Am. Chem. Soc.* **70**, 3965 (1948).
3. SINGLETERRY, C. R., AND WEINBERGER, L. A., *J. Am. Chem. Soc.* **73**, 4574 (1951).
4. MATTOON, R. W., AND MATHEWS, M. B., *J. Chem. Phys.* **17**, 496 (1949).
5. JONES, E. R., AND BURY, C. R., *Phil. Mag.* **4**, 841 (1927).
6. GRINDLEY, J., AND BURY, C. R., *J. Chem. Soc.* **1929**, 679.
7. MURRAY, R. C., AND HARTLEY, G. S., *Trans. Faraday Soc.* **31**, 183 (1935).
8. MURRAY, R. C., *Trans. Faraday Soc.* **31**, 206 (1935).
9. HARTLEY, G. S., *Aqueous Solutions of Paraffin Chain Salts*. Hermann et Cie, Paris, 1936.
10. ALEXANDER, A. E., AND JOHNSON, P., *Colloid Science*, p. 672. Oxford, New York, 1949.
11. BAKER, H. R., AND ZISMAN, W. A., *Ind. Eng. Chem.* **40**, 2338 (1948); *ibid.* **41**, 137 (1949).
12. BAKER, H. R., AND ZISMAN, W. A., *Lubrication Eng.* **7**, 117 (1951).
13. ARKIN, L., AND SINGLETERRY, C. R., *J. Colloid Sci.* **4**, 537 (1949).
14. KLEVENS, H. B., *J. Phys. & Colloid Chem.* **51**, 1143 (1947).
15. SHEPPARD, S. E., AND GEDDES, A. L., *J. Chem. Phys.* **13**, 63 (1945).
16. CORRIN, M. L., KLEVENS, H. B., AND HARKINS, W. D., *J. Chem. Phys.* **14**, 480 (1946).
17. LEWIS, G. N., GOLDSCHMID, O., MAGEL, T. T., AND BIGELEISEN, J., *J. Am. Chem. Soc.* **65**, 1150 (1943).
18. TIMBERS, A. M., AND LINGAFELTER, E. C., *J. Am. Chem. Soc.* **71**, 4155 (1949).
19. RAMART-LUCAS, P., GRUMEZ, M., AND MARTYNOFF, M., *Bull. soc. chim. France (Mémoires)* **8**, 554 (1941).
20. RAMART, P., GRUMEZ, M., AND MARTYNOFF, M., *Compt. rend.* **207**, 1106 (1938).
21. BRICE, B. A., HALWER, M., AND SPEISER, R., *J. Optical Soc. Am.* **40**, 768 (1950).
22. DAVIS, M.[†]M., *J. Am. Chem. Soc.* **71**, 3544 (1949).

THE SPREADING OF LIQUIDS ON LOW-ENERGY SURFACES. V. PERFLUORODECANOIC ACID MONOLAYERS ¹

Fred Schulman

*Georgetown University, Washington, D. C., and Office of Naval Research,
Washington, D. C.*

W. A. Zisman

Naval Research Laboratory, Washington, D. C.

Received April 21, 1952

INTRODUCTION

It has been shown in previous papers of this series (1, 2, 3) that the equilibrium contact angles of most liquids on smooth, organic solid surfaces vary regularly in a manner which can be correlated with the nature of the compounds or groups of atoms comprising the surface. Thus for surfaces consisting essentially of $-\text{CF}_2$ -groups (1), $-\text{CH}_3$ groups (2), and $-\text{CH}_2$ -groups (3), the contact angle (θ) decreases in the order $\theta_{\text{CF}_2} > \theta_{\text{CH}_3} > \theta_{\text{CH}_2}$. This is a report on the wetting properties of the oriented close-packed monolayers consisting of $-\text{CF}_3$ groups created by the adsorption of perfluorodecanoic acid on smooth surfaces of platinum, brass, copper, and glass.

EXPERIMENTAL TECHNIQUE

The *n*-perfluorodecanoic acid $\text{CF}_3(\text{CF}_2)_8\text{COOH}$ used was a pure crystalline, white solid (m.p. 79–80°C.) supplied through the courtesy of the Minnesota Mining and Manufacturing Company. It is sparingly soluble in water and in aromatic solvents at 20°C. and is somewhat more soluble in lower *n*-aliphatic solvents, halogenated liquids, and formamide. The "pseudoperfluoro" alcohols, $\text{CHF}_2-(\text{CF}_2)_n-\text{CH}_2\text{OH}$, were pure research samples made available through the kindness of the late W. S. Calcott of the Du Pont Organic Chemicals Department. Many of the organic liquids listed in Tables I–III are identical with those described in previous

¹ Abstracted from a dissertation submitted by Fred Schulman to the Faculty of the Graduate School of Georgetown University in partial fulfillment of the requirements for the Ph.D. degree in Chemistry, 1951.

Presented before Colloid Division, American Chemical Society, Buffalo, New York, March 27, 1952.

studies (1, 2, 3). They were derived from the sources listed in the footnotes to the tables. Each liquid was percolated through a long column packed with "Florosil," activated silica gel, or alumina to remove highly adsorbable polar impurities, while the higher boiling liquids were first stripped of more volatile impurities at 100°C. and 5 mm. pressure using a countercurrent of CO₂ to carry off any more volatile components.

The majority of the measurements of contact angles were made on platinum surfaces which had been covered by an oriented monolayer of perfluorodecanoic acid. Generally the platinum surfaces were smooth strips of foil prepared as described earlier (1, 2, 4). In measuring contact angles of water and ethylene glycol it was necessary to anchor the acid monolayer to a more reactive surface than platinum in order to avoid dissolving the film. The surfaces of copper and instrument brass used were polished to mirror brightness on a polishing wheel of silk impregnated with 1500-mesh diamond dust and then were degreased by continuous extraction for 20 min. with boiling c.p. benzene in a modified Soxhlet apparatus.

Monolayers of perfluorodecanoic acid were prepared by immersing the smooth solid in a solution containing 4×10^{-4} mole/l. of the acid in *n*-decane. A close packed monolayer was formed in less than 1 sec. The "multiple dip" method (4) was used to prove that the adsorbed film was an oriented monolayer. It was found that the dipper emerged dry and the contact angle against hexadecane was constant after each dip until the 54th dip. After each subsequent dip the contact angle decreased gradually until complete wetting occurred at the 66th dip. Therefore, the acid was adsorbed from the decane solution as a closely packed film in each of the first 54 dips. Only at the 63rd dip did diffuse patches of liquid remain on the dipper indicating the solute was nearly exhausted. Dips 64-66 had even larger wet patches and are assumed to average one-half of a close-packed monolayer each. Assuming that approximately one additional monolayer remained in the exhausted bulk solution because the latter was too dilute to permit adsorption within a reasonable time, the total area coated in the series of dips was 1024 cm.² Corrections due to adsorption on non-dipper surfaces were 49 cm.² Thus the total area occupied by the solute (4.65×10^{17} molecules) was approximately 1073 cm.² and, with the indicated approximation relating to the last few dips, the average cross-sectional area of the acid was 23 Å.²

The contact angle of a sessile drop of each liquid on the monolayer-covered surface was measured as before (1, 2, 3). When the contact angle did not change with successive small increases in the size of the drop, it was assumed that the advancing contact angle was obtained with the system close to mechanical equilibrium (5). When contact angles of drops of volatile liquids were measured, they were also observed through the

windows of a closed glass cell filled with the saturated vapor of the liquid. Each angle given is the result of measurements of at least six drops on two different platinum surfaces. Advancing and receding contact angles were the same except with a few liquids like water which were able to penetrate the pores of the monolayer (2). Even then the receding contact angle was reproducible and agreed with the advancing contact angle for water on a previously saturated monolayer. Measurements were made at $20 \pm 0.1^\circ\text{C}$. and 50% relative humidity. Under these conditions it was possible to obtain readings reproducible to $\pm 1^\circ$. Surface tensions were measured at 20.0°C . with an uncertainty of $\pm 0.3\%$ by the capillary rise and ring methods applying the usual corrections. The Fox and Chrisman corrections (6) were applied to the highly fluorinated liquids.

Associated liquids like water and glycerol were found to dissolve the perfluorodecanoic acid monolayer, presumably due to the highly hydrophilic character of its strongly acid group. This effect can be lessened when homologs of greater chain length become available. However, since leaching of the monolayer by the liquid had been effectively stopped by using a test drop of liquid which had already been saturated with the polar compound (2), a few experiments were performed under similar conditions. With saturated solutions of perfluorodecanoic acid in decane and in hexane, this procedure caused the contact angles to increase a maximum of about 3° . This is indicated for decane by the half-shaded circle in Fig. 1. It did not prove helpful with water drops presumably due to the resulting decrease of about 50 dynes/cm. in the surface tension of the aqueous solution. Saturated solutions of perfluorodecanoic acid in 12 different organic liquids were tried. As no significant change in the contact angle or in the surface tension of the liquid was observed, it was decided that this technique was neither advantageous nor necessary for most non-aqueous liquids.

RESULTS ON WETTING

Tables I-III summarize: the values of (γ_{LV}°) the surface tension of each pure liquid at 20°C .; the average value of the measured equilibrium contact angle (θ_E) ; and the calculated values of (S_{LV}°/S_V°) the final spreading coefficient of each of the liquids investigated.

It is believed that the higher-boiling liquids in contact with low-energy solids have negligible values of f_{SV}° . The correctness of this assumption was shown by Fox and Zisman (1) for hexadecane on TFE (polytetrafluoroethylene). Inasmuch as the surfaces studied here are even less wettable than TFE, the assumption of $f_{SV}^\circ = 0$ is even more justifiable. Therefore, in the usual equations the term f_{SV}° has been neglected; and by using measurements of contact angles and surface tensions of the pure liquids studied, it was possible as in Refs. (1), (2), and (3) to compute W_A and f_{SL} . The data of Tables I-III were calculated without requiring the

TABLE I

Surface Energy Data for Alkanes, Ethers, Alkylbenzenes and Glycols on a Close-Packed Monolayer of Perfluorodecanoic Acid at 20°C.^a

Compound and source	γ_{LV}^o and reference dynes/cm.	θ_E deg.	S_{LV}^o/SV^o ergs/cm. ²
<i>n-Alkanes</i>			
Hexadecane ^b	27.6 (9)	72	-19.1
Tetradecane ^b	26.7 (9)	69	-17.1
Dodecane ^c	25.4 (10)	67	-15.5
Heptadecane ^c	24.7 (10)	64	-13.9
Decane ^c	23.9 (10)	62	-12.7
Nonane ^d	22.9 (10)	59	-11.1
Octane ^c	21.8 (10)	56	-9.6
Heptane ^c	20.3 (10)	52	-7.8
Hexane ^c	18.4 (9)	41	-4.5
<i>Di(n-alkyl)ethers</i>			
Decyl ^e	28.4 extrap.	69	-18.2
Octyl ^e	27.7 (11)	65	-16.0
Heptyl ^f	27.0 (11)	62	-14.3
Amyl ^e	24.9 (11)	54	-10.3
Butyl ^e	22.8 (11)	47	-7.0
Propyl ^e	20.5 (11)	31	-2.9
<i>Di(isoalkyl)ethers</i>			
Amyl ^e	23.0 (11)	49	-7.9
Propyl ^e	17.8 (11)	10	-0.3
<i>Alkylbenzenes</i>			
Decylbenzene ^b	31.2	73	-22.1
Hexylbenzene ^g	30.0 (12)	69	-19.3
Butylbenzene ^b	29.2 (13)	63	-16.0
Propylbenzene ^b	29.0 (13)	59	-14.1
Ethylbenzene ^b	29.0 (13)	58	-13.6
Methylbenzene ^b	28.5 (14)	48	-9.5
Benzene ^b	28.9 (14)	58	-15.6
<i>Glycols</i>			
Glycerol ^f	63.4 (15)	89	-62.3
Thiodiglycol ^{h, i}	54.0	77	-41.8
Ethylene glycol ^c	47.7 (15)	81	-40.3
Tetramethylene glycol ^j	44.6	80	-36.8
Diethylene glycol ^{i, k}	44.4	76	-33.7
Pentamethylene glycol ^j	43.4	82	-37.3

^a Underlying surface is platinum unless otherwise indicated.

^b American Petroleum Institute Spectrographic Standards (National Bureau of Standards).

^c Eastman "White Label" grade.

^d Kaiser Wilhelm Institut ("Reinst" grade).

^e Connecticut Hard Rubber Company.

^f Wallace and Tiernan Co.

^g National Defense Research Committee (NDRC) preparation by Prof. Homer Adkins.

^h Preparation of Naval Research Laboratory.

ⁱ Underlying surface is copper.

^j Columbia Organic Chemical Co.

^k Union Carbide and Carbon Corp.

assumption that $f_{SV}^\circ = 0$; however, in order to plot and interpret conveniently some of the graphical data in the figures presented later, that assumption will be introduced in the appropriate places.

No simple general quantitative relation was found for the contact angles of the entire group of liquids studied. One can only say that as the surface tension increases, the contact angles tend to rise. How-

TABLE II

Surface Energy Data for Halocarbons on a Close-Packed Monolayer of Perfluorodecanoic Acid at 20°C.

Compound and source	γ_{LV}° and reference dynes/cm.	θ_F deg.	SLV°/SV° ergs/cm. ²
<i>Fluorocarbons</i>			
$\text{CCl}_3\text{—CF}_2\text{—CCl}_3^a$	32.6	60	−16.3
$\text{CFCl}_2\text{—CF}_2\text{—CCl}_3^a$	27.8	56	−12.3
$\text{CF}_2\text{Cl—CCl}_2\text{—CF}_2\text{Cl}^a$	22.8	29	−2.8
$\text{H}(\text{CF}_2)_2\text{CH}_2\text{OH}^b$	27.6	32	−4.0
$\text{H}(\text{CF}_2)_4\text{CH}_2\text{OH}^b$	24.5	55	−10.4
$\text{H}(\text{CF}_2)_6\text{CH}_2\text{OH}^b$	23.8	62	−12.6
<i>p</i> -Difluorobenzene ^b	27.0	32	−4.1
FCD 330 Fluorolube ^b	20.2	31	−2.9
boiling range 60–130° at 10 mm.			
Perfluorokerosene ^b	18.1	26	−1.8
Perfluorotrihexylamine ^c	18.3	42	−4.7
Perfluorotributylamine ^c	16.3	26	−1.7
Perfluorotripropylamine ^c	15.2	5	−0.1
Perfluoromethylcyclohexane ^b	14.7	11	−0.3
Perfluorodibutyl ether ^c	13.4	8	−0.1
<i>Nonfluoro halocarbons</i>			
Methylene iodide ^d	50.8 (15)	90	−50.8
<i>sym</i> -Tetrabromoethane ^e	49.7 (15)	87	−47.1
Aroclor 1242 (trichlorobiphenyl) ^b	45.3 (1)	90	−45.3
α -Bromonaphthalene ^d	44.6 (15)	84	−40.7
Aroclor 1248 (tetrachlorobiphenyl) ^b	44.2 (1)	92	−45.7
Methylene bromide ^d	39.0	67	−23.8
Hexachloropropylene ^g	38.1 (1)	58	−17.9
Perchlorocyclopentadiene ^h	37.5 (1)	73	−26.6
<i>sym</i> -Tetrachloroethane ^e	36.3 (15)	36	−6.9
Hexachlorobutadiene ^g	36.0 (1)	77	−27.9
Tetrachloroethylene ⁱ	31.7 (15)	35	−5.8
Carbon tetrachloride ^d	26.8 (15)	60	−13.4

^a Preparation of Prof. A. L. Henne (Ohio State University).

^b E. I. du Pont de Nemours and Company.

^c Minnesota Mining and Manufacturing Co.

^d Eastman "White Label" grade.

^e Eastman "Practical" grade.

^f Monsanto Chemical Company.

^g Hooker Electrochemical Company.

^h Synthesized at the Naval Research Lab.

ⁱ Commercial C.P. grade.

TABLE III

Surface Energy Data for Miscellaneous Fluids on a Close-Packed Monolayer of Perfluorodecanoic Acid at 20°C.^a

Compound and source	γ_{LV}^o and reference dynes/cm.	θ_E deg.	SLV^o/SV^o ergs/cm. ²
Mercury ^b	485 (16)	152	-913
Water ^c	72.8 (16)	102	-88.1
Aniline ^b	42.6 (15)	51	-15.8
<i>tert</i> -Butylnaphthalene ^d	33.7 (1)	71	-22.7
Carbon disulfide ^b	31.4 (15)	59	-15.2
Polyethylene SS903 ^e	30.4	80	-24.5
<i>o</i> -Xylene ^f	30.1 (16)	59	-14.6
1,3,5-Triethylbenzene ^f	29.1	78	-23.0
Methylphenylsiloxane dimer ^g	29.0 (1)	52	-11.1
<i>sec</i> -Butylbenzene ^f	28.7	65	-16.6
<i>n</i> -Heptylic acid ^d	28.3 (15)	44	-8.0
<i>m</i> -Xylene ^d	28.9 (16)	71	-19.5
Polyethylene V120 ^e	27.8	75	-20.6
<i>n</i> -Butylcyclohexane ^f	26.9	63	-14.7
<i>n</i> -Propylcyclohexane ^f	26.2	61	-13.5
<i>n</i> -Butylcyclopentane ^f	25.9	61	-13.3
Cyclohexane ^h	25.0 (14)	62	-7.2
Polyethylsiloxane ^g	23.3 (17)	79	-18.9
Methyl alcohol	22.6 (15)	15	-0.8
2,2-Dimethylbutane ^f	16.3	41	-4.0
<i>Linear Polymethyl siloxanes</i>			
Heptadecamer ^g	19.9 (17)	62	-10.4
Dodecamer ^g	19.6 (17)	61	-10.1
Nonamer ^g	19.2 (17)	59	-9.3
Heptamer ^g	18.6 (17)	56	-8.3
Hexamer ^g	18.5 (17)	52	-7.1
Pentamer ^g	18.1 (17)	48	-6.0
<i>Esters</i>			
Tricresyl phosphate ⁱ	40.9 (1)	82	-35.2
Tetra (mixed phenyl cresyl)silicate ^j	39.8	93	-42.0
Butylphenylhendecanoate ^k	38.0	76	-28.8
Benzylphenylhendecanoate ^k	37.7 (1)	85	-34.4
Bis(2-ethylhexyl)phthalate ^k	31.2 (1)	71	-21.0
Bis(2-ethylhexyl)sebacate ^k	31.1 (1)	70	-20.5
Pentaerythritol tetracaproate ⁱ	30.4 (1)	69	-19.5
1,6-Hexamethylene glycol bis-2-ethyl hexanoate ^k	30.2 (1)	66	-17.9
Tris-(2-ethylhexyl)tricarallylate ^k	29.6 (1)	65	-17.1
Hexa(2-ethyl-1-hexoxy)disiloxane ^j	26.8	75	-19.9
Hexa(2-ethyl-1-butoxy)disiloxane ^j	26.1	73	-18.5

^a Underlying surface is platinum unless otherwise indicated.

^b Commercial, C.P. grade.

^c Underlying surface is copper.

^d Eastman "White Label" grade.

^e U. S. Naval Technical Mission in Europe.

^f American Petroleum Institute spectroscopic standard samples from National Bureau of Standards.

^g Dow-Corning Company.

^h Phillips Petroleum Co., Pure Grade, 99 mole per cent minimum.

ⁱ Monsanto Chemical Company.

^j California Research Corporation.

^k Synthesized at Naval Research Laboratory.

^l Hercules Powder Company.

ever, simple relations are observed when members of homologous series are compared. For example graphs of $\cos \theta_E$ vs. γ_{LV}° for *n*-alkanes, diethers, methyl silicones, alkylbenzenes, pseudoperfluoroalcohols and perfluoroamines all plot as straight lines. Except for the pseudoperfluoroalcohols, all other homologous series show a decrease in $\cos \theta_E$ as γ_{LV}° increases. Despite the wide variety of liquids studied not one was found which would spread on the surfaces covered with this type of oriented monolayer. Extrapolation of the straight line for a homologous series as in Fig. 1 to $\cos \theta_E = 1$ yields a value which has been defined (1) as the critical surface tension for that series. Thus the critical surface tensions are about 11.0 dynes/cm. for the alkanes, 15.3 for the methyl silicones, 15.7 for the perfluoroamines, 16.7 for the dialkyl ethers, and 27.5 for the alkyl benzenes.

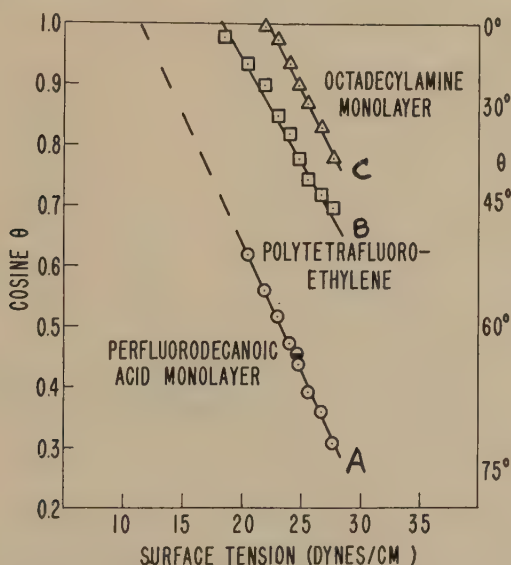


Fig. 1. Comparison of $\cos \theta$ vs. γ_{LV}° of *n*-alkanes on low-energy surfaces.

Figure 1 shows a comparison of $\cos \theta_E$ vs. γ_{LV}° for (a) a perfluorodecanoic acid monolayer, (b) solid polytetrafluoroethylene, and (c) an octadecylamine monolayer using data for the *n*-alkanes. The data for the latter two surfaces were taken from the results of the first two reports of the series (1, 2). It is obvious that the perfluorodecanoic acid monolayer coating was the most organophobic surface of the three. Polyethylene was the fourth surface compared; but it was the least organophobic of the four surfaces since the alkanes spread upon it (3). An essentially similar but displaced group of curves is obtained in plotting the data for the series of *n*-alkyl benzenes. At the higher surface tensions (corresponding

to compounds with longer alkyl chains), the curve for the perfluorodecanoic acid monolayer deviates from linearity and asymptotically approaches the *n*-alkanes line. This behavior is to be expected since the higher alkylbenzenes should approach the alkanes in properties.

A comparison of the contact angles of various fluids on the four surfaces is shown in Fig. 2. The order of increasing contact angles is roughly the same for all four surfaces with the highly associated liquids exhibiting the highest contact angles. Note that, excluding the hydrogen-bonded liquids (water, glycerol, and ethylene glycol), the surface coated with the perfluorinated monolayer is the most organophobic studied. However, it is slightly less hydrophobic than TFE but of the same order of magnitude as the surface coated with the octadecylamine monolayer. The greater hydrophobicity of TFE is believed to be due to the closer

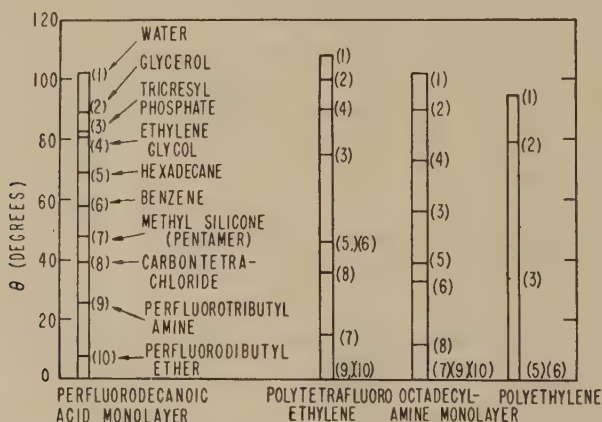


Fig. 2. Comparison of contact angles of various liquids on several low-energy surfaces.

packing of the molecules in the solid as compared with the monolayer. Despite the attack of the hydrogen-bonded liquids on the monolayer coating adsorbed on platinum, it was possible to obtain the correct contact angles for such liquids by using techniques described in the experimental section.

Since $W_A - W_C$ is equal to the final spreading coefficients when $f_{SV}^\circ = 0$, the values in the last column of Tables I-III are equal to $W_A - W_C$. Therefore, in plotting the data for the *n*-alkanes, the ordinate ($W_A - W_C$) in Fig. 3 was taken directly from Tables I-III. It will be noted that the spreading coefficients are lowest for the surface coated with the fluorinated monolayer and highest for the octadecylamine monolayer. Spreading coefficients for these liquids on polyethylene must be still higher and positive. A similar plot of all the members of the *n*-alkylbenzene series showed that they did not have the same value of f_{SL} for

any of the three surfaces since they had different y -intercepts. The spreading coefficients of the n -alkyl ethers approach the values of the n -alkanes at higher chain lengths. The ether oxygen can be considered to be equivalent to a $-\text{CH}_2-$ group in comparing some physicochemical properties of alkyl ethers and alkanes. Thus the spreading coefficients of di- n -heptyl ether and the extrapolated value for n -pentadecane are approximately the same. As the surface tensions of these liquids are reduced, differences in the spreading coefficients become evident. This may be attributed to the higher proportion of oxygen atoms in the lower ethers and to the dominating influence of the oxygen atoms on the surface properties. In general,

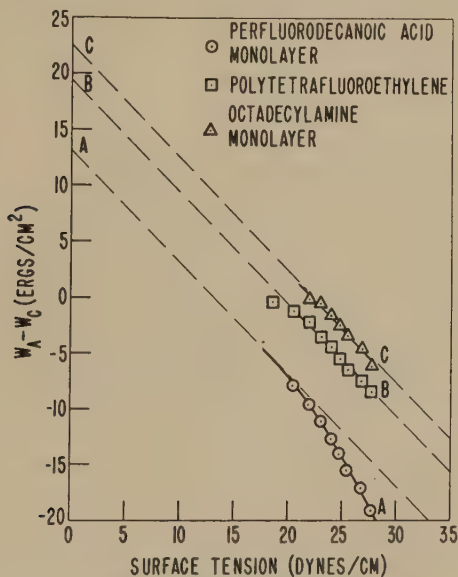


FIG. 3. Comparison of the spreading coefficients of n -alkanes on low-energy surfaces.

the fluorocarbons have higher spreading coefficients than do the other halocarbons. This is due to the greater attraction of fluorinated compounds for the fluorinated monolayer, and this is believed to be an example of electronic resonance increasing the intensity of the van der Waals' cohesive forces between like atoms. Hexachloropropylene, hexachlorobutadiene, perchlorocyclopentadiene, and *sym*-tetrachloroethane attacked the film, and hence their contact angles are somewhat unreliable. The reported data for these liquids all were obtained within as short a time as possible in order to minimize this difficulty.

When all the liquids studied were plotted on one graph, no such simple relations were found between the spreading coefficient and the surface tension. But it was apparent that as the surface tension increased, the spreading coefficient decreased.

In Fig. 4 is a comparison of the values of W_A for the n -alkanes on various low-energy surfaces; and it is evident that W_A increases in the order: perfluorodecanoic acid monolayer coating, solid polytetrafluoroethylene, and octadecylamine monolayer coating. W_A is so large for solid polyethylene that all alkanes from hexane through hexadecane spread on it. Also, W_A for the higher alkanes is about 10 ergs/cm.² larger for a TFE surface than for the surface coated with the perfluorodecanoic acid monolayer; in case of the octadecylamine monolayer coating, W_A is about 2.5 ergs/cm.² greater than for TFE, and, therefore, it has a work of adhesion about 12.5 ergs/cm.² greater than for the fluorinated monolayer coating. It will be noticed that curves B and C are approximately parallel straight

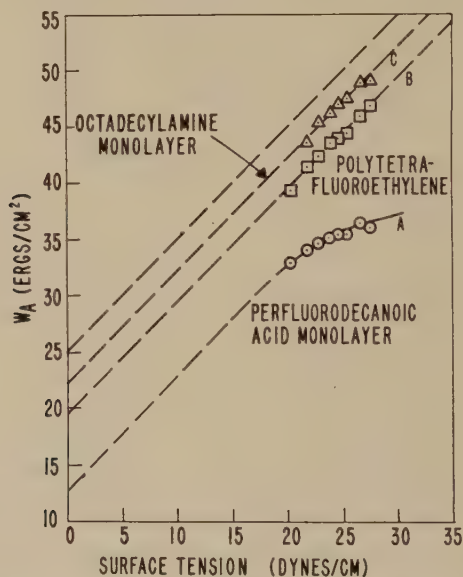


FIG. 4. Comparison of the work of adhesion of n -alkanes on low-energy surface.

lines, but curve A is definitely convex and approaches a maximum at high values of γ_{LV}° . This is to be expected, for it is a consequence of the linearity of the $\cos \theta_E$ vs. γ_{LV}° curve just as was shown in Refs. (2) and (3) for a surface of $-\text{CH}_3$ groups.

A large spread was found in the work of adhesion of the liquids studied. Thiodiglycol had the highest value (66.2 ergs/cm.²) and perfluorodibutyl ether the lowest (26.7 ergs/cm.²). The bulk of the compounds were within the range of 35–45 ergs/cm.² Introduction of an aromatic nucleus raises the value of W_A considerably. The W_A vs. γ_{LV}° curve is the steepest of any homologous series excluding the pseudoperfluoroalcohols. The methylphenylsiloxane dimer has a work of adhesion of 46.9 ergs/cm.² which

places this compound directly on the curve for the alkylbenzenes, indicating the phenyl group is the determining factor for this surface property.

The free energy decrease on immersion (f_{SL}) can be calculated from the data in Tables I-III, since neglecting f_{SV}° results in the convenient approximation

$$f_{SL} = \gamma_{LV}^\circ \cos \theta_E. \quad (1)$$

The value of f_{SL} of nearly all the liquids is between 10 and 20 ergs/cm.² although the spreading coefficients vary from 0.1 to 40 ergs/cm.². The lowest values of f_{SL} observed were those for water ($f_{SL} = -15.3$ ergs/cm.²) and mercury ($f_{SL} = -428$ ergs/cm.²). It was observed that the non-fluorinated halocarbons had a common value of f_{SL} of about 2 ergs/cm.², while the fluorocarbons and derivatives (excluding the pseudoperfluoroalcohols) had a common value of about 15 ergs/cm.² It is not surprising that the pseudoperfluoroalcohols do not have a constant free energy of immersion since the ratio of fluorine to hydrogen atoms is markedly different for each member of the series. Simple calculations from the data of Tables I-III show that f_{SL} does not exceed 25 ergs/cm.² Since $f_{SL} = \gamma_S^\circ - \gamma_{SL}$, the maximum value of f_{SL} would be γ_S° . Hence the small experimental range of values of f_{SL} is good evidence that γ_S° is that small, also. It can be concluded that the external surface of an oriented close-packed monolayer of perfluorodecanoic acid has the lowest surface energy per unit area of all solids studied, and it may well be impossible to obtain lower values except by solidifying one of the inert gases.

A progressive change in slope was observed for each homologous series of liquids in going from surfaces coated with a film of oriented perfluorodecanoic acid to TFE and to an oriented coating of octadecylamine. In every case, the perfluorodecanoic acid-coated surface had the lowest values of f_{SL} and the octadecylamine-coated surface the highest. Analogous curves for polyethylene cannot always be given since for many of these liquids $\theta_E = 0$. Obviously, f_{SL} for polyethylene must be larger than for the other three surfaces considered. None of the curves obtained with the perfluorinated acid-coated surface were parallel to the axis of abscissas. This is indicative of the sensitivity of the contact angle on such a surface to minor differences in the structure of the liquid molecule; whereas, on TFE (and to some extent on the octadecylamine coating) the curves exhibit nearly constant values of f_{SL} for a wide variety of liquids.

In general, except for certain highly fluorinated liquids, f_{SL} decreases with increasing surface tension. When f_{SL} is plotted as a function of γ_{LV}° as in Fig. 5, simple curves are obtained for each homologous series of liquids studied. At low values of γ_{LV}° it is apparent that values of f_{SL} for the alkanes and ethers are depressed below the extrapolated straight lines which fit the curves at high values of γ_{LV}° . This indicates that a surface made up of methyl groups has a lower free surface energy than

one made up of methylene groups. As the chain length is increased slightly, the $-\text{CH}_3$ group still dominates, and the slope is either zero or nearly so. However, when the chain length has increased sufficiently, the influence of the two end methyl groups is lessened because of the higher proportion of methylene groups. Thus, if a liquid can be obtained which has more methyl groups but the same surface tensions as any of the n -alkanes or di- n -alkyl ethers shown, it should have a lower value of f_{SL} because of the presence of the extra methyl groups. This is shown to be the case for the two isoethers which are below the curve for the n -ethers and also for 2,2-dimethylbutane (neohexane) which is about 0.6 ergs/cm.² below the extrapolated curve for the n -alkanes. The alkylbenzenes do not exhibit a similar curvature because of the pronounced ability of the aromatic

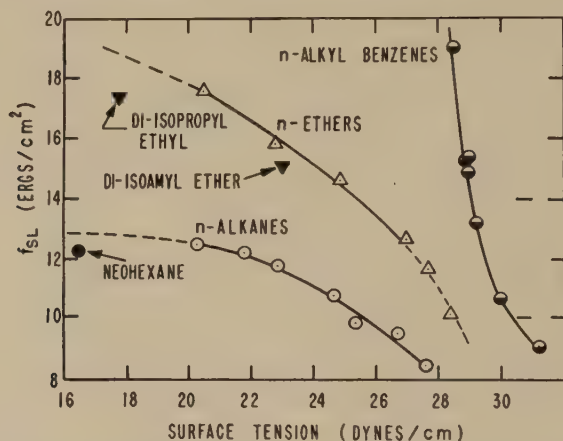


FIG. 5. Free energy decrease on immersion of n -alkanes, n -ethers, and n -alkylbenzenes on an oriented monolayer of perfluorodecanoic acid.

nucleus to raise f_{SL} considerably. If higher members could be obtained, the curve would probably tend to level off somewhat when the alkyl chain is sufficiently long to overcome the influence of the benzene ring. This tendency becomes apparent in decylbenzene.

DISCUSSION

It might be expected that an important variable would be the nature of the underlying solid. Fortunately, most of the liquids studied did not attack or dissolve the adsorbed monolayer. Hence, the contact angles obtained were generally the same with substrates as different as polished platinum, copper, brass, and fire-polished glass. Since particular precautions have been taken here to prepare smooth surfaces, it is believed that the Wenzel's roughness factor (7) is considerably below 1.07 and that surface roughness is not great enough to cause serious error. The effect of

surface roughness was further decreased here as in the study of monolayers of octadecylamine (2) by the action of any coherent monolayer of forming a carpet over higher prominences of the surface resulting in a new surface which is even smoother than the underlying surface. Since fire-polished glass is one of the smoothest surfaces obtainable, a number of measurements were made of the contact angles of several liquids on this surface coated with a monolayer of perfluorodecanoic acid. Upon comparison of these with the contact angles of the same liquids on the film-covered platinum foil, no significant differences were observed. The results demonstrate that either the metal foil was sufficiently smooth or else bridging effects had nullified the differences in roughness of the foil and the glass.

The most remarkable result of this investigation is that despite the wide variety of liquids studied, no liquids were found which would spread on a polished surface coated with an oriented, close-packed monolayer of perfluorodecanoic acid. It should be noted that the organic liquids studied exhibited the largest contact angles ever reported for them on any smooth surface. The inert behavior of the " CF_3 surface" makes apparent the appropriateness of our assumption that f_{SV}° is zero for such surfaces for all except the lowest boiling liquids. It has been recognized since the early work of Hardy (8) that the spreading of liquids on smooth surfaces is aided by a process of evaporation and subsequent condensation. Evidently, this process cannot be responsible for the spreading of liquids on the surface of oriented closely packed $-\text{CF}_3$ groups because of the low adsorptivity of the surface for such vapors. The analogy between the wetting properties of surfaces made up of packed $-\text{CH}_3$ or $-\text{CH}_2-$ groups on one hand and of $-\text{CF}_3$ or $-\text{CF}_2-$ groups on the other hand has proved to be sound. The bar chart of Fig. 2 or the data of Tables I-III show that replacing $-\text{CH}_2-$ by $-\text{CH}_3$ groups or $-\text{CF}_2-$ by $-\text{CF}_3$ groups in the surface of the solid usually causes a decrease in wettability by liquids. This means that an oriented and closely packed monolayer of $-\text{CF}_3$ groups forms a surface which is more nonwetable than TFE. Presumably, the former surface is even less reactive chemically than TFE provided no film penetration occurs. Even more nonreactive and nonwetable would be the close-packed arrangement of $-\text{CF}_3$ groups in the appropriate surface of a single crystal of a long-chain perfluorinated *n*-alkane (if such could be prepared), since that would be the most closely packed arrangement possible without external pressure.

A noteworthy homologous series studied is that of the three pseudo-perfluoroalcohols in which the members differ from each other by increments of $-\text{CF}_2-\text{CF}_2-$. In this series the behavior of the surface tension as a function of chain length is the opposite of that usually encountered in homologous series. The small change in surface tension per $-\text{CF}_2-$

group is the result of two competing effects. The first is the normal increase in surface tension with the addition of a $-\text{CH}_2-$ group. The second and the much larger effect of the two is the large decrease in surface tension contributed by the replacement of the two methylene hydrogen atoms by fluorine atoms to form the $-\text{CF}_2-$ group. The net effect is a reduction in surface tension with increasing length of the fluorinated carbon chain.

It is interesting to note that the polyethylene liquids have surface tensions and contact angles which indicate that the liquids are homologs (or nearly so) of the higher n -alkanes. As the chain length of the diethers and alkylbenzenes is increased, the variables $\cos \theta_E$, W_A , $W_A - W_C$, and f_{SL} all approach the values for the n -alkanes as limits. The presence of an aromatic ring raises the contact angle of the liquid. Examples are: tricresyl phosphate, benzyl phenyl hendecanoate, and *tert*-butylnaphthalene which are among the most nonwetable hydrocarbon compounds or derivatives studied. It is interesting to compare the wettability properties of the following C_6 hydrocarbons: n -hexane ($\gamma_{LV}^\circ = 18.4$; $\theta_E = 41^\circ$), cyclohexane ($\gamma_{LV}^\circ = 25.0$; $\theta_E = 62^\circ$) and benzene ($\gamma_{LV}^\circ = 28.9$; $\theta_E = 58^\circ$). The rise in contact angles in going from n -hexane to cyclohexane is expected from the increase in surface tension, but the fact that benzene, which has an even higher surface tension, has a slightly lower contact angle than cyclohexane may be due to the greater adhesion of the resonating structure to the solid surface.

The ester group and the ether oxygen atom do not have particularly important effects on the wetting properties of liquids on perfluorodecanoic acid films. Thus benzylphenylhendecanoate approximates the properties of an alkylbenzene of the same surface tension, and the higher members of the diethers have nearly the same properties as the n -alkanes of the same chain length. In general, liquids containing aliphatic carbon atoms, hydrogen atoms, and only a small proportion of oxygen atoms have nearly the same value of f_{SL} . All the silicones and silicate esters listed in Table III exhibited high contact angles and low spreading coefficients. The influence of a silicon atom on the spreading of liquids on a perfluorodecanoic acid film is slight. In tetra (mixed phenylcresyl) silicate, the aromatic groups were the most important in determining the wetting properties. This compound may be located approximately on the charts by extending the curves of the alkylbenzenes to the surface tension of the silicate.

The comparative behavior of the polymethylsiloxanes and n -alkanes is interesting. Since the surface tension of the former is lower than an n -alkane of the same number of monomers, the contact angles are lower. However, the exterior of a polymethylsiloxane molecule is covered with methyl groups, and the low surface tensions of such fluids are primarily

due to the highly localized van der Waals' cohesive forces between the methyl groups of adjacent molecules, and hence the lower members of the polymethylsiloxane and *n*-alkane families approach each other in properties. This is not surprising, because at the lower end of the *n*-alkane series there is a higher proportion of methyl to methylene groups. Since a methylsilicone behaves like an alkane, a methylphenylsilicone should behave like an alkylbenzene; and this is found to be true, because the methylphenylsiloxane dimer lies on the $\cos \theta$ vs. γ_{LV}° curve for the family of alkylbenzenes.

Of the halogenated compounds studied, the contact angle for the oriented perfluorodecanoic acid film appears to increase in the order $\theta_F < \theta_{Cl} < \theta_{Br} < \theta_I$. Perfluorokerosene, which contains perfluoroalkanes of chain length approximately C_{12} – C_{16} , had a contact angle of only 26° as compared with 69° for the nonfluorinated C_{14} alkane. The analogs *sym*-tetrabromoethane and *sym*-tetrachloroethane had contact angles of 87° and 36° , respectively, while W_A was 20 ergs/cm.² higher for the latter. Methylene iodide had a contact angle of 90° as compared with 67° for methylene bromide. Introduction of a fluorine atom into an aromatic ring increases the wettability of the fluid. Thus f_{SL} , W_A , and $W_A - W_C$ for *p*-difluorobenzene are much greater than those of benzene.

In Fig. 5 it is seen that for the alkanes on a perfluorodecanoic acid coating, f_{SL} or $\gamma_S^\circ - \gamma_{SL}$ is a monotone decreasing function of γ_{LV}° . As γ_S° is a constant, it follows that γ_{SL} must be a monotone increasing function of γ_{LV}° ; therefore, liquids of higher surface tension in a homologous series should have higher values of γ_{SL} . This conclusion cannot at present be verified experimentally, for there are no reliable data on the interfacial energy of the solid-liquid interface. But analogous reasoning applies equally to the oil-water interface; and upon plotting the interfacial tensions of the *n*-alkanes against water versus the surface tension of the alkanes, it is found that $\gamma_{oil-water}$ is a monotone increasing function of γ_{LV}° .

Since methyl substituents are more effective than methylene in rendering a liquid more inert to a solid, it would seem that the higher alkanes should have much larger values of f_{SL} than the lower members. The opposite is true, however. This may be a result of the masking effect of the surface tension variable, for f_{SL} decreases as the surface tension of the liquid increases (as discussed above). This decrease has a larger effect on f_{SL} than does the increase which would be expected to result from increasing the number of $-\text{CH}_2$ -groups. Thus, the small surface chemical effects due to structural differences in the molecules may easily be counterbalanced by the effect due to increased surface tension of the liquids. This may be the reason why 2,2-dimethylbutane, which has four $-\text{CH}_3$ groups, has a considerably lower value of f_{SL} than the *n*-alkane of corre-

sponding surface tension (Fig. 5). Similarly, in the same figure, it is seen that the two isoethers (which have more $-\text{CH}_3$ groups than their n -alkyl analogs) have also lower values of f_{SL} than the di- n -ethers of the same surface tensions.

The $-\text{CF}_3$ group may be expected to occupy an interesting and unique place in surface chemistry. By employing it properly it is possible to obtain a maximum in organophobic behavior. In synthesizing surface-active compounds, it has always been essential to have hydrophilic and hydrophobic groups in opposite portions of the molecule. Synthesis of surface-active compounds with $-\text{CF}_3$ groups and hydrophilic or other adsorbable polar groups at opposite portions of the molecule should result in a new class of compounds with useful and interesting properties.

ACKNOWLEDGMENTS

The cooperation of H. W. Fox and Elaine Shafrin and the assistance of Alfred H. Ellison in measuring some of the surface tensions are sincerely appreciated.

SUMMARY

The wettability of more than 90 pure liquids on oriented close-packed monolayers of perfluorodecanoic acid adsorbed on platinum, copper, brass, and glass has been studied. Comparison with results reported earlier for solid polyethylene, oriented monolayers of octadecylamine, and solid polytetrafluoroethylene shows that oriented, close-packed monolayers of perfluorodecanoic acid are the most nonwetable surfaces ever found and that for most liquids in contact with these surfaces the contact angle (θ) decreases in the order $\theta_{\text{CF}_3} > \theta_{\text{CF}_2} > \theta_{\text{CH}_3} > \theta_{\text{CH}_2}$.

Values of the work of adhesion, the initial and final spreading coefficients, and the free energy decrease on immersion, f_{SL} , were computed from contact angle measurements and surface tensions using the assumption justified by experiment that $f_{SV}^\circ = 0$. From the values of f_{SL} , it has been possible to estimate the free surface energy of the surfaces prepared from films of perfluorodecanoic acid.

Structural differences determining the wetting properties of liquids are presented, and the effect of increase in surface tension of higher members in a homologous series is discussed. Observed modifications of the wetting properties of high-energy solids by adsorption of a single monolayer, demonstrate beyond doubt the short-range nature of the forces involved in wetting.

In view of the remarkable resistance to wetting shown by surfaces of close-packed perfluoromethyl groups, surface-active compounds with $-\text{CF}_3$ groups and hydrophilic groups at opposite ends of the molecule should have unusual and valuable properties, and they deserve to be treated as a special class of surface-active compounds.

REFERENCES

1. FOX, H. W., AND ZISMAN, W. A., *J. Colloid Sci.* **5**, 514 (1950); *ibid.* **7**, 109 (1952).
2. SHAFRIN, E. G., AND ZISMAN, W. A., *J. Colloid Sci.* **7**, 166 (1952).
3. FOX, H. W., AND ZISMAN, W. A., *J. Colloid Sci.* **7**, 428 (1952).
4. BIGELOW, W. C., PICKETT, D. L., AND ZISMAN, W. A., *J. Colloid Sci.* **1**, 513 (1946).
5. SUMMER, C. G., *Wetting and Detergency*. Chemical Publishing Co., New York, 1937.
6. FOX, H. W., AND CHRISMAN, C. H., *J. Phys. Chem.* **56**, 284 (1952).
7. WENZEL, R. N., *Ind. Eng. Chem.* **29**, 988 (1936).
8. HARDY, W. B., *Collected Scientific Papers*. Cambridge Univ. Press, London, 1936.
9. VOGEL, A. I., *J. Chem. Soc.* **1946**, 133.
10. QUAYLE, O. R., DAY, R. A., AND BROWN, G. M., *J. Am. Chem. Soc.* **66**, 938 (1944).
11. VOGEL, A. I., *J. Chem. Soc.* **1948**, 616.
12. QUAYLE, O. R., private communication.
13. QUAYLE, O. R., Technical Report to O.N.R. (Contract N8-onr 525-Emory Univ.), June 1, 1949 (available from Library of Congress).
14. DOSS, M. P., *Physical Constants of the Principal Hydrocarbons*, 4th Ed. The Texas Company, 1943.
15. WASHBURN, E. W. (ed.), *International Critical Tables of Numerical Data*, Vol. 4, p. 446. McGraw-Hill, New York (1928).
16. HODGMAN, C. D., *Handbook of Chemistry and Physics*, 30th Ed. Chem. Rubber Pub. Co., Cleveland, Ohio, 1947.
17. FOX, H. W., TAYLOR, P. W., AND ZISMAN, W. A., *Ind. Eng. Chem.* **39**, 1401 (1947).

STUDIES OF SURFACE POTENTIALS. I. EFFECT OF SALTS AND THE NATURE OF THE INTERFACE UPON THE SURFACE POTENTIALS OF INSOLUBLE MONOLAYERS

B. D. Powell¹ and A. E. Alexander

*Department of Colloid Science, Cambridge, England; and Department of Chemistry,
New South Wales University of Technology, Sydney, Australia*

Received December 7, 1951; revised May 22, 1952

ABSTRACT

A systematic study of the surface potentials of both insoluble and adsorbed monolayers has been undertaken, and of their relation to electrophoretic (zeta) potentials. It is shown how zeta-potentials may be obtained from the effect of salts on the magnitude of the surface potential.

INTRODUCTION

The "surface potential" ΔV [$\Delta V = V$ (film) - V (water)] is a definite physical quantity, being independent of the method used for its measurement, and has proved to be useful in the study of the structure and reactions of both insoluble and adsorbed monolayers at the air/water interface (1). At the oil/water interface the data are scanty and refer almost entirely to adsorbed films, although some preliminary work upon insoluble monolayers has been reported (2).

In the present investigation we have examined how the concentration of the salts present in the aqueous phase, and the nature of the non-aqueous phase, affect the surface potential of insoluble monolayers of copolymers. The contribution made by the electrokinetic (zeta) potential to the surface potential has been measured and compared with experimental values.

EXPERIMENTAL

The air/water and oil/water potentials were determined with a vacuum tube electrometer using mesothorium bromide as the ionizing source and a silver wire coated with silver chloride as the half-cell. The aqueous phase was a solution of either KCl, NaCl, or HCl.

Oil/water potentials were measured in a small cylindrical glass dish of ca. 9 cm. diameter. The surface of the aqueous phase was cleaned by "sucking off" before adding the thin layer (usually ca. 1 mm.) of oil. The micrometer syringe used for spreading purposes was held in an adjustable arm so that the tip could be suitably positioned at the interface.

¹ Present address: National Research Council of Canada, Ottawa, Canada.

At the air/water surface either the above dish was employed or a rectangular glass tray, *ca.* 14×25 cm., and, in the latter case, the surface was cleaned by sweeping with glass barriers. The method of successive additions was used to vary the concentration, the surface potential (ΔV) being measured at suitable intervals.

Potentials were found to be independent of the size of the air gap and of the oil layer thickness (up to 2 mm.).

The electrophoretic mobility of Nujol particles (a highly refined mineral oil) on which the copolymers could be adsorbed, was found by measurements made in a microelectrophoresis apparatus (3). A single tube cell of cylindrical section was used and allowance made for the refraction error pointed out by Henry (4). To reduce contamination by tap grease the glass tubes carrying the electrodes of platinum black were ground in to serve as stoppers. The preparation of the suspensions was necessarily

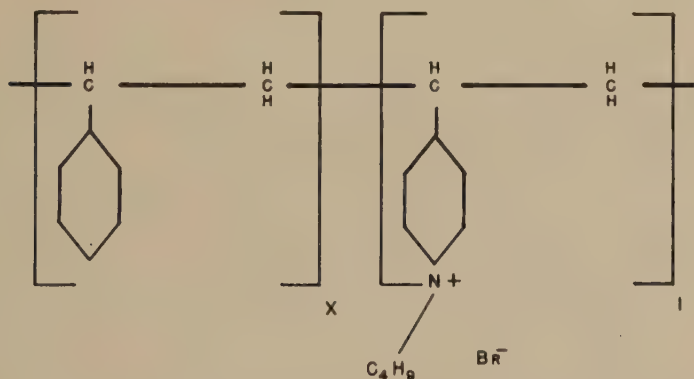


FIG. 1. General formula of the copolymers.

different for the two copolymers used. With compound C125B (see below) a stock suspension of Nujol in water was made by the method of Powney and Wood (5), and suitable amounts of an aqueous solution of C125B were added. With compound D41 (see below), a solution in chloroform was added to hot Nujol, poured into hot water, boiled to drive off the chloroform, and the resulting suspension was separated in a funnel from excess Nujol.

The substances used for spreading were kindly given by Dr. Fuoss (6), two of a series of copolymers of vinylpyridine and styrene having chains containing different proportions of ionogenic groups. They were prepared by copolymerizing vinylpyridine with styrene, followed by treatment with *n*-butyl bromide, and have the general formula given in Fig. 1. According to Fuoss their structure in solution is that of an open coil which is more diffuse than that of compounds like polystyrene because

the positively charged pyridonium ions which are attached to the chain by valency links repel one another. The bromide ions fall into two categories, those in the solvent between the polymeric cluster ions and the others near or inside the positive polyion.

Compound D41 contains 13 mole % of vinylpyridine (calculated from the percentage bromide) and being insoluble in water was spread from a 40:60 isopropyl alcohol-chloroform mixture, a very satisfactory agent shown to produce no change in surface potential itself. Further, "runs" with solutions of D41 in this mixed solvent at widely differing concentrations yielded coincident ΔV -surface concentration plots.

C125B, the other compound in the series studied, contained 58.3 mole % of vinylpyridine and was water-soluble; it is nevertheless convenient to include it here in the insoluble film section with D41 because of its similarity. The maximum surface potential at the various interfaces was

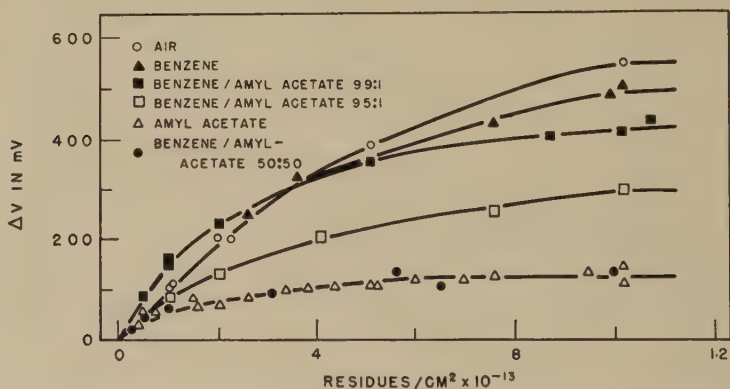


FIG. 2. Surface potential of D41 at various interfaces plotted against surface concentration. Aqueous phase, 0.001 *N* HCl.

therefore determined by dropping a small crystal into the interface and measuring the resulting change.

RESULTS

Figure 2 shows the effect of the nature of the interface on the relation between surface potential (ΔV) and the surface concentration (n) for D41 spread on dilute (0.001 *N*) HCl (n is the number of pyridonium groups/cm.² since we assume that the nonpolar styrene residues will make a negligible contribution to ΔV in comparison with the ionic pyridonium groups). For the nonaqueous phase, air, benzene, amyl acetate, and amyl acetate-benzene mixtures were used. ΔV is seen to rise fairly rapidly initially; at the higher surface concentrations it approaches a constant value, the magnitude of which decreases in the following order: air > ben-

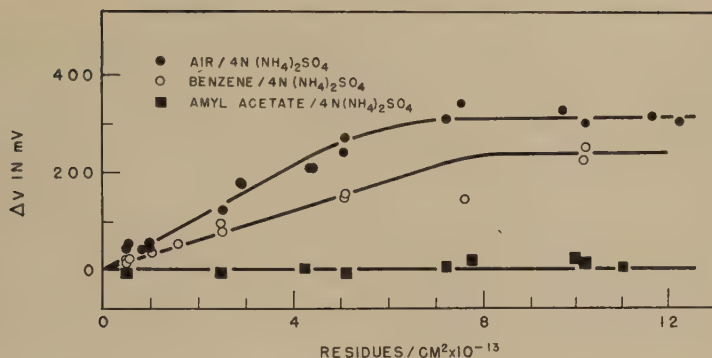


FIG. 3. Surface potential of D41 at various interfaces plotted against surface concentration. Aqueous phase, 4 N $(\text{NH}_4)_2\text{SO}_4$ solution.

zene > 99% benzene-1% amyl acetate > 95% benzene-5% amyl acetate > 50% benzene-50% amyl acetate; and amyl acetate (the last two coincide).

In Fig. 3 are plotted the ΔV - n curves for the various interfaces, when the previously used dilute HCl solution was replaced by a strong salt solution. With air and benzene as the nonaqueous phase the curves resemble those of Fig. 2, although the maximum ΔV is lower in each case; with amyl acetate no change of potential could be detected.

The ΔV - n curves for D41 at the air/HCl solution interfaces is given in Fig. 4, the concentration of HCl in the aqueous phase ranging from N to 0.001 N . Replacement of HCl by KCl was found to have little effect upon ΔV .

All the above curves were from measurements in the small cylindrical dish. Using the larger rectangular tray, and salt solutions ranging from

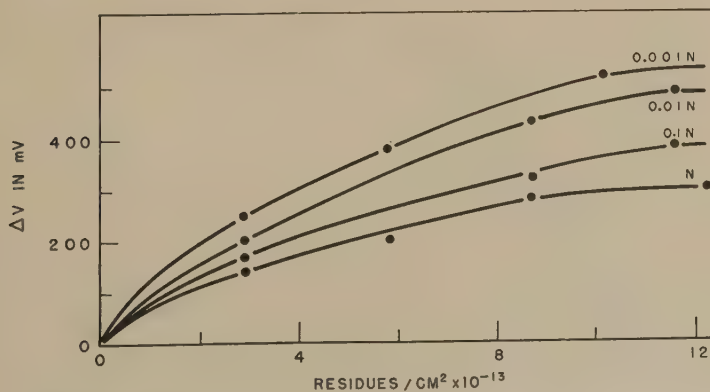


FIG. 4. Surface potential of D41 at the air/water interface plotted against surface concentration. Aqueous phase, HCl at various concentrations.

2×10^{-6} to $5 N$, the results shown in Fig. 5 were obtained. These clearly resemble in general those of Fig. 4, although all potentials were appreciably higher, probably due to edge effects with the smaller dish. (In the large tray a barrier was used for sweeping, and in the experiments the area would vary, depending on the position in which it was left, from about 14×25 cm. to about 14×20 cm. Potential-surface concentration plots were always the same, and the distance of the glass surface from the air electrode would be at least double in the case of the tray, so that any edge effects would be correspondingly diminished.) For this reason the ΔV values of Fig. 5 are more reliable and are therefore used for the quantitative calculations below.

As regards electrophoretic results, a complete mobility-concentration curve could be obtained for C125B, as is shown in Fig. 6, by the methods detailed earlier. Initially the Nujol particles have a negative charge which is reduced and then reversed in sign by C125B in low concentration, and at high concentration an approximately constant value of $8.8 \mu/\text{sec.}/\text{v.}/\text{cm.}$ was found, corresponding to a particle surface saturated with C125B. The insolubility of D41 made a mobility-concentration curve impracticable; therefore only the mobility for the saturated particle surface could be determined at all readily, the value found being $11.2 \mu/\text{sec.}/\text{v.}/\text{cm.}$ From the electrokinetic mobility (v) the ζ -potential was calculated by means of the equation:

$$v = \frac{D\zeta}{4\pi\eta}$$

The maxima were D41, $+165$ mv.; and C125B, $+130$ mv.

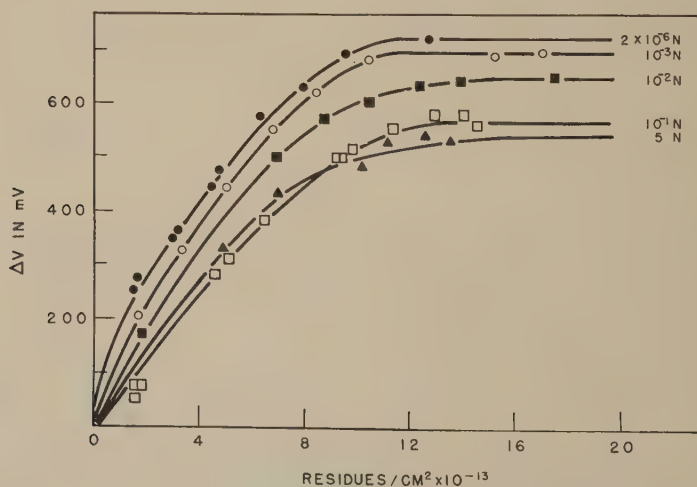


FIG. 5. As Fig. 4, but experiment carried out in large rectangular tray.

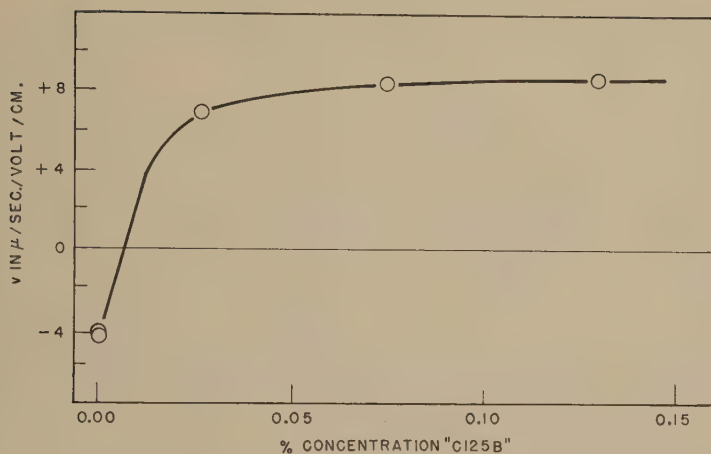


Fig. 6. Electrophoretic mobility of Nujol particles in solutions of C125B plotted against concentration.

The case of D41 and C125B illustrates well the difficulty of this work. A compound insoluble in water is easier to study for surface potential (since it can be spread) than for electrophoretic mobility; whereas, a soluble compound, simple for electrophoresis, makes for difficulties when used for surface potential measurements. A compound equally convenient for both techniques was not found.

DISCUSSION

From the above results there would seem to be five major points to be discussed:

1. The general form of the ΔV - n curve.
2. The effect of salts in reducing ΔV at a given value of n .
3. The smaller ζ -potential of C125B, which has the greater vinylpyridine content.
4. The dipole potentials (see below) of C125B and D41.
5. The effect of the nature of the nonaqueous phase on the ΔV - n curve.

The surface potential is due to the existence of an electrical double layer, which generally can arise by any or all of three processes:

1. The interface is more permeable to ions of one sign than to the other—a diffusion potential.
2. Ions of one sign tend to be adsorbed more strongly than those of the other—an adsorption potential.

3. Ions or molecules containing electrical dipoles are adsorbed and orientated at the interface—a dipole potential.

In none of the systems studied here were the potentials found to be time dependent, so presumably *diffusion potentials* were not involved. A reading could be taken within half a minute of setting up the system and it remained constant for the longest time during which it was ever observed—several hours. (It is not advisable to wait too long lest impurities diffuse to the interface and give spurious effects.) The potential changes are therefore made up of two contributions: (a) from the *dipoles* in the pyridonium ions; and (b) from a diffuse double layer in the aqueous phase caused by *preferential adsorption* of the polymeric ion. The former will depend on the surface concentration and orientation of the pyridonium ions and the latter upon the surface concentration of the pyridonium ions and the salt concentration in the aqueous phase.

1. The General Form of the ΔV - n Curve

Let us consider first the general form of the ΔV - n curve which, as Figs. 2, 3, 4, and 5 show, is approximately Langmuirian in shape, i.e., at low values of n it is linear and tends to a constant value of ΔV at the higher values, when n exceeds about 11×10^{13} pyridonium ions/cm.² If intermolecular interactions were absent the ΔV - n curve would be linear, as indeed it is when n is small.

The decrease in slope at higher n indicates that intermolecular effects are becoming increasingly important, reducing the contribution from each ionic group. The constant value of ΔV at about $n = 11 \times 10^{13}$ pyridonium residues/cm.² indicates that polar groups are being removed from the interface, and the area at which it occurs, ca. 90 Å.² per pyridonium residue, is close to the value anticipated from the molecular constitution of seven styrene to one pyridonium residue.

2. The Effect of Salts in Reducing ΔV at a Given n

The effect of increased salt concentration is always to reduce ΔV at a given n , as shown by a comparison of Figs. 2 and 3, and also Figs. 4 and 5. If, as is suggested, part of the total surface potential comes from the diffuse electrical double layer, addition of salts would reduce and eventually eliminate this contribution, just as increase of salt concentration will reduce a ζ -potential to zero. The electrokinetic (zeta) potential is very difficult to measure at the air/water interface, but for surfaces covered with ionic polymers the values would not be expected to differ greatly from those for the Nujol/water interfaces, which can readily be determined. For D41 and C125B the experimental results are:

Polymer D41

Maximum potential on very dilute salt solution, air/water interface:	+715 mv.
Maximum potential on strong salt solution, air/water interface:	+545 mv.
Difference; the decrease in surface potential on salt addition at the air/water interface:	170 mv.
Zeta-potential of Nujol particles covered with D41 in very dilute salt solution:	+165 mv.

Polymer C125B

Maximum potential, dilute salt, air/water:	+600 mv.
Maximum potential, strong salt, air/water:	+470 mv.
Decrease in surface potential on salt addition at:	
air/water interface:	130 mv.
benzene/water interface:	137 mv.
octyl alcohol/water interface:	120 mv.
Zeta-potential of Nujol particles at saturation (see Fig. 6):	+130 mv.

It is seen from the figures above that in both instances the ζ -potential deduced from electrophoretic mobility determinations is numerically very close to the decrease in the surface potential, brought about when the concentration of salt in the aqueous phases increases from a very low to a very high value. This close agreement would seem to provide adequate proof that both potentials arise from the same cause, namely, a diffuse double layer. Further, the ζ -potential is independent of the nature of the nonaqueous phase; proceeding from air to benzene to amyl alcohol to Nujol-C125B, and from air to Nujol-D41, although the surface potential varies greatly. Since the ζ -potential is due to the diffuse double layer in the aqueous phase, the observation is not unexpected. Abramson (7) and others have shown that particles such as those of Pyrex glass, mineral oil, carbon, collodion, or quartz, all have the same electrophoretic mobility (and the same ζ -potential) as each other and as the dissolved protein when coated with a film of (say) egg albumin in solutions of the same ionic strength—an interesting behavior parallel to that of these polymers.

3. Zeta-Potentials of D41 and C125B

The ζ -potential of C125B is less than that of D41, although it contains a greater percentage of vinylpyridine. This suggests that ion-pair formation is occurring to a greater extent in C125B; the more pyridonium groups in the chain, the higher the positive charge density and more bromide ions are brought into the neighborhood of the cation, and so the

mobility does not increase in proportion to the number of ionic groups. Cathers and Fuoss (8) came to the same conclusion from a consideration of the conductivity of solutions of the polymers in various solvents as a function of salt concentration, dielectric constant of the solvent, and copolymer composition. For instance, in a given solvent at a fixed salt concentration the conductivity decreased with increasing vinylpyridine content, whereas the opposite effect would be anticipated and especially at infinite dilution. They were unable to extrapolate their results to this dilution but did make their measurements at low concentration. Viscosity change, they showed, was not the explanation, but increased association, due to the greater charge density in the coil which predominated over opposing effects.

4. Dipole Potentials of D41 and C125B

The surface potential measured on a strong salt solution is in reality a dipole potential (see definitions above), for our failure to detect any time effects has ruled out diffusion, and the high salt concentration has reduced the ζ -potential to zero. At high surface concentration the dipole potentials of D41 and C125B are 545 mv. and 470 mv., respectively, due to the dipoles of the vinyl pyridonium group. In the C125B molecule the length of the styrene chain between adjacent vinyl pyridonium groups is shorter and the steric hindrance to the orientation of these groups with their dipoles vertical is greater—a fact most easily demonstrated with molecular models. Hence the vertically resolved component of the dipole in C125B will be numerically smaller, and correspondingly also, the dipole potential. Allen and Alexander (9) who studied the whole range of these compounds had occasion to measure the initial slope of the ΔV - n curve for C125B on strong salt solution, and it was less than that for D41. As they point out, this initial slope is a measure of the dipole moment ($\Delta V = 4\pi n\mu$) of the polar groups when only intramolecular effects are operating, of which the most important will be the lengths of the connecting links of styrene groups between adjacent vinylpyridines.

5. Effect of the Nature of the Nonaqueous Phase on the ΔV - n Curve

All the ΔV -curves have the same general shape: after the rapid initial rise the curve flattens progressively and eventually approaches a constant value of ΔV . At a given concentration of D41, ΔV is less at an oil/water than at an air/water interface, that is at the former, D41 is "less effective." It suggests that when a molecule of D41 is spread at the oil/water interface it replaces one or more oil molecules with a resulting net reduction in the magnitude of the dipole moment per unit area.

Let μ_0 and A_0 be, respectively, the dipole moment and area occupied at the interface by one molecule of oil, and let μ_P and A_P be the corresponding quantities for polymer D41.

Now $\Delta V = 4\pi n\mu = 4\pi\mu/A$; therefore $\mu_0 = (A_0 \times \Delta V_0)/4\pi$, and $\mu_P = (A_P \times \Delta V_P)/4\pi$. If the area A_P of a molecule of D41 is N times greater than the area of an oil molecule A_0 the change $\Delta\mu$ in the dipole moment at the interface on spreading a molecule of D41, which will replace N molecules of oil, is: $\Delta\mu = \mu_P - N\mu_0$. Substituting for μ_P and μ_0 ,

$$\Delta\mu = \frac{A_P \times \Delta V_P}{4\pi} - \frac{A_0 \times \Delta V_0}{4\pi} \times N = \frac{A_P}{4\pi} [\Delta V_P - \Delta V_0]$$

If we define $\Delta\Delta V$ as the maximum change in ΔV when D41 is spread at an oil/water interface, then $\Delta\Delta V = (4\pi \times \Delta\mu)/A_P$. Hence on substituting, $\Delta\Delta V = \Delta V_P - \Delta V_0$, and this equation can be tested. Collecting the definitions:

$\Delta\Delta V$: Maximum surface potential observed when D41 is spread at a given oil/water interface, i.e., the net change in potential.

ΔV_0 : Change in potential observed when an oil is put onto a water surface, i.e., the surface potential of the oil at an air/water interface.

 TABLE I^a

Interface	Salt concentration	$\Delta\Delta V$ (Exptl.)	ΔV_0 (Exptl.)	ΔV_P (Calcd.)	ζ (Exptl.)	$\Delta V_P'$ (Calcd.)
(a) Benzene/water	Strong	230	310	540	0	540
	Dilute	500	216	716	170	546
(b) Air/water	Strong	—	—	545 ^b	0	545
	Dilute	—	—	715 ^b	170	545
(c) Amyl acetate/ water	Strong	0	295	295	0	295
	Dilute	120	335	455	170	285

$$\Delta\Delta V + \Delta V_0 = \Delta V_P$$

$$\Delta V_P = \zeta + \Delta V_P'$$

^a All potentials in the table are positive and in millivolts.

^b Experimental, too, of course.

ΔV_P : Change in potential that the spreading of D41 causes at an air/water interface. On strong salt solutions it will be a dipole potential $\Delta V_P'$; on dilute salt, a dipole plus an adsorption (or zeta) potential ($\Delta V_P' + \zeta$).

From the figures in Table I the following conclusions may be drawn:

1. At the benzene/water interface the dipole potential of D41 is independent of the salt concentration and approximates to the air/water value. The orientation of the dipoles must therefore be similar in both cases.

2. At the amyl acetate/water interface the dipole potential is again independent of salt concentration, but smaller in magnitude. The dipole orientation is more random at this interface of low energy.

3. The equation $\Delta\Delta V + \Delta V_0 = \Delta V_P$ is verified and the theory on which it is based shown to be valid.

In line (c) of Table I, $\Delta\Delta V = 0$ for D41 at the amyl acetate/strong salt solution interface. This figure is surprising, but is not due to imperfect spreading at an interface of such low interfacial tension, as has been shown by another author (9).

REFERENCES

1. ALEXANDER, A. E., *Ann. Rept. on Progress Chem. (Chem. Soc. London)* **41**, 5 (1944).
2. ALEXANDER, A. E., AND TEORELL, T., *Trans. Faraday Soc.* **35**, 727 (1939).
3. ALEXANDER, A. E., AND SAGGERS, L., *J. Sci. Instruments* **25**, 374 (1948).
4. HENRY, D. C., *J. Chem. Soc.* **1938**, 997.
5. POWNY, J., AND WOOD, L. J., *Trans. Faraday Soc.* **36**, 57 (1940).
6. FUOSS, R. M., AND CATHERS, G. I., *J. Polymer Sci.* **4**, 97 (1949).
7. ABRAMSON H. A., MOYER L. S. AND GORIN M., *Electrophoresis of Proteins*, Chap 4. Reinhold, New York, 1942.
8. CATHERS, G. I., AND FUOSS, R. M., *J. Polymer Sci.* **4**, 121 (1949).
9. ALLEN, G., AND ALEXANDER, A. E., *Trans. Faraday Soc.* **46**, 316 (1950)

STUDIES OF SURFACE POTENTIALS. II. EFFECT OF SALTS AND THE NATURE OF THE INTERFACE UPON THE SURFACE POTENTIALS OF SOLUBLE MONOLAYERS

B. D. Powell,¹ and A. E. Alexander

*Department of Colloid Science, Cambridge, England; and Department of Chemistry,
New South Wales University of Technology, Sydney, Australia*

Received December 7, 1951; revised May 22, 1952

ABSTRACT

The work described in part I is continued with soluble monolayers of a cationic and an anionic soap, respectively: investigating the effect of salt concentration in the aqueous phase and the nature of the nonaqueous phase on their surface potentials. Confirmation is obtained of the conclusions drawn therein, and the results are compared with those of Dean and the theory of Dean, Gatty, and Rideal.

INTRODUCTION

The cationic soap CTAB (hexadecyltrimethylammonium bromide) was studied at the air/water, amyl acetate/water and *sec*-octyl alcohol/water interfaces, and for comparison, AOT (the dioctyl ester, 2-ethyl-1-hexanol, of sodium sulfosuccinic acid) an anionic soap, at the air/water interface only. In every case but one (below) the aqueous phase was 0.001 *N* HCl.

EXPERIMENTAL

Surface potentials were determined as in part I (1), with necessary modifications, the interfacial tensions of the same solutions (though not simultaneously) with the ring detachment apparatus, and the electrophoretic mobility of suspensions of Nujol particles in CTAB solution and AOT solution, respectively, in the microelectrophoresis cell. On strong (4 *N*) potassium chloride solution, CTAB could be spread from a solution in water expelled from a micrometer syringe in the usual manner for insoluble monolayers. The CTAB used was a very pure specimen kindly given by Imperial Chemical Industries Ltd. (Dyestuffs Division); the AOT was 100% material kindly supplied by the American Cyanamid Co.

¹ Present address: National Research Council of Canada, Ottawa, Canada.

RESULTS

The surface potentials (ΔV) were found to be independent of time, after a few minutes, and of oil-layer thickness, but the behavior of the octyl alcohol/water interface was exceptional in one particular; the potential, relative of course to the Ag/AgCl electrode, of the octyl alcohol/water interface fell slightly over a period of some 30 min. when clean and also when an adsorbed film of CTAB was present. Both potential/time plots were parallel straight lines, and so ΔV was independent of time. Figure 1 for CTAB at the air/water interface is typical of the other cases and the upper curve, "the zero," was frequently checked during a "run."

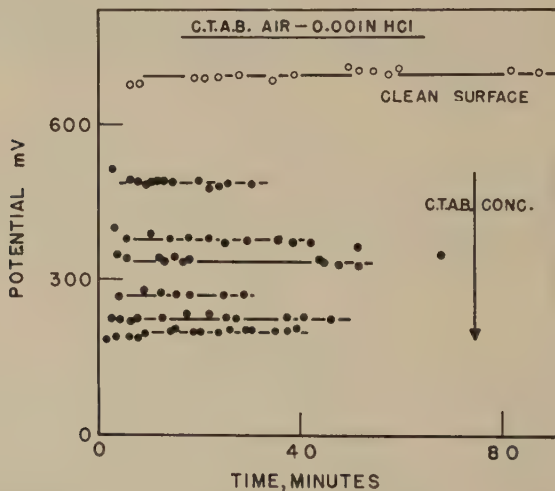


FIG. 1. Surface potential of CTAB adsorbed at the air/0.001 *N* HCl interface, for various bulk concentrations, plotted against time.

Figure 2 shows the ΔV - n curves for CTAB at the several interfaces which were obtained thus: direct experiment gave the ΔV - c curve, the Gibbs equation applied to the γ - c measurements, an n - c curve, and hence one of ΔV against n ; n and c are the surface and bulk concentrations, respectively (the former in molecules/cm.²). Initially the surface potential rises rapidly with n but eventually approaches a constant value and replacement of air by amyl acetate or octyl alcohol reduces the surface potential, for a given n , in the order air > amyl acetate > octyl alcohol. The surface potential is also reduced by increase of salt concentration. AOT gave curves of similar shape with a maximum surface potential of 300 mv. at the air/water interface.

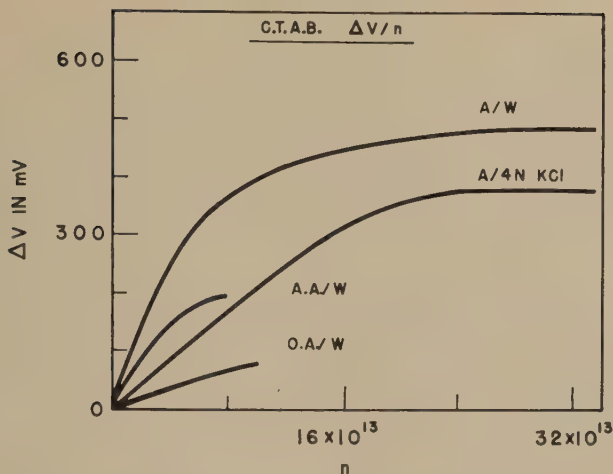


Fig. 2. Surface potential of CTAB at various interfaces plotted against surface concentration n in molecules/cm.² (A = air, AA = amyl acetate, and OA = octyl alcohol).

In Table I are the mobility-concentration observations for CTAB adsorbed onto Nujol (liquid petrolatum) particles suspended in 0.001 *N* HCl.

Note the very small concentration of CTAB required to change the sign of the Nujol particle from its original negative to a high positive value.

DISCUSSION

The major points to be discussed are:

1. The general shape of the ΔV - n curve.
2. The effect of salts in reducing ΔV at a given n .
3. The effect of the nature of the nonaqueous phase on ΔV .

Points (1) and (2) can be explained as in part I, where the same observations were recorded on polymer D41. On 0.001 *N* HCl, CTAB adsorbed from solution gave a maximum positive surface potential of 500 mv., and on 4 *N* potassium chloride it fell to 385 mv., a decrease of

TABLE I

Conc. CTAB %	Mobility (μ /sec./v./cm.)
0.0	-4.2
0.0003	+8.4
0.005	+8.1
0.001	+8.5
0.0039	+8.6
0.0097	+8.5

115 mv. Following the earlier reasoning, the ζ -potential is 115 mv. on 0.001 N HCl.

The mobility of Nujol droplets suspended in CTAB solution, made up, again, in 0.001 N HCl reached a steady value of $8.6 \mu/\text{sec.}/\text{v.}/\text{cm.}$, to which a ζ -potential of 125 mv. corresponds, in good agreement with the value from salt addition experiments on the surface potential. This serves as further proof that both these ζ -potentials arise from the diffuse double layer.

The third point: at a given n , ΔV is less, in the order air > amyl acetate > octyl alcohol, which is also the order of decreasing interfacial tension. The results are similar to those for D41 at various interfaces, where the surface potential at a given n also fell in the order of decreasing tension, and thus support the theory in part I.

The surface potential of AOT is 300 mv. positive, and the ζ -potential is about 140 mv. negative. To the surface potential, the contribution (a dipole potential) of the two ester groups is positive upwards and greater than the ζ -potential (an adsorption potential) which is negative upwards due to the preferential adsorption of the organic anion. On strong salt solutions this latter, zeta, potential will be zero and the surface potential should be about 140 mv. more positive, i.e. 440 mv., which is experimentally found.

Surface Potentials Measured by the Hanging Drop Apparatus

Some time was spent experimenting with a hanging drop apparatus of the type described by Dean (2), though unfortunately it was not found possible to obtain from it reproducible results. AOT was studied at the octyl alcohol/water interface, but all that could be said was that the surface potentials were very erratic and time dependent.

McMullen (3) however, with this apparatus, adsorbed dyes, anionic soaps, and more usefully, from our point of view, CTAB, at oil/water interfaces, which he observed for surface potential as a function of concentration, time, and oil-layer thickness, and he too, found great difficulty in securing stable potentials when using these surface-active materials. Initially CTAB gave a high potential (*ca.* 300 mv.) which rapidly decayed to a low value (*ca.* 50 mv.), and the curve of surface potential against percentage concentration either decreased thereafter to a more or less constant value or showed a definite maximum, and then a falling off. Which alternative was followed seemed to be governed by the extent to which the cleaning of the *reference* interface was carried—i.e., the one at which the soap was *not* adsorbed—and the difference between the two curves became great at high concentration of CTAB.

At the amyl acetate/water interface the same rapid decay of the initial potential was observed and, further, they were found to vary both with time and oil-layer thickness. These results then are not in agreement

with the ones given by the present (radioactive air electrode) method where it will be recalled, mention was made of the possible "edge effects" of small dishes. The diameters of the tips on which the upper drop could be used in the hanging drop apparatus were 1 and 4 mm., respectively, and it is suggested that many of the above results would not be obtained if the apparatus could be used with tips of say 12 cm. radius which, of course, would be a hydrostatic impossibility. Also, in this apparatus we are liable to experience contamination at two interfaces, instead of one, and uncertain liquid junction potentials in the side arms. Thus it is thought that the differences between the results from the hanging drop and dish techniques are due to the nature of the former apparatus, which is unsuitable.

Much experimental work has been reported on the potentials between water and organic liquids, very little on insoluble and soluble films at the oil/water interface² and none has been found where the effect of the nature of the nonaqueous phase and salt concentration in the aqueous phase were studied systematically. For many years, discussions raged as to the origin of these potentials, but it is now accepted that they are those enumerated in part I.

Dean, Gatty, and Rideal (4), by a thermodynamic argument, showed that the potentials concerned in this paper—those set up by the preferential adsorption of ions (adsorption potentials) or by the adsorption of particles containing dipoles (dipole potentials)—will not be permanent if ions can pass across the interface and come to equilibrium on both sides, for then a compensating electrical double layer will be set up in the oil phase. (Air/water surface potentials will be permanent because no compensating double layer can be built up.) Dean (2), for example, has done experiments with a hanging drop apparatus, which though similar, was not the one used by us, and they support this theory. Thermodynamic equilibrium may take a very long time to attain and so the fact that the surface potentials in these papers showed no time effects, over the periods involved, does not enable one to say with certainty that the results are in disagreement with the theory of Dean, Gatty, and Rideal, and the observations of Dean.

ACKNOWLEDGMENT

One of us (B.D.P.) is indebted to the D.S.I.R. for a grant in Cambridge, and to the British Council (Fund for Commonwealth University Interchange) and the Zinc Corporation Ltd., for grants in New South Wales.

REFERENCES

1. POWELL, B. D., AND ALEXANDER, A. E., *J. Colloid Sci.* **7**, 482 (1952).
2. DEAN, R. B., *Trans. Faraday Soc.* **36**, 166 (1940).
3. McMULLEN, A. I., Ph.D. dissertation, Part I. University of Cambridge, 1948.
4. DEAN, R. B., GATTY, O., AND RIDEAL, E. K., *Trans. Faraday Soc.* **36**, 161 (1940).

² For reviews, see Refs. (2) and (4).

VISCOSITIES OF CONCENTRATED POLYMER SOLUTIONS.

II. POLYISOBUTYLENE ¹

Myrle F. Johnson,² Warren W. Evans,³ Ivo Jordan,⁴ and John D. Ferry

Department of Chemistry, University of Wisconsin, Madison, Wisconsin

Received April 21, 1952

INTRODUCTION

Measurements of the viscosities of concentrated polyvinyl acetate solutions and their dependence on temperature, concentration, choice of solvent, and molecular weight have been reported in a previous communication (1). In the present paper, a similar study of polyisobutylene solutions is described. These measurements of steady-flow viscosity were undertaken in part for correlation with dynamic mechanical properties of the same solutions (2, 3). They were made under conditions of low stress such that the flow was essentially Newtonian.

MATERIALS AND METHODS

Eight different samples of polyisobutylene were studied. Their viscosity-average molecular weights, given below, were determined from intrinsic viscosity measurements in diisobutylene and in xylene (Table I). The intrinsic viscosities were obtained for two samples in both these solvents; the ratios of $[\eta]$ in diisobutylene at 20°C. to $[\eta]$ in xylene at 25°C. were 1.07 (4) and 1.03, respectively. A ratio of 1.05 was assumed for samples A, B, N, W-3, and E-1 to convert from xylene to diisobutylene⁵ in order to calculate the molecular weights from the formula of Flory (6). The latter formula was applied directly to measurements in diisobutylene on the other samples both at 20° and at 25°, since the work of Fox and Flory (5) indicates very little temperature dependence of intrinsic viscosity in this solvent.

¹ Reference (1) is considered to be Paper I of this series.

² Present address: Southwest Missouri State College, Springfield, Missouri.

³ Minnesota Mining and Manufacturing Company Fellow, 1951-52.

⁴ Escola Politecnica, Universidade de São Paulo, São Paulo, Brazil; Fellow of the Rockefeller Foundation, 1950-52.

⁵ Fox and Flory (5) have shown that the ratio of intrinsic viscosities in two solvents should depend somewhat on molecular weight; however, such dependence should be slight for diisobutylene and xylene, since the exponents in the empirical $M-[\eta]$ equations for diisobutylene and toluene are not very different (0.64 and 0.66 at 20°).

Sample *N*, 1.1 million, was kindly furnished by Dr. John Rehner, Jr., Esso Laboratories; its dynamic mechanical properties have been described elsewhere (2). Two other unfractionated samples, originally from Dr. Rehner's laboratory, were given us by Dr. Rodney D. Andrews, then at Princeton University: *A*, 0.54 million; and *B*, 0.78 million. These were cleaned by dissolving in benzene at a concentration of 5%, filtering through Republic⁶ S-1 filter pads under pressure, and precipitating with methanol, followed by vacuum desiccation at 60°C. Sample NBS was a standard unfractionated sample distributed by Dr. Robert S. Marvin, National Bureau of Standards, for measurements of mechanical properties in different laboratories. Its viscosity-average molecular weight was 1.35

TABLE I
Intrinsic Viscosities at 25°

Sample	$M_{\eta} \times 10^{-6}$	Intrinsic viscosity in			
		DIB ^a	Xylene	Decalin ^b	D-C ^c
Unfractionated					
<i>A</i>	0.54	—	1.60	—	—
<i>B</i>	0.78	—	2.03	—	—
<i>N</i>	1.1	—	2.49	—	—
Rough fractions					
<i>W-3</i>	0.32	—	1.16	—	—
<i>W-2</i>	2.51	4.53	—	5.15	3.57
<i>E-1</i>	4.0	—	5.76	—	—
Sharper fraction					
<i>FJ</i>	1.00	2.5	—	—	—

^a Diisobutylene.

^b Decahydronaphthalene.

^c Decalin 69.9%-cyclohexanol 30.1%.

million, but the weight-average value was 1.56 million (7). This difference of 16% is about twice as great as would be expected for a "most probable" distribution of molecular weights, and much greater than could exist in even a rough fraction. Since the viscosities of concentrated polymer solutions and melts are generally considered to depend on the weight-average molecular weight, the value of 1.56 million has been chosen for comparing sample NBS with the others.

Three rough fractions were employed, obtained by precipitation with acetone from benzene solution. Fraction *E-1*, 4.0 million, was obtained from Vistanex of grade *B-100* (given by the Esso Laboratories) as the first cut comprising 28% of the total material. Fractions *W-2*, 2.5 million; and *W-3*, 0.32 million; were obtained from Vistanex of grade *B-120* (given by the Enjay Company, Inc.) as the second and third cuts comprising

⁶ Republic Filter Corp., Newark, N. J.

56% and 20%, respectively, of the total material, after removal of a first cut of 13%. (The residual low-molecular-weight material was discarded.) Finally, one fairly sharp fraction, *FJ*, 1.00 million, was obtained from Vistanex *B-120* by two fractional precipitations. In the first fractionation, carried out on two batches, 38 and 30%, respectively, of high- and 24 and 45%, respectively, of low-molecular-weight material were rejected. The middle cuts of 38 and 25%, respectively, were combined and refractionated with rejection of 24% of low- and 28% of high-molecular-weight material. On the basis of total weight, the final fraction *FJ* comprised 15% of the original sample. Its weight-average molecular weight by light scattering⁷ was 0.98 million; this agreement with the viscosity-average is consistent with the expectation of a fairly sharp distribution, although it is not a critical test. All fractions were dried by vacuum desiccation at 60°C.

The xylene was a commercial product of analytical reagent grade. The decahydronaphthalene (Decalin) was redistilled through a 30-plate Oldershaw column; its density corresponded to a mixture of 89% of the *cis* isomer and 11% of the *trans* (8). The cyclohexanol was redistilled through the Oldershaw column, with a boiling range of about 1°.

Solutions were made up by weight. Those in Decalin contained 0.1% of "Deenax," calculated on the weight of the polymer, to prevent possible oxidative degradation.

Viscosity measurements were made by both falling-ball and capillary methods, exactly as described in the previous study of polyvinyl acetate (1). In calculations of the falling-ball measurements on xylene solutions, the Ladenburg correction for the wall effect (1) was used; for the Decalin solutions, the Faxén formula was used, since it has better theoretical justification (9), although under our conditions the difference between the two equations is negligible. Since in both methods the maximum stresses are of the order of 100 dynes/cm.² (1), no significant deviations from Newtonian behavior are to be expected.

RESULTS

Samples *A*, *B*, *N*, *E-1*, and *W-3* were studied in xylene; samples *NBS*, *W-2*, and *FJ* in Decalin; and sample *W-2* in a mixture of 69.9% Decalin and 30.1% cyclohexanol. The latter was chosen as a poor solvent in which the polymer would be on the verge of precipitation; phase separation occurs in this solvent at 2°C. at a concentration of 20%, and at -10°C. at a concentration of 11%. Data for concentrated solutions for the three solvents are given in Tables II, III, and IV, where w_2 denotes weight fraction of polymer. Some additional values for dilute solutions in the

⁷ We are much indebted to Dr. Sidney Katz and Mr. Malcolm L. Williams for this measurement.

TABLE II
Viscosities of Solutions in Xylene

Sample and $M_{\eta}/10^6$	w_2	Method ^a	η , in poises at			Q_{η} at 25°C. kcal.
			15.2°	25.0°	35.2°	
W-3	0.130	C	4.16	3.49	2.94	3.04
0.32	0.174	F	19.0	15.5	12.8	3.46
	0.239	F	106	83.2	66.7	4.05
	0.297	F	397	303	236	4.57
	0.345	F	1,122 ^b	757	635 ^c	5.00
	0.400	F	3,240 ^b	2,080	1,700 ^c	5.55
A	0.064	C	1.22	1.05	0.92	2.46
0.54	0.097	C	6.84	5.81	4.94	2.87
	0.119	C		18.3		
	0.166	F		94.5		
	0.224	F		471		
	0.240	F		983		
B	0.051	C	0.96	0.84	0.74	2.27
0.78	0.064	C	3.45 ^d	2.98	2.59 ^e	2.54
	0.085	C	14.58 ^d	12.28	10.48 ^e	2.93
	0.142	F		94.8		
	0.181	F		419		
	0.250	F		2,533		
N	0.050	C	2.86	2.48	2.19	2.35
1.1	0.070	C	10.95	9.44	8.12	2.61
	0.090	F	49.3	41.5	35.4	2.91
	0.120	F	138.8	115.1	97.0	3.15
E-1	0.058	F	413	354	303	2.77
4.0	0.084	F	3,040 ^b	2,400	2,140 ^c	3.03
	0.120	F	19,100 ^b	14,800	12,900 ^c	3.40
	0.152	F	65,200 ^b	49,000	43,300 ^c	3.70

^a C = capillary, F = falling ball.

^b At 12.2°C.

^c At 32.1°C.

^d At 15.0°C.

^e At 35.0°C.

latter two solvents, obtained in connection with intrinsic viscosity measurements, are presented in Table V.

Typical plots of the logarithm of viscosity against the reciprocal absolute temperature are shown in Figs. 1 and 2. As in the previous study on concentrated polyvinyl acetate solutions (1), such a plot approximates linearity over a narrow temperature range, but over a wider range (Fig. 2) there is a distinct upward curvature [this is also perceptible in Fig. 4 of Ref. (1)]. This departure from linearity has been noted for various liquids

TABLE III

Viscosities of Solutions in Decalin

Sample and $M\eta/10^5$	w_2	Method ^a	η , in kilopoises, at					$Q\eta$ at 25°C.
			-5°	10°	25°	40°	45°	
NBS	0.125	F	16.15	8.60	5.43	—	3.14	kcal. 5.47
1.35	0.152	F	46.85	25.34	15.35	—	8.50	5.70
	0.180	F	117.4	62.2	36.3	—	20.2	5.87
	0.221	F	399	200	114	—	61.1	6.25
W-2	0.0050	C	0.000318	0.000217	0.000156	0.000114	—	3.72
2.51	0.0101	C	0.00120	0.000815	0.000575	0.000426	—	3.82
	0.0154	C	0.00384	0.00254	0.00178	0.00130	—	3.85
	0.0200	C	0.00748	0.00483	0.00345	0.00258	—	3.88
	0.0292	F	0.0414	0.0268	0.0181	0.0131	—	4.13
	0.040	F	0.175	0.112	0.0738	0.0522	—	4.33
	0.049	F	0.510	0.313	0.205	0.144	—	4.46
	0.066	F	2.43	1.46	0.942	0.666	—	4.64
	0.098	F	18.8	10.7	6.73	4.49	—	5.05
	0.112	F	50.2	28.3	17.8	11.7	—	5.19
	0.143	F	174	93.6	52.3	33.9	—	5.69
	0.175	F	516	254	152	97.1	—	5.96
	0.200	F	945	493	268	172	—	6.33
FJ	0.158	F	15.30	7.94	4.63	—	2.56	5.81
1.00	0.192	F	45.7	23.4	13.58	—	6.88	6.34
	0.2185	F	93.8	48.2	27.8	16.86	—	6.51
	0.248	F	206	100	54.1	33.4	—	6.69

^a C = capillary, F = falling ball.

TABLE IV

Viscosities of Solutions in Decalin-Cyclohexanol

(Sample W-2, falling ball method)

w_2	η , in kilopoises, at					$Q\eta$ at 25°C. kcal.
	10°	20°	25°	30°	40°	
0.0300	0.0454	0.0317	0.0277	0.0242	0.0184	5.47
0.0402	0.193	0.134	0.113	0.0980	0.0740	5.64
0.0508	0.613	0.448	0.361	0.314	0.235	5.88
0.074	5.34	3.50	2.95	2.45	1.76	6.38
0.099	17.6	11.5	9.13	7.63	5.56	6.96
0.126	63.6	41.1	32.5	26.7	18.7	7.20
0.151	171	106	82.0	67.1	49.4	7.38
0.173	351	231	174	141	97.5	7.60
0.203	901	505	425	323	223	7.87

TABLE V

Relative Viscosities of Dilute Solutions in Decalin and Decalin-Cyclohexanol

(Sample W-2, capillary method, at 25°C.)

Decalin		Decalin-Cyclohexanol	
$\frac{c}{g/cc.}$	η_r	$\frac{c}{g/cc.}$	η_r
0.000408	1.227	0.000409	1.155
.000543	1.311	.000546	1.210
.000815	1.485	.000818	1.326
.001304	1.857	.001169	1.488
.001630	2.125	.001637	1.740
		.002046	2.012

and solutions (10, 11, 12). In undiluted bulk polyisobutylenes, the logarithm of the viscosity has been found to be a linear function of the *square* of the reciprocal absolute temperature (11, 12). Plots of the data of Tables III and IV against $1/T^2$ are more nearly linear than against $1/T$, but not exactly so. The apparent heats of activation, Q_η , have been calculated for comparison with other studies by measuring the slopes of plots against $1/T$ at 298°K.

For polyvinyl acetate solutions, plots of logarithm of relative viscosity (η_r) against the square root of the volume concentration, c_2 (grams of

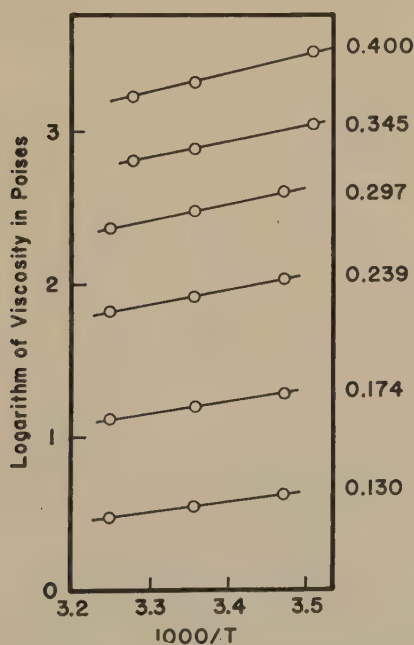


FIG. 1. Logarithm of viscosity plotted against reciprocal of absolute temperature for solutions of sample W-3 in xylene. Figures denote weight fraction of polymer.

polymer per cubic centimeters solution) were found to be approximately linear, with a slight upward curvature (1). To test this function for polyisobutylene solutions, relative viscosities at 25°C. were calculated from the data of Tables II-V, taking the viscosities of xylene, Decalin, and the mixture to be 0.0058, 0.0233, and 0.041 poises, respectively; the first value was taken (for *m*-xylene) from the International Critical Tables, and the others were measured directly. Volume concentrations were calculated from the densities of polymer and solvents (at 25°C., 0.91 and 0.860, 0.890, and 0.902, respectively) by assuming the volumes of polymer

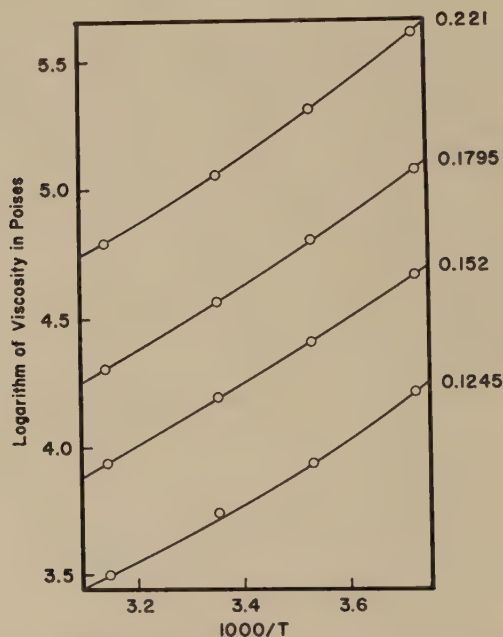


FIG. 2. Logarithm of viscosity plotted against reciprocal of absolute temperature for solutions of samples NBS in Decalin. Figures denote weight fraction of polymer.

and solvent to be additive. The results for all eight samples are shown in Fig. 3. Polyisobutylene differs from polyvinyl acetate in that at high concentrations there is downward rather than upward curvature. At low concentrations there is upward curvature, as exemplified by *W*-2, and necessarily by the other samples to reach the origin, with an inflection region of approximate linearity between.

For polyvinyl acetate, the function of Fig. 3 was found to be approximately independent of the nature of the solvent. In the present study, only one sample (*W*-2) has been measured in more than one solvent (Decalin and the mixture), and in this case the same conclusion is reached. It may

be further concluded that Decalin and xylene are equivalent on this basis, since the curves of Fig. 3 show a regular dependence on molecular weight. Thus, the logarithms of η_r interpolated at three selected concentrations are plotted against $\log M$ in Fig. 4, and at each concentration the points for the two solvents fall together on a single line.

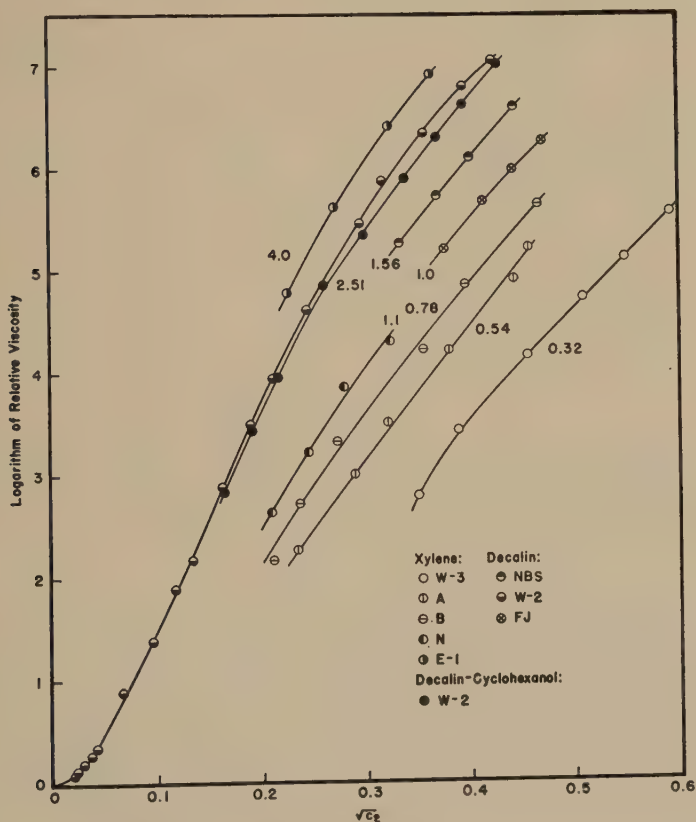


FIG. 3. Logarithm of relative viscosity at 25°C. plotted against square root of concentration in g./cc. for eight samples. Figures denote molecular weight in millions; weight-average for NBS, viscosity-average for the others.

Figure 4 also shows that, except for the lowest molecular weights at the lowest concentration, the dependence of $\log \eta_r$ on $\log M$ (viscosity-average for all samples except NBS; weight-average for the latter) at constant concentration can be approximated by a straight line with a slope of 3.4. An identical empirical dependence of viscosity on molecular weight was found for undiluted bulk polyisobutylenes by Fox and Flory (11).

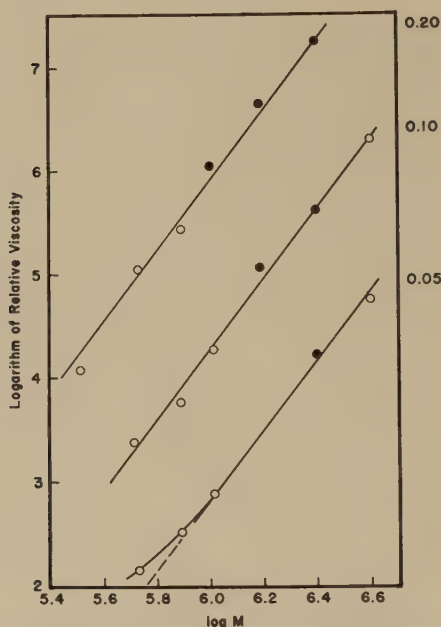


FIG. 4. Logarithm of relative viscosity at 25°C. plotted against logarithm of molecular weight at constant concentration (denoted by figures at right). Lines are drawn with a slope of 3.4. Open circles, in xylene; solid circles, in Decalin.

DISCUSSION

The apparent activation energies for viscous flow are plotted against concentration in Fig. 5. As found for polyvinyl acetate, this quantity increases roughly linearly with c_2 (except at low c_2), and increases only slightly with molecular weight. The values for *E*-1 and *W*-3, whose molecular weights differ by a factor of 12, are only about 0.5 kcal. apart. Fox and Flory (11) found the temperature dependence of viscosity of bulk polyisobutylene to be independent of molecular weight for $M > 17,000$. The presence of a slight molecular weight effect in solutions at much higher values of M might be thought of as due to an upward shift of this limit due to presence of solvent.

While Fig. 4 provides one empirical expression for the dependence of viscosity on molecular weight, an alternative method is suggested by the obvious relation between abscissas and slopes in Fig. 3. Weissberg, Simha, and Rothman (13), in treating the viscosity of moderately concentrated polymer solutions, recently utilized a reduced concentration $c_2 [\eta]$, and have shown that, when the viscosity is expressed as a function of this variable, curves for different molecular weights in the same solvent fall fairly close to each other. For combining data in different solvents, it

would not be appropriate to use $[\eta]$, since this depends on the solvent (Table I) and would cause the reduced concentration scale to vary in proportion, whereas in fact $\log \eta_r$ is approximately the same function of c_2 independent of the choice of solvent. Accordingly we try c_2 times some function of M as a reduced concentration. Empirically it is found that the choice of $c_2 M^{0.68}$ makes the data for all eight samples superpose rather closely on a single curve, as shown in Fig. 6 where $\log \eta_r$ is plotted against the square root of $c_2 M^{0.68}$.

It is interesting that the exponent 0.68 expresses almost exactly the dependence of intrinsic viscosity on molecular weight; at room temperature in cyclohexane and toluene (5), which closely resemble Decalin and xylene, respectively, the exponents a in the equation $[\eta] = KM^a$ are 0.69 and 0.67. It might be supposed, therefore, that the factor $M^{0.68}$ in

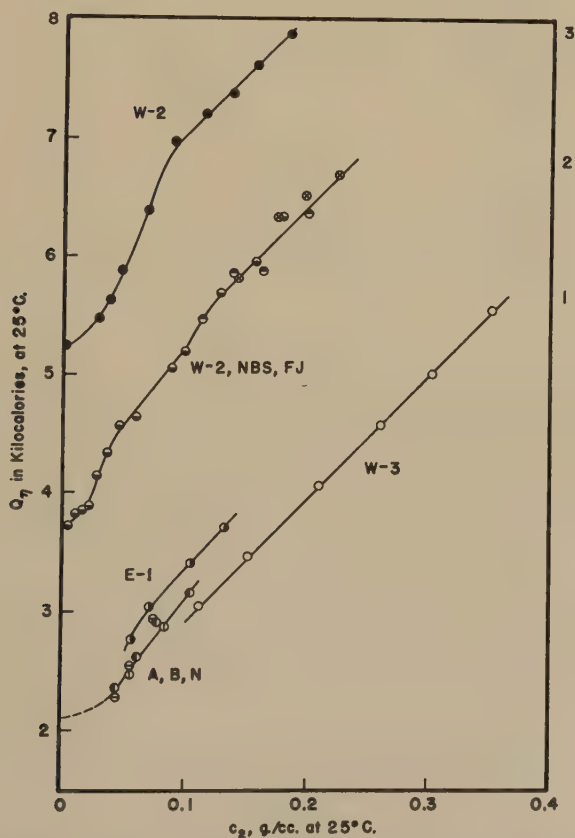


FIG. 5. Apparent activation energy for viscous flow at 25°C. plotted against concentration in g./cc. Symbols denote samples; key same as in Fig. 3. Curve 1, solutions in xylene; 2, in Decalin; 3, in Decalin-cyclohexanol.

our reduced concentration reflects the dimensions of the polymer coil (as measured, for example, by the radius of gyration, s), which in *dilute* solution are related in a simple manner to the intrinsic viscosity (14); specifically, s is proportional to $([\eta] M)^{\frac{1}{2}}$, or in this case $M^{0.56}$. However, in *concentrated* solution it is expected that, as in undiluted bulk polymer (15), the coil configuration would be more nearly random and its radius of gyration proportional to $M^{0.50}$. The significance of the exponent 0.68 is not yet clear, therefore.

If $\log \eta_r = f(c_2 M^{0.68})$ as indicated by Fig. 6 and $(\partial f / \partial \log M)_c = 3.4$ as indicated by Fig. 4, it must follow that $f = \text{const.} + 5.0 \log (c_2 M^{0.68})$, so that at constant molecular weight the relative viscosity is proportional

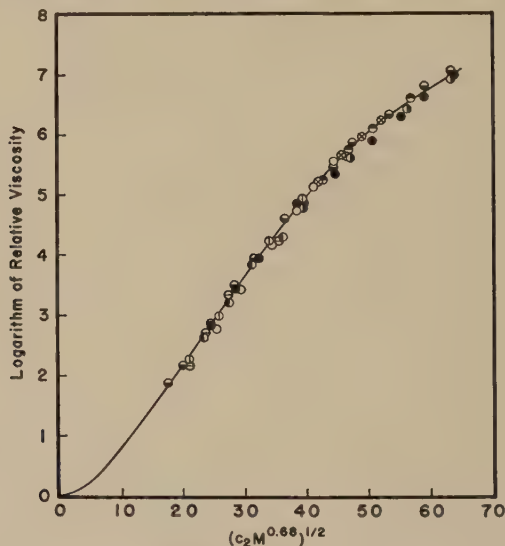


FIG. 6. Logarithm of relative viscosity at 25°C. plotted against the square root of $c_2 M^{0.68}$ for eight samples. Key same as in Fig. 3.

to the fifth power of the concentration. It is doubtful whether this relation has any theoretical significance, but it leads to the following empirical equation for dependence of viscosity at 298°K. on molecular weight and concentration:

$$\log \eta_{298} = \log \eta_0 - 11.0 + 5.0 \log c_2 + 3.4 \log M \quad [1]$$

where η_0 is the viscosity of the solvent at 298°K. This equation expresses the data of Fig. 6 within a logarithmic error of about 0.1 over the viscosity range from 1 to 10^6 poises.

In the first paper of this series (1), it was noted that the slope $d \log \eta / dc_2^{\frac{1}{2}}$, measured at $c_2 = 0.16$, is about $10 \text{ (g./cc.)}^{-\frac{1}{2}}$ for a variety of

polymer-solvent systems reported in the literature. This relation can be shown to be a consequence of a fifth power dependence on concentration; differentiation of Eq. [1] gives $d \log \eta / dc_2^{\frac{1}{5}} = 10/2.303 c_2^{\frac{1}{5}}$, which for $c_2 = 0.16$ equals 10.9. A dependence of the viscosity on the fifth power of concentration in polyisobutylene solutions has also been observed by DeWitt and Morrison (16). It should be noted, however, that this does not apply to either polyvinyl acetate (1) or polystyrene (17).

Equation [1] does not hold for moderately dilute or very dilute solutions, where the polymer coils overlap only partly or not at all and the hydrodynamic situation is quite different (13). It cannot hold in the concentration range approaching the pure polymer either, since the term $\log \eta_0$ must be eliminated as c_2 approaches ρ , the density of undiluted polymer. Nevertheless, it should serve for approximate prediction of viscosities of a wide variety of polyisobutylene systems.

It is of particular interest that the mixed solvent Decalin-cyclohexanol, though so poorly matched in cohesive energy density [as in the system polyvinyl acetate-diisopropyl ketone previously reported (1)], shows no abnormal viscosity behavior in the region in which Eq. [1] holds.

ACKNOWLEDGMENTS

This work was supported in part by the Research Committee of the Graduate School of the University of Wisconsin from funds supplied by the Wisconsin Alumni Research Foundation, and in part by a grant from Research Corporation. We are indebted to Mr. Lester D. Grandine, Jr., for assistance with calculations.

SUMMARY

The steady-flow viscosities of solutions of eight samples of polyisobutylene (four unfractionated, three rough fractions, and one sharp fraction), ranging in viscosity-average molecular weight from 0.32 to 4.0 million, have been measured in three solvents: five samples in xylene, three in Decalin, and one in a mixture of Decalin and cyclohexanol. The logarithm of the viscosity is not quite a linear function of the reciprocal absolute temperature. The apparent heat of activation for viscous flow at 25°C. increases with concentration in each solvent, approximately linearly with c_2 (grams of polymer per cubic centimeters of solution) above $c_2 = 0.1$. The dependence of viscosity in poises at 25° on concentration, molecular weight (M), and solvent viscosity (η_0) can be expressed by the empirical equation $\log \eta = \log \eta_0 - 11.0 + 5.0 \log c_2 + 3.4 \log M$, over a range of $\log \eta$ from 0 to 6. The relations between this equation and other empirical viscosity expressions are discussed.

REFERENCES

1. FERRY, J. D., FOSTER, E. L., BROWNING, G. V., AND SAWYER, W. M., *J. Colloid Sci.* **6**, 377 (1951).

2. FERRY, J. D., FITZGERALD, E. R., JOHNSON, M. F., AND GRANDINE, L. D. JR., *J. Applied Phys.* **22**, 717 (1951).
3. JORDAN, I., AND EVANS, W. W., unpublished experiments.
4. ASHWORTH, J. N., AND FERRY, J. D., *J. Am. Chem. Soc.* **71**, 622 (1949).
5. FOX, T. G., JR., AND FLORY, P. J., *J. Phys. & Colloid Chem.* **53**, 197 (1949).
6. FLORY, P. J., *J. Am. Chem. Soc.* **65**, 372 (1943).
7. MARVIN, R. S., Interim Report, National Bureau of Standards, April 25, 1951; and private communications.
8. SEYER, W. F., AND WALKER, R. D., *J. Am. Chem. Soc.* **60**, 2125 (1938).
9. BACON, L. R., *J. Franklin Inst.* **221**, 251 (1936).
10. DOOLITTLE, A. K., *J. Applied Phys.* **22**, 1031, 1471 (1951).
11. FOX, T. G., JR., AND FLORY, P. J., *J. Phys. & Colloid Chem.* **55**, 221 (1951).
12. LEADERMAN, H., private communication.
13. WEISSBERG, S. G., SIMHA, R., AND ROTHMAN, S., *J. Research Natl. Bur. Standards* **47**, 298 (1951).
14. FLORY, P. J., AND FOX, T. G., JR., *J. Am. Chem. Soc.* **73**, 1904 (1951).
15. FLORY, P. J., *J. Chem. Phys.* **17**, 303 (1949).
16. DEWITT, T. W., private communication.
17. FERRY, J. D., GRANDINE, L. D., JR., AND UDY, D. C., to be submitted to *J. Colloid Sci.*

STUDIES ON ION-EXCHANGE RESINS. V. WATER VAPOR SORPTION ¹

Harry P. Gregor, Benson R. Sundheim,² Kalman M. Held,³
and Monroe H. Waxman ⁴

Department of Chemistry, Polytechnic Institute of Brooklyn, Brooklyn, New York

Received February 26, 1952

INTRODUCTION

The thermodynamics of the water sorption process (sorption being defined as total uptake of water vapor by an absorbent) was studied for ion-exchange resins to establish relationships between structure, physical properties, and exchange properties. The reaction of ion-exchange resins with water involves solvation of ionic charges, swelling (presumably against entropy springs), and entropy of mixing. The system is too complex for a direct and exact theoretical approach. While the statistics of cross-linked nonionic polymers have been studied, this treatment is not applicable to strong acid ion-exchange resins because these systems are concentrated strong electrolytes, and involve the interaction of water dipoles with fixed charges, as well as the interaction of fixed charges among themselves. The general literature has been discussed by McLaren and Rowen (25) and Hermans (20); some sorption data on ion-exchange resin systems has appeared (16, 26).

Experimental data have been obtained which allow the calculation of changes in the entropy, free energy, and heat content of the system during the sorption process. This paper reports the results of preliminary studies using a number of commercially available resins, including a cross-linked (10%), sulfonated polystyrene resin in a number of ionic states, a series of the same type of resins with varying degrees of cross-linking, a carboxylic acid resin, and a quaternary amine resin.

¹ The authors thank the Office of Naval Research for the support given to this work.

² Present address: New York University, N. Y.

³ A portion of this work is abstracted from the dissertation of Kalman M. Held submitted in partial fulfillment of the requirements for the degree of Doctor of Philosophy in Chemistry, Polytechnic Institute of Brooklyn, June, 1951. The author was the recipient of an Atomic Energy Commission Pre-Doctoral Fellowship.

⁴ A portion of this work is abstracted from the dissertation of Monroe H. Waxman submitted in partial fulfillment of the requirements for the degree of Doctor of Philosophy in Chemistry, Polytechnic Institute of Brooklyn, June, 1952.

EXPERIMENTAL METHODS

A. Resins

Three different types of resins were used. A series of sulfonated polystyrene-divinylbenzene copolymers (Dowex 50, Dow Chemical Co.) containing different amounts of the cross-linking agent are referred to by their designated percentages of divinylbenzene, as DVB 1, 2, etc., but are not the resins described earlier (14). The resins were conditioned, put in the hydrogen state, and dried to constant weight in a vacuum oven at 40°C. (15). One of these resins, DVB 10 (commercial Dowex 50), was put into ten different ionic states, and then dried in an oven at higher temperatures. The hydrogen resin reached the same, constant weight at 112°C. as under vacuum at 40°C.

The capacity of DVB 10 hydrogen resin was 4.80 mequiv./g. dry hydrogen resin, corresponding to an equivalent weight of 208.3 g. This resin in various cationic states was dried at temperatures ranging from 112 to 140°C. Two-gram samples were kept for 1 month at 120°C. without loss in weight (< 1 mg.). Thus it may be seen that the dry weight of the resin is a well-defined experimental value; the difficulties encountered in the case of protein systems (1) are not met.

A carboxylic cation-exchange resin (Amberlite IRC-50, Rohm and Haas Company) was used. This resin is similar to those prepared by copolymerization of methacrylic acid with 10% divinylbenzene. The resin was used in the hydrogen state, in the potassium state (prepared by neutralization with the base), and in partially neutralized states.

A quaternary base anion-exchange resin (Dowex 2, Dow Chemical Co.) was studied in the chloride and iodate states. This resin contains about 10% cross-linking; its exchange groups are the benzyl-dimethylethanolammonium ion.

B. Water Sorption Apparatus

The sorption of water was measured using both a humidistat and a McBain balance. The humidistat in which isopiestic studies were made consisted of a set of eight 10-in. Pyrex desiccators mounted in a large enclosed tank, the lower portion of which was filled with water to a depth of 6 in. Both the water and the air above the desiccators were supplied with appropriate heaters and cooling and circulating devices so that the temperature was maintained at $25.0 \pm 0.1^\circ\text{C}$. Each desiccator contained approximately 1 l. of sulfuric acid at a concentration appropriate to the desired relative humidity (21).

Both the acid solutions and the air in the desiccators were continually stirred by means of propellers attached to a vertical metal shaft. This shaft passed through an Oilite bearing mounted in the desiccator top; the seal proved to be sufficiently air-tight to maintain a constant relative

humidity in each desiccator over a period of months. For example, in a desiccator where the relative humidity (R.H.) was 2%, there was no appreciable change ($< \pm 0.1\%$ R.H.) over a period of a few months.

Samples of the resin (0.5–2.0 g.) were weighed into 60×30 mm. low-form weighing bottles; equilibrium, indicated by the sample coming to constant weight, was attained in 2 to 5 days. The weight fluctuations with time were studied and are discussed later.

To determine the effect of permanent gases in the system, a sorption curve was also run for a typical resin, DVB 10 in the hydrogen state, in a McBain balance which employed quartz springs with an evacuated system. The quartz spirals were similar in characteristics to those described by McBain and Bakr (24); the experimental vapor pressures were read directly using a mercury manometer.

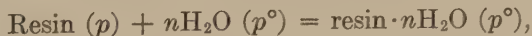
C. Volume Measurements

The specific resin volumes were determined pycnometrically, using centrifugation as described by Gregor, Held, and Bellin (16); determinations for resins at relative humidities less than 100% used octane as the inert liquid.

D. Calorimetric Measurements

The calorimeter employed was of the isothermal Bunsen type (2); the dilatometric and heat-transfer medium was diphenylmethane (DPM) (7, 27) having a phase change at $24.48^\circ\text{C}.$, at which temperature measurements were made. The calorimeter proper was immersed in a large Dewar flask filled with DPM slush, the entire apparatus being contained in an air thermostat at $24.48^\circ\text{C}.$ This apparatus was calibrated electrically using a standard circuit described by Daniels, Mathews, and Williams (3). Thermal equilibrium was established within 20 min. The average error for each determination was $\pm 3.0\%$. Heats varying from 20 to 500 cal. could be measured with this apparatus.

The heat of sorption was measured by mixing a 2–4 g. sample of resin (equilibrated in the humidistat at a specific relative humidity) with an excess (20 g.) of water in the calorimeter chamber. The reaction measured was



with p/p° varying from zero to unity. The reproducibility of this measurement is satisfactory; seven duplicate determinations made with dry DVB 10-*K* resin ($p = 0$) gave a mean value of -21.71 ± 0.56 cal./g. dry resin. All experiments were performed at $25^\circ\text{C}.$, unless otherwise stated.

EXPERIMENTAL RESULTS

In evaluating sorption data on high polymeric systems, it is essential to establish the presence or absence of hysteresis (25). For the experi-

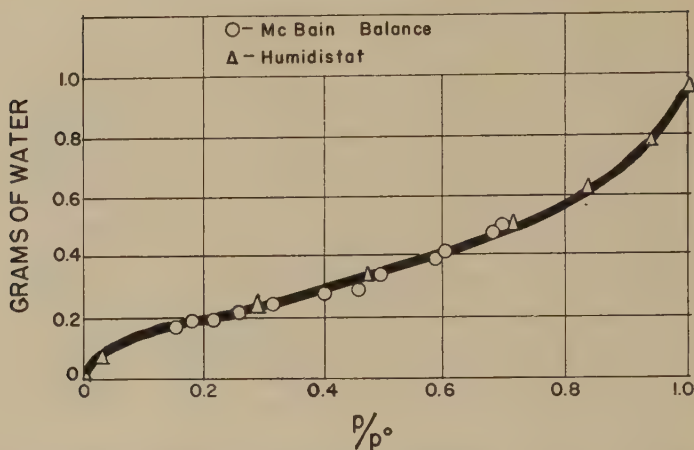


FIG. 1. Sorption of water by 1 g. DVB 10-*H*, measured by McBain Balance (O) and Humidistat (Δ).

ments performed thus far, there appears to be a small but consistent difference between the ascending and descending curves, the former being lower than the latter. At any given relative humidity this difference is never more than 1%. Since the reproducibility of each determination is about $\pm 0.4\%$, it appears that the hysteresis effect is real but extremely small. It remains to be determined if this is a rate process.

A comparison of results obtained with the humidistat and with the McBain balance with DVB 10-*H* are shown in Fig. 1. Satisfactory agreement is observed. Evidently the presence of air does not affect the sorption of water. Although the McBain balance system does come to equilibrium more rapidly than does the humidistat, the latter allows the simultaneous measurement of many samples at one time.

TABLE I

Moles of Water Sorbed at Various Relative Humidities by Equivalent Weights of Resin DVB 10

Ionic state	Per cent relative humidity						
	2.5	29	47	71	83	94	100
H ⁺	1.08	2.84	4.00	5.85	7.24	9.15	10.18
K ⁺	0.60	1.61	2.27	3.35	4.32	6.14	7.63
Na ⁺	0.72	1.95	2.76	4.23	5.49	7.49	8.83
Li ⁺	0.93	2.22	3.17	5.02	6.49	8.63	10.05
NH ₄ ⁺	0.65	1.63	2.31	3.48	4.51	6.11	7.78
Ag ⁺	0.58	1.46	1.94	2.74	3.40	4.59	6.73
(CH ₃) ₄ N ⁺	0.58	1.83	2.54	3.93	4.86	5.93	6.72
Mg ⁺⁺	1.90	3.09	4.00	5.52	6.57	7.91	10.03
Ca ⁺⁺	1.18	2.29	3.01	4.28	5.41	6.92	8.81
Ba ⁺⁺	1.09	2.13	2.78	3.76	4.46	5.41	7.18

TABLE II

Grams of Water Sorbed at Various Relative Humidities Per Gram of Hydrogen Resin Having Different Degrees of Cross-Linking

DVB	Per cent relative humidity							
	66.3	75.8	77.7	83.6	88.0	92.0	95.5	97.4
0.5	0.510	0.645	0.691	0.822	0.961	1.218	1.920	2.296
1	0.477	0.624	0.662	0.778	0.906	1.115	1.733	2.043
2	0.488	0.616	0.677	0.788	0.908	1.131	1.643	1.924
4	0.478	0.617	0.657	0.757	0.867	1.051	1.415	1.543
8	0.480	0.618	0.627	0.709	0.787	0.888	1.036	1.083
12	0.431	0.541	0.540	0.580	0.614	0.664	0.715	0.731
16	0.323	0.387	0.416	0.444	0.468	0.503	0.537	0.550
24	0.216	0.235	0.246	0.243	0.246	0.261	0.283	0.287

Data for the sorption of water by DVB 10 in ten different cationic states are tabulated in Table I. The data are presented in terms of n , the moles of water sorbed per equivalent of resin; and as a function of p/p° , the relative humidity, hereafter referred to as x . The equivalent weight was determined by titration of the hydrogen state, as described by Gregor and Bregman (12). The capacity of the resin is the same for all cations (14).

Water sorption data for sulfonic acid resins with different degrees of cross-linking are shown in Table II. Here water uptake is shown as grams of water per gram of dry hydrogen resin. Relative humidities from 66 to 97% are shown here; this range was selected because the effect of cross-linking is most noticeable in this region. Extensive studies over the entire x range with the resins in various states are to be presented in a later paper.

Fluctuations in the weights of resin samples at different relative humidities were studied to determine the precision of the measurements. All values given in this paper represent the average of at least ten weighings, made after the system reached constant weight. The relative average

TABLE III

Moles of Water Sorbed at Various Relative Humidities by Equivalent Weights of Carboxyl Resin

x	H ⁺	70% H ⁺ , 30% K ⁺	40% H ⁺ , 60% K ⁺	K ⁺
0.04	0.11	0.07	0.23	0.30
0.15	0.33	0.44	1.04	1.28
0.28	0.48	0.70	1.45	1.82
0.47	0.70	1.10	2.35	3.09
0.73	1.09	1.91	3.79	4.79
0.83	1.42	2.56	5.30	6.29
0.95	1.95	4.49	7.71	8.73
1.00	3.82	—	—	11.30

TABLE IV

Moles of Water Sorbed at Various Relative Humidities by Equivalent Weights of Quaternary Base Resin

Moles of water sorbed		
x	Cl^-	IO_3^-
0.04	0.27	0.27
0.15	1.11	1.25
0.28	1.45	1.92
0.47	2.50	3.31
0.73	4.00	5.74
0.83	5.92	8.49
0.95	8.54	12.10
1.00	14.14	17.65

deviations due to fluctuations range from a minimum of 0.5% in the case of DVB 24 at the lowest relative humidities to a maximum of 4% in the case of DVB 0.5 at the highest relative humidities. Therefore the highest relative standard deviations are 1.1%, and very much less than this value in all but the case of the highest relative humidities.

Sorption data for the carboxyl resin are presented in Table III as moles of water sorbed per equivalent of resin. The exchange capacity of this resin is 9.32 mequiv./g. hydrogen resin. Data for the quaternary base anion-exchange resin are shown in Table IV; here the capacity of the resin was 2.26 mequiv./g. in the dry chloride state.

Volume data are expressed as milliliters per gram of resin in the hydrogen state. The specific volumes of resin DVB 10 in various dry states are: H^+ , 0.696; Li^+ , 0.702; Na^+ , 0.730; K^+ , 0.763; NH_4^+ , 0.792; $(\text{CH}_3)_4\text{N}^+$, 1.130; Ag^+ , 0.685; Mg^{++} , 0.707; Ca^{++} , 0.720; Ba^{++} , 0.726. Table V shows the increase in volume over that of the dry state ($V - V_m$) at various relative humidities for this resin.

TABLE V

Change in Volume in Milliliters per Gram of H^+ Resin ($V - V_m$) with Relative Humidity for Resin DVB 10

Ionic state	Per cent relative humidity						
	2.5	29	47	71	83	94	100
H^+	0.102	0.206	0.296	0.453	0.567	0.728	0.828
Li^+	0.063	0.155	0.234	0.383	0.508	0.692	0.801
Na^+	0.037	0.120	0.180	0.298	0.406	0.572	0.688
K^+	0.034	0.102	0.150	0.238	0.321	0.473	0.594
Mg^{++}	0.120	0.191	0.280	0.402	0.491	0.602	0.794
Ca^{++}	0.072	0.147	0.199	0.299	0.391	0.513	0.652
Ba^{++}	0.065	0.139	0.182	0.257	0.315	0.392	0.538
Ag^+	0.038	0.096	0.134	0.197	0.249	0.347	0.524
NH_4^+	0.043	0.106	0.154	0.254	0.338	0.474	0.617
$(\text{CH}_3)_4\text{N}^+$	0.032	0.119	0.182	0.298	0.374	0.470	0.493

TABLE VI

Integral Heat of Sorption for Resin DVB 10

x	Calories per equivalent dry resin
0.040	-2321
0.150	-3754
0.280	-4515
0.475	-4804
0.725	-5265
0.825	-5391
0.947	-5379
1.000	-5265

The heat of hydration of DVB 10-*K* was calculated for the process,



where p/p° varies from 0 to 1. Calculations were made using Hess's law; these values are shown in Table VI in terms of calories per equivalent of dry resin.

DISCUSSION

This discussion will consider first the general characteristics of the water vapor sorption curves of sulfonic acid resins. There exists a striking analogy between the sorption curves for cross-linked polystyrene sulfonic acid and certain low-molecular-weight strong electrolytes. Of the compounds available for this purpose, *p*-toluenesulfonic acid is chemically the most similar to the resin, but cannot be used because of its limited solubility. On the other hand, the bisulfate ion, present in concentrated solutions of sulfuric acid, is sufficiently like the aromatic sulfonate ion for purposes of comparison.

In order to use the vapor pressure curve of sulfuric acid, the osmotic equivalent weight rather than the molecular weight must be taken. The osmotic equivalent weight of sulfuric acid is taken as half the molecular weight because the secondary ionization is negligible in concentrated solutions.

Low-molecular-weight sulfonic acids clearly have a dissociation number (ν) of two. Although in cross-linked systems the sulfonic acid group maintains its high degree of dissociation (as shown by titration (12) and conductivity curves), it is not likely that in the cross-linked resin the fixed sulfonic acid ions are still osmotically active.

In order to clarify this point, the vapor pressure curves of DVB 10-*H* are presented in Fig. 2, as moles of water sorbed per equivalent (n) against x . Curves are shown assuming ν to be one and two, respectively. The sorption curve for sulfuric acid is shown for purposes of comparison, with ν equal to two. The data clearly show that the value of ν equal to one must be selected for closest fit with sulfuric acid.

It is seen from Fig. 2 that the curves for the resin ($\nu = 1$) and sulfuric acid are very similar for values of x less than 0.7; this latter point corresponds to about 5 molal sulfuric acid and 10 molal polystyrene sulfonic acid resin. At higher relative humidities the sulfuric acid curve rises sharply while the resin reaches a state of limited swelling. At the point x equals 0.8, the bisulfate ion is about 5% ionized, enough to lower the vapor pressure perceptibly, and the choice of a dissociation number of two for sulfuric acid is no longer valid.

The data of Fig. 2 are also shown as a Raoult's law plot in Fig. 3, for ν equal to one and two, corresponding to one and two osmotic equiv-

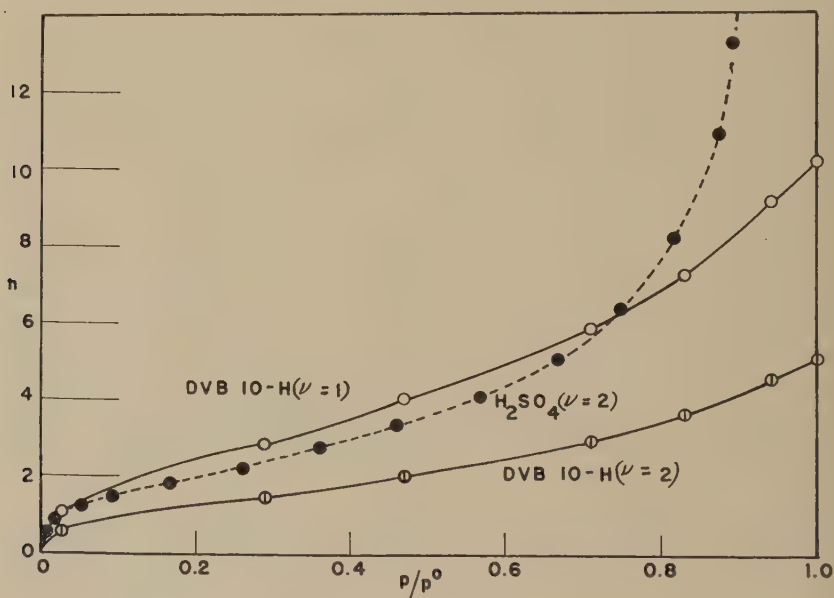


FIG. 2. Moles of water sorbed per mole of DVB 10-H calculated as $\nu = 1$ (O), $\nu = 2$ (⊙), and per half mole of sulfuric acid (●).

alents. Here again, a value of one for ν for the resin is definitely the best. It may be well to emphasize that the value of $\nu = 1$ for DVB 10-H is in no way connected with association or ion-pair formation; rather the significance must lie in the immobility of the fixed anionic group.

Other authors have pointed out the parallelism between the sorption of water by various adsorbents, such as cellulose, and by sulfuric acid (22, 28); comparisons have been made by fitting curves and selecting values of ν which are much less than unity in terms of each monomeric group. In this work the obvious value of ν gives excellent agreement between acid and polymer.

The plot of Raoult's law points up an unusual feature of this system, namely that the components, resin and water, are completely miscible at low water mole fractions, but become completely immiscible at higher mole fractions, where the resin-rich phase is completely insoluble in water.

These special properties of the resin-water systems make it impossible to utilize standard thermodynamic methods of calculating ν which involve

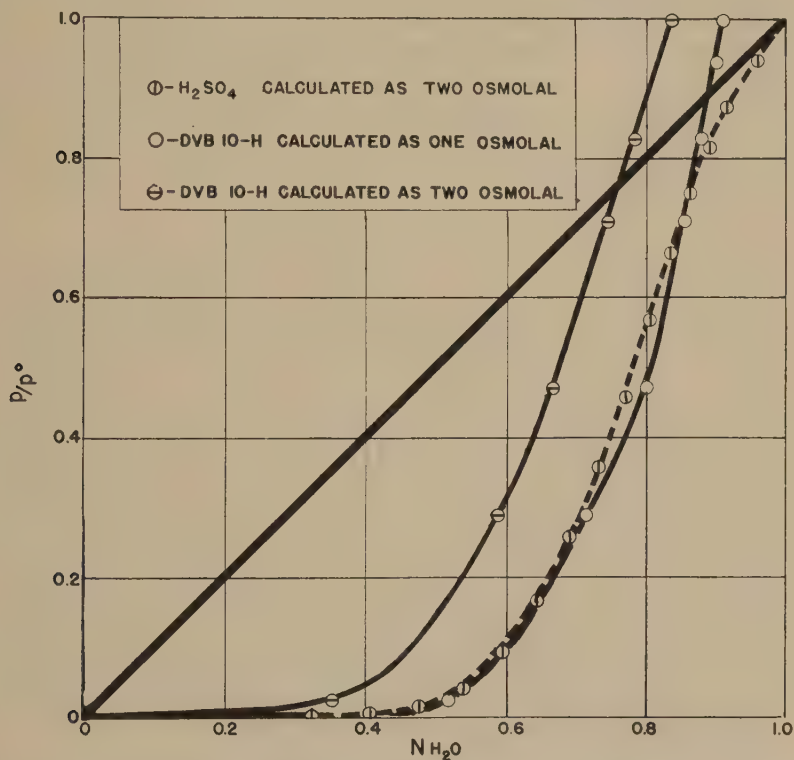


FIG. 3. Raoult's law plot of the systems: sulfuric acid-water calculated as two osmolal (\oplus); DVB 10-*H*-water calculated as one (\circ) and two (\ominus) osmolal.

extrapolation to infinite dilution. For example, one cannot make use of the concept of the osmotic coefficient

$$\phi\nu = - \frac{128.2 \log_{10} a_1}{m_2}$$

where ϕ is the practical osmotic coefficient, and the subscripts 1 and 2 refer to solvent and solute phases respectively (18). This type of calculation for sulfuric acid and DVB 10-*H* is shown in Fig. 4, where the ordinate values for sulfuric acid have been divided by 2. In concentrated sulfuric

acid solutions ν is equal to 2, and since ν is 1 for the resin, the two curves are identical for concentrations greater than $16m$. The sulfuric acid curve begins to approach $\phi\nu = 1$, but rises sharply in dilute solutions, approaching 1.5 ($3\phi/2$) at infinite dilution, because of the secondary ionization. The resin curve drops sharply because of limited swelling, intersecting the abscissa at finite concentrations.

This behavior must be shown by all cross-linked resins; the value of m_2 corresponding to $\phi\nu = 0$ will decrease with less cross-linking. Therefore values of ν for cross-linked resins cannot be determined by extrapolation techniques, because the extrapolation refers to a state which is not even conceptually possible. Gleuckauf and Duncan (8) have attempted to calculate values of ν by such extrapolation techniques for lightly cross-linked resins.

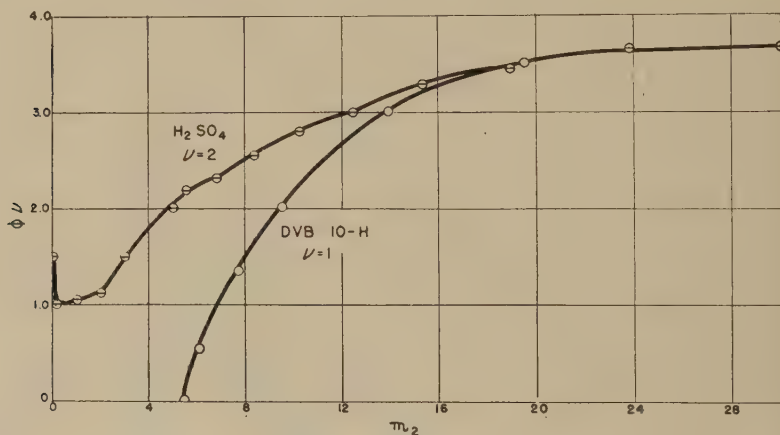


FIG. 4. Osmotic coefficient plots for sulfuric acid (\ominus) and DVB 10-H resin (\circ). Experimental values of $\phi\nu$ for sulfuric acid have been divided by two.

Thus it appears that cross-linked polystyrene sulfonic acid systems behave as simple, strong electrolytes over an extraordinarily wide range of concentrations, with the sulfonate groups exhibiting essentially no osmotic activity.

The data of Table I are shown plotted in Figs. 5, 6, and 7. The four curves in Fig. 5 form a family ($H^+ > Li^+ > Na^+ > K^+$) in that the resin containing the ion which is most heavily hydrated in aqueous solution sorbs the most water. The principal differences between the curves may thus be ascribed to the hydration of the cations or, in more formal terms, the mean activity coefficient of the polyelectrolyte. Therefore, there seems to be no specific chemical interaction between the ions and the resin matrix for these systems.

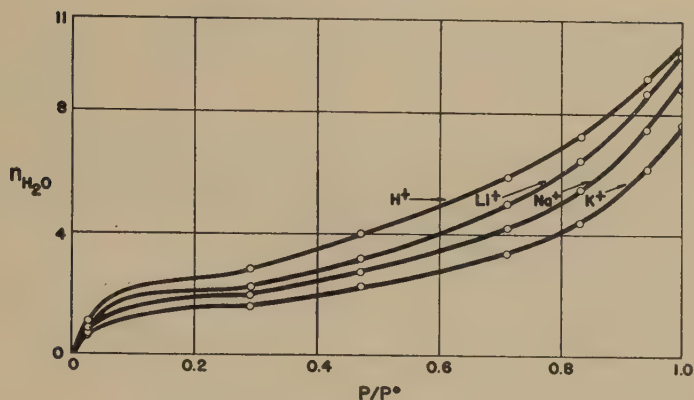


FIG. 5. Moles of water sorbed by one equivalent of DVB 10 resin in the hydrogen and alkali metal states.

For the bivalent ions shown in Fig. 6 (Mg^{++} , Ca^{++} , Ba^{++} , K^+), the most strongly hydrated, Mg^{++} , gives a very sharp initial uptake, considerably higher than that observed with the univalent cations. This is to be expected from the hydration series [see for example the hydration numbers calculated by Stokes and Robinson (29)]. The curve for Ca^{++} falls under the Mg^{++} curve as expected and has a similar shape. However, for the Ba resinate, this curve starts similarly to the Ca resinate, but as the relative humidity is increased it falls lower than would be expected if it followed the family of bivalent resinate curves. A possible explanation of this behavior lies in the comparative values of the activity coefficients of the alkaline earth salts in aqueous solutions (17). The activity coefficients of Ba^{++} salts fall considerably below those of the Mg^{++} and Ca^{++}

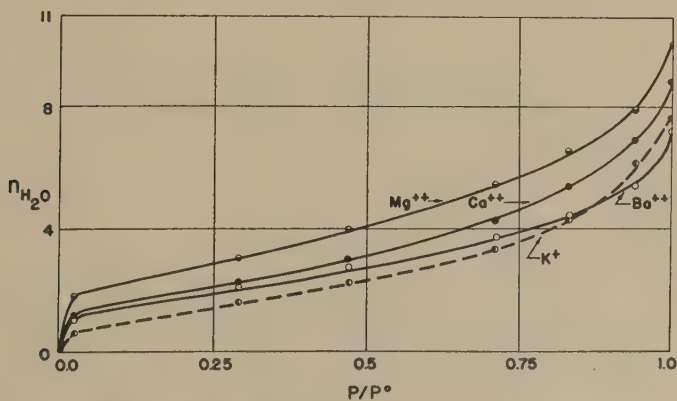


FIG. 6. Moles of water sorbed by one equivalent of DVB 10 resin in various bivalent cationic states.

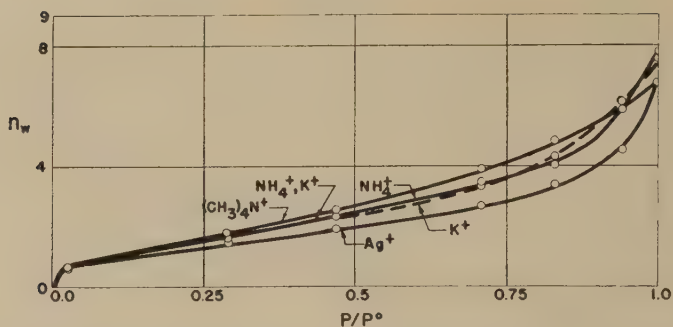


FIG. 7. Moles of water sorbed by one equivalent of DVB 10 resin in the NH_4^+ , Ag^+ , and $(\text{CH}_3)_4\text{N}^+$ states.

salts; the activity of water in the Ba resinate will be correspondingly raised. It is also possible that the barium ion forms associated ion-pairs with the fixed, exchange groups (9, 15). In this case the degree of dissociation of the ion-pair would increase with increasing dilution of the resin phase, making for increased water sorption.

As shown in Fig. 7, the curves for the K^+ and NH_4^+ resins are almost the same, in accordance with the fact that in aqueous solutions these ions behave similarly, their hydrated ionic volumes being almost identical. In the case of silver there is probably a specific interaction

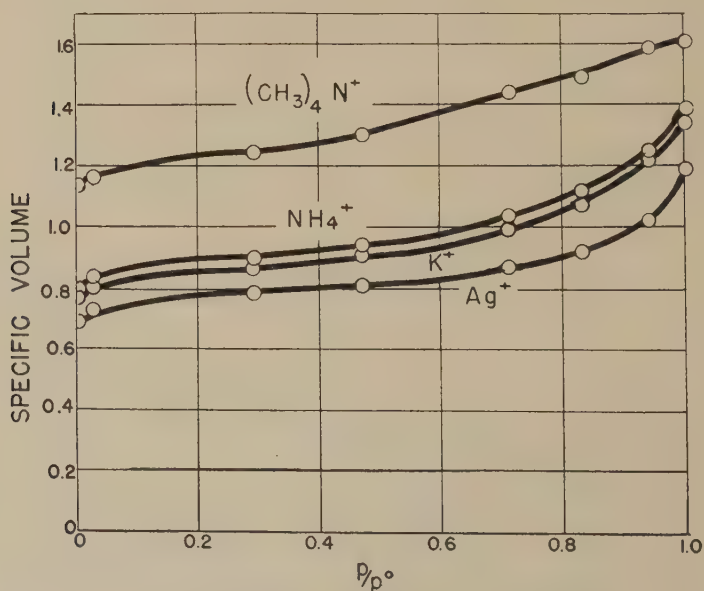


FIG. 8. Specific volumes in milliliters of DVB 10 resins as a function of relative humidity.

between the sulfonate and silver ions; studies of distribution coefficients and resin volumes with the silver ion (4, 15) are indicative of ion-pair formation.

The tetramethylammonium curve is quite different from those for the other systems; it is distinctive largely because its slope is very much lower at high relative humidities. Three explanations suggest themselves: While activity coefficient effects may be responsible, the data available from the literature are inadequate. Second, the abnormally high osmotic

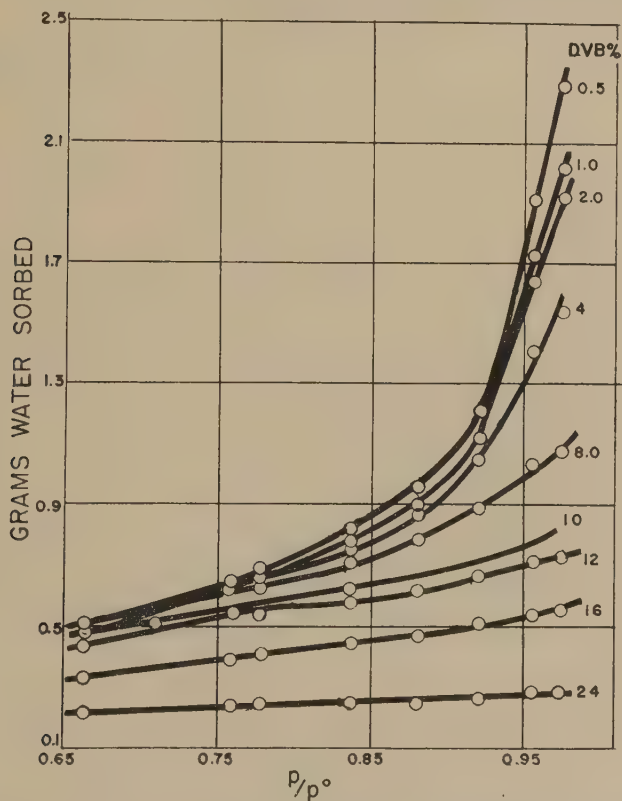


FIG. 9. Grams of water sorbed by 1 g. of various DVB resins in the hydrogen state.

pressures which result because the ion itself is so large, reduce water uptake; Fig. 8 shows specific resin volumes as a function of x . Third, the organic cation is known to be adsorbed onto the resin matrix (13). It may be that this adsorptive effect increases as the resin imbibes more water, thus making for less water uptake.

Data for the sorption of water by hydrogen resins having varying degrees of cross-linking are shown in Fig. 9. Each curve has the same,

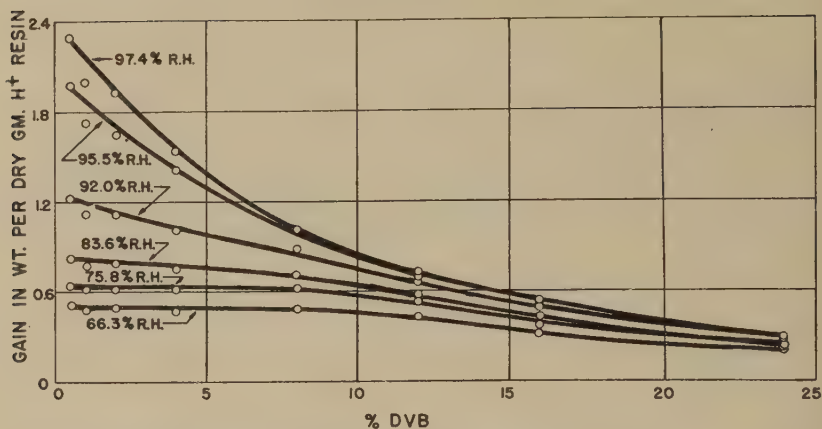


FIG. 10. Sorption of water by 1 g. of various DVB resins in the hydrogen state, plotted as a function of per cent DVB.

general shape as that for DVB 10; the sorption of water follows directly with decreasing degree of cross-linking. These data can also be plotted as the gain in weight *vs.* the percentage of DVB for individual values of x ; this is shown in Fig. 10. From Figs. 9 and 10 it may be observed that resin DVB 1 does not fall into its proper position. This resin may have been mislabeled by the manufacturer. While there is obviously a relationship between the degree of cross-linking of a resin and its sorption characteristics, no theoretical treatment is as yet available.

Sorption data for the carboxylic resin in the hydrogen and potassium states, also for two resins representing partially neutralized states, are presented in Fig. 11. The positions of the K^+ and H^+ curves are reversed from the order found with sulfonic acid resins because here the H^+ state

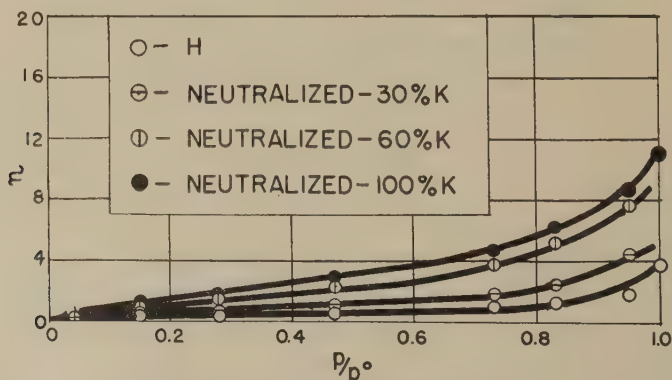


FIG. 11. Moles of water sorbed per mole of carboxylic acid resin in the hydrogen state (O), neutralized 30% (⊖), 60% (⊕), and 100% (●) with potassium hydroxide.

is relatively undissociated. Another point of interest is that the general shape of these sorption curves does not exhibit the sharp, initial rise observed with the sulfonic resins. They may be due partly to the low degree of hydration of the potassium ion and partly to some hydration of the sulfonic acid group.

Sorption data for the quaternary ammonium resin in the Cl^- and IO_3^- states are shown in Fig. 12. Here, too, the general shape of the curves is different from those for the sulfonic acid resins, particularly in the region of low relative humidity, where it is similar to those for the carboxyl resins. The resin in the iodate state sorbs considerably more

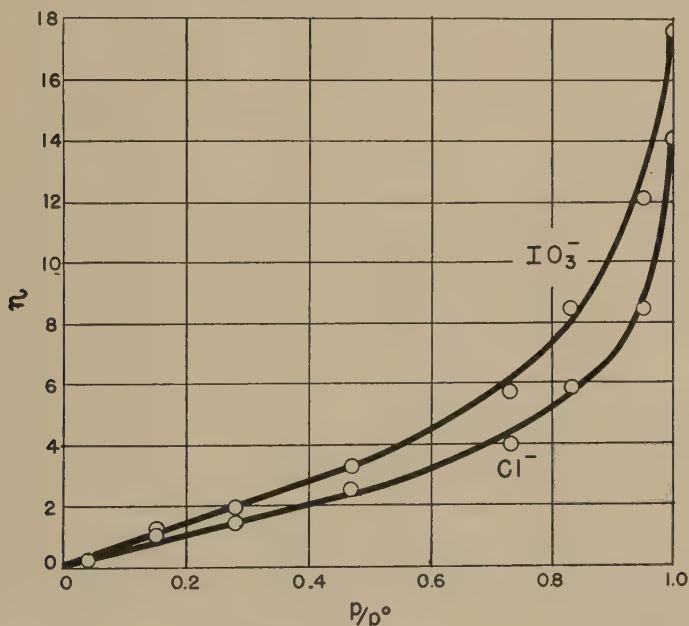


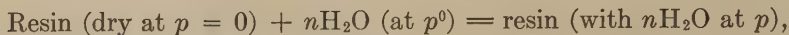
FIG. 12. Moles of water sorbed per mole of quaternary ammonium resin in the chloride and iodate states.

water than the resin in the chloride state. It is unlikely that these effects are due to differences in hydration. It can be postulated that this effect is due to the formation of an ion-pair between the Cl^- and the exchange group. A considerable body of independent evidence in terms of selectivity coefficient data exists to support this hypothesis (10, 11).

Attempts have been made to fit the various sorption curves presented in this paper with various theoretical adsorption isotherms. The Langmuir isotherm obviously does not apply; the two-parameter Brunauer-Emmett-Teller (B.E.T.) isotherm can be fitted to curves for the carboxyl and quaternary ammonium resins, but not to data for the sulfonic acid resins. A

three-parameter isotherm of the type developed by White and Eyring (30) can be applied to both types of curves. This treatment will be presented in a later paper.

From the water sorption data, it is possible to calculate the free energy of sorption of water vapor by the resins; this method is described by Bull (1) and by Dole and McLaren (6). The reaction under consideration is



where p/p^0 varies from 0 to 1. For this reaction, the partial molar free energy increase $\Delta\bar{F} = RT \ln x$. It can be shown (6) that the integral free

TABLE VII
Decrease in Free Energy for the Water Sorption Process with DVB 10 in Various Cationic States

x	Ca^{++}	Mg^{++}	Ag^+	NH_4^+	Li^+
0.025	3330	5553	1668	1881	2653
0.29	5680	7446	3451	3645	5188
0.47	6126	7989	3768	4073	5848
0.71	6667	8568	4055	4485	6478
0.83	6876	8804	4185	4697	6775
0.94	7034	8990	4319	4854	7017
1.00	7083	9040	4356	4897	7076
x	$(\text{CH}_3)_4\text{N}^+$	Na^+	Ba^{++}	H^+	K^+
0.025	1678	2076	3093	3061	1250
0.29	3822	4240	5362	6523	3680
0.47	4316	4764	5773	7289	4080
0.71	4816	5257	6131	7965	4495
0.83	5015	5505	6292	8258	4620
0.94	5158	5694	6399	8435	4780
1.00	5211	5753	6466	8484	4846

energy change is

$$\Delta F = -RT \int_x^1 n d \ln x + n RT \ln x.$$

Thus by graphical integration of the plot of $-nRT/x$ against x and addition of the term $nRT \ln x$, the free energies of hydration can be calculated; this has been done for several of the resin systems described in this paper. The results of these calculations are shown in Table VII, and are plotted in Figs. 13 and 14.

A comparison of the sequence of free energies of hydration for the cationic states of DVB 10 with the Stokes-Robinson (29) hydration numbers is presented in Table VIII. Since the free energies have been calculated in terms of calories per equivalent of resin, the Stokes-Robinson molar hydration number for the cations Mg^{++} , Ca^{++} , and Ba^{++} have

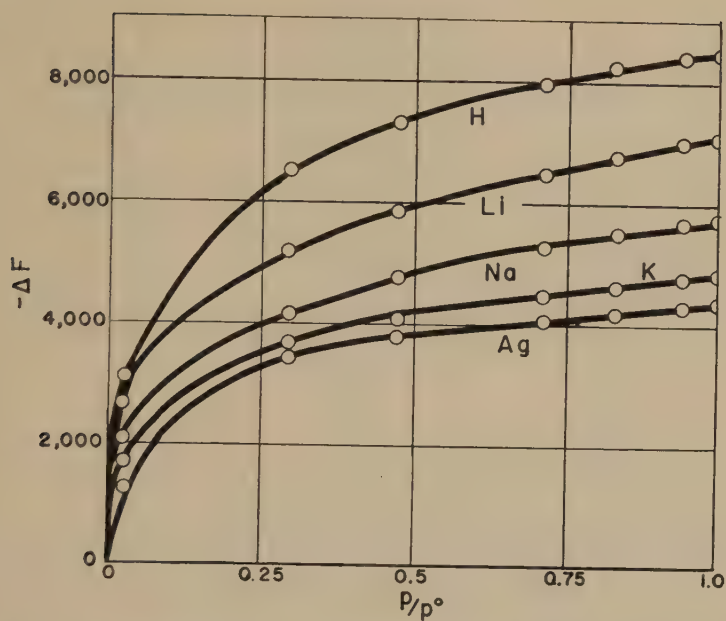


FIG. 13. Free energy changes of water sorption process by DVB 10; H^+ , Li^+ , Na^+ , K^+ , and Ag^+ in calories per equivalent of resin.

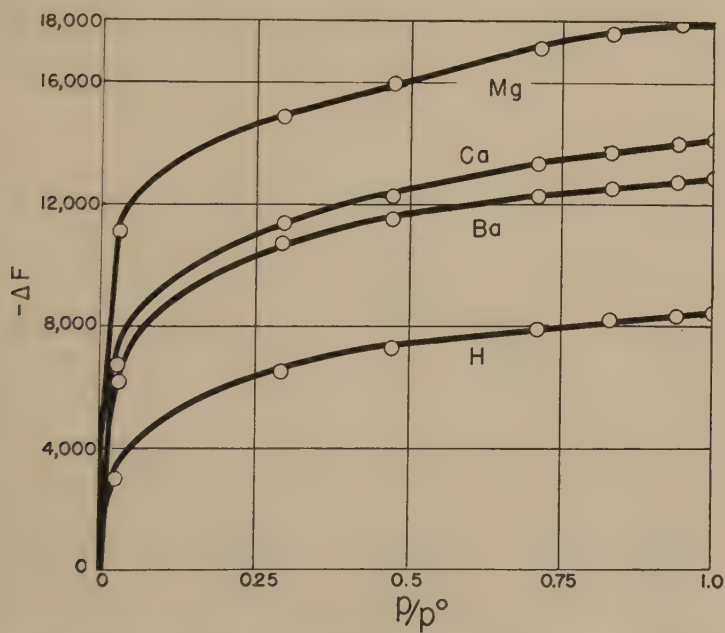


FIG. 14. Free energy changes of water sorption process by DVB 10; Mg^{++} , Ca^{++} , Ba^{++} , and H^+ in calories per equivalent of resin.

TABLE VIII

Comparison of Free Energies of Hydration of DVB 10 in Various Cationic States with Hydration Number (from Stokes-Robinson) of Cations

Ion	$\Delta F(\text{hydration})$ cal./equiv. resin	Stokes-Robinson hydration No. "n"
Mg ⁺⁺	-9040	7.0
H ⁺	-8484	7.3
Ca ⁺⁺	-7083	6.0
Li ⁺	-7076	6.5
Ba ⁺⁺	-6466	4.2
Na ⁺	-5753	3.5
(CH ₃) ₄ N ⁺	-5211	—
NH ₄ ⁺	-4897	—
K ⁺	-4846	1.9
Ag ⁺	-4356	—

been halved. It can be concluded that the sequence of ΔF_{hyd} follows the hydration series for the cations studied with DVB 10.

Figure 15 shows the free-energy curve for the carboxylic resin in the hydrogen state. As expected from the previous data, the total free energy is very low compared to the same state with DVB 10, namely about -1000 cal. per equivalent of resin.

The change in entropy of the water sorption reaction of DVB 10-K has been calculated, and is shown in Fig. 16 together with the changes in free energy and heat content. Consideration of the variation of the entropy with the number of moles of water sorbed, and of the partial molar entropy

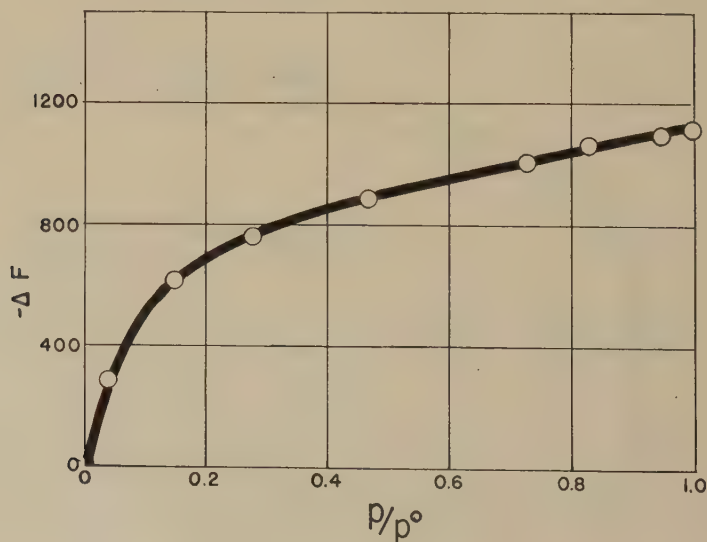


FIG. 15. Free energy changes of water sorption process by carboxylic acid resin.

obtained by graphical differentiation of this curve permit a few qualitative deductions. First, the net entropy change is negative. This is the usual case for sorption since the leading term is the ordering of the sorbed material. The sharp initial rise in $-\Delta S$ may be associated with the formation of a hydrate which is analogous to sorption on localized sites. The following rise is slower, and eventually the net entropy becomes more positive. Davis and McLaren (5) find a similar curve for salmine. They suggest the positive trend in the entropy as being due to incipient solution. In more concrete terms, it might be a positive contribution due to mixing, for since the major nonideal entropy contribution is in the beginning of the curve, it is likely that the smaller entropy of mixing becomes felt at larger n 's. A contribution from the stretching of the

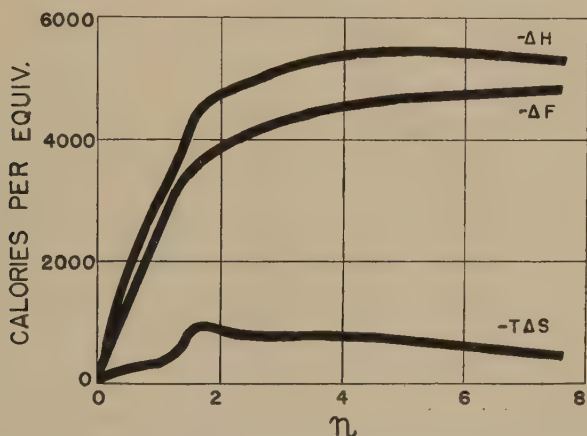


FIG. 16. Changes in free energies, heat content and entropy of DVB 10-K for reaction. Resin ($p = 0$) + $n\text{H}_2\text{O}$ (at p°) = resin $\cdot n\text{H}_2\text{O}$ (at p), with p/p° varying from 0 to 1.

matrix, expected to be positive and then negative in sign (19), is not seen. It is clear that the entropy curve is the resultant of many factors such as the entropy of sorption (or of hydration of the ions) and stretching of the resin network. In addition, only the gross character of the curve is reliable. There is no certainty as to the reality of the minor variations on the curve.

The variation of the external volume of an ion-exchange resin with the amount of sorbed water may be expected to give some indication as to the nature of the interaction between the resin and the water. From the data of Table V, by graphical differentiation, it is possible to calculate the partial molal volume of the water (\bar{V}_w) in resins in various states. It is also possible to calculate the partial molal volume of the resin itself in these systems and to test its variation with the ionic state.

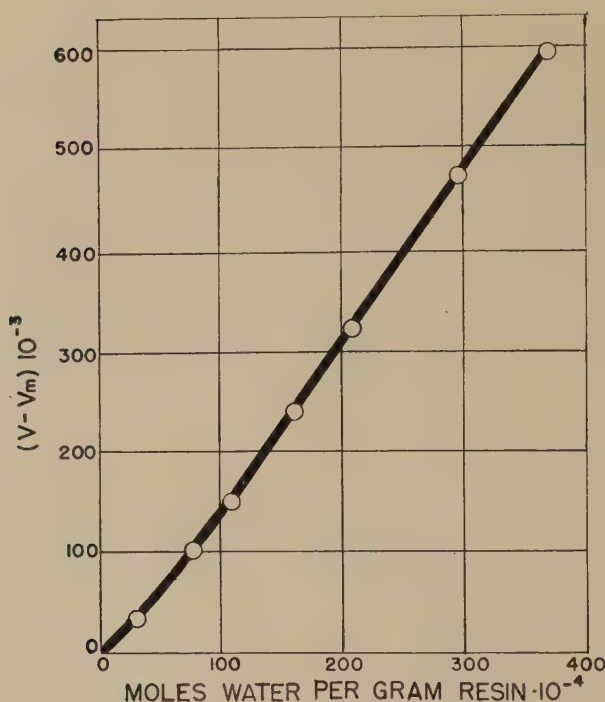


Fig. 17. Increase in volume of DVB 10-K over that of the dry state as a function of sorbed water.

Plots of $(V - V_m)$, the increase in volume of the resin over that of the dry state in ml./g. of H^+ resin, against n , number of moles of water sorbed per gram of resin referred to the hydrogen state, were made. The resulting curves for all ten ionic species are similar in nature; Fig. 17 shows a typical curve for the K resinate. \bar{V}_w increases as p/p° changes

TABLE IX

Partial Molal Volumes of Water (\bar{V}_{H_2O}) in DVB 10 as a Function of Ionic State (in Range $p/p^\circ = 0.45 - 1.00$)

Ionic state	\bar{V}_{H_2O} ml./mole H_2O
H^+	16.85
Li^+	17.55
Na^+	17.35
$(CH_3)_4N^+$	17.15
NH_4^+	17.16
K^+	17.25
Ag^+	17.00
Mg^{++}	16.85
Ca^{++}	16.90
Ba^{++}	16.25

from 0 to about 0.45; in the range 0.45 to 1 it is constant. The value of \bar{V}_w increases as p/p° changes from 0 to about 0.45; in the range 0.45 to 1 it is constant. The values of \bar{V}_w in the latter range have been calculated and are presented in Table IX.

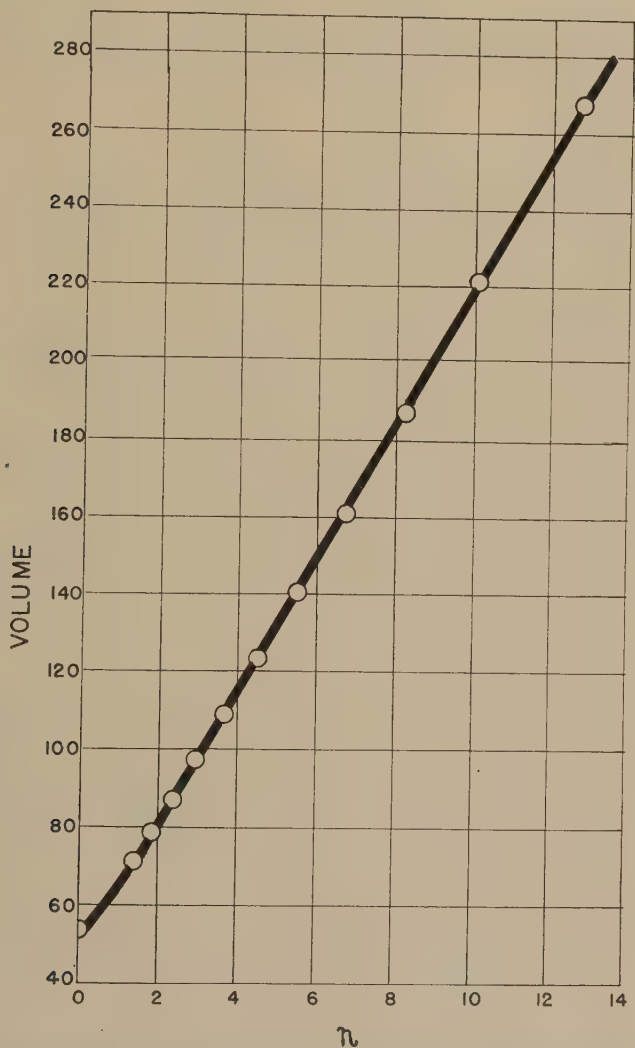


FIG. 18. Volume per mole of sulfuric acid plotted against n , the number of moles of water per mole of sulfuric acid.

Data from the literature (23) for sulfuric acid have been treated in a similar fashion, and the volume of solution per mole of sulfuric acid has been plotted against n , the number of moles of water per mole of sulfuric acid, in a concentration range of from 40.8 to 3.40 molal. The latter range

TABLE X

Calculated Partial Molal Volumes (\bar{V}_2) and Dry Volumes (V_2°) of the DVB 10 Resinates with Same Values for Sulfuric Acid

State	\bar{V}_2 (ml./mole)	V_2° (ml./mole)	$\bar{V}_2 - V_2^\circ$ (ml./mole)
H ⁺	138.2	145.2	-7.0
Li ⁺	139.1	146.5	-7.4
Na ⁺	144.5	152.3	-7.8
K ⁺	152.5	159.2	-6.7
NH ₄ ⁺	159.9	165.2	-5.3
(CH ₃) ₄ N ⁺	227.5	235.7	-8.2
Ag ⁺	140.5	143.0	-2.5
Mg ⁺⁺	142.5	147.5	-5.0
Ca ⁺⁺	155.5	150.3	+5.2
Ba ⁺⁺	180.5	151.7	+28.8
H ₂ SO ₄	46.0	53.5	-7.5

was selected so as to make the concentrations approximately the same as those found in the resin systems. It can be seen from Fig. 18 that \bar{V}_w over this range for the sulfuric acid-water system is constant and equal to 17.18 ml./mole of water. Thus the behavior of the H resinate again is shown to be very similar to sulfuric acid since \bar{V}_w for the former system was 16.85 ml./mole of water.

In view of the fact that these values were obtained by graphical differentiation, the difference between the two values mentioned is scarcely greater than the expected error. It will also be noted that not only for the acid but also for all the resin systems \bar{V}_w shows an initial increase before the constant value obtained.

The values of \bar{V}_w vary with the ion and with the charge on the ion in a fashion which seems to offer no clear-cut sequence. It is felt that the basic explanation for the individual values of \bar{V}_w for the various resin systems lies in the behavior of simple strong electrolytes and is not particularly related to the presence of the resin network for the first 80% of the curve.

As mentioned above, the partial molal volume of the solid phase (\bar{V}_2) may be calculated from the same data, and is shown in Table X. These volumes are also sensibly constant as would be expected from the constancy of \bar{V}_w . It is of interest to compare the \bar{V}_2 's with the volumes of the dry resins (V_2°) also shown in Table X. It will be noted that the univalent ions with the exception of Ag⁺ give an average value of $\bar{V}_2 - V_2^\circ$ of -7.5 ml./mole, the standard deviation being ± 0.4 ml./mole. Both \bar{V}_2 and V_2° increase in the sequence of the increasing ionic crystal volumes for these ions. (The hydrated volumes would be incorrect here because both V_2° and \bar{V}_2 are calculated in regions of low water content.)

The value of $\bar{V}_2 - V_2^\circ$ for sulfuric acid has also been calculated, and

is equal to -7.5 . Thus this difference appears to stem from properties of solutions of strong electrolytes. It would be no more correct to speak of "pore volume" here than in sulfuric acid.

In the case of Ag^+ the unusually low value of $\bar{V}_2 - V_2^\circ$ is undoubtedly connected with resin-ion interaction as has been mentioned previously. The explanation of the $\bar{V}_2 - V_2^\circ$ values obtained for the alkaline-earth ions apparently is connected with the valence in a way which is not clear.

SUMMARY

1. Water vapor sorption studies on a series of ion-exchange resins are presented. The systems investigated include sulfonic acid cation-exchange resins of various degrees of cross-linking, a carboxylic acid resin, and a quaternary ammonium anion-exchange resin.

2. Some direct calorimetric measurements of heats of sorption are presented. Free energies, heats of sorption, and entropies are calculated.

3. The sorption behavior of sulfonic acid resins is compared with that of sulfuric acid. It is concluded that the sulfonic acid groups are osmotically inactive. For the sulfonic acid resins, variations in sorption with ionic state are discussed and interpreted. The partial molal volumes of the hydrated resin systems are studied.

4. The behavior of the cross-linked polystyrene sulfonic acid resins is discussed from the point of view of simple, strong electrolytes in aqueous media. This interpretation is valid for the range 0–75% relative humidity; the influence of cross-linking makes itself felt above this point.

REFERENCES

1. BULL, H. B., *J. Am. Chem. Soc.* **66**, 1499 (1944).
2. BUNSEN, R., *Ann. Physik* **141**, 1 (1870).
3. DANIELS, F., MATHEWS, J. H., AND WILLIAMS, J. W., *Experimental Physical Chemistry*, 3rd Ed., p. 352. McGraw-Hill Co., Inc., New York.
4. DAVIDSON, A. W. AND ARGERSINGER W. J., JR., *J. Phys. Chem.* **56**, 92 (1952).
5. DAVIS, S., AND McLAREN, A. D., *J. Polymer Sci.* **3**, 16 (1948).
6. DOLE, M., AND McLAREN, A. D., *J. Am. Chem. Soc.* **69**, 651 (1947).
7. EUSTROPIEV, K. S., *J. Phys. Chem. U.S.S.R.* **8**, 130 (1936).
8. GLEUCKAUF, E., AND DUNCAN, J. F., paper presented at the 120th National Meeting of the Amer. Chem. Soc., New York, Sept. 1951.
9. GREGOR, H. P., *J. Am. Chem. Soc.* **70**, 1293 (1948).
10. GREGOR, H. P., *J. Am. Chem. Soc.* **73**, 3537 (1951).
11. GREGOR, H. P., AND BELLE, J., in preparation.
12. GREGOR, H. P., AND BREGMAN, J. I., *J. Am. Chem. Soc.* **70**, 2370 (1948).
13. GREGOR, H. P., AND BREGMAN, J. I., *J. Colloid Sci.* **6**, 323 (1951).
14. GREGOR, H. P., BREGMAN, J. E., GUTOFF, F., BROADLEY, R. D., BALDWIN, D. E., AND OVERBERGER, C. G., *J. Colloid Sci.* **6**, 20 (1951).
15. GREGOR, H. P., GUTOFF, F., AND BREGMAN, J. I., *J. Colloid Sci.* **6**, 245 (1951).
16. GREGOR, H. P., HELD, K. M., AND BELLIN, J., *Anal. Chem.* **23**, 620 (1951).
17. HARNED, H. S., AND MASON, C. M., *J. Am. Chem. Soc.* **54**, 1439 (1932).

18. HARNED, H. S., AND OWEN, B. B., *Physical Chemistry of Electrolytic Solutions*, p. 15. Reinhold, New York, 1950.
19. HERMANS, J. J., *Trans. Faraday Soc.* **299**, 591 (1947).
20. HERMANS, P. H., *Colloid Science*, Vol. II, Chap. XII. Elsevier Pub. Co., 1949.
21. *International Critical Tables*, Vol. III, p. 303. McGraw-Hill Co., Inc., New York, 1928.
22. KATZ, J. R., *Ergeb. exakt. Natur.* **3**, 372 (1924); *ibid.* **4**, 197 (1925).
23. LANGE, N. A., *Handbook of Chemistry*, p. 1319. Handbook Pub., Inc., Sundusky, Ohio, 1946.
24. MCBAIN, J. W., AND BAKR, A. M., *J. Am. Chem. Soc.* **48**, 690 (1926).
25. McLAREN, A. D., AND ROWEN, J. W., *J. Polymer Sci.* **7**, 289 (1951).
26. PEPPER, K. W., *J. Applied Chem.* **1**, 124 (1951).
27. SCHÜKAREV, A. N., KRIVOBABKO, I. P., AND SCHÜKAREVA, L. A., *Physik. Z. Sowjetunion* **5**, 722 (1934).
28. STAMM, A. J., AND LOUGHBOROUGH, W. K., *J. Phys. Chem.* **39**, 121 (1935).
29. STOKES, R. H., AND ROBINSON, R. A., *J. Am. Chem. Soc.* **70**, 1870 (1948).
30. WHITE, H. J., AND EYRING, H., *Textile Research J.* **17**, 523 (1947).

THE STATISTICS OF THE ADSORPTION OF ROD-SHAPED MOLECULES IN CONNECTION WITH THE STABILITY OF CERTAIN COLLOIDAL DISPERSIONS

E. L. Mackor and J. H. van der Waals

Koninklijke/Shell-Laboratorium, Amsterdam, Holland

Received May 15, 1952

1. INTRODUCTION

Colloidal dispersions of carbon black particles in liquid paraffins can be stabilized by the adsorption of aromatic molecules with a long aliphatic side chain, e.g. of dodecylbenzene (1). As has recently been shown (2) this stabilizing effect can be quite simply accounted for by considering the decrease in the number of configurations of the adsorbed molecules due to steric hindrance of the aliphatic side chains when the particles approach each other. This decrease causes an increase in the configurational free energy and hence leads to a repulsive force which at short distances may dominate over the long-range van der Waals-London type of attractive forces between the colloidal particles.

The previous treatment using continuous distribution functions was restricted to surface coverages by the adsorbed molecules sufficiently small to justify their mutual interactions to be neglected. By using the quasi-lattice model, however, we are now able to give a treatment which is also valid for higher coverages. The present derivation is essentially an extension of Prigogine's theory of surface tension of solutions of molecules different in size (3), and we have used a similar notation.

In the first paragraphs the adsorption isotherm and surface tension are determined for the adsorption of rod-shaped solute molecules onto a single adsorbing plane. For a few selected examples the adsorption isotherm is numerically evaluated and compared with a simple Langmuir isotherm; the comparison clearly shows that the determination of the active area of an adsorbent from an apparent maximum in the adsorption isotherm of elongated molecules may be quite unreliable.

In the last two paragraphs the same statistical technique is used for a calculation of the repulsive term in the free energy of interaction of two parallel planes due to adsorption. Combination of the repulsive term with the attractive term corresponding to van der Waals-London forces between the planes shows that colloidal dispersions in nonpolar media may be markedly stabilized by the adsorption of elongated molecules.

2. DEFINITION OF THE MODEL

We consider a single plane in a solution onto which elongated solute molecules are being adsorbed.

The treatment is based on the quasi-crystalline model of the liquid state and in particular on the following assumptions which may be illustrated by Fig. 1.

1. The solution consists of spherical solvent molecules *A* each occupying one site and dumbbell solute molecules *B* each occupying two sites. Of the two ends of each solute molecule one is preferentially adsorbed by the plane (these active ends are marked + in the figure). The cooperative free energy of adsorption per active group is equal to χ .¹

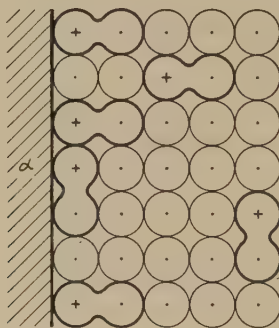


FIG. 1. Use of lattice model in describing adsorption of dumbbell solute molecules onto adsorbing plane α .

2. The lattice can be divided into layers of lattice sites parallel to the plane α . If the coordination number of the lattice is z we assume that each site in a layer has lz nearest neighbor sites in the same layer and mz such neighbors in each of the two adjacent layers. Hence,

$$l + 2m = 1. \quad [1]$$

3. All configurations of the molecules on the lattice in which n active groups are adsorbed on the plane α have equal statistical weight, $\exp(-n\chi/kT)$. This implies that the cooperative free energy of adsorption of the inactive ends of the solute molecules is equal to that of the solvent molecules.

4. We restrict our treatment to cases where the solution is so dilute that one may neglect the interaction between adsorbed and nonadsorbed solute molecules. In some cases recently reported (1) this condition will

¹ χ roughly corresponds to the average energy gain when bringing a solute molecule from the interior of the solution with its active end onto the plane, thereby displacing two solvent molecules (4).

approximately be satisfied because χ/kT is relatively large and a considerable surface concentration of B still corresponds to a very dilute solution.

3. STATISTICAL DETERMINATION OF ADSORPTION ISOTHERM AND SURFACE TENSION

We consider the system of the first two layers parallel to the plane α , each containing N lattice sites, and we determine the partition function of N_A molecules A and N_B molecules B on these $2N$ sites. The following notation is introduced. The number of A molecules in the first and second layer is denoted by $N_A^{(1)}$ and $N_A^{(2)}$, respectively. The B molecules may be adsorbed in two manners having equal energy, viz. parallel to the plane with both ends in the first layer (" B_2 molecules"), or pointing away from the plane with the active end in the first layer and the other one in the second layer (" B_1 molecules"); the numbers of these are N_{B_2} and N_{B_1} , respectively with $N_{B_1} + N_{B_2} = N_B$. (Since we neglect configurations with unadsorbed B molecules in the first two layers we have omitted the superscript (1) in the latter cases.)

The numbers just defined are not independent variables but have to obey certain relations expressing that the total number of lattice sites occupied in each layer should be equal to N ,

$$\begin{aligned} \text{1st layer, } N_A^{(1)} + N_{B_1} + 2N_{B_2} &= N \\ \text{2nd layer, } N_A^{(2)} + N_{B_1} &= N. \end{aligned} \quad [2]$$

One could use $N_A = N_A^{(1)} + N_A^{(2)}$, N_{B_1} , N_{B_2} as independent variables but the success of the statistical calculations is essentially based on the choice of N , N_{B_1} , and N_{B_2} as independent variables (5).

Let $g(N, N_{B_1}, N_{B_2})$ further denote the number of distinct configurations of the system for the set of values (N, N_{B_1}, N_{B_2}) .

The configurational part of the partition function for our system can then be written as

$$g(N, N_{B_1}, N_{B_2}) \exp[-(N_{B_1} + N_{B_2})\chi/kT] = \exp[-F/kT]. \quad [3]$$

F is the configurational free energy and since we are not interested in the effect of temperature variations we may express F as a function of N , N_{B_1} , N_{B_2} . The other contributions to the partition function² will not be considered here since these are either assumed not to change on adsorption, or may formally be accounted for by the constant χ [cf. Ref. (4)].

F should obey the following equilibrium conditions,

$$(\partial F / \partial N_{B_1})_{N, N_{B_2}} = (\partial F / \partial N_{B_2})_{N, N_{B_1}} = kT (\ln a_B - 2 \ln a_A). \quad [4]$$

² E.g., those corresponding to the internal degrees of freedom of the molecules.

The first one of these equalities directly follows from the minimum condition for the free energy and is identical with that which would obtain for a chemical equilibrium between two different species, B_1 and B_2 , according to $B_1 \rightleftharpoons B_2$. The second one is necessary if there is to be equilibrium between the surface phase considered and the bulk of the solution since both derivatives in [4] correspond to the exchange of a B molecule with two A molecules.

We now come to the statistical construction of the free energy function; as shown later the surface tension can then simply be found by taking the derivative $(\partial F / \partial N)_{N_{B_1}, N_{B_2}}$. The present derivation essentially is a generalization of Guggenheim's theory (5) for the free energy of mixing of binary solutions of molecules different in size.

Consider the process of replacing two A molecules in the first layer by a B_2 molecule, symbolically written as $2A^{(1)} \rightarrow B_2$. By this process a configuration of the "set" (N, N_{B_1}, N_{B_2}) is transformed into one belonging to the set $(N, N_{B_1}, N_{B_2} + 1)$. Every configuration of the latter set can thus be generated in $(N_{B_2} + 1)$ different ways from those of the former set since each of the $(N_{B_2} + 1)$ molecules B_2 may have replaced the two A molecules. Hence one can write

$$g(N, N_{B_1}, N_{B_2}) \times \lambda = g(N, N_{B_1}, N_{B_2} + 1)(N_{B_2} + 1), \quad [5]$$

where λ is the average number of pairs of sites in the set (N, N_{B_1}, N_{B_2}) occupied by A molecules but so located that they can accommodate a B_2 molecule.

The number λ can be found as follows. We factorize

$$\lambda = (lz N) \times \nu_P^{(1)} \times \nu_Q^{(1)}. \quad [6]$$

In this expression $lz N$ is the total number of pairs of neighboring lattice sites PQ^3 in the first layer, $\nu_P^{(1)}$ is the average probability that P is occupied by an A molecule and $\nu_Q^{(1)}$ is the average probability that Q is occupied by another A molecule *when P is known to be already occupied by an A molecule* (5).

Obviously $\nu_P^{(1)} = N_A^{(1)} / N$, but $\nu_Q^{(1)}$ is somewhat larger since one has to account for the fact that the occupation of P by an A molecule excludes the possibility of the point Q being occupied by a B_2 molecule having its other end at P . There are $2N_{B_2}$ such pairs PQ , each occupied by a single B_2 molecule; of the remaining $(lz N - 2N_{B_2})$ pairs, $lz N_A^{(1)}$ have an A molecule at Q . Hence,

$$\nu_Q^{(1)} = \frac{lz N_A^{(1)}}{lz N - 2N_{B_2}} \quad [7]$$

³ For convenience we have omitted a symmetry factor $\frac{1}{2}$, and we consequently distinguish between the pair PQ and the pair QP .

and

$$\lambda = \frac{N_A^{(1)2} (lz)^2}{lz N - 2N_{B_2}}. \quad [8]$$

Since N_{B_2} is a large number a differential equation for F can now be found by comparing the partition function [3] with that which obtains for the set $(N, N_{B_1}, N_{B_2} + 1)$ and by using the relation [5]

$$(1/kT)(\partial F/\partial N_{B_2})_{N, N_{B_1}} = - \ln \left\{ \frac{g(N, N_{B_1}, N_{B_2} + 1)}{g(N, N_{B_1}, N_{B_2})} \right. \\ \left. \times \exp(-\chi/kT) \right\} = \ln(N_{B_2} + 1) - \ln \lambda + \chi/kT. \quad [9]$$

Substitution of the value of λ Eq. [8], expressing $N_A^{(1)}$ in the variables N, N_{B_1}, N_{B_2} according to [2], and replacing $N_{B_2} + 1$ by N_{B_2} then leads to

$$(1/kT)(\partial F/\partial N_{B_2})_{N, N_{B_1}} = \ln N_{B_2} - 2 \ln(N - N_{B_1} - 2N_{B_2}) \\ - 2 \ln lz + \ln(lz N - 2N_{B_2}) + \chi/kT. \quad [10]$$

An analogous differential equation for $(\partial F/\partial N_{B_1})_{N, N_{B_2}}$ can be found by considering a second elementary process whereby two neighboring A molecules, one from the first layer and the other from the second layer, are replaced by a B_1 molecule, $A^{(1)} + A^{(2)} \rightarrow B_1$. The equation equivalent to [5] is

$$g(N, N_{B_1}, N_{B_2}) \times \lambda = g(N, N_{B_1} + 1, N_{B_2}) (N_{B_1} + 1). \quad [11]$$

For this case $\lambda = (mz N) \times \nu_P^{(1)} \times \nu_Q^{(2)}$, with

$$\nu_P^{(1)} = N_A^{(1)}/N, \quad \nu_Q^{(2)} = mz N_A^{(2)}/(mz N - N_{B_1}),$$

and hence

$$\lambda = \frac{N_A^{(1)} N_A^{(2)} (mz)^2}{mz N - N_{B_1}}. \quad [12]$$

The counterpart of Eq. [10] is thus found to be

$$(1/kT)(\partial F/\partial N_{B_1})_{N, N_{B_2}} = \ln N_{B_1} - \ln(N - N_{B_1} - 2N_{B_2}) \\ - \ln(N - N_{B_1}) - 2 \ln mz + \ln(mz N - N_{B_1}) + \chi/kT. \quad [13]$$

Equations [10] and [13] are the fundamental differential equations of our problem. Integration under the appropriate boundary conditions will give the value of the free energy and hence of the surface tension; but before we do so we shall first derive the adsorption isotherm directly from [10] and [13] and the equilibrium conditions of [4]. Equating the right-hand sides of [10] and [13] accordingly, one obtains

$$\frac{N_{B_1}}{N_{B_2}} = \frac{N - N_{B_1}}{N - N_{B_1} - 2N_{B_2}} \times \frac{m}{l} \times \frac{N - (2N_{B_2}/lz)}{N - (N_{B_1}/mz)}.$$

When expressing the concentrations in the adsorbed layer, in the new variables,

$$\theta_1 = N_{B_1}/N \quad \text{and} \quad \theta_2 = N_{B_2}/N,$$

this can further be written as

$$\theta_1/\theta_2 = \frac{1 - \theta_1}{1 - \theta_1 - 2\theta_2} \times \frac{m}{l} \times \frac{1 - (2\theta_2/lz)}{1 - (\theta_1/mz)}. \quad [14]$$

On the other hand substitution of [10] into the second equality of [4] gives

$$\frac{a_B}{a_A^2} \exp(-\chi/kT) = \frac{\theta_2[1 - (2\theta_2/lz)]}{lz(1 - \theta_1 - 2\theta_2)^2}. \quad [15]$$

Equations [14] and [15] enable us to determine the adsorption isotherm as a function of the activities in the solvent and energy parameter χ ; at the same time they inform us about the ratio of B_1 to B_2 molecules adsorbed.

In order to find the surface tension γ —in our case equal to the free energy per unit area—we could now integrate the set of Eqs. [10] and [13] and then differentiate the result with respect to N . The mathematical work involved can be considerably reduced, however, by reversing the order of integration and differentiation. We have

$$dF = \gamma d\Omega + kT \sum_{i=A,B} \ln a_i dN_i,$$

which for our system may be written as

$$dF = (\gamma/N^s) dN + kT[\ln a_A dN_A + \ln a_B(dN_{B_1} + dN_{B_2})],$$

where N^s is the number of lattice sites per unit area of the planes. Evidently,

$$(\partial F/\partial N)_{N_{B_1}, N_{B_2}} = \gamma/N^s + 2kT \ln a_A, \quad [16]$$

since $2N = N_A + N_{B_1} + 2N_{B_2}$. Taking the derivative with respect to N in [10] and [13] gives

$$\frac{1}{kT} \left(\frac{\partial^2 F}{\partial N \partial N_{B_2}} \right)_{N_{B_1}} = \frac{-2}{N - N_{B_1} - 2N_{B_2}} + \frac{lz}{lz N - 2N_{B_2}}, \quad [17]$$

$$\begin{aligned} \frac{1}{kT} \left(\frac{\partial^2 F}{\partial N \partial N_{B_1}} \right)_{N_{B_2}} &= \frac{-1}{N - N_{B_1} - 2N_{B_2}} - \frac{1}{N - N_{B_1}} \\ &\quad + \frac{mz}{mz N - N_{B_1}}. \end{aligned} \quad [18]$$

Integration of [17] and [18] gives

$$\begin{aligned} \frac{1}{kT} \left(\frac{\partial F}{\partial N} \right)_{N_{B_1}, N_{B_2}} &= \ln \frac{(N - N_{B_1} - 2N_{B_2})(N - N_{B_1})}{N^2} \\ &\quad - \frac{lz}{2} \ln \frac{lz N - 2N_{B_2}}{lz N} - mz \ln \frac{mz N - N_{B_1}}{mz N}. \end{aligned} \quad [19]$$

The integration constant has been so determined that each term vanishes when $N_{B_1} = N_{B_2} = 0$, because in that case there is only one configuration and hence $(\partial F/\partial N)_{0,0}$ must be zero.

Substitution from [16] and again using θ_1, θ_2 as variables leads to

$$\gamma/N^s kT = \ln(1 - \theta_1 - 2\theta_2)(1 - \theta_1) - \frac{lz}{2} \ln[1 - (2\theta_2/lz)] \\ - mz \ln[1 - (\theta_1/mz)] - 2\ln a_A. \quad [20]$$

With the aid of [14] and [15], Eq. [20] can be solved numerically to give $\gamma/N^s kT$ as a function of a_A and a_B . It should be realized that γ is *not* the surface tension but the excess surface tension relative to that of the pure solvent A , because it has been derived from the configurational part of the free energy only.

By using the same type of argument one can derive analogous formulas for the adsorption of rigid solute molecules with an arbitrary number of segments n . One finds

$$\theta_1/\theta_2 = (m/l) \left\{ \frac{[1 - \theta_1][1 - 2(n-1)(\theta_2/lz)]}{[1 - \theta_1 - n\theta_2][1 - (\theta_1/mz)]} \right\}^{n-1}, \quad [21]$$

$$a_B/a_A^n \times \exp(-\chi/kT) = \frac{\theta_2}{lz} \frac{[1 - 2(n-1)(\theta_2/lz)]^{n-1}}{(1 - \theta_1 - n\theta_2)^n}, \quad [22]$$

$$\gamma/N^s kT = -n \ln a_A + \ln(1 - \theta_1 - n\theta_2) \\ + (n-1) \ln(1 - \theta_1) - mz(n-1) \ln[1 - (\theta_1/mz)] \\ - lz/2 \{ \ln[1 - 2(n-1)(\theta_2/lz)] \}. \quad [23]$$

4. DISCUSSION OF ADSORPTION ISOTHERM

In Fig. 2 we have plotted the value of $\theta = \theta_1 + \theta_2$ as a function of concentration for adsorption of dimers according to [14] and [15], and for that of tetramers according to [21] and [22] with $n = 4$. The calculations have been made for a close-packed lattice with $z = 12$, $lz = 6$, and $mz = 3$, and the concentrations have been expressed by means of a function X defined as

$$X = (a_B/a_A^n) \exp(-\chi/kT). \quad [24]$$

For $n = 4$ we have also plotted θ_1 and θ_2 separately. At extremely low concentrations $\theta_2/\theta_1 = l/m = 2$, but owing to the interaction, θ_2 soon falls below θ_1 and reaches a very flat maximum at about $X = 0.4$.

The most remarkable feature is the very slow rise of the total fraction θ with concentration at the higher concentrations. This is even better revealed on comparing the present curves with the simple Langmuir isotherm found when the mutual interaction of the adsorbed molecules is neglected (marked "Langmuir" in Fig. 2, and derived from the partition function for an ideal localized monolayer allowing for the fact that each

adsorbed molecule still has $lz + mz = 9$ possible orientations on a close-packed lattice).

Figure 2 is qualitatively in agreement with the results found by van der Waarden (1) when measuring the adsorption isotherm of naphthalene and various alkyl-substituted naphthalenes on carbon black. For the molecules with long side chains the steric hindrance is such that very high solute activities are necessary to attain a nearly complete surface coverage. The latter requires $\theta_1 \rightarrow 1$ and $\theta_2 \rightarrow 0$, which is yet very far from being realized in Fig. 2. One may thus conclude that it is unreliable to determine the active area of an adsorbent from the maximum value of the adsorption isotherm of elongated molecules: the flattening out of this

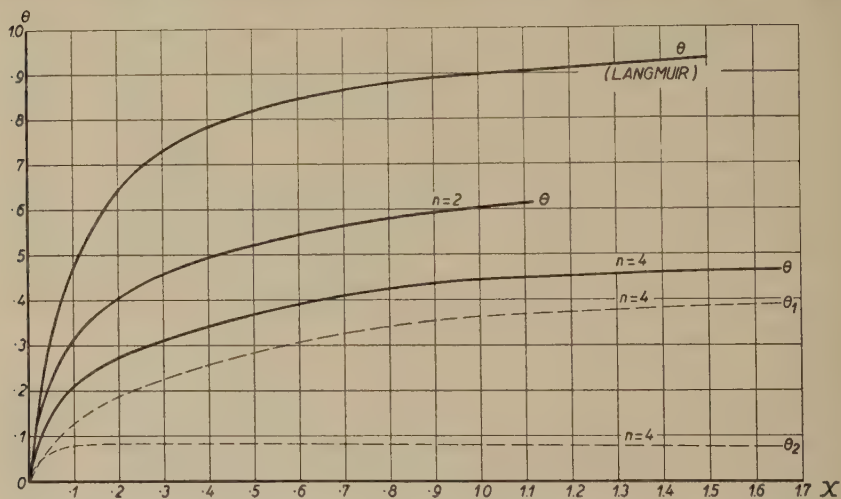


FIG. 2. Adsorption isotherms of rod-shaped molecules occupying two or four lattice sites, respectively.

isotherm at relatively low surface coverages may easily be mistaken for an asymptotic behavior.

5. INTERACTION BETWEEN TWO ADSORBING PLANES

In order to explain the stability of a colloidal dispersion by adsorption of rod-shaped molecules we again use the model of two parallel adsorbing planes (2) and further base our treatment on the assumptions introduced in sec. 2.

We consider two such planes α and β —each with a surface area Ω —in an infinite amount of solution of dumbbell solute molecules B and spherical solvent molecules A . Let our system contain n_A , n_B molecules of species A and B , respectively, and let their chemical potentials be μ_A , μ_B . When the number, d , of layers of lattice sites separating the two

planes is large no interaction between the adsorbed layers occurs and the adsorption isotherm and surface tension will be determined by the formulas derived above; the values of various functions for this case will further be denoted by marking these functions with an asterisk. We now bring the planes closer together: as soon as $d < 4$ interaction sets in and manifests itself as a repulsion between the two planes. In order to calculate the free energy of repulsion we successively consider the three states of our system illustrated in Figs. 3a, 3b, and 3c, where d equals 3, 2, or 1, respectively. The difference in free energy between any of the states illustrated in Fig. 3a-c and that of large separation can formally be written as

$$F - F^* = 2\Omega (\gamma - \gamma^*)_{n_A, n_B} + \sum_{i=A, B} n_i (\mu_i - \mu_i^*). \quad [25]$$

The first term is due to the change in surface tension from a value γ^* to a value γ , and the latter term corresponds to the changes in chemical

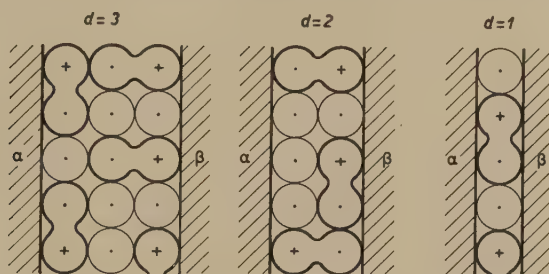


FIG. 3. (a) Two adsorbing planes separated by three layers of lattice sites.
(b) Two adsorbing planes separated by two layers of lattice sites.
(c) Two adsorbing planes separated by one layer of lattice sites.

potentials of the components due to the desorption of B molecules from the planes when these are brought closer together. Subscripts n_A , n_B are attached to the parentheses enclosing $\gamma - \gamma^*$ as a reminder that this difference should be taken at constant n_A , n_B and hence variable μ_A , and μ_B . But in the case where one has an infinite amount of solution it can be shown that [25] is equal to

$$F - F^* = 2\Omega (\gamma - \gamma^*)_{\mu_A^*, \mu_B^*}, \quad [26]$$

where the difference $\gamma - \gamma^*$ is now to be taken at constant values of the chemical potentials, μ_A^* and μ_B^* .

The proof is as follows. We split the total numbers of molecules, n_A , n_B into those in the first two adsorbed layers, $2\Omega \Gamma_A$, $2\Omega \Gamma_B$, and those in the remainder of the solution, m_A , m_B . Hence Γ_A , Γ_B are the amounts adsorbed per unit area, and $2\Omega \Gamma_A + m_A = n_A$ as well as $2\Omega \Gamma_B + m_B = n_B$. Equation [25] can then be written as

$$F - F^* = 2\Omega [(\gamma - \gamma^*)_{n_A, n_B} + \sum_{i=A, B} (\Gamma_i \mu_i - \Gamma_i^* \mu_i^*)] + \sum_{i=A, B} (m_i \mu_i - m_i^* \mu_i^*).$$

We introduce the abbreviation $\mu_i - \mu_i^* = \Delta\mu_i$, and expand the right hand side of the expression for $F - F^*$ in a Taylor series with respect to the variables μ_i . One obtains

$$F - F^* = 2\Omega \left[(\gamma - \gamma^*)_{\mu_A^*, \mu_B^*} + \sum_{i=A, B} \left\{ \frac{\partial \gamma}{\partial \mu_i} \Delta\mu_i + (\Gamma_i - \Gamma_i^*) \mu_i^* + \Gamma_i \Delta\mu_i \right\} \right] \\ + \sum_{i=A, B} \{ (m_i - m_i^*) \mu_i^* + m_i \Delta\mu_i \}.$$

Since $2\Omega(\Gamma_i - \Gamma_i^*) = -(m_i - m_i^*)$ two terms cancel out and hence

$$F - F^* = 2\Omega \left\{ (\gamma - \gamma^*)_{\mu_A^*, \mu_B^*} + \sum_{i=A, B} \left[\frac{\partial \gamma}{\partial \mu_i} \Delta\mu_i + \Gamma_i \Delta\mu_i \right] \right\} + \sum_{i=A, B} m_i \Delta\mu_i.$$

This completes the proof as the first sum vanishes according to the relation of Gibbs-Duhem for surface phases⁴ and the second sum vanishes according to the same relation for the solution.

The problem which we have to solve has thus been reduced to a determination of the difference in surface tension between each of the three cases illustrated in Fig. 3 and that found in sec. 3 for a single plane.

By using the same statistical technique as before one can determine the value of γ and the adsorption isotherm for each of the cases shown in Fig. 3a, 3b, and 3c. We consider the layers of sites between the planes α and β and we again construct a set of two simultaneous differential equations for the free energy of this surface phase by studying the two elementary processes $2A^{(1)} \rightarrow B_2$ and $A^{(1)} + A^{(2)} \rightarrow B_1$; the case given in Fig. 3c ($d = 1$) is a very simple one since then the first process only is possible, $N_{B_1} \equiv 0$ and hence only one differential equation remains.

Since the mathematical technique is exactly the same as before we shall only quote the relevant relations analogous to [2] for each case, the new values of λ to be taken and the ultimate formulas for the adsorption isotherms and surface tension. For the sake of convenience we shall denote the analog of formula [2] for the case of Fig. 3b by [2b], etc.

$d = 3$ (Fig. 3a)

The layers 1 and 3 are taken together, so that $N_A^{(1)}$ and N_{B_2} are the numbers of A molecules and B_2 molecules in both these layers together; N_{B_1} is the total number of B_1 molecules, i.e. adsorbed onto either α or β . We then have

$$\left. \begin{aligned} N_A^{(1)} &= 2N - N_{B_1} - 2N_{B_2} \\ N_{A^{(2)}} &= N - N_{B_1} \end{aligned} \right\} \quad [2a]$$

The fractions θ_1 , θ_2 are now defined as

$$\theta_1 = N_{B_1}/2N \text{ and } \theta_2 = N_{B_2}/2N,$$

$$2A^{(1)} \rightarrow B_2, \lambda = (2lzN) \times \frac{N_A^{(1)}}{2N} \times \frac{lz N_A^{(1)}}{2lzN - 2N_{B_2}} = \frac{N_A^{(1)2} \times (lz)^2}{2lzN - 2N_{B_2}} \quad [8a]$$

$$A^{(1)} + A^{(2)}, \lambda = (2mzN) \times \frac{N_A^{(1)}}{2N} \times \frac{2mz N_A^{(2)}}{2mzN - N_{B_1}} = \frac{2N_A^{(1)} N_A^{(2)} (mz)^2}{2mzN - N_{B_1}}, \quad [12a]$$

⁴ Cf. Ref. (10), formula (1.55.2), p. 39, $dp = dT = 0$.

$$\theta_1/\theta_2 = \frac{1 - 2\theta_1}{1 - \theta_1 - 2\theta_2} \times \frac{m}{l} \times \frac{1 - (2\theta_2/lz)}{1 - (\theta_1/mz)}, \quad [14a]$$

$$\frac{a_B}{a_A^2} \exp(-\chi/kT) = \frac{\theta_2}{lz} \times \frac{[1 - 2\theta_2/lz]}{(1 - \theta_1 - 2\theta_2)^2}, \quad [15a] \equiv [15]$$

$$(\partial F/\partial N)_{N_{B_1}, N_{B_2}} = 2\gamma/N^s + 3kT \ln a_A, \quad [16a]$$

$$\begin{aligned} \gamma/N^s kT = -(3/2) \ln a_A + \ln(1 - \theta_1 - 2\theta_2) + (1/2) \ln(1 - 2\theta_1) - mz \ln[1 - (\theta_1/mz)] \\ - (lz/2) \ln[1 - (2\theta_2/lz)]. \end{aligned} \quad [20a]$$

$$d = 2 \text{ (Fig. 3b)}$$

The total numbers of A , B_1 , and B_2 molecules are denoted by N_A , N_{B_1} , and N_{B_2} , respectively; we do not distinguish between B molecules adsorbed on α and those adsorbed on β . We have

$$N_A = 2N - 2N_{B_1} - 2N_{B_2}, \quad [2b]$$

and we again define

$$\theta_1 = N_{B_1}/2N \text{ and } \theta_2 = N_{B_2}/2N.$$

$$2A \rightarrow B_2, \lambda = (2lz/N)(N_A/2N)[lz N_A/(2lz N - 2N_{B_2})], \quad [8b]$$

$$2A \rightarrow B_1, \lambda = (2mz/N)(N_A/2N)[mz N_A/(2mz N - 2N_{B_1})] \quad [12b]$$

$$\theta_1/\theta_2 = \frac{m}{l} \times \frac{1 - (2\theta_2/lz)}{1 - (2\theta_1/mz)}, \quad [14b]$$

$$(a_B/a_A^2) \exp(-\chi/kT) = \frac{\theta_2}{lz} \times \frac{1 - (2\theta_2/lz)}{(1 - 2\theta_1 - 2\theta_2)^2}, \quad [15b]$$

$$(\partial F/\partial N)_{N_{B_1}, N_{B_2}} = 2\gamma/N^s + 2 \ln a_A, \quad [16b]$$

$$\begin{aligned} \gamma/N^s kT = -\ln a_A + \ln(1 - 2\theta_1 - 2\theta_2) - (mz/2) \ln[1 - (2\theta_1/mz)] \\ - (lz/2) \ln[1 - (2\theta_2/lz)]. \end{aligned} \quad [20b]$$

$$d = 1 \text{ (Fig. 3c)}$$

For the sake of completeness we also consider this rather exceptional case. Since the active groups of the B molecules are now simultaneously in contact with both α and β it should be realized that our use of $\exp(-N_B \chi/kT)$ as the appropriate weighting factor in the partition function is subject to severe criticism. Since we are only interested in the principle of the present phenomenon we shall, nevertheless, make this arbitrary choice.

We have N_A and $N_{B_2} = N_B$ molecules A and B in the one layer under consideration. One has

$$N_A = N - 2N_B \quad [2c]$$

and

$$\theta_2 = N_B/N \quad (\theta_1 \equiv 0),$$

$$2A \rightarrow B, \lambda = (lz/N)(N_A/N)[lz N_A/(lz N - 2N_{B_2})] = \frac{N_A^2 (lz)^2}{lz N - 2N_{B_2}}, \quad [8c]$$

$$\frac{a_B}{a_A^2} \exp(-\chi/kT) = \frac{\theta_2}{lz} \times \frac{1 - (2\theta_2/lz)}{(1 - 2\theta_2)^2}, \quad [15c]$$

$$(\partial F/\partial N)_{N_B} = 2\gamma/N^s + kT \ln a_A, \quad [16c]$$

$$\gamma/N^s kT = -(1/2) \ln a_A + (1/2) \ln(1 - 2\theta_2) - (lz/4) \ln[1 - 2\theta_2/lz]. \quad [20c]$$

6. NUMERICAL RESULTS FOR FREE ENERGY OF INTERACTION

The formulas derived in the preceding section have been worked out numerically for two cases, viz., (a) simple cubic lattice: $z = 6$, $lz = 4$, $mz = 1$; and (b) close-packed lattice: $z = 12$, $lz = 6$, $mz = 3$.⁵ Both for the case without interaction ($d \geq 4$) and for that where $d = 3, 2$, and 1 , respectively, we first determined the values of θ_1 and θ_2 corresponding to a few selected values of the generalized concentration X . Using these values of θ_1 and θ_2 we could then determine those of the dimensionless quantities γ^*/N^*kT and γ/N^*kT from formulas [20] and [20a], [20b], and [20c], respectively. We thereby assumed the solution to be so dilute that the terms involving $\ln a_A$ may be neglected in these formulas, because $a_A \sim 1$.

One has according to [26] and putting $\Omega = 1$,

$$2(\gamma(d)/N^*kT - \gamma^*/N^*kT) = \Delta F_R(d)/N^*kT \quad [27]$$

where ΔF_R is the free energy of repulsion per unit area; both γ and ΔF_R are functions of d .

In Fig. 4a we have plotted $\Delta F_R/N^*kT$ for various values of X as a function of d for a simple cubic lattice; in Fig. 4b we have done the same for a close-packed cubic lattice. In these figures one can distinguish two regions: (a) the region where the repulsion is only due to steric hindrance of the molecules adsorbed onto the one plane by those adsorbed onto the other one (i.e., for $d = 3$ and 2), and (b) the case where $d = 1$ for which even at very high dilution the number of configurations is considerably reduced because the molecules adsorbed on either of the planes are hindered by the other plane itself. The lattice model with its very limited number of orientations for a molecule adsorbed onto a given site is evidently ill-suited for a description of the latter region.

In order to get a better insight into the first region we have further made some calculations for rigid molecules consisting of four segments and adsorbed onto two parallel planes in the close-packed lattice (b). The calculations were performed with the aid of [21], [22], and [23], putting $n = 4$, and analogous formulas—not quoted here—derived for the case where two adsorbed layers interact (i.e. for $d < 8$).

In Fig. 5 we have plotted the resulting free energy of repulsion $\Delta F_R/N^*kT$ as a function of d for $X = 0.1, 0.4$, and 1.0 , respectively. It is evident from the graphs that a considerable repulsion occurs even for com-

⁵ The adsorbing plane is taken to coincide with the (111) plane of the face-centered cubic lattice; hence the adsorbing sites are arranged in equilateral triangles and the sites in the next layer form regular tetrahedra with the sites in the adsorbing layer. It should be mentioned that one could equally well assume a coincidence of the adsorbing plane with the (100) plane in which case $lz = 4$, $mz = 4$. For a given concentration the latter model would lead to an even greater repulsion between the planes than found for $lz = 6$, $mz = 3$.

paratively large d values. We recall that for $d = 3$ the repulsive term $\Delta F_R/N^s kT$ vanishes proportional to the concentration at extremely low surface coverages because the distance between the two planes is smaller than the length of the molecules. For $d \geq 4$, however, the interaction is only due to the mutual hindrance of the molecules in the two adsorbed layers which vanishes proportional to the square of the concentration at infinitely low surface coverage. This behavior is clearly indicated by the relatively rapid disappearance of the "tail" of the curves when going to smaller X values.

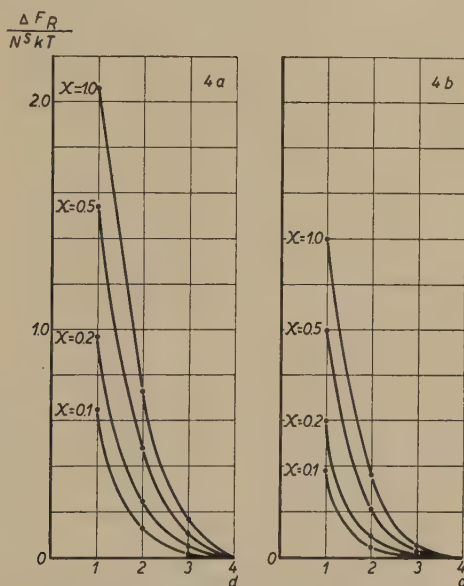


FIG. 4. The free energy of repulsion between two adsorbing planes as a function of distance for adsorption of dumbbell molecules. (a) Close-packed cubic lattice. (b) Simple cubic lattice.

In order to assess the physical consequences of the repulsion, ΔF_R should be compared with the van der Waals-London type energy of attraction per unit area, ΔF_A , for two infinite plates at the same distance.

According to de Boer (6) and Hamaker (7), ΔF_A can be written as

$$\Delta F_A = -A/12\pi r^2, \quad [28]$$

where A is a numerical constant and r the distance between the two planes in units of length. For convenience we restrict our further considerations to the close-packed lattice (b) in which the distance between nearest neighbors be a . The distance between two adjacent layers of sites is $\frac{1}{3} a\sqrt{6}$ (height of a tetrahedron with side a), and hence

$$r = \frac{1}{3} \sqrt{6} (ad). \quad [29]$$



FIG. 5. Total free energy of interaction between two adsorbing planes and its separate terms as a function of d for adsorption of rigid linear tetramers.

- (a) The dotted curve below the axis represents the attractive term $\Delta F_A/N^s kT$ for $A/kT = 50$.
 (b) The dotted curves above the axis represent the repulsive term $\Delta F_R/N^s kT$ for various values of X .
 (c) The full-drawn curves are the corresponding curves for the total interaction, $\Delta F/N^s kT = (\Delta F_R/N^s kT) + (\Delta F_A/N^s kT)$.

The lattice model further requires a relation between N^s and a . When the minimum distance between two adsorbing sites is equal to a , then the number of sites per unit area, N^s , follows from

$$N^s = \left(\frac{1}{2} \sqrt{3} a^2\right)^{-1}. \quad [30]$$

Substitution from [30] into [29] and thence into [28] leads to

$$\Delta F_A = -N^s A \sqrt{3}/16\pi d^2,$$

which can also be written as

$$\Delta F_A/N^s kT = - (0.03446 A/kT) \times 1/d^2. \quad [31]$$

Little is known about the precise value of the dimensionless constant A/kT to be taken for colloidal systems. Verwey and Overbeek (8) assumed a value of $2 \times 10^{-12}/4 \times 10^{-14} = 50$ for aqueous systems; according to more recent work (9) this value gives too large an attraction at short distances. Even less is known about values of this constant in non-polar systems.

The lower curve in Fig. 5 represents $\Delta F_A/N^s kT$ for $A/kT = 50$. Summation of a repulsive and an attractive term according to

$$(\Delta F_R/N^s kT) + (\Delta F_A/N^s kT) = \Delta F/N^s kT$$

gives $\Delta F/N^s kT$ which measures the total free energy of interaction per unit area.

As can be seen from the solid curves in the graph, stabilization occurs even for a relatively low concentration of $X = 0.1$, and notwithstanding the very high A/kT value which is thought to be a safe upper limit for the real value.

The order of magnitude of the effect considered may also be illustrated by reducing the dimensionless vertical scale to a proper energy value. In the case of van der Waarden's experiments (1), for instance, $N^s \approx 10^{-14} \text{ cm.}^{-2}$ and $kT = 4 \times 10^{-14} \text{ ergs}$, so a value of $\Delta F/N^s kT = 0.1$ corresponds to about 0.4 erg/cm.^2 .

Per carbon black particle there are of the order of 1000 adsorbing sites; if in our model the two planes each had 1000 adsorbing sites, $\Delta F/N^s kT = 0.1$ would already be equivalent to a stabilization of 100 kT ! Although the stabilization of the actual, i.e. roughly spherical, particles must be expected to be only a fraction of this it will still be considerable.

Considering the scarcity of relevant experimental data a further discussion does not seem warranted.

ACKNOWLEDGMENT

The authors wish to express their gratitude to the Management of the Koninklijke/Shell-Laboratorium, Amsterdam, for giving them the opportunity of carrying out this research.

SUMMARY

The adsorption of rod-shaped molecules from a solution onto an adsorbent is studied. Expressions for the adsorption isotherm and surface tension are given using the model of a localized monolayer, and allowing for the interaction between the adsorbed molecules due to steric hindrance. Examination of the adsorption isotherm reveals that its slope becomes extremely small at high concentrations, long before the surface is completely covered.

The same statistical technique is then applied to the model of two parallel adsorbing planes. When the planes are brought closer together

the free energy of the system rises due to the interaction of the two adsorbed layers; an expression for the free energy of repulsion is given. Comparison with some experimental data shows that this effect must be responsible for the stabilization of certain colloidal dispersions in non-polar media.

REFERENCES

1. WAARDEN, M. VAN DER, *J. Colloid Sci.* **5**, 317 (1950); *ibid.* **6**, 443 (1951)
2. MACKOR, E. L., *J. Colloid Sci.* **6**, 492 (1951).
3. PRIGOGINE, I., *J. chim. phys.* **47**, 33 (1950); PRIGOGINE, I., AND SAROLEA, L., *J. chim. phys.* **47**, 890 (1950).
4. GUGGENHEIM, E. A., *Trans. Faraday Soc.* **44**, 1007 (1948).
5. GUGGENHEIM, E. A., *Proc. Roy. Soc. (London)* **A183**, 203 (1944).
6. BOER, J. H. DE, *Trans. Faraday Soc.* **32**, 21 (1936).
7. HAMAKER, H. C., *Physica* **4**, 1058 (1937).
8. VERWEY, E. J. W., AND OVERBEEK, J. TH. G., *Theory of the Stability of Lyophobic Colloids*. Elsevier, Amsterdam, 1948.
9. MACKOR, E. L., *Rec. trav. chim.* **70**, 857 (1951).
10. GUGGENHEIM, E. A., *Thermodynamics*. North-Holland Publishing Company, Amsterdam, 1950.

LETTER TO THE EDITORS

THE "CRITICAL POINT"

There is a certain amount of divergence in current interpretations of phenomena in the critical region which, I wish to suggest, might be minimized by a more explicit recognition of the fact that different criteria for locating a "critical point" do not necessarily lead to the same result. These criteria or definitions for a critical point include the following: (a) The first and second derivatives of pressure with respect to volume, in the case of liquid-vapor systems, or of activity with respect to composition, in the case of liquid-liquid systems, are both equal to zero. (b) The two phases attain the same density. (c) The interfacial tension and energy become zero. (d) The appearance of a "fog" or "emulsion" as temperature is raised or lowered.

Definition (a) offers a thermodynamic basis for theoretical treatment of the problem, not a convenient experimental criterion. The rectilinear diameter law of Cailletet and Mathias makes (b) the best means for fixing critical volume or composition respectively, but a poor one for fixing critical temperature. Criterion (c) is an obvious consequence of (b), but it cannot be fixed by direct measurement, nor by extrapolation, because the linear relation between the "molecular surface energy" and temperature, formulated by the old rule of Ramsay and Shields breaks down in the critical region. My experience with (d), applied to liquid-liquid systems, has convinced me that it is not free from a subjective element, because the opacity persists through a small range of temperature.

I suggest the following microscopic picture of the changes occurring at an interface as the temperature approaches the critical. As the densities of the two phases rapidly approach each other with rising temperature, a sort of Brownian movement occurs at the surface, corresponding to standing waves, increasing till small regions of "clusters" or "globules" of one shoot into the other sufficient to be observable as the "fog" or "emulsion" referred to above. If a sealed tube of the system in this interval is gently rocked, the whole contents become opaque. These clusters rapidly become smaller and less sharply defined as temperature is further raised until they may be more appropriately regarded as local fluctuations in density. If this is a reasonably accurate kinetic description of the process, there would seem to be room for slight disagreement as to a precise value for a critical temperature, particularly if we remember

that we are observing the effects of small differences in density, which depend upon the gravitational field and could be markedly changed in a centrifugal field. The possible slowness in attaining equilibrium by reason of the small density gradient may be avoided, while investigating light scattering, by gentle stirring.

I suggest, finally, that the variations in other thermodynamic quantities in this region might prove enlightening, particularly the entropy, in view of the profound changes which are occurring in the structure of the two phases.

*Department of Chemistry,
University of California,
Berkeley 4, California
Received June 9, 1952*

JOEL H. HILDEBRAND

Book Review

Diffusion in Solids, Liquids, Gases. By W. Jost. Academic Press, Inc., New York, 1952. 558 pp. Price \$12.00.

In the last 10–15 years alone, several hundred publications devoted to the problems of diffusion in solids, liquids, and gases have appeared in numerous journals. The need for a book summarizing systematically the modern outlook on the diffusion problem as set forth in these scattered publications is evident. The book under review fills this gap to a great extent. The author does not pretend to give an exhaustive account of the diffusion problem, and his chief aim is “to assist in planning, evaluating and understanding diffusion experiments, at the same time giving a survey of the result to date.” The author has used, in part, the first three chapters of his book *Diffusion und chemische Reaktion in festen Stoffen* (published in 1937).

The first chapter describes the general theory of diffusion and gives solutions of differential equations including a great number of special cases: for example, the cases where diffusion is complicated by chemical reactions and convection, diffusion in systems consisting of more than one phase, etc. This chapter also contains tables of Stefan and Kawalki and tables of error functions.

Chapters II through IX are devoted to the problem of diffusion in solids and deal with a theory of disorder in crystals, general theory of diffusion in solids, electrolytic conduction and diffusion in ionic crystals, diffusion in metals and in nonpolar crystals, solubility in solids, permeation and diffusion of gases in solids, mobility of ions in solid and molten metals and alloys, and surface reaction of metals.

Diffusion in gases is the subject of the tenth chapter; diffusion in liquids is treated in the eleventh chapter. The twelfth chapter deals with thermal diffusion and gives the theory of Clusius' separation tube.

It can be seen from this short list of contents that the main part of the book is devoted to diffusion in solids and only about one-fifth of the book deals with diffusion in liquids and gases and with thermal diffusion. Accordingly, such problems of diffusion in liquids as, for example, diffusion in colloids, self-diffusion in liquids, and application of isotopes, are not treated.

The remark of the author that Matano in 1933 was the first to apply Boltzmann's solution of diffusion differential equation is inaccurate. This solution was applied previously (1925) by Fürth and his co-workers, and in 1930 by D. Krüger and M. Grunsky.

The references at the end of every chapter are numerous, totaling over 2000. The book is written clearly and comprehensively, and can be recommended to anyone interested in the modern situation in the field of diffusion.

VADIM DROZIN, New York, New York

XIIIth International Congress of Pure and Applied Chemistry

**Stockholm July 29th—August 4th and
Uppsala August 5th—7th, 1953**

The Congress will comprise a Physical Chemistry Section and a Symposium on the Chemistry of Wood and Wood Constituents, both in Stockholm from July 29th to August 4th and a Symposium on Macromolecules in Uppsala from August 5th to 7th. Further information and the First Circular and preliminary application forms can be obtained from

***XIIIth International Congress of Pure and Applied Chemistry,
Stockholm 70, Sweden.***

THE VISCOELASTIC BEHAVIOR OF POLYMETHYL METHACRYLATE

J. R. McLoughlin and A. V. Tobolsky

The Frick Chemical Laboratory, Princeton University, Princeton, New Jersey

Received May 2, 1952

ABSTRACT

Complete stress relaxation data for polymethyl methacrylate are presented covering behavior of this linear amorphous polymer from the rubbery state to the glassy state. The effect of water on stress relaxation rates in the glassy state and in the transition region is shown. Fast cooling is shown to increase subsequent stress relaxation rates in the glassy state.

The complete pattern of viscoelastic behavior may be represented by a master stress relaxation curve holding for all temperatures, but shifting along the logarithmic time scale with temperature change.

The master stress relaxation curve can be represented by a distribution of relaxation times. This distribution has been derived from the master stress relaxation curve, and the master curve recalculated from the distribution has been shown to agree with the experimental master curve. The method used in calculating the distribution of relaxation times is described and can be applied generally.

INTRODUCTION

In a previous publication (1) we have discussed the fundamental principles involved in extension of the time scale in elastoviscous data by the use of experimental results obtained at various temperatures. We showed that a master stress relaxation curve could be used to explain the stress relaxation data for various temperatures by shifting the position of this master curve along the time axis with temperature. The function $\kappa(T)$ was defined such that the stress relaxation curves at all temperatures are identical if plotted versus time divided by $\kappa(T)$. The master relaxation curves for polyisobutylene and for polymethyl methacrylate were presented and plots of the functions $\kappa(T)$ for each polymer were shown.

The present paper deals with the details of the investigation of polymethyl methacrylate and presents a method for deriving a continuous distribution of relaxation times from the master stress curve.

Our investigation of polymethyl methacrylate covers a broad temperature range such that its behavior in the rubbery state, in the glassy state, and in the transition region between is well defined. Previous investigations of polyisobutylene (1) did not extend down into the glassy state of

the polymer because of the difficulty of making measurements at such low temperatures. From the measurements made with polymethyl methacrylate it has been possible to obtain the complete master stress relaxation curve for one polymeric material, and to show that the principle of translation of the master curve along the logarithmic time axis still applies reasonably well throughout the transition region.

EXPERIMENTAL

The techniques used in the measurement of stress relaxation in the rubbery state where the modulus ranges from 10^7 to $10^{7.5}$ dynes/cm.² have been described elsewhere (2,3). These techniques may be extended to cover measurements through some of the transition region, but with increasing difficulty as the modulus increases because of the small size of the elongations which can be produced. Because of these small elongations, the maintenance of constant strain during the stress relaxation, the measurement of strain, and the control of temperature all become more difficult problems. A special relaxometer was devised for stress relaxation measurements in this glassy state, or region of high modulus, and has been described elsewhere by one of us (4). The stress measurement was carried out by means of accurate measurement of a low deflection spring system, using a linear differential transformer as the sensitive element, coupled to a recorder. Strain was measured by an optical extensometer utilizing two rollers with attached mirrors and reading rotational angles with a telescope. The sample and clamps were enclosed inside a thermostated air oven consisting of an inner and outer air chamber surrounded by 3 in. of glass wool insulation. The temperature regulator was based on a mercury expansion element which had minimum temperature drift over the long periods of time necessary to run the experiments.

In carrying out the measurements on polymethyl methacrylate, several precautions were necessary which had not previously been found to be of importance in work on polyisobutylene and rubbers. Polymethyl methacrylate absorbs water, and it was found that it was necessary to dry the samples thoroughly before making measurements and to dehydrate the sample chamber by use of trays of calcium chloride to prevent reabsorption of water during the measurements. These precautions were necessary in the range of glassy behavior largely because absorption of water caused the sample to swell and caused a change in stress at constant strain during the measurements. Consequently, variations in room humidity from day to day caused irregularities in the stress relaxation curves when such precautions were not followed.

At higher temperatures, in the transition region, water had a slightly different effect on the results. In this temperature region it was found that samples which were not initially dried before beginning a stress relaxation

run showed a lower value of the stress for a given strain and faster stress decay than they did after drying out the water by holding them in the oven for a number of hours. Figure 1 shows the results obtained on the same sample which had been initially saturated with water and then stretched successively a number of times in the oven. The results show that as the water is driven out the sample gets stiffer. When the sample was then resoaked in water and tested again, its modulus started out

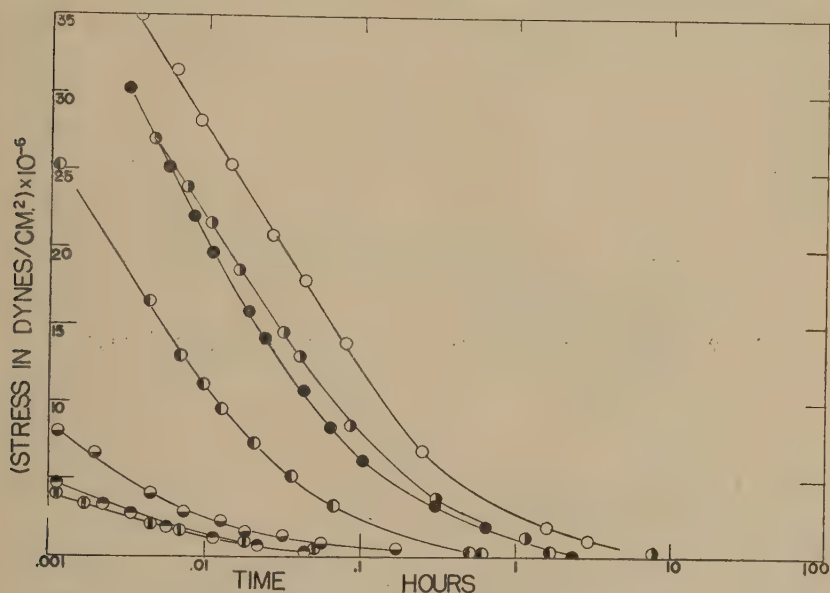


FIG. 1. Effect of water content on stress relaxation of polymethyl methacrylate at 108°C.

First series: ● 23 minutes in oven
 ● 37 minutes in oven
 ● 73 minutes in oven
 ● 249 minutes in oven
 ○ 1,162 minutes in oven

Second series: ⊕ 16 minutes in oven
 ● 1,150 minutes in oven

(All runs with same elongation.)

again at the low level. Figure 2 shows a plot of the loss of weight of water of a wet sample at this temperature compared with the change in the value of the modulus after various lengths of time in the oven. It seems clear-cut that the change in modulus follows the water loss. Evidently, water plasticizes polymethyl methacrylate effectively in the transition region.

During the investigation of methods of drying polymethyl methacry-

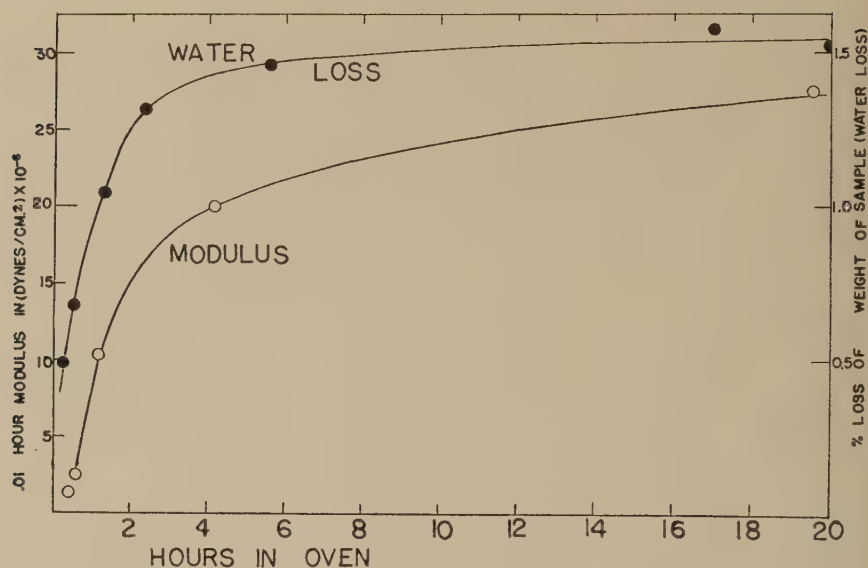


FIG. 2. Effect of water content on polymethyl methacrylate at 108°C.

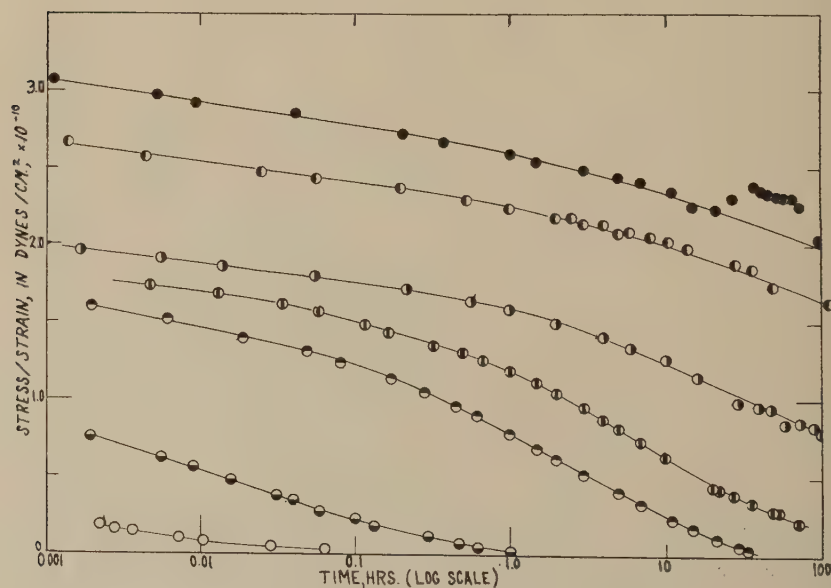


FIG. 3. Stress relaxation of polymethyl methacrylate.

- | | |
|---------|----------|
| ● 30°C. | ● 100°C. |
| ● 50°C. | ● 110°C. |
| ● 80°C. | ○ 112°C. |
| ○ 92°C. | |

late samples for use in measurements made in the region of glassy behavior, it was found that the rate of cooling of the samples from temperatures above the transition had a pronounced effect on the stress relaxation curves in the glassy state. This has been mentioned by us briefly in a recent communication (5). We found that samples cooled rapidly exhibited a faster rate of stress relaxation than samples cooled slowly through the transition region. The faster rate of stress relaxation for samples cooled rapidly may be related to less ordered and less compact packing during cooling at the faster rate, allowing more room for chains

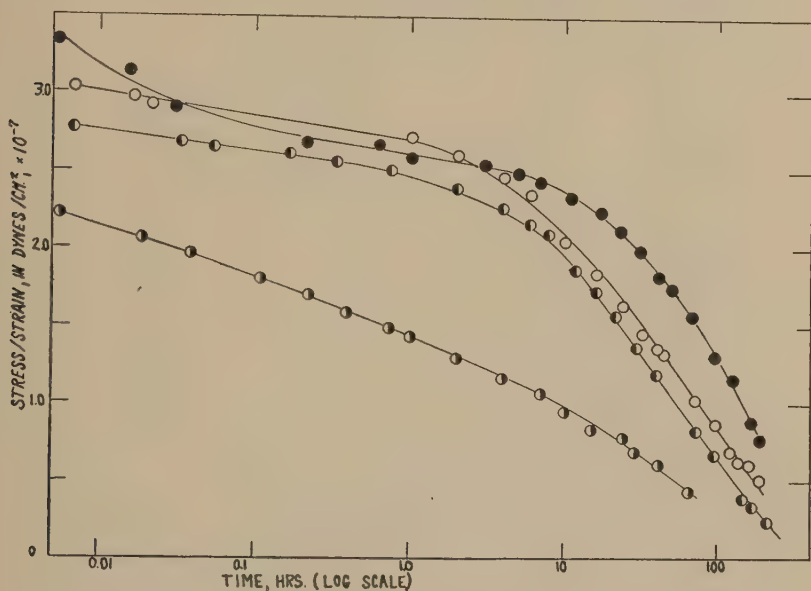


FIG. 4. Stress relaxation of polymethyl methacrylate.

● 125°C. ● 135°C.
○ 135°C. ● 155°C.

to rearrange when the sample is later stretched and thus causing a faster rate of stress relaxation. If this is the case, it should be possible to pick up a difference in specific volume on cooling at different rates. This has already been done by Alfrey, Goldfinger, and Mark (6) for polystyrene and they showed that, indeed, samples cooled more rapidly had a higher specific volume at any given temperature below the transition temperature region. Boyer and Spencer (7) and Rynkiewicz (8) showed similar effects. In addition to a faster rate of stress relaxation, polymethyl methacrylate samples cooled rapidly exhibited a smaller initial modulus than those cooled slowly.

All of the samples whose stress relaxation curves are shown in Fig. 3 were dried thoroughly by holding in a desiccator for a week and were all cut from the same sheet, and hence all had the same past thermal history. Thus Fig. 3 shows the family of stress relaxation curves in the glassy state. Relaxation in the rubbery state is shown in Fig. 4. The complete behavior of the polymer, all the way from the glassy state to the rubbery state, is shown in Fig. 5. Here the logarithm of the stress/strain has been

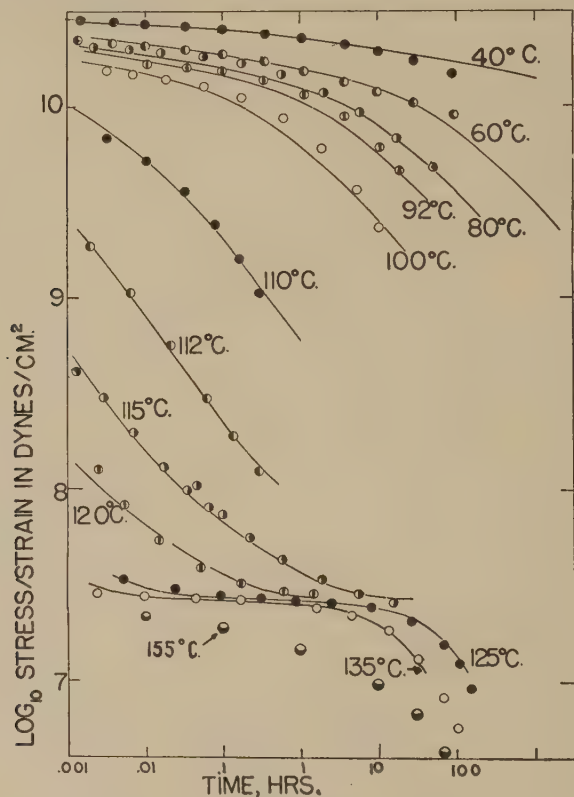


FIG. 5. Comparison of experimental curves and master stress relaxation curve for polymethyl methacrylate.

plotted against the logarithm of the time. The experimental results are shown as points. The solid lines are all parts of the same master relaxation curve which has been shifted along the time axis to match the experimental curves at each temperature. The accuracy of the fit of the master relaxation curve can be judged from this figure. The function $\kappa(T)$, mentioned previously, describes the amount of the shift of the master curve along the logarithmic time axis from one temperature to another. It was tabulated previously for polymethyl methacrylate in our last

TABLE I

Dependence of $\kappa(T)$ on Temperature for Polymethyl Methacrylate

T °C.	κ	$\log_{10} \kappa$	$-\frac{d \log_{10} \kappa}{dT}$
40	4.0×10^6	6.60	0.105
60	3.2×10^4	4.50	0.045
80	4.0×10^3	3.60	0.038
92	1.4×10^3	3.15	0.118
100	1.6×10^2	2.20	0.220
110	1.0	0	0.925
112	1.4×10^{-2}	-1.85	0.417
115	8.0×10^{-4}	-3.10	0.240
120	5.0×10^{-5}	-4.30	0.280
125	2.0×10^{-6}	-5.70	0.055
135	5.60×10^{-7}	-6.25	

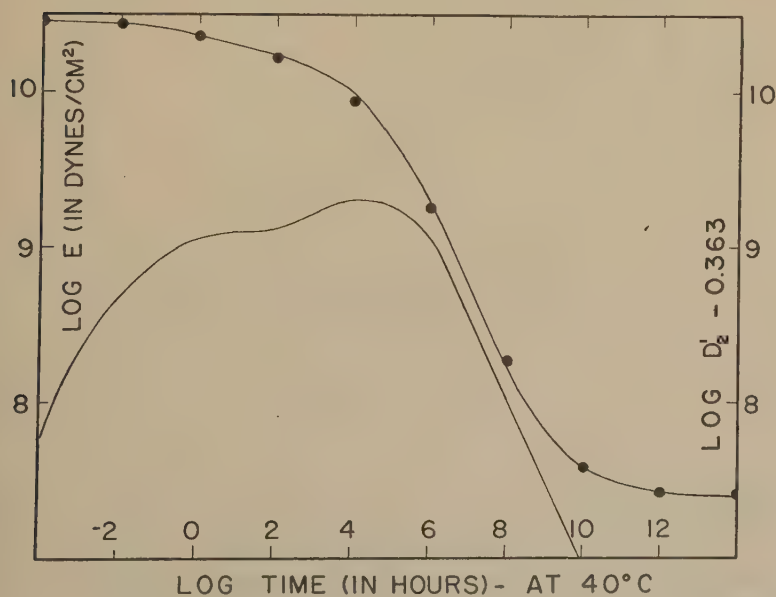


FIG. 6. Comparison of master stress relaxation curve, calculated from the distribution of relaxation times (shown beneath it), with the experimentally determined master stress relaxation curve which is represented by the points (●).

paper (1), but is included again for convenience in Table I. The whole master relaxation curve is shown in Fig. 6 together with the distribution of relaxation times corresponding to the master relaxation curve. The method of deriving the distribution of relaxation times from the master relaxation curve is discussed later.

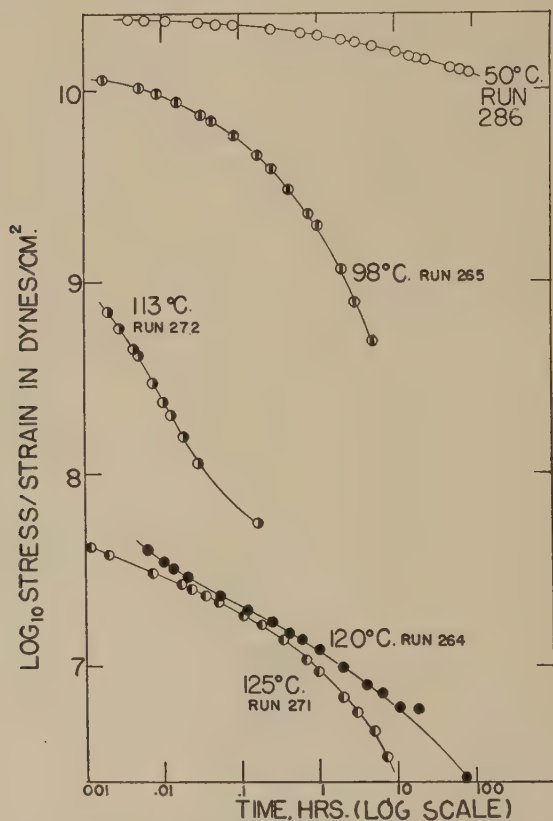


FIG. 7. Stress relaxation of low molecular weight polymethyl methacrylate.

- 50°C. ● 120°C.
 ⊙ 98°C. ● 125°C.
 ○ 113°C.

In addition to the above data on a polymethyl methacrylate sample which had an average molecular weight of 3,600,000 as determined by intrinsic viscosity measurements, a further series of relaxation experiments was run on a sample with a molecular weight of 150,000. The results obtained are shown in Fig. 7. The pattern is very similar to the pattern for high molecular weight methyl methacrylate in the glassy region and in the transition region. Only in the rubbery state does mole-

cular weight have any pronounced effect on the stress relaxation curves. Here the lower molecular weight material exhibits a faster decrease of stress with time for any given temperature as well as a lower modulus for any given point on the time scale at that temperature. This agrees very well with the effects in the rubbery state produced by molecular weight changes in polyisobutylene. The whole master curve for low molecular weight polymethyl methacrylate bears a greater resemblance to polyisobutylene than does the higher molecular weight polymethyl methacrylate which deviates slightly from the principle of transposition along the logarithmic time axis in the temperature range from 125 to 155° C. (see Fig. 5). Figure 8 shows the master relaxation curve for polymethyl

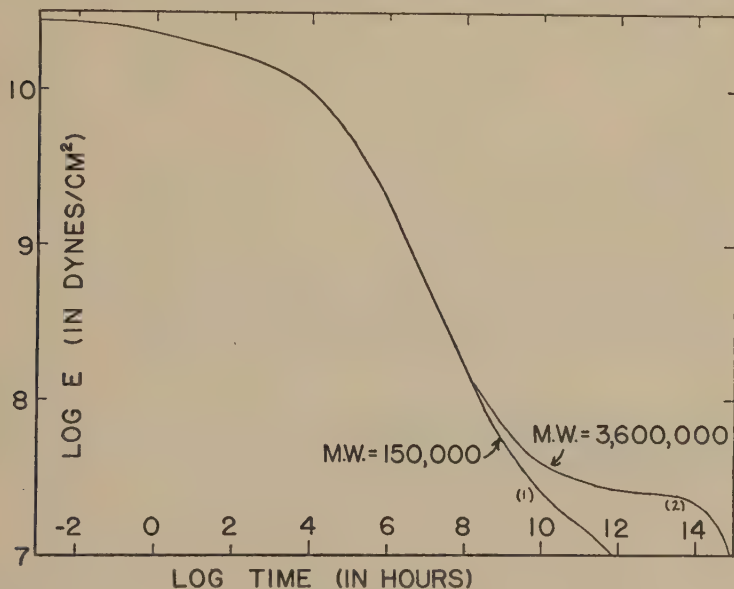


FIG. 8. Master stress relaxation curves for low molecular weight (m.w. 150,000 shown on left), and high molecular weight (m.w. 3,600,000, shown on right) polymethyl methacrylate.

methacrylate of molecular weight 3,600,000 compared with the master curve for methyl methacrylate of molecular weight 150,000. The curve for the higher molecular weight is necessarily inaccurate in the rubbery region where the deviation mentioned above occurs, but illustrates how increasing molecular weight extends the "flat" on the master curve at a modulus $10^{7.4}$ dynes/cm.². The presence of this "flat" is characteristic of an elastic rubber with very little plastic flow.

The function κ which defines the transposition of the master relaxation curve along the time scale with temperature has been tabulated. The logarithm of κ represents the magnitude of shift along the logarithmic

time scale and $-d \log_{10} \kappa/dT$ represents the temperature dependence of the relaxation rate. This quantity has been plotted against temperature in Fig. 9, illustrating that the most rapid change with temperature is in the middle of the transition region, that is, at 111°C . The change with

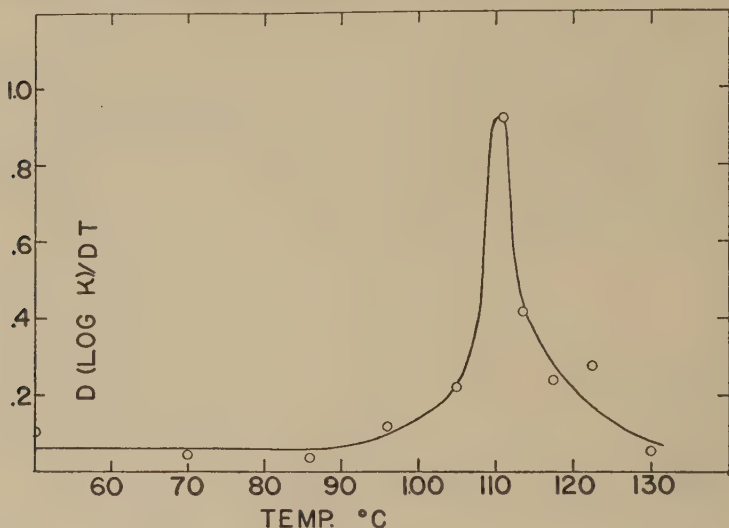


FIG. 9. Temperature dependency of stress relaxation for polymethyl methacrylate.

temperature in the transition region is much sharper for polymethyl methacrylate than for polyisobutylene.

DISTRIBUTION OF RELAXATION TIMES

First Approximation

The distribution of relaxation times $D(\tau)$ is defined in terms of the stress relaxation modulus $E_r(t)$ as follows:

$$E_r(t) = \int D(\tau) \exp(-t/\tau) d\tau. \quad [1]$$

The function $D'(\log \tau)$ which expresses the distribution function of relaxation times in terms of the argument $\log \tau$ is related to $D(\tau)$ by means of the equation

$$D'(\log \tau) = 2.303 \tau D(\tau). \quad [2]$$

The first approximation for $D'(\log \tau)$ is (9,10,11):

$$D'(\log \tau) = - \left[\frac{\partial E_r(t)}{\partial \log t} \right]_{t=\tau} = - 2.303 \left[\frac{E_r(t) d \log E_r(t)}{d \log t} \right]_{t=\tau}. \quad [3]$$

TABLE II
Tabulated Calculations for Derivation of Distribution of Relaxation Times from Master Stress Relaxation Curve
 (Time values correspond to 40°C. position of master curve)

$\log_{10} t$ t in hr.	E (exptl.) dynes/cm. ² $\times 10^7$	$\frac{E - E_2}{E - 2.54 \times 10^7}$ $\times 10^7$	$\log_{10} (E - E_2)$	$-\frac{d \log_{10} (E - E_2)}{d \log_{10} t}$	$\log_{10} D_1'$	$\log_{10} (E - E_2)$ (calcd.)	$\log_{10} (E - E_2)$ calcd. from shifted dis- tribution	$E - E_2$ calcd. from shifted distribution $\times 10^7$
(-5) ^a	(2,851)	2,849	10.4547	0.0000	8.216	10.457	10.460	2,884
(-4)	(2,851)	2,849	10.4547	0.0025	8.813			
-3	2,819	2,817	10.4498	0.0100	9.099	10.429	10.432	2,704
-2	2,723	2,721	10.4347	0.0200	9.347			
-1	2,571	2,569	10.4098	0.0375	9.444	10.352	10.363	2,307
0	2,291	2,289	10.3597	0.0526	9.446			
1	2,018	2,016	10.3045	0.0600	9.492	10.209	10.220	1,660
2	1,738	1,736	10.2396	0.0775	9.584			
3	1,413	1,411	10.1495	0.1178	9.702	9.921	9.943	877.0
4	1,012	1,010	10.0043	0.2158	9.631			
5	524.8	522.3	9.7179	0.3549	9.347	9.196	9.248	177.0
6	199.5	197.0	9.2945	0.4887	8.861			
7	57.55	55.01	8.7404	0.5727	8.246	8.117	8.209	16.18
8	16.60	14.10	8.1492	0.5416	7.739	6.996	7.107	1.279
9	7080	45.40	7.6571	0.5241	7.266			
10	3802	1.262	7.1011	0.6331	6.513	5.757	5.875	0.075
11	2786	0.246	6.3909	0.5734	5.977	3.4	3.5	0.0003
12	2.630	0.090	5.9542	0.4569	5.519			
13	2.570	0.030	5.4771	0.4771	3.741			
14	(2,541)	0.001	4.0000	0.2385				
15	(2,541)	0.001	4.0000	0.0000				

^a Values in parentheses are extrapolated.

In this paper we are only concerned with the distribution of relaxation times corresponding to the transition region—in which the modulus varies between $10^{7.4}$ dynes/cm.² and $10^{10.5}$ dynes/cm.². Accordingly, to obtain the first approximation for $D'(\log t)$ according to Eq. [3] we subtracted the quantity $E_2 = 10^{7.4}$ dynes/cm.² from all values of $E_r(t)$. This is equivalent to assuming that the Maxwellian distribution of relaxation times is a bimodal distribution one portion of which has a total modulus of $10^{7.4}$ dynes/cm.² and a set of very long relaxation times. It is the other portion of the bimodal distribution, i.e., the portion with the smaller relaxation times and which is relatively independent of molecular weight that concerns us here. The value of E_2 (namely, $10^{7.4}$ dynes/cm.²) was obtained by observation of the second "flat" in Fig. 6.

In Table II we have tabulated the values of $E_r(t)$ which are shown in Fig. 6 for various times (at 40°C.). The next columns give the values of $E - E_2$, $\log_{10}(E - E_2)$, $d \log_{10}(E - E_2)/d \log_{10} t$, and $\log_{10} D_1'(\log \tau)$ where

$$D_1'(\log \tau) = -2.303 [E_r(t)] \frac{d \log [E_r(t)]}{d \log t} \quad [4]$$

The notation $D_1'(\log \tau)$ signifies the first approximation to the distribution of relaxation times corresponding to the transition region of viscoelastic behavior.

Second Approximation

In order to obtain a second approximation to the distribution function $D'(\log \tau)$, the stress relaxation curve $E_r(t)$ corresponding to $D_1'(\log \tau)$ was computed and compared with the time experimental values. The computation of $E_r(t)$ that corresponds to $D_1'(\log \tau)$ was accomplished as follows: the logarithmic time axis was divided into intervals 0.2 units wide (i.e., two-tenths of a logarithmic cycle). The value of $D_1'(\log \tau)$ at the center of each of these logarithmic time intervals was interpolated from Table II, and D_1' was assumed to have that value from one end of the interval to the other. The result is a staircase type of distribution with the discontinuities from one interval to the next quite small. The distribution obtained within each interval is a so-called "box" distribution whose properties have been described at length previously (11). The relaxation modulus $E_r(t)$ corresponding to a "box" distribution can be evaluated by means of tabulated exponential integral functions. A systematic calculation of $E_r(t)$ was set up by computing the contribution from each "box" of the staircase function. Twenty evaluations of the exponential integral were made at 20 points covering four cycles of logarithmic time change. Where $t > 10 \tau_m$ (τ_m being the upper limit of the box) relaxation is essentially complete. Where $t < 0.001 \tau_i$ (τ_i being the lower limit of the box) the relaxation is essentially negligible. The contribution from each

box of the staircase is then summed up to give the computed values of $E_r(t)$ at each of the time intervals (spaced two-tenths of a logarithmic cycle apart on the log time axis).

The values of $\log(E - E_2)$ thus obtained from the staircase distribution corresponding to $D_1'(\log \tau)$ are shown in Table II where they may be compared with the experimental $\log(E - E_2)$ values. It was found that the calculated values would be closer to the experimental values if the whole distribution curve, and corresponding values of $\log(E - E_2)$ obtained from it, would be moved 0.2 logarithmic time units toward the longer time side. This was accordingly done, and E_2 was added to the calculated $E - E_2$ values, giving values of E which can be compared with the experimental values as shown in Tables II and III. The second ap-

TABLE III

Master Stress Relaxation Curve for Polymethyl Methacrylate and Distribution of Relaxation Times Calculated from It

(Time values correspond to 40°C. position for master curve)

$\log_{10} t$ <i>t in hr.</i>	$\log_{10} E$ (exptl.) <i>dynes/cm.²</i>	$\log_{10} E$ calcd. from dis- tribution of relaxation times	$\log_{10} D_2'$ (distribu- tion of relax- ation times)
(-4) ^a	(10.455)	10.460	8.097
-2	10.435	10.432	9.042
0	10.360	10.363	9.424
2	10.240	10.221	9.482
4	10.005	9.944	9.678
6	9.300	9.254	9.403
8	8.220	8.272	8.369
10	7.580	7.582	7.360
12	7.420	7.416	6.084
(14)	(7.405)	7.405	4.096

^a Values in parentheses are extrapolated.

proximation for the distribution function $D_2'(\log \tau)$, obtained by moving the distribution $D_1'(\log \tau)$ 0.2 logarithmic units to the right, is also shown. The agreement between the experimental points and the relaxation curve calculated from $D_2'(\log \tau)$ is shown in Fig. 6. Further improvement in the distribution function by a successive approximation was not felt to be warranted in view of the recognized approximations used in deriving the master stress relaxation curve from the experimental data.

ACKNOWLEDGMENTS

We should like to acknowledge the cooperation of Drs. W. F. Bartoe and T. F. Protzman of the Rohm and Haas Chemical Company in supplying us with samples and in determining intrinsic viscosities. We are indebted to Professor W. J. Kauzmann for helpful discussions, and to the Princeton Plastics Laboratory for partial support of this work.

REFERENCES

1. TOBOLSKY, A. V., AND McLOUGHLIN, J. R. *J. Polymer Sci.* **5**, 543 (1952).
2. TOBOLSKY, A. V., PRETTYMAN, I. B., AND DILLON, J. H., *J. Applied Phys.* **15**, 380 (1944).
3. STEIN, R. S., AND SCHAEVITZ, H., *Rev. Sci. Instruments* **19**, 835 (1948).
4. McLOUGHLIN, J. R., *Rev. Sci. Instruments* **23**, 459 (1952).
5. McLOUGHLIN, J. R., AND TOBOLSKY, A. V., *J. Polymer Sci.* **7**, 658 (1951).
6. ALFREY, T., GOLDFINGER, G., AND MARK, H. *J. Applied Phys.* **14**, 700 (1943).
7. BOYER, R. F., AND SPENCER, R. S. *J. Applied Phys.* **17**, 398 (1946).
8. CLASH, R. F., AND RYNKIEWICZ, L. M., *Ind. Eng. Chem.* **36**, 279 (1944).
9. ALFREY, T., *Mechanical Behavior of High Polymers*. Interscience Publishers, New York, 1948.
10. FERRY, J. D., SAWYER, W. M., BROWNING, G. V., AND GROTH, A. H., *J. Applied Phys.* **21**, 513 (1950).
11. TOBOLSKY, A. V., DUNELL, B., AND ANDREWS, R. D., *Textile Research J.* **21**, 404 (1951).

SELF-PLASTICIZATION OF POLYMERS

Kurt Ueberreiter and Gerhard Kanig

Kaiser-Wilhelm Institute for Physical Chemistry, Berlin-Dahlem, Germany

Received May 5, 1952

A. INTRODUCTION

Because of their polymolecularity, polymers contain small proportions of components with very low molecular weights such as monomers, dimers, trimers, tetramers, etc. These act as plasticizers and it therefore seems reasonable to speak of a self-plasticization of the high polymer. As far as we know there have been no previous experiments carried out with this point of view. Some investigations have been published, however, concerning the plasticization of polystyrene with monostyrene and of polymethyl methacrylate with monomethyl methacrylate by Alexandrov and Lazurkin (1) and of polystyrene with ethylbenzene (as a substance similar to styrene) by Ueberreiter (2). But the plasticization by monomers shall not be considered by us.

Only the investigations of Fox and Flory (3) involving three different mixtures of fractionated polystyrenes with molecular weights of 85,000, 4810, and 3540 are in a closer relationship to the experiments described in this paper.

B. EXPERIMENTAL

Polystyrene previously investigated (4) had been polymerized thermally without the use of catalyst at 220 and 300°C. Eighteen fractions with degrees of polymerization of 2–900 had been separated from these polymers. The experimental results from these fractions are used in this paper. Using varying proportions and different combinations of these fractions, 12 mixtures of widely varying composition were prepared (see Table I for composition). The homologous polystyrenes were taken either from the above mentioned fractions or from a series prepared in the same way.

Molecular weights up to 1000 have been cryoscopically determined, the higher ones with the viscometric method following a formula of Bamford and Dewar (5):

$$[\eta] = 2.92 \times 10^{-4} \times M^{0.65}.$$

The recently developed formula of Pepper (6) might be even better

$$[\eta] = 2.7 \times 10^{-4} \times M^{0.66},$$

TABLE I—Data Summary

No.	w^a	P^b	N_e^c	$(dv/dT)_{liq.} \times 10^{14d}$	$(dv/dT)_{sol.} \times 10^{14d}$	t_g^e	v_g^f	$v_{(0)liq.}^g$	$v_{(0)sol.}^h$	$v_g - v_{(0)sol.}$
Pure polystyrene fractions										
1	1.0	2	1	7.11		°C.				
2		2	1	7.50	3.28	-78	0.9130	0.7667	0.8473	0.0657
3		3.1	0.667	6.53	2.78	-40	0.9245	0.7724	0.8614	0.0631
4		3.2	0.623	6.70						
5		3.3	0.597	6.56		-45	0.9215	0.7719		
6		4.1	0.485	6.24	2.25	-25	0.9267	0.7719	0.8710	0.0557
7		6.9	0.292	6.04		+19	0.9370	0.7606		
8		8.1	0.248	5.81	2.21	+11	0.9383	0.7733	0.8753	0.0630
9		12	0.172	5.66	2.05	+38	0.9465	0.7705	0.8829	0.0636
10		25	0.081	5.64	2.08	+63	0.9555	0.7694	0.8860	0.0695
11		45	0.045	5.68	1.88	+80	0.9660	0.7655	0.8996	0.0664
12		81	0.025	5.58	1.75	+87	0.9650	0.7641	0.9020	0.0630
13		140	0.014	5.52	1.80	+87	0.9650	0.7663	0.8912	0.0738
14		252	0.008	5.49	1.77	+96	0.9685	0.7659	0.9032	0.0653
15		292	0.007	5.55	1.80	+89	0.9670	0.7661	0.9015	0.0655
16		311	0.006	5.69	1.95	+91	0.9663	0.7591	0.8954	0.0709
17		400	0.005	5.41	1.78	+97	0.9685	0.7683	0.9026	0.0659
18		900	0.002	5.47	1.85	+98	0.9682	0.7653	0.8986	0.0696
Mixtures of fractions: $w_{[39-4]} + w_{[8-1]}$										
$w_{[39-4]} \quad \bar{P}_n$										
19	0.10	8.8	0.228	6.02	2.03	+15	0.9350	0.7616	0.8765	0.0585
20	0.25	10	0.199	5.82	2.02	+24	0.9360	0.7631	0.8760	0.0600
21	0.50	13	0.149	5.83	1.96	+40	0.9465	0.7640	0.8852	0.0613
22	0.75	20	0.100	5.55	1.84	+60	0.9530	0.7682	0.8917	0.0613
23	0.90	29	0.070	5.50	1.81	+72	0.9585	0.7687	0.8961	0.0624
Mixtures of fractions: $w_{[928]} + w_{[8-3]}$										
$w_{[928]}$										
24	0.243	4.4	0.453	6.08	2.33	-11	0.9285	0.7692	0.8675	0.0610
25	0.50	6.7	0.300	6.03	2.17	+13	0.9370	0.7645	0.8749	0.0621
26	0.75	13	0.151	5.60	2.08	+47	0.9465	0.7673	0.8799	0.0666
27	0.90	32	0.062	5.52	1.90	+71	0.9585	0.7686	0.8931	0.0654
Mixtures of fractions: $w_{[48-1]} + w_{[2]}$										
$w_{[2]}$										
28	0.374	5.0	0.400	6.04		-16	0.9300	0.7747		
29	0.197	8.7	0.230	5.68	2.33	+16	0.9380	0.7738	0.8707	0.0673
Mixtures of fractions: $w_{[222]} + w_{[2]}$										
$w_{[2]}$										
30	0.516	3.8	0.520	6.13		-24	0.9260	0.7734		
										0.7674
										0.0646

^a w [degree of polymerization] = weight fraction of a polystyrene fraction in a mixture.^b P = degree of polymerization.^c N_e = mole fraction of chain end groups.^d $(dv/dT)_{liq.}$ and $(dv/dT)_{sol.}$ = volume-temperature coefficient of liquid and solid states.^e t_g = second-order transition temperature.^f v_g = specific second-order transition volume.^g $v_{(0)liq.}$ = extrapolated specific liquid volume at absolute zero point.^h $v_{(0)sol.}$ = extrapolated specific solid volume at absolute zero point.

covering the molecular weight range 1000–2,000,000. Both equations are valid for fractionated polystyrenes. It did not prove necessary to use the last equation as the results differ by only a negligible amount.

Volume-temperature curves of the mixtures were taken and used to calculate the specific volumes, the thermal expansion coefficients, and the second-order transition temperatures in the same way described in the previous paper (4), which contains further details.

C. RESULTS

1. *Polymers as Mixtures of End and Middle Groups*

(a) *Thermal Expansion Coefficients.* It could be proven (4) that above the second-order transition temperature in the liquid state, and below this temperature in the solid state, the expansion coefficients $(dv/dT)_{\text{liq.}}$ or $(dv/dT)_{\text{sol.}}$ (change of specific volume with temperature) can be composed additively from the expansion coefficients of the end and middle groups of the chain molecules. The end groups have a greater expansion coefficient according to an improved mobility which is due to their privileged position. It is not possible to compare monostyrene with these groups as its movements are entirely different. The result was:

$$(dv/dT) = (dv_m/dT) + [(dv_e/dT) - (dv_m/dT)] 2/P \quad [1]$$

and introducing the mole fractions of the end and middle groups

$$N_e = 2/P$$

and

$$N_m = (P - 2)/P \quad [2]$$

one obtains either

$$(dv/dT) = (dv_m/dT) + [(dv_e/dT) - (dv_m/dT)] N_e \quad [3a]$$

or

$$(dv/dT) = N_e \times (dv_e/dT) + N_m \times (dv_m/dT). \quad [3b]$$

These equations should remain the same even if fractions of different degree of polymerization were to be mixed. In this case it is only necessary to determine N_e or N_m .

The total number of chain groups in a mixture of two fractions, calculated in basic moles of styrene, is

$$n_{\text{st}} = n_1 P_1 + n_2 P_2.$$

Hence

$$N_e = \frac{2n_1 + 2n_2}{n_1 P_1 + n_2 P_2}$$

$$\text{or} \quad N_e = 2 \left(\frac{w_1}{P_1} + \frac{w_2}{P_2} \right) \quad (w_1 \text{ and } w_2 = \text{weight fraction}) \quad [4a]$$

as practically the same molecular weight can be used for the end and middle groups with the polymerization being carried out without catalyst. For i components of mixtures,

$$N_e = 2 \sum_1^i \frac{w_i}{\bar{P}_i} \quad [4b]$$

With the number-average degree of polymerization

$$\bar{P}_n = \frac{1}{\sum_1^i \frac{w_i}{\bar{P}_i}}$$

Eqs. [4a] and [4b] can be expressed as

$$N_e = 2/\bar{P}_n \quad [5]$$

The value of N_e in unfractionated polymers is therefore easily obtained by cryoscopic, osmotic, or end group determination of the number-average degree of polymerization \bar{P}_n .

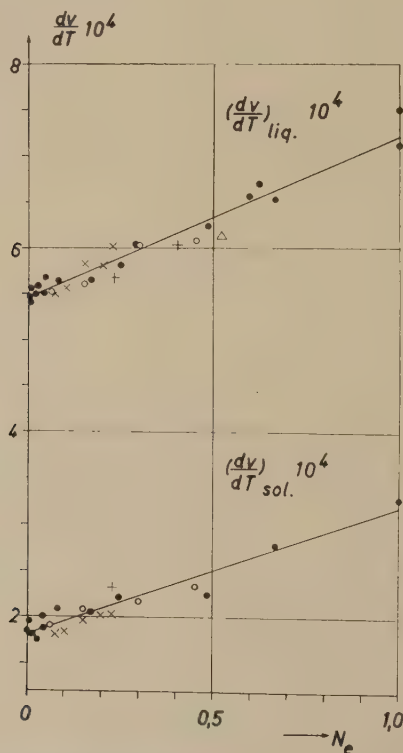


Fig. 1. The expansion coefficients of pure polystyrene fractions and mixture of fractions vs. mole fraction of chain end groups (for symbols see Fig. 6).

Table I shows the various mixtures with their experimental data. Figure 1 shows the dependence of $(dv/dT)_{\text{liq.}}$ and $(dv/dT)_{\text{sol.}}$ on N_e in both pure fractions and mixtures (4). The result is evident that the expansion coefficients of the mixtures show the same linear dependence on the composition as the pure fraction. Including all of the experimental data one obtains

$$(dv/dT)_{\text{liq.}} = 5.46 \times 10^{-4} + 1.74 \times 10^{-4} N_e, \quad [6a]$$

$$(dv/dT)_{\text{sol.}} = 1.81 \times 10^{-4} + 1.38 \times 10^{-4} N_e. \quad [6b]$$

Both equations are identical with Eq. [3a]. Specially for the end groups one obtains therefore

$$(dv_e/dT)_{\text{liq.}} = 7.20 \times 10^{-4} \text{ and}$$

$$(dv_e/dT)_{\text{sol.}} = 3.19 \times 10^{-4} \quad [7a]$$

and for the middle groups

$$(dv_m/dT)_{\text{liq.}} = 5.46 \times 10^{-4} \text{ and}$$

$$(dv_m/dT)_{\text{sol.}} = 1.81 \times 10^{-4}. \quad [7b]$$

Substituting [5] into [6a] and [6b] one obtains

$$(dv/dT)_{\text{liq.}} = 5.46 \times 10^{-4} + (3.48 \times 10^{-4})/\bar{P}_n, \quad [8a]$$

$$(dv/dT)_{\text{sol.}} = 1.81 \times 10^{-4} + (2.76 \times 10^{-4})/\bar{P}_n. \quad [8b]$$

(b) *The Volumes.* An important result of the previous paper (4) was the fact that all the volume-temperature curves of the liquid state above the transition temperature if they are extrapolated intersect each other practically at the same point, at absolute zero temperature. The volume at this point is

$$v_{(0)\text{liq.}} = 0.7674 \text{ cm.}^3/\text{g.} \quad (\text{See Table I.})$$

As the curves for the mixtures of the fractions intersect each other also at the same point if extrapolated, the conclusion of equal behavior to the pure fractions is obvious. Integration of [8a] gives for pure and mixed fractions the equation

$$v_{\text{liq.}} - 0.7674 = \left(5.46 \times 10^{-4} + \frac{3.48 \times 10^{-4}}{\bar{P}_n} \right) T. \quad [9]$$

This means isothermals of a functional dependence

$$v_{\text{liq.}} = a + (b/P) \quad [10]$$

which could be found in different homologous and polymer-homologous series and which are the result of the additivity of the molar volumes of end and middle groups (3, 7).

It is quite evident that these simple relations hold only for corresponding states of molecular motion. These exist, beginning with the corresponding transition temperature, obviously in a large temperature range.

Accepting the theories (8) of the thermal volume expansion of liquids, the decrease of the specific volume of polymers with decreasing temperature can be explained (3) with the increase of density of packing of the chain units or segments. This is combined with an increase of the degree of order of the spatial arrangement and the "short range" order. No change of the intermolecular distance of the chain units occurs thereby according to x-ray investigations of polystyrenes by Krimm and Tobolsky (9). This seems to be the case as long as the volume-temperature coefficient above the transition temperature remains constant. This temperature range is quite large. The position of this temperature range

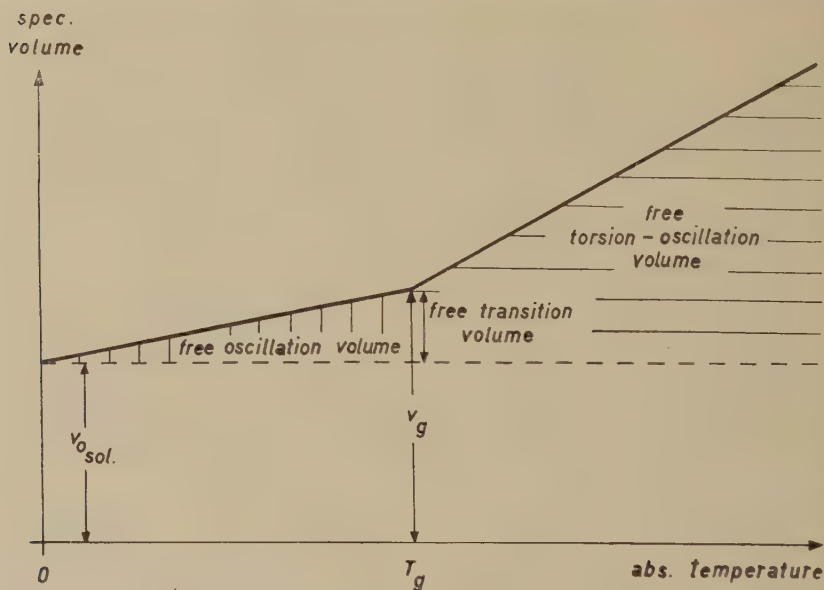


FIG. 2. Free volumes.

naturally depends upon the transition temperature and therefore upon the chain length of the particular fraction.

At higher temperatures a noticeable deviation from the linearity of the $v_{liq.}-T$ equations is observed. Krimm and Tobolsky explain this fact with the increase of the intermolecular distance of the chain units. The $v-T$ curves by Fox and Flory of polystyrene fractions with molecular weights 3000 to 85,000 deviate at 160°C. from a straight line, while the three fractions with molecular weights of 32,400, 14,500, and 4600, the volume curves of which have been investigated up to 270°C. by us, do not deviate under 240°C. from a linear relationship. Trimeric styrene shows a deviation at 140°C. and the dimer at *ca.* 80°C. But it could be proven experimentally that, with the exception of the dimer, all these deviations

from a straight line are caused by the beginning of degradation of the polystyrene.

As the polymer is cooled to its transition temperature the chains become closer packed due to changes in the chain configuration. The motions of the chain units—in a previous paper explained as torsion oscillations (10)—freeze in, and therefore the structure existing at that point is retained practically to absolute zero (11).

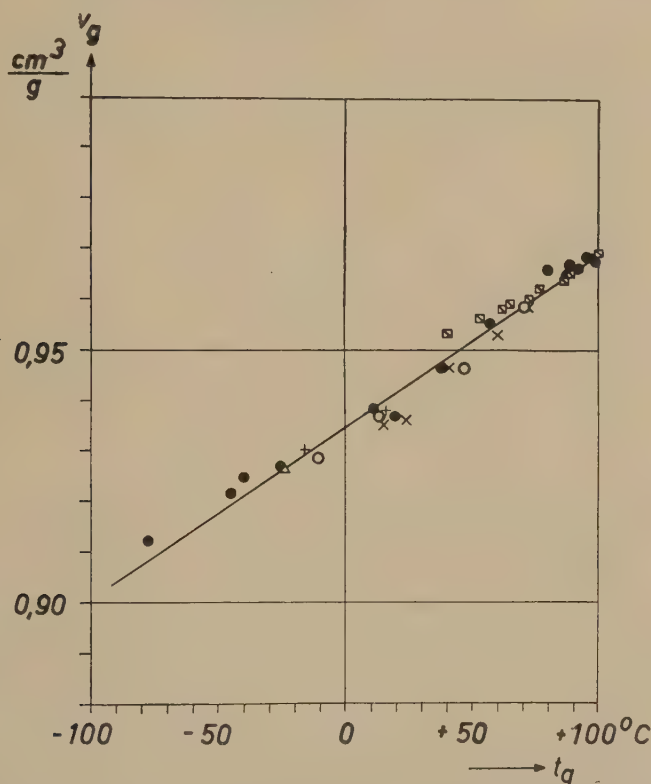


FIG. 3. Second-order transition temperature of pure polystyrene fractions and mixtures of fractions vs. second-order transition volume (for symbols see Fig. 6).

The volume available for torsion oscillations above the transition temperature at a temperature T is (Fig. 2)

$$v_{\text{free tor. oscil.}} = v_{\text{liq.}} - v_{(0)\text{sol.}} \quad [11]$$

and shall be called "free torsion oscillation volume." This definition differs from the Fox and Flory "free volume" as shall be described later. The volume changes below the transition temperature also, although at a much lower rate (see Eq. [8b] and Fig. 1). This is due to the oscillations

of the frozen-in system (10) similar to those of a crystal lattice. By extrapolating the volume curves below the transition temperature to absolute zero, $v_{(0)\text{sol.}}$ data can be found, which depend only on the frozen-in state of order, according to the corresponding transition temperature

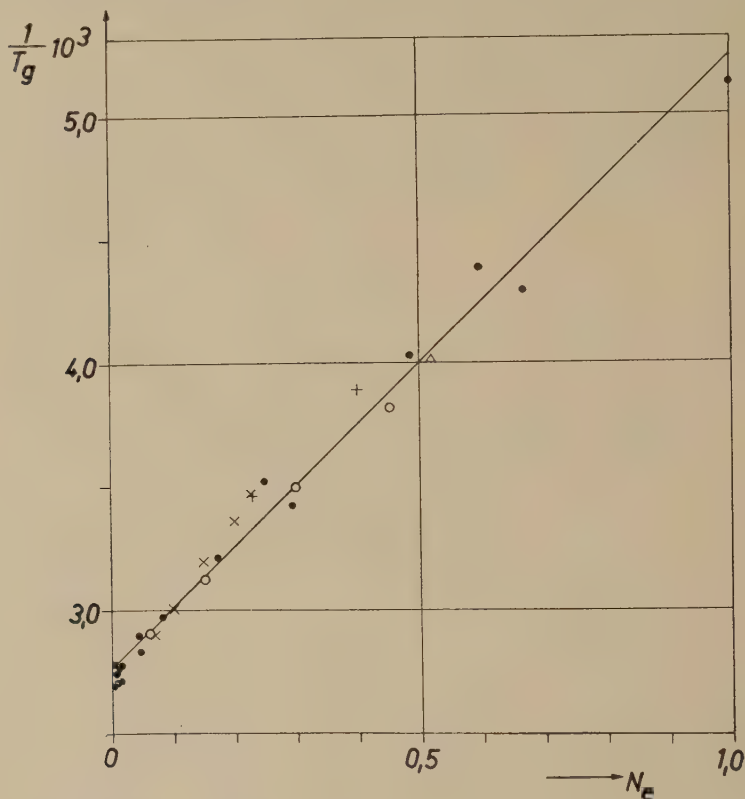


FIG. 4. Second-order transition temperature of pure polystyrene fractions and mixtures of fractions vs. mole fraction of chain end groups (for symbols see Fig. 6).

T_g . $v_{(0)\text{sol.}}$ is a function of \bar{P}_n and T_g since the state of order is dependent on the chain length.

Integrating [8b] one obtains

$$v_{\text{sol.}} - v_{(0)\text{sol.}}(T_g, \bar{P}_n) = \left(1.81 \times 10^{-4} + \frac{2.76 \times 10^{-4}}{\bar{P}_n} \right) T \quad [12]$$

with

$$v_{\text{free oscil.}} = v_{\text{sol.}} - v_{(0)\text{sol.}}, \quad [13]$$

the volume available for oscillations [see Ref. (12)]. Using Eqs. [9] and [12] for the special value T_g and eliminating the resulting v_g from both

equations, an equation for $v_{(0)\text{sol.}}$ can be derived:

$$v_{(0)\text{sol.}} = \left(3.65 \times 10^{-4} - \frac{0.72 \times 10^{-4}}{\bar{P}_n} \right) T_g + 0.7674. \quad [14]$$

The isothermals of Eq. [12] do not show the simple form of Eq. [10], i.e. the volumes of a polymer-homologous series within the amorphous solid state cannot be treated as ideal mixture volumes of end and middle groups as one finds by substituting [14] into [12].

2. Chain End Groups Acting as Plasticizers

The second-order transition volumes of the mixtures are also represented practically by the same v_g-t_g curve (4) as the pure fractions, as

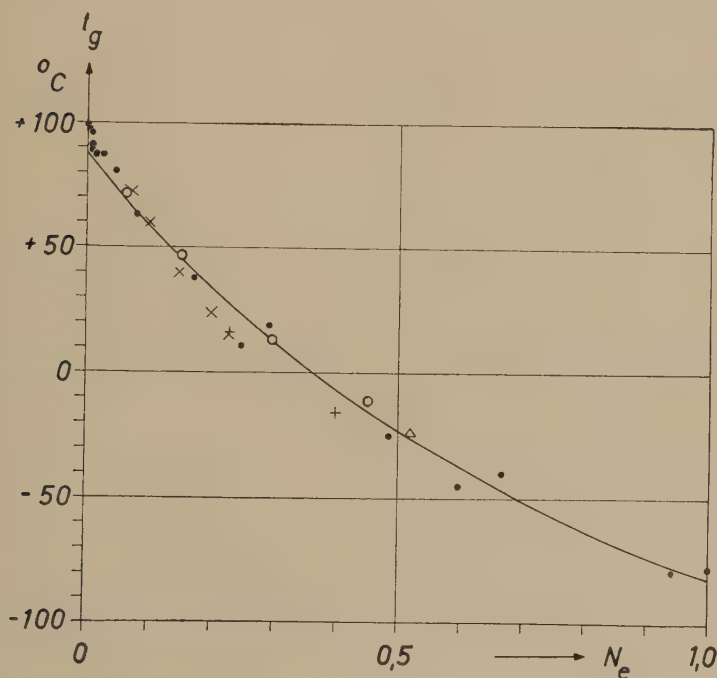


Fig. 5. Second-order transition temperature of pure polystyrene fractions and mixtures of fractions vs. mole fraction of chain end groups (for symbols see Fig. 6).

shown by Fig. 3 and Table I. Using the results of the mixtures too, the relation may be represented by the equation (Fig. 3 and Table I):

$$v_g = 0.9346 + 3.45 \times 10^{-4} t_g. \quad [15]$$

Putting v_g and T_g (see Table I) into Eq. [9] and introducing N_e with the help of [2] and [5], one obtains, using Eq. [15],

$$1/T_g = 0.002753 + 0.002384 \times N_e \quad [16a]$$

which is identical within the limits of experimental accuracy with the empirically determined relationship (Fig. 4)

$$1/T_g = 0.002768 + 0.002477 \times N_e. \quad [16b]$$

Accepting the idea of a binary system made up of end and middle groups [16b] the second-order transition point diagram can be represented like

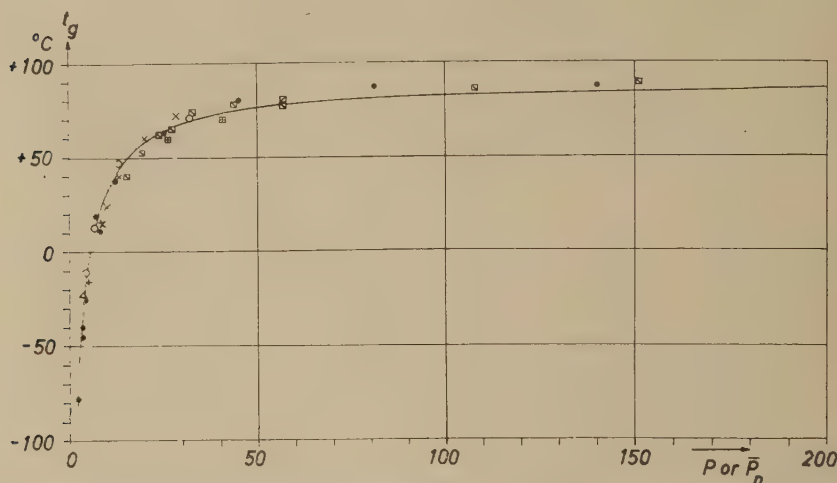


FIG. 6. Second-order transition temperature of pure polystyrene fractions and mixtures of fractions vs. degree of polymerization P or number-average degree of polymerization \bar{P}_n .

- pure fractions.
- × mixtures of fractions $P = 39.4$ and 8 .
- mixtures of fractions $P = 928$ and 3.3 .
- + mixtures of fractions $P = 48.1$ and 2 .
- △ mixtures of fractions $P = 222$ and 2 .

Measurements by Fox and Flory (3) [molecular weights converted with formula of Bamford and Dewar (5)]:

- pure fractions.
- ▤ mixtures of fractions $P = 724$ and 27.5 .
- ▥ mixtures of fractions $P = 724$ and 19.4 .

the ordinary melting point diagrams for binary systems of micromolecules, as shown in Fig. 5. Equation [16b] and Figs. 4 and 5 show the decrease of the transition temperature with an increase of the number of end groups (N_e). It therefore seems reasonable to treat the end groups as plasticizers. They cause the self-plasticization of the unfractionated polymer.

By substituting [2] or [5] into [16b] the dependence of the transition

temperature on the degree of polymerization may be described by

$$\frac{1}{T_g} = 0.002768 + \frac{0.004954}{\bar{P}_n} \quad [17]$$

(Fig. 6). An explanation for this equation may be found in the following fact:

A comparison of the difference $v_g - v_{(0)\text{sol.}}$ of the single fractions and fraction mixtures shows a practically constant volume difference of 0.0646 (Table I). In combination with [13] this results in

$$v_{\text{max. oscil.}} = v_g - v_{(0)\text{sol.}} = 0.0646 \text{ cm.}^3/\text{g.} \quad [18]$$

This volume difference is the space which, in the amorphous solid, is available for oscillations at the transition temperature. It is at the same time the maximum value for oscillations, and therefore there exists an "iso-oscillation volume" at the transition temperature for all degrees of polymerization. As the expression [18] follows from [11], one can conclude also a state of an "iso-torsion oscillation volume" at the transition temperature for all degrees of polymerization. Fox and Flory (3) define in a different way a "free volume" v_f as the specific liquid volume above the transition temperature minus the specific solid volume extrapolated to the same temperature above the transition temperature. This means that their free volume at the transition temperature should be zero for all kind of glasses. It is not clear how they find a state of iso-free volume from this.

The oscillations in the solid body cause a certain enlargement of the structure which seems necessary for the torsion oscillations (10) at the transition point. The necessary enlargement is, counting from the absolute zero point, constant for this polymer-homologous series, i.e. independent of the degree of polymerization. This means that end groups as well as middle groups in starting the torsion oscillation motion which causes a rearrangement of the groups need the same minimum volume for this displacement. The same shape of end and middle groups of nonpolar polymers might be the reason for it.

Substituting [18] into Eq. [12] gives in good agreement with [17]

$$\frac{1}{T_g} = 0.002801 + \frac{0.004260}{\bar{P}_n} \quad [19]$$

Different authors have tried with the help of viscometric data to derive relationships between the chain length and the transition temperature or the softening temperature which because of experimental conditions is always somewhat higher for long chains than the transition temperature. For a polystyrene fraction of molecular weight 420,000 Alexandrov and Lazurkin (1) found a softening temperature of about 106°C. whereas

Fox and Flory (3) found 99°C. for one of molecular weight 300,000. Alexandrov and Lazurkin reported a softening temperature of -80°C . for the dimer, while we found a transition temperature of -78°C . R. F. Tuckett (13) treated the softening temperature as an "isoviscous state" (14-17) and used a viscosity relationship for linear polyesters found by Flory (7) to derive the equation

$$\sqrt{P_w} = \frac{H}{R \times T_s} + G$$

which he tried to confirm by experiments with various polyvinyl acetates.

Fox and Flory (3), on the contrary, were able to prove with viscometric data from fractionated polystyrenes (range of mol.-weight 3000-

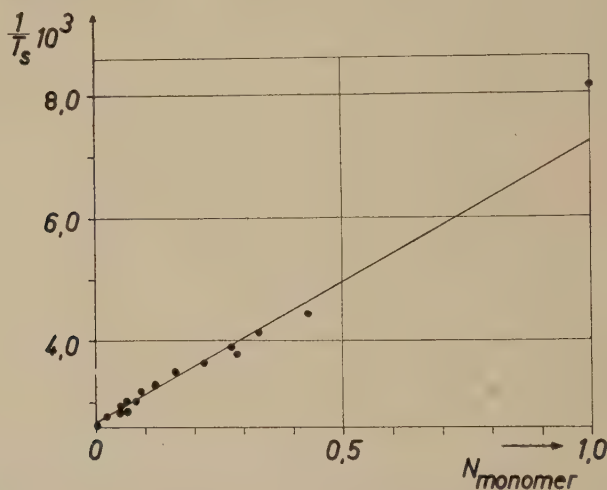


FIG. 7. Softening temperature of various polystyrene fractions (range of molecular weights 27,000-420,000) vs. mole fraction of monomer. Measurements by Alexandrov and Lazurkin (1).

300,000) that no isoviscous state exists at the transition temperature or softening point within a polymer homologous series. They however found a constancy of the viscosity-temperature coefficient or the "apparent energy of activation for viscous flow" (18) at the transition temperature:

$$R \times \frac{d \ln \frac{\eta_T}{\eta_{217}}}{d \frac{1}{T}} = E_T = 110 \text{ kcal./mole.}$$

By means of this result they derived from their empirical relationship

$$\log \frac{T}{217} = 2.92 \times 10^{16} \left(\frac{1}{T^6} - \frac{1}{490^6} \right) e^{-2530/M} \quad [20]$$

the equation

$$T_g = 373 - (1814/P).$$

But this may only be applied for the range of molecular weights investigated by them. It cannot be used for smaller molecular weights, for example the dimer which would receive an "apparent energy of activation" of 0.015 kcal./mole, which differs too much from the accepted constant value of 110 cal.

3. Monomers Acting as Plasticizers

The softening action of the chain end groups can be neglected in very high molecular weight polymers because of their small concentration

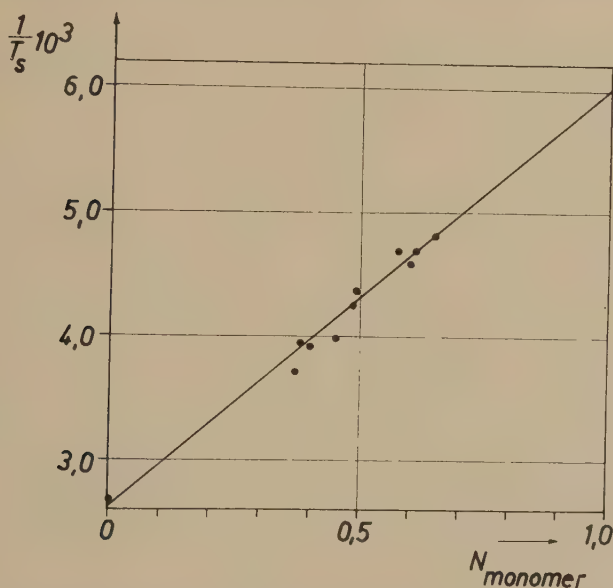


Fig. 8. Softening temperature of various polymethyl methacrylate fractions (range of molecular weights 20,000–135,000) vs. mole fractions of monomer. Measurements by Alexandrov and Lazurkin (1).

(Eq. [16b]). The statement of Alexandrov and Lazurkin (1) therefore does not seem surprising that polystyrene of a molecular range from 27,000 to 420,000 plasticized by monostyrene possesses softening temperatures which do not depend on the molecular weight of the high polymer but only on the content of monomer. Polymethyl methacrylates of molecular weights from 20,000 to 135,000 plasticized by monomers show the same result.

One can expect that plasticizers in externally plasticized (19, 20) substances act in a similar manner to the end groups. Here, finally, linear re-

lationships like [16b] between $1/T_g$ or $1/T_s$ and N_{pl} . (mole fraction of plasticizer) should be obtained too if the plasticizers are chemically and sterically similar to the chain units. Figures 7 and 8 illustrate this statement for the above-mentioned polymers plasticized by their monomers. Only the data for monostyrene differ to a larger extent from linearity. Unfortunately, the paper of Alexandrov and Lazurkin (1) gives no further details about the measurement of the softening temperature of monostyrene, while figures exist for the deformation curves of all other mixtures.

Further generalization still awaits an extension of experimental material.

SUMMARY

Using varying proportions and different combinations of polystyrene fractions with degrees of polymerization 928, 222, 48, 39, 8, 3.3, and 2, twelve mixtures of widely varying composition were prepared. The same conclusions could be drawn from the volume-temperature curves of these mixtures as were drawn from the data for pure fractions in an earlier paper. Regarding the thermal expansion coefficients $(dv/dT)_{liq.}$ and $(dv/dT)_{sol.}$ and the specific volumes above the transition temperature $v_{liq.}$, the mixtures behave as ideal mixtures composed of chain end and middle groups.

The end groups act as plasticizers and cause the "self-plasticization" of the polymer. From the fact of an "iso-oscillation volume" at the transition temperature, a relationship between second-order transition temperature, T_g , and the mole fraction of the end groups, N_e , was derived.

An explanation is given for the statements of Alexandrov and Lazurkin that high polymers plasticized by their monomers show softening temperatures which are independent of the molecular weight of the high polymer and depend only on the percentage of monomer.

REFERENCES

1. ALEXANDROV, A. P., AND LAZURKIN, J. S., *Compt. rend. acad. sci. U.S.S.R.* **43**, 376 (1944).
2. UEBERREITER, K., *Angew. Chem.* **53**, 247 (1940).
3. FOX, T. G., AND FLORY, P. J., *J. Applied Phys.* **21**, 581 (1950).
4. UEBERREITER, K., AND KANIG, G., *Z. Naturforsch.* **6a**, 551 (1951).
5. BAMFORD, C. H., AND DEWAR, M. J., *Proc. Roy. Soc. (London)* **A192**, 329 (1948).
6. PEPPER, D. C., *J. Polymer Sci.* **6**, 347 (1951).
7. FLORY, P. J., *J. Am. Chem. Soc.* **62**, 1057 (1940).
8. BERNAL, J. D., *Trans. Faraday Soc.* **33**, 27 (1937).
9. KRIMM, S., AND TOBOLSKY, A. V., *J. Polymer Sci.* **6**, 667 (1951).
10. UEBERREITER, K., AND NENS, S., *Kolloid-Z.* **123**, 92 (1951).
11. UEBERREITER, K., *Z. physik. Chem.* **B45**, 361 (1940); *ibid.* **B46**, 157 (1940).
12. UEBERREITER, K., AND ORTHMANN, H.-J., *Kolloid-Z.* **123**, 84 (1951).

13. TUCKETT, R. F., *Trans. Faraday Soc.* **39**, 158 (1943).
14. TAMMANN, G., AND HESSE, W., *Z. anorg. u. allgem. Chem.* **156**, 245 (1926).
15. JENCKEL, E., AND UEBERREITER, K., *Z. physik. Chem.* **A182**, 361 (1938).
16. BERGER, E., THOMAS, M., AND TURNER, W. S., *Glastech. Ber.* **12**, 172 (1934).
17. JENCKEL, E., AND SCHWITTMANN, A., *Glastech. Ber.* **16**, 163 (1938).
18. FOX, T. G., AND FLORY, P. J., *J. Am. Chem. Soc.* **70**, 2384 (1948).
19. UEBERREITER, K., *Kunststoffe* **30**, 170 (1940).
20. UEBERREITER, K., *Kolloid-Z.* **102**, 272 (1943).

SOME PROPERTIES OF ETHYL CELLULOSE FILMS¹

Howard C. Haas, Leonard Farney, and Claude Valle, Jr.

*The Chemical Research Laboratories of Polaroid Corporation,
Cambridge, Massachusetts*

Received February 14, 1952

INTRODUCTION

During a research program designed to study and compare the low-temperature strength properties of films of various cellulosic derivatives, it was found necessary to investigate some of the variables which have an effect on these properties. Before conclusions could be drawn regarding the comparative strengths of different materials, those conditions of film preparation which lead to maximum strength had to be established. It has been recognized for some time that the mechanical properties of films depend on the solvent used for casting. Sheppard and Newsome (1), Yamada (2), and Spence (3) have found, for example, that films of cellulose esters are more brittle when cast from polar solvents, this resulting from a larger degree of crystallinity. Other workers (4, 5, 6) have also studied the effect of solvent composition on film properties. The Hercules Powder Co. brochure on ethyl cellulose recognizes that flexible films of maximum strength are obtained when nonpolar solvents which have little or no affinity for water constitute a major portion of the solvent at the moment the film sets to a gel. Since effects of this nature are extremely important, the work described herein is primarily concerned with solvent composition and film properties. Ethyl cellulose, a good low-temperature polymer and representative of the type in which we were interested, was chosen for study. Specifically, an ethyl cellulose, which is commercially available from the Dow Chemical Company, containing 48.0–49.5% ethoxyl content and of the 100 centipoises viscosity type was employed. The investigation consisted of preparing films from a limited number of solvents of different dielectric constant and making a fairly detailed study of these films. Where possible, correlations have been drawn between film properties and other properties of the polymer-solvent systems.

Films of ethyl cellulose were prepared by castings on glass from benzene, 1:1 benzene-carbon tetrachloride, chlorobenzene, and 2-nitropro-

¹ This work was carried out under Quartermaster Corps Contract No. W-44-109-qm-2007; and presented at the Gordon Research Conferences, American Association for the Advancement of Science, July, 1951.

pane. After appropriate drying, the residual solvent contents of these films were determined. The ultimate strengths of these films were measured by a modified A.S.T.M. brittle-point test and by stress-strain measurements at 25° and -50°C. using a constant rate of elongation. Film densities, softening points, and moduli of flexure were also investigated. X-ray diffraction and birefringence measurements were employed to obtain an insight into film structure. The solvent power of these solvents for ethyl cellulose was estimated from dilute solution viscosity behavior and from the swelling of a cross-linked ethyl cellulose film in these solvents. The effects of annealing glass casts by holding them at their softening points for 18 hr. has been observed. Films have also been prepared by casting on mercury and their properties compared with those of glass casts.

EXPERIMENTAL METHODS

Preparation of Films

Solutions of ethyl cellulose in benzene, benzene-carbon tetrachloride, chlorobenzene, and 2-nitropropane were prepared by dissolving 90 g. of polymer in 510 g. of solvent. The solutions were filtered under pressure and allowed to stand until entrapped air escaped. Casts were made on carefully cleaned, level glass surfaces at doctor settings of 0.070 in. The casts were then covered with a frame of polyvinyl alcohol to maintain a solvent atmosphere during evaporation. After such time that a major portion of the solvent had evaporated and the films had a certain degree of strength, a second layer was cast over the first at doctor settings of 0.070 in. plus the film thickness. The films were again covered and allowed to dry in air for 24 hr. The films were then heated while still on glass for 48 hr. at 60°C. and then stripped from the glass and dried for 4 days at 60°C. under vacuum. The finished films were clear and had thicknesses ranging from 15 to 17 $\times 10^{-3}$ in.

Films were prepared on mercury as follows: Solutions containing 4.5 g. of ethyl cellulose in 70 ml. of solvent were poured on a mercury surface 6 in. in diameter, the mercury being contained in a glass evaporating dish. After the solutions had gelled, they were cut away from the sides of the dishes, and the remainder of the solvent evaporation was accompanied by unrestrained shrinkage in the planar dimensions of the films. This technique yielded films comparable in thickness to the films prepared on glass.

Residual Solvent Contents of Films Cast on Glass²

By analyzing the 2-nitropropane film for nitrogen and the films from chlorobenzene for chlorine, the residual solvent contents were calculated.

² Analyses were performed by Dr. C. Fitz.

Carbon and hydrogen analyses on the film from benzene and on the original ethyl cellulose powder were used to calculate the residual benzene content. The data are at best approximate because of the small quantities involved.

Brittle-Point Determinations³

The method and specifications of the test as we have carried it out were essentially those of Clash and Berg (7). These authors modified the tentative A.S.T.M. method D746-43T. A constant anvil velocity of 16.4 ft./sec. and an arbitrary span length of 0.045 in. were employed by us in order that thin films could be tested. The test pieces were $1.5 \times 0.05 \times 0.016 \pm .001$ in. and were conditioned prior to testing at 25°C. and 50% relative humidity for a minimum of 40 hr. Some samples were also tested after conditioning at room temperature and 0% relative humidity and after 1 week of cold storage (-40°C.). The brittle temperature was determined as the lowest temperature of nonfailure of five consecutive test specimens. The samples were allowed to remain for 15 min. at the test temperature before being struck. Although these brittle points are not standard, the data are comparable among themselves and serve the required purposes.

Tensile Stress—Elongation Measurements

Stress-strain measurements were made at 25° and -50°C. The measurements at room temperature were carried out on an Instron machine. Samples 2 in. in length were used (the jaws were set accurately at an initial separation of 2 in.), and a constant rate of elongation of 1 in./min. was employed. The -50°C. measurements were made on a Baldwin instrument; the same rate of elongation was employed. The samples were conditioned at -50°C. for 30 min. prior to measurement.

Moduli of Flexure³

Our instrument for measuring the modulus of flexure over a wide temperature range embodies the same parts as the Olsen stiffness tester (8). Moduli were calculated from plots of torque versus angle data. Samples were preloaded slightly to eliminate the difficult determination of the zero-point load. Prior to testing, all films were conditioned at room temperature and 40% relative humidity. Measurements were made from -50° to 80°C., the samples being held at each temperature for 20 min. before being measured.

Film Densities

Small strips of film were dried for 1 week over concentrated sulfuric acid in a vacuum desiccator. The densities were determined at 20°C.

³ These test methods were developed by personnel associated with the contract for the evaluation of thin films of cellulosic materials.

by displacement of a dilute solution of a non-sudsing wetting agent, Antaron L-250.

Softening Points

These measurements were made according to the directions of E. J. Lorand (9). The most characteristic point, which was taken as the softening point, was that temperature at which the thermometer under its own weight seemed to stick slightly to the packed material. The method enabled us to check the values given by the Dow Chemical Company brochure for its medium and standard ethoxy ethylcelluloses.

Dilute Solution Viscosity

Dilute solution viscosity measurements on ethyl cellulose in the four solvents were carried out at 30°C. using an Ostwald viscometer. The Huggins-Kraemer (10) viscosity equation

$$\eta_{sp}/c = [\eta] + k'[\eta]^2c \quad [1]$$

has been applied to the data.

X-ray Diffraction

X-ray photographs of the films cast on glass from benzene, chlorobenzene, and 2-nitropropane were taken. A double-film technique was used to cover the range of intensities. The samples were mounted on a fiber camera ($d = 57$ mm.) and exposure times of 1 hr. were employed. Cu(Ni) radiation was used.

Cross-Section Birefringence

The four films cast on glass were inspected for their cross-section birefringence. The sheet directions were defined so that x is in the direction of sheet thickness and y and z lie in the plane of the film. For these films $n_x = n_y$, i.e. the refractive index is independent of angle for light vibrating parallel to the plane of the film. The method consisted essentially of obtaining retardation data as a function of angle of rotation about either y or z . The plastic sheet was immersed in mineral oil ($n_D = 1.481$) and inspected in a crossed polariscope illuminated by a diffused AH_4 source and filtered by $xG14L$ ($\lambda = 546.1$ m μ). The cross-section birefringence ($\Delta n = n_x - n_z$) was obtained by extrapolation of a Δn vs. $\cos^2 \theta$ plot to $\theta = 90^\circ$ according to the method of Spence (11).

Swelling Measurements

A film of cross-linked ethyl cellulose was prepared by casting a solution of 38.2 g. of ethyl cellulose and 0.84 g. of hexamethylene diisocyanate⁴ (12) in 216 g. of benzene at 0.100 in. The film was allowed to

⁴ Hexamethylene diisocyanate was obtained as an experimental sample from the Hooker Electrochemical Co.

air-dry for 24 hr. at room temperature and baked for 78 hr. at 60°C. under vacuum. The cross-linked film was then extracted with benzene and again dried. Nitrogen analyses² on the film before and after extraction gave a value of 0.4% N which corresponds closely to the amount of diisocyanate employed. The swelling measurements were made by allowing strips of the dry cross-linked film to swell in the solvents for 48 hr. at 50°C. and for 48 hr. at 25°C. To ascertain whether equilibrium swelling had been reached, strips were also allowed to swell for 96 hr. at 50°C. and 48 hr. at 25°C. Since the films undergo anisotropic swelling, the

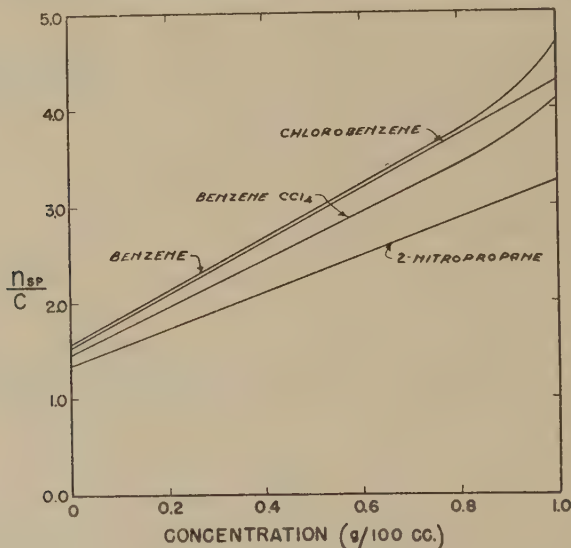


FIG. 1. Dilute solution viscosity behavior of ethyl cellulose.

volume fractions of the polymer at equilibrium swelling were calculated from weight measurements according to the following equation (13):

$$v_2 = 1/1 + \frac{\rho_2}{\rho_1} \left(\frac{W_a}{W_b} \right) - \frac{\rho_2}{\rho_1} \quad [2]$$

where ρ_2 and ρ_1 are the densities of the pure polymer and solvent, respectively, and W_b and W_a are the weights of the polymer strips before and after swelling.

Annealing Glass Casts

Films cast on glass were annealed by holding them at their softening points (134–5°C.) for 18 hr. in a hot-air oven. The films were held between glass plates separated by 0.022 in. Dimensional changes including a decrease in the planar dimensions and an increase in the thickness occurred. Surface irregularities as a result of annealing prevented reliable data from being obtained for changes in thickness.

EXPERIMENTAL RESULTS

Figure 1 is a plot of η_{sp}/c vs. c for ethyl cellulose in the solvents we have studied. The intrinsic viscosities and k' values are given in Table I.

Table II contains the results of swelling measurements carried out on a cross-linked film of ethyl cellulose. Equation [2] has been used to calculate the volume fraction of the polymer at equilibrium swelling, v_2 , at 25°C.

TABLE I

Dilute Solution Viscosity Behavior of Ethyl Cellulose at 30°C.

Solvent	$[\eta]$	k'
2-Nitropropane	1.35	1.04
Chlorobenzene	1.52	1.21
Benzene-carbon tetrachloride	1.46	1.20
Benzene	1.57	1.12

X-ray diffraction photographs of the films from 2-nitropropane, chlorobenzene, and benzene have not been reproduced. However, very diffuse rings were obtained indicating the absence of any high degree of crystalline order; all three films give rise to diffraction maxima of the same diffuseness. A more sensitive measurement, the birefringence has also been employed to study film structure. Inspection between crossed polar-

TABLE II

Swelling Measurements on a Cross-Linked Ethyl Cellulose Film at 25°C.

Solvent	Volume fraction of polymer v_2 after swelling for	
	48 hr. at 50°C., 48 hr. at 25°C.	96 hr. at 50°C., 48 hr. at 25°C.
2-Nitropropane	0.013	Film disintegrated
Chlorobenzene	0.033	0.037
Benzene	0.041	0.043

izers of the films cast on glass has shown that the films are uniaxial and have a high cross-section birefringence. The actual values of the cross-section birefringence appear in Table III.

Table IV contains the densities and the softening points of the four ethyl cellulose films. Flotation experiments employing a concentrated aqueous solution of sodium sulfate were capable of distinguishing between the film from 2-nitropropane and the three other films.

TABLE III

Cross-Section Birefringence of Ethyl Cellulose Films, Glass Casts

Film from	$\Delta n = n_x - n_z$ $\times 10^{-3}$
2-Nitropropane	-5.75
Chlorobenzene	-6.65
Benzene-carbon tetrachloride	-7.95
Benzene	-7.40

TABLE IV

Densities and Softening Points of Ethyl Cellulose Films, Glass Casts

Film from	Density _{20°C.}	Lorand softening point °C.
2-Nitropropane	1.114	131-3
Chlorobenzene	1.119	132-3
Benzene-carbon tetrachloride	1.124	132-4
Benzene	1.120	132-5

The ultimate strength properties of the films cast on glass are tabulated in Tables V and VI. The residual solvent contents of these films are reported in Table VII.

Figure 2 contains plots of moduli of flexure as a function of temperature for the four ethyl cellulose films cast on glass.

The effect of annealing glass casts by holding them at their softening point for 18 hr. has been studied. The brittle-point data on the annealed

TABLE V

*Tensile Stress-Strain Measurements at 25°C. and -50°C.,^a
Ethyl Cellulose, Glass Casts*

Film from	25°C.					-50°C.	
	Young's modulus $\times 10^{-5}$	Ultimate tensile strength	Per cent elonga- tion	Yield stress	Yield strain	Ultimate tensile strength	Per cent elonga- tion
2-Nitropropane	2.36	7,430	26.7	5,950	5.1	11,245	10.8
Chlorobenzene	2.45	7,515	25.0	6,050	4.8	10,730	7.3
Benzene-CCl ₄	2.23	7,940	29.4	6,150	5.0	10,885	8.3
Benzene	2.71	8,560	33.8	6,300	5.6	11,510	10.0

^a Moduli, tensile strengths, and yield stresses are in lb./in.².

TABLE VI

Brittle-Point Temperatures of Ethyl Cellulose Films, Glass Casts

Film from	Solvent properties		T_B (°C.)		
	B.P. °C.	ε _{25°C.}	0% R.H.	50% R.H.	Cold storage
2-Nitropropane	120	~25	-10	-10(-47)	-13
Chlorobenzene	132	5.4	-17	-16(-27)	-17
Benzene-carbon tetrachloride	—	—	-38	-34(-68)	-31
Benzene	80	2.3	-64	-40(< -75)	-48

TABLE VII

Residual Solvent Contents of Ethyl Cellulose Films, Glass Casts

Film from	N %	Cl %	C %	H %	Ash %	Residual solvent %
2-Nitropropane	0.2					
Chlorobenzene		0.0				1.3
Benzene			57.1	8.9	0.0	0.0
Original ethyl cellulose powder			56.8	9.0	0.6	0.8

films and the decrease in planar area as a result of annealing are given in Table VIII. Inspection of the annealed films between crossed polarizers shows that the long-range high cross-section birefringence is no longer present. The films now consist of randomly oriented regions of frozen-in stress imbedded in an isotropic matrix.

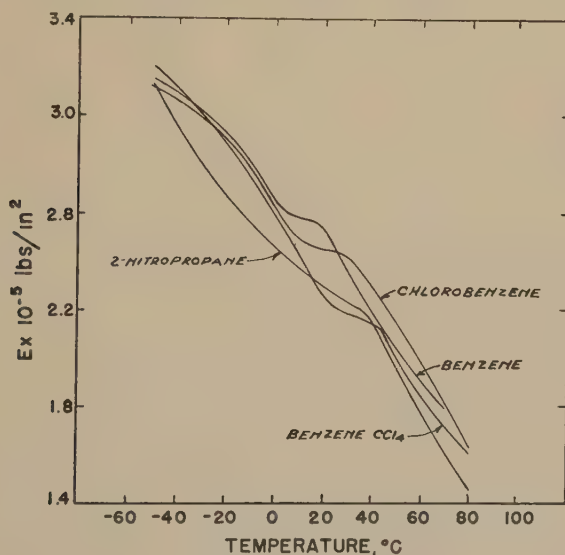


Fig. 2. Moduli of flexure as a function of temperature for ethyl cellulose films prepared by casting on glass from several different solvents.

TABLE VIII

Heat Treatment of Ethyl Cellulose Films, Glass Casts

Film from	Decrease in area %	T_B (original) °C.	T_B (heat-treated) °C.
2-Nitropropane	Low	-10	Very brittle
Chlorobenzene	12.7	-16	-60
Benzene-carbon tetrachloride	18.2	-34	-60
Benzene	19.8	-40	-91

TABLE IX

Brittle-Point Temperatures of Ethyl Cellulose Films, Mercury Casts

Film from	T_B °C.
2-Nitropropane	-66
Chlorobenzene	-70
Benzene-carbon tetrachloride	-75--82
Benzene	-68

Films prepared by casting on mercury surfaces have been found to be essentially isotropic. Table IX contains brittle-point data on films cast from the four different solvents on mercury. The stress elongation data of Table X illustrate the difference between glass and mercury casts.

TABLE X

Stress-Strain Behavior of Ethyl Cellulose Films, 25°C., Glass and Mercury Casts^a

Film from	Young's modulus $\times 10^{-6}$	Ultimate tensile strength	Per cent elonga- tion	Stress yield	Strain yield
80:20 toluene- alcohol on glass	2.72	6,665	13.2	6,475	5.7
80:20 toluene- alcohol on mercury	1.94	5,315	36.1	4,875	5.0
Benzene on glass	2.49	7,020	20.6	6,275	5.2
Benzene on mercury	1.87	5,540	50.5	4,510	4.3

^a Moduli, tensile strengths, and yield stresses are in lb./in.².

DISCUSSION

The dilute solution viscosity behavior of ethyl cellulose was studied in benzene, benzene-carbon tetrachloride, chlorobenzene, and 2-nitropropane (Fig. 1 and Table I). All intrinsic viscosities fall between 1.35 and 1.57. This agrees with the results of Frith (14) and of Spurlin, Martin, and Tennent (15) who have found that for celluloses the intrinsic viscosity is comparatively independent of solvent composition. It has also been generally accepted that the slope of the η_{sp}/c vs. c curve provides a better measure of the solvent power than the $[\eta]$ in the case of non-flexible polymers. Spurlin *et al.* (15) and Alfrey (16) are of the opinion that the steepest slope corresponds to the poorest solvent. Sufficient scatter is present in our data so that considerable error may be associated with the k' values. If one speaks in terms of slopes and assumes that higher slopes are associated with intermolecular association and poorer solvent properties, it can be seen from the data that 2-nitropropane is the best solvent for ethyl cellulose. The slopes for the benzene and chlorobenzene solutions are quite similar. Considerable positive deviation from linearity is present at 1 g./100 ml. in the benzene-containing solutions

however, and it may be concluded that ethyl cellulose approaches a gel structure much more rapidly in these two solvents. During the preparation of casting solutions it was observed that benzene and benzene-carbon-tetrachloride solutions of ethyl cellulose showed a certain amount of thixotropic behavior. Thus, we feel that the order of increasing solvent power is benzene, chlorobenzene, and 2-nitropropane.

In view of a more recent publication by Evans and Spurlin (17) concerning the effect of bound metal in ethyl cellulose on dilute solution properties, additional work was carried out to determine the relative solvent power of these solvents for ethyl cellulose. In the treatment of polymer solutions, Huggins (18) has introduced the quantity μ as the coefficient of the square term of the volume fraction of polymer v_2 in the expression for the logarithm of the activity

$$\ln a_1 = \ln (1 - v_2) + \left(1 - \frac{\bar{V}_1}{\bar{V}_2}\right) v_2 + \mu v_2^2 \quad [3]$$

and for dilute solutions

$$-\Delta \bar{F}_1 = RT \frac{\bar{V}_1}{\bar{V}_2} v_2 + RT[(1/2) - \mu] v_2^2 + RT \frac{v_2^3}{3}. \quad [4]$$

Except for the effect of molecular weight, μ determines the value of $-\Delta \bar{F}_1$ and this in turn determines whether or not a liquid will be a solvent or nonsolvent for a given polymer. Therefore μ can serve as a measure of polymer-liquid interaction and solvent power. With the development of the Flory-Rehner (19, 20) theory for the swelling of three-dimensional gel structures, the determination of μ has been simplified. Their equation is as follows:

$$\mu v_2^2 = -\ln (1 - v_2) - v_2 - \rho_2 V_1 v_2^{1/3} / M_c \quad [5]$$

where v_2 is the volume fraction of the polymer at equilibrium swelling, ρ_2 is the density of pure polymer (taken as 1.12 for ethyl cellulose), V_1 is the molar volume of the solvent, and M_c is the average molecular weight between cross-links. Thus if a polymer is cross-linked and M_c known, μ follows from the determination of v_2 . We have used a film of ethyl cellulose cross-linked with hexamethylene diisocyanate for the determination of the equilibrium swelling (cf. Table II). Since under the experimental conditions which were employed, it is highly probable that the diisocyanate was not completely utilized as a cross-linking agent, we cannot calculate M_c from the nitrogen analysis of this film. If however we may assume a value of 87,000 for M_c , μ values falling in the expected range are obtained (Table XI). Although the Flory-Rehner theory is probably not completely applicable to rigid polymers of the ethyl cellulose type, the results at least lend qualitative substantiation to the solvency power as determined from viscosity measurements.

The x-ray diffraction diagrams indicate that films from all solvents are essentially amorphous. This is in agreement with the results of Iznairskaya (21) who has shown that ethyl cellulose of comparable ethoxyl content yields diffuse diffraction patterns and that crystalline character becomes strongly apparent only when triethyl cellulose is approached.

Inspection of the films cast on glass has shown them to be uniaxial and to have a high degree of cross-section birefringence. The data are contained in Table III. Since n_z or n_y minus n_x is always a relatively large positive number, the refractive index of these films is greater in the plane of the sheets than normal to it. This can only result if there is a tendency for the principal valence chains to be confined to the plane of the films or to lie at such an angle that their contribution to the refractive index is greatest in the z and y direction. The data of Table III also indicate that the poorer solvents, which happen to be the more nonpolar solvents, lead to films of highest birefringence. This may probably be explained as follows. As will be discussed later, casting on mercury leads to films which

TABLE XI
Mu Values for Ethyl Cellulose-Solvent Systems

Solvent	Average v_2 (25°C.)	V_1 (25°C.)	μ
2-Nitropropane	0.013	90.3	-4.38
Chlorobenzene	0.035	102.1	+0.17
Benzene	0.042	89.4	+0.30

$M_c = 87,000$

are essentially isotropic. This strongly suggests that the large value of Δn of glass casts results from the stresses set up because of the inability of the cast to contract in the plane of the sheet during solvent evaporation, the planar dimensions of the film being determined at the time of casting. All subsequent shrinkage due to solvent loss is normal to the plane of the film and is similar to a force being applied normal to the sheet thus forcing the chains into the plane of the film and accounting for the high birefringence of glass casts. Sometime during solvent evaporation and at a certain concentration, a gel structure will set up. The concentrations of polymer at which this occurs depends on the solvent in question, the solution gelling at a higher dilution in a poorer solvent. In a poor solvent such as benzene, there is considerably more intermolecular association than in 2-nitropropane which has the ability to solvate the ethyl cellulose chains. With continued evaporation, those films already existing as a gel will be subjected to a considerably more uniform stress, the entire gel network shrinking perpendicular to the plane of the film and forcing chains into the plane of the film. In the case

of 2-nitropropane, solvated chains will be more or less independent of each other until a much later time during solvent evaporation leading to a lower value for Δn .

The densities of the films prepared by casting on glass (Table IV) indicate that benzene and benzene-carbon tetrachloride lead to higher film densities. This is probably associated with a greater degree of shrinkage of the gel network resulting in a more compact structure in the case of thermodynamically poorer solvents.

It is of interest to compare the results we have obtained with this sample of ethyl cellulose, which we believe is essentially noncrystalline, with the results obtained on a crystalline polymer, cellulose triacetate. Spence (3), utilizing x-ray and birefringence methods, has made a detailed study of the effect of solvent composition on films of the latter material. Briefly, he found that the highly polar solvents lead to films of a greater degree of intercrystallite orientation and this higher crystallinity restricts a greater portion of the principal valence chains to the

TABLE XII
Cross-Section Birefringence of Cellulose Acetate Films
Glass Casts^{a, b}

Solvent	ϵ	$\Delta n = n_x - n_z$ $\times 10^{+3}$
Ethylene chlorohydrin	25.8 (24.5°C.)	-2
Methylene chloride	8.93 (24.8°C.)	-0.8
Chloroform	5.05 (20°C.)	+0.4

^a According to Spence (3).

^b n_x and n_z correspond respectively to Spence's n_e and n_o .

plane of the sheet. Thus unlike ethyl cellulose, films of higher cross-section birefringence are obtained from the more polar solvents in the case of cellulose triacetate (Table XII).

It is our opinion that this generalized behavior is probably followed by all polymeric materials when films are prepared on glass. For essentially crystalline materials, the more polar solvents will lead to a more highly crystalline modification. In the case of essentially amorphous polymers, sheet structure is determined by the solvent power of the solvent for the polymer in question.

To determine whether any correlation exists between the ultimate strengths of ethyl cellulose films and the casting solvents, the brittle temperatures and the stress-strain behavior have been studied. The stress-strain data obtained at 25°C. (Table V) show quite clearly that the poorer solvents for ethyl cellulose, i.e., benzene and benzene-carbon tetrachloride, lead to films of higher tensile strength, yield stress, per cent elongation at break, and total energy required for breaking. Since these films also have the highest cross-section birefringences, one may consider

them as being modifications of the films from 2-nitropropane and chlorobenzene, obtained by applying a uniform bilateral stretch in the plane of the films. In this way, the results observed with ethyl cellulose are comparable to those obtained by Nielsen and Buchdahl (22) during a study of oriented polystyrene. These authors observed that the ultimate tensile strength, per cent elongation at break, and area under the stress-strain curve increased in the direction of stretch. Brittle-point data (Table VI) indicate that the films from the poorer solvents are also better low-temperature films. It is of interest to note that the brittle temperatures for films preconditioned at 50% relative humidity are higher than those conditioned at 0% relative humidity. Furthermore, it is seen that the lower the brittle temperature, the more detrimental the effect of moisture. The cold-storage values indicate that little or no change has taken place except a possible slight lowering of T_B due to a drying out of the sample. Other series of films cast from these solvents on glass have been studied. Another typical set of data are included in parentheses in Table VI. A large degree of scatter was observed in the absolute values of the brittle temperatures in these series. It has been pointed out however that the ultimate strength of a material depends largely on such factors as crystal size, mosaic structure, the presence of flaws and imperfections, and slight variations in prevailing conditions during film formation. Thus, it is felt that the scatter we observe is inherent in this type of testing. It may be concluded from our data however that the films from benzene and benzene-carbon tetrachloride consistently have lower brittle-point temperatures.

Stress-strain measurements performed at -50°C . (Table V) show a large increase in tensile strength accompanied by a decrease in elongation, in agreement with the data of Carswell and Nason (23). The apparently anomalous behavior of the film from 2-nitropropane which now shows an elongation comparable to that of the film from benzene may be associated with the residual solvent content of the film from 2-nitropropane which was found to be more than 1% (Table VII). This residual solvent may exert a plasticizing action which does not show up in the rapid brittle-point test or a room temperature stress elongation experiment in which elongations are of the order of 25–35%. However, at low temperature using a slower type of test the effect of this plasticizing action may be magnified.

Moduli of flexure (Fig. 2) as a function of temperature are very similar for the four ethyl cellulose films. The films from benzene and chlorobenzene show slightly higher moduli and the values at 25°C . compare favorably with Young's modulus at 25°C . (Table V). Otherwise, solvent appears to have little effect on this property. In a similar manner,

the softening point of these films (Table IV) appears independent of casting solvent composition.

Baker, Fuller, and Pape (24) have employed annealing and quenching techniques to obtain crystalline and randomly oriented modifications of cellulosic ester films. We thought it would be of interest to study the effect of a heat treatment on the ethyl cellulose films cast on glass. The heat treatments resulted in contraction in the planar dimensions of the films accompanied by an increase in thickness. This contraction must result from the alleviation of stress present in the plane of the film, a more disordered film resulting. As one would expect, the decreases in area parallel the cross-section birefringence measurements, the more highly birefringent films undergoing the greatest amount of shrinkage (Table VIII). A considerable lowering of T_B accompanies the heat treatment in all cases except the films from 2-nitropropane. The latter films become very brittle. This may also be associated with the presence of residual nitro compounds which are causing oxidation and breakdown of polymer at the elevated temperatures. Work which has not been reported here has shown that a 0 to 20% decrease in modulus also results from the heat treatment. As seen between crossed polarizers, the long-range order (high cross-section birefringence) was destroyed, and the treated films now consist of randomly oriented regions of frozen-in stress imbedded in an essentially isotropic medium. This structure apparently results from incomplete annealing. Somewhat similar observations have been made by Spurlin *et al.* (15) during a study of the dimensional stability of molded objects.

Kozlov (25) has cast films on mercury surfaces to avoid what he terms anomalies in optical anisotropy. We have used mercury casting surfaces in order to obtain other modifications of ethyl cellulose films. If after the film has set to a gel it is cut away from the sides of the container and allowed to undergo unrestrained shrinkage in the plane of the film, essentially isotropic ethyl cellulose films are obtained. Even when cutting from the container sides is omitted, the films are essentially isotropic except for a small area around the circumference. Since other metallic surfaces, for example polished chromium, lead to highly birefringent films similar to those obtained on glass, it must be the mobility of the mercury surface which allows planar shrinkage. The brittle-point temperatures (Table IX) of these isotropic films all fall in the same range, and it appears that the effect of solvent composition observed with glass casts has largely disappeared. Changing from mercury to glass resulted in a greater lowering of the brittle point for films cast from the better solvents for ethyl cellulose. Isotropic films from mercury have been found to have lower moduli, lower ultimate tensile strengths and yield stresses but considerably greater elongations at break than films cast on glass

(Table X). For films cast on glass, higher birefringence was associated with greater elongation at break and one might consider the results obtained with mercury casts anomalous in this respect. However, in systems of this type, an infinite number of gel structures can exist each with its own specific mechanical properties and it is not always possible to consider one type of structure as a modification of another.

ACKNOWLEDGMENTS

The authors are indebted to Mr. Albert Makas for carrying out the birefringence measurements and to Mr. Peter Riesz for the x-ray diffractions.

SUMMARY

An investigation of the properties of ethyl cellulose films prepared by casting on glass from a limited number of different solvents has been carried out. It appears that the solvent power of a given solvent for ethyl cellulose may be the prime factor which determines film properties in essentially amorphous polymers of this type. Briefly, it has been found that thermodynamically poorer solvents for ethyl cellulose lead to films of higher birefringence, higher densities, lower brittle-point temperatures, and in general greater toughness. Modulus of flexure and the softening point appear to be relatively independent of solvent composition. A simple theory has been proposed to correlate solvent power and cross-section birefringence. More random modifications of ethyl cellulose films have been obtained by annealing glass casts. As one would expect, the shrinkage in the plane of the films parallels the cross-section birefringence. These annealed films have lower moduli and lower brittle-point temperatures, and the long-range high birefringence of glass casts has disappeared. An exceedingly low brittle-point temperature has been obtained by annealing films cast from benzene on glass. Essentially isotropic films prepared on a nonrigid surface, i.e. mercury, also have lower moduli than glass casts, and a considerable change in the stress-elongation curve has been observed, a decrease in yield stress and tensile strength being accompanied by more than a twofold increase in elongation. The noticeable effect of solvent composition on film properties when films are prepared on rigid casting surfaces largely disappeared when films were prepared on mercury. Lower brittle-point temperatures appear to be associated with the more isotropic films obtained by annealing or by casting on mercury.

REFERENCES

1. SHEPPARD, S. E., AND NEWSOME, P. T., *J. Soc. Chem. Ind. (London)* **56**, 256T (1937).
2. YAMADA, T., *J. Soc. Chem. Ind. (Japan)* **46**, 281 (1943).
3. SPENCE, J., *J. Phys. Chem.* **45**, 401 (1941).
4. CENTROLA, G., *Ann. chim. applicata* **28**, 463 (1938).

5. MOISEEV, A., AND ROGOVIN, J., *J. Applied Chem.* (U. S. S. R.) **14**, 579 (1941).
6. REINHART, F. W., AND KLINE, G. M., *Ind. Eng. Chem.* **31**, 1522 (1939).
7. CLASH, R. F., AND BERG, R. M., *Modern Plastics* **21**, No. **11**, 119 (1944).
8. TINIUS OLSEN TESTING MACHINE COMPANY, Bulletin 35.
9. LORAND, E. J., *Ind. Eng. Chem.* **30**, 527 (1937).
10. HUGGINS, M. L., *J. Am. Chem. Soc.* **64**, 2716 (1942).
11. SPENCE, J., *J. Phys. Chem.* **43**, 865 (1939).
12. BAYER, O., *Modern Plastics* **24**, No. **10**, 149 (1947).
13. DOTY, P., AND ZABLE, H. S., *J. Polymer Sci.* **1**, 90 (1946).
14. FRITH, E. M., *Trans. Faraday Soc.* **41**, 90 (1945).
15. SPURLIN, H. M., MARTIN, H. F., AND TENNENT, H. G., *J. Polymer Sci.* **1**, 63 (1946).
16. ALFREY, T., JR., *J. Colloid Sci.* **2**, 99 (1947).
17. EVANS, E. F., AND SPURLIN, H. M., *J. Am. Chem. Soc.* **72**, 4750 (1950).
18. HUGGINS, M. L., *Ann. N. Y. Acad. Sci.* **43**, 1 (1942).
19. FLORY, P. J., AND REHNER, J., *J. Phys. Chem.* **11**, 512 (1945).
20. FLORY, P. J., AND REHNER, J., *J. Phys. Chem.* **11**, 521 (1945).
21. IZNAIRSKAYA, N. I., *J. Gen. Chem.* (U. S. S. R.) **17**, 367 (1947).
22. NIELSEN, L. F., AND BUCHDAHL, R., *J. Applied Phys.* **21**, 488 (1940).
23. CARSWELL, T. S., AND NASON, H. K., Symposium on Plastics. Philadelphia District Meeting, American Society for Testing Materials, Feb., 1944.
24. BAKER, W. O., FULLER, C. S., AND PAPE, N. R., *J. Am. Chem. Soc.* **64**, 776 (1942).
25. KOZLOV, P. V., *Trudy Konferents. Vysokomolekulyar. Soedineniyam* **1**, 12 (1943).

ELECTROPHORESIS MEASUREMENTS IN BENZENE— CORRELATION WITH STABILITY.

I. DEVELOPMENT OF METHOD¹

J. L. van der Minne and P. H. J. Hermanie

Koninklijke/Shell-Laboratorium, Delft, Holland

Received September 18, 1951; revised May 2, 1952

INTRODUCTION

The stability (peptizing behavior) in aqueous colloid systems is correlated principally with the electrophoretic velocity and the derived electrokinetic potential (ζ), which correlation has proved to be very fruitful, although recent development indicates that it is not so simple as originally supposed.

As to the existence and the significance of electrophoresis in non-aqueous colloids the following may be stated. In the lower alcohols, acetone, nitrobenzene, and several other liquids, generally electrophoresis can be measured normally and in the same way as in aqueous systems. The dielectric constant (ϵ) is the determining factor, and, roughly stated, in liquids where this constant is larger than a certain limit, which may roughly be put at 10 to 15, electrophoresis measurement is feasible with normal apparatus (i.e. constructed for aqueous colloids) and correlation with stability is known to exist. In liquids with dielectric constant lower than 10 (especially lower than 5, e.g. hydrocarbons having a constant of 2), when one is working with normal apparatus instead of the regular electrophoretic movement, irregular movements, to be referred to later, turn up, and consequently electrophoretic movement cannot be observed; thus many authors consider ζ -potential nonexistent in such liquids. Generally this goes together with the notion that ions are not present in liquids with such low dielectric constants. The work of Walden, of La Mer and Downes (1), and of Fuoss and Kraus (2) has apparently not permeated enough. Their work makes it clear that even in solutions of hydrocarbons ions exist; evidently this has been too much ignored.

In an investigation which the authors carried out several years ago they came across the curious fact that peptization of suspensions in mineral oil of material resembling carbon black was promoted by calcium

¹ Paper presented at the XIIth International Congress of Pure and Applied Chemistry (Section of Physical and Inorganic Chemistry), New York, Sept. 10–13, 1951.

soaps and also by oil-soluble oxidation products of such an oil,* but that when both these substances were added together flocculation of the suspension ensued (3). Only when one of the two peptizing substances was present in excess could the suspension be peptized again. When using benzene instead of the mineral oil the authors observed exactly the same phenomena; only here the flocculation of the suspension takes much less time owing to the much lower viscosity. The two substances apparently did not react with each other, which would have given the easiest explanation. The explanation of such phenomena in aqueous suspensions would be simply the presence of opposite charges due to the addition of various electrolytes. A similar explanation in the case of suspensions in oil was at that time not acceptable, because, although for other reasons it was considered the most likely one, there was no evidence of charged particles. Since then considerable effort has been devoted to investigating the possibility of measuring electrophoresis.

While experimenting on the reversal of emulsions, one of us had found (4) that water drops in organic liquids did not give normal electrophoretic movement of the particles when the organic liquid had a low dielectric constant (hydrocarbon oil, $\epsilon = 2.3$). (For the case of water drops in nitrobenzene ($\epsilon = 36$) perfect electrophoresis could be observed, the water drops moving to the positive pole.) A microscopic cell was used. The criteria for real electrophoresis are that: (a) the motion of the particles should be rectilinear between electrodes and uniform; (b) the velocity should be independent of the position in the electric field; and (c) the velocity should be proportional to the field strength and should reverse on reversal of the field.

All these criteria follow from Helmholtz's (or Smoluchowski's) equation $v = \frac{\zeta \epsilon E}{4\pi\eta}$ in which v = velocity, E = field strength, ϵ = dielectric constant, and η = viscosity of continuous phase. What actually was observed upon the application of an electric field of say 100 v./cm. d.c. (two electrodes at a distance of 2 cm.) was that irregular (not linear) movements of the particles occur midway between the electrodes and that particles just near the electrodes ($< 50 \mu$) are attracted by them and after touching them are violently repelled; some particles are seen to vibrate between a coalesced water drop on the glass plate and the electrode. Also chains are formed which start from the electrodes; loose water drops are likewise attracted and repelled by these chains. These phenomena are the same near both electrodes. On reversal of the field some particles continue their irregular movement and some reverse their movement for a moment, after which they continue in the same way as before. This behavior reminds us of experiments in induction (influence) and

* So called oxidation resin.

static electricity, in which a rubbed glass or rosin rod is seen alternately to attract and repel small particles. As is known, these phenomena are governed by the dielectric polarization occurring in divergent electric fields in which dE/dx is not a constant (E = field strength; voltage applied divided by distance x). Particles having a higher dielectric constant than the continuous phase are always moving to the place of highest field energy (proportional to E^2) which is often the same thing as moving to the electrode).² The velocity of this displacement is proportional to $\frac{\alpha}{2} \frac{dE^2}{dx}$, in which α is dependent on the difference between the two dielectric constants (dielectric constant of particles and of liquid). The fact that this velocity is proportional to the second power of E , whereas the electrophoretic velocity is proportional to the first power of E means that at lower field strengths electrophoresis wins. The way to obtain pure electrophoresis and to eliminate polarization is to make dE/dx equal to zero by making the electric field homogeneous; our attempts were made in this way.

Before describing these experiments we would refer to literature on electric phenomena in liquids of low dielectric constant, mainly hydrocarbons.

LITERATURE REVIEW

This review deals with the influence of electric currents on suspensions in hydrocarbons.

Pohl (5) also considered both phenomena but contrary to us he especially wanted to study and to apply the dielectric polarization. For this purpose he constructed a cell with a strong divergent field. He has coined the word "dielectrophoresis" for it, in contrast to electrophoresis. The migration velocity of the former is proportional to the square of the particle diameter, a fact which he makes use of for removing coarser particles.

The dielectric polarization may cause the particles to arrange themselves in lines (chain formation). Hollmann (6) investigated the effects of chain formation of carbon black suspensions in mineral oil in respect to electric conductivity, and Winslow (7) in respect to the viscosity and the stiffening of concentrated suspensions.

Putilova and Gindin (8) described the formation of chains in suspensions of zinc and barium stearates in gasoline and mineral oil, which takes place at a field strength of 7500 v./cm. Conductivity is thereby increased considerably. Further, Gindin (9) studied chain formation in suspensions of aluminum in gasoline; he found that these chains caused short-circuiting.

² The occasional repulsion of the particles from the electrodes is due to the fact that after touching they have obtained a free charge either of ions or of electrons.

The fact that electrophoretic velocity in hydrocarbons is small compared with that in water because it is proportional to the dielectric constant of the liquid, often induces experimenters to apply large field strengths; by so doing they promote polarization. An instructive example is to be found in the work of Soyenkoff (10), who applied at least 5000 v./cm. on many organosols, principally in benzene, toluene, and xylene. His conclusion (1931) was that "electrical factors of stability are shown to be unimportant in hydrocarbons as dispersion media" (p. 3009). A somewhat similar conclusion was recently arrived at by Hayek (11). Although the latter was out to measure electrophoresis, it follows from his description that in his cell there occurred polarization phenomena such as nonuniform mobility, and the movement of particles from one electrode to the other. Therefore the mobilities quoted are not those of electrophoresis alone.

Amongst various other authors we would mention Terada and Kahn (12), who studied suspensions of carbon, sulfur, sulfides, and oxides in mineral oil, and Reising (13), who studied paints. They all found dielectric polarization (or electrostatic phenomena as they are sometimes called) to be the predominant phenomenon in liquids of low dielectric constant.

Only Gemant (14), who made use of the fact that dielectric polarization is zero when the dielectric constant of both phases is the same and who chose a suspension in which this condition was fulfilled (polystyrene in a hydrocarbon mixture) showed that electrophoresis did occur in hydrocarbons. He used a glass cell in which two copper electrodes were separated by a distance that was small relative to their distance from the walls. We found that carbon suspensions in mineral oil did not, however, show real electrophoresis in this cell even at lower field strengths than he applied; only dielectric polarization phenomena were observed.

Humphry and Jane (15) also made use of this principle of equality of the dielectric constant for both phases in their investigation on rubber solutions in benzene. When some water was present and they made this sol flow out in pure benzene between two electrodes they found that particles moved to both the electrodes. In this case the migration was due neither to electrophoresis nor to polarization phenomena, but to the different electric conductivities of wet rubber sol and the pure benzene. This has been pointed out by Buchner and Van Royen (16).

Somewhat more evidence of the occurrence of electrophoresis in hydrocarbons in those cases where dielectric constants are not the same was obtained from the early work of Quincke (17), who observed uniform motion of all sorts of particles (platinum and other metals, quartz, starch) in turpentine ($\epsilon = ca. 2.3$).

PRELIMINARY EXPERIMENTS

A very simple device due to Kerkvoort³ produced evidence of electrophoresis in hydrocarbons. In a rectangular cell made of two parallel microscope slides 0.3 cm. apart, two copper wires were placed parallel to the length of the slides and 0.6 cm. apart. When the cell was filled with a carbon black suspension (0.1% in benzene) peptized with 0.03% of calcium soap (calcium diisopropyl salicylate, abbr.: Ca dips) and a voltage was applied to the copper wires the following was observed. After some time, in the field between the two poles a clear zone was formed along the length of the positive pole. This zone increased with time, but apparently owing to convection currents, only to a certain width. On reversal of the current the same took place at the other copper wire (now the positive pole). Adding oxidation resin instead of Ca dips to the carbon suspension produced the opposite result: a zone at the negative pole became clear. The migration observed, being unidirectional in regard to the field, was indicative of real electrophoresis. Apparently with Ca dips as a peptizer carbon particles were positively charged and with oxidation resin negatively. This would at once explain why each of these substances was able to peptize the suspensions and why both together produced flocculation. Of course this experiment is at most an indication, no quantitative measurement being possible on account of the convection currents interfering with the movement and the electric field not being well defined.

When higher field strengths were applied polarization phenomena occurred and predominated over the electrophoresis. One of the polarization phenomena is the formation of chains. These chains in the case of the positively charged suspension reached from the negative pole to near the positive pole. The carbon was considered to be positively charged because the "electrophoretic" motion at the lower voltage was directed away from the positive pole. Round the positive pole a strong whirling of the liquid (or the particles) was observed. Separate chains with irregular motions and unattached to the poles were also observed. Very sudden and rapid attraction took place; on reversing the field one often observed the chains to explode and split up into separate particles, and shortly afterwards to reform. Sometimes flocculation of the suspension was fostered. These phenomena also occurred in a carbon suspension without any addition. Generally on the addition of more Ca dips more electrophoresis and less dielectric polarization were observed. The same applied to the negatively charging oxidation resin. Chains then generally start from the positive pole, while there is an accompanying whirling movement at the negative pole.

It appeared that the field strengths necessary to bring about these polarization phenomena were very different for different grades of carbon

³ Personal communication.

black; they ranged from 20 v./cm. (for Micronex MPC and EPC grade) up to 150 v./cm. and higher. The particular carbon black used in this investigation (see below) did not show polarization phenomena.

The indications obtained with the simple cell described above of the existence of electrophoresis checked so well with the peptization and flocculation of the carbon suspension in benzene as to induce us to try to put this electrophoresis on an exact quantitative basis.

DEVELOPMENT OF A MICROSCOPIC ELECTROPHORESIS CELL FOR QUANTITATIVE MEASUREMENT IN BENZENE

In view of the evidence from the literature and our own previous experience it was considered necessary that very strict criteria should be applied to make sure of measuring only real electrophoresis and of eliminating other effects. To that end the criteria mentioned on p. 601 were applied (uniform rectilinear motion, proportionality to the field strength, no polarization phenomena such as chain formation, moreover no free charge transfer except very close to the electrodes).

Suspension Used

The suspension chosen was one that was well peptized and made of a carbon black known from preliminary experiments to exhibit no polarization phenomena. The concentration of carbon black ranged from 0.003 to 0.05%, larger concentrations interfering with microscopic observation. The suspension was peptized by small amounts of calcium diisopropyl salicylate. Mostly 0.03% (or 600×10^{-6} mole/l.) was taken, which was above the necessary minimum. This particular product was used in the peptizing experiments because it dissolves better in benzene, and because its properties, such as electric conductivity (*ca.* $2 \times 10^{-12} \Omega^{-1} \text{ cm.}^{-1}$ in a 0.03% solution in benzene), are more reproducible than those of other calcium soaps, e.g. calcium oleate, which in solution is rather undefined.

The carbon black came from a used engine oil from a diesel engine running under smoky conditions and was obtained by filtration and extraction with benzene, alcohol, and mixtures of benzene and alcohol, with and without hydrochloric acid. Elementary analysis: C, 85.0%; S, 1.1%; H, 1.3%; N, 0.2%; O (by difference), 10.8%; ash, traces; H₂O, 1.6%. This carbon black is among the best-peptizable, especially by agents other than Ca dips. The particle size of the suspension was *ca.* 0.5 μ .

Cell Development

Numerous designs of cell were tried and gradually a clue was obtained which in the end led to our constructing a usable cell.

It was necessary to use cells of the most simple design, as appeared after experiments with open or semiopen cells [design of Smith and Lisse

(18) and of Rutgers and one of the authors (19)]; these cells, however useful for aqueous solutions, caused extra complications when used with benzene. A capillary is suitable; as no gas evolution occurs in hydrocarbons it may be used with both sides closed; this construction is simple.

In order that the criteria for pure electrophoresis can be measured and checked as exactly as possible, the distance between the electrodes should be large.

As is known, electroösmotic flow along the wall of a closed capillary causes the liquid to flow back and set up a parabolic velocity distribution over the depth of the capillary. The observed velocity of the particles is the sum of the liquid velocity and the electrophoretic velocity. At a distance $\frac{1}{2}r\sqrt{2} = 0.71r$ from the axis, liquid velocity is zero and the velocity of the particles at that level is the real electrophoretic velocity. This is often made use of in studying aqueous systems. However, in our case, in order to make sure that no other phenomena than electrophoresis and electroösmosis come into play and to have a better check on the criteria for pure electrophoresis, it was found necessary to measure particle velocity at various depths and thus to verify the parabolic velocity distribution. The electrophoretic velocity (and also the electroösmotic velocity along the wall) can then be calculated.

A 10-cm. long glass capillary was taken; it had an internal diameter of 2 mm. and an external diameter of 8 mm., and two platinum wires 8 cm. apart were fitted as electrodes. For making microscopic observation possible up to the bottom of the capillary, it was in this case only necessary to provide the glass capillary with a flat polished surface at the top, since the refractive indices of benzene and glass are nearly the same. The capillary has on both sides filling vessels which can be closed by stopcocks.

With the suspension described above and an electric field of 25 v./cm. movement was observed, but condition (b) (p. 601) was not fulfilled: closer to the electrodes, velocity was higher and not always rectilinear.

Closer investigation revealed that part of the electric current found its way through the glass wall, thus causing a nonhomogeneous field to be set up. The conductivity of the suspension is $2 \times 10^{-12} \Omega^{-1} \text{ cm.}^{-1}$ and of glass *ca.* $10^{-14} \Omega^{-1} \text{ cm.}^{-1}$; the cross section of the glass is, however, much larger than that of the liquid. A quartz capillary, although having a lower conductivity, was also unsatisfactory.

Therefore we took a glass capillary of the same internal diameter (2 mm.) but having a wall only about 0.2 mm. thick; the length was 13 cm., and spiral platinum electrodes were introduced so that the ends were 4 cm. apart. This thin-walled capillary was enclosed in a jacket which could be evacuated or could be filled with various substances, see Fig. 1. The jacket was provided with a flat glass plate at the top for good

microscopic observation; for the same reason the capillary had a flat plane. The ends of the capillary were connected as before to filling vessels closed by stopcocks.

Under similar conditions as before, with an electric field of 40 v./cm. it appeared that when the jacket was evacuated velocities at different points in the field were more nearly equal than in the thick-walled capillary (condition (b)) but not yet the same.

When the jacket was filled with ethyl alcohol (conductivity $3 \times 10^{-7} \Omega^{-1} \text{ cm.}^{-1}$) no movement at all could be observed. The explanation is that in this case the current made its way through the alcohol, and just near each of the electrodes, where it passed through the glass wall, a region of relatively large voltage drop was formed, so that over nearly the whole

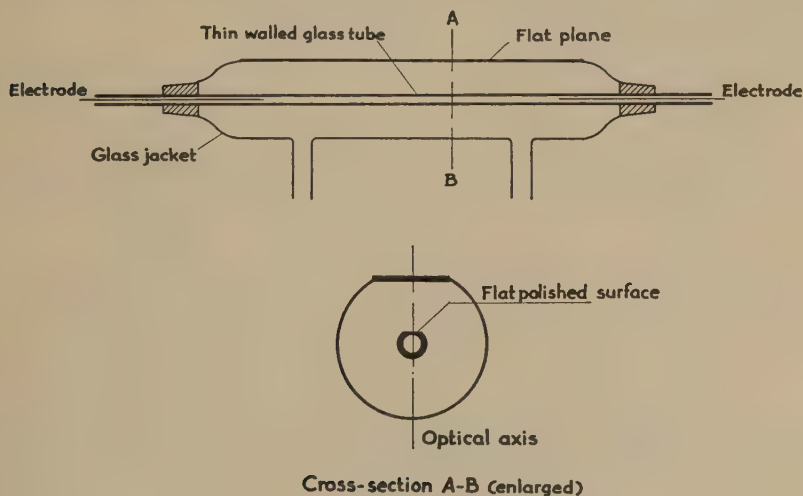


FIG. 1. Electrophoresis cell.

length of the capillary there was too small a field strength left for any movement to be observed. For various data obtained with these and other fillings of the jacket, such as benzene and air, see Fig. 2; the velocities given are those observed in the axis and are the sum of electrophoretic velocity and electroosmotic velocity. Indications were obtained that the surface conductivity of the glass wall still had an influence (see for instance the difference between jacket evacuated and jacket filled with air).

Therefore the outer surface of the capillary was treated for half an hour with silicones at 350°C. , which is a known procedure for eliminating surface conductivity of glass (20). The results obtained with this capillary were what was to be expected of real electrophoresis in a homogeneous field. No difference greater than the experimental error (5%)

was in this case found between the velocities near the electrodes and those midway between them (see Fig. 2). Not only that, but also the other conditions were fulfilled, including that of the parabolic velocity distribution over the depth of the capillary. As regards the also required proportionality of velocity with field strength it was found that within the regions of field strength of 12 to 150 v./cm. the values obtained on the suspensions containing 0.03% Ca dips (= 600 μ moles/l.) ranged from 0.12 to 0.16 μ /sec./v./cm. approximately, and on a suspension containing 0.003% Ca dips values ranged from 0.065 to 0.085; in both cases particles were positively charged.

As soon as the absolute voltage exceeded 900 v., jerky movements, apparently due to electric leakage inside the vacuum jacket, were observed, and the mean velocity decreased. This did not occur when air at atmospheric pressure was present in the jacket.

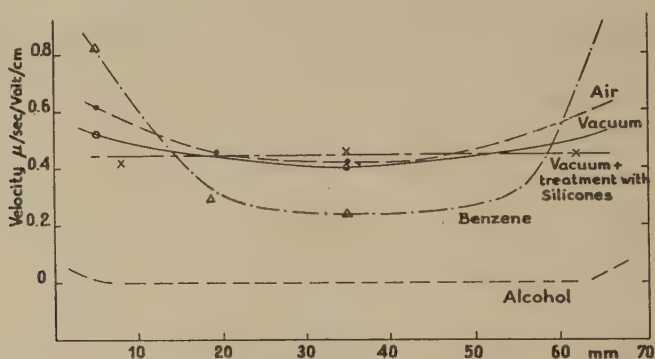


FIG. 2. Velocities (in axis) of particles in different parts of cell. Jacket evacuated or filled with various substances.

For our definitive apparatus the principle of the cell of Fig. 1 has proved very suitable.

One important change has been made, viz. instead of the glass capillary a quartz capillary is used, the reason for this change being the following.

When electrophoresis of the carbon suspensions was measured in benzene with addition of negatively charging substances (the oxidation resin gave a negative charge) very irregular motion was obtained in glass capillaries. The parabolic velocity distribution was much impaired and was very irregular. As soon as a suspension with Ca dips was tried everything became normal again. The irregularities are attributed to the presence of surface inhomogeneities in the particular glass capillary, and it is supposed that weakly adsorbing agents such as oxidation resin cannot overcome these inhomogeneities. Irregularities also come to the fore in

the particular pattern that carbon particles, lying in the bottom of the capillary, form in this case during electrophoresis. The pattern consists of patches and canals of microscopic dimensions (a few microns). This never occurs with the suspension to which Ca dips, which is much more strongly adsorbed, is added. Higher concentrations of oxidation resin (0.3%) do not show it either. Cleaning of the glass did not help, nor did silicone treatment of the inner surface make any difference. The only remedy was the use of quartz, which thanks to its simpler composition might be supposed to give a more homogeneous surface. Actually, in our experiments the quartz capillaries never gave rise to any irregularity.

To repeat, these irregularities between the glass surface and benzene are ascribed to irregularity of ζ -potential at microscopically visible distances. As far as we know this has never been encountered with water. It is realized that the irregularities may also be caused by differences in surface conductivity of the interface glass-benzene solution. Variations in the latter may be responsible for a disturbance of the electric field, with the same result. Then differences in surface conductance will go together with differences in ζ -potential. Fortunately, by using quartz capillaries such irregularities were avoided.

DEFINITIVE APPARATUS

The apparatus is shown in Fig. 3. The principle is that of the cell of Fig. 1, mentioned before, with the difference that a quartz capillary is used instead of the glass one, for the reason stated.

Further, both the filling vessels have been provided with very narrow capillaries (diameter 0.3 mm.) for equalizing pressure differences due to temperature changes. The flow resistance of these is so high that the principle of the closed cell is not violated. The quartz capillary is fixed into the jacket by a water glass-talc cement. Of course, there is no connection between the inside of the capillary and the contents of the jacket. The capillary is 13 cm. long and the distance between the ends of the electrodes is 4 cm.

It must be stated that quartz capillaries with thin walls are very difficult to make, above all because they have to be provided with a polished concave surface. In the case of glass this must be flat, but because quartz has a lower refractive index (*ca.* 1.46) than the benzene solution (*ca.* 1.50) it is necessary to apply a correcting lens in the form of a concave cylindrical surface in order to be able to observe microscopically through the whole depth of the capillary.⁴

In aqueous solutions one very often observes a solution with a re-

⁴For best results the radius of the cylindrical surface in this case should be:

$$\frac{1.46 - 1}{1.50 - 1.46} = 11.5$$
 times that of the radius of the internal capillary.

fractive index of 1.33 (n_D water) in a glass capillary of refractive index *ca.* 1.50. The consequence is that normally only the upper half of the capillary can be observed when there is a flat-topped surface. This is sufficient for computing electrophoretic velocity, because in aqueous electrokinetics all peculiarities are known; hundreds of experimenters have already explored this field.

In electrophoresis in benzene solution one has constantly to be on the alert for snags; several of these have been described. It is considered necessary to make quite certain that for each determination of electrophoretic velocity a velocity distribution curve is made from the roof to the bottom of the capillary and only those where this distribution is parabolic are accepted.

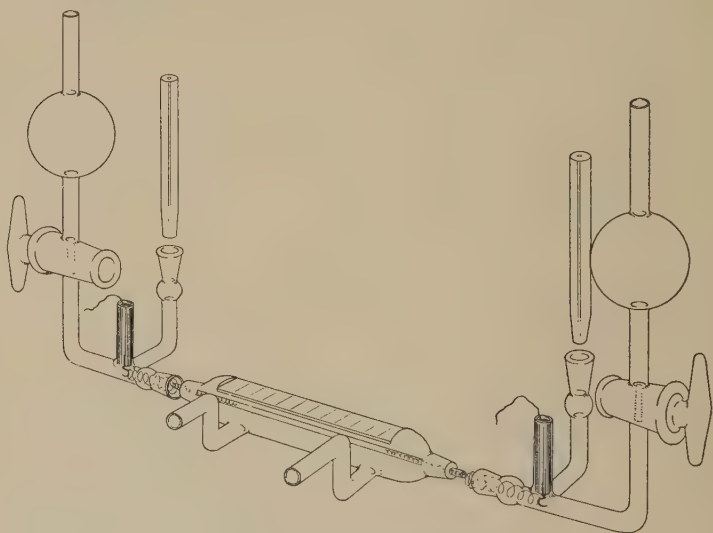


FIG. 3. Definitive apparatus.

Velocities are measured by observing with a stop watch the time a particle takes to travel a fixed distance on an ocular scale. Many determinations are made, the potential being reversed after each one and a mean value being taken.

The velocities at various depths are plotted according to a method which Van Gils (21) has described. On the x -axis are plotted the velocities observed at the various levels. On the y -axis are plotted the squares of the relative distances from the axis. In this way a parabola gives two straight lines and a diagram is obtained for a certain measurement, as given in Fig. 4. At $\frac{1}{2}r\sqrt{2}$, indicated by crosses, a parallel line is drawn. The electrophoretic velocity v_e is thus determined, and by combining it

with the velocity at the wall or with the velocity in the axis the electro-osmotic velocity is determined as well (indicated as v_0).

Velocity distributions that are not symmetrical or that are otherwise irregular are discarded. The method allows of obtaining good mean values of all observed points without undue calculation.

Further attention must be paid to the vertical adjustment and the elimination of irregularities of the micrometer screw of the microscope.

In cases where liquids of higher specific conductivity have to be investigated not all the above features need be applied. In the case described the conductivity of the suspension was $2 \times 10^{-12} \Omega^{-1} \text{ cm.}^{-1}$. It was raised by the addition of nitrobenzene, 5% increasing the conductivity to $2.5 \times 10^{-10} \Omega^{-1} \text{ cm.}^{-1}$. Electrophoresis of this suspension could

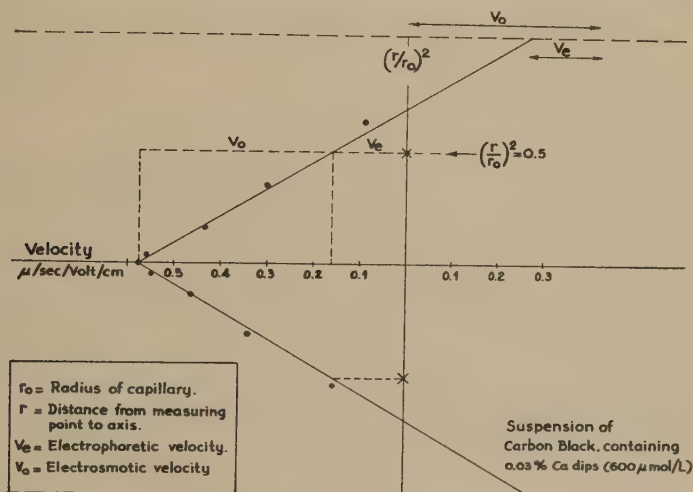


FIG. 4. Velocities in an electrophoresis cell. Parabolic distribution of velocity along a line perpendicular to the axis.

very well be measured in one of the simple glass capillaries described on p. 606. In this case the dielectric constant was only raised to 3.2. Apparently the conductivity is the most important factor. The addition of 3.0% nitrobenzene raised the conductivity to 1.0×10^{-10} but this appeared to be insufficient ($\epsilon = 2.85$).

EXPERIMENTS ON SUSPENSIONS OF VARIOUS OTHER MATERIALS

Having developed this method of electrophoresis measurement we were very much interested to know the range over which it could be applied.

Therefore a number of substances were dispersed in benzene to which 0.03% (600 $\mu\text{moles}/\text{l.}$) of Ca dips had been added. This soap was added

in order to increase the electric conductivity and to provide a ζ -potential such as would make conditions as favorable as possible for electrophoresis. *Rutile* (TiO_2), *lead chloride*, and *water*⁵ were chosen for their very high dielectric constants (ϵ of ca. 100, 33, and 80, respectively) and *aluminum* and *antimony* for their very high electric conductivity. Rather coarse suspensions were made by mechanical means and the coarsest particles were allowed to settle out. The particles were more or less globular.

All these suspensions showed perfect electrophoresis, no chain formation, and no other electrostatic phenomena and no turbulence till very near the electrodes. The electrophoretic velocities (v_e) obtained for the substances mentioned were in the above order: 0.28, 0.24, 0.15, 0.26, and 0.29 $\mu/\text{sec.}/\text{v.}/\text{cm.}$ (positive charge). Field strength applied: 100–200 $\text{v.}/\text{cm.}$

Then an aluminum suspension was made from aluminum powder as used for paint. The particles have the shape of leaflets. The powder was purified by extraction with ethyl alcohol. Contrary to the suspension of the globular aluminum, strong chain formation was observed already at 100 $\text{v.}/\text{cm.}$ and also other electrostatic phenomena such as attraction and repulsion. Electrophoresis was also observed, the velocity (v_e) of incidentally occurring loose particles being: 0.33 $\mu/\text{sec.}/\text{v.}/\text{cm.}$; loose chains also showed electrophoresis but at a different velocity. Although these experiments are preliminary we may draw the following conclusion.

Provided a homogeneous electric field is applied ($dE/dx = \text{constant}$), pure electrophoresis exists, independent of differences in dielectric constant (ϵ) and of electric conductivity (σ) between dispersed phase and continuous phase. Whether or no polarization phenomena occur appears to depend on the shape of the particles.

DEVIATION FROM NORMAL BEHAVIOR IN THE NEW APPARATUS AT VERY LOW ELECTROLYTE CONCENTRATIONS

Whereas particles in a suspension of carbon black in benzene to which 0.03% (600 $\mu\text{moles/l.}$) of Ca dips has been added start moving immediately after the field is applied, at lower concentrations the following is observed.

At a concentration of 0.007% (140 $\mu\text{moles/l.}$) and 0.003% (60 $\mu\text{moles/l.}$), immediately after application of the field no motion is observed; then, very slowly, motion begins and it takes ca. 10–15 sec. before a uniform motion sets in, which uniform motion then lasts as long as the potential remains on the electrodes. When the current is interrupted the motion continues and it takes approximately the same time before the particles come to a standstill. Also, on reversal of the current the particles first continue their former movement, then stop, and then gradually acquire

⁵ In this case 0.5% of cetyl alcohol had been added to the benzene solution.

velocity in the opposite direction. These observations were all made midway between the poles.

It should be noted that the same lapse of time is found over the whole depth of the capillary. Therefore electroendosmotic velocity and electrophoretic velocity must both undergo this change with time, and it therefore follows that there is no specific influence of either the quartz wall or the carbon particle.

On the other hand, the kind of electrolyte added does have an effect.

With the following substances in a concentration of *ca.* 10 μ moles/l. (allowing for adsorption by the carbon) these "running-in times" are:

tetraisoamylammonium picrate:	10 sec. (conductivity $1.5 \times 10^{-12} \Omega^{-1}/\text{cm.}^{-1}$)
calcium diisopropyl salicylate:	15 sec. (conductivity $0.5 \times 10^{-12} \Omega^{-1}/\text{cm.}^{-1}$)
oxidation resin:	100 sec. (conductivity $10^{-13} \Omega^{-1}/\text{cm.}^{-1}$).

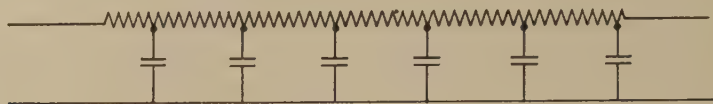
At higher concentrations, corresponding to conductivities of approximately 5×10^{-12} these "running-in times" disappear with all three electrolytes.

Considering: (a) this dependence on conductivity of the liquid; (b) the fact that in a badly insulated cell such as that described above these effects are much more in evidence; and (c) that both electroendosmotic and electrophoretic velocity show this same time effect; "running-in" effects are thought to be due to the time necessary to charge the small-capacitor formed by the electrophoresis cell. The quartz or glass tube with the space between the two electrodes filled with a benzene solution has a certain capacitance with respect to the surroundings. In order to build up the electric field a certain very small current has to pass through the liquid. It is known that the time necessary to build up the electric field is of the order of magnitude of $R \times C$, in which R is the resistance (in this case of the liquid) and C the capacitance of the capacitor. In a very simple case the part of the capacitor charged is:

$$1 - e^{-\frac{t}{RC}} \text{ in which } t \text{ is time.}$$

This capacitance C of the capillary certainly is small, but the resistance R of the very dilute solutions (see preceding) becomes considerable, and rough calculations on the basis of the data on conductivity and dimensions of the cell indicate that in such an electrical system a charging time (so-called RC time) of the order of a few seconds may be expected. This hypothesis was corroborated by a few preliminary experiments made in our laboratory by J. M. L. Janssen and H. H. Idzerda in an electrical

setup composed of resistances and capacitances as follows:



They found a charging time of this order. In electrotechnics this effect is considered as a special case of Heaviside's telegraph equation.

Extrapolating to the supposed conductivity of pure benzene ($10^{-17} \Omega^{-1}/\text{cm.}^{-1}$) the running-in or the running-down time would become very large and in a liquid of zero conductivity it is to be expected that no electrophoresis will take place even at infinity. This is the same conclusion that we arrived at in Part II of this series (22) from experimental evidence that when no ions are present in the continuous phase no electrophoresis occurs.

CONCLUSIONS

It was known that for enabling electrophoresis measurement in liquids of low dielectric constant, a homogeneous electric field must be built up, and dielectric polarization phenomena must be avoided.

The homogeneous field was obtained by increasing the resistance of the cell walls by diminishing the thickness of the glass or quartz wall and eliminating the surface conductance by treating the walls with silicones and applying a vacuum jacket. It is considered possible that a good result might also be obtained with conducting cell walls, provided that their conductivity is homogeneous. As soon as the conductivity of the liquid becomes of the order of 10^{-10} to 10^{-9} special designs of the glass or quartz cell cease to be necessary, so that a glass cell of simple design can be used.

Polarization phenomena are avoided by applying a relatively low electric field strength; however, in a reasonably homogeneous field such as we have obtained, a field strength of 200 v./cm. might be applied, the limit being set by the nature of the suspended material. In this respect the form of the particles is of much more importance than the differences in dielectric constant or in conductivity between the particles and the dispersion medium.

REFERENCES

1. LA MER, V. K., AND DOWNES, H. C., *J. Am. Chem. Soc.* **53**, 888 (1931); *ibid.* **55**, 1840 (1933); *Chem. Revs.* **13**, 47 (1933).
2. FUOSS, R. M., *Chem. Revs.* **17**, 27 (1935); STRONG, L. E., AND KRAUS, C. A., *J. Am. Chem. Soc.* **72**, 166 (1950).
3. MINNE, J. L. VAN DER, *Rec. trav. chim.* **65**, 549 (1946).
4. MINNE, J. L. VAN DER, Thesis: Over Emulsies. Utrecht, Holland, 1928.
5. POHL, H. A., *J. Applied Phys.* **22**, 869 (1951).

6. HOLLMANN, H. E., *J. Applied Phys.* **21**, 402 (1950).
7. WINSLOW, W. M., *J. Applied Phys.* **20**, 1137 (1949).
8. PUTILOVA, J. N., AND GINDIN, L. G., *Doklady Akad. Nauk, S.S.S.R.* **71**, 81 (1950).
9. GINDIN, L. G., *Doklady Akad. Nauk, S.S.S.R.* **72**, 671 (1950).
10. SOYENKOFF, B. C., *J. Phys. Chem.* **35**, 2993 (1931).
11. HAYEK, M., *J. Phys. & Colloid Chem.* **55**, 1527 (1951).
12. TERADA, AND KAHN, T., *C. A.* **42**, 1105 (1948).
13. REISING, J. A., *Ind. Eng. Chem.* **29**, 565 (1937).
14. GEMANT, A., *J. Phys. Chem.* **43**, 743 (1939).
15. HUMPHRY, R. H., AND JANE R. S., *Trans. Faraday Soc.* **22**, 420 (1926).
16. BUCHNER, E. H., AND VAN ROYEN, A. H. H., *Kolloid-Z.* **49**, 249 (1929).
17. QUINCKE, G., *Pogg. Ann.* **113**, 513 (1861).
18. SMITH, M. E., AND LISSE, M. W., *J. Phys. Chem.* **40**, 399 (1936).
19. RUTGERS, A., FACQ, L., AND MINNE, J. L. VAN DER, *Nature* **166**, 100 (1950).
20. JOHANSSON, O. K., AND TOROK, J. J., *Proc. Inst. Radio Eng.* **34**, 296 (1946).
21. VAN GILS, G. E., AND KRUYT, H. R., *Kolloid-Beihefte* **45**, 60 (1937).
22. MINNE, J. L. VAN DER, *J. Colloid Sci.*, in press.

PRODUCTION OF MONODISPERSE LIQUID PARTICLES BY ELECTRICAL ATOMIZATION

Bernard Vonnegut and Raymond L. Neubauer

General Electric Research Laboratory, Schenectady, New York

Received October 1, 1952

ABSTRACT

Streams of highly electrified uniform droplets about 0.1 mm. in diameter can be produced by applying potentials of 5-10 kv. a.c. or d.c. to liquids in small capillaries. Monodisperse aerosols having a particle radius of a micron or less can be formed if the capillary is positively charged and if liquids having low electrical conductivity are used. Aerosols formed in this way show the colors of higher-order Tyndall spectra.

INTRODUCTION

As the result of a suggestion made by Dr. W. R. Whitney, some qualitative experiments have been made concerning the effects of high voltage on the formation of water drops. It has been felt worth while to describe some of the phenomena which have been observed, even though much more work must be done before they are satisfactorily understood.

EXPERIMENTAL

Most of the work has been done with the simple apparatus shown in Fig. 1. A glass tube drawn down to a capillary having a diameter of the

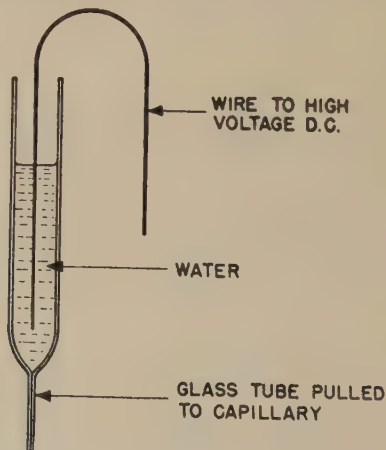


FIG. 1. Apparatus for electrical atomization.

order of a few tenths of a millimeter is filled with water or some other liquid. The liquid is connected with a source of variable high d.c. voltage

by a wire placed in the tube. Before voltage is applied, the liquid in the tube slowly comes out of the capillary and forms drops about a millimeter in diameter which fall off the tip at the rate of a few per minute. As the potential is raised to a few thousand volts, the droplets at the end of the capillary become smaller and smaller and come off at a much higher fre-



FIG. 2. Stream of droplets from capillary.

quency. At about 5000 v. and higher, the droplets are so small and are coming off with such speed that they appear to be a fine line. This is shown in Fig. 2. If water colored with ink is used and a piece of paper is moved around in the stream, the individual droplets leave a fine line of spots such as that shown in Fig. 3. The droplets in the stream are of the order of $100\ \mu$ in diameter and are produced at the rate of about 100/sec. Depending on the voltage and the characteristics of the capillary, one

or more streams can be produced. The droplets are highly charged. If an insulated rod is held in the stream for a few seconds, it quickly acquires such a high charge that the stream of drops is repelled and bounces off without touching the rod. If a high-voltage, 60-cycle a.c. source is brought

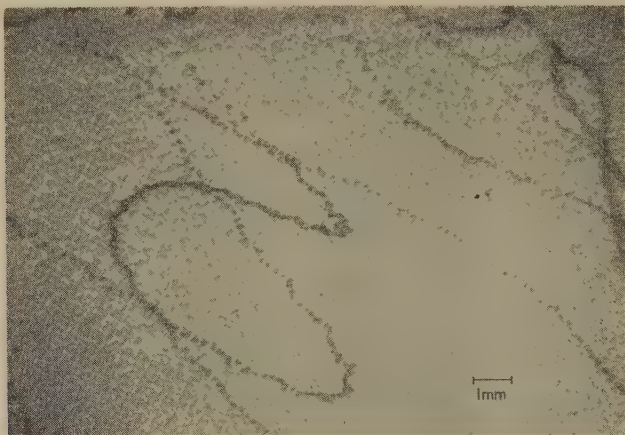


FIG. 3. Spots produced by spraying ink from capillary.

near to the stream, the droplets begin to move in bizarre, zigzag sinusoidal paths in the 60-cycle electrostatic field. Individual drops can be seen sometimes that are vibrating back and forth under the influence of the field so that they appear to be little fibers floating in the air.

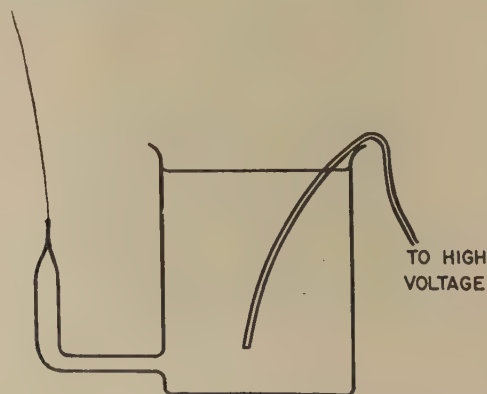


FIG. 4. Electrostatic fountain.

An electrostatic fountain shown in Fig. 4 was made by pointing the capillary tube up instead of down. In order for the fountain to operate, it is necessary to have the level of the water in the vessel about a centimeter above the capillary tip. This fountain rose to a height of about 30 cm. above the level of the water in the vessel. By placing a grounded funnel

near the stream, it was possible to catch the drops and allow the water to drip back into the vessel.

When a high voltage source of 60-cycle a.c. is applied to the capillary arrangement shown in Fig. 1, it produces one or more fine streams of droplets very similar in appearance to that formed using direct current.

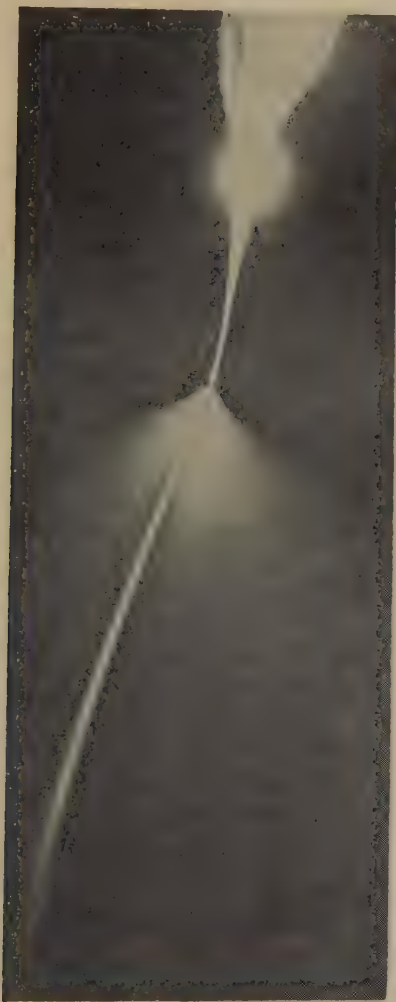


FIG. 5. Simultaneous production of stream of droplets and smoke.

It can be demonstrated that the stream carries no net charge by holding an insulated rod in it. The drops continue to hit the rod and are not deflected as was the case when direct current was used. It can be shown that the individual drops are charged by bringing a charged plastic pocket

comb near the stream. This causes it to separate into two streams, one of which is attracted and the other repelled by the comb.

The behavior of the stream with an alternating voltage suggests that by the use of a.c. or a pulsed d.c. it should be possible to control accurately the frequency of drop formation.



FIG. 6. Production of smoke alone.

Another phenomenon, quite different from the foregoing, has been observed with d.c. It was found in some cases that, in addition to the stream of drops coming off of the capillary tip, there was also a smoke of fine particles coming off through a solid angle of almost 180° , as is shown in Fig. 5. By trial and error, it was found possible to produce the smoke alone without the main stream, as is shown in Fig. 6.

When the smoke is illuminated with a beam of parallel light, it is beautifully colored—red, green, or orange—the colors depending on the angle of observation. This phenomenon, known as “higher-order Tyndall spectra” (1,2), indicates that the particles are of the order of $1\ \mu$ in diameter and that they are very uniform in size. The particle size is sensitive to voltage, and the color of the smoke when viewed from a given angle can be varied by changing the voltage. When two capillaries each producing smoke are brought close to each other, the fact that both smokes are highly charged with the same sign prevents them from mixing. With the proper lighting, one can see a thin boundary of smoke-free air between them.

It was found that the smoke of fine uniform particles could be produced only with liquids having a very low conductivity, such as distilled water, lubricating oil, alcohol, etc. Furthermore, it was not possible to produce the smoke except when the capillary was positively charged.

It is easy to see in a qualitative way how electric charge can cause the convex surface of a liquid to disperse into small droplets. The charges which go to the liquid surface repel each other and cause a force opposing surface tension. With sufficient charge, the forces of surface tension are overcome, and the liquid disperses as small droplets. Putting it another way, if a volume of liquid has a sufficiently large charge, the state of lowest energy will be one in which the liquid is in the form of many small drops, rather than in one large drop as is the equilibrium case when there is no charge.

If one assumes that by some mechanism it is possible for an electrically charged volume of water to break up into independent uniform droplets, one can compute the equilibrium value for the droplet radius by calculating the condition for minimum energy.

Consider a volume of liquid, V , having a surface tension, γ , and carrying a total charge, Q . Assume that by some mechanism the liquid is dispersed into N equal droplets of radius r , each carrying the same charge. Further assume that these droplets are far enough apart so that their electrical interaction can be neglected. The total energy, E , of the system is the sum of the surface energy and the electrical energy. It can be shown that

$$E = \frac{3V\gamma}{r} + \frac{2}{3} \frac{\pi r^2 Q^2}{KV} \quad [1]$$

where K is the constant relating the capacitance of a sphere to its radius. If we take the derivative of the total energy with respect to the radius and set it equal to zero for the condition of equilibrium, we find

$$r = \left(\frac{9KV^2\gamma}{4\pi Q^2} \right)^{\frac{1}{3}} \quad [2]$$

or if we solve for n , the equilibrium number of particles,

$$n = \frac{Q^2}{3KV\gamma} \quad [3]$$

It is possible to check Eq. [3] against the rather rough experimental data which have been obtained. It was found that with a current of 0.9×10^{-6} amp. and a flow rate of 5×10^{-6} cm.³/sec. the capillary produced a fine mist having a particle diameter estimated to be of the order of a few tenths of a micron. This means that drops were being formed at the rate of perhaps 10^8 /sec. When the figures for the flow rate and the current are used in Eq. [3], one obtains a value of 10^{10} particles/sec. The agreement between theory and experiment is not too bad in view of the fact that much of the measured current may have been lost as corona, and there is certainly a strong electrostatic interaction between the particles.

The foregoing discussion does not tell anything about how the smoke is produced. It is hard to visualize exactly how the uniform particles are formed, and further work must be done to understand the mechanism.

It was thought that possibly the smoke might be formed by evaporation and condensation of the liquid at the capillary tip. This explanation seems ruled out by the fact that it is possible to make smokes of liquids containing nonvolatile components, such as sugar solutions and suspensions of fine inorganic powders in liquids of low conductivity.

A few experiments have been made in which a drop of water is placed on a wire and the voltage steadily increased. Phenomena similar to those occurring with the capillary are observed. At about 5000 v. or more, the water drop develops a tiny sharp bump, and at this point it can be seen that small droplets or mist particles are being ejected.

It seems reasonable to suppose that in the high electrostatic fields under thunderstorms similar atomization of water might take place from drops on foliage and perhaps from the crests of waves. Also, if large, highly charged drops from a thunderstorm fall into dry air and evaporate, it is to be expected that as the drops get smaller the charge density on their surface will reach sufficiently high values to cause rapid breakup or even atomization.

ACKNOWLEDGMENTS

The authors wish to thank Mr. P. Pallett for taking the original photographs in color and Mr. K. Maynard for his help in making the black and white prints used in this report. The authors also gratefully acknowledge the sponsorship of this work by the U. S. Signal Corps and the Office of Naval Research under Contract No. W-36-039-sc-38141.

REFERENCES

1. LA MER, V. K., *Proc. Natl. Air Pollution Symposium, 1st Symposium, Pasadena, Calif.* 1, 5-13 (Nov. 1949); *J. Phys. & Colloid Chem.* **52**, 65 (1948); *J. Am. Chem. Soc.* **69**, 1184 (1947).
2. LA MER, V. K., AND SINCLAIR, D., *Chem. Revs.* **44**, 245 (1949).

THE SURFACE TENSION AND SURFACE POTENTIAL OF AQUEOUS SOLUTIONS OF NORMAL ALIPHATIC ALCOHOLS

A. M. Posner, J. R. Anderson, and A. E. Alexander

*The Department of Colloid Science, Cambridge, England; and the School of Applied
Chemistry, New South Wales University of Technology, Sydney, Australia*

Received November 26, 1951; revised May 26, 1952

I. INTRODUCTION

When a capillary-active substance is dissolved in water, the surface tension and the phase boundary potential fall to equilibrium values which depend on the bulk concentration. The difference between the values for the pure medium and the solution are respectively termed the surface pressure (Π) and the surface potential (ΔV). Little systematic work has been done on these quantities for a homologous series of normal aliphatic alcohols, though some earlier work (1) has demonstrated a constant increase in surface activity per additional CH_2 group, as the series is ascended. The work of Addison (2), who studied the surface tension of solutions of alcohols up to octyl alcohol, was limited to one temperature, and the temperature dependence study of Addison and Hutchinson (3) was limited to solutions of decyl alcohol.

The changes in surface tension and phase boundary potential are due to the adsorption of an excess of solute molecules at the surface. It has been suggested (4,5) that this excess forms a monolayer of much the same type as that formed by spreading certain insoluble substances at the air/water interface. The present experiments, on normal aliphatic alcohols, were undertaken originally in connection with our studies of the kinetics of adsorption (6).

II. EXPERIMENTAL

The alcohols were distilled twice before use and had boiling points within 1°C . of those given in the literature. Solutions were made up in 0.001 *N* HCl.

(a) Surface Tension

(i) *Maximum Bubble Pressure Method.* The method of Sugden (7) was used, the cell being immersed in a thermostat, constant to $\pm 0.2^\circ\text{C}$. The air used for blowing the bubbles was preheated by passing it through a coil placed in the thermostat. Bubbles were blown at the rate of about one per 15 sec. and the pressure differences read with a cathetometer on

an alcohol manometer. The method had an accuracy of ± 0.05 dyne/cm. Excellent values were obtained for pure liquids and for solutions of C_2 , C_3 , and C_4 alcohols; the higher alcohols showed a tendency to age.

(ii) *Drop Volume Method.* For C_5 and higher alcohols, the drop volume method was adopted, using a micrometer syringe with a ground-glass tip (8). The syringe dipped well into a closed glass cell containing some of the liquid under test, thus enabling the determination to be carried out in an atmosphere saturated with the vapor of the solution. The cell was immersed in a thermostat constant to $\pm 0.1^\circ C.$, and allowed to stand for 15 min. before a reading was made. Approximately 95% of the drop was formed rapidly, allowed to stand for 1 min., and the rest formed slowly, the whole operation taking about 2 min. Before use, the syringe was calibrated with solutions of ethyl alcohol of known surface tension. Values for other solutions were interpolated from this calibration curve, after making appropriate density corrections. The method was accurate to ± 0.2 dyne/cm.

(b) *Surface Potential*

This was measured using a circuit containing a vacuum tube electrometer of the type designed by Compton and Haring (9). The air electrode used for making the air gap conducting consisted of a silver wire bent in the form of an L, with two one-millicurie mesothorium bromide tubes attached to its end. The standard half-cell was of the Ag/AgCl type.

The glass trough (housed in a screened wooden box) was first filled with the 0.001 *N* HCl medium, the surface swept clean with waxed glass slides, and its contact potential (V_1) determined after lowering the air electrode to within 2 mm. of the surface. The trough was then emptied, filled with the solution under test, and its contact potential (V_2) determined as before. The difference in contact potentials ($V_1 - V_2$) gave the surface potential (ΔV).

The temperature of the trough was kept constant to $\pm 0.5^\circ C.$ by immersing it to within 3 mm. of its top in a thermostat. The air in the box was maintained at $2^\circ C.$ above the thermostat temperature by electrical heating pads, and kept saturated with vapor by having, in the box, vessels containing some of the solution under examination.

The contact potential could be determined to ± 0.5 mv. Solutions having Π within the range of 0 to 35 dynes/cm. were studied, and were prepared by successive dilution. Two initial solutions were used, the concentration of one being $\frac{3}{4}$ of the other, and no further experiments were done if the two sets of readings fell on the same smooth curve. Experiments were done at 12, 25, and $39^\circ C.$

III. RESULTS AND DISCUSSIONS

(a) *Normal Aliphatic Alcohols*

The data are recorded in Table I. Where comparable, the values for surface tension are in agreement with those of Addison and Hutchinson (3) and Hutchinson (10).

TABLE I

	Concentration <i>g. mole/l.</i>	Surface pressure		
		12°C. <i>dynes/cm.</i>	25°C. <i>dynes/cm.</i>	39°C. <i>dynes/cm.</i>
<i>n</i> -Butyl alcohol	0.4060	33.6	—	34.7
	0.2700	27.5	26.4	28.8
	0.2030	25.3	22.3	24.9
	0.1350	20.4	19.1	19.8
	0.1020	17.3	15.4	16.6
	0.0675	13.5	11.5	12.6
	0.0510	11.1	9.6	9.0
	0.0338	8.4	6.4	7.6
	0.0260	6.2	5.0	5.8
	0.0169	4.1	3.0	3.1
	0.0130	2.9	2.0	—
	0.0085	2.9	—	2.5
	0.0064	2.2	1.0	—
	0.0048	1.1	—	0.9
	0.0032	1.2	—	—
<i>n</i> -Amyl alcohol	0.1200	—	34.0	31.4
	0.0852	—	31.3	28.7
	0.0600	—	25.4	23.0
	0.0426	—	20.5	19.4
	0.0300	—	16.7	14.3
	0.0213	—	13.1	11.9
	0.0150	—	10.3	8.2
	0.0107	—	7.6	—
	0.0075	—	5.3	3.8
	0.0054	—	3.7	—
	0.0038	—	2.8	1.7
	0.0027	—	2.0	—
	0.0019	—	1.6	—
	0.02940	—	32.5	31.4
	0.01960	—	27.6	24.7
	0.01470	—	24.3	20.8
	0.00980	19.4	19.2	16.8
	0.00740	—	15.0	13.3
	0.00686	16.3	—	—
	0.00490	13.4	10.9	9.7
	0.00370	—	8.7	7.6

TABLE I (Continued)

		Surface pressure		
Concentration		12°C.	25°C.	39°C.
g. mole/l.		dynes/cm.	dynes/cm.	dynes/cm.
<i>n</i> -Hexyl alcohol	0.00343	9.4	—	—
	0.00250	7.9	5.5	5.0
	0.00185	—	—	3.3
	0.00172	5.7	—	—
	0.00125	3.9	2.6	—
	0.00093	—	—	1.3
	0.00081	2.5	—	—
	0.00062	2.3	1.3	—
	0.00047	—	—	0.6
	0.00032	—	0.6	—
<i>n</i> -Heptyl alcohol	0.00690	32.4	31.5	28.6
	0.00516	29.0	27.0	23.7
	0.00345	23.2	21.6	18.0
	0.00258	19.9	17.9	14.2
	0.00173	15.3	14.1	10.1
	0.00129	12.0	12.9	8.1
	0.00087	8.6	7.4	4.8
	0.00065	5.9	6.0	2.4
	0.00044	3.9	3.0	2.0
	0.00033	2.7	2.3	—
<i>n</i> -Octyl alcohol	0.00022	2.3	—	0.6
	0.00017	1.9	0.8	—
	0.00011	1.3	—	—
	0.00308	40.2	38.3	38.0
	0.00231	35.6	—	29.6
	0.00192	—	31.3	—
	0.00154	30.4	26.4	24.2
	0.00116	25.6	—	19.0
	0.00096	—	20.1	—
	0.00077	21.4	18.1	14.3
<i>n</i> -Octyl alcohol	0.00058	17.8	—	9.1
	0.00048	—	11.5	—
	0.00038	12.8	10.6	7.3
	0.00029	9.8	—	4.2
	0.00024	—	5.4	—
	0.00019	6.8	4.0	—
	0.00014	4.4	—	1.2
	0.00012	—	1.8	—
	0.00010	2.1	1.1	—
	0.00007	1.9	0.8	—
	0.00005	1.5	—	0.6

Figure 1 shows a typical Π vs. concentration (c) curve for *n*-heptyl alcohol at 12, 25, and 39°C. $d\Pi/dc$ is initially constant (0–10 dynes/cm.), followed by a continuous decrease. Increase in temperature causes a

slight decrease in Π , the temperature coefficient of the Traube constant α being about 0.2×10^3 dynes/cm./mole/deg. over the range of 0–10 dynes/cm., where the Traube rule, $\Pi = \alpha c$, holds.

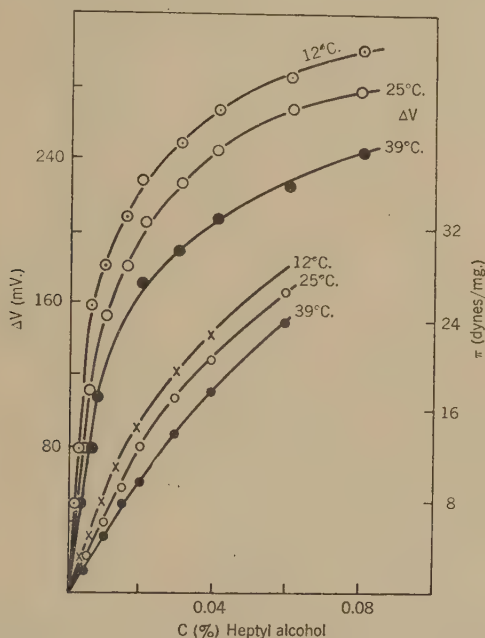


FIG. 1. Surface pressure (Π) plotted against bulk concentration (c in %).

n -heptyl alcohol $\left\{ \begin{array}{l} \times 12^\circ\text{C.} \\ \circ 25^\circ\text{C.} \\ \bullet 39^\circ\text{C.} \end{array} \right.$

Surface potential (ΔV) plotted against bulk concentration (c in %) for n -heptyl alcohol solution.

n -heptyl alcohol $\left\{ \begin{array}{l} \circ 12^\circ\text{C.} \\ \circ 25^\circ\text{C.} \\ \bullet 39^\circ\text{C.} \end{array} \right.$

Figure 2 shows Π vs. $-\log_{10} c$ curves at 25°C. for C_2 – C_8 alcohols inclusive. For $\Pi > 10$ dynes/cm. the curves form a series of approximately equidistant parallel lines. Below $\Pi = 10$, the curves assume considerable curvature going off, asymptotically, to infinity at $\Pi = 0$. Curves similar in shape to that at 25°C. are shown for n -heptyl alcohol at 12°C. and 39°C. The curves of ΔV vs. c (Fig. 1) and ΔV vs. $-\log_{10} c$ (Fig. 3) show similar characteristics to those of Π vs. c and Π vs. $-\log_{10} c$ (see below).

The Traube rule, $\Pi = \alpha c$, holds in the region 0–10 dynes/cm. for all the alcohols. It is also valid from 0 to 100 mv. when written in the form $\Delta V = \beta c$.

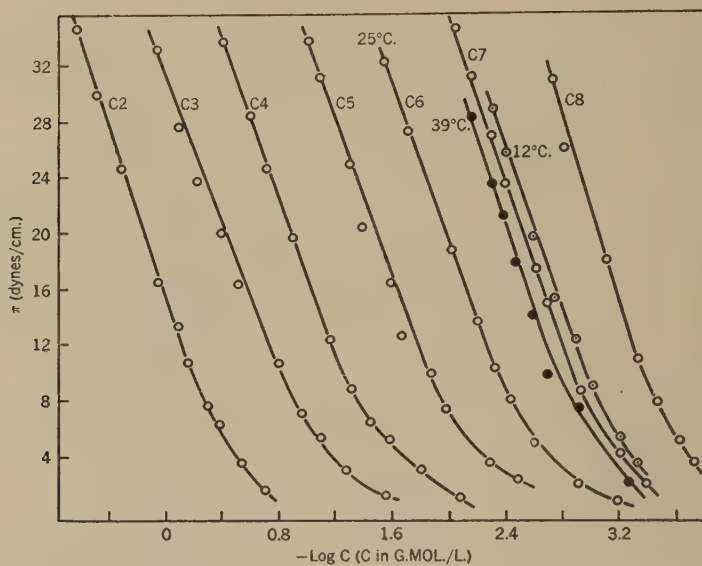


FIG. 2. Surface pressure (Π) plotted against $-\log_{10} c$ (c = concentration in g. moles/l.) for the normal alcohols C_2 - C_8 inclusive).

○ 25°C.
○ 12°C.
● 39°C.

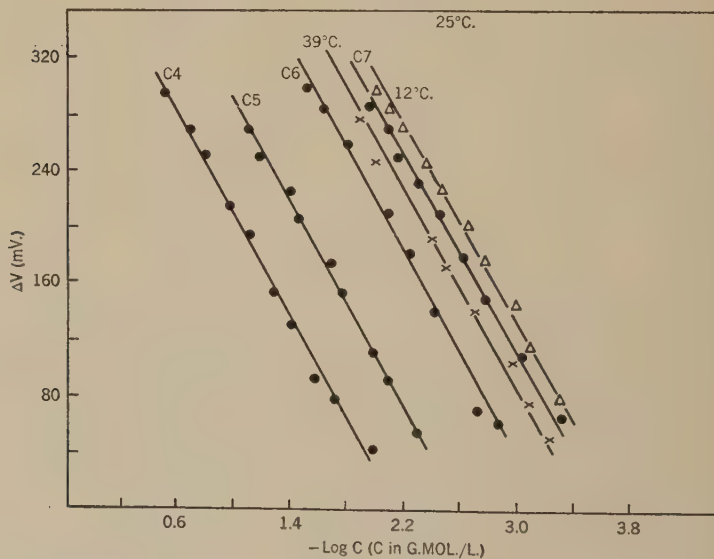


FIG. 3. Surface potential (ΔV) plotted against $-\log_{10} c$ (c = concentration in g. moles/l.) for the normal alcohol solutions C_4 , C_5 , C_6 , and C_7 .

● 25°C.
× 39°C.
△ 12°C.

As expected $\alpha_n/\alpha_{n-1} \approx 3$ (where n is the number of carbon atoms in the molecule); a similar value for β_n/β_{n-1} was also obtained. Values of the Traube constants were obtained in the higher concentration region by considering the relative concentrations of alcohol to produce the same Π or ΔV . Mean values of the ratios α_n/α_{n-1} and β_n/β_{n-1} were obtained from the slope of the straight line plot of $\log_{10} \alpha$ or $\log_{10} \beta$ vs. number of carbon atoms per molecule. The results are shown in Table II.

TABLE II

$\frac{n}{n-1}$	25°C.				39°C.	
	$\frac{\alpha_n}{\alpha_{n-1}}$ 0-10 dynes/cm.	$\frac{\beta_n}{\beta_{n-1}}$ 0-100 mv.	$\frac{\alpha_n}{\alpha_{n-1}}$ 32 dynes/cm.	$\frac{\beta_n}{\beta_{n-1}}$ 240 mv.	$\frac{\alpha_n}{\alpha_{n-1}}$ 0-10 dynes/cm.	$\frac{\beta_n}{\beta_{n-1}}$ 0-100 mv.
3/2	2.92	—	3.24	—	—	—
4/3	3.03	—	3.31	—	—	—
5/4	3.24	2.63	3.80	3.0	2.63	—
6/5	3.32	4.07	3.24	3.6	3.62	—
7/6 ^a	4.20	2.84	3.10	2.75	3.6	3.03
8/7 ^a	3.42	—	3.55	—	2.60	2.66
Mean	3.5 ₀	3.2 ₇	3.4 ₀	3.1 ₀	3.1 ₀	3.0 ₄

^a Mean values, based on these two readings at 12°C., for $\alpha_n/\alpha_{n-1} = 3.3_8$; for $\beta_n/\beta_{n-1} = 2.5_1$.

(b) *The Surface Pressure (II) vs. Surface Area (A) Relationship*

The surface concentration N_s (where $N_s = 1/A$) vs. Π curve can be obtained with the aid of the Gibbs Adsorption Isotherm,

$$N_s = \frac{c}{kT} \frac{d\Pi}{dc} \quad [1]$$

assuming that the activity coefficient is constant over the range of concentrations concerned (11). The tangents $d\Pi/dc$ are best drawn with the aid of a small mirror. However, for values of Π exceeding about 20 dynes/cm. the method of drawing tangents is of insufficient accuracy for constructing the Π vs. A diagram in this region. The films in the region 0-10 dynes/cm. are all gaseous, becoming more expanded as the homologous series is descended and the temperature raised.

Studies on insoluble monolayers (12) and some adsorbed films (1) show that for $\Pi > ca. 15$ dynes/cm., many films obey a modified form of the two-dimensional perfect gas law, namely,

$$\Pi(A - A_0) = xkT \quad [2]$$

where A_0 is the co-area of the molecule and x is a measure of the lateral adhesion of the molecules in the film, being unity when there is no adhesion and decreasing as the adhesion increases.

Combination of this equation with the Gibbs adsorption isotherm, followed by integration, leads to the result (13):

$$\ln \Pi' = \frac{\Pi A_0}{kT} + x \ln \Pi \quad [3]$$

where Π' is the pressure the film would have if it were perfectly gaseous. Application of this equation to the experimental results enables A_0 and x to be determined. Table III gives the values of x and A_0 thus found.

TABLE III

No. of C atoms per molecule	x			A_0		
	12°C.	25°C.	39°C.	12°C.	25°C.	39°C.
4	0.84	0.88	0.93	17.8	17.0	18.0
5	—	0.88	0.88	—	16.0	14.8
6	0.86	0.84	0.84	17.8	16.0	15.0
7	0.80	0.80	0.81	17.0	16.0	15.8
8	0.78	0.84	0.70	17.8	16.0	16.0

There is a tendency for x to decrease with increasing chain length, corresponding to the increased lateral adhesion in the film. A_0 is approximately constant at each temperature and independent of the chain length. This is not surprising for A_0 depends primarily on the end-group. The slight decrease with increasing temperature is unexpected but may not be significant.

The agreement is good between the Π vs. A curve derived from the equation of state and that obtained by direct application of the Gibbs adsorption isotherm.

(c) *The Surface Potential (ΔV) vs. Surface Concentration (N_s) Relationship*

Figure 4 shows the plot of ΔV vs. N_s for *n*-heptyl and butyl alcohol solutions at 25°C.; the values of N_s were obtained from the equations of state determined above. The curves are linear within experimental error, similar curves being obtained for all the other alcohols studied.

Drawing the usual analogy between the electrical double layer existing at the surface and a parallel plate condenser we have

$$\Delta V = \frac{4\pi\mu N_s}{\epsilon} \quad [4]$$

where μ is the vertical component of the dipole moment of the film molecules and ϵ the dielectric constant of the surface phase. The linear relationship between ΔV and N_s is therefore not unexpected on the basis of the above equation. The linearity over a wide range of surface concentrations indicates that μ changes but little as the film is compressed.

Table IV shows the values of μ for the normal alcohol films, taking the dielectric constant as unity. They are all of the order 0.2 D.,¹ indi-

¹ D (Debye unit) = 10^{-18} (e.s.u.) (cm.).

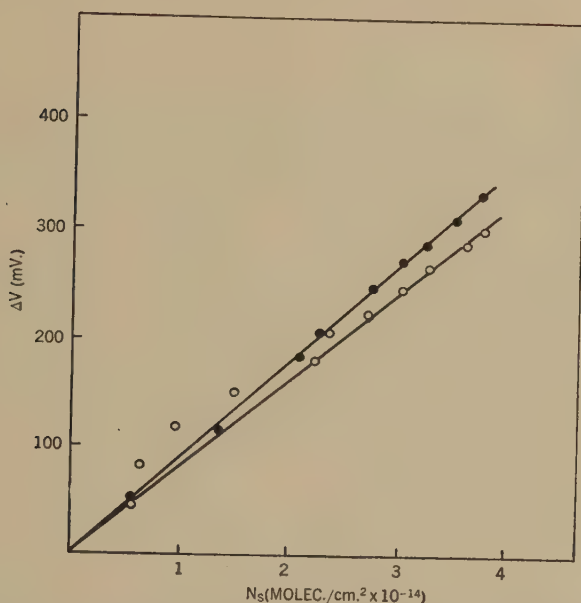


Fig. 4. Surface potential (ΔV) plotted against surface concentration (N_s).

● *n*-butyl alcohol solution (25°C.)

○ *n*-heptyl alcohol solution (25°C.)

cating that μ is largely determined by the end-group $-\text{OH}$. The values are in good agreement with the figures of about 0.22 D. quoted by Adam (14). In the gaseous region of the film,

$$\Pi = N_s kT \quad \text{and} \quad \Pi = \alpha c, \quad \text{i.e.,} \quad N_s kT = \alpha c.$$

From Eq. [4] we have

$$\Delta V = \frac{4\pi\alpha\mu}{kT} c. \quad [5]$$

TABLE IV

No. of C atoms	12°C.	μ (D) 25°C.	39°C.
4	0.24	0.24(0.20)	0.24
5	—	0.22(0.22)	—
6	0.26	0.24(0.20)	0.21
7	0.22	0.20(0.19)	0.20
8	0.21	— —	0.17

As expected from this equation, ΔV vs. c is a straight line in the initial region (0–100 mv.), from the slope of which μ can readily be calculated. This method of determining μ is of course identical with the one used above.

Examination of Eq. [5] shows why

$$\alpha_n / \alpha_{n-1} \approx \beta_n / \beta_{n-1},$$

for

$$\beta_n/\beta_{n-1} = (\alpha_n/\alpha_{n-1}) \times (\mu_n)/(\mu_{n-1}),$$

and since $\mu_n \approx \mu_{n-1}$ it follows that $\beta_n/\beta_{n-1} \approx \alpha_n/\alpha_{n-1}$.

Application of the Langmuir theory to the surface equilibrium and the direct proportionality between ΔV and N_s , leads (15) to the equation,

$$c/\Delta V = \frac{1}{4\pi\mu A} + Bc/4\pi\mu A; \quad [6]$$

thus a plot of $c/\Delta V$ vs. c should be a straight line of slope $B/4\pi\mu A$. Typical results of such a plot for the normal alcohols are shown in Fig. 5 (hexyl, heptyl). The curves are all linear, except perhaps in the very initial region where $\Delta V = \beta c$. From the slopes of these curves and assuming that $B/A = 20 \text{ \AA.}^2$ values of μ were calculated. The results are shown in brackets in Table IV; the agreement between the two methods of obtaining μ is quite good.

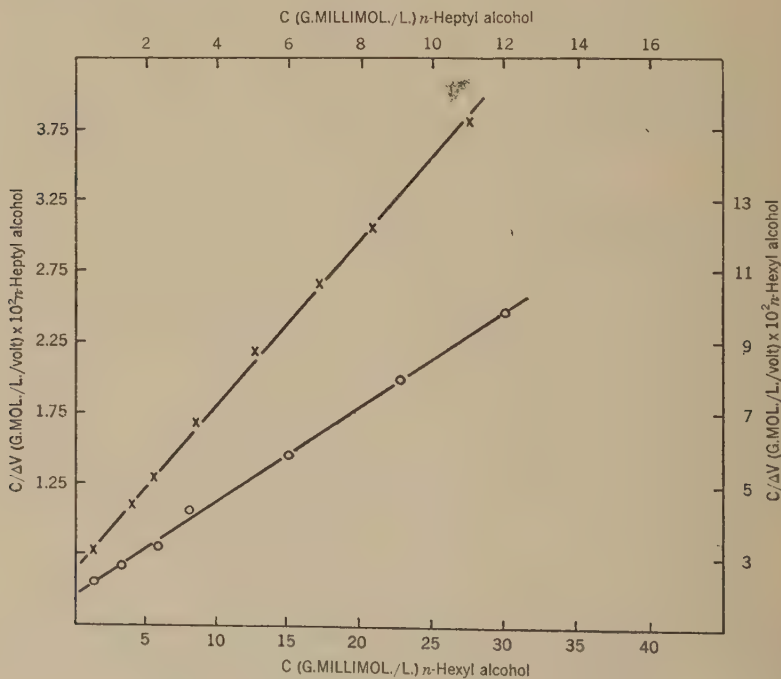


FIG. 5. $c/\Delta V$ plotted against concentration c .

× *n*-heptyl alcohol.

○ *n*-hexyl alcohol.

The above experiments and results thus provide good evidence for the direct proportionality between ΔV and N_s for these adsorbed alcohol films.

IV. THE ENTROPY OF ADSORPTION AT THE AIR WATER INTERFACE

Considerable interest has been shown recently in the entropy changes associated with adsorption from the gas phase onto solid or mercury surfaces (16), whereas adsorption at the air water interface appears to have been completely neglected.

The data about adsorption at the gas mercury interface will be used later for comparison. The results of Kemball and Rideal (K-R) (17) and of Kemball (18,19) are summarized in Table V [see Ref. (16)].

TABLE V

Surface Standard State: $\Pi = 0.0608$ dynes/cm.

Bulk standard state: 1 atm. pressure

All values at 25°C.

	$-\Delta H^\circ$ kcal./mole	$-\Delta G^\circ$ kcal./mole	$-\Delta S^\circ$ e.u./mole	$-(\Delta S_{\text{trans.}} - \Delta S_{\text{trans.}})$ e.u./mole
Benzene	16.4	8.51	26.6	9.0
Toluene	21.2	9.63	39.6	9.1
<i>n</i> -Heptane	13.4	8.82	15.3	9.1
Methyl alcohol	15.9	7.88	27.2	8.1
Ethyl alcohol	11.4	8.06	11.2	8.4
<i>n</i> -Propyl alcohol	10.8	8.45	7.9	8.7
<i>n</i> -Butyl alcohol	18.1	9.82	27.8	9.0
<i>n</i> -Amyl alcohol	19.2	10.51	29.0	9.2
<i>n</i> -Hexyl alcohol	21.2	11.23	33.4	9.3
Water	17.6	6.85	35.9	

In col. 5 of Table V is recorded the calculated loss of entropy for the loss of one degree of translational freedom. The experimental entropy loss is considerably greater than this calculated value, and the fact was interpreted by K-R as being due to loss of rotational and vibrational degrees of freedom on adsorption onto the mercury surface. On this basis, the cases of benzene and toluene were calculated in detail by Kemball, and good agreement was obtained between the observed and calculated entropy changes. However, the alcohols and heptane could be treated in a qualitative manner only.

(a) *Calculation of Entropy from Surface Tension Measurements,
and the Definition of Standard States*

The standard states used by K-R were: (a) ideal gas phase: 1 atm. pressure; (b) surface: a film pressure (Π) 0.0608 dyne/cm. This value is chosen so that on the assumption that the film thickness is 6 Å., the volume per molecule is the same as that for an ideal gas at 1 atm. This choice is an attempt to make the conditions as regards concentration in the bulk and in the surface correspond as closely as possible, a feature which is desirable in the choice of all such standard states.

Using a film thickness of δ cm. so that concentrations in the surface may be expressed as bulk concentrations, and adopting the standard states of 1 molecule/cc. in both the bulk and the surface, the standard free energy of adsorption is readily expressible (20) as

$$\Delta G^0 = -RT \ln \frac{\alpha}{kT\delta} \quad [7]$$

where the concentrations are sufficiently low for activity coefficients to be set equal to unity. In [7] α is the Traube constant in dynes/cm./molecule/cc.

In Table VI are recorded the values of ΔG^0 calculated using Eq. [7], and also the ΔH^0 values calculated from the temperature variation of the

TABLE VI
Alcohols, Bulk to Surface

No. of carbon atoms	Temp. °C.	δ^a A.	$10^{-2} \frac{\alpha}{KT\delta}$	$-\Delta H^0$ (mean) kcal./mole	$-\Delta G^0$ kcal./mole	$-\Delta S^0$ (± 0.1) e.u./mole
4	12		1.20			
	25	8.8 ₉	0.90	2.6 ₈	2.66	0.1
	39		0.80			
5	25		2.99			
	39	9.5 ₃	2.14	4.4 ₁	3.36	3.5
6	12		13.5			
	25	9.9 ₂	9.5	3.8 ₈	4.05	-0.6
	39		7.5			
7	12		39.5			
	25	10.1 ₂	29.6	4.2 ₂	4.72	-1.7
	39		20.8			
8	12		142.			
	25	10.2 ₄	97.7	4.8 ₇	5.42	-1.8
	39		67.4			

^a Obtained from the most probable lengths of the hydrocarbon chain (20) and taking the length of the OH group as 2.5 Å.

equilibrium constant $\alpha/kT\delta$. The corresponding entropy changes were calculated using the relation: $\Delta G^0 = \Delta H^0 - T\Delta S^0$.

In the final analysis we wish to obtain information about the state of the molecules in the surface by comparing the surface (by a thermodynamic method) with the reference state for the bulk solution. To compare the surface with the vapor phase we shall use the results of Butler (11).

Butler calculated the free energy change for vapor to solution from the equation:

$$\Delta G_B^0 = RT \ln \frac{p}{x} \quad [8]$$

where p is the partial pressure of the alcohol vapor above the solution and x is the mole fraction of alcohol in the solution. The standard states thus employed were (a) vapor: 1 atm. pressure; (b) bulk: an infinitely dilute solution where it was assumed that $x = a$. To make use of Butler's results it is necessary to recalculate them using the standard states of (a) bulk: 1 molecule/cc., and (b) vapor: 1 molecule/cc.; or to be consistent with the usual convention for defining standard states of gases in terms of pressure, a pressure in atmospheres such that the volume per molecule is 1 cc. assuming ideal behavior of the gas.

The pressure in atmospheres required to give a volume per molecule of 1 cc. is given by: $p = kT$ when k is the Boltzmann constant in cc. atm./molecule/deg. The conversion from mole fraction x to concentration (c) in molecules/cc. is effected by the relation (for very dilute solutions) $x = C M_w / N$ where M_w is the molecular weight of the solvent (water) and N is Avogadro's number. Thus, Eq. [8] becomes

$$\Delta G_B^0 = RT \ln (pN/C M_w). \quad [9]$$

Hence, if we write ΔG_B^0 for Butler's values, the standard free energy change per mole (ΔG^0) from vapor to bulk under the new standard states is given by:

$$\Delta G^0 = \Delta G_B^0 - RT \ln (kTN/M_w)$$

or at 298°K.

$$\Delta G^0 = \Delta G_B^0 - 1359 \log_{10} 1360. \quad [10]$$

The values of ΔG_B^0 and ΔG^0 are shown in Table VII with the corresponding ΔH^0 and ΔS^0 values. The differences between corresponding bulk \rightarrow surface and bulk \rightarrow vapor data give values for the vapor \rightarrow sur-

TABLE VII
Alcohols, Vapor to Bulk at 25°C.

No. of carbon atoms	$-\Delta G_B^0$ kcal./mole	$-\Delta G^0$ kcal./mole	$-\Delta H^0$ kcal./mole	$-\Delta S^0$ e.u./mole
4	0.41	4.66	15.94	37.9
5	0.17	4.42	17.50	43.9
6	0.06	4.31	19.08 ^a	49.6
7	-0.06	4.19	20.67 ^a	55.3
8	-0.21	4.04	22.25 ^a	61.1

^a Obtained by linear extrapolation of data for C₁-C₅.

face transition (now termed ΔG_{vs}^0 , etc.). Calculated values of ΔG_{vs}^0 , ΔH_{vs}^0 , and ΔS_{vs}^0 are given in Table VIII.

Using the Sackur-Tetrode equation for three dimensions, the classical entropy due to three degrees of translational freedom (${}_3S_{trans}$) may be

calculated. The two-dimensional analog of the Sackur-Tetrode equation developed by Kamball (18)

$${}_2S_{\text{trans.}} = R \ln MTA + 65.80$$

where A is the accessible area per molecule in cm.^2 , enables the entropy of a perfect two-dimensional gas (${}_2S_{\text{trans.}}$) to be calculated. The values of (${}_3S_{\text{trans.}} - {}_2S_{\text{trans.}}$) so obtained are all close to 9 e.u. for the present series of alcohols.

TABLE VIII
Alcohols, Vapor to Surface at 25°C.

No. of carbon atoms	$-\Delta H_{\text{VS}}^0$ kcal./mole	$-\Delta G_{\text{VS}}^0$ kcal./mole	$-\Delta S_{\text{VS}}^0$ (± 0.2) e.u./mole
4	18.6 ₂	7.32	38.0
5	21.9 ₁	7.78	47.4
6	22.9 ₂	8.36	49.0
7	24.8 ₀	8.91	53.6
8	26.9 ₃	9.46	59.3

Now the agreement found by Kamball between the observed and calculated entropy change for benzene and toluene where a rigorous calculation is possible leads to the conclusion that on a mercury surface it is justifiable to treat the accessible area per molecule as the total area per molecule. In other words the surface phase may be considered as a true two-dimensional perfect gas. However, if we compare the entropy decrease for adsorption of alcohols on mercury with corresponding adsorption at the air water interface (Fig. 8) it will be seen that the latter values are considerably greater. This could be accounted for, at least in part, if the accessible area per molecule at the air water interface were considerably less than the apparent total area per molecule. This is precisely what is to be expected if the adsorbed molecule is still considerably immersed in the water for then the movement of the adsorbed molecule in the plane of the surface will be restricted. This is analogous to the way in which a solute molecule is restricted by the cage of solvent which surrounds it in the bulk. Taking the simplest picture one may now define a *free area* A' , which is the effective area in which an adsorbed molecule is free to move in the plane of the surface, and it is the appropriate value of A' which should be inserted in the two-dimensional Sackur-Tetrode equation to obtain ${}_2S_{\text{trans.}}$. We make the assumption that adsorption involves the complete loss of one degree of translational freedom, and although this will be replaced by a vibration perpendicular to the surface, we assume that this makes a negligible contribution to the entropy of the adsorbed molecule. This approximation, which is probably a fairly good one, was also made by Kamball.

Table VI shows that the entropy change going from bulk to surface is close to zero. This is at first surprising since one might have expected a small entropy decrease due to localization of the molecules in one plane and further restriction of rotation. That no decrease is found is in our

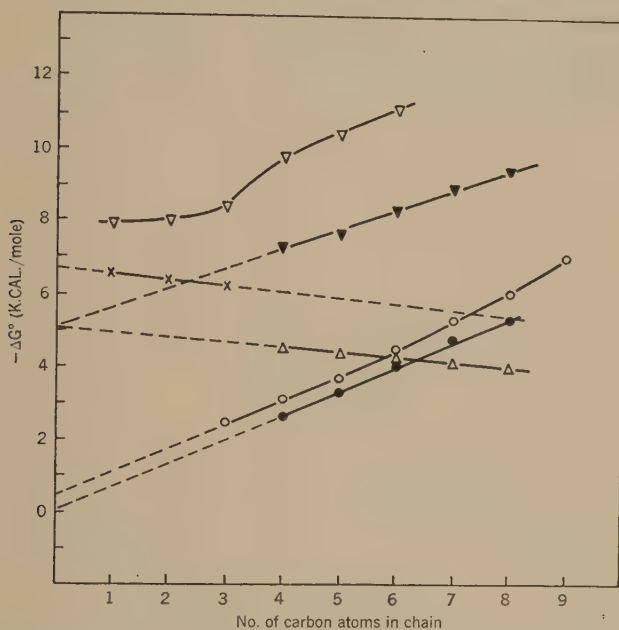


FIG. 6. Standard free-energy change ($-\Delta G^0$) plotted against number of carbon atoms in chain.

- ▽ alcohols (vapor) onto mercury
- acids, vapor to surface
- × acids, vapor to bulk
- acids, bulk to surface
- △ alcohols, vapor to bulk
- alcohols, bulk to surface
- ▼ alcohols, vapor to surface.

view associated with a corresponding small increase in internal degrees of freedom of the hydrocarbon portion of the molecule when it reaches its equilibrium position in the interface. Nevertheless, these opposing changes are no doubt small in such a system and it must be concluded that in the surface the hydrocarbon chain is still considerably immersed in the water, and the surface state far more closely resembles the solution than the vapor. It is clear therefore, that the value of A' will be much less than the total area per molecule. However it is not possible as yet in such a complex system to evaluate A' quantitatively. In the closely related case of the bulk solution, Frank and Evans (21) have discussed in detail the entropy of solution (from the vapor) of the alcohols in water

using the free volume theory and have shown that the large negative entropy changes cannot be explained on this theory alone. They suggest that the abnormally high loss of entropy is due not only to hydrogen bonding through the hydroxyl group, but also to "iceberg" or "cluster" formation in the water immediately in contact with the solute molecule. The same idea has recently been applied by Bohon and Claussen (22) to explain a similar large entropy of solution of aromatic hydrocarbons in water. It seems possible that this mechanism is also operating to some

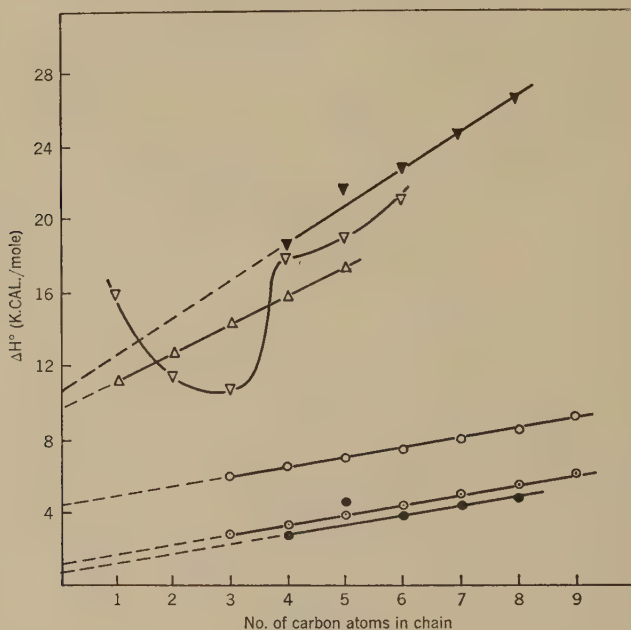


FIG. 7. Heat content change ($-\Delta H^0$) plotted against number of carbon atoms in chain.

- ∇ alcohols (vapor) onto mercury
- \circ acids, bulk to surface as calculated by Ward
- \odot acids, bulk to surface as calculated on p. 641
- \triangle alcohols, vapor to bulk
- \bullet alcohols, bulk to surface
- \blacktriangledown alcohols, vapor to surface.

extent with an adsorbed molecule. In addition to this factor there is also the probable loss of entropy due to restriction of the internal degrees of freedom of the hydrocarbon chain on adsorption. In the gas phase a hydrocarbon chain is certainly not fully extended (23,24); nevertheless, when it enters water as in the solution of the alcohols, the cage of solvent molecules which surrounds the solute molecule probably leads to very considerable tightening of the hydrocarbon coil. This would be reflected in restriction of internal degrees of freedom and loss of entropy. Both

of these effects should increase with increase of chain length. The conclusion, viz. of a coiled-up hydrocarbon chain considerably immersed in the water, agrees with the picture suggested by Ward (25) from surface energy considerations.

In Figs. 6 to 8 are plotted the various thermodynamic quantities as functions of the length of the hydrocarbon chain, for adsorption at both water and mercury surfaces. The results for mercury vary with chain length in a complex manner. The most striking feature is the pronounced

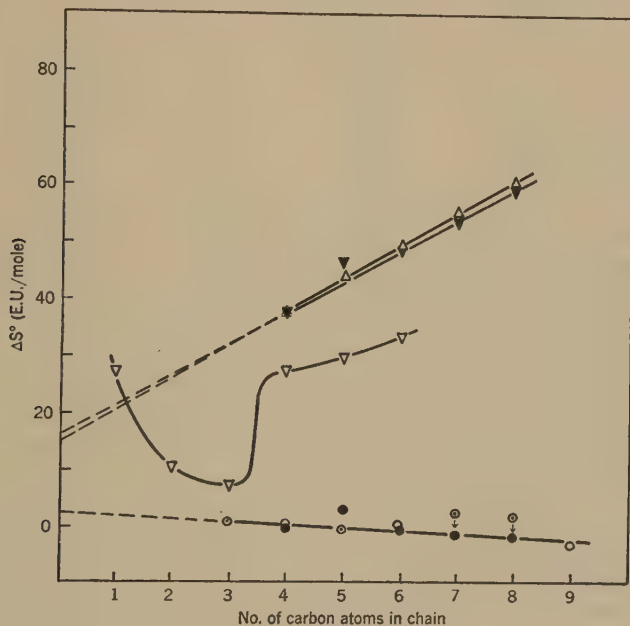


FIG. 8. Standard entropy change ($-\Delta S^\circ$) plotted against number of carbon atoms in chain.

- ▽ alcohols (vapor) onto mercury
- acids, bulk to surface, calculated using ΔH°
as calculated on p. 641
- △ alcohols, vapor to bulk
- alcohols, bulk to surface
- ▼ alcohols, vapor to surface.

trough in the ΔH° curve. This was interpreted by Kemball as being due to variations in orientation of the adsorbed molecules at the interface, and this was supported by co-area data.

With the alcohols adsorbed on water we find a linear variation with chain length, this probably indicating that the orientation is the same in all cases. Assuming that the extrapolation is justified we can obtain values for the end-groups. In this way we obtain for the *OH* group the

data set out in Table IX. From the slopes of the curves one may obtain the ΔH^0 , ΔG^0 , and ΔS^0 per CH_2 group. The results so obtained are recorded in Table X.

TABLE IX

	$-\Delta H^0$ kcal./mole	$-\Delta G^0$ kcal./mole	$-\Delta S^0$ e.u./mole
Bulk \rightarrow surface	0.5	0	2
Vapor \rightarrow surface	10.2	5.3	17
Vapor \rightarrow bulk	9.7	5.3	15

TABLE X

	$-\Delta H^0$ kcal./mole	$-\Delta G^0$ kcal./mole	$-\Delta S^0$ e.u./mole
Bulk \rightarrow surface	0.5	0.6	-0.5
Vapor \rightarrow surface	2.1	0.5	5.8
Vapor \rightarrow bulk	1.5	-0.1	5.3

Of the results for the OH group we remark that the free energy change for bulk to surface is zero as might be expected. The heat and entropy changes for the same process are both small but not zero, although in view of the experimental error and the extrapolation involved the deviations may not be significant. The free energy change accompanying the processes vapor to surface and vapor to bulk is much greater for an OH group than for a CH_2 group. This reflects the greater interaction between an OH group and water (through hydrogen bonding) than between a CH_2 group and water.

Some recent work of Bartell, Thomas, and Fu (26) has for the first time provided data for the adsorption of butyl alcohol from aqueous solution onto graphite and blood char, from which may be calculated the standard entropy of adsorption. Using the same standard states as in the present paper the ΔG^0 , ΔH^0 , and ΔS^0 values at 25°C. are: for graphite, -2.43 kcal./mole, -0.82 kcal./mole, and 5.4 e.u./mole; and for blood char, -3.54 kcal./mole, -0.73 kcal./mole, and 9.4 e.u./mole. These values may be compared with the corresponding data for the air water interface; however a detailed discussion is best left until more data have been obtained.

(b) The Acid Series

An attempt has been made to analyze the data available for the corresponding series of aliphatic acids. Calculations of ΔG^0 were carried out by Ward and Tordai (20) using Eq. [7]; the results are recorded in Table XI.

The values of ΔH^0 bulk to surface are not available from experiment; those given in col. 2 of Table XI were calculated by Ward (25) from surface energy considerations (assuming that there was no contribution to ΔH^0 because of the polar part of the molecule; see however, below).

Reference to Fig. 7 will show that the plot of this ΔH^0 against chain length gives a line of the same slope as the experimental alcohol curve. However, extrapolation to zero chain length gives ΔH^0 for adsorption of a COOH group as -4.3 kcal., a value which seems very high particularly when compared with the value of -0.55 kcal. for an OH group. This

TABLE XI

Adsorption of Acids, Bulk to Surface at 25°C.

No. of C atoms	$-\Delta H^0$ calcd. by Ward kcal./mole	$-\Delta H^0$ calcd. as below kcal./mole	$-\Delta G^0$ calcd. using Eq. (7) kcal./mole	$-\Delta S^0$ using $-\Delta H^0$ from col. 2 e.u./mole	$-\Delta S^0$ using $-\Delta H^0$ from col. 3 e.u./mole
3	5.95	2.75	2.45	11.7	1.0
4	6.46	3.26	3.18	11.0	0.3
5	6.91	3.71	3.72	10.7	0.0
6	7.48	4.28	4.52	9.9	-0.8
7	8.10	4.90	5.40	9.1	-1.7
8	8.64	5.44	6.10	8.5	-2.2
9	9.31	6.11	7.06	7.6	-3.2

is also in conflict with Ward's original assumption. The ΔH^0 of adsorption of a COOH group has been estimated by the following procedure. It is reasonable to assume that for the process bulk to surface, the ratio ΔH^0 acid/ ΔH^0 alcohol will be the same as for the process vapor to bulk. Now it will be seen from results given later in this section that this ratio for the process vapor to bulk is close to 2. Hence the value for the ΔH^0 of adsorption of a COOH from bulk to surface is found to be approximately -1.1 kcal./mole. Using this value with the known dependence of ΔH^0 on chain length, the values given in col. 3 of Table XI have been obtained. In Table XI are given the values of ΔS^0 calculated using (a) the ΔH^0 values of Ward (col. 5), and (b) the ΔH^0 values calculated by the above procedure (col. 6).

In comparing the alcohols and acids it will be seen that the slopes of the ΔG^0 vs. chain length curves are almost the same (the acid curve deviates from the parallel slope only in the higher members, but even here the deviation is not great). Extrapolation to zero chain length gives the ΔG^0 of adsorption of a COOH group as -0.40 kcal. For the acids, the ΔS^0 values obtained by using the revised ΔH^0 values agree very closely with the ΔS^0 results for the corresponding alcohols, and the discussion given previously for the alcohols applies here and will not be repeated.

The free energy of transfer from vapor to bulk solution is known in three cases only (11). However, since these values lie on a line which is parallel to the corresponding alcohol curve, it appears safe to obtain free energy data for the other acids by extrapolation. The values plotted in Fig. 6 were corrected to the new standard states.

The heat content data are far more incomplete. One may obtain the ΔH^0 of transfer from vapor to bulk solution by combining the latent heat of vaporization with the heat of solution. This has been done for the cases where satisfactory data are available, and the results are given in Table XII.

TABLE XII

No. of C atoms	Latent heat of vaporization ^a kcal./mole	Heat of solution at infinite dilution kcal./mole	$-\Delta H^0$ vapor to bulk kcal./mole
3	12.5	1.1 ^c	11.4
4	18.6	(0.68) ^d	17.9
5	25.8	0.91 ^b	24.9

^a Calculated from vapor pressure data from *International Critical Tables*, Vol. 3, p. 215.

^b Calculated from solubility data of Ralston and Hoerr (27).

^c *International Critical Tables*, Vol. 5, p. 148.

^d The value is given for isovaleric acid (*I.C.T.*) in the absence of a value for *n*-valeric acid.

Despite the inaccuracy of these data it is evident that the slope of the line obtained by plotting ΔH^0 against chain length is very much different from the case of the alcohols (cf. Fig. 7). The most likely reason is that, unlike the alcohols, the acids are appreciably associated (dimerized) in the vapor phase. This means that latent heat data calculated from saturated vapor pressures gives a ΔH^0 characteristic of that mixture of monomer and dimer which is in equilibrium under the given conditions. Since the ΔH^0 of the change dimer \rightarrow monomer is large (7–8 kcal./mole of monomer) this will make a large error in the previous calculations, for the mole fraction of monomer will increase as the vapor pressure decreases, that is as we go up the acid series, temperature remaining constant.

The equilibrium constant Kp defined as $Kp = (p_{\text{monomer}})^2/p_{\text{dimer}}$ has been obtained by MacDougall (28,29) for acetic and propionic acids at varying temperatures. Given in Table XIII are the values calculated for the latent heat of vaporization (to give the monomer in the vapor phase).

Inspection of col. 4 of Table XIII will show that the apparent latent heat of vaporization (L.H.V.) of propionic acid is abnormally high. It is apparent that not much *quantitative* reliance can be placed upon the L.H.V. values in the last column. In view of the difference between the Kp for acetic acid and propionic acid, it is an uncertain procedure to use the Kp for propionic acid for the higher acids. The corrected latent heat of vaporization of acetic acid appears somewhat too large. The heats of solution at infinite dilution in all cases are comparatively small and are given in Table XIII together with the calculated ΔH^0 's of hydration. Nevertheless, we can at least say that *making the above correction brings*

the ΔH^0 values for the acids into qualitative agreement with the alcohols (i.e., not as strongly dependent on chain length as indicated in Table XII).

An outstanding feature of the above results is that the order of magnitude of the ΔH^0 vapor to bulk for the acids is much greater than for

TABLE XIII
Temperature 25°C.

Acid	Remarks (for col. 5)	Heat of soln. at infinite dilution	L.H.V. ^a from satd. vap. press.	L.H.V. ^a for monomer	$-\Delta H^0$ vap. to bulk soln.
		kcal./mole	kcal./mole	kcal./mole	kcal./mole
Acetic	Calcd. using Kp for acetic	0.24 ^b	10.1	27.2	27.0
Propionic	Calcd. using Kp for propionic	0.62 ^b	21.2	22.7	22.1
Butyric	Calcd. using Kp for propionic	1.1 ^b	12.5	24.8	23.7
Valeric	Calcd. using Kp for propionic	(0.68) ^c	18.6	34.6	33.9

^a L.H.V. = latent heat of vaporization.

^b *International Critical Tables*, Vol. 5, p. 148.

^c See Table XII.

the alcohols, and this must be due to the greater heat of hydration of the carboxyl group. The corresponding entropy change will thus also be considerably greater.

ACKNOWLEDGMENTS

We wish to thank Dr. K. Sutherland, Mr. J. Barker, and Professor E. A. Guggenheim for helpful discussions, and the D.S.I.R. for a maintenance grant to one of us (A. M. Posner).

SUMMARY

Surface tension and surface potential measurements have been made as functions of concentration and temperature for a homologous series of normal aliphatic alcohols. The results are fitted to a two-dimensional equation of state and the surface tension measurements are checked for consistency with the corresponding surface potential results. From the temperature dependence of the surface tension the quantities ΔH^0 , ΔS^0 , and ΔG^0 for the adsorption process are calculated. These results are correlated with corresponding solution thermodynamics. The molecular configuration in the surface has been tentatively deduced. The surface phase more closely resembles the bulk solution than the vapor. The negative entropy of adsorption from the vapor is very large and it is suggested that the additional factors responsible for the high values are changes in internal degrees of freedom of the hydrocarbon portion of the molecule, and "cluster" formation in the water in the immediate neighborhood of the solute molecule.

REFERENCES

1. ADAM, N. K., *Physics and Chemistry of Surfaces*, 3rd Ed., p. 121. Oxford Univ. Press, London, 1941.
2. ADDISON, C. C., *J. Chem. Soc.* **1945**, 98.
3. ADDISON, C. C., AND HUTCHINSON, S. K., *J. Chem. Soc.* **1949**, 3387, 3395.
4. ADAM, N. K., *loc. cit.*, p. 118.
5. ALEXANDER, A. E., *Trans. Faraday Soc.* **38**, 54 (1942).
6. POSNER, A. M., AND ALEXANDER, A. E., *Trans. Faraday Soc.* **45**, 651 (1949), and unpublished results.
7. SUGDEN, S., *J. Chem. Soc.* **1922**, 858.
8. ADAM, N. K., *loc. cit.*, p. 379.
9. COMPTON, K. G., AND HARING, H. E., *Trans. Electrochem. Soc.* **62**, 345 (1932).
10. HUTCHINSON, E., *J. Colloid Sci.* **3**, 418 (1948).
11. BUTLER, J. A. V., *Chemical Thermodynamics*, p. 385. Macmillan, New York, 1946.
12. ADAM, N. K., *loc. cit.*, p. 42.
13. ALEXANDER, A. E., AND POSNER, A. M., *Nature* **166**, 1932 (1950).
14. ADAM, N. K., *loc. cit.*, p. 136.
15. PHILLIPS, J. N., private communication.
16. KEMBALL, C., in *Advances in Catalysis*, Vol. II, Chap. 7. Academic Press Inc., New York, 1950.
17. KEMBALL, C., AND RIDEAL, E. K., *Proc. Roy. Soc. (London)* **A187**, 53 (1946).
18. KEMBALL, C., *Proc. Roy. Soc. (London)* **A187**, 73 (1946).
19. KEMBALL, C., *Proc. Roy. Soc. (London)* **A190**, 117 (1947).
20. WARD, A. F. H., AND TORDAI, L., *Trans. Faraday Soc.* **42**, 408 (1946).
21. FRANK, H. S., AND EVANS, M. W., *J. Chem. Phys.* **13**, 507 (1945).
22. BOHON, R. L., AND CLAUSSEN, W. F., *J. Am. Chem. Soc.* **73**, 1571 (1951).
23. MELAVEN, R. M., AND MACK, E., *J. Am. Chem. Soc.* **54**, 888 (1932).
24. LASKOWSKI, L., AND BURK, R. E., *J. Chem. Phys.* **7**, 465 (1939).
25. WARD, A. F. H., *Trans. Faraday Soc.* **42**, 399 (1946).
26. BARTELL, F. E., THOMAS, T. L., AND FU, Y., *J. Phys. & Colloid Chem.* **55**, 1456 (1951).
27. RALSTON, A. W., AND HOERR, C. W., *J. Org. Chem.* **7**, 546 (1942).
28. MACDOUGALL, F. H., *J. Am. Chem. Soc.* **58**, 2585 (1936).
29. MACDOUGALL, F. H., *J. Am. Chem. Soc.* **63**, 3420 (1941).

Book Reviews

Chemistry of Carbon Compounds. Vol. I, part A. Edited by E. H. Rodd. The Elsevier Press, Houston, Texas, 1951. xxi + 777 pp. Price \$20.75.

This volume is part of a major work presented as a successor to Richter's *Organic Chemistry* and consisting of five volumes in six or seven parts. Volume IA appeared in November, 1951, Volume IB is just out, and the rest of the series is promised at intervals of about ten months.

Richter's classification of organic compounds (to which the reader is referred for the arrangement of the material in this and subsequent volumes) has been maintained throughout, although the whole work has been rewritten. This is particularly true of the "General Introduction" (pp. 2-217) which, after brief chapters on "Nomenclature and Documentation" (E. H. Rodd), contains discussions on "Micro- and Semi-micro Methods" (R. Belcher), the "Physical Properties of Carbon Compounds" (H. D. Springall), "Crystallography" (A. F. Wells), "Absorption of Light by Carbon Compounds" (E. A. Braude), "Acids and Bases" (H. D. Springall), "Mechanism of Reactions" (E. D. Hughes; aromatic substitution is reserved for Vol. III), "Stereochemistry" (an excellent treatment along classical lines by E. E. Turner, in which some recent concepts such as those related to "conformation" and to stereospecific reactions are very briefly mentioned though not elaborated to any extent), and "Free Radicals and Homolytic Reactions" (D. H. Hey and W. A. Waters). As can be seen in the above selection, the list of 23 contributors to Vol. IA includes outstanding names in various fields. The Editor has been advised by a group of eminent British chemists under the chairmanship of Sir Robert Robinson.

The purely descriptive material is a model of compactness and of thorough coverage. Among the uniformly excellent chapters on aliphatic compounds to which the volume is devoted, mention should be made of an up-to-date section on alkanes (A. W. Johnson) and of a comprehensive discussion of organometallic compounds (J. Chatt). Abundant cross references lend unity to the whole, and a suitable subject index is provided. It is planned to provide a General Index in Vol. V. The inclusion of physical properties of an abundant number of representatives of each class of compounds enhances the value of the book as a reference work. The stated goal of serving as a bridge between the Beilstein-type compilation or the Grignard-type encyclopedia and the more modest textbooks seems to have been approached closely in this volume.

The material appears in general to be up to date judging by the documentation which includes references through 1951. A few slight incongruities were noted (for example, obsolete diagrams dealing with melting point determinations, p. 42). In a few cases (for example, in the brief discussion of the Beckmann transformation, pp. 386, 524, and of the addition and condensation reactions of carbonyl compounds, pp. 187, 470), the treatment is sketchy to the point of oversimplification, and the selection of key references points with emphasis to early work. This is perhaps inherent to the stated scope of the work and it seems difficult to conceive of a more skillful utilization of the 777 pages of the present volume.

While a final judgment on this difficult enterprise must obviously await completion of the series, it seems apparent that the literature of organic chemistry has been greatly enriched by the appearance of this valuable and handsomely printed and bound volume.

FAUSTO RAMIREZ, New York, New York.

The Chemistry of Wood. By ERIC HÄGGLUND, Swedish Forest Products Laboratory, Stockholm. Academic Press Inc., New York, 1951. x + 631 pp. Price \$13.50.

This book is a revised and enlarged English version of *Holzchemie*, which was published in German in 1928, a second German edition appearing in 1939.

In the beginning of the book the author defines wood and describes in some detail the general structure, the characteristics of the various wood elements, and the growth of wood. Excellent diagrams accompany the discussion, though the photomicrographs are, in general, disappointing. Compression wood and tension wood, not mentioned in the previous German edition, are treated very briefly at the close of the chapter. Following this is a discussion of the physical properties of wood covering a very limited part of this field. Only information on the specific gravity and moisture content and the relationship between these factors is included.

The third chapter, entitled "The Wood Components and Their Physical Properties," constitutes well over half the book with the references divided into two very long lists. From the standpoint of locating various subjects and particularly in checking references, division into short chapters might have been preferable. The part devoted to cellulose is well coordinated. It is not, however, nearly as extensive as the portion devoted to lignin, in spite of the fact that the latter material constitutes a smaller percentage of the wood and is industrially relatively unimportant. The lignin part is, perhaps, the outstanding portion of the text. It contains much of the more recent important discoveries in this field, including work in the author's laboratory which was not yet published when the book was in preparation. Frequent cross references aid in the evaluation of points under discussion.

The section on wood polyoses points out the advantages of using the terms "wood polyoses" and "polyuronic acids" to avoid confusion arising from the use of the older term "hemicellulose." The information on the individual wood polyoses and their occurrence in different woods is probably the most comprehensive review published so far. An up-to-date section on minor wood components, a section on analyses of wood, and one on the structure of the cell wall complete the chapter.

The remainder of the book is devoted largely to the chemistry of pulping and other technological processes in which wood serves as the principal raw material. The author's widely known theory of sulfite pulping, as well as his newer hypothesis on sulfate pulping, is well presented. European practice influences the discussion on all phases of pulping, so that emphasis and statements are sometimes at variance with practice in this country.

While it is no longer possible to completely encompass the entire field of wood chemistry in a single volume, the author has managed to compress a large amount of useful information into his book. For the student and the reader who wish to obtain a bird's-eye view of the many facets of the subject, the book is excellent. The specialist will find the more extensive parts on cellulose, wood polyoses, pulping, and especially on lignin very usable for quick reference.

The translation of the German avoids awkward phraseology and the typography is excellent.

JOHN C. PEW, Madison, Wisconsin

Phase Transformations in Solids. Edited by R. SMOLUCHOWSKI, J. E. MAYER, and W. A. WEYL. A Symposium held at Cornell University, August 23-26, 1948; sponsored by the Committee on Solids, Division of Physical Sciences, National Research Council. J. Wiley and Sons, Inc., New York, 1951. 660 pp. Price \$9.50.

This book consists of a collection of seventeen papers on various topics related to phase transformations in solids which were presented at a 1948 symposium sponsored by the National Research Council. The first six papers are fairly general in character; they are followed by eleven papers of a more specialized nature.

The first paper of the symposium, by Laszlo Tisza, presents a general thermodynamic theory of phase transitions. He extends the treatment of Gibbs to include second-order transitions for which energy and volume change continuously, in contrast to the discontinuous changes associated with the usual first-order transitions. This paper is followed by one by J. E. Mayer which presents a general method of treating phase transitions of crystals which contain imperfections in thermodynamic equilibrium. Then J. G. Kirkwood presents a new statistical-mechanical treatment of crystallization as a cooperative phenomenon.

The fourth paper of the volume is a review and critical analysis of the theory of diffusion in solids, with particular reference to the atomic mechanisms, by F. Seitz. This paper is somewhat out of date, as Seitz and others have made important contributions to this topic since the symposium, but it remains a valuable summary. The Volmer-Becker theory of nucleation is summarized by R. Smoluchowski, and discussed in relation to the problem of nucleation in solids. In the final general paper, M. J. Buerger presents a comprehensive classification and discussion of the crystallographic aspects of transformations.

The general papers are followed by six that deal with transitions in nonmetals. These include "The Solid-Liquid Transition in Argon," by O. K. Rice; a discussion of transitions in silver halides, by Huggins; and papers on transformations in silicate systems and glasses, by Kracek, Schairer, and Weyl. In the final paper of this group, Matthias briefly reviews our knowledge of phase transitions in ferroelectrics.

The final group of five papers is concerned with transitions in metals. The most comprehensive of these is a lengthy (160-page) review of precipitation from solid solutions by A. H. Geisler. Transitions in pure metals, order-disorder transitions, and martensite transformations are reviewed by C. S. Barrett, S. Siegel, and M. Cohen, respectively. The kinetics of eutectoid decomposition are covered by Mehl and Dubé.

It is unfortunate that it was not possible to publish this book immediately after the 1948 symposium, as some of the papers now seem out of date. Some of the authors did, however, take advantage of the delay in publication to revise their papers in the light of more recent work. But in spite of this objection, the book is a very valuable summary of our state of knowledge in this field.

T. A. READ, New York, New York

Physical Chemistry of the Hydrocarbons. Edited by A. FARKAS. Academic Press Inc., New York, 1950. x + 453 pp. Price \$9.50.

There has been a trend in book publishing in this country toward increasing numbers of comprehensive treatises produced as the cooperative effort of several specialists in different branches of a field. Books of this type are welcome as reference works because they collect much widely scattered information. The present book is an excellent example of a compilation of this type.

A good idea of the scope and authority of the material may be obtained from the Table of Contents, which is as follows:

1. "The Chemical Bond in Hydrocarbon Molecules" by G. W. Wheland
2. "The Molecular Structure of Hydrocarbons as Determined by Spectroscopy and Electron and X-Ray Diffraction" by M. H. Jellinek
3. "Mass Spectroscopy in Hydrocarbon Analysis" by J. J. Mitchell
4. "Optical Properties of Hydrocarbons: Infrared Absorption, Raman, and Ultra-violet Absorption Spectroscopy" by Norman D. Coggeshall
5. "Optical Methods of Hydrocarbon Analysis" by Norman D. Coggeshall
6. "Electrical Properties of Hydrocarbons" by Andrew Gemant
7. "Solvent Extraction of Hydrocarbons" by Alfred W. Francis

8. "Solid-Liquid Equilibria of Hydrocarbons" by M. R. Cines
9. "Chemical Thermodynamic Equilibria among Hydrocarbons" by Frederick D. Rossini

A particularly pleasing feature of the book, which does credit to its editor, is the uniformity of style and the lack of overlap of the contributions of the authors. The book, in fact, almost reads as though it were the work of a single writer.

Though the book is not large, it contains more detail than is useful for a textbook. It could, however, serve as auxiliary reading for a course in petroleum chemistry. Its real value, this reviewer believes, will be in petroleum laboratories as a general purpose reference book; as such, it will probably be a classic for a long time.

JOHN R. BOWMAN, Pittsburgh, Pennsylvania

Inorganic Chemistry. An Advanced Textbook. By THERALD MOELLER. John Wiley and Sons, Inc., New York, 1952. 966 pp. Price \$10.00.

Fashions in chemistry change periodically. At the beginning of modern chemistry, inorganic materials received the primary attention. Then classical physical chemistry dominated the scene, followed after World War I by the pre-eminence of organic chemistry. Today the pendulum is swinging back toward inorganic chemistry with emphasis upon its physicochemical aspects rather than upon a purely descriptive treatment.

The present work is offered as a textbook "to survey the field from this modern point of view and to acquaint students with existing problems and current investigations."

Part I outlines the necessary principles with considerable factual material for purposes of illustration. Part II treats the elements and their compounds by families in a somewhat unconventional but nevertheless logical and teachable manner in the light of these principles.

Part I opens with an extensive discussion of atomic nuclei, their instabilities and related problems; electronic configurations; periodic classifications, importance of radii, ionization potentials, and hydrogen and covalent bonds. Problems of geometry and stereoisomerism come next, followed by oxidation potentials and acid-base concepts.

An elaborate author and subject index contributes to the value of both parts. The book is a welcome addition to our knowledge and will be of value to workers in Colloid Science as a convenient source book of reference.

VICTOR K. LA MER, New York, New York

The Chemistry of Lignin. By F. E. BRAUNS. Academic Press Inc., New York, 1952. xv + 808 pp. Price \$14.50.

This first book written in English devoted exclusively to lignin chemistry should be warmly welcomed by wood, lignin, and paper chemists.

In the first chapter, the author calls attention to the little-recognized importance of lignin, the fact that the essential structure of the substance is still unknown, and the confusion which exists in lignin terminology. A system is suggested "to try to bring order into lignin nomenclature" and is used with effectiveness throughout the book.

This introduction is followed by a review of over 2200 literature references on the distribution, isolation, determination, physical properties, and chemical properties of lignin, as well as theoretical concepts regarding this substance. The summaries are brief, but concise, and appear invariably to include the source and kind of lignin when such information is available in the original article. The author frequently compares the results with the findings of others and offers critical comment. In many cases, the data are assembled into tables to aid in comparison. The material as a whole is exceedingly well classified and adequately indexed. An outstanding feature of the book is the facility with which various subjects may be located from a detailed table of contents covering nine pages.

The book covers the period from 1811 through 1949. Inclusion of some of the older experimental work, particularly theories regarding lignin, may be questioned in the light of present-day concepts. While this should be no disadvantage to the lignin chemist, the uninitiated may place undue reliance on some of the more fanciful ideas of the past. It is to be regretted that important developments since 1949 are not included, but this is understandable in a work of this magnitude.

The author is to be congratulated on an excellent piece of work.

JOHN C. PEW, Madison, Wisconsin

AUTHOR INDEX

A

- ADAMS, MABELL E. See Karon, 407
 ALEXANDER, A. E. See Posner, 623
 See Powell 482, 493
 ANDERSON, J. R. See Posner, 623
 ASBECK, W. K., LAIDERMAN, D. D., AND
 VAN LOO, M. A high shear method of
 rating brushability of paints, 306

B

- BARON, THOMAS. See Whitfield, 268
 BARTELL, F. E., AND BOWER, JOHN E.
 Adsorption of vapors by silica gels of
 different structures, 80
 BASU, SADHAN, AND DAS GUPTA, PARES
 CH. Studies on polyelectrolytes. I.
 Sodium carboxymethylcellulose, 53
 BEYER, C. E., AND TOWSLEY, F. E. The
 flow of polystyrene through rectangular
 channels, 236
 BIRDSALL, D. H. See Hotten, 284
 BLACK, S. A. See Mooney, 204
 BOSE, S. See Chatterjee, 414
 BOWER, JOHN E. See Bartell, 80
 BRIDGMAN, P. W. Acceptance of Bingham
 medal, 202

C

- CAPPS, WEBSTER. Viscosity of glass, 334
 CHATTERJEE, B., AND BOSE, S. The electro-
 chemical properties of humid acid, 414
 CONRAD, CARL M., AND ZIIFLE, HILDA M.
 Implications of Philippoff flow curves
 for the determination of intrinsic vis-
 cosity of high polymer nitrocellu-
 loses, 227
 COPLEY, ALFRED L. The rheology of blood.
 A survey, 323

D

- DAHLQUIST, C. A., AND HATFIELD, M. R.
 Constant stress elongation of soft poly-
 mers: time and temperature studies, 253

- DAOUST, HUBERT, AND RINFRET, MARCEL.
 Solubility of polymethyl methacrylate
 and polyvinyl acetate, 11
 DAS GUPTA, PARES CH. See Basu, 53
 DESAI, R. L. See Prasad, 178
 DINEGAR, ROBERT H., AND SMELLIE,
 ROBERT H. Stability of monodispersed
 sulfur hydrosols, 370

E

- ELTON, G. A. H. The surface tension of
 solids, 450
 EVANS, WARREN W. See Johnson, 498

F

- FARNEY, LEONARD. See Haas, 584
 FARRAR, J., AND NEALE, S. M. The distri-
 bution of ions between cellulose and
 solutions of electrolyte, 186
 FERRY, JOHN D., AND WILLIAMS, MAL-
 COLM L. Second approximation methods
 for determining the relaxation time
 spectrum of a viscoelastic material, 347
 See Johnson, 498
 FOX, H. W., AND ZISMAN, W. A. The
 spreading of liquids on low-energy sur-
 faces. II. Modified tetrafluorethylene
 polymers, 109
 AND ZISMAN, W. A. The spreading of
 liquids of low-energy surfaces. III. Hy-
 drocarbon surfaces, 428

G

- GREGOR, HARRY P. see Sollner, 37
 SUNDHEIM, BENSON R., HELD, KALMAN
 M., AND WAXMAN, MONROE H. Studies
 on ion-exchange resins. V. Water
 vapor sorption, 511

H

- HAAS, HOWARD C., FARNEY, LEONARD,
 VALLE, CLAUDE, JR. Some properties of
 ethyl cellulose films, 584

- HATFIELD, M. R. See Dahlquist, 253
- HELD, KALMAN M. See Gregor, 511
- HENNIKER, JOHN C. Retardation of flow in narrow capillaries, 443
- HERMANIE, P. H. J. See van der Minne, 600
- HILDEBRAND, JOEL H. The "critical point," 551
- HILL, TERRELL L. Comments on the preceding note by W. B. Innes, 449
- HOLZMAN, G. R., AND MOORE, K. H. An electron diffraction study of the re-orientation of certain alkali halides deposited on mica and on mica surfaces covered by organic films, 396
- HOTTEN, B. W., AND BIRDSALL, D. H. Fine structure and rheological properties of lithium soap-oil dispersions, 284
- HULL, HARRY H. The band viscometer, 316
- HUTCHINSON, E., AND RANDALL, D. An application of the Gibbs' adsorption theory to films at oil-water interfaces, 151
- I
- INNES, W. B. The treatment of complex absorbates as a single phase, 447
- J
- JOHNSON, MYRLE F., EVANS, WARREN W., JORDON, IVO, AND FERRY, JOHN D. Viscosities of concentrated polymer solutions. II. Polyisobutylene, 498
- JONES, S. P., AND TYSON, J. K. The rheology of a lubricating oil at temperatures below the pour point, 272
- JORDAN, IVO. See Johnson, 498
- K
- KANEKAR, C. R. See Prasad, 178
- KAPLAN, J. GORDIN. The activity of catalase unfolded at the air-water interface, 382
- KARON, MELVIN L., ADAMS, MABELLE E., AND NEWMAN, SEYMOUR. The effect of temperature on the electrophoretic analysis of cottonseed meal extracts, 407
- KAUFMAN, SAMUEL, AND SINGLETERRY, CURTIS R. The critical range for micelle formation by an oil-dispersible soap in a hydrocarbon solvent, 453
- KUHNS, PERRY W. See Weltmann, 218
- L
- LAIDERMAN, D. D. See Asbeck, 306
- M
- MACKOR, E. L., AND VAN DER WAALS, J. H. The statistics of the adsorption of rod-shaped molecules in connection with the stability of certain colloidal dispersions, 535
- MANLEY, R. ST. J., AND MASON, S. G. Particle motions in sheared suspensions. II. Collisions of uniform spheres, 354
- MARECHAL, J. See Prigogine, 122
- MARKWOOD, W. H., JR., AND SPURLIN, H. M. Residual stresses and strains in molded plastics, 244
- MARON, SAMUEL H., AND MOORE, CARL. Morphologic changes in gelled synthetic latices, 94
- MASON, S. G. See Manley, 354
- McLOUGHLIN, J. R., AND TOBOLSKY, A. V. The viscoelastic behavior of polymethyl methacrylate, 555
- MOMMAERTS, W. F. H. M. The measurement of lightscattering intensities according to Brice, 71
- MOONEY, M., AND BLACK, S. A. A generalized fluidity power law and laws of extrusion, 204
- MOORE, CARL. See Maron, 94
- MOORE, K. H. See Holzman, 396
- N
- NEALE, S. M. See Farrar, 186
- NEUBAUER, RAYMOND, L. See Vonnegut, 616
- NEWMAN, SEYMOUR. See Karon, 407
- NUTTING, G. C. Effects of electrolytes on the viscosity of potato starch pastes, 128
- O
- OVERBEEK, J. TH. G., AND SPARNAAY, M. J. Experiments of long-range attractive forces between macroscopic objects, 343
- P
- POSNER, A. M., ANDERSON, J. R., AND ALEXANDER, A. E. The surface tension and surface potential of aqueous solutions of normal aliphatic alcohols, 623

- POWELL, B. D., AND ALEXANDER, A. E.
 Studies of surface potentials. I. Effect
 of salts and the nature of the interface
 upon the surface potentials of insoluble
 monolayers, 482
 II. Effect of salts and the nature of the
 interface upon the surface potentials of
 soluble monolayers, 493
- PRASAD, MATA, AND SWAMINATHAN, V.
 Study of the extinction coefficients of
 gels during mutual gelation, 20
 AND SWAMINATHAN, V. Studies in
 mutual gelation, 25
 SUBRAMANIAN, K. E., DESAI, R. L.,
 AND KANEKAR, C. R. Light scattering by
 some thixotropic gels, 178
- PRIGOGINE, I., AND MARECHAL, J. The
 influence of differences in molecular size
 on the surface tension of solutions.
 IV, 122
- R
- RANDALL, D. See Hutchinson, 151
 RINFRET, MARCEL. See Daoust, 11
- S
- SCHULMAN, FRED, AND ZISMAN, W. A. The
 spreading of liquids on low-energy sur-
 faces. V. Perfluorodecanoic acid mono-
 layers, 465
- SHAFRIN, ELAINE G., AND ZISMAN, WIL-
 LIAM A. The spreading of liquids on
 low-energy surfaces. IV. Monolayer
 coatings on platinum, 166
- SINGLETERRY, CURTIS R. See Kauf-
 man, 453
- SLATER, J. C. Presentation of Bingham
 medal to P. W. Bridgman, 199
- SMELLIE, ROBERT H. See Dinegar, 370
- SOLLNER, KARL, AND GREGOR, HARRY P.
 The electrochemistry of permselective
 protamine collodion membranes. III.
 The electrical resistance of several types
 of permselective protamine collodion
 membranes in solutions of various elec-
 trolytes, 37
- SPARNAAY, M. M. See Overbeek, 343
- SPURLIN, H. M. See Markwood, 244
- SUBRAMANIAN, K. E. See Prasad, 178
- SUNDHEIM, BENSON R. See Gregor, 511
- SURIANI, LOUIS R. See Voet, 1
 SWAMINATHAN, V. See Prasad, 20, 25
- T
- TOBOLSKY, A. V. See McLoughlin, 555
 TOWSLEY, F. E. See Beyer, 236
 TYSON, J. K. See Jones, 272
- V
- VALLE, CLAUDE, JR. See Haas, 584
 VAN DER MINNE, J. L., AND HERMANIE,
 P. H. J. Electrophoresis measurements
 in benzene-correlation with stability.
 I. Development of method, 600
- VAN DER WAALS, J. H. See Mackor, 535
 VAN DER WAARDEN, M. The process of
 spontaneous emulsification, 140
 VAN LOO, M. See Asbeck, 306
- VOET, ANDRIES, AND SURIANI, LOUIS R.
 Dielectric characteristics of pigment dis-
 persions, 1
- VOLD, MARJORIE J. Molecular cross sec-
 tions in films of fatty acids on water, 196
- VONNEGUT, BERNARD, AND NEUBAUER,
 RAYMOND, L. Production of mono-
 disperse liquid particles by electrical
 atomization, 616
- W
- WAXMAN, MONROE H. See Gregor, 511
 WELTMANN, RUTH N., AND KUHN, PERRY
 W. Effect of shear temperature on vis-
 cosity in a rotational viscometer meas-
 urement, 218
- WEST, W. J. Size determinations of clay
 particles in water suspensions by use of
 low-angle x-ray diffraction, 295
- WHITFIELD, H. B., AND BARON, THOMAS.
 Application of Eyring's rate equation
 to viscometric data on paraplex, 268
- WILLIAMS, MALCOLM L. See Ferry, 347
- Z
- ZIFFLE, HILDA M. See Conrad, 227
 ZISMAN, W. A. See Fox, 109
 See Shafrin, 166
 See Fox, 428
 See Schulman, 465

SUBJECT INDEX

A

- Adsorbates, treatment of complex—as a single phase, INNES, 447; HILL, 449
 Adsorption (see also *Films, Silica gel*); —and colloidal dispersions, MACKOR AND VAN DER WAALS, 535
 Alcohols, surface tension and surface potential at aqueous solutions of normal aliphatic —, POSNER *et al.*, 623
 Alkali halides (iodides), electron diffraction of the reorientation of — — deposited on mica (covered by organic films), HOLZMAN AND MOORE, 396
 Antonoff rule, see *Surface*
 Atomization, see *Electrical*
 Attractive forces, between macroscopic objects, OVERBEEK AND SPARNAAY, 343

B

- Bingham medal, presentation to P. W. Bridgman, SLATER, 199; acceptance, BRIDGMAN, 202
 Blood, rheology of —, a survey, CO-PLEY, 323
 Brushability, see *Paints*

C

- Capillaries, retardation of flow of Newtonian liquids in narrow —, HENNIKER, 443
 Catalase, activity of — unfolded at the air-water interface, KAPLAN, 382
 Cellulose (see also *Ethyl cellulose; Polyelectrolytes*); distribution of ions between — and solutions of electrolyte, FARRAR AND NEALE, 186
 Channels, see *Polystyrene*
 Clay, size determinations of — particles in water suspensions by x-ray diffraction, WEST, 295
 Coatings, see *Polymers*
 Collision, see *Particle*
 Collodion, see *Membranes*

Colloid, see *Sulfur*

- Colloidal dispersions, stability, MACKOR AND VAN DER WAALS, 535
 Cottonseed, effect of temperature on the electrophoretic analysis of — meal extracts, KARON *et al.*, 407
 Critical point, HILDEBRAND, 551

D

- Dielectric, see *Dispersions*
 Diffraction, see *Alkali halides*
 Dispersions (see also *Adsorption, Colloidal, Electrical, Lithium, Micelle, Sulfur*); dielectric characteristics of pigment —, VOET AND SURIANI, 1

E

- Electrical atomization, production of monodisperse liquid particles by — —, VONNEGUT AND NEUBAUER, 616
 Electrochemistry, see *Humic, Membranes*
 Electrolyte, see *Cellulose*
 Electrophoresis, electrophoretic analysis of cottonseed meal extracts, KARON *et al.*, 407; — studies, VAN DER MINNE AND HERMANIE, 600
 Emulsification, spontaneous, VAN DER WAARDEN, 140
 Ethyl cellulose, properties of — — films, HAAS *et al.*, 584
 Extinction, see *Gels*
 Extrusion, see *Fluidity*

F

- Fatty acids, molecular cross sections in films of — — in water, VOLD, 196
 Films, application of the Gibbs' adsorption theory to — at oil-water interfaces, HUTCHINSON AND RANDALL, 151
 Flow, — in capillaries, HENNIKER, 443
 Fluidity, — power law and law of extrusion, MOONEY AND BLACK, 204

G

- Gels (see also *Light, Silica*); extinction coefficients, PRASAD AND SWAMINATHAN, 20; mutual gelation, PRASAD AND SWAMINATHAN, 25; morphologic changes in gelled synthetic latices, MARON AND MOORE, 94
Glass, viscosity, CAPPS, 334

H

- Humic acid, electrochemical properties, CHATTERJEE AND BOSE, 414
Hydrocarbons (see also *Micelle*); spreading of liquids on low-energy surfaces, surfaces (and surface tensions) of —, FOX AND ZISMAN, 428
Hydrosols, see *Sulfur*

I

- Interfaces, oil-water —, see *Films*
International Congress, XIIIth of Pure and Applied Chemistry, 554
Iodides, see *Alkali halides*
Ions, see *Cellulose*

L

- Latex, see *Gel*
Light (see also *Clay*); — scattering measurement, MOMMAERTS, 71; — scattering by thixotropic gels, PRASAD *et al.*, 178
Liquids, see *Capillaries, Hydrocarbons, Spreading*
Lithium soap, — — — oil dispersions, HOTTEN AND BIRDSALL, 284
Lubricating oil, rheology of — — at temperatures below the pour point, JONES AND TYSON, 272

M

- Membranes, electrochemistry of permselective protamine collodion —, SOLLNER AND GREGOR, 37
Methacrylate, see *Polymethyl . . .*
Mica, see *Alkali halides*
Micelle, — formation by an oil-dispersible soap in a hydrocarbon solvent, KAUFMAN AND SINGLE-TERRY, 453
Monolayer, see *Polymers, Spreading, Surface*
Motion, see *Particle*

N

- Nitrocellulose, see *Viscosity*

O

- Oil, see *Films, Lithium*

P

- Paints, high shear method of rating brushability of— (viscometer), ASBECK *et al.*, 306
Paraplex, see *Viscosity*
Particle (see also *Clay, Electrical*); — motions in sheared suspensions, collisions of uniform spheres, MANLEY AND MASON, 354
Perfluorodecanoic acid, see *Spreading*
Permselective, see *Membranes*
Phases (see also *Adsorbates*); critical point, HILDEBRAND, 551
Philippoff flow curves, see *Viscosity*
Pigment, see *Dispersions*
Plastic(s), stresses and strains in molded —, MARKWOOD AND SPURLIN, 244
Plasticization, see *Polymers*
Platinum, see *Polymers*
Polyelectrolytes, sodium carboxymethylcellulose, BASU AND DASGUPTA, 53
Polyisobutylene (see also *Polymers*); viscosities, JOHNSON *et al.*, 498
Polymers (see also *Spreading*); solubility of polymethyl methacrylate and polyvinyl acetate, DAoust AND RINFRET, 11; spreading of liquids on low-energy surfaces, modified tetrafluoroethylene —, FOX AND ZISMAN, 109; monolayer coatings on platinum, SHAFRIN AND ZISMAN, 166; stress elongation of soft —, time and temperature studies, (polyisobutylene and rubber), DAHLQUIST AND HATFIELD, 253; self-plasticization, UEBERREITER AND KANIG, 569
Polymethyl methacrylate (see also *Polymers*); viscoelasticity, McLoughlin AND TOBOLSKY, 555
Polystyrene, flow of—through rectangular channels, BEYER AND TOWSLEY, 236
Potato, see *Starch*
Protamine, see *Membranes*

R

- Relaxation, second-approximation methods for determining the—time spectrum of a viscoelastic material, FERRY AND WILLIAMS, 347
 Resins, ion-exchange —, water vapor sorption, GREGOR *et al.*, 511
 Rubber, see *Polymers*

S

- Shear, see *Paints, Particle, Viscosity*
 Silica gel, vapor adsorption by — —, BARTELL AND BOWER 80
 Society of Rheology, annual meeting, Oct., 1951, 199
 Soap, see *Lithium, Micelle*
 Solids, see *Surface*
 Solubility, see *Polymers*
 Solutions, see *Alcohols, Surface*
 Sorption, see *Resins*
 Spectrum, see *Relaxation*
 Spreading (see also *Hydrocarbons, Polymers*); — of liquids on low-energy surfaces, FOX AND ZISMAN, 109, 428; SHAFRIN AND ZISMAN, 166; perfluorodecanoic acid monolayers, SCHULMAN AND ZISMAN, 465
 Starch, viscosity of potato — pastes, NUTTING, 128
 Strain, see *Plastics*
 Stress, see *Plastics, Polymers*
 Sulfur, stability of monodispersed — hydrosols, DINEGAR AND SMELLIE, 370
 Surface (see also *Alcohols, Catalase, Films, Hydrocarbons, Polymers, Spreading*); — tension of solutions, PRIGOGINE AND

- MARECHAL, 122; — tension of solids Antonoff's rule), ELTON, 450; critical point, HILDEBRAND, 551
 Surface potentials (see also *Alcohols*); — — of insoluble monolayers, POWELL AND ALEXANDER, 482; — — of soluble monolayers, POWELL AND ALEXANDER, 493

Suspension, see *Particle*

T

- Tetrafluoroethylene, see *Polymers*
 Thixotropic gels, see *Light*

V

- Vapor adsorption, see *Silica gel*
 Viscoelastic, see *Relaxation*
 Viscometer (see also *Paints, Viscosity*); band —, HULL, 316
 Viscosity (see also *Polyisobutylene, Starch, Viscometer*); shear temperature and — in a rotational viscometer measurement, WELTMANN AND KUHN, 218; — of nitrocelluloses and Philippoff flow curves, CONRAD AND ZIIFLE, 227; Eyring's rate equation, and Paraplex, WHITEFIELD AND BARON, 268; — of glass, CAPPS, 334

W

- Water, oil — interfaces, see *Films*
 Water, sorption, see *Resins*

X

- X-ray diffraction, see *Clay*

INDEX OF BOOK REVIEWS

- | | |
|---------------------------------------------------------------------------------------------------------------------------------------------------------------------------------------------------------------------------------------------------------------------------------------------------------------------------------------------------------------------------------------------------------------------------------------------------------------------------------------------------------------------------------------------------------------------------------------------------------------------------------------------|------------------------------------------------------------------------------------------------------------------------------------------------------------------------------------------------------------------------------------------------------------------------------------------------------------------------------------------------------------------------------------------------------------------------------------------------------------------------------------------------------------------------------------------|
| <p>BRAUNS, F. E., The Chemistry of Lignin (PEW, J. C.), 648</p> <p>BRUYNE, N. A. DE, AND HOUWINK, R. (ed.), Adhesion and Adhesives (BIKERMAN, J. J.), 103</p> <p>BUCHTHAL, F., AND KAISER, E., The Rheology of the Cross Striated Muscle Fibre (HILL), 452</p> <p>FARKAS, A. (ed.), Physical Chemistry of the Hydrocarbons (BOWMAN, J. R.), 647</p> <p>GREENBERG, D. M. (ed.), Amino Acids and Proteins. Theory. Methods. Application (STEINHARDT, J.), 105</p> <p>HÄGGLUND, E., The Chemistry of Wood (PEW, J. C.), 646</p> <p>HUSEMANN, E. (ed.), Die Makromolekulare Chemie, Band VI, Staudinger Festband, MÄRZ 1951 (MARK, H.), 104</p> | <p>JOST, W., Diffusion in Solids, Liquids, Gases (DROZIN, V.), 553</p> <p>KERTESZ, Z. I., The Pectic Substances (OWENS, H. S.), 104</p> <p>KUBASCHEWSKI, O., AND EVANS, E. LL., Metallurgical Thermochemistry (BIRCHENALL, C. E.), 106</p> <p>MOELLER, T., Inorganic Chemistry. An Advanced Textbook (LAMER, V. K.), 648</p> <p>RODD, E. H. (ed.), Chemistry of Carbon Compounds. Vol. I, part A (RAMIREZ, F.), 645</p> <p>SMOLUCHOWSKI, R., MAYER, J. E., AND WEYL, W. A. (ed.), Phase Transformations in Solids (READ, T. A.), 646</p> |
|---------------------------------------------------------------------------------------------------------------------------------------------------------------------------------------------------------------------------------------------------------------------------------------------------------------------------------------------------------------------------------------------------------------------------------------------------------------------------------------------------------------------------------------------------------------------------------------------------------------------------------------------|------------------------------------------------------------------------------------------------------------------------------------------------------------------------------------------------------------------------------------------------------------------------------------------------------------------------------------------------------------------------------------------------------------------------------------------------------------------------------------------------------------------------------------------|

JOURNAL OF COLLOID SCIENCE

Editor-in-Chief

VICTOR K. LA MER, Columbia University, New York

Advisory Board

C. O. BECKMANN	J. TH. G. OVERBEEK
KATHARINE B. BLODGETT	R. RUYSSSEN
K. F. BONHOEFFER	E. K. RIDEAL
M. L. CORRIN	WILLIAM SEIFRIZ
P. J. W. DEBYE	LEO SHEDLOVSKY
JOHN T. EDSALL	THEODORE SHEDLOVSKY
I. FANKUCHEN	ROBERT SIMHA
JOHN D. FERRY	JACINTO STEINHARDT
A. R. GORDON	THE SVEDBERG
WILFRIED HELLER	HUGH S. TAYLOR
ERIC HUTCHINSON	ARNE TISELIUS
JOHN G. KIRKWOOD	ROBERT D. VOLD
E. C. LINGAFELTER	BERNARD VONNEGUT
L. G. LONGSWORTH	RALPH W. G. WYCKOFF
J. W. MCBAIN	BRUNO H. ZIMM

VOLUME 7

1952

ACADEMIC PRESS INC., PUBLISHERS
NEW YORK, N. Y.

Copyright 1952, by Academic Press Inc.
Made in United States of America

CONTENTS OF VOLUME 7

NUMBER 1, FEBRUARY, 1952

ANDRIES VOET AND LOUIS R. SURIANI. Dielectric Characteristics of Pigment Dispersions	1
HUBERT DAOUST AND MARCEL RINFRET. Solubility of Polymethyl Methacrylate and Polyvinyl Acetate	11
MATA PRASAD AND V. SWAMINATHAN. Study of the Extinction Coefficients of Gels During Mutual Gelation	20
MATA PRASAD AND SWAMINATHAN. Studies in Mutual Gelation	25
KARL SOLLNER AND HARRY P. GREGOR. The Electrochemistry of Permselective Protamine Collodion Membranes. III. The Electrical Resistance of Several Types of Permselective Protamine Collodion Membranes in Solutions of Various Electrolytes	37
SADHAN BASU AND PARES CH. DAS GUPTA. Studies on Polyelectrolytes. I. Sodium Carboxymethylcellulose	53
W. F. H. M. MOMMAERTS. The Measurement of Lightscattering Intensities According to Brice	71
F. E. BARTELL AND JOHN E. BOWER. Adsorption of Vapors by Silica Gels of Different Structures	80
SAMUEL H. MARON AND CARL MOORE. Morphologic Changes in Gelled Synthetic Latices	94
BOOK REVIEWS	103

NUMBER 2, APRIL, 1952

H. W. FOX AND W. A. ZISMAN. The Spreading of Liquids on Low-Energy Surfaces. II. Modified Tetrafluoroethylene Polymers	109
I. PRIGOGINE AND J. MARECHAL. The Influence of Differences in Molecular Size On the Surface Tension of Solutions. IV.	122
G. C. NUTTING. Effect of Electrolytes on the Viscosity of Potato Starch Pastes	128
M. VAN DER WAARDEN. The Process of Spontaneous Emulsification	140
E. HUTCHINSON AND D. RANDALL. An Application of the Gibbs' Adsorption Theory to Films at Oil-Water Interfaces	151
ELAINE G. SHAFRIN AND WILLIAM A. ZISMAN. The Spreading of Liquids on Low-Energy Surfaces. IV. Monolayer Coatings on Platinum	166
MATA PRASAD, K. E. SUBRAMANIAN, R. L. DESAI AND C. R. KANEKAR. Light Scattering by Some Thixotropic Gels	178
J. FARRAR AND S. M. NEALE. The Distribution of Ions Between Cellulose and Solutions of Electrolyte	186
LETTER TO THE EDITORS:	
MARJORIE J. VOLD. Molecular Cross Sections in Films of Fatty Acids on Water	196

NUMBER 3, JUNE, 1952

J. C. SLATER. Presentation of Bingham Medal to P. W. Bridgman	199
P. W. BRIDGMAN. Acceptance of the Bingham Medal	202
M. MOONEY AND S. A. BLACK. A Generalized Fluidity Power Law and Laws of Extrusion	204

RUTH N. WELTMANN AND PERRY W. KUHN. Effect of Shear Temperature on Viscosity in a Rotational Viscometer Measurement	218
CARL M. CONRAD AND HILDA M. ZIFLE. Implications of Philippoff Flow Curves for the Determination of Intrinsic Viscosity of High Polymer Nitrocelluloses	227
C. E. BEYER AND F. E. TOWSLEY. The Flow of Polystyrene through Rectangular Channels	236
W. H. MARKWOOD, JR. AND H. M. SPURLIN. Residual Stresses and Strains in Molded Plastics	244
C. A. DAHLQUIST AND M. R. HATFIELD. Constant Stress Elongation of Soft Polymers: Time and Temperature Studies	253
H. B. WHITFIELD AND THOMAS BARON. Application of Eyring's Rate Equation To Viscometric Data on Paraplex	268
S. P. JONES AND J. K. TYSON. The Rheology of a Lubricating Oil at Temperatures Below the Pour Point	272
B. W. HOTTEN AND D. H. BIRDSALL. Fine Structure and Rheological Properties of Lithium Soap-Oil Dispersions	284
W. J. WEST. Size Determinations of Clay Particles in Water Suspensions by Use of Low-Angle X-Ray Diffraction	295
W. K. ASBECK, D. D. LAIDERMAN AND M. VAN LOO. A High Shear Method of Rating Brushability of Paints	306
HARRY H. HULL. The Band Viscometer	316
ALFRED L. COPLEY. The Rheology of Blood. A Survey	323
WEBSTER CAPPS. Viscosity of Glass	334
LETTER TO THE EDITORS:	
J. TH. G. OVERBEEK AND M. J. SPARNAAY. Experiments on Long-Range Attractive Forces between Macroscopic Objects	343

NUMBER 4, AUGUST, 1952

JOHN D. FERRY AND MALCOLM L. WILLIAMS. Second Approximation Methods for Determining the Relaxation Time Spectrum of a Viscoelastic Material	347
R. ST. J. MANLEY AND S. G. MASON. Particle Motions in Sheared Suspensions. II. Collisions of Uniform Spheres	354
ROBERT H. DINEGAR AND ROBERT H. SMELLIE. Stability of Monodispersed Sulfur Hydrosols	370
J. GORDIN KAPLAN. The Activity of Catalase Unfolded at the Air-Water Interface	382
G. R. HOLZMAN AND K. H. MOORE. An Electron Diffraction Study of the Reorientation of Certain Alkali Halides Deposited on Mica and on Mica Surfaces Covered by Organic Films	396
MELVIN L. KARON, MABELLE E. ADAMS AND SEYMOUR NEWMAN. The Effect of Temperature on the Electrophoretic Analysis of Cottonseed Meal Extracts	407
B. CHATTERJEE AND S. BOSE. The Electrochemical Properties of Humid Acid	414
H. W. FOX AND W. A. ZISMAN. The Spreading of Liquids on Low Energy Surfaces. III. Hydrocarbon Surfaces	428
JOHN C. HENNIKER. Retardation of Flow in Narrow Capillaries	443
LETTERS TO THE EDITORS:	
W. B. INNES. The Treatment of Complex Absorbates as a Single Phase	447
TERRELL L. HILL. Comments on the Preceding Note by W. B. Innes ..	449
G. A. H. ELTON. The Surface Tension of Solids	450
BOOK REVIEW:	
TERRELL L. HILL. The Rheology of the Cross Striated Muscle Fibre ..	452

NUMBER 5, OCTOBER, 1952

SAMUEL KAUFMAN AND CURTIS R. SINGLETERRY. The Critical Range for Micelle Formation by an Oil-Dispersible Soap in a Hydrocarbon Solvent	453
FRED SCHULMAN AND W. A. ZISMAN. The Spreading of Liquids on Low-Energy Surfaces. V. Perfluorodecanoic Acid Monolayers	465
B. D. POWELL AND A. E. ALEXANDER. Studies of Surface Potentials. I. Effect of Salts and the Nature of the Interface upon the Surface Potentials of Insoluble Monolayers	482
B. D. POWELL AND A. E. ALEXANDER. Studies of Surface Potentials. II. Effect of Salts and the Nature of the Interface upon the Surface Potentials of Soluble Monolayers	493
MYRLE F. JOHNSON, WARREN W. EVANS, IVO JORDAN, AND JOHN D. FERRY. Viscosities of Concentrated Polymer Solutions. II. Polyisobutylene	498
HARRY P. GREGOR, BENSON R. SUNDHEIM, KALMAN M. HELD, AND MONROE H. WAXMAN. Studies on Ion-Exchange Resins. V. Water Vapor Sorption	511
E. L. MACKOR AND J. H. VAN DER WAALS. The Statistics of the Adsorption of Rod-Shaped Molecules in Connection with the Stability of Certain Colloidal Dispersions	535
LETTER TO THE EDITORS:	
JOEL H. HILDEBRAND. The "Critical Point"	551
BOOK REVIEW:	
VADIM DROZIN. Diffusion in Solids, Liquids, Gases	553

NUMBER 6, DECEMBER, 1952

J. R. McLOUGHLIN AND A. V. TOBOLSKY. The Viscoelastic Behavior of Polymethyl Methacrylate	555
KURT UEBERREITER AND GERHARD KANIG. Self-Plasticization of Polymers	569
HOWARD C. HASS, LEONARD FARNEY, AND CLAUDE VALLE, JR.	584
J. L. VAN DER MINNE AND P. H. J. HERMANIE. Electrophoresis Measurements in Benzene Correlation with Stability	600
BERNARD VONNEGUT AND RAYMOND L. NEUBAUER. Production of Monodisperse Liquid Particles by Electric Atomization	616
A. M. POSNER, J. R. ANDERSON AND A. E. ALEXANDER. The Surface Tension and Surface Potential of Aqueous Solutions of Normal Aliphatic Alcohols	623
BOOK REVIEWS:	
FAUSTO RAMIREZ. Chemistry of Carbon Compounds. Vol. I, part A.	645
JOHN C. PEW. The Chemistry of Wood	646
T. A. READ. Phase Transformations in Solids	646
JOHN R. BOWMAN. Physical Chemistry of the Hydrocarbons	647
VICTOR K. LA MER. Inorganic Chemistry. An Advanced Textbook	648
JOHN C. PEW. The Chemistry of Lignin	648
AUTHOR INDEX	650
SUBJECT INDEX	653
INDEX OF BOOK REVIEWS	656

